CRUSTAL EVOLUTION IN NORTHWEST AUSTRALIA: EVIDENCE FROM SEISMIC REFRACTION DATA

A thesis submitted for the degree of

DOCTOR OF PHILOSOPHY

in the

AUSTRALIAN NATIONAL UNIVERSITY

by

BARRY JOHN DRUMMOND

JUNE 1982

STATEMENT

The studies described in this thesis were undertaken while I was a full-time research scholar in the Research School of Earth Sciences of the Australian National University during the period September 1979 to June 1982.

Except where mentioned in the text or in the acknowledgements, the research described in this thesis is my own.

This thesis has never been submitted to another University or similar institution.

. . . . . .

BARRY JOHN DRUMMOND

Canberra June 1982

ACKNOWLEDGEMENTS

The work described in this thesis was supervised by Dr K.J. Muirhead of the Research School of Earth Sciences, to whom I express my gratitude. Dr C. Wright also made many useful comments during the latter part of the project, and critically read the manuscript. Emeritus Professor A.L. Hales was involved in the initial shaping of the project, and I benefitted greatly from the friendship and gentle guidance of the late Dr J.R. Cleary.

Of course, research based on the interpretation of seismic data is impossible without data, and in this respect I acknowledge the considerable effort of my friends and colleagues of the Bureau of Mineral Resources, Geology and Geophysics, during the collection of the data in 1977. In particular, I thank D.M. Finlayson and P. Wellman, who supervised the field work, J.B. Connelly, C.D.N. Collins and J.W. Williams for the efforts they made in collecting the seismic data, and Heather McCracken Shelley for collecting the gravity data. The staff of the iron mining companies of the Pilbara, notably Goldsworthy Mining Limited, Cliffs Robe River Associates, Hamersley Iron Pty Ltd, and Mount Newman Mining Company Pty Ltd often gave of their own time in order to allow us to time their mining blasts and to ensure that our seismic survey ran smoothly. Emeritus Professor A.L. Hales made available the data from his recorders deployed throughout the region at the time of the BMR survey.

During the interpretation of the seismic data, I used numerous computer programs, several of which were made available by my colleagues. Dr K.J. Muirhead and C.D.N. Collins gave me ray tracing programs. S.P. Mathur made available his program for intercept method inversion and the time term inversion programs were written by Dr J. Leven. The synthetic seismogram program was written by Professor K. Fuchs and Dr G. Muller of the University of Karlsruhe, Federal Republic of Germany and converted to the RSES computer by Dr J. Leven. D.R. Christie gave me useful hints for writing my own programs.

Financial support for this research came in the form of an Australian Public Service Board Postgraduate Scholarship. All Bureau of Mineral Resources data and Figure 46 are used with the permission of the Director, Bureau of Mineral Resources.

Finally, I wish to thank my wife and children for their support during this project.

ABSTRACT

A seismic refraction and detailed gravity survey was undertaken in 1977 in the northwestern part of the Precambrian shield of Australia to study the structure of the Archaean Pilbara and Yilgarn Cratons which crop out in the area. Most of the traverses were across the Pilbara Craton, but some results are available from the northern Yilgarn Craton. The older Pilbara Craton has a much thinner crust than the Yilgarn Craton. The different crustal thicknesses, when considered with isostatic models of the region, imply that the upper mantle under the Pilbara Craton is less dense than the upper mantle under the Yilgarn Craton. Thus the upper mantle is implicated as the source of the huge amounts of iron in the banded iron formations of the Hamersley Basin which formed across the Pilbara Craton in the late Archaean and early Proterozoic.

Sediments of the Proterozoic Capricorn Orogenic Belt overlap the margins of the cratons and mask their structural relations. The northern margin of the Yilgarn Craton was deformed along a zone 50 km wide during the Proterozoic orogeny, but no such zone is recognisable in the seismic models of the southern edge of the Pilbara Craton. The lower crust of the Carpricorn Orogenic Belt has high seismic velocities and is dense, probably due either to higher metamorphic grades or mafic intrusions caused by the Proterozoic tectonics.

The seismic velocities in the crust of the Pilbara Craton imply that the upper crust is of granitic composition. At 10-15 km depth, it is metamorphosed to felsic granulite. Below this depth, the amount of garnet increases, causing an increase in the seismic velocity. The mafic content also increases, causing a further increase in the amount of garnet, until the lower crust of the craton is of dioritic composition. The crust/mantle boundary under the craton must be a chemical discontinuity. The lower crust of the Pilbara Craton is much less mafic than the lower crust in younger regions of Australia implying that different tectonic processes were active in the Archaean.

The Pn seismic velocity under the craton is anisotropic with the direction of maximum velocity at right angles to the axis of the Hamersley Basin along the azimuth N30^{o}E. The anisotropy is probably due to the realignment of olivine crystals in the upper mantle by syntectonic recrystallisation and/or power law creep in the tensional environment caused at the base of the lithosphere by flexure during loading by the Hamersley Basin strata. Another boundary occurs 15 km below the crust/mantle boundary throughout the region. It exhibits topography and the velocity below it is also anisotropic, with the apparent direction of maximum velocity between north and 40 degrees west of north. This direction correlates loosely with trends of geological features in the Hamersley Basin and in the younger Capricorn Orogenic Belt, suggesting that the anisotropy below the sub-Moho boundary is a younger feature than that below the crust/mantle boundary. This is consistent with the notion that the lithosphere was thinner in the Precambrian and implies that the base of the Archaean lithosphere is the velocity increase which is now at 45 km depth under the Pilbara Craton. The current base of the lithosphere may be below 200 km depth.

The seismic models limit the types of evolutionary processes that can be applied to the formation of the Hamersley Basin. The most likely are: (a) isostatic adjustment of an initial depression gradually filled with sediments. The initial depression may have been formed by any or all of (i) thermal uplift followed by erosion and then cooling and contraction, (ii) a metamorphic change within the crust to a denser, less voluminous phase, and (iii) a mass transfer process in which volcanic rocks were taken from the upper mantle and deposited on the land surface; and/or (b) compression and folding of the thin lithosphere by a compressive stress, causing the basin to form out of isostatic equilibrium.

TABLE OF CONTENTS

LIST OF TABLES

ABBREVIATED FIGURE CAPTIONS

Page

Page

1. INTRODUCTION

The history of the earth's crust is important, because the crust contains all of the minerals and energy resources necessary for man's existence. It also contains rocks from deep within the earth, and therefore provides us with a window to the interior of the earth. The history of the crust is imprinted in its rocks; rocks forming at the surface of the earth today carry the marks of the processes that formed them within the earth and carried them to the surface.

None of the primaeval crust of the earth remains. It was all either recycled through the mantle by the hot, active processes which must have prevailed during the first few hundred million years of the earth's existence, or was destroyed, or at least its character so altered that it is no longer recognisable, by meteorite bombardments, the evidence of which is still preserved on the surface of the moon. The oldest remnants of the earth's crust are the few Archaean cratons now exposed around the world, and it is from the geology and geochemistry of these cratons that we must piece together the earliest history of the earth.

The Archaean cratons are very old, perhaps older than 3500 m.y., and are often metamorphosed. As well, the cratons are composed of domes of granitoid that intruded sequences of volcanic and sedimentary rocks, now called greenstones, and these granitoid/greenstone terrains are unknown in younger regions. This poses problems for those who are studying the cratons and need to apply the principles of uniformitarianism.

While evidence for plate tectonics in the middle to late Precambrian can be found in the geochemistry of some lavas (eg. Loberg, 1980) and in the geographical distribution, stratigraphy, composition and evolutionary characteristics of other lavas and sediments (eg. Waters, 1976), the style, geochemistry and age relationships of the oldest Precambrian rocks fail attempts to unequivocally assign a plate tectonic history to the early Precambrian (eg. Groves & others, 1978; Grachev & Fedorovsky, 1981).

An example of the difficulty of studying Archaean cratons and deriving a model of Archaean crustal development is evidenced by the fact that many different theories exist for the development of the greenstone belts.

Four of them are currently regarded as plausible. Green (1972) suggested that the volcanics of the greenstone belts were the terrestrial equivalents of the lunar maria, formed by volcanism caused by the meteorite impact. Anhaeusser (1973) suggested they were formed by the protonucleation of ancient arcs, while Hunter (1974) preferred a model of small volcanic basins that formed between the uplifting granitoid magmas which were partial melts of a hydrous basaltic lithosphere. Glikson (1975) proposed that the greenstone belts are the relics of the ocean floor from which the granitoids were derived by partial melting. Within these four processes can be seen the uncertainty over whether the granitoids predated, were coeval with, or postdated the greenstones. Clearly, it is not easy to make unequivocal interpretations of the origins of Archaean cratons through the fog of time, tectonism and metamorphism.

The geology and geochemistry of the surface rocks can tell us much about the origins of the cratons, but before a full picture of the earliest evolution of the earth can be drawn, the interior of the crust must also be studied, for the processes which shaped the surface of the crust also modified its interior.

The rock types within the crust can sometimes be inferred from the surface geology. Lava flows, plutonic rocks and dyke swarms might have originated as partial melts of the lower crust, so their chemistry can indicate the rock types of the lower crust, and the tectonics of their emplacement can give inference to the stress state during their emplacement. Kimberlitic rocks which originated in the upper mantle often have inclusions of the lower crustal country rocks through which they passed to reach the surface.

However, in some cases, the lower crust in the areas of interest is not sampled by any of these means. For example, there may be no igneous rocks whose origins were undeniably in the lower crust, or perhaps there are no kimberlite pipes. In these regions, the physical properties of the lower crust crust can only be sampled by geophysical surveys.

The oldest exposed crust in the world exists in the South African Craton, the North Atlantic Craton of North America and Greenland, and in the Pilbara and Yilgarn Cratons of Western Australia. In 1977, the Australian Bureau of Mineral Resources, Geology and Geophysics (BMR) and the Research School of Earth Sciences of the Australian National University (ANU) undertook a geophysical study of the portion of the northwest part of Australia

containing the Pilbara Craton and the northern part of the Yilgarn Craton. The aims of the survey were to investigate the major structures within the Pilbara Craton and, if possible, those of the northern Yilgarn Craton, and to investigate the structures in the mobile belt which lies between the cratons to determine the mechanism of the its formation.

Some of the data from the survey were interpreted using the intercept method (Ewing & others, 1938; Dooley, 1952; Mota, 1954) and the results published by Drummond (1979b; 1981) and Drummond & others (1981). Drummond & Shelley (1981) considered the gravity field of the region, and Drummond & others (1982) studied structures deeper in the mantle. The purpose of this thesis is to paraphrase the results in those papers, and to present the results of a time term interpretation and a study of the seismic amplitudes of some of the data. From the models so derived, inferences are drawn about the the nature of the crust in the cratons, and about the formation of the crust of northwest Australia during the Precambrian. The results may be of use to geoscientists studying similar cratons in other parts of the world where geophysical data are not yet available.

2. GEOLOGY AND GEOCHRONOLOGY OF THE PRECAMBRIAN SHIELD OF NORTHWEST AUSTRALIA.

The geology of Western Australia is most completely described in GSWA (1975). More up to date, though brief, descriptions of the Precambrian shield are given by Gee (1979a; 1979b; 1980), Horwitz & Smith (1978), and Hallberg & Glikson (1981). Summaries of the geochronology of the region are to be found in Compston & Arriens (1968), Arriens (1971), de Laeter & others (1974), Richards (1977) and de Laeter, Libby & Trendall (1981). Brief descriptions of the geology and geochronology of the area of the 1977 seismic survey are in Drummond (1979b; 1981) and Drummond & others (1981) which appear in this thesis as Appendices 1, 2 and 3, respectively. The purpose of this chapter is to present a succinct description of those features of the geology relevant to future discussions in this thesis. As such, it is an expanded version of the chapters on geology in the first three appendices. However, before the geology and geochronology are described, a few notes on tectonic and time nomenclature are in order.

2.1 NOMENCLATURE

The tectonic nomenclature used below mostly follows that of Gee (1979a; 1979b). Accordingly, a block is that portion of an old, stabilised region of the basement now exposed at the surface. If the buried portion of the basement can be delineated, the total extent of the stabilised region is known as a craton. Consequently, the Pilbara Block discussed below is the exposed part of the Pilbara Craton, whose limits below the younger cover rocks can be interpreted with confidence from geological and geophysical data.

Mobile belts bound some of the margins of the cratons in the Western Australian shield. Mobile belts are elongate regions in which crustal mobility is expressed by magmatism, metamorphism and deformation. If the mobile belt also has a thick pile of flysch-type sedimentary rocks in an elongate depositional trough, it is called an orogen.

The entire survey area is in a region of outcropping Precambrian rocks. The Precambrian is traditionally subdivided into the older Archaean era and the younger Proterozoic era. Permeating the literature on the geology of Western Australia is the sense that granitoid/greenstone terrains are Archaean

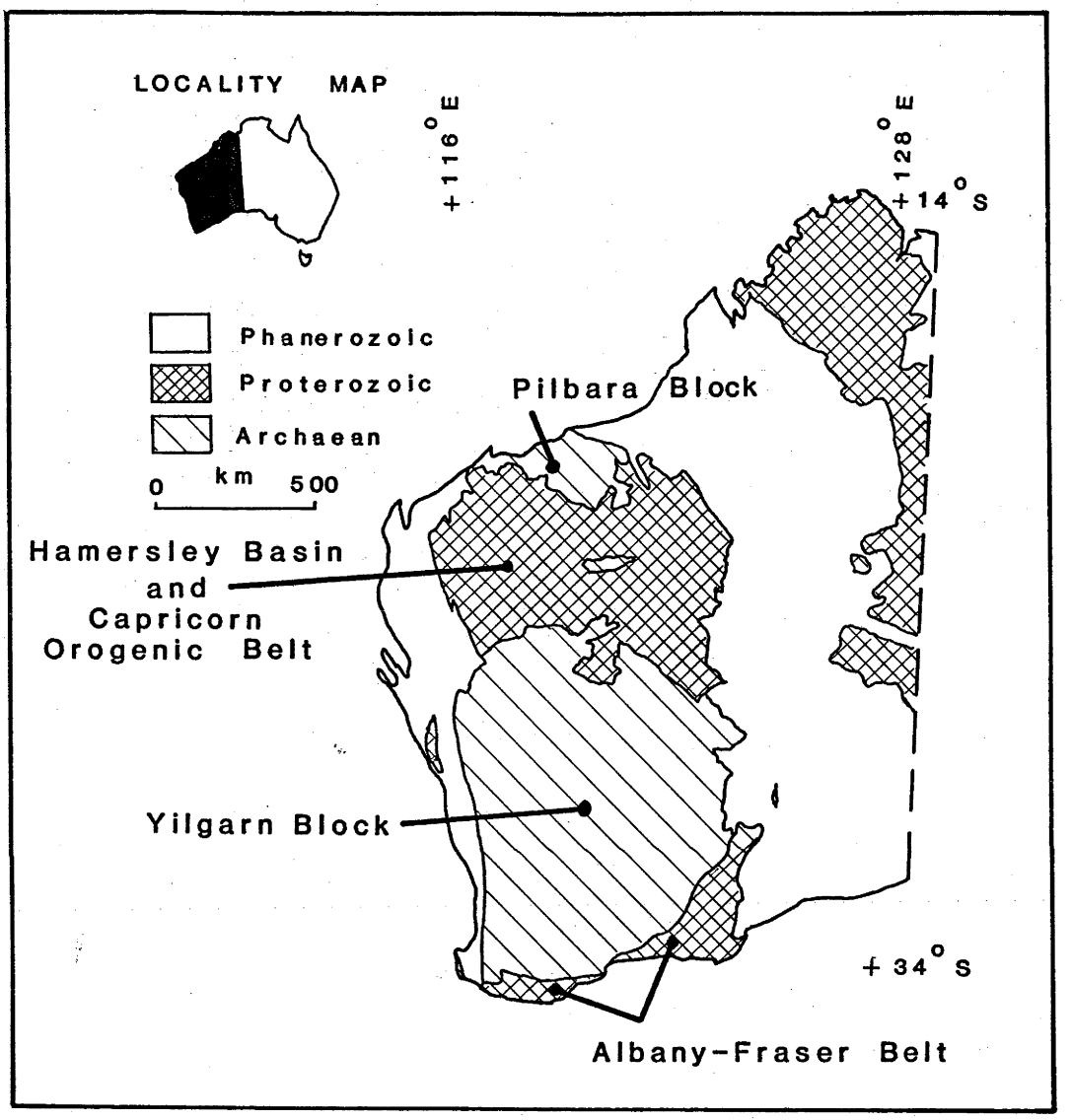

Figure 1: Distribution of Precambrian rocks in Western Australia.

and all younger Precambrian rocks are Proterozoic. On this basis, Trendall (1975a) set the Archaean/Proterozoic boundary at 2400 m.y., while Proterozoic rocks are between 2400 and 600 m.y. old. The terms 'early', 'middle' and 'late' give the rock ages relative to these time boundaries, and the terms 'lower', 'middle' and 'upper' refer to the positions of the rocks in the stratigraphic column.

With the increasing flood of isotope geochronological ages, the basal rocks of the Hamersley Basin, which unconformably overlie the granitoid/greenstone terrains of the Pilbara Craton, appear to be older than many of the granitoids and greenstones of the Yilgarn Craton. Thus, Gee (1980) revised the adopted time of the Archaean/Proterozoic boundary to 2500 m.y. Further revisions will probably be necessary as more isotopic dates become available, and this means that literature assigning some rocks to one or the other era will become outdated as the boundary is moved backwards and forwards in time.

The problem of defining the Archaean/Proterozoic boundary in time would not exist if the original definition of the term 'Archaean' was applied. Holmes (1965, p165) wrote: "The term ARCHAEAN refers to the oldest known Precambrian crystalline rocks of a given region and has no other age significance" (my underling). Thus, in the strictest usage, the Archaean rocks of a region can be Proterozoic, in which case the expression 'Archaean/Proterozoic boundary' is meaningless. The Archaean/Proterozoic time boundary probably varies from continent to continent, and, within the shield of Western Australia, from one craton to another. For this reason, I have tried to avoid using the terms 'Archaean' and 'Proterozoic' as indicators of time in the following discussion, and generally rely on the use of absolute isotopic ages. Where the term 'Archaean' is used, it refers to the oldest recognisable cratonic core, as inferred from Holmes' definition.

2.2 GEOLOGICAL DESCRIPTION

The survey area is part of the Western Shield of Western Australia, shown in Figure 1, and composed of two Archaean blocks, the Pilbara and Yilgarn Blocks, whose structural relations are masked by the younger Proterozoic cover rocks of the Hamersley Basin and Capricorn Orogenic Belt. Another mobile belt, the Albany-Fraser Belt, bounds the southern margin of the Yilgarn Block. The Darling Fault forms the western margin of the Yilgarn Block, but younger, Phanerozoic cover rocks unconformably overlie all other boundaries. The full extent of the Precambrian basement below the Phanerozoic regions is

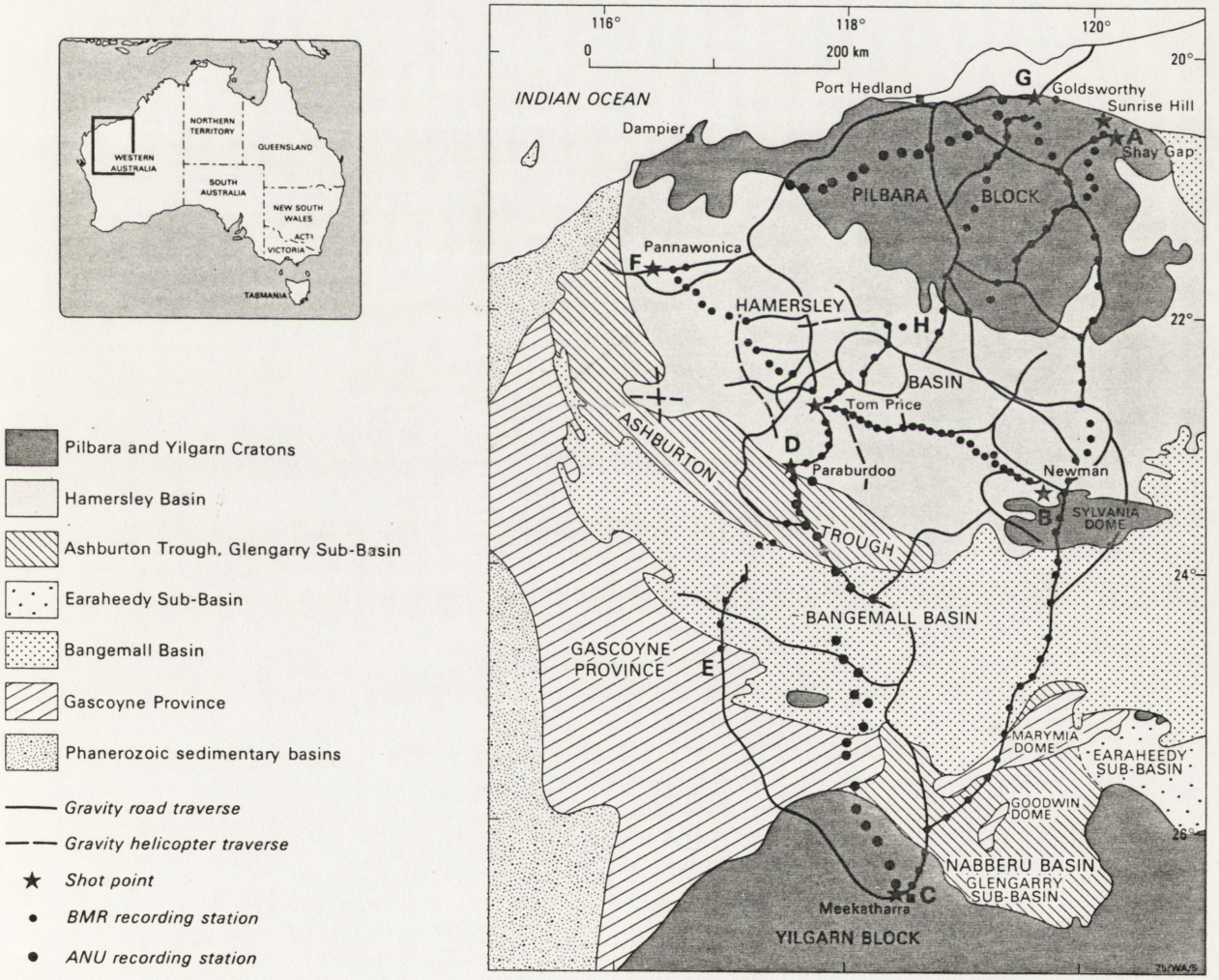

Figure 2: Geology of the survey region, and survey design.

not known. The exposed part of the Western Shield measures approximately 1500 km from north to south and about 700 km from east to west. The survey area covered the northern half of the Western Shield.

The geology of the survey area is shown in slightly more detail in Figure 2. The oldest isotopic dates yet recorded in Australia are in the range 3400 to 3600 m.y. and are for rocks in the greenstone belts of the Pilbara Block (Richards, 1977; Pidgeon, 1978a; Hamilton & others, 1980). The greenstone belts are composed of volcanic rocks of mainly ultrabasic and basic composition, although rocks of acid and intermediate composition are also present, with associated volcaniclastic rocks and clastic sediments. They sinuously enclose large ovoid domes of younger granitoid, with isotopic ages grouped around 3000 m.y. (Oversby, 1976; Pidgeon, 1978b; de Laeter & Blockley, 1972; de Laeter, Libby & Trendall, 1981; Cooper & others, 1980). These granitoids were probably derived directly from the mantle, or had very little crustal prehistory before intrusion into the upper crust (de Laeter & Blockley, 1972), and were intruded into the greenstone strata with broadly concordant contacts. The granitoid domes and the greenstone belts were further intruded by younger granitoids, with ages grouped around 2600 to 2800 m.y. (Oversby, 1976; de Laeter & Blockley, 1972; de Laeter, Libby & Trendall, 1981), which probably resulted from the partial melting of the lower crust (de Laeter & Blockley, 1972).

The Yilgarn Block also has a granitoid/greenstone stratigraphy, but whereas the granitoids of the Pilbara Block are ovoid in shape, the granitoids and greenstones of the Yilgarn Block are elongate with a general north/south trend. Gee (1979a) defined the Western Gneiss Zone, a region of high metamorphic grade gneisses and granulites along the western margin of the Yilgarn Block, in which the granitoid ages fall in the range 3000 to 3400 m.y. (Arriens, 1971; de Laeter , Fletcher & others, 1981). For the rest of the Yilgarn Block, most isotopic ages for granitoids fall about 2600 .m.y. The ages can generally be interpreted as close to the time the granitoids were derived from the mantle, although Oversby (1975) was able to postulate a possible crustal prehistory of up to 700 m.y. for some granites in the Norseman and Kalgoorlie regions. The greenstones may predate the granitoids by no more than 100 m.y. (Turek, 1966; Cooper & others, 1978; Hallberg & others, 1976).

Thus the bulk of the granitoids in the Yilgarn Block appear to be the same age as the thermal event which remelted the lower crust in the Pilbara Block. Figure 3 is a modified version of Figure 4 of de Laeter , Libby &

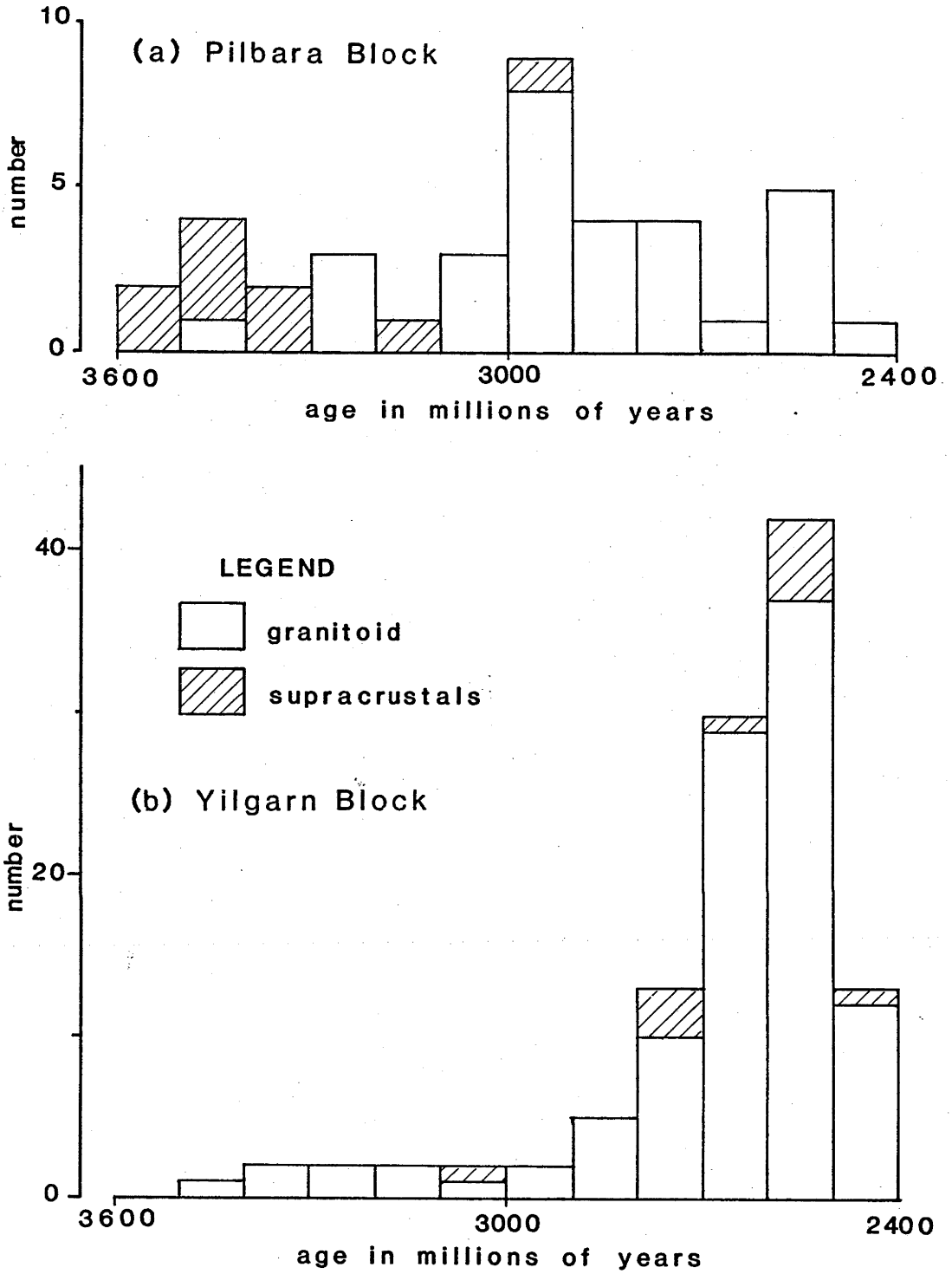

Figure 3: Histograms of presently available isotopic ages of Precambrian rocks in the Pilbara and Yilgarn Blocks.

Trendall (1981), and shows histograms of the available isotopic ages from the Pilbara and Yilgarn Blocks. It differs from Figure 4 of de Laeter & others in several ways. The ages of rocks from the Hamersley Basin are not included with those from the Pilbara Block; Oversby's (1975; 1976) lead ages, and not her Rb/Sr ages were used; the ages from Leggo & others (1965), Cooper & others (1980), Richards & others (1981), and Richards (1982) are included in the data for the Pilbara Block, and those of de Laeter, Fletcher & others (1981), Chapman & others (1980), Nieuwland & Compston (1980), Pidgeon (1973), Mc Culloch & Wasserburg (1978) and Mc Culloch & Compston (1981) were included in those of the Yilgarn Block; and, where several rocks from the same locality gave similar ages, or where several isotopic techniques were applied, only one result was included. The histograms do not show the ages of the cratons. The dates plotted include the times that some rocks were derived from the mantle, but they also include the times some rocks were formed by remelting the lower crust, and metamorphic dates. The histograms may also be influenced by the uneven areal sampling of the blocks.

The histograms are, however, very useful indicators of thermal events. The greenstones of the Pilbara Block have ages which are generally older than the granitoids, and older than the bulk of the ages in the Yilgarn Block. The histogram of the ages in the Yilgarn Block peaks at 2500 to 2600 m.y., at or just after the time of partial melting of the lower crust of the Pilbara Block.

The rocks of the Hamersley Basin unconformably overlie the southern margin of the Pilbara Block. Inliers of basement rock within the basin suggest that the Pilbara Craton forms the basement of the basin. The Sylvania Dome in Figure 2 is the only inlier large enough to plot at the scale of Figure 2. Trendall (1979) defined the type areas and revised the stratigraphy of the Hamersley Basin. It is made up of the basal Fortescue Group, composed mainly of basalts and mudstones, the Hamersley Group, with banded iron formations of remarkable lateral extent and continuity (Trendall, 1975b), clastic sediments, and the acid Woongarra Volcanics, and the uppermost Turee Creek Group, of clastic sediments. Together, these three groups comprise the Mount Bruce Supergroup.

The structure of the Hamersley Basin was described by Trendall (1975b). In the north of the present day outcrop area of the basin, the strata dip southwards at no more than a few degrees. South of the axis of the basin, which lies just to the northeast of a line joining Pannawonica to Newman in Figure 2, the dips are gentle, but to the north. Farther south,

however, the intensity of folding increases, with the strata folded on approximate east/west axes. Coupled with this folding is a regular plunge undulation, forming synclines and anticlines, with the synclines passing along strike into anticlines. Archaean basement has either been exposed by erosion or can be inferred from gravity data (Fraser, 1979a) in the cores of the anticlines. Along the southern margin of the basin, the dips are very steep, often near vertical, and some overturning has occurred.

The basal rocks of the Fortescue Group are probably 2700 to 2800 m.y. old (Trendall, 1975c; Richards, 1977; Richards & others, 1981; Richards, 1982; Hickman & de Laeter, 1977; R.T. Pidgeon, ANU, personal communication, 1978). The Woongarra Volcanics, near the top of the Hamersley Group are about 2200 m.y. old (Leggo & others, 1965), which is consistent with an age of about 2200 m.y. for the underlying Weeli Wolli Formation (de Laeter & others, 1974). However, these are probably minimum ages for these formations. Blockley & others(1980) suggested that the Sylvania Dome was uplifted about 2200 m.y. ago. Thus, the Hamersley Basin was active for a period of 500 to 600 m.y. This represents a time interval equal to the entire Phanerozoic.

The flysch-type clastic sediments of the Ashburton Trough (the Wyloo Trough of Horwitz & Smith, 1978), which abuts the southern margin of the Hamersley Basin, were originally included with the Turee Creek Group and called the Wyloo Group of the Mount Bruce Supergroup of the Hamersley Basin (Trendall, 1975b), but they are now recognised as younger than the Hamersley Basin strata (Gee, 1979a). Isotopic dates for granite plutonism lie in the range 1700 to 1800 m.y. (de Laeter, 1976; Leggo & others, 1965; Williams & others, 1978), and provide a minimum age for trough sedimentation. A tuffaceous siltstone within the trough sediments is 1850 m.y. old (Leggo & others, 1965).

Gee (1979b) has the Ashburton Trough coeval with the Nabberu Basin. The structural and time relations between the two provinces are masked by younger cover rocks. Horwitz (1975) reported a minimum K/Ar age of 1680 m.y. for a glauconite schist in the Nabberu Basin. The stratigraphy of the Nabberu Basin was described in detail by Hall & Goode (1978). The basin is composed of two sub-basins - the Earaheedy Sub-basin in the east and the Glengarry Sub-Sub-basin in the west. The Glengarry Sub-basin lies in the survey area and contains a thick geosynclinal sequence (Gee, 1979c) . The strata dip gently northwards off the Yilgarn Block which they unconformably overlie, but the intensity of folding increases to the north. The Stanley Fold Belt along the northern and northwestern margins of the basin contains intensely folded strata,

with the Archaean basement often involved in the deformation. Horwitz (1975) commented on the mirror-image symmetry of folding in the Nabberu and Hamersley Basins. Gee (1979a) included the Nabberu Basin and Ashburton Trough geosynclinal sequences in the Capricorn Orogen.

The Bangemall Group, which fills the Bangemall Basin and masks the structural relations between the Ashburton Trough and Nabberu Basin is composed of fine grained sedimentary rocks, with minor conglomerates, breccias, tuffaceous sandstones and acid volcanics. The basin formed over a cratonic crust (Gee, 1979a). Changes in the structureal style and facies within the basin implied to Brakel & Muhling (1976) that stable basement paralleled the southern boundary of the Pilbara Craton in the north, and the northern boundary of the Yilgarn Block in the south, while the central and western portions of the basin had active basement.

Gee (1980) placed the age of the basal unconformity of the Bangemall Basin at 1100 m.y., based on the results of Gee & others (1976) and Compston & Arriens (1968). Richards (1982) derived an age of 1580 m.y. for galenas from a basement high in the basin, but he does not say whether the samples are from the basement or from basal rocks of the basin exposed near the high. The basin may have been uplifted between 700 and 800 m.y. ago (de Laeter, 1976).

The Gascoyne Province in the west of the survey area contains reworked and metamorphosed Archaean basement rocks, and folded and metamorphosed rocks of the Bangemall and Nabberu Basins and the Ashburton Trough (Daniels, 1975). The province underwent a major dynamothermal event 1700 to 1800 m.y. ago, and a thermal event 700 m.y. ago. Granitoids which crop out within the province were derived from partially melted basement granitoids mixed with younger magmatic and supracrustally reworked material (de Laeter, 1976; Williams & others, 1978).

The entire survey area has been a positive landmass since the Precambrian. It is now mostly arid semi-desert covered by a thin veneer of Tertiary and Quaternary sand and soil. Rejuvenated erosional surfaces testify to regional uplift on several occasions since the Tertiary (Hickman & Lipple, 1975).

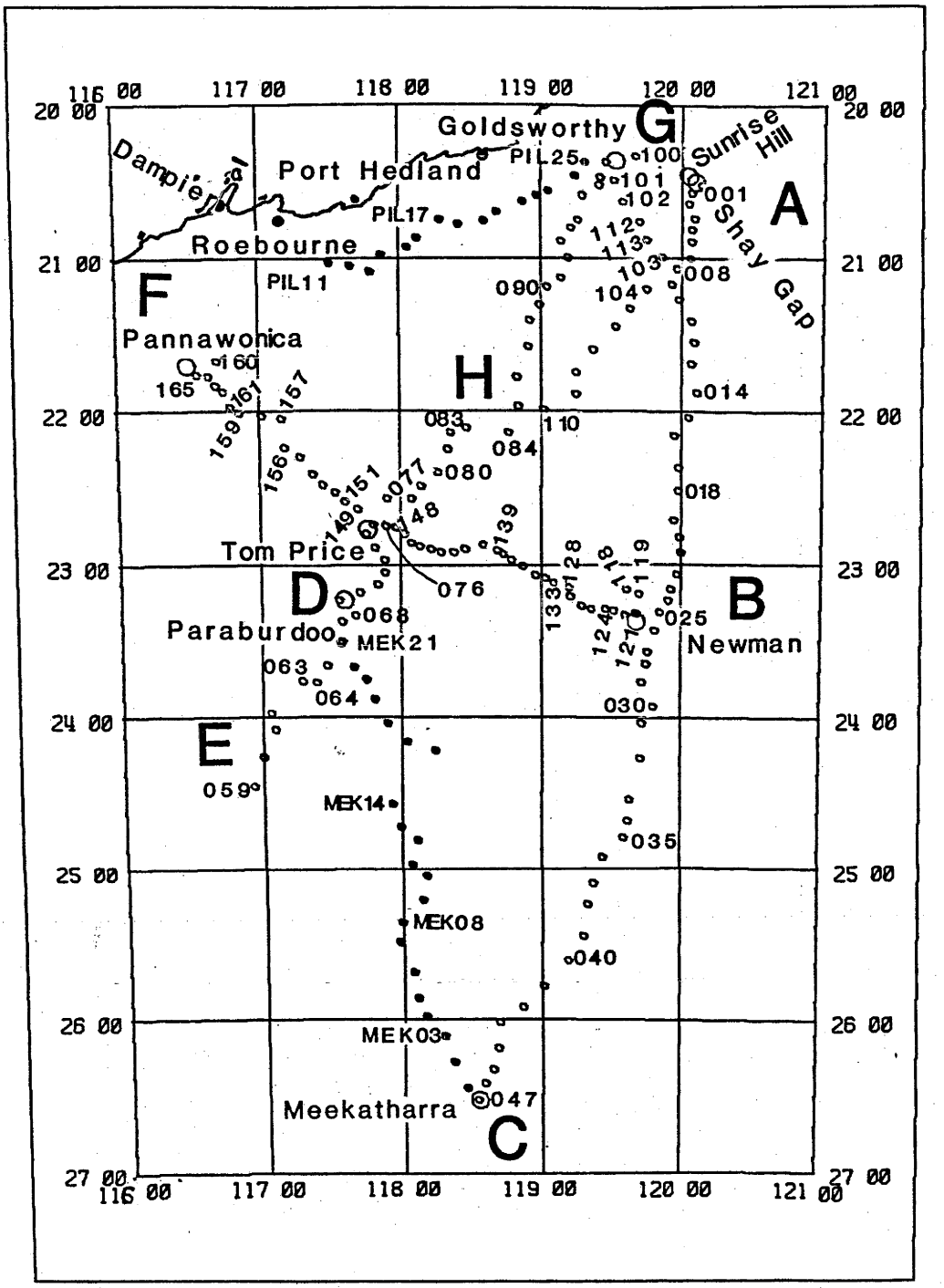

Figure 4 Survey design. Large circles indicate the shot sites. Those at Goldsworthy (G), Shay Gap and Sunrise Hill (A), Newman (B), Tom Price and Paraburdoo (D) and Pannawonica (F) were quarrying blasts at the iron ore mines. The blast at Meekatharra (C) was especially prepared for the survey. Small circles with a three digit number are BMR recording stations; dots with a two digit number and a prefix of three alphabetic characters are ANU stations.

3 THE SURVEY

Full details of the 1977 BMR field work are given in Drummond (1979c). Brief summaries are given in Drummond (1979a; 1979b; 1981), Drummond & others (1981) and Drummond & Shelley (1981). Drummond (1979a) gave some details of the the ANU field recording. The following description is included to make this report complete.

One hundred and fifteen quarry blasts at the seven open-cut iron ore mines in the Pilbara region were used as seismic sources. The mines are at Goldsworthy (G in Figures 2 & 4), Shay Gap and Sunrise Hill (A), Newman (B), Tom Price and Paraburdoo (D) and Pannawonica (F). The first three mines quarry iron ore in banded iron formations in the greenstone belts of the northern Pilbara Block. The Newman, Tom Price and Paraburdoo mines are in the banded iron formations of the Hamersley Group in the Hamersley Basin, and the mine at Pannawonica is in Tertiary laterites deposited along ancient stream beds, but now exposed as the caps of mesas in the western Hamersley Basin.

The mining blasts varied in size from a few tonnes to nearly 600 tonnes. However, the blasts were designed to break rock, and not to produce seismic energy; in fact, the seismic energy was often kept to a minimum to avoid damage to buildings near the mines. Many of the blasts had large delays between charges, and were spread over several benches within the mines; for example, one Pannawonica blast had a total burning time of more than 2 s, while areal extents greater than 10 km were common. Consequently, the blasts were not efficient sources of seismic energy. The seismic energy was assumed to originate from the centre of the blast pattern, so that some errors may occur in the adopted effective position of some of the blasts.

Seismographs set up near the mines were used to time the explosions. The travel times to these mine monitors were calibrated by recording at least one blast simultaneously on the monitor recorder and on a chart recorder placed as near as practicable to the blast. The time base used for all survey work was the standard frequency and time signal transmission on radio station VNG, on 4.5, 7.5 and 12 MHz.

A blast of 11 tonnes of explosives was prepared and fired in an abandoned mine shaft at Meekatharra in the northern Yilgarn Block (C in Figures 2 & 4). The blast was used to reverse the recording lines which extended the survey south of the Pilbara Craton to the northern Yilgarn Craton.

Arrays of portable seismographs were deployed to record the blasts. Recorders were set up at each station and left until sufficient blasts had been recorded. The arrays were then moved to the next set of stations. Several types of recorders were used. The BMR recorders were single (vertical) component slow speed frequency modulated tape recording seismographs, described by Finlayson & Collins (1980). The ANU seismographs were updated versions of the slow speed, direct record tape recorders described by Muirhead & Simpson (1972), recording either one or three components at three gain levels.

The recording stations were positioned with an accuracy of 100 m or better using aerial photographs and topographic maps at 1:100 000 scale from which the coordinates could be scaled. In some cases, greater accuracy was obtained by setting up stations near surveyed road bench marks. The station spacing was generally less than 20 km. Near the shotpoints, a spacing of 5 km was used; the maximum spacing along line BD was 8 km.

The station numbers of Drummond (1979c) are shown in Figure 4. The 137 BMR stations sre shown as small circles with three digit numbers, and the 37 ANU stations as dots with two digit station numbers with prefixes of three alphabetic characters. A few of the stations failed, either partially or entirely.

During playback of the BMR tapes in the laboratory, the seismic signals were first anti-alias filtered at 20 Hz, and then digitised at 16 ms intervals. This meant that the Nyquist frequency of about 31 Hz was well beyond the limits of the remaining seismic signals. After anti-alias filtering, The ANU tapes were sampled at about 25 samples per second, depending on the instantaneous tape speed. Record sections were then produced for the seismic interpretation.

Gravity coverage of the region had previously been at the reconnaissance scale of readings on an 11 km grid (Fraser, 1979a; 1979b). During the survey, more than 2000 gravity measurements were made at intervals of less than 4 km along roads and tracks in the area. Total magnetic intensity was also measured at each of these gravity stations. As well, 109 gravity readings were made in inaccessible regions using a helicopter for transport.

Heat flow was measured in several drill holes in the region; Cull & Denham (1979) reported the results.

Wherever possible, fresh rock samples were collected at recording sites and from road and railway cuttings. The specific gravity and compressional wave velocities at standard temperature and pressure were measured for these samples in the laboratory after the field work. Drummond (1979c) tabulated the results, and Drummond & others (1981) presented some of the results as a bar graph (their Figure 5, repeated later as Figure 8 of this thesis).

4. PRELIMINARY INTERPRETATION OF THE SEISMIC DATA.

4.1 DATA

In the following discussion, all of the data are represented as record sections. Unless stated otherwise in the figure captions, all data were digitally filtered for display purposes in the bandpass 0.5 to 8.0 Hz, and no changes were made to the relative amplitudes of the traces; ie. no adjustments were made for the effects of different shot weights, recorder gains, or for the effects of geometrical spreading of the wave fronts with distance from the shotpoint. All record sections have a reduced time scale, with a reduction velocity of 8.0 km s^{-1}. All times referred to in this chapter are reduced times.

The measurements errors in the measured travel times should be less than 0.05 s, this being the cumulative error in scaling both the shot and arrival times, and in applying corrections for parallax between the channels in the tape recorder, and in adjusting for clock drift. However, the subjective nature of picking arrivals, especially when they are emergent, means that the actual errors on the observed times could have been as much as 0.2 s.

No time corrections were made for the effects of topography in these, or in any other data in this thesis. While the maximum topographic relief over the survey area is about 1000m, from around sea level to the top of the highest mountains, the maximum variation in shot and recorder heights was about 500m. The error due to topographic relief would depend on the angle of emergence, and this in turn would vary with the wavegroups. The maximum efect would be about 0.14 s for the P* phase from the lower crust, and less for other wavegroups. Therefore, the effects of topography are small and were neglected.

4.2 METHOD

The seismic survey yielded a vast amount of seismic data from which it was hoped a time term interpretation and a study of seismic wave amplitudes would be made. However, both of these methods require that there is very little refractor topography, and it was therefore decided that the first approach to interpreting the data would be made using the intercept method (Ewing & others, 1938; Dooley, 1952; Mota, 1954). It requires that data fall along linear profiles, and that the refractors are continuous planar surfaces between the

shotpoints. It gives the refractor depths and dips from an input of reversed pairs of intercept times and apparent velocities. A computer program written by S.P. Mathur of BMR (personal communication, 1976) automated the technique and simplified its application.

The theoretical travel times from the models of the intercept method inversion were then calculated using a computer program for ray tracing through flat earth models of arbitrary two-dimensional polygonal cross section (C.D.N. Collins, BMR, personal communication, 1978). The theoretical times were compared with the record sections, and the models further perturbed until a reasonable match was obtained. In this way, topography on the refractor surfaces could be introduced.

The theoretical times for the models generally agree to within about 0.2 s with the observed times, which is about the magnitude of the maximum timing uncertainties. Errors of about 0.2 s imply inaccuracies in the modelled refractor depths of 1 or perhaps 2 km. Larger errors in the refractor depths probably arose from the assumption that the velocities within the refractors did not vary with depth (Berry, 1971). This is discussed further in future chapters.

4.3 SEISMIC WAVEGROUP NOMENCLATURE

The seismic wavegroup nomenclature used in the following discussion, and in Figures 5, 7, 11, 12, 13 and 15 is as follows:

- Pg - Direct waves, which travel through the near-surface crystalline basement with velocities of 6.0-6.2 km s^{-1}.
- P* - Waves critically refracted at an intracrustal boundary, and with velocities of 6.4-6.55 km s^{-1}.
- P^I - Waves reflected from the intracrustal boundary and travelling with velocities intermediate between those of the Pg and P* wavegroups.
- Pn - Waves critically refracted at the crust/mantle boundary, and having apparent velocities in the range 7.6-8.6 km s^{-1}.
- P^M - Waves reflected from the crust/mantle boundary, and with apparent velocities intermediate between those of the P* and Pn wavegroups.
- P_1, P_2 - Near-surface wavegroups observed where the Hamersley Basin strata are underlain by lower velocity rocks. P_1 waves have velocities of about 5.9 km s^{-1}, and P_2 waves have velocities of 6.3-6.7 km s^{-1}.
- P^L - Near-critical reflections from a deep crustal layer in the northern Yilgarn Craton and the Capricorn Orogenic Belt. They have velocities of about 7.0 km s^{-1}.

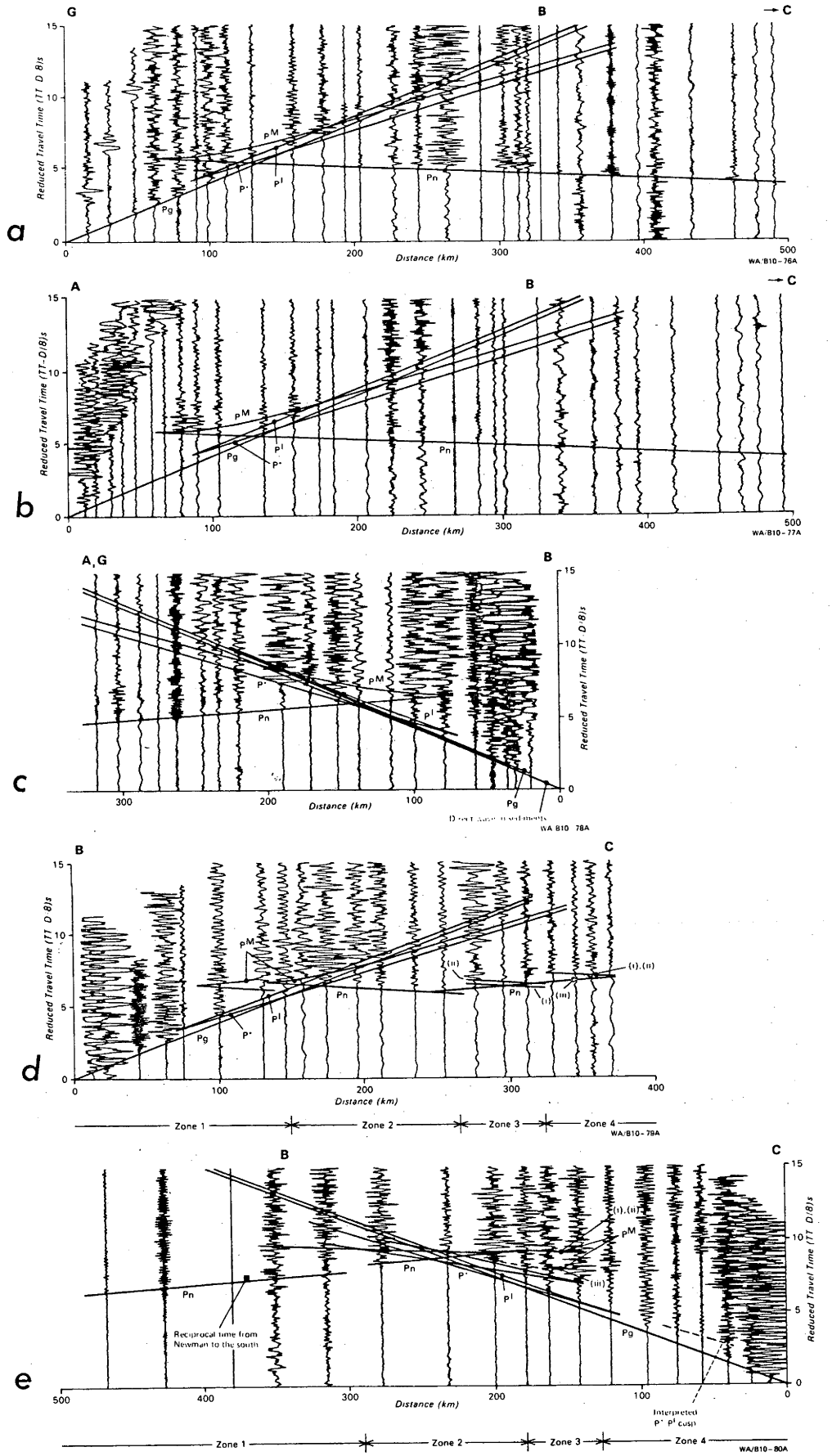

Figure 5: Record sections along line ABC. The record sections are for: (a) shot point G (Goldsworthy) southwards; (b) shotpoint A (Shay Gap & Sunrise Hill) southwards; (c) shotpoint B (Newman) northwards; (d) shotpoint B (Newman) southwards; and (e) shotpoint C (Meekatharra) northwards. The superimposed travel time curves are for the models in Figure 6 (part 1); the curves numbered i, ii, and iii are for models A, B and C, respectively. The zones marked in this figure are described in Appendix 1 (Drummond, 1979b) , of which this diagram is Figure 3.

4.4 RESULTS

NOTE: Throughout this thesis, sections from the papers appearing in the first five appendices were quoted directly to avoid having to rewrite them. In those quotes, all figure numbers were altered to the figure numbers of this thesis, and the references were changed to agree with those in the reference list (Chapter 11) of this thesis.

4.4.1 Line ABC (and GBC)

The interpretation of the data from line ABC (and GBC) formed the basis of an earlier Master of Science degree (Drummond, 1979a) and is therefore non-examinable as part of this thesis. A description of that interpretation is given by Drummond (1979b), which forms Appendix 1 of this thesis. However, the results of the earlier study are of use in forming a picture of the tectonic framework of the region, and in studying crustal evolutionary history of the area, so a brief summary of the results of Drummond (1979b) is appropriate.

The record sections for line ABC (and line GBC) are given in Figure 5. Crustal models derived from these data are given in Figure 6.

Line ABC was originally interpreted in two segments: AB and BC. The models were then joined to make a crustal cross-section for the whole of line ABC, resulting in a mismatch of some of the refractor depths where the models were joined (Figure 6, part 1). Drummond (1979b) wrote: "The step in the refractor under Newman in the models results from the process in which segments AB and BC were interpreted independently. It is probably not real, and the refractor is probably continuous between Goldsworthy and Meekatharra."

To avoid the risk of any significance being attributed to the step in the refractor, Drummond & others (1981) modified the models in two ways (Figure 6, part 2). The 5.86 km s^{-1} material was extended 15 km farther south to agree more closely with the Hamersley Basin outcrop area, and wedges out, also in closer agreement with the geology. Secondly, the step in the refractor in the middle crust is smoothed out over a zone, arbitrarily set at 100 km wide, extending 50 km either side of the original step. The theoretical travel times for the revised models fall within 0.1 s of the times for the original. Note that if the intracrustal boundary had been shallowed over a 50 km wide

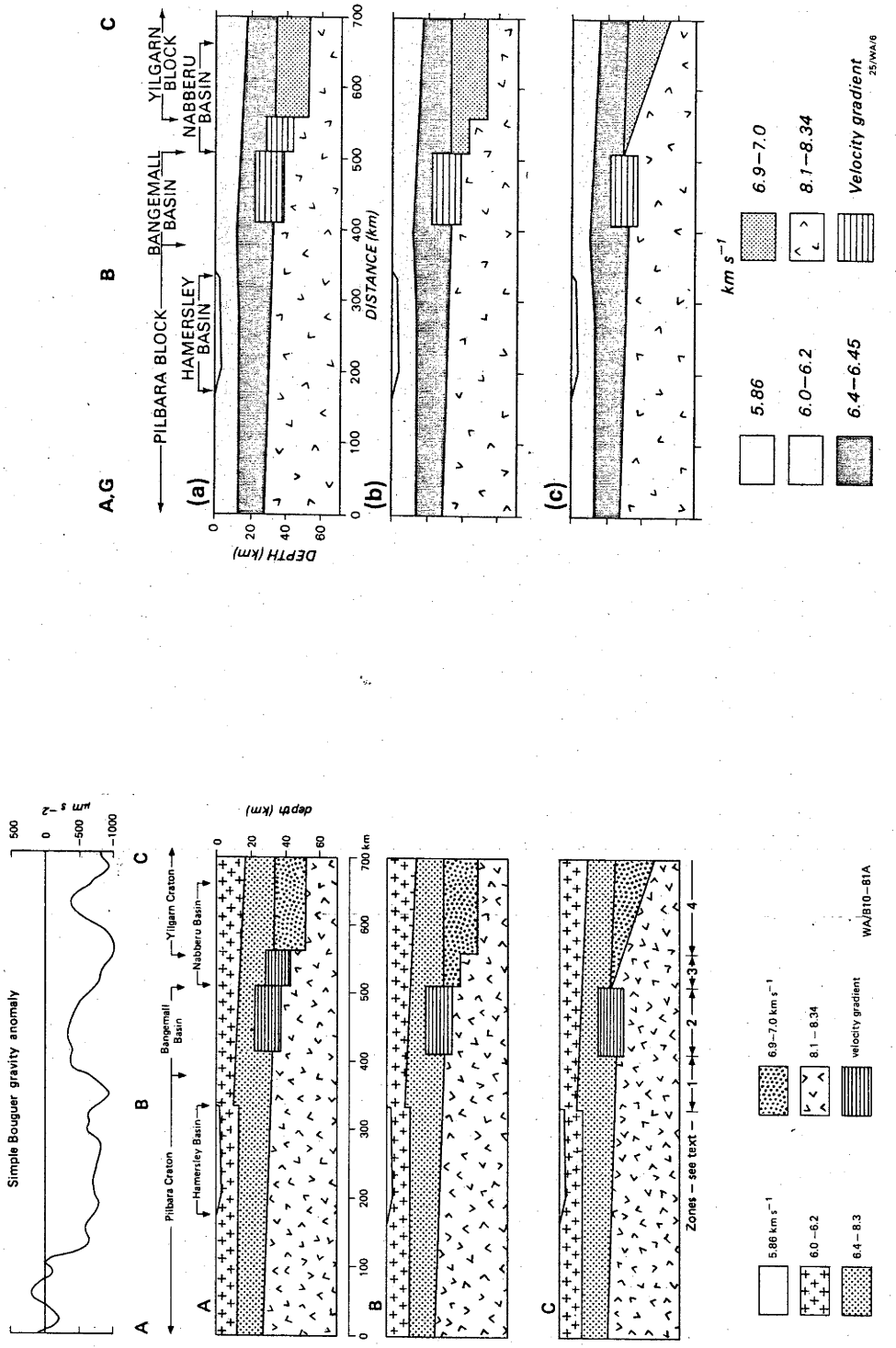

Figure 6: Alternative models for line ABC. Part 1 is Figure 3 of Drummond (1979b); Part 2 is Figure 2 of Drummond & others (1981).

TABLE 1: Seismic velocities and intercepts. The references are: 1 Drummond (1979b), (Appendix 1); 2 Drummond & others, 1981, (Appendix 2); 3 Drummond (1981), (Appendix 3). The values from reference 1 were calculated by linear regression analysis and have errors at the 95% confidence levels. The values from references 2 & 3 were scaled from record sections and therefore have no estimated errors.

Shotpoint & direction		Line	Phase	Velocity km s^{-1}	(Std. error)	Intercept s	(Std. error)	Reference
G Goldsworthy	south	GBC	Pg	6.01	(0.02)	0.03	(0.09)	1
G Goldsworthy	south	GBC	Pn[1]	8.20	(0.05)	5.92	(0.17)	1
A Sunrise Hill	south	ABC	Pg	6.01	(0.02)	0.18	(0.04)	1
A Shay Gap	south	ABC	Pg	6.05	(0.02)	0.19	(0.04)	1
A Shay Gap	south	ABC	Pn	8.18	(0.11)	5.68	(0.40)	1
B Newman	north	BA	Pg	5.86	(0.04)	-0.13	(0.09)	1
B Newman	north	BA	Pn	8.49	(0.05)	6.99	(0.17)	1
B Newman	south	BC	Pg	6.08	(0.04)	0.04	(0.10)	1
B Newman	south	BC	Pn[2]	8.46	(0.07)	7.73	(0.19)	1
B Newman	south	BC	Pn[3]	7.25	(0.05)	2.75	(0.31)	1
C Meekatharra	north	CBA	Pg	6.12	(0.02)	0.17	(0.06)	1
C Meekatharra	north	CBA	Pn	8.68	(0.11)	10.60	(0.58)	1
C Meekatharra	south		Pn	8.08	(0.03)	6.37	(0.22)	1
F Pannawonica	southeast	FDB	Pg	6.07		0.00		2
F Pannawonica	southeast	FDB	P*	6.51		1.20		2
F Pannawonica	southeast	FDB	Pn	7.64		5.50		2
D Tom Price	northwest	DF	P_2	6.32		0.00		2
D Tom Price	northwest	DF	P*[4]	6.54		0.60		2
D Tom Price	northwest	DF	P*[5]	6.57		1.20		2
D Tom Price	northwest	DF	Pn	8.00		6.10		2
D Tom Price	southeast	DB	P_1	5.88		-0.31		2
D Tom Price	southeast	DB	P_2	6.49		0.42		2
D Tom Price	southeast	DB	P*	6.39		0.91		2
B Newman	northwest	BDF	P_2	6.76		0.10		2
B Newman	northwest	BDF	P*	6.77		3.10		2
B Newman	northwest	BDF	Pn	7.96		6.00		2
G Goldsworthy	south	GD	Pg	6.11		0.00		3
G Goldsworthy	south	GD	P*	6.36		1.00		3
G Goldsworthy	south	GD	Pn	8.13		5.50		3
A Shay Gap	south	AD	Pg	6.15		0.00		3
D Tom Price	north	DA	Pg	6.10		0.00		3
D Tom Price	north	DA	P*	6.55		1.60		3
D Tom Price	north	DA	Pn	8.23		6.20		3
D Paraburdoo	north	DA	P_2	6.19		0.00		3
D Paraburdoo	north	DA	P*	6.54		1.20		3
D Paraburdoo	north	DA	Pn	8.23		6.20		3
D Tom Price	south	DE	P_2	6.25		0.00		3
D Paraburdoo	south	DE	P*	6.25		1.20		3
D Tom Price	south	DC	P*	6.54		1.30		3
D Tom Price	south	DC	P^L	6.99		3.40		3
D Tom Price	south	DC	Pn	7.89		6.23		3
D Paraburdoo	south	DC	P*	6.54		1.30		3
D Paraburdoo	south	DC	P^L	6.99		3.40		3
D Paraburdoo	south	DC	Pn	7.89		6.80		3
C Meekatharra	north	CD	Pg	6.13		0.00		3
C Meekatharra	north	CD	P*	6.37		0.85		3
C Meekatharra	north	CD	P^L	7.04		4.46		3
C Meekatharra	north	CD	Pn[6]	8.17		10.15		3
C Meekatharra	north	CD	Pn[7]	8.12		8.70		3

Notes:

1. Data north of Newman.
2. Data between 175 & 255 km.
3. Data beyond 255 km.
4. Between 0 & 90 km.
5. Beyond 90 km.
6. Based on later arrivals between 120 & 180 km.
7. Based on first arrivals beyond 180 km.

zone, ie. 25 km either side of the original step, there would have been no change to the theoretical times for P*, and the change to Pn would have been negligible, as the change in refractor depths would have been entirely within the cone of emergence of P*.

The most concise description of the models for line ABC (and line GBC) was given by Drummond (1981):

"In the north, along segment Shay Gap-Newman, the crust is 28 km thick at Shay Gap, 32 km thick at Newman, and is two-layered. The upper crust has a seismic velocity of 6.0 km s^{-1}, and at about 13 km depth the velocity increases to 6.4 km s^{-1}. The upper mantle velocity is 8.34 km s^{-1}. The Hamersley Basin north of Newman is represented by a thin layer with a low velocity (5.86 km s^{-1})

Along the segment from Newman to Meekatharra, the Pn arrivals are delayed beyond 250 km (Figure 5, section d, this thesis), and as no such delay is apparent in the Pn data in the reverse direction (Figure 5, section e), crustal thickening to the south is inferred. Crustal thickening is consistent with intercept times from recordings of Newman and Meekatharra shots, and with delays of teleseismic arrivals from earthquakes in the Fijiian region (Drummond 1979a), and the Indonesian Arc to the north (Drummond & others, 1982). Ray tracing has shown that, in the most likely models, the crust thickens from about 33 km south of Newman to more than 50 km at Meekatharra. The principal differences in the models occur in the lower crust along the segment between Newman and Meekatharra.

The seismic velocity in the upper crust between Newman and Meekatharra is 6.1-6.2 km s^{-1}. At 10 km depth in the north and 16 km depth in the south, the velocity increases to 6.4 km s^{-1}. In the south of segment BC, a lower crustal layer, with a velocity of about 7 km s^{-1}, is implied by a band of large amplitude reflections at about 7s and 140-200 km (the P^L phase in Figure 5, section e). The crust in the south is therefore three-layered. The upper mantle velocity may decrease from 8.34 to 8.1 km s^{-1} southward along segment BC."

4.4.2 Line FDB

Line FDB lies along the axis of the Hamersley Basin. An intercept method interpretation of the data from line FDB was given by Drummond & others, (1981), but because of space limitations they did not give a detailed description of their data. A more comprehensive description now follows.

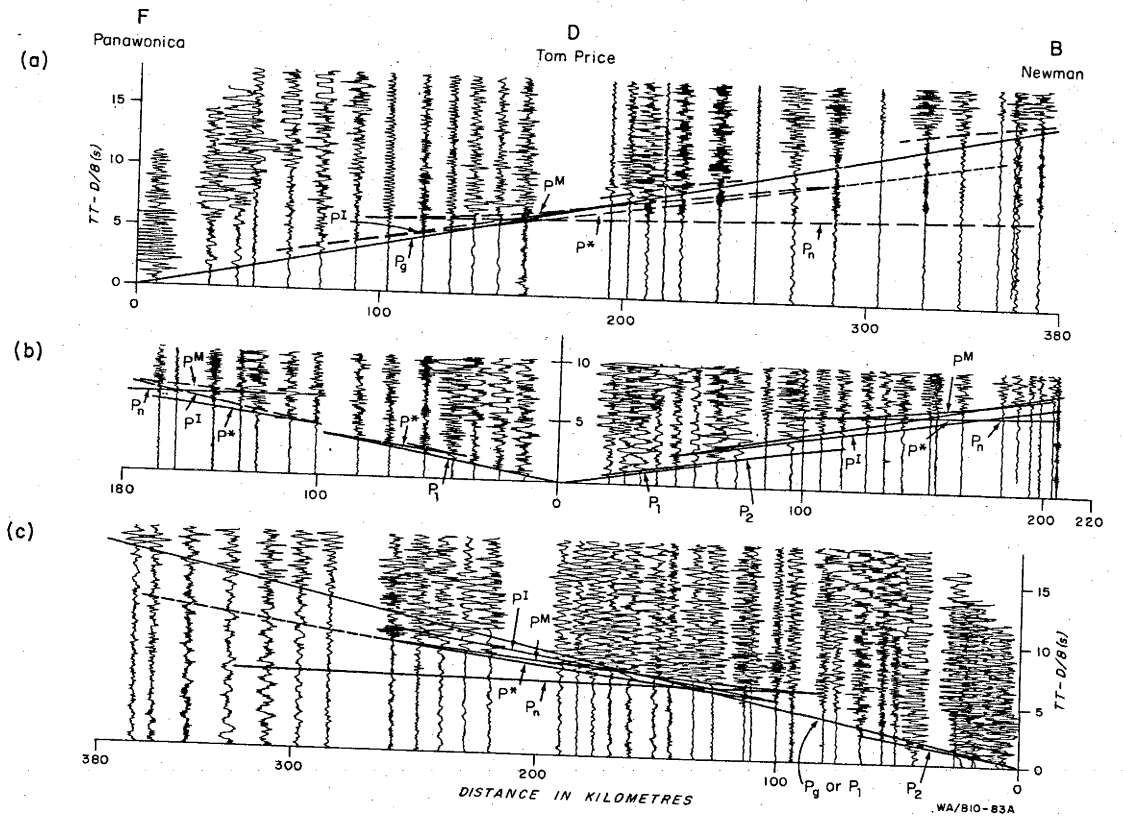

Figure 7: Seismic record sections along line FDB of blasts at (a) shotpoint F (Pannawonica) to the southeast towards Newman; (b) shotpoint D (Tom Price) to the northwest towards Pannawonica (left hand side) and to the southeast towards Newman (right hand side); and (c) shotpoint B (Newman) to the northwest towards Pannawonica. The amplitudes of the traces are as recorded, except in (c), where they have been modified so that all traces have the same maximum amplitudes in order to enlarge the phases beyond 270 km. The superimposed travel time curves are for the model in Figure 10 (Drummond & others, 1981, Figure 3).

Figure 7 contains record sections from line FDB. The seismic velocities and intercept times of the identified phases are given in Table 1.

Shotpoint F, at Pannawonica, is at the western end of the line. A record section of recordings of blasts at shotpoint F is given in Figure 7a. Only two Pannawonica blasts were recorded along line FDB, one at stations between 0 and 160 km, and the other at stations between 190 and 370 km. The second blast had a large areal extent, and a burning time of more than 2 s, so that arrivals from the blast were emergent and had several phases; for example, in Figure 7a, the phases between 200 and 380 km and 7 to 15 s begin with high frequency, small amplitude movements and end with longer period, large amplitude movements. This makes correlation of the phases between traces difficult, especially in the places where several phases overlap.

The upper crustal Pg phase has an apparent velocity of 6.07 km s^{-1}. Beyond 160 km, the first arrivals are interpreted as Pn, although they have a low apparent velocity of 7.64 km s^{-1}. A lower crustal P* phase (6.51 km s^{-1}) is present as second arrivals along the section, with a retrograde cusp at about 50 km and 3 s, and a forward cusp at 250 km and 9 s.

The Pannawonica crustal data are reversed by Tom Price shots (at D, Figure 2), recordings of which are displayed on the left of Figure 7b. Tom Price first arrival data to 60 km have an apparent velocity of 6.3 km s^{-1}, and are interpreted as the P_2 phase (not P_1 as in the diagram). Beyond 60 km, the P_2 phase is either absent or weak, and the P* phase (6.54 km s^{-1}), with a retrograde cusp as second arrivals at 2 s and 45 km becomes the dominant phase. It is offset in time at about 90 km, implying a deepening of the lower crustal layer to the west. The record section is not long enough for sub-Moho refractions to be observed as first arrivals, but a band of mantle reflections, and some arrivals which could be sub-Moho refractions have been identified as second and later arrivals.

Figure 7c is a record section of Newman blasts recorded to the northwest, reversing the Moho arrivals of Pannawonica blasts in Figure 7a. The P^M arrivals have stronger amplitudes than in Figure 7a, but the mantle refractions (Pn) are weak. Near Newman, a band of strong arrivals with a high apparent velocity (6.76 km s^{-1}) and a small intercept (0.1 s), and interpreted as the P_2 phase, is recorded to 60 km, beyond which its amplitudes drop until it is not recorded. It implies the presence immediately to the west of Newman

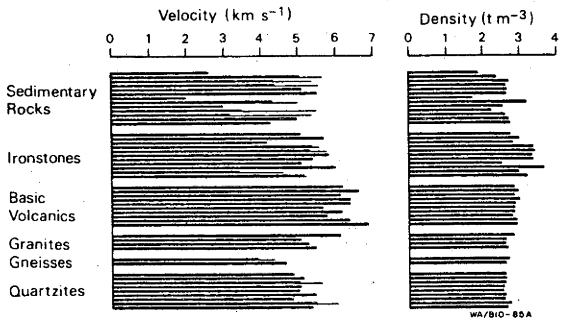

Figure 8: Bar graph of laboratory measurements of seismic velocities and densities, at standard temperature and pressure, of 49 fresh hand samples from the survey region. Seismic velocity was measured both parallel and at right angles to the layering in layered samples, and is illustrated in the figure by the split ends of some of the velocity bars (Drummond & others, 1981, Figure 5).

of shallow, high velocity rocks underlain by material of lower velocity. Arrivals which may be the P* phase are observed at 4 to 5 s between 80 and 120 km

The crustal phases recorded from the Newman blasts are reversed by the blasts at Tom Price, shown on the right hand side of Figure 7b. Near Tom Price, a P_1 phase (5.9 km s^{-1}) with a negative intercept time implies increasing sediment thickness to the east. Beyond 60 km, the first arrivals are from the P_2 phase (6.46 km s^{-1}), but they weaken beyond 100 km. The P* phase, with a lower apparent velocity of 6.39 km s^{-1} becomes dominant beyond 80 km, implying dips on the crustal layers.

The interpretation of the phases into wavegroups was based on the apparent velocities of the wavegroups and their stratigraphic positions. Not all of the phases were recognised on all record sections. Although some of the reciprocal times agree within experimental error, others do not. Lateral inhomogeneities are therefore likely in the crust along the section.

The P_1 phase velocity of 5.9 km s^{-1} to the east of Tom Price is similar to the apparent velocity of first arrivals north of Newman on line ABC, and the P_2 phase is observed both to the east and west of Tom Price and to the west of Newman. Inversion of the travel time data suggests that the P_2 phase results from a shallow, high velocity layer 0.5 to 1.0 km deep near Newman, and 2 to 3 km deep east of Tom Price. West of Tom Price, it is interpreted as being at the surface, and extending west for 60 km. It is not possible to calculate the thickness of the high velocity layer because it is underlain by rocks of lower velocity.

The rocks which outcrop in the area are predominantly Fortescue Group basic volcanics, and banded iron formations and sediments of the Hamersley group which may have an average total thickness of up to several kilometres (Daniels & MacLeod, 1965; Mac Leod & de la Hunty, 1966; de la Hunty, 1965). Drummond (1979c) reported the compressional wave velocities and densities of hand specimens collected in the survey area during the field work in 1977. In Figure 8, the velocities and densities of the specimens with clearly defined rock types are plotted as bars in their approximate stratigraphic position: the basement in the region is Archaean granitoid and its metamorphosed equivalents, gneisses and quartzites; it is overlain unconformably by the volcanic rocks of the Fortescue Group and the banded iron formations and sedimentary rocks of the Hamersley Group. The samples of volcanic rocks and banded ironstones have the highest

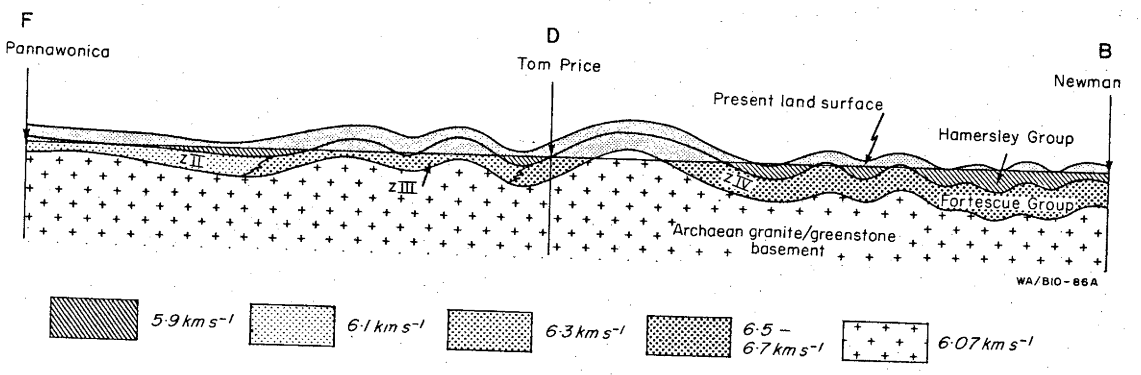

Figure 9: Diagrammatic cross-section along line FDB illustrating the increase in metamorphic grade from the northwest to the southeast. The metamorphic grades are: ZII pumpellyite-epidote zone; ZIII pumpellyite-actinolite zone; and ZIV actinolite zone (Drummond & others, 1981, Figure 6).

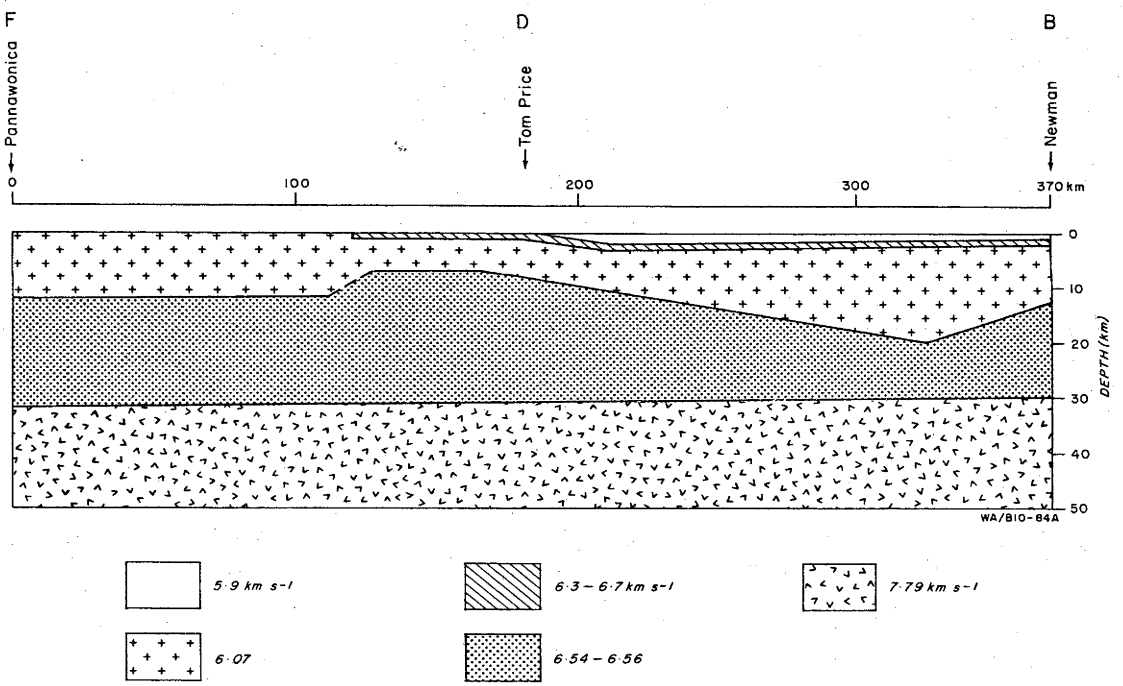

Figure 10: Crustal model along line FDB based on the seismic data in Figure 7 (Drummond & others, 1981, Figure 4).

densities and velocities in the region. It might be argued that, because the velocities were measured at only one atmosphere of pressure, they do not represent the velocities of these rocks at depth, where the effects of confining pressure would close the thin cracks in the rocks. The confining pressure at a few kilometres depth would be only about 0.1 GPa, and this is unlikely to be enough to close the cracks and pore spaces (see Chapter 6). Thus, the laboratory measured velocities might reasonably be argued to be true indicators of the velocities of these rocks near the surface, and imply that the velocity inversion near the surface results from the Hamersley Basin rocks overlying the Archaean granitoid basement.

The P_2 apparent velocity increases from east to west across the region. Immediately to the east of Pannawonica, it is indistinguishable from the basement velocity. It is 6.32 km s^{-1} west of Tom Price, 6.49 km s^{-1} to the east of Tom Price, and 7.76 km s^{-1} west of Newman. Drummond & others (1981) proposed that the increase in velocity from west to east was a result of increasing metamorphic grade of Hamersley Basin rocks along the traverse, caused by the increasing depth of burial from west to east. Four zones of burial metamorphism are recognised in the region (Horwitz & Smith, 1978). They are, in increasing order of grade, ZI, the pumpellyite-prehnite zone, which is to the north of line FDB, ZII, the pumpellyite-epidote zone, in the west of line FDB, ZIII, the pumpellyite-actinolite zone, in the centre of the line, and ZIV, the actinolite zone, in the east of the line. Figure 9 shows diagrammatically the distribution along line FDB of the metamorphic zones in the now folded, uplifted and eroded Hamersley Basin strata.

Figure 10 shows the crustal model derived from the seismic data. The Hamersley Basin strata are shown in the centre and southeast as 5.9 km s^{-1} rocks overlying a high velocity layer with a velocity of 6.3 to 6.7 km s^{-1}. No estimate can be made of the thickness of the high velocity layer. It was set at 1 km thick, so that the combined thickness of the near surface layers would approach that likely from the geological mapping.

No estimate of the velocity in the material below the Hamersley Basin rocks is possible in the east. In the modelling, 6.07 km s^{-1} was used; it is the value measured east from Pannawonica, and is in general agreement with the uppercrustal velocities along line ABC (Figure 6). Inversion of the P* data gave a lower crustal layer 12 km deep under Pannawonica. About 60 km west of Ton Price, it shallows to 7 km. The nature of the shallowing is unclear from the seismic data, and the layer is shown in Figure 10 shallowing over a 20 km

wide zone. The structure could equally be vertical, or even overthrust, but there is no evidence for such structures in the 1:250 000 regional geological maps (de la Hunty, 1965). The screening effect of the P_2 phase makes estimates of the depth of the mid-crustal boundary difficult. The boundary in Figure 10 is based on the tentative interpretation of the P* phases listed in Table 1 for segment DB; they have equal reciprocal times and may therefore be indeed be P*. East of Tom Price, the lower crustal layer deepens, possibly reaching 20 km before shallowing again to 13 km depth, a depth constrained by the depth along line ABC. The velocity in the lower crustal layer is 6.55 km s^{-1}.

Pn arrivals along line FDB, and especially those from the Newman blasts, are much weaker than along line ABC, and the very low apparent velocity of 7.65 km s^{-1} from the Pannawonica blasts to the southeast makes the interpretation of the phase as Pn seem uncertain. However, inversion of these data as Pn arrivals gives a Moho 31 km deep under Pannawonica and 32 km deep under Newman, in good agreement with the model for line ABC. The Moho velocity is only 7.8 km s^{-1} for the centre of line FDB, which seems anomalously low when compared with the velocities for line ABC, and considered in the context of the the regional heat flow for the region (Cull & Denham, 1979). This will be discussed again later.

4.4.3 Lines GDE (and ADE) and DC

The record sections of the seismic data from lines GDE)and ADE) and DC are given in Figures 11, 12 and 13. They were interpreted by Drummond (1981), whose models appear in Figure 14. The travel time curves superimposed on the record sections are those for the models in Figure 14. The apparent velocities and intercept times for the identified phases are listed in Table 1. A full description of the seismic phases identified and their interpretation is given by Drummond (1981).

The Pg phase is recognised on all record sections, except on those where the shotpoints are in the Hamersley Basin (Figures 11d; 12a,b; 13a,b). For these, the P_2 phase is the near source first arrival, screening the Pg phase. On all record sections, P* phases are clear, especially near their retrograde cusp. The P^M phase is the most obvious phase, and Pn arrivals are generally weak. Dots in Figure 11 indicate Pn arrivals picked on these or other large amplitude records. Along lines DE and DC (Figures 12 and 13), the P^L phase can be identified as large amplitude arrivals on some traces.

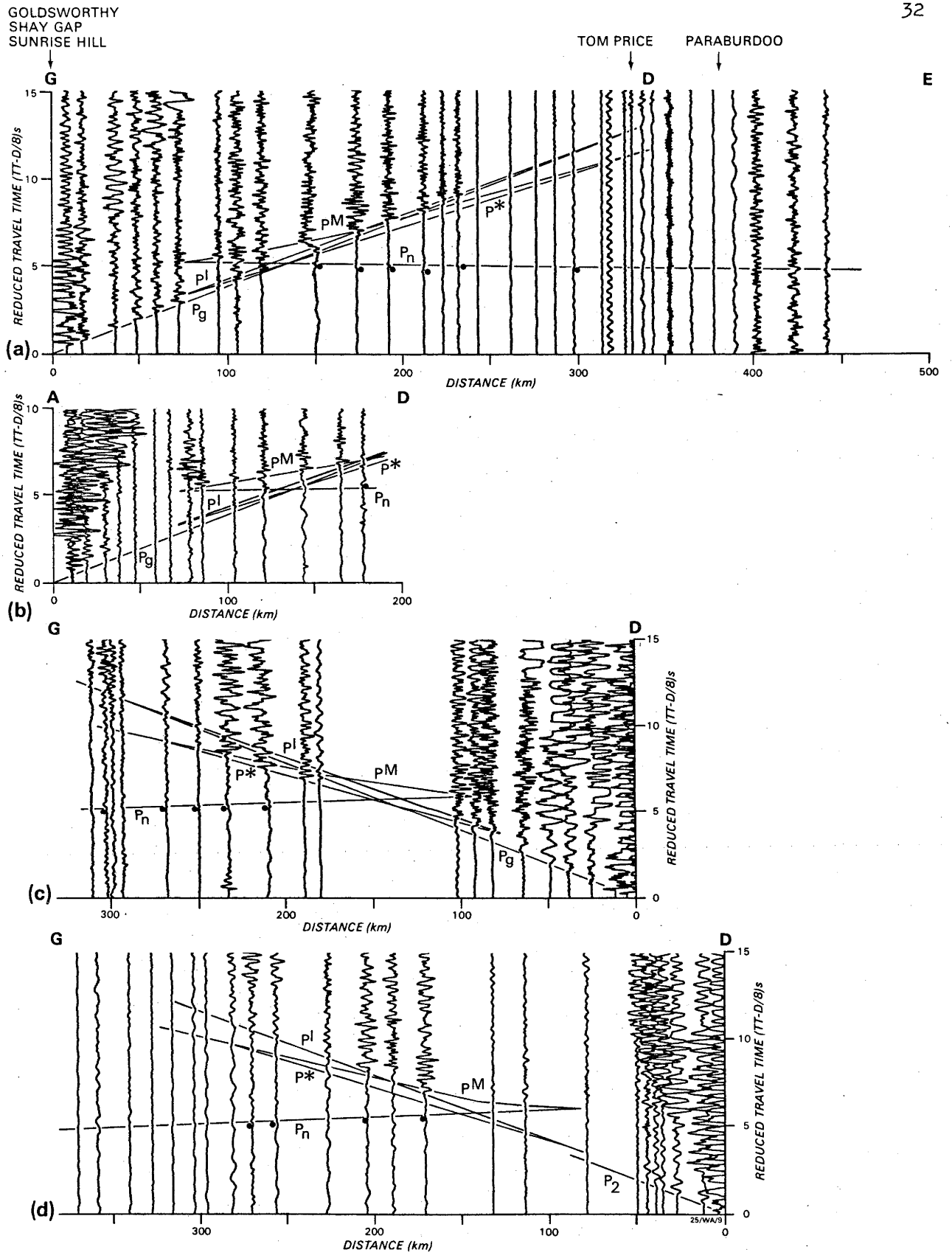

Figure 11: Record sections for line GD. Sections a, b, c and d are for shot-points G (Goldsworthy) southwards; shotpoint A (Shay Gap & Sunrise Hill) southwards; shotpoint D (Tom Price) northwards; and shotpoint D (Para-burdoo) northwards, respectively. The superimposed travel time curves are for the right hand side of the model in Figure 14a. The dots indicate the times of Pn arrivals picked from these and large ampltitude records (Drummond, 1981, Figure 4).

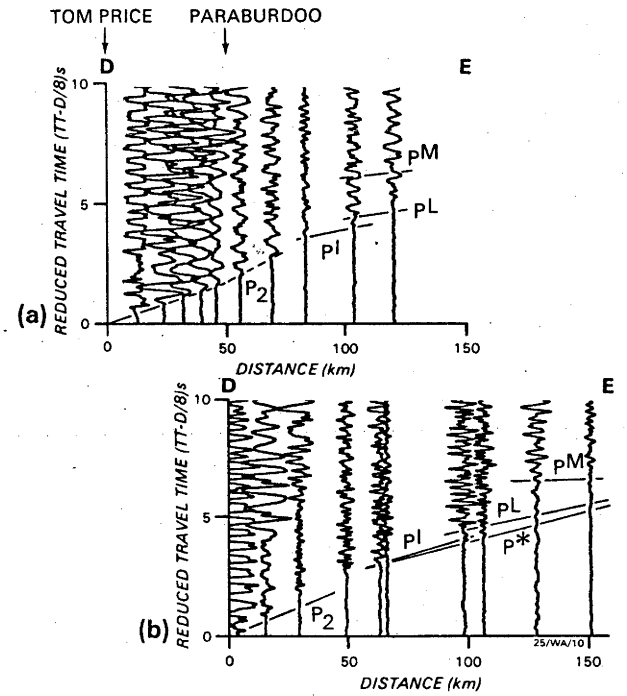

Figure 12: Record section for line DE. Section a is for shotpoint D (Tom Price) southwards, and section b is for shotpioint D (Paraburdoo) southwards. The superimposed travel time curves are for the model in Figure 14b (Drummond, 1981, Figure 5).

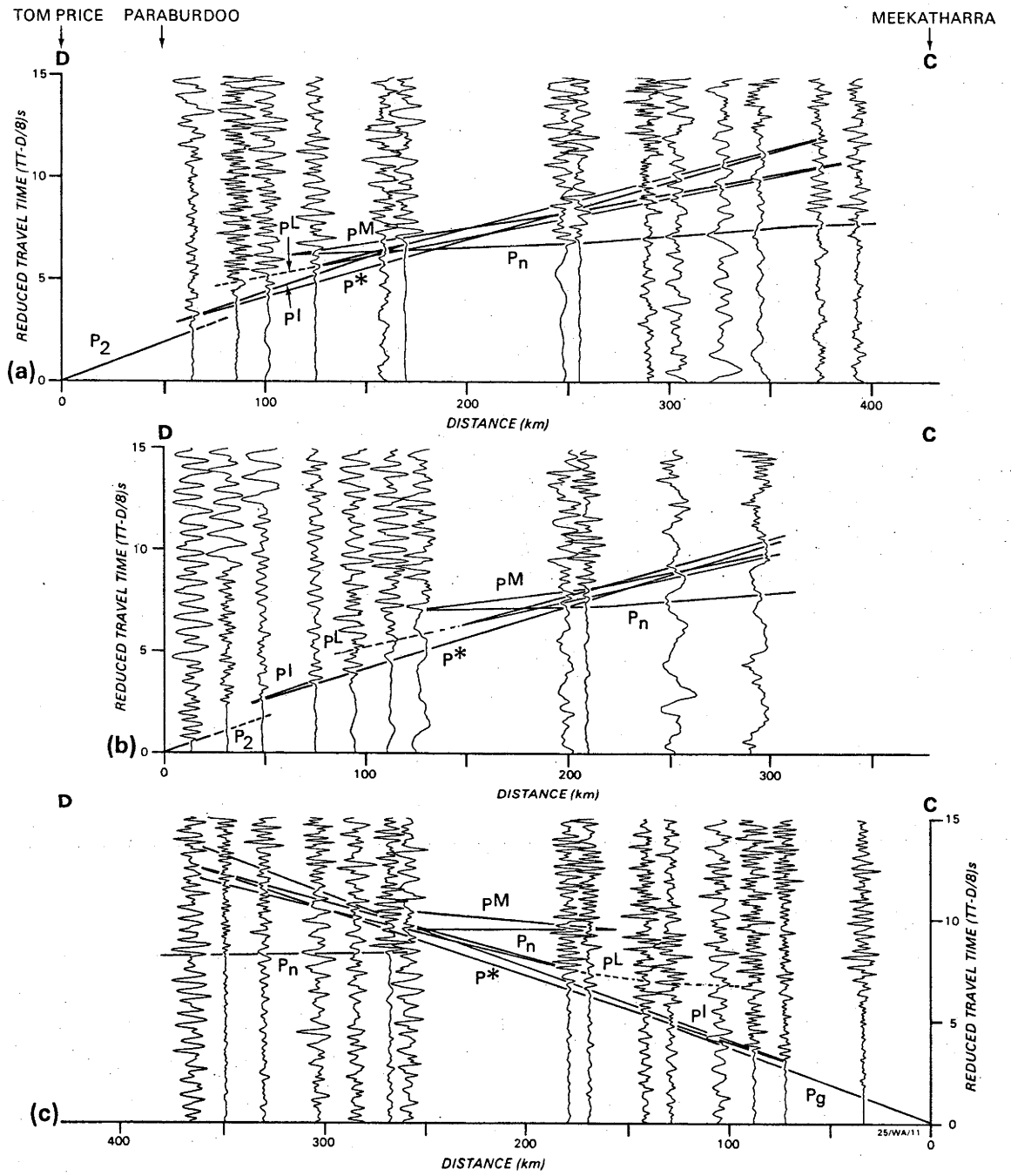

Figure 13: Record sections for line DC. Sections a, b, and c are for shotpoint D (Tom Price) southwards; shotpoint D (Paraburdoo) southwards and shotpoint C (Meekatharra) northwards, respectively. The superimposed travel time curves are for the right hand side of the model in Figure 14a. The trace amplitudes have been normalised so that the maximum amplitude is the same for all traces; the traces are unfiltered, except in section c, where they were filtered in the bandpass 1.0 to 8.0 Hz. For some recorders, one of the horizontal components had clearer arrivals than the vertical component, and was plotted in its place. Note that the P^L cusp (the dashed curve) is closer to the shotpoint than predicted by the model (Drummond , 1981, Figure 6).

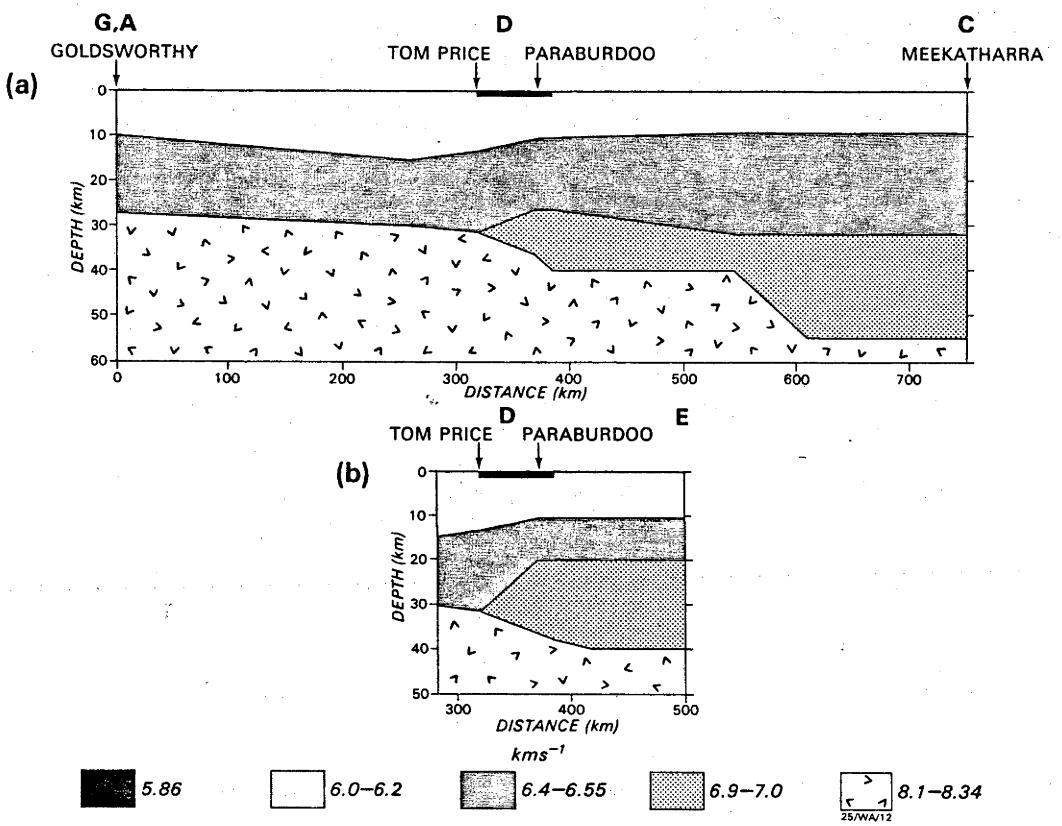

Figure 14: Seismic models for lines GDC and DE. Model a is for line GDC, and Model b is for line DE (Drummond, 1981, Figure 7).

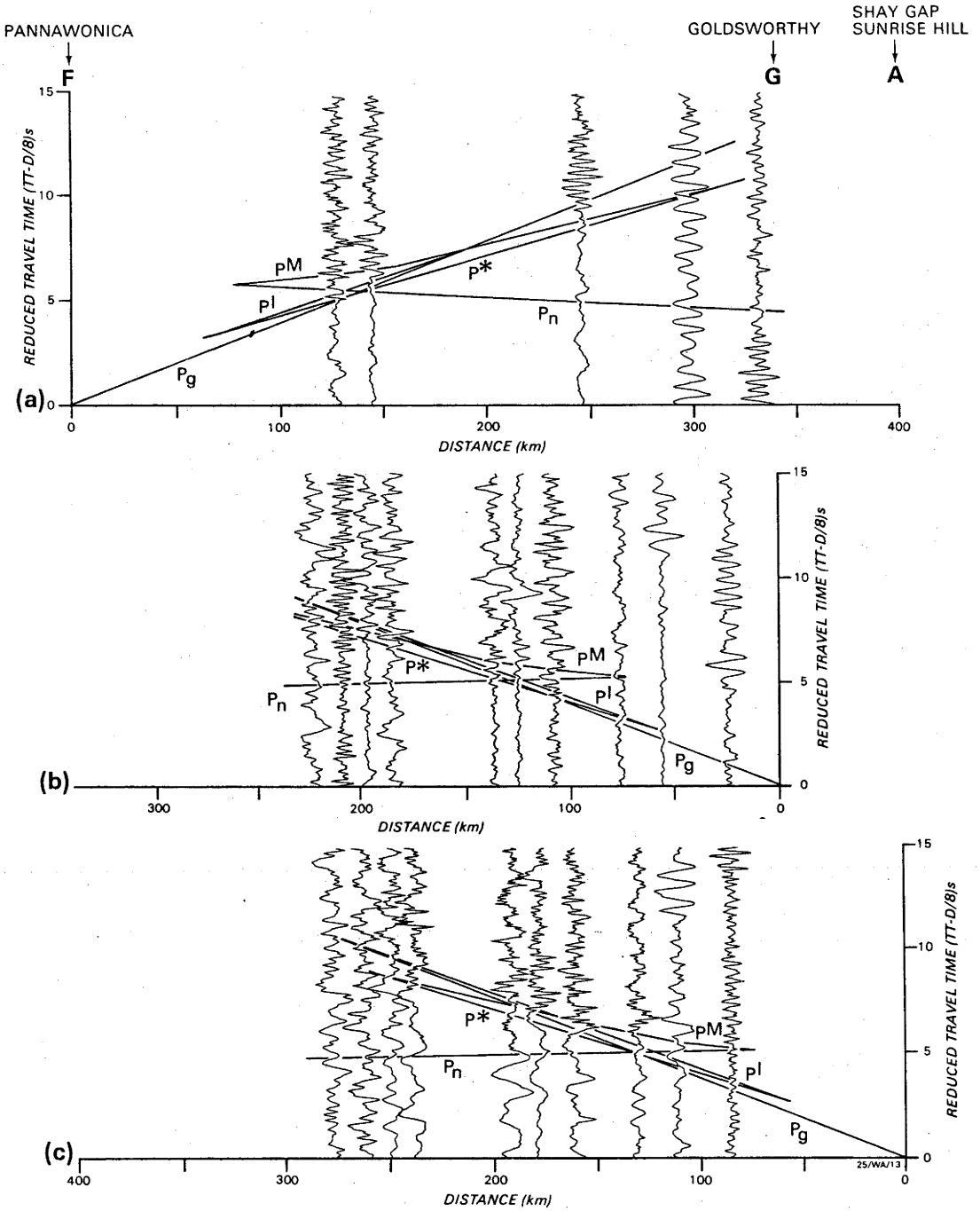

Figure 15: Record sections for line FG. Sections a, b, and c are for shotpoint F (Pannawonica) northeast; shotpoint G (Goldsworthy) southwest; and shotpoint A (Shay Gap and Sunrise Hill) southwest, respectively. The trace amplitudes are normalised as in Figure 13, and are unfiltered. For some recorders, one of the horizontal components had clearer arrivals than the vertical component, and was plotted in its place. The superimposed travel time curves are for the model in Figure 16.
(Drummond, 1981, Figure 8).

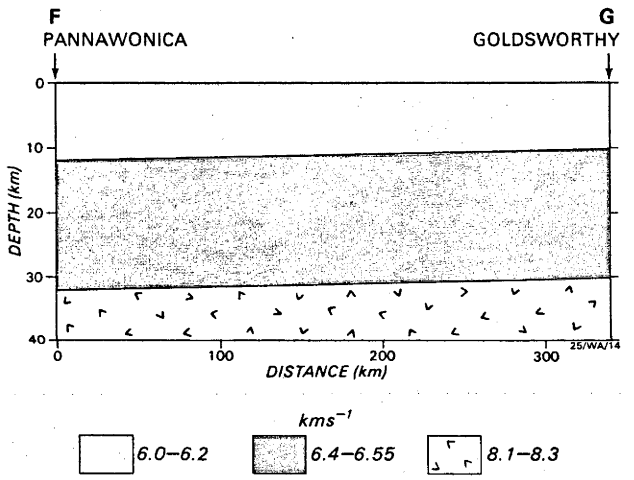

Figure 16: Seismic model for line FG. The model was based on the models for the northern end of of line GDC and the western end of line FD, and is broadly consistent with the data shown in Figure 15 (after Drummond, 1981, Figure 9).

Drummond's (1981) description of the models in Figure 14 follows: "The upper crustal velocity along the profile is 6.0-6.1 km s^{-1}. In the centre of the profile, near Tom Price (D), a thin, near-surface layer corresponds to the Hamersley Basin rocks. It has been modelled as 1 km thick, but it may be thicker. Assessment of the thickness of such layers is difficult with ray tracing alone, and further modelling with synthetic seismograms is required. A lower crustal layer, with velocities of 6.37-6.55 km s^{-1} is present along the profile. It is 10 km deep under shotpoint G at Goldsworthy, deepens to 15 km about 260 km south of G, but then shallows again to 10 km between Tom Price and Meekatharra (DC). An even deeper crustal layer, with a velocity of 6.7-7.0 km s^{-1} is present along DC. It is 10 km thick south of Tom Price (D), and thickens rapidly in the centre of the line, to be 20-25 km thick under Meekatharra (C). The interpreted upper mantle velocity along the Goldsworthy - Tom Price - Meekatharra line varies between 8.0 and 8.2 km s^{-1}. The crust/mantle boundary is 28 km deep under Goldsworthy, deepens steadily to 31.5 km under Tom Price, and then rapidly to 40 km , and then to 55 km southwards towards Meekatharra.

The model for line DE (Figure 14b) is similar to the equivalent part of of line DC to the east, except that the lowermost, 6.98 km s^{-1}, crustal layer layer is thicker. This may not be significant, because the seismic line is unreversed."

4.4.4 Line FG

Only 15 recording stations were set up along line FG. All were confined to the northeast part of the line, and several of them failed to operate. The available data from those that did operate are shown in Figure 15. It is not possible to interpret these data with any degree of confidence. Drummond 's (1981) model for the line is shown in Figure 16 and was derived by taking the refractor depths at shotpoint F (Pannawonica) from the model for FDB (Figure 10) and those at shotpoint G from the model for line GDC (Figure 14), and velocities which were averages of those for the corresponding layers in the two models. The theoretical travel times for the model agree in general with phases that can be identified in the record section, and the model is regarded as the best available.

5. AMPLITUDES

5.1 THE NEED TO USE AMPLITUDES

Berry (1971) emphasised the importance of recognising, and correlating between seismic traces, later arrivals which can be used to define in more detail the velocity structure with depth. He also stressed the importance of recognising and matching the position of the critical cusps. Mueller & Landisman (1971) suggested that the dynamic properties of seismic arrivals, that is, their amplitudes, phases and frequencies, and not just their travel times should be considered in the seismic interpretation.

A study of the dynamic properties of seismic arrivals is inextricably linked to a study of secondary arrivals, because the secondary, wide - angle and near critical reflections off seismic discontinuities are nearly always of higher amplitude, and therefore more easily identified, than the refracted head waves from the layers above and below the interface (Braile & Smith, 1975). However, although generally small, the amplitudes of head waves are greatly affected by velocity gradients in the refracting medium.

The models from the intercept method interpretation presented in Chapter 4 were based principally on the travel times of the refraction branches. Little attention was given to the times or amplitudes of the reflection branches. Drummond (1979b, 1981) noted that the times of the reflection branches derived by ray tracing through his models did not always match the recorded times; nor was the position of the critical, or retrograde cusp always accurately portrayed by the travel time curves for the models. Consequently, the depths in the models derived from the intercept method interpretation may be somewhat in error (Drummond, 1979b; 1981; Drummond & others, 1981). It was hoped that a study of the amplitudes of the seismic arrivals would help to more accurately model the velocity/depth profile of the region and correct the defects in the seismic models.

Several computer programs are now available for calculating synthetic seismograms for short period seismic refraction data. The most popular are based on generalised ray theory (eg. Wiggins & Helmberger, 1974) and the reflectivity method (Fuchs & Muller, 1971). In the study discussed below, the reflectivity method was used for several reasons. Firstly, a computer program was readily available. Secondly, the computer program is easy to apply.

Collins (1979) described the input parameters for a version which he uses on another computer system, and those parameters, with only a few minor changes are the same in the version of the program used in this study. However, the computer program was made more computer-time efficient by incorporating the modification suggested by Kind (1976).

Thirdly, and most importantly, the program has found widespread acceptance. It has been used extensively in the interpretation of seismic refraction data in Europe (see Giese , Prodehl & Stein, 1976), North America (for example, Prodehl, 1977), and elsewhere in Australia (for example, Finlayson & others, 1980). Braile & Smith (1975) used it to calculate the examples of synthetic seismograms in their 'Guide to the interpretation of crustal refraction profiles'. The general acceptance of the reflectivity method, and of this computer program in particular, therefore provides a basis for comparison of seismic models of many parts of the world.

Before discussing the application of synthetic seismograms to the analysis of actual data, some limitations of using the synthetic seismogram technique should be discussed. Firstly, the method requires that the phases be correlated from trace to trace. Mueller & Landisman (1971) suggested that a station spacing of 3 km or less is required or phases will be missed or incorrectly correlated. In this study, the station spacing was between 5 km near the shotpoints and 25 to 30 km in the middle of some of the profiles. It is therefore possible that some travel time branches were not recognised, or incorrect correlations made. However, within the data currently available, most of the recognised phases have been interpreted, and it seems unlikely that any major wave groups were missed.

Secondly, the computer program assumes that the earth is composed of flat-lying, homogeneous, isotropic layers; zones of vertical velocity gradients may be represented by thin laminae of such layers (Fuchs, 1968). This is usually an oversimplification, as any geological, gravity or magnetic map will reveal. For example, in the survey area, the geological map reveals several Archaean cratons, each with large, low density granitoids intruding denser greenstone belts and separated by Proterozoic mobile belts. The first impression is therefore of lateral , and not vertical, structure. The seismic signature of flat-lying, vertically stratified structure must therefore overprint that of the lateral structure before it can be accurately interpreted. As well, the effects of refractor topography can often appear to come from vertical structure (Mereu, 1969; see also Section 5.4).

The use of synthetic seismograms should therefore be limited to regions of limited lateral structure, where a network of traverses can be used to distinguish lateral structure from vertical structure. Within the survey area, these criteria are met only within the confines of the Pilbara Craton (lines AB, FDB and GHD). That the velocity/depth models derived for all of the seismic profiles over the Pilbara Craton by synthetic seismogram modelling, and about to be described below, are similar suggests that the technique is generally applicable to the interpretation of vertical structure in the craton.

5.2 DATA PROCESSING

All data are presented in the form of record sections with a reduction velocity of 8 km s^{-1}. Most data are digitally bandpass filtered in the range 0.5 to 8.0 Hz. This passband removed much of the long period background noise, as well as high frequency local wind noise, while leaving the character of the principal seismic signal inviolate. When plotting the data, corrections were made for recorder gain, so that all traces in each record section are as if recorded at the same gain level.

In the majority of cases, a correction proportional to the epicentral distance was applied to all data beyond the interpreted P^M/Pn cusp to account for the geometrical spreading of the wavefronts. Between the shot and about 100 km, which is about the position of the P^M/Pn critical cusp, the seismic traces were often distorted by overmodulation of the seismic channels because of the large shot sizes. Correction of these amplitudes for geometrical spreading would have been meaningless, and, at worst, misleading. The P^M/Pn cusp was usually, though not always characterised by large, clear and therefore easily recognised arrivals, and was therefore a useful datum to which the arrivals on the other traces could be related. In a few cases, additional adjustments were made to the trace amplitudes. These were generally of the form of a reduction of anomalously large amplitude arrivals which obscured arrivals on adjacent traces, and are clearly marked on the diagrams, and in a few cases discussed in the text.

Braile & Smith (1975) and Berry & Fuchs (1973) also used a correction factor to amplitudes for geometrical spreading proportional to epicentral distance, but other workers, for example Mereu & others (1977), prefer the square of the distance. When a factor proportional to distance squared was

used on these data, the ampitudes of the recorded signals, and especially those of the reflected waves, increased interminably with distance, which cannot happen in nature, firstly because of the natural attenuation processes, and secondly because it would imply that seismic waves could gain energy with distance from the blast.

An intermediate factor might be more appropriate. The geometrical spreading of head waves at great distances is proportional to distance squared, and, to a first approximation, the decay of reflected waves is proportional to distance (Aki & Richards, 1980). An intermediate factor might be more appropriate for diving waves, which are intermediate between reflections and refractions, returning to the surface from regions of high velocity gradient.

It may be possible to use different correction factors for different wave groups, although, because the identification of wavegroups relies heavily on the observed amplitudes, the argument could become circular and it is doubtful whether a better definition of the velocity/depth function would result from such a contentious process.

No amplitude corrections were made for shot weight. Many of the blasts have individual source characteristics; see for example the different waveforms for the blasts at Shay Gap (Figure 18) and Pannawonica (Figure 24). The differences in the waveforms are usually in the frequency and time duration of the signal, and not in its amplitude. No simple relationship links the observed amplitudes to the amounts of explosives used in the blasts (see also Berry & Fuchs, 1973, for similar observations of blasts specially prepared for seismic surveys). This probably stems from the practice of firing the quarrying blasts one mining bench at a time, with delays between the benches. The delays mean that the amplitude of the seismic energy is related more to the quantity of explosives in each bench than the total quantity of explosives in the blast.

The seismic amplitudes were often dependent on the order of firing of the benches. For example, in the mine at Newman, the practice was to fire from the northern benches progressively to the south. For the near surface phase which travelled approximately horizontally, this appeared to increase the amplitudes recorded at stations south of the mine, but to decrease those to the north. At some of the other mines, most noteably the Goldsworthy mine, small blasts commonly produced greater seismic amplitudes than larger blasts.

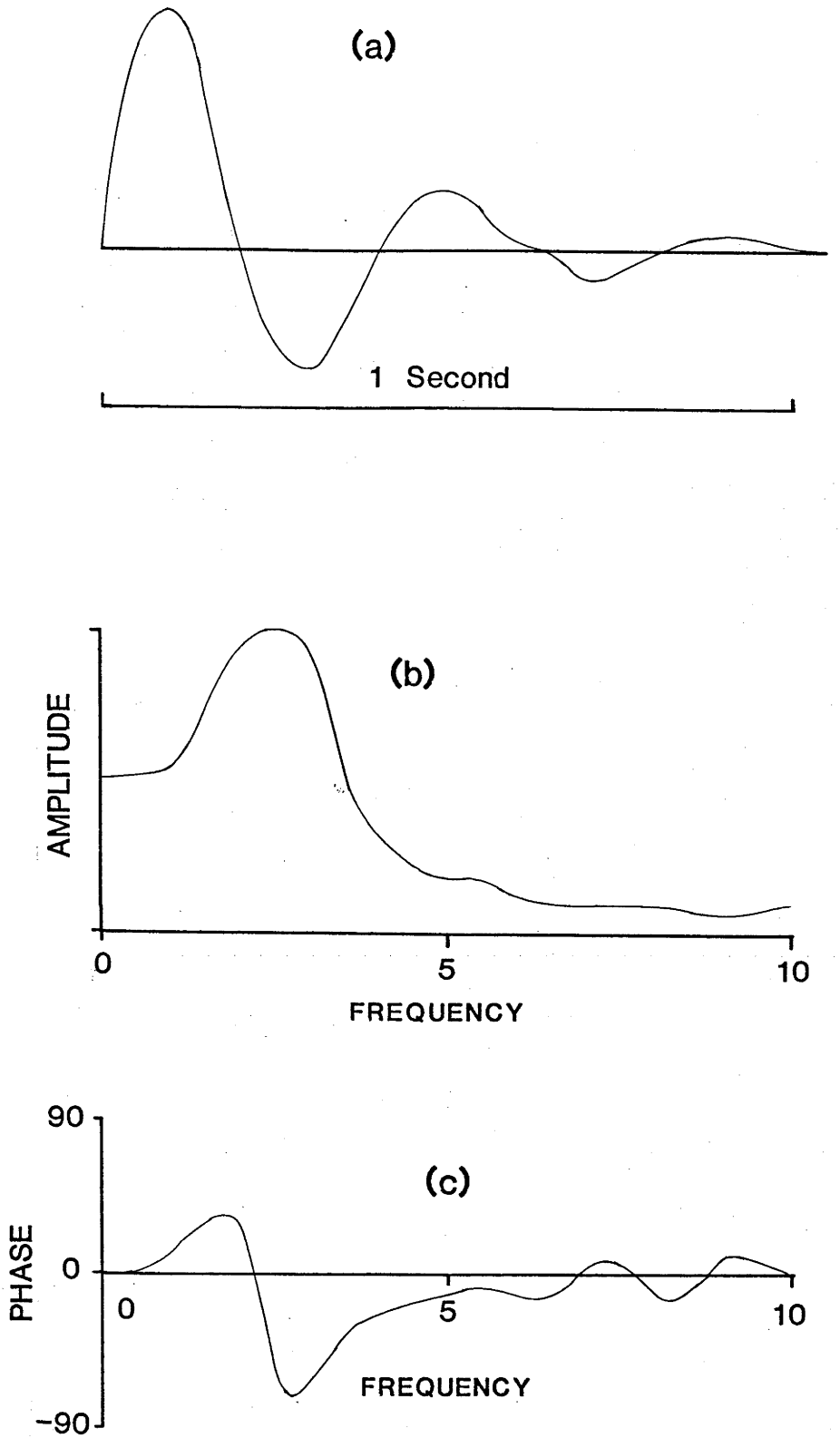

Figure 17. Source wavelet for synthetic seismogram modelling. (a) time domain wavelet; (b) amplitude spectrum; (c) phase spectrum.

The wavelet in Figure 17 was used for all of the synthetic seismogram modelling. It is a minimum delay wavelet whose frequency peaks between 2 and 3 Hz.

For simplicity, the travel time cusps in the following discussion are denoted by the letters A, B, C etc., so that branch AB is the Pg phase, BC is the P^I reflection from the intracrustal boundary, CD is the P* phase, DE the P^M phase, and EF the Pn phase. The model in Figure 20h has an extra lower crustal triplication labelled DC'D', and the model in Figure 19c has an extra upper mantle triplication labelled FGH.

5.3 SYNTHETIC SEISMOGRAM MODELLING

5.3.1 Shotpoint A (Sunrise Hill & Shay Gap), along line AB

Because of the overmodulation of the near-source recordings due to the large quarrying blasts used for the seismic survey, very little is known about the amplitudes of the Pg phase, and the P^I/P* cusp. Some of the smaller blasts at Shay Gap, Sunrise Hill and Goldsworthy, however, did not overmodulate the traces, and the record section of one such blast is shown in Figure 18b. The location of the profile is shown in Figure 18a.

The Pg phase decays by a factor intermediate between distance and distance squared. This implies that there is probably very little attenuation of the seismic energy, and that no upper crustal low velocity channel similar to that found in both young and old regions elsewhere in the world (eg. Mueller & Landisman, 1966; Berry & Fuchs, 1973; Finlayson & others, 1980) can be implied. Rather, positive velocity gradients can be inferred to limit the decay to between distance and distance squared.

The amplitude of the P^I/P* cusp (C) is also further evidence that no upper crustal low velocity channel is present in the region. Mueller & Landisman (1966) suggested that the large amplitudes of the P^I phase relative to the Pg phase in the data that they studied was evidence for the low velocity zone - the low velocity zone brought the intracrustal boundary in their model closer to the surface, and moved the P^I/P* cusp closer to the blast. In the record section in Figure 18b, the arrowed P^I arrivals in each trace have about twice the amplitude of the Pg phase in that trace. However, the full interp-

Figure 18. Model for shotpoint A (Sunrise Hill and Shay Gap), along line AB. (a) location diagram for the record section in Figure 18b; (b) record section southwards from A. The superimposed travel time curves are for the model in Figure 18e; (c) synthetic seismogram record section and travel time plot for the model in Figure 18e, but with the Pg phase omitted; (d) location diagram for the record section in Figure 18e; (e) record section southwards from A. The superimposed travel time curves are for the model in Figure 18f; (f) velocity/depth model for the profile AB; (g) p versus distance plot for the model in Figure 18f; (h) synthetic seismogram record section and travel time plot for the model in Figure 18(f).

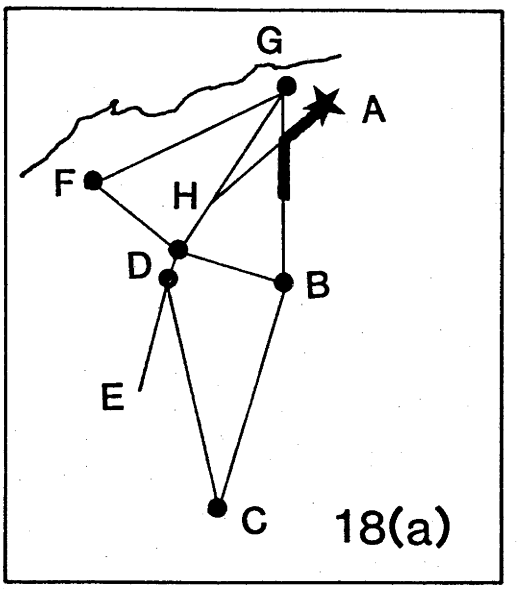
G
A
F
H
D
B
E
C
18(a)

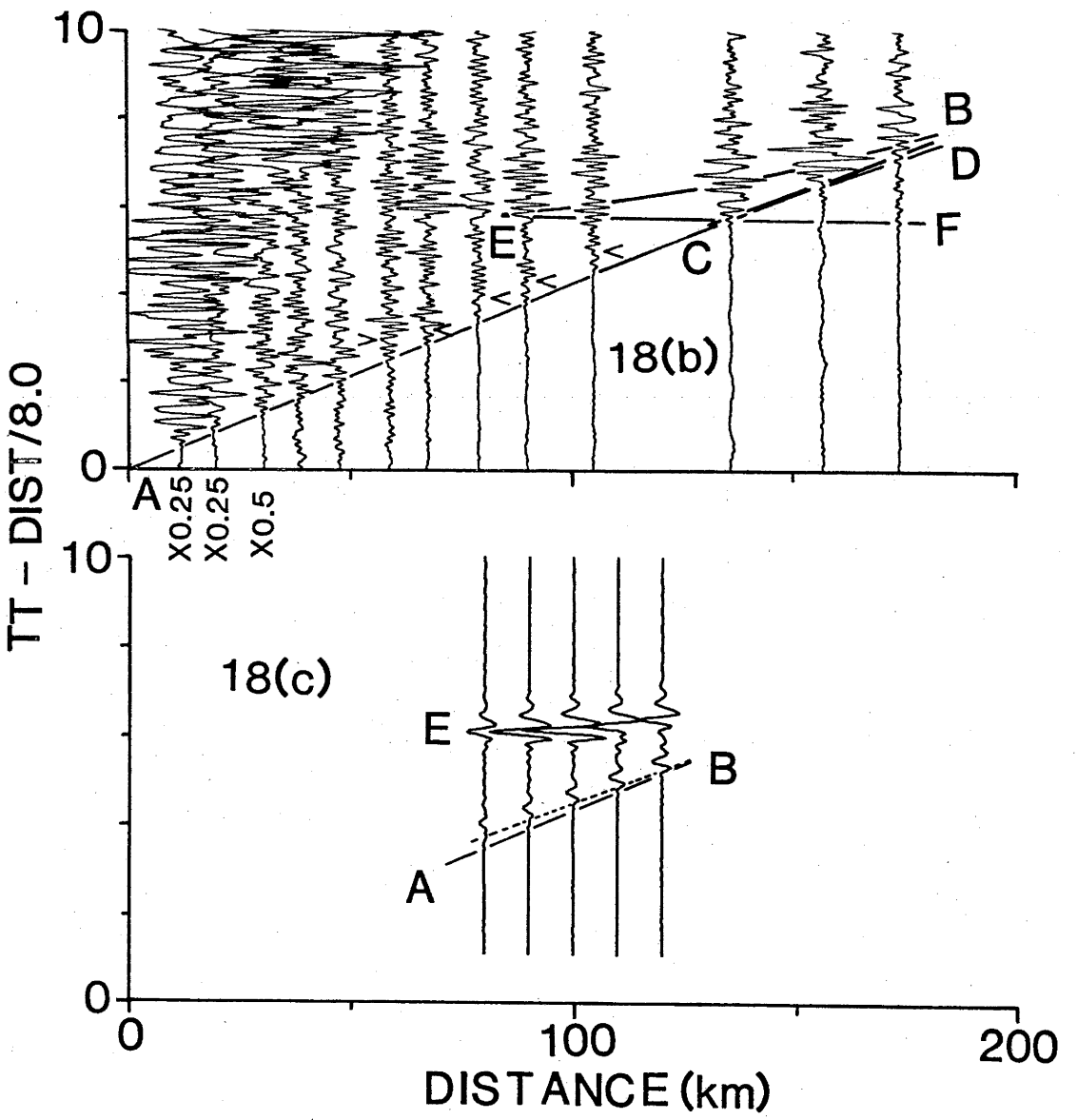
10
0
B
D
F
E
C
18(b)
A
X0.25
X0.25
X0.5
10
0
18(c)
E
B
A
0
100
200
DISTANCE (km)
TT - DIST/8.0

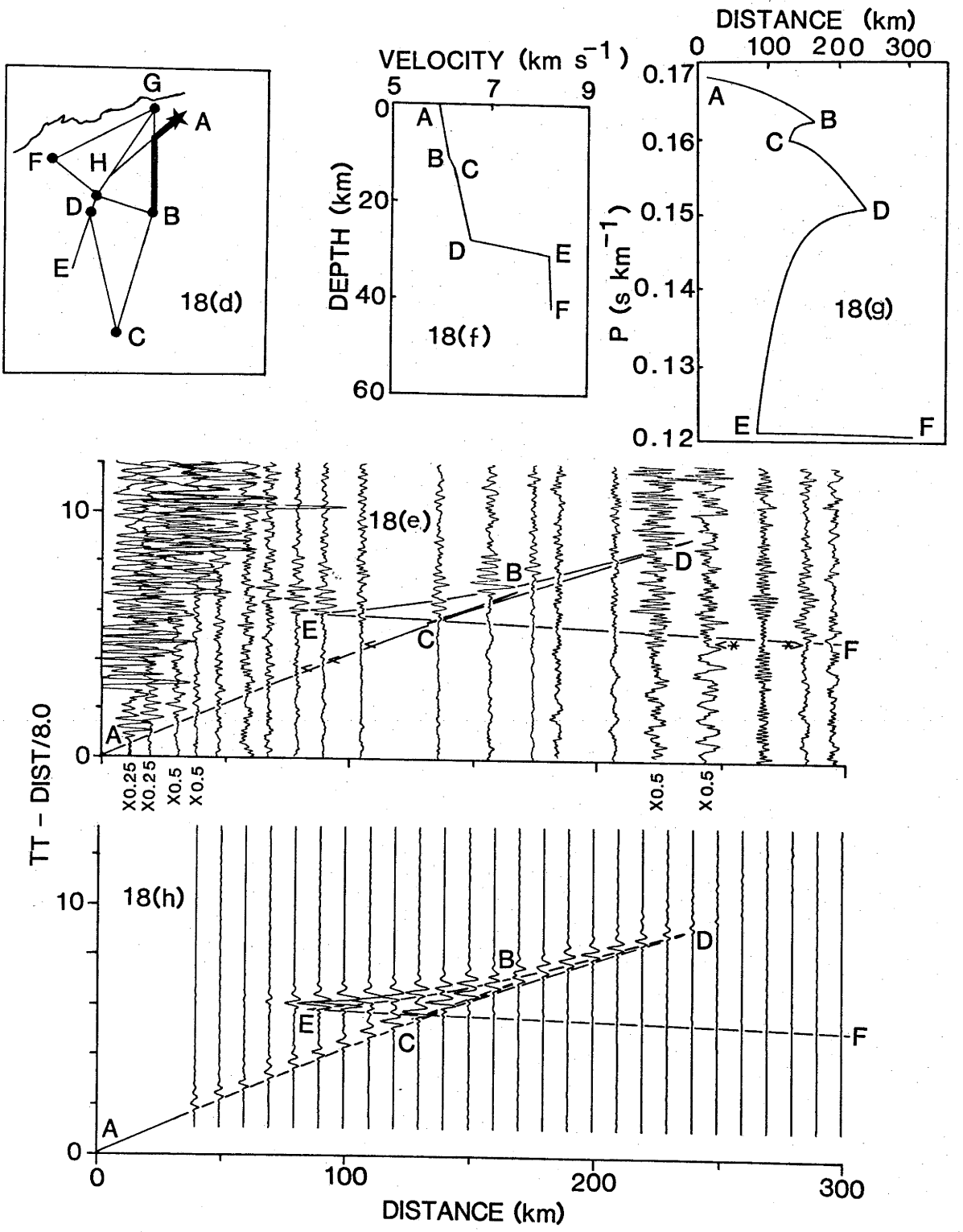
G
A
F
H
D
B
E
C
18(d)
VELOCITY (km s^{-1})
5
7
9
0
20
40
60
DEPTH (km)
A
B
C
D
E
F
18(f)
DISTANCE (km)
0
100
200
300
0.17
0.16
0.15
0.14
0.13
0.12
P (s km^{-1})
18(g)
18(e)
10
0
TT - DIST/8.0
X0.25
X0.25
X0.5
X0.5
X0.5
X0.5
18(h)
0
100
200
300
DISTANCE (km)

TABLE 2 - Velocity/depth model for the profile:
Shotpoint A (Sunrise Hill and Shay Gap), along line AB

Velocity ($km\ s^{-1}$)	Depth (km)	Travel-time curve cusps
5.950	0.0	A
6.150	11.0	B
6.250	13.0	C
6.600	28.0	D
8.200	31.0	E
8.250	42.0	F

retation of the P^I/P^* cusp cannot be made without comparing it to the P^M/Pn cusp. Between about 80 and 120 km, the arrivals of the P^I/P^* cusp have about one third to one quarter the amplitude of those near the P^M/Pn cusp (E).

The P^M/Pn cusp is shown again in the record section of a different blast in Figure 18e, the location of which is shown in Figure 18d. Figure 18e also shows seismic traces beyond 200 km. Note the different frequency contents of the source signals in Figures 18b and 18e. In Figure 18e, the P^I cusp (C) is difficult to define, because the arrivals have a much lower frequency than in Figure 18b, and are difficult to distinguish from the weak Pg phase (AB). The amplitudes of the interpreted P^I phase (arrowed) is very small compared to the amplitudes of the P^M/Pn cusp (E). The velocity/depth function derived from these record sections therefore had to model the amplitudes of the P^I/P^* cusp relative to the Pg phase, as well as its amplitudes relative to the P^M/Pn cusp (E). The amplitudes of the cusp at E are more easily defined than those of the Pg phase (AB), so most emphasis was placed on the comparison of the P^I/P^* cusp (C) with the P^M/Pn cusp (E). The resulting model does, however, give a fair match of the amplitudes of the Pg phase and the P^I phase when the uncertainties in the method due to lateral heterogeneities in the upper crust are considered.

The proposed model for profile AB is shown in Figure 18f and listed in Table 2; the ray parameter (p) versus distance plot is shown in Figure 18g. The travel time curves for the model, derived by ray tracing through the model, are superimposed on the record sections in Figures 18b and 18e. The synthetic seismogram record section, with superimposed travel time curves, are illustrated in Figure 18c and 18h. In the synthetic seismograms of Figure 18c, the Pg phase was omitted because, as can be seen in the synthetic seismograms of Figure 18h which contains the Pg phase, the Pg and P^I phases constructively interfere so that no meaningful comparison of the P^I and P^M phases can be made. The comparison can be made in Figure 18c, where the ratio of the amplitudes of the phases is about one third to one quarter, as noted previously in the recorded data in Figure 18b.

The amplitudes of the P^I/P^* cusp (C) were reduced relative to those of the P^M/Pn cusp (E) by (i) including velocity gradients above and below the intracrustal boundary, thus forcing energy which would otherwise fall on the reflection branch onto the forward (refraction) branches either side of the reflection branch, and (ii) making the boundary gradational, thereby forcing the ray theoretical cusp further from the blast. Without the gradients above

Figure 19. Model for shotpoint G (Goldsworthy), along line GBC. (a) location diagram for the record section in Figure 19b; (b) record section southwards from G. The superimposed travel time curves are for the model in Figure 19c; (c) velocity/depth model for profile GBC; (d) p versus distance plot for the model in Figure 19c; (e) synthetic seismogram record section and travel time curves for the model in Figure 19c; (f) synthetic seismogram record section for the sub-Moho phases.

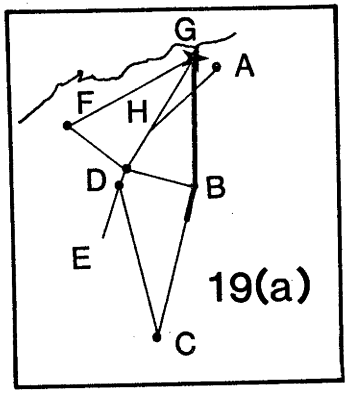
G
A
F
H
D
B
E
C
19(a)

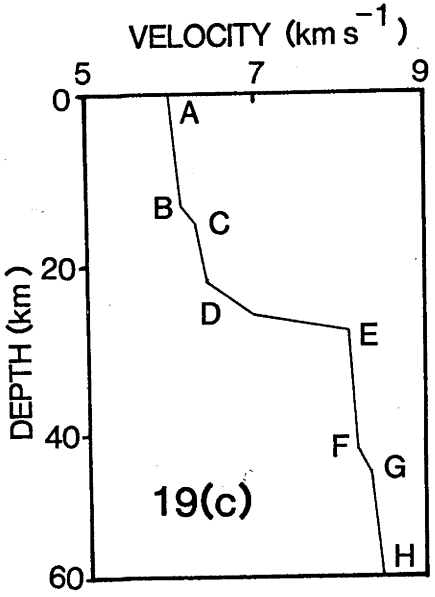
VELOCITY (km s^{-1})
5
7
9
0
20
40
60
DEPTH (km)
A
B
C
D
E
F
G
H
19(c)

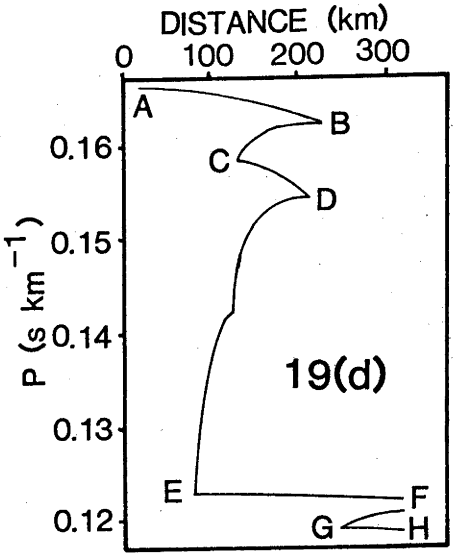
DISTANCE (km)
0
100
200
300
P (s km^{-1})
0.16
0.15
0.14
0.13
0.12
A
B
C
D
E
F
G
H
19(d)

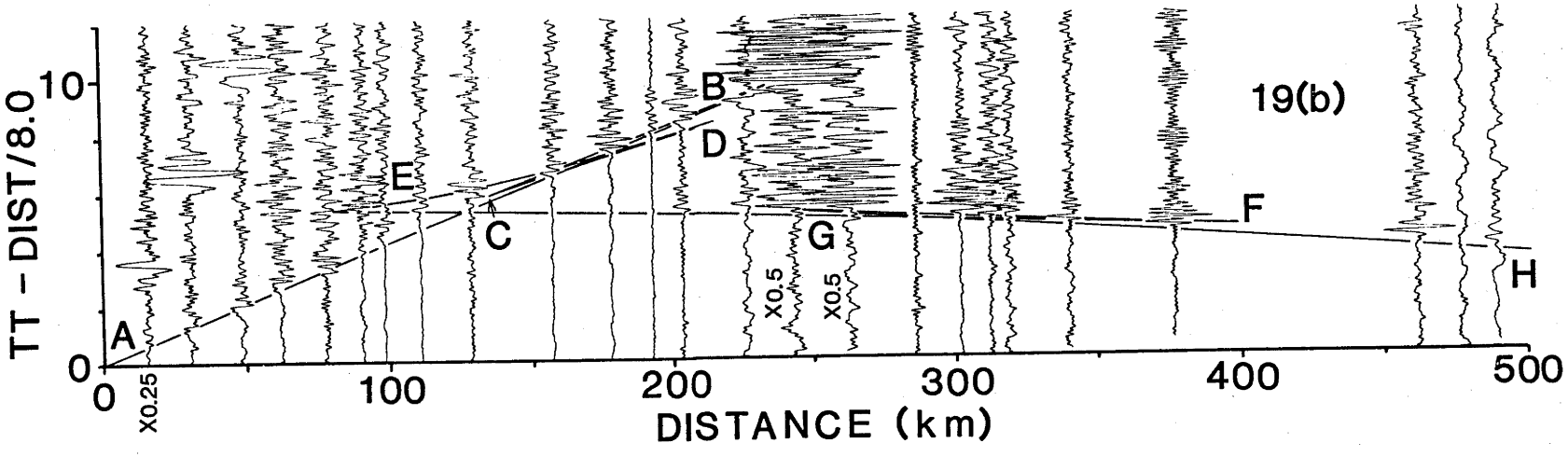
TT - DIST/8.0
10
0
0
X0.25
100
200
300
400
500
DISTANCE (km)
A
B
C
D
E
F
G
H
X0.5
X0.5
19(b)

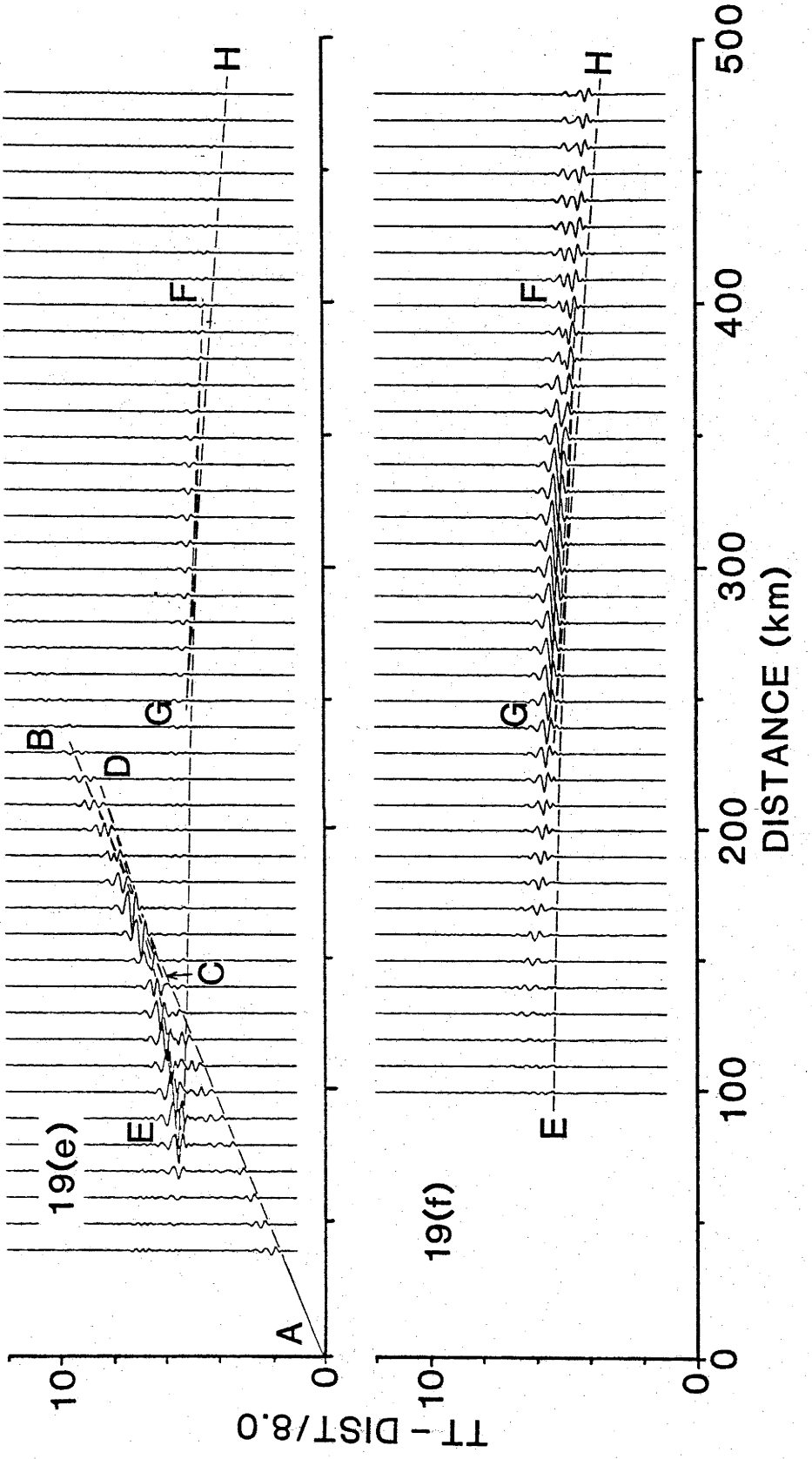
19(e)
19(f)
A
B
C
D
E
F
G
H
TT - DIST/8.0
DISTANCE (km)
0
10
100
200
300
400
500

and below the boundary, and with a sharper boundary, the amplitudes of the P^I/P^* cusp were too large compared to the P^M/Pn cusp. The intracrustal boundary creates a small triplication in the travel time curve, and the arrowed P^I phases in Figures 18b and 18e are assumed to be sub-critical reflections.

Several arrivals which could be part of the forward Pg/P^I cusp (B) can be interpreted in Figure 18e, but no convincing correlations can be made. The arrivals are generally small. The model gives a correspondingly small cusp at B (Figure 18h).

The PM phase weakens beyond about 180 km in the data, and beyond about 200 km in the synthetic record section. Note that the Pn phase is weak in the data, although some arrivals (arrowed, with an asterisk in Figure 18e) can be interpreted. This is an important factor in the interpretation of the data from shotpoint G at Goldsworthy along line GBC.

5.3.2 Shotpoint G (Goldsworthy), along line GBC

The record section of the recordings of a blast at shotpoint G southwards along line GBC is shown in Figure 19b. Figure 19a gives the location of the profile. Note that in this record section, two traces at about 250 km were reduced in amplitude by 50%. When these traces were adjusted for gain , etc., they became anomalously large. These stations were situated within the alluvial deposits of the Fortescue River valley. Very little information is available about the thickness and seismic velocity of the alluvium, but it is thick enough to contain extensive aquifers used for water supply by the local cattle stations and the township of Newman. If the velocity in the alluvium is about 3 km s^{-1}, and if it overlies a basement with a velocity of 6 km s^{-1}, a Pn wave transmitted through the laterite would undergo an increase of 55% in amplitude; the reduction of the recorded amplitudes to half means that they now have approximately the same amplitudes as the traces on either side.

The Pg phase (AB) has large, often overmodulated arrivals out to the crossover distance with Pn, and the arrivals at cusp E in the distance range 90 to 100 km are overmodulated. Consequently, the interpretation of the near-surface phases is difficult, so an upper crustal model similar to that in Figure 18e was adopted for this profile.

The P^M reflection branch (DE) maintains fairly large amplitudes to

TABLE 3 - Velocity/depth model for the profile:
Shotpoint G (Goldsworthy), along line GBC

Velocity ($km\ s^{-1}$)	Depth (km)	Travel-time curve cusps
6.010	0.0	A
6.150	13.0	B
6.300	15.0	C
6.450	22.0	
7.000	26.0	D
8.100	28.0	E
8.200	42.0	F
8.350	44.5	G
8.500	57.0	H

about 300 km. Note that the Pn arrivals (EF) are fairly small between 130 and 200 km, but beyond 200 km very large sub-Moho phases are evident. The sub-Moho arrivals have amplitudes comparable to those of the P^M phases in the same traces.

Except for the stations in about the first 100 km of the profile, the stations used in Figure 19b are the same as those used in Figure 18e for the record section of blasts at shotpoint A. In Figure 18e, the P^M arrivals are small beyond about 200 km, and only small sub-Moho phases are evident. The blast recorded beyond 200 km in Figure 19b had three times the amount of explosives but only one eleventh of the turning time of the blast recorded beyond 180 km in Figure 18e. It is therefore apparent that source effects have contributed to the large amplitudes in Figure 19b.

A triplication FGH can be interpreted in the travel time curves at about 300 km in Figure 19b, and defines a boundary in the upper mantle about 14 km under the Moho. The triplication is probably present in Figure 18e, corresponding to the arrivals arrowed with an asterisk, but it is not clear because of the small amplitudes.

The model for line GBC is shown in Figure 19c and listed in Table 3, and the ray parameter versus distance plot is shown in Figure 19d. In the model, the velocity increases steadily through the crust, and the Moho is transitional over several kilometres. Between 42 and 45 km depth, a slight increase in velocity marks an upper mantle discontinuity which causes the triplication FGH in the travel time curve. Velocity gradients above and particularly below the discontinuity maintain the amplitudes of the refracted phases along travel time branches EF and GH, respectively.

In the synthetic seismogram record section in Figure 19e, the amplitudes of the arrivals around cusp G are similar to those around cusps B and and D, but the absolute amplitudes are more akin to those in Figure 18d than those in Figure 19e. Figure 19f shows the amplitudes of the curves EFGH in more detail.

5.3.3 Shotpoint B (Newman), along line BG

The record section of blasts at shotpoint B northwards along line BG is presented in Figure 20b. The location of the profile is shown in Figure 20a. It reverses the profile on Figure 19b, and it differs from it in several ways.

Figure 20. Models for shotpoint B (Newman), along line BG.
(a) location diagram for the record section in Figure 20b; (b) record section northwards from B. The superimposed travel time curves are for the model in Figure 20d; (c) diagrammatic sketches illustrating two ways of obtaining negative intercept times from regression analysis of travel time data: (i) thickening wedge of near surface, low velocity rocks, and (ii) thin, high velocity, near surface layer; (d) model 1 for profile GB; (e) p versus distance plot for the model in Figure 20d; (f) synthetic seismogram record section and travel time curves for the model in Figure 20d; (g) record section northwards from shotpoint B. The superimposed travel time curves are for the model in Figure 20h; (h) model 2 for profile GB. Note that only the amplitudes for the lower crust have been modelled accurately; the model for the upper crust and below the Moho was derived to fit the observed travel times only; (i) p versus distance plot for the model in Figure 20h; (j) synthetic seismogram record section and travel time curves for the model in Figure 20h.

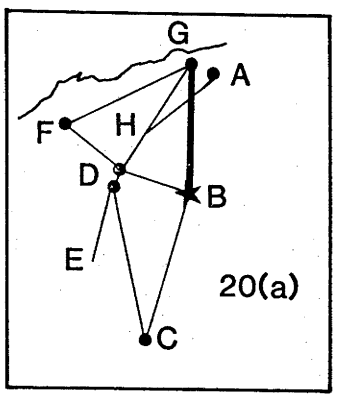
G
A
F
H
D
B
E
C
20(a)

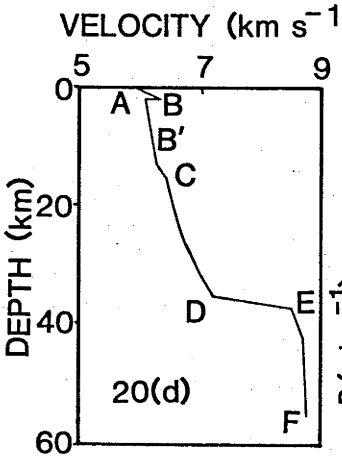
VELOCITY (km s⁻¹)
5
7
9
0
20
40
60
DEPTH (km)
A
B
B′
C
D
E
F
20(d)

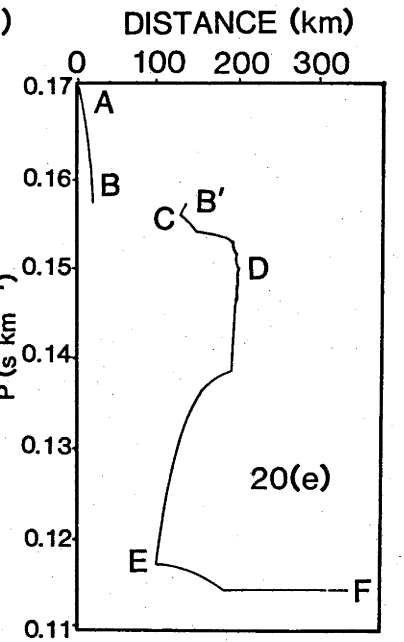
DISTANCE (km)
0
100
200
300
0.17
0.16
0.15
0.14
0.13
0.12
0.11
P (s km⁻¹)
A
B
C
B′
D
E
F
20(e)

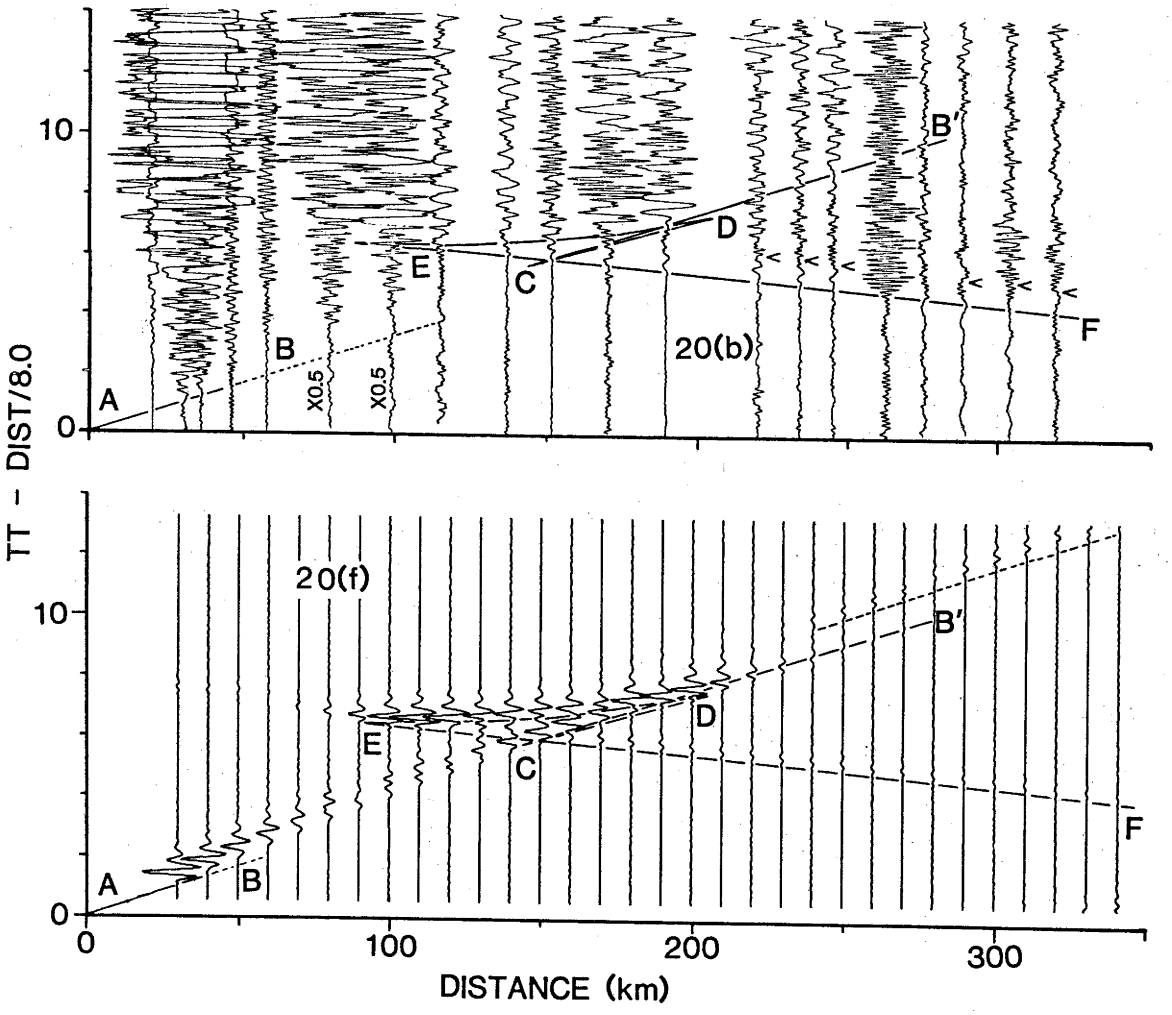
TT - DIST/8.0
10
0
A
B
X0.5
X0.5
E
C
D
B′
F
20(b)
20(f)
0
100
200
300
DISTANCE (km)

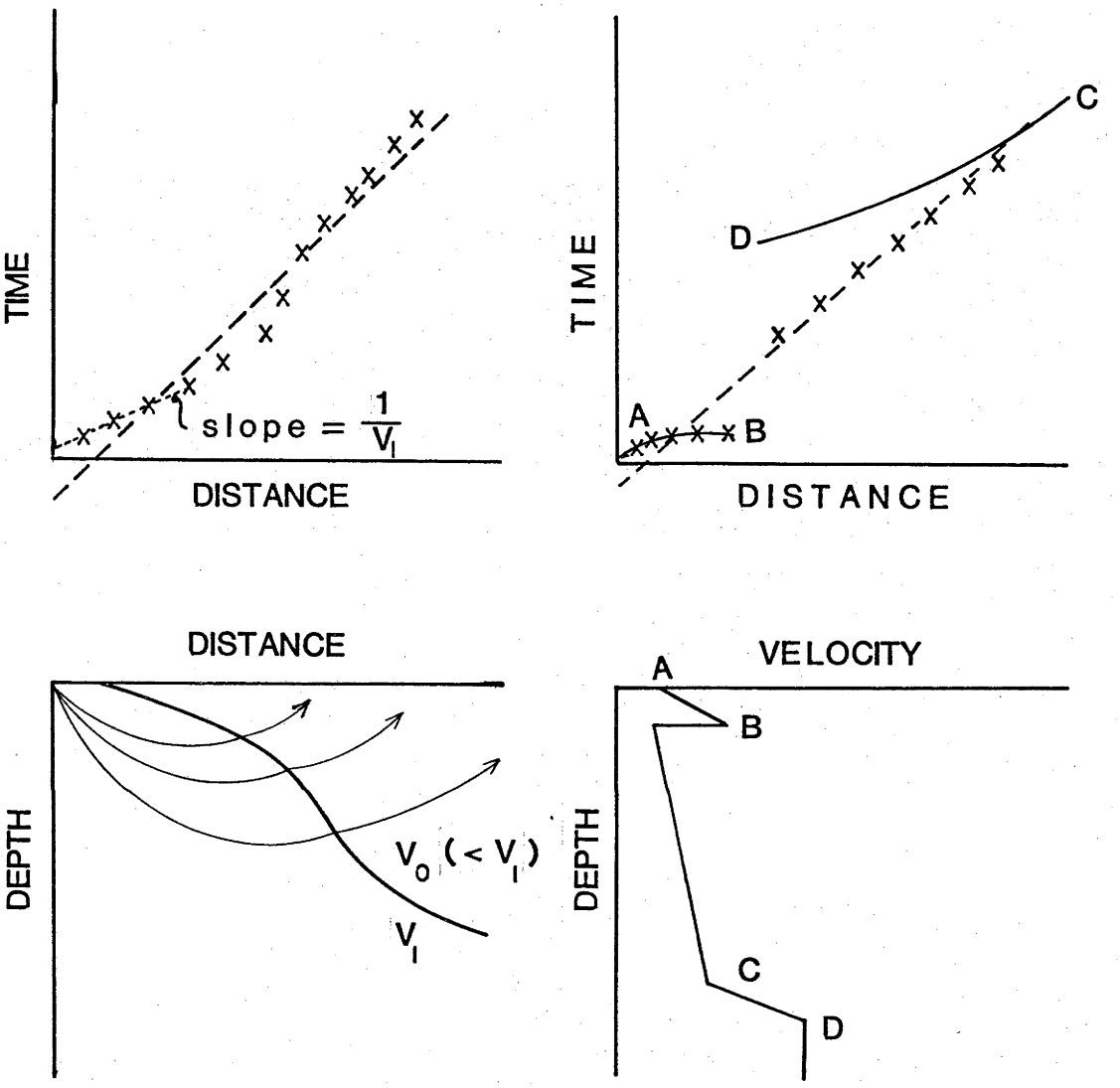

20(c)

Part 1 Part 2

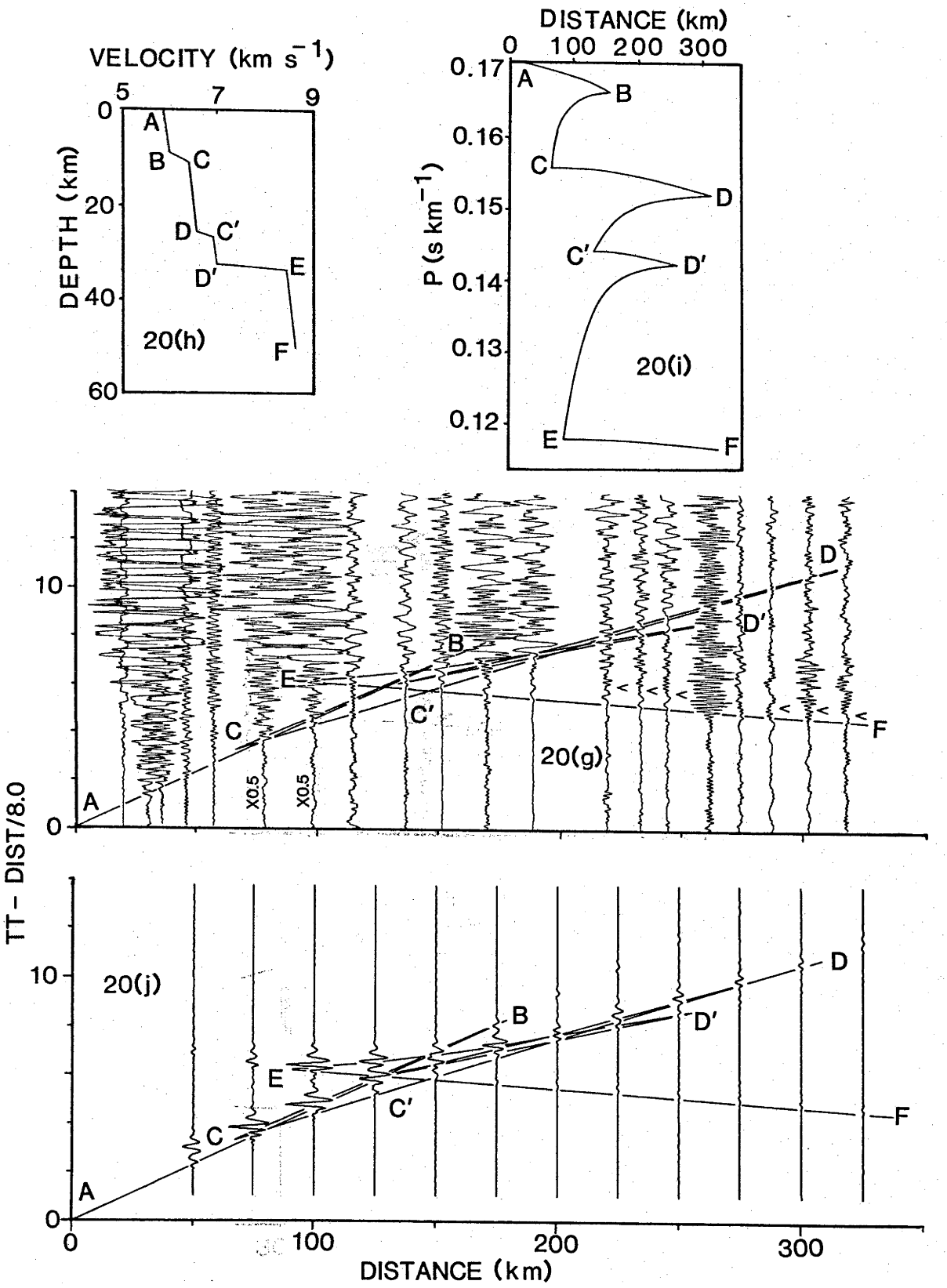
VELOCITY (km s^{-1})
5
7
9
0
20
40
60
DEPTH (km)
A
B
C
D
C′
D′
E
F
20(h)
DISTANCE (km)
0
100
200
300
0.17
0.16
0.15
0.14
0.13
0.12
P (s km^{-1})
20(i)
10
0
X0.5
X0.5
20(g)
TT - DIST/8.0
20(j)
DISTANCE (km)

TABLE 4 - Regression analyses of travel-time data for the phase Pg from shotpoint B northwards along lines BA and BG. The errors are at the 95% confidence level. The RMS residuals are in seconds. (after Drummond, 1979a)

Shot number	Velocity ($km\ s^{-1}$)	(Std error)	Intercept (s)	(Std error)	RMS residual	No. of points
083	5.922	(0.052)	-0.018	(0.112)	0.132	7
088	5.804	(0.052)	-0.207	(0.093)	0.097	7
089	5.844	(0.110)	-0.261	(0.295)	0.234	6
all data	5.864	(0.037)	-0.134	(0.090)	0.197	20

The first arrivals along curve AB, ie. the Pg phase, are weak and emergent, and have a negative (-0.13 s) intercept time (Drummond, 1979a,b). The P^M branch is very clear, with the amplitudes decaying abruptly at 200 km, forming a bright cusp similar to that observed in the Canadian Shield by Berry & Fuchs (1973). The Pn phase (EF) is clear, but no triplication similar to FGH in Figure 19b can be interpreted. One feature of the Pn phase originally noted by Drummond (1979a, b) was that on most traces beyond 150 km a phase (arrowed) could be picked 0.6 s after the Pn arrival. The five traces beyond 250 km are from a different blast from those between 150 and 250 km and were plotted to show that the effect is independent of the blast used. Linear regression analyses of the travel times of the two phases yielded statistically indistinguishable apparent velocities for the phases. It is possible that the second phase forms part of the triplication FGH, and its apparent velocity is rendered the same as Pn by the effects of refractor topography. Alternatively, the second arrival may be a multiple from a structure unique to the crust near shotpoint B.

Drummond (1979a) reported the results of separate linear regression analyses of the data from three blasts, and they are repeated in Table 4. The intercepts are all very small, and are generally of the same order of magnitude as the error at the 95% confidence level. However, the intercepts are consistently negative, even when all of the data are regressed together.

The negative intercept time from the regression analysis of the upper crustal phases northwards from shotpoint B may be caused by the same feature which causes the weak and emergent Pg phase arrivals. While it is possible that the weak arrivals of upper crustal phases north from Newman may be caused by the practice of firing the mining benches from north to south, thus reinforcing seismic energy propagating southwards and destructively interfering with the energy propagating northwards, a number of other reasons can be proffered. Figure 20c illustrates two ways of obtaining negative intercept times. In part 1, which is the model preferred by Drummond (1979b), the the Pg phase is increasingly delayed with distance because of thickening low velocity, near surface rocks. Drummond (1979b) nomimated the thickening Hamersley Basin sediments wedging northwards off the Sylvania Dome as the thickening low velocity rocks. However, although Drummond & others (1981) confirmed the presence of low velocity (5.9 km s^{-1}) rocks in the Hamersley Basin, these rocks were usually underlain by a high velocity sheet of volcanics and banded iron formations. In the Newman area, the velocity in the high velocity layer may reach 6.7 km s^{-1}.

TABLE 5 - Velocity depth models for the profile:
Shotpoint B (Newman), along line BG

MODEL 1			MODEL 2		
Velocity (km s^{-1})	Depth (km)	Travel-time curve cusps	Velocity (km s^{-1})	Depth (km)	Travel-time curve cusps
5.860	0.0	A	5.860	0.0	A
6.350	2.0	B	6.000	9.0	B
6.050	2.0		6.400	11.0	C
6.250	13.0	B'	6.550	26.0	D
6.400	15.0	C	6.910	27.0	C'
6.475	17.0		7.000	33.0	D'
6.500	18.5		8.450	34.0	E
6.531	20.0		8.600	50.0	F
6.583	22.0				
6.645	24.0				
6.718	26.0				
6.801	28.0				
6.847	29.0				
6.895	30.0				
6.946	31.0				
7.000	32.0				
7.057	33.0				
7.116	34.0				
7.178	35.0	D			
8.500	37.0	E			
8.700	42.0				
8.750	55.0				

In part 2 of Figure 20c, a high velocity, near surface layer generates a forward branch AB. If the high velocity layer has infinite lateral extent, much of the energy which propagates in the upper crust will be trapped under the high velocity lid, and will only emerge as weak arrivals where local structures, such as basement domes, form windows in the high velocity layer. As well, in the Hamersley Basin, the high velocities are found only in the southeast (Drummond & others, 1981), and it is possible that, to the north along line BG, rays which bottom within the upper crust will return to the surface beyond the edge of the high velocity lid as Pg arrivals. Their travel times, when regressed with those of branch AB may give negative intercepts.

The present data do not distinguish which, if either of these models is correct. A high velocity, near surface layer is included in Model 1 of Figure 20d and Table 5, but it must be remembered that the effects of the high velocity layer are applied to both the downgoing and upgoing rays by the synthetic seismogram program, whereas it is likely that beyond 50 or 100 km from the blast the true effect would be on the downgoing ray only. The structure of the upper crust and the intracrustal boundary (B'C in Figure 20d) is similar to that in Figure 18f.

Bullen (1960) showed that large amplitude forward cusps such as the one at D can be produced if the velocity increases continuously with depth. In such a model, rays which penetrate deeper, rather than emerging at greater distances, meet higher velocities and are bent back to the surface faster than those which bottom at shallower depths, so that rays are focussed at one distance.

In Model 1 (Figure 20d), the lower crust has a second order increase of velocity with depth. This causes all of the rays with ray parameters between about 0.153 and 0.138 s km^{-1} and which bottom between 15 and 35 km to emerge between 190 and 205 km; note the broad cusp at D in the p versus distance plot in Figure 20e, and compare it with the sharp cusps at D in Figures 18f and 19e. The model gives large amplitudes at cusp D to about 200 to 210 km, after which they decay rapidly (Figure 20f).

A zone of high velocity gradient (EF) below the Moho, which is transitional over 2 km, maintains the amplitudes of the Pn phase; it may extend to greater depths but the profile is too short to provide the relevant information.

The dotted travel time curve later than and beyond B' in Figure 20f are multiples from the high velocity, near surface layer. The data are too poor to verify whether or not they are observed.

Several second and later arrivals in the distance range 130 to 200 km are difficult to correlate and it is possible that they imply a lower crustal boundary, similar to that in the Capricorn Orogen in the south, which gives rise to the P^L phase. In Figure 20g, a triplication DC'D' has been tentatively interpreted.

Model 2, in Figure 20h and Table 5 shows the structure of the lower crust required to produce the triplication DC'D'. It must be stressed, however, that the structure of the upper crust and below the Moho is designed to fit the measured travel times but not the amplitudes of the record section. The p versus distance plot is shown in Figure 20i, and the synthetic seismogram seismogram record section in Figure 20j. Note that constructive interference between branches DC' and D'E produces large amplitudes to 180 km, and destructive interference beyond 180 km produces small amplitudes on the D'E branch. This may be fortuitous, because the effects of destructive and constructive interference are critically dependent on the separation of the interfering branches, and on the frequency content and phases of the interfering wavelets.

The model provides an alternative to Model 1 in Figure 20d, but is not preferred because there is no evidence for the P^L phase elsewhere in the Pilbara Craton; there are other bright cusps observed in the craton; and the nature of the interference that produces the bright cusp is apparently fortuitous.

5.3.4 Shotpoint G (Goldsworthy), along line GHD

The record section of shotpoint G recorded to the southwest along line GHD is shown in Figure 21b. The location of the profile is shown in Figure 21a.

The Pg phase has large, overmodulated arrivals on most traces out to the crossover distance with Pn at about 130 km. The trace at about 95 km is

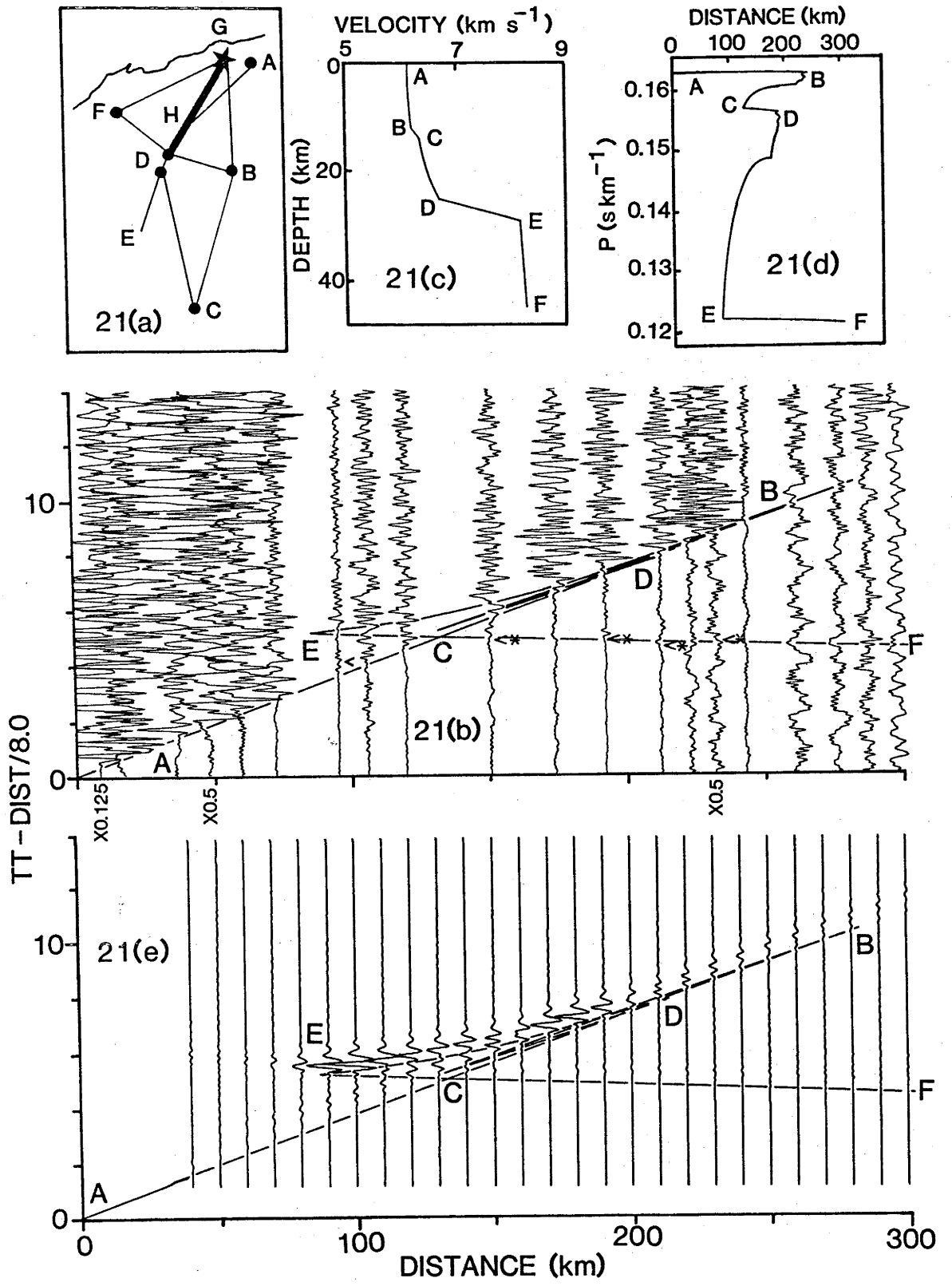

Figure 21. Model for shotpoint G (Goldsworthy), along line GHD. (a) location diagram for the record section in Figure 21b; (b) record section southwards from G. The superimposed travel time curves are for the model in Figure 21c; (c) velocity/depth model for profile GHD. (d) p versus distance plot for the model in Figure 21c; (e) synthetic seismogram record section and travel time curves for the model in Figure 21c.

TABLE 6 - Velocity/depth model for the profile:
Shotpoint G (Goldsworthy), along line GHD

Velocity ($km\ s^{-1}$)	Depth (km)	Travel-time curve cusps
6.130	0.0	A
6.130	2.0	
6.131	3.0	
6.137	5.0	
6.142	6.0	
6.156	8.0	
6.164	9.0	
6.174	10.0	
6.185	11.0	
6.200	12.0	B
6.350	14.0	C
6.377	16.0	
6.420	18.0	
6.480	20.0	
6.515	21.0	
6.555	22.0	
6.600	23.0	
6.648	24.0	
6.700	25.0	D
8.150	29.0	E
8.250	45.0	F

not overmodulated, and has a clear second arrival (arrowed) interpreted as a sub-critical P^I reflection. The forward cusp D does not have any convincing arrivals beyond 180 km where it blends with the large amplitude P^I arrivals of the branch BC, which maintains large amplitudes to about 230 km.

The P^M phase between the forward cusp D and retrograde cusp E is clear, with large amplitudes. Pn is generally weak but is observed (arrowed, with an asterisk) on some traces between 150 and 240 km. Note that there are no large amplitudes which identify an upper mantle triplication similar to FGH observed from this shotpoint southwards along line GB in Figure 19b.

The model for this profile is shown in Figure 21c and listed in Table 6; the p versus distance plot for the model is shown in Figure 21d, and the synthetic seismogram record section in Figure 21e.

The overmodulation of the Pg phases within 130 km of the blast means that no estimate of the gradient in the upper crust is possible. The blast used to construct the first 210 km of the record section was large, with a very short burning time. The Pg phase is well recorded to about 230 km, so it is reasonable to assume that the large amplitudes near the blast are due to blasting effects and not high velocity gradients in the upper crust. This means that the model can have low velocity gradients in the upper crust to allow the Pg phase to propagate beyond 200 km without being turned back to the surface. Gradients are needed just above the intracrustal boundary to focus the Pg energy at about 200 to 230 km - note the broad cusp B in the p versus distance plot in Figure 21d.

The intracrustal boundary is gradational so that the amplitudes of the subcritical P^I reflections at cusp C are not too large. Below the intracrustal boundary, a second order velocity gradient focusses the P* phase at about 180 to 190 km (Figure 21d) to account for the large observed amplitudes at D. Note the broad cusp D in Figure 21d.

The model has a broad Moho (over 4 km depth) to fit the travel time data and to move the largest amplitudes at the cusp E away from the blast. Below the Moho, a very small gradient accounts for the observed weak Pn arrivals.

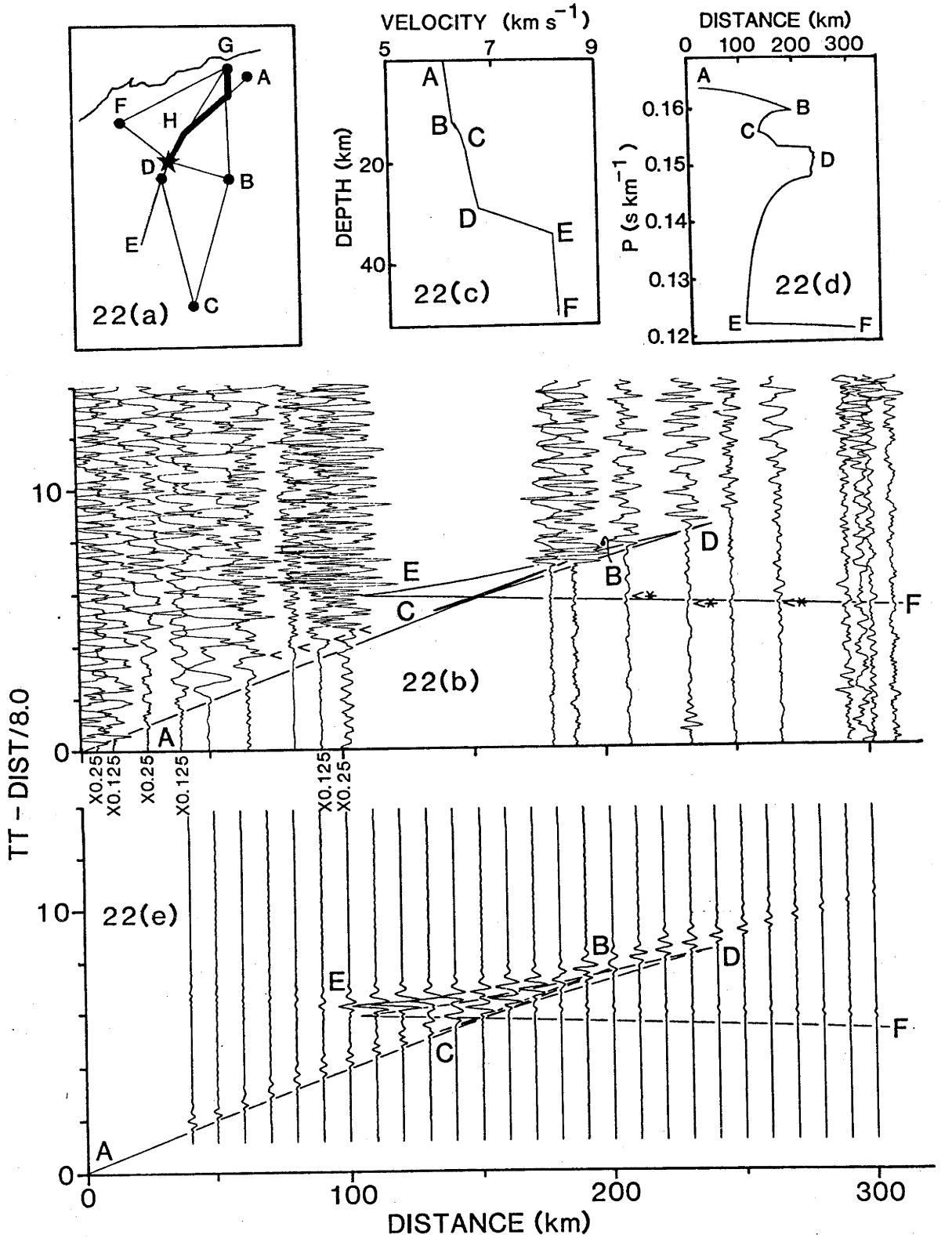

Figure 22. Model for shotpoint D (Tom Price), along line DHG. (a) location diagram for the record section in Figure 22b; (b) record section northwards from Tom Price, at D. The superimposed travel time curves are for the model in Figure 22c; (c) velocity/depth model for profile DHG, from blasts at Tom Price; (d) p versus distance plot for the model in Figure 22c; (e) synthetic seismogram record section and travel time curves for the model in Figure 22c.

TABLE 7 - Velocity/depth model for the profile:
Shotpoint D (Tom Price), along line DHG

Velocity (km s^{-1})	Depth (km)	Travel-time curve cusps
6.100	0.0	A
6.250	11.5	B
6.400	14.5	C
6.500	18.0	
6.520	20.0	
6.550	22.0	
6.589	24.0	
6.638	26.0	
6.696	28.0	
6.728	29.0	D
8.150	34.0	E
8.250	50.0	F

5.3.5 Shotpoint D (Tom Price), along line DHG

The record section of Tom Price blasts northeast along line DHG (Figure 22b, location diagram Figure 22a) reverses the profile of Goldsworthy blasts in Figure 21b. The record section has a gap between 100 and 180 km across which the correlation of phases is tentative, but the correlations made seem realistic.

The Pg phase (AB) has strong, low frequency arrivals between the blast and 100 km. It is not clear as later arrivals beyond 180 km. This record section has some of the clearest evidence for P^I reflections from the intracrustal boundary. They appear as high frequency arrivals (arrowed) up to a second after Pg in the four traces between 60 and about 100 km.

The P^M phase must be correlated across the gap in the recordings. It is fairly weak around the retrograde cusp at E, but strong arrivals with an apparent velocity of about 6.5 km s^{-1} are observed on cusp D out to about 240 km, after which they decay rapidly. The Pn phase is weak, although some arrivals (arrowed, with an asterisk) may be interpreted.

The model derived from the record section in Figure 22b is shown in Figure 22c and listed in Table 7; the p versus distance plot is shown in Figure 22d and Figure 22e is the synthetic seismogram record section derived from the model.

The model has a high velocity gradient in the upper crust to maintain the amplitudes of the Pg phase, a transitional intracrustal boundary to ensure that the P^I phase at the retrograde cusp C is not too large relative to the P^M phase at cusp E, and a second order increase of velocity with depth in the lower crust to focus the P* phase at about 240 km. Note the broad cusp D in Figure 22d, and the fairly rapid decay of amplitudes beyond 240 km at cusp D in Figure 22e.

5.3.6 Shotpoint D (Paraburdoo), along line DHG

Recordings of the blasts at the mine at Paraburdoo at shotpoint D northwards along line DHG comprise the record section in Figure 23b. The location of the profile is shown in Figure 23a. As with the record section of Tom Price blasts (Figure 22b), also from shotpoint D, this record section has significant gaps. The most important are in the distance range 50 to

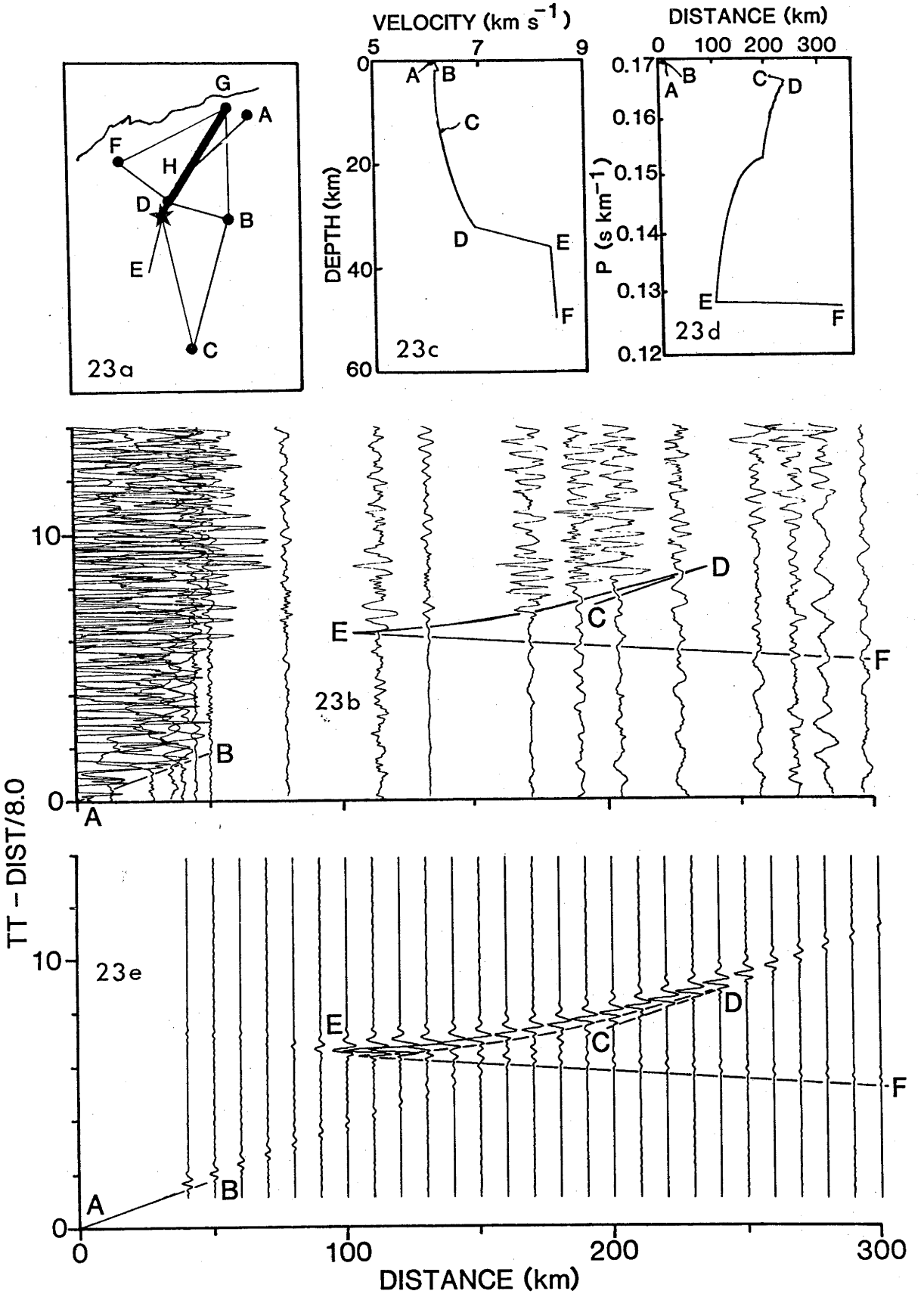

Figure 23. Model for shotpoint D (Paraburdoo), along line DHG. (a) location diagram for the record section in Figure 23a; (b) record section northwards from Paraburdoo, at D. The superimposed travel time curves are for the model in Figure 23c; (c) velocity/depth model for profile DHG, from blasts at Paraburdoo; (d) p versus distance plot for the model in Figure 23c; (e) synthetic seismogram record section and travel time curves for the model in Figure 23c.

TABLE 8 - Velocity/depth model for the profile:
Shotpoint D (Paraburdoo), along line DHG

Velocity (km s^{-1})	Depth (km)	Travel-time curve cusps
6.190	0.0	A
6.300	2.0	B
6.190	2.0	
6.200	8.0	
6.209	9.0	
6.219	10.0	
6.230	11.0	
6.300	14.0	C
6.325	16.0	
6.360	18.0	
6.406	20.0	
6.462	22.0	
6.529	24.0	
6.606	26.0	
6.648	27.0	
6.693	28.0	
6.741	29.0	
6.791	30.0	
6.844	31.0	
6.900	32.0	D
8.350	36.0	E
8.450	50.0	F

170 km, where only three recording stations successfully monitored Paraburdoo blasts.

The Pg phase, where observed, decays rapidly near the blast, probably because of the near surface high velocity Hamersley basin rocks noted above in Section 5.3.3 for Newman blasts along line BG, and by Drummond (1981) in the intercept method interpretation of this record section. The high velocity layer extends about 60 km north of Paraburdoo, and so does not affect the upgoing rays for most of this profile.

Clear arrivals with an apparent velocity of about 6 km s^{-1}. and therefore attributed to the Pg phase or its asymptote, the P^I phase, are observed as later arrivals between 220 and 270 km. They may be caused by energy trapped below the high velocity Hamersley Basin lid, and propagated in the uppermost crust before escaping beyond the edge of the basin, and/or the upper crust below the near surface high velocity Hamersley Basin cover rocks may have low velocity gradients to allow the Pg phase to propagate to such distances.

The intracrustal boundary must be included in the model because this profile duplicates much of that included in Figure 22b, where very clear subcritical reflections off the boundary were noted, but there is very little evidence for the boundary in this record secion at this scale. The boundary is modelled (Figure 23c, Table 8) as very gradational, with velocity gradients above and below to cause only a small triplication CD.

The P^M branch DE has clear, large amplitude arrivals which blend with branch BC beyond 220 km. A second order increase of velocity with depth is invoked for the lower crust to focus the energy of the P* phase at 220 km (Figure 23d). The Pn phase is weak and implies a very low velocity gradient in the upper mantle.

Except for the near surface high velocity layer, the model in Figure 23c is very similar in form to that in Figure 21c, for which this profile is the reverse.

5.3.7 Shotpoint F (Pannawonica), along line FDB

Two blasts at shotpoint F were used to construct the record section along line FDB, shown in Figure 24b. Figure 24a shows the location of the profile. The blast used to construct the record section from 190 to 370 km

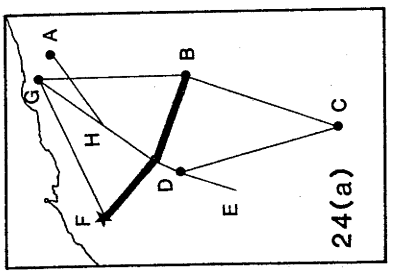
A
B
C
D
E
F
G
H
24(a)

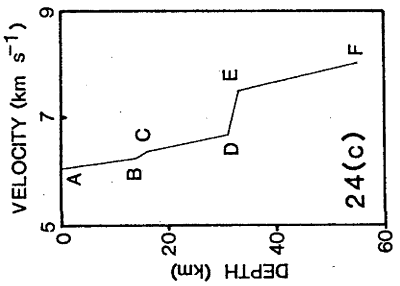
VELOCITY (km s^{-1})
DEPTH (km)
A
B
C
D
E
F
24(c)

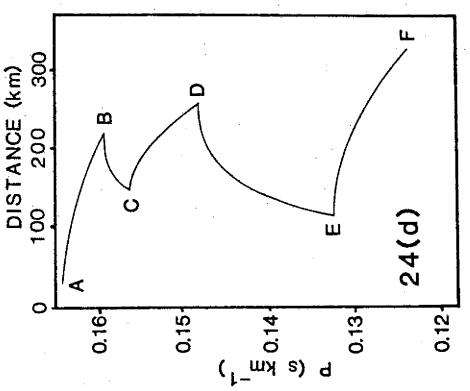
DISTANCE (km)
p (s km^{-1})
A
B
C
D
E
F
24(d)

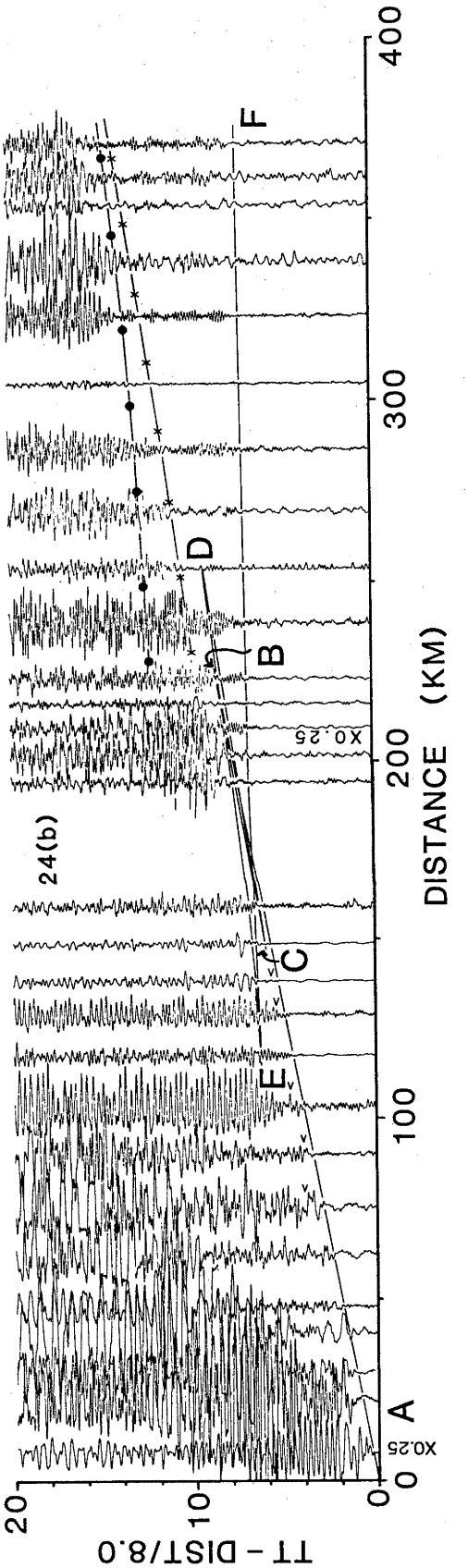
TT - DIST/8.0
DISTANCE (KM)
XO.25
X0.25
A
B
C
D
E
F
24(b)

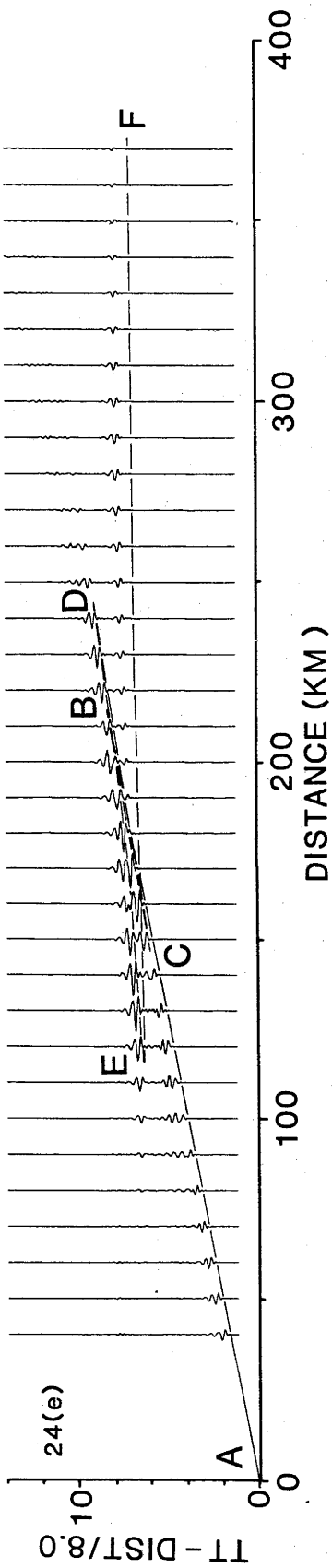

Figure 24. Model for shotpoint F (Pannawonica), along line FDB.
(a) location diagram for the record section in Figure 24b; (b) record section southeastwards from F. The superimposed travel time curves are for the model in Figure 24c; (c) velocity/depth model for profile FDB. (d) p versus distance plot for the model in Figure 24c; (e) synthetic seismogram record section and travel time curves for the model in Figure 24c.

TABLE 9 - Velocity/depth model for the profile:
Shotpoint F (Pannawonica), along line FDB

Velocity (km s^{-1})	Depth (km)	Travel-time curve cusps
6.070	0.0	A
6.250	14.0	B
6.370	16.0	C
6.700	31.0	D
7.500	33.0	E
8.000	55.0	F

was large (484 tonnes of explosives), dispersed over several kilometres, and had a burning time of 2.17 s. Consequently, the seismic energy from the blast is not a clear, sharp pulse but an oscillating, high frequency wavelet of over a second's duration, and it is not easy to distinguish on all traces beyond 190 km the onset of secondary pulses whose arrivals are buried in the coda of previous phases.

The Pg phase is well observed between the blast and the crossover with Pn, which is at about 170 km. P^I reflections (arrowed) follow the Pg phase on traces between 75 and 140 km. The forward cusps B and D are difficult to interpret because of the nature of the arrivals beyond 190 km, but they are interpreted as falling at about 220 and 250 km, respectively. The P^M phase has large amplitude arrivals, and the Pn phase appears as a low apparent velocity (7.6 km s^{-1}), high amplitude (compared to Pn on other profiles) phase (EF).

The model for the profile is shown in Figure 24c and Table 9, the p versus distance plot in Figure 24d, and the synthetic seismogram record section in Figure 24e. The model has a high velocity gradient in the upper crust to maintain the amplitudes of the Pg phase (AB), a transitional intracrustal boundary to restrict the amplitudes of the P^I phase near cusp C, and gradients in the lower crust to limit the forward cusp D to 250 km. The Moho is transitional over several kilometres and the upper mantle has a high velocity gradient to produce and maintain the large Pn amplitudes. The upper mantle velocity gradient also increases the upper mantle velocity from a modelled value of 7.5 km s^{-1} below the Moho to 8.0 km s^{-1}, a value more like that on some of the other profiles, at 55 km depth.

Several large amplitude phases are observed as later arrivals beyond 190 km in Figure 24b. They have apparent velocities similar to that of the Pg phase, and are reminiscent of the multiples Mereu & others (1977) observed from the Moho under the Rocky Mountains of Canada. It will be shown later that these arrivals are probably multiples from the intracrustal boundary and Moho reflected as underside reflections off the Hamersley Basin cover rocks. The travel time curves with the crosses and the dots are the times of the multiples off the intracrustal boundary and the Moho, respectively, reflected off the underside of the high velocity layer, assuming that the velocity in the high velocity layer at the point of reflection approximately half way along the profile is 6.3 km s^{-1} (Drummond & others, 1981), and that the layer is 2 km thick. The modelled travel times are in reasonable agreement

with the observed times; no attempt was made at more accurate modelling because of the lateral changes known to occur in the high velocity layer (Section 4.4.2).

5.3.8 Shotpoint B (Newman), along line BDF

The location of profile BDF, along which blasts at the Newman mine at shotpoint B were recorded, is shown in Figure 25a. The record section is presented in Figures 25b and 25g, on which the superimposed travel time curves are for two alternative velocity/depth models derived for the profile.

The record section, has a very high (6.65 km s^{-1}) velocity branch (AB) near the source. The large amplitudes of branch AB, which is the P_2 phase of Drummond & others (1981) and Drummond (1981), decay rapidly beyond 50 km, and imply a near surface high velocity layer.

The Pg, P^I and P* phases are difficult to identify in the record section. While the near surface, high velocity layer might be expected to mask out all of the effects of the upper crust, the P_2 phase velocity decreases to the northwest, and the high velocity layer pinches out in places against basement domes, so that there are windows in the high velocity layer through which the crustal phases can reach the surface. Such arrivals can be seen (arrowed) in the distance range 60 to 140 km in Figure 25b, although correlation between them is difficult.

The P^M phase (DE) is clearly observed with large amplitudes which decay abruptly beyond cusp D at 260 km. The Pn phase is observed on some traces (arrowed, with an asterisk, in Figure 25b), to 250 km, beyond which it is not observed.

Because of the screening effect of the near surface, high velocity layer, it is not possible to derive a unique model of the crust from this record section, so two models are presented. Many others would fit the data equally as well.

Model 1 is presented in Figure 25c and Table 10. The p versus distance ance plot for the model is in Figure 25d, and the synthetic seismogram record section in Figure 25e. Model 1 is based on the model in Figure 20d for the record section for the same shotpoint to the north along line BG, although some changes were necessary to account for different apparent velocities of

TABLE 10 - Velocity/depth models for the profile:
Shotpoint B (Newman), along the line BDF

MODEL 1			MODEL 2		
Velocity (km s^{-1})	Depth (km)	Travel-time curve cusps	Velocity (km s^{-1})	Depth (km)	Travel-time curve cusps
5.950	0.0	A	5.900	0.0	A
6.650	2.0	B	6.650	2.0	B
6.050	22.0		6.100	2.0	
6.250	16.0		6.250	14.0	
6.550	20.0		6.370	16.0	
6.565	22.0		6.700	31.0	D
6.591	24.0		7.750	35.0	E
6.627	26.0		7.850	39.0	F
6.674	28.0	D	7.850	50.0	
6.732	30.0				
6.800	32.0	E			
7.750	35.0				
7.850	39.0	F			
7.850	50.0				

Figure 25. Models for shotpoint B (Newman), along line BDF.
(a) location diagram for the record section in Figure 25b; (b) record section northwestwards from B. The superimposed travel time curves are for the model in Figure 25c. Those marked with dots indicate the first multiple from the Moho, and those marked with crosses the first multiple from the intracrustal boundary, reflected as underside reflections from the near surface, high velocity layer; (c) Model 1 for profile BDF; (d) p versus distance plot for the model in Figure 25c; (e) synthetic seismogram record section and travel time curves for the model in Figure 25c. The multiples are as for Figure 25c. Part 1:amplitudes relative to the largest overall peak to trough amplitude, Part 2: trace normalised, so that the maximum peak to trough amplitude is the same for all traces; (f) ratios of reflected and refracted P-wave energy to incident P-wave energy, plotted as a function of angle of incidence: (i) wave in a medium of 6.65 km s^{-1} velocity incident at the free surface, (ii) wave in a medium of 6.10 km s^{-1} velocity incident on a medium of 6.65 km s^{-1} velocity, and (iii) wave in a medium of 6.10 km s^{-1} velocity incident on a medium of 6.30 km s^{-1} velocity; (g) record section northwestwards from B. The superimposed travel time curves are for the model in Figure 25h. See Figure 25b for a description of the multiples; (h) Model 2 for profile BDF; (i) p versus distance plot for the model in Figure 25h; (j) synthetic seismogram record section and travel-time curves for the model in Figure 25h. See Figure 25b for a description of the multiples, Parts 1 and 2 as for Figure 25e.

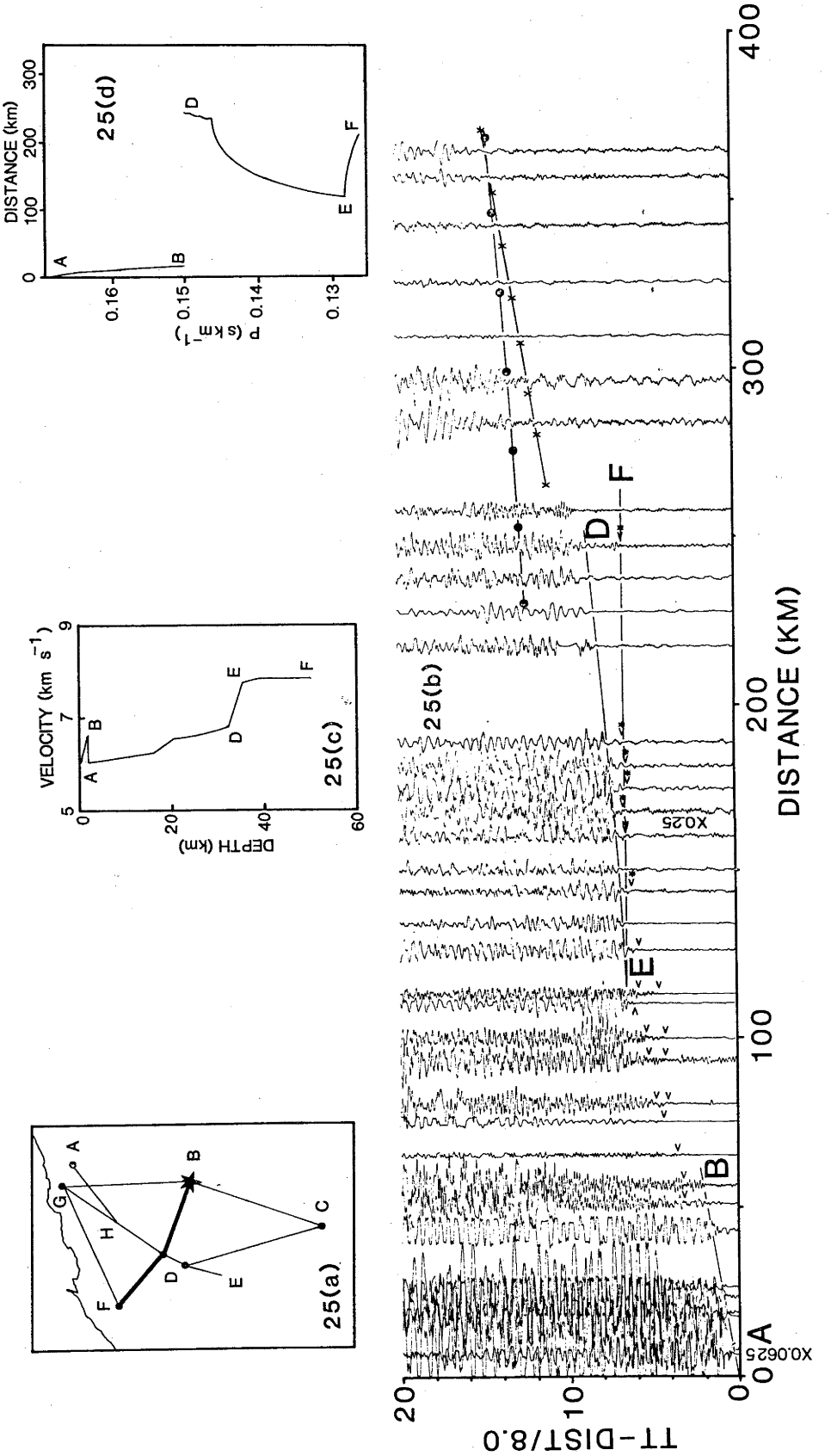
25(a)
A
B
C
D
E
F
G
H
25(b)
TT-DIST/8.0
DISTANCE (KM)
XO.0625
XO25
25(c)
VELOCITY (km s^{-1})
DEPTH (km)
25(d)
DISTANCE (km)
p (s km^{-1})

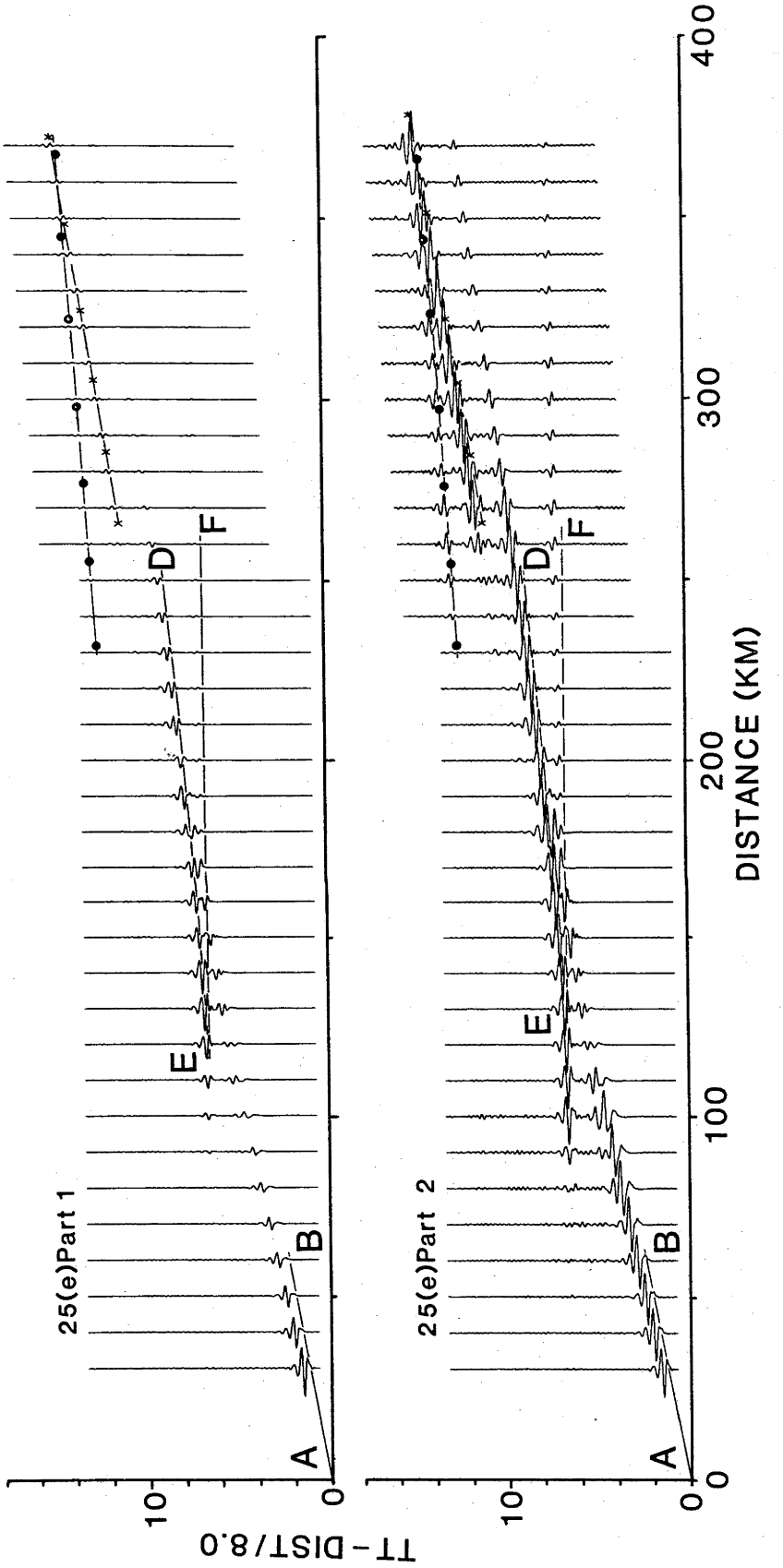
25(e)Part 1
25(e)Part 2
A
B
D
E
F
0
100
200
300
400
DISTANCE (KM)
10
TT - DIST/8.0

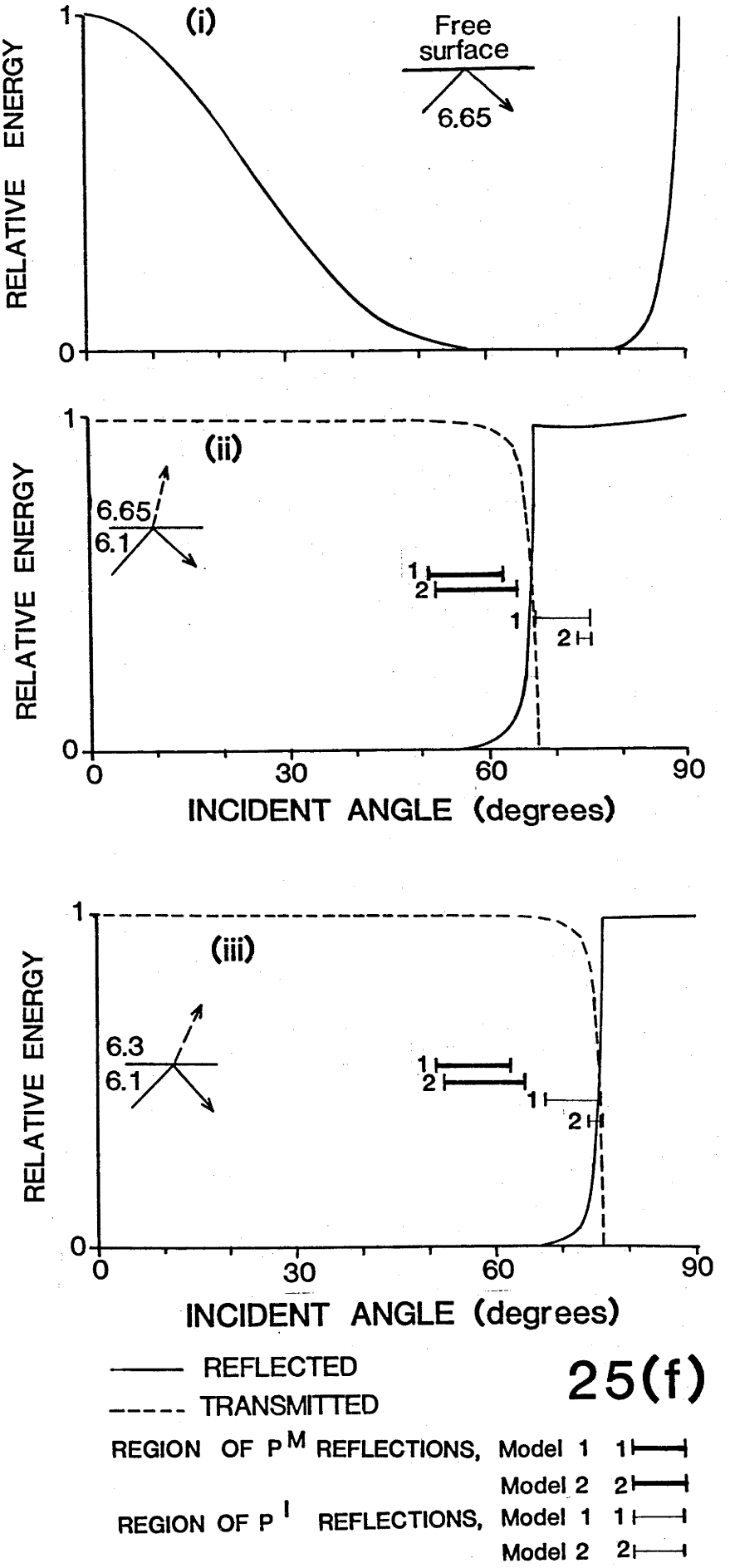
(i)
Free surface
6.65
RELATIVE ENERGY
1
0
(ii)
6.65
6.1
1
2
1
2
RELATIVE ENERGY
0
30
60
90
INCIDENT ANGLE (degrees)
(iii)
6.3
6.1
1
2
1
2
RELATIVE ENERGY
0
30
60
90
INCIDENT ANGLE (degrees)
REFLECTED
TRANSMITTED
REGION OF P^M REFLECTIONS, Model 1 1
Model 2 2
REGION OF P^I REFLECTIONS, Model 1 1
Model 2 2

25(f)

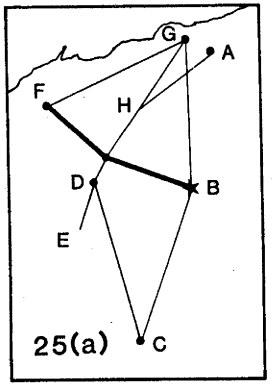
G
A
F
H
D
B
E
C
25(a)

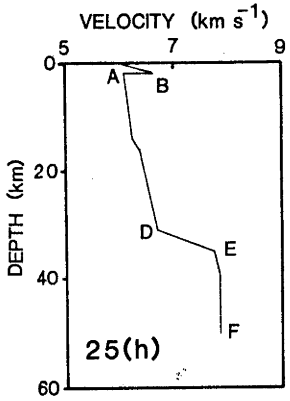
VELOCITY (km s^{-1})
5
7
9
0
20
40
60
DEPTH (km)
A
B
D
E
F
25(h)

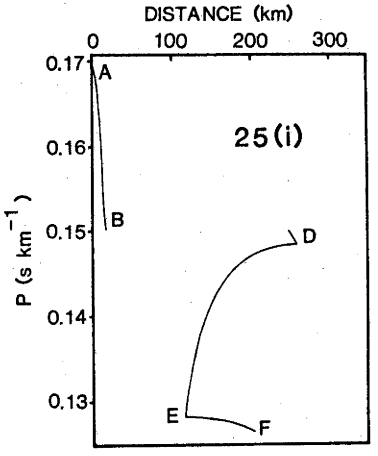
DISTANCE (km)
0
100
200
300
0.17
0.16
0.15
0.14
0.13
P (s km^{-1})
A
B
D
E
F
25(i)

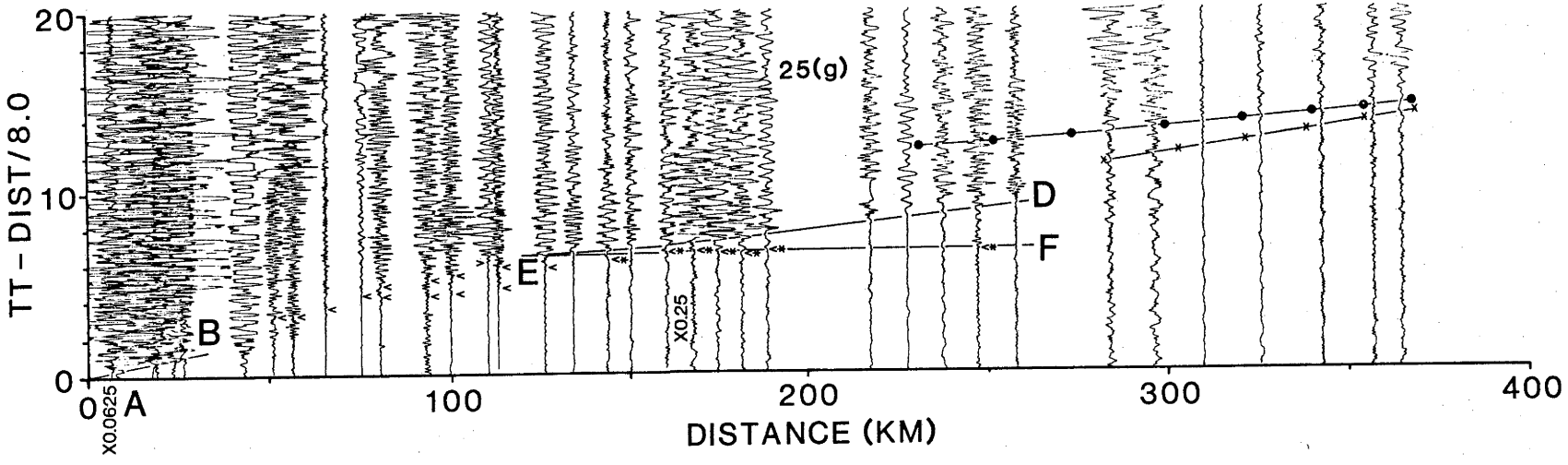
20
10
0
TT - DIST/8.0
25(g)
B
E
D
F
X0.25
X0.0625
0
A
100
200
300
400
DISTANCE (KM)

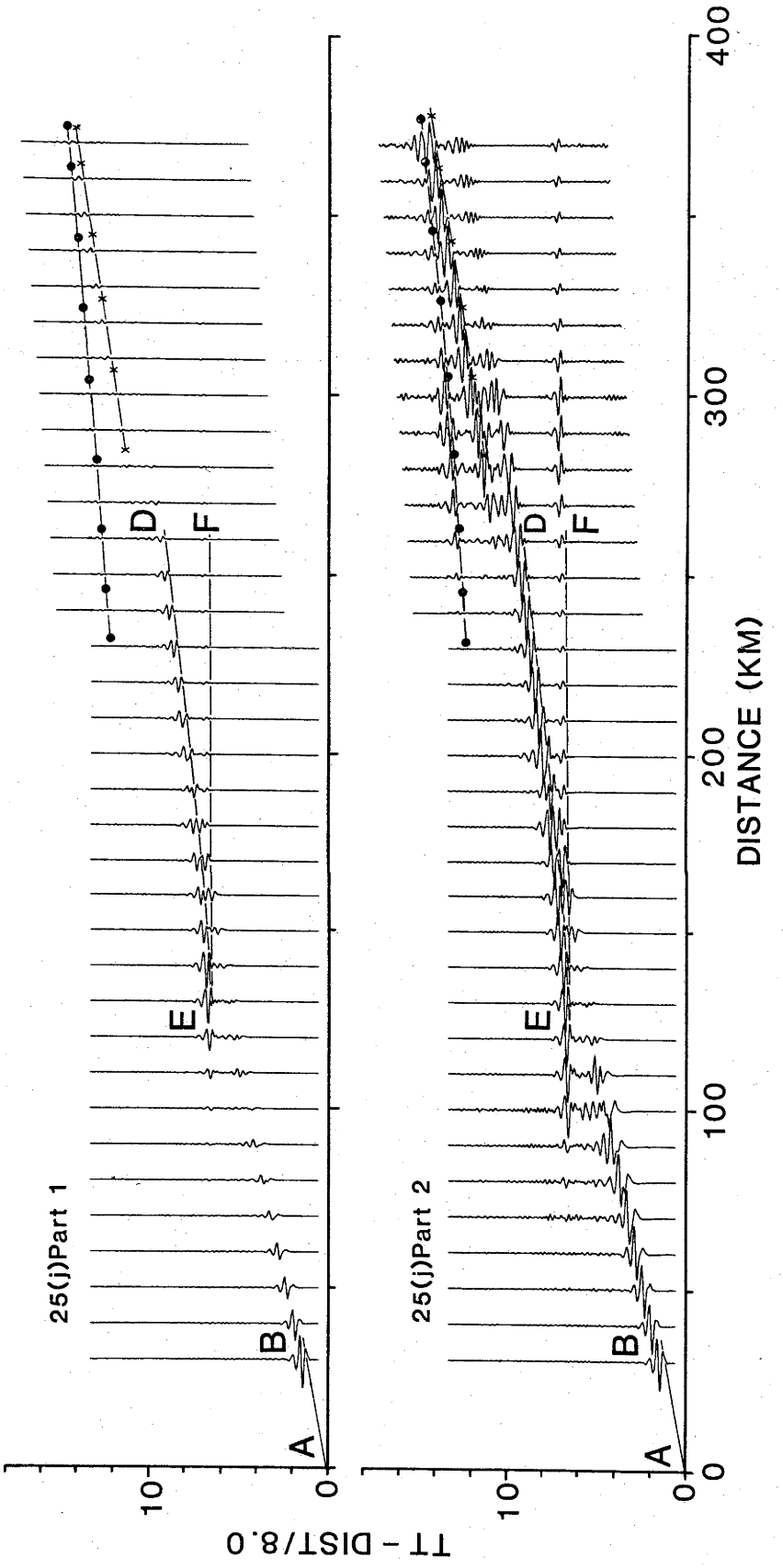
25(j)Part 1
25(j)Part 2
A
B
D
E
F
0
10
TT - DIST/8.0
0
100
200
300
400
DISTANCE (KM)

the phases AB, DE and EF, and their intercept times.

One feature arising from the synthetic seismogram record section in Figure 25e is the production of multiples from the intracrustal boundary and the Moho. They are especially evident on the trace normalised synthetic seismogram record section (Figure 25e, part 2) and correlate with a band of recorded arrivals which have considerable energy (Figure 25b). They are similar to those noted in Figure 24b for the reversed profile from shotpoint F, and are also similar to the multiples recorded in Canada by Mereu & others (1977).

Mereu & others (1977) interpreted their multiples as phases focussed at the surface oy strong gradients in the lower crust and then internally reflected at the free surface. In Figure 25f, part i, the energy reflected at the free surface, expressed as a fraction of the incident p-wave energy, is plotted as a function of the angle of incidence. As noted by Mereu & others (1977), the angle of incidence must be small if most energy is to be reflected and multiples created. In Model 1, rays which reflect off the intracrustal boundary and the Moho, and which reach the surface as multiples within 400 km of the shotpoint, have angles of incidence at the free surface between 49 and 74 degrees. These rays will not be reflected at the free surface.

Figure 25f, part ii, illustrates the partitioning of energy into reflected and transmitted phases at the base of the high velocity layer in Model 1. Also marked are the angles of incidence at the base of the high velocity layer of the waves which reflect off the intracrustal boundary and the Moho. The angles of incidence of these rays fall in that part of the energy partitioning curves where some energy will be transmitted and some reflected. For example, most P^M energy will be transmitted through the high velocity layer to the surface, and will be recorded at the free surface, while a smaller proportion will be reflected to be returned to the surface as multiples. Most energy reflected off the intracrustal boundary will be internally reflected at the high velocity layer.

The amplitudes of the multiples in the synthetic seismogram record section are much smaller than the observed multiples, and in the synthetic section the multiples from the intracrustal boundary are larger than those from the Moho, whereas in the data the Moho multiples are larger. No attempt was made to model the amplitudes of the multiples because of the lateral changes in the velocity in the high velocity layer (Drummond & others, 1981) and

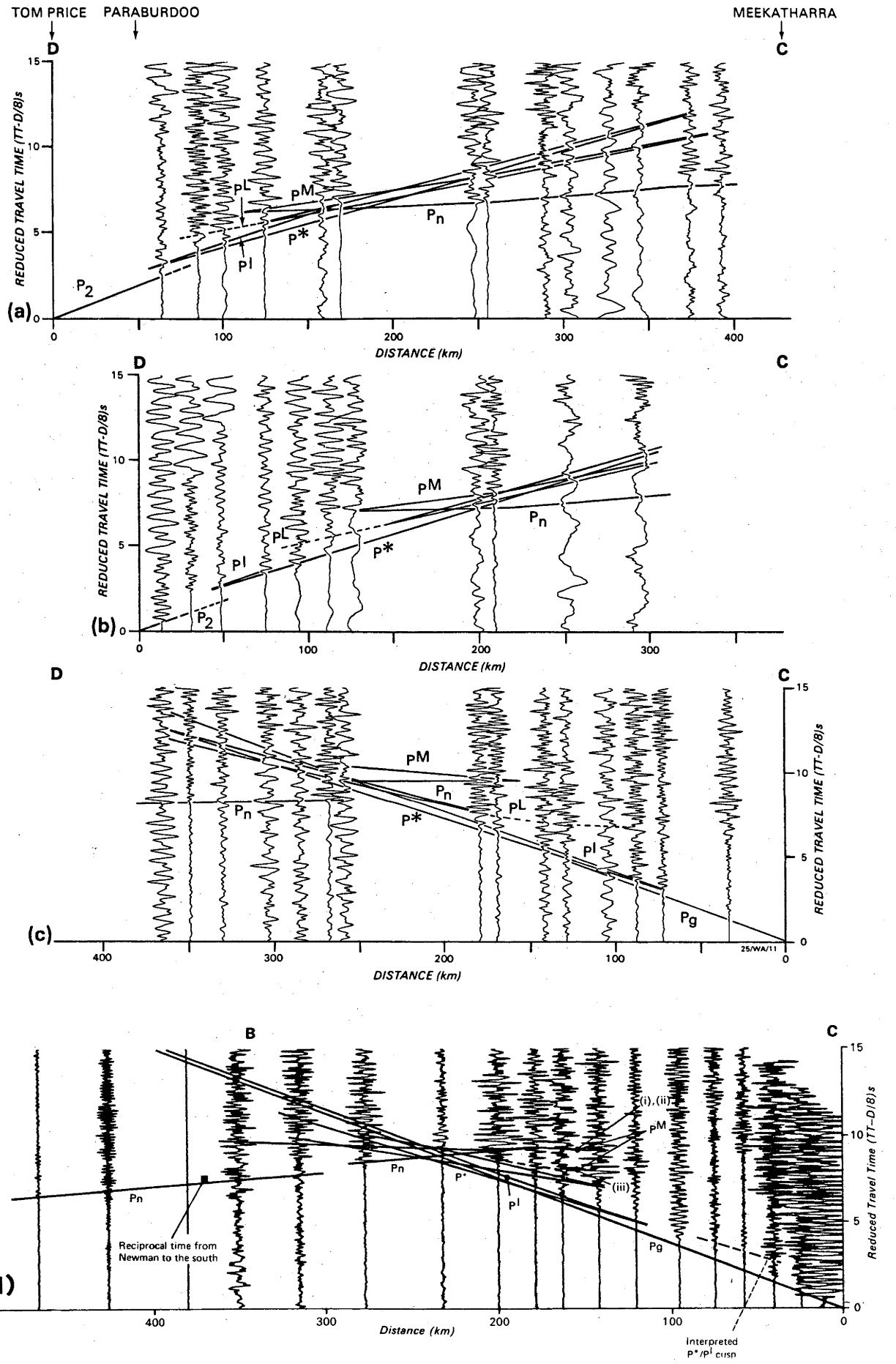

Figure 26. Record sections across the Capricorn Orogen comparing the positions of the observed P^L and P^I/P^* cusps with the positions of those from the models of the intercept method interpretation. Parts a, b & c are from Drummond (1981), and part d is from Drummond (1979b), Figure 3e.

the irregular nature of the boundary between the high velocity layer and the underlying basement. For example, in Figure 25f, part iii, the energy partitioning of a wave incident on a high velocity layer with a velocity of only 6.3 km s^{-1} is shown. This is the velocity in the high velocity layer in the centre of the profile. In this case, all energy returned from the intracrustal boundary will be partitioned approximately equally into transmitted and reflected phases.

Clearly, the modelled amplitudes of the multiples are so critically dependent on the velocity in the high velocity layer, and the structure within boundaries, which determines the angle of incidence at the base of the high velocity layer, that to try to model them with a program that allows only laterally homogeneous models would be fruitless.

Model 2 for this profile, presented in Figure 25h and Table 10, is based on the model for the reversed profile from shotpoint F towards shotpoint B (Figure 24). The high velocity, near surface layer has been included, and the structure at and below the Moho changed to suit the apparent velocity and amplitudes of the Pn phase. The p versus distance plot is presented in Figure 25i, and the synthetic seismogram record section in Figure 25j.

It is not possible on the basis of the present data to give preference to either Model 1 or Model 2 for this profile. Both are based on models from other profiles in the region, and both fit the data for this profile equally well.

5.3.9 Observed amplitudes within the Capricorn Orogen.

While it is not possible to use current synthetic seismogram techniques in the Capricorn Orogen (lines BC and DC) because of the extreme lateral structure, some observations can be made about the nature of the boundaries based on the fit to the observed data of the ray theoretical cusps from the models from the intercept method of interpretation.

Drummond (1981) noted that the P^L phase, assumed to be reflections from the lowermost crust, occurred much closer to the blast than expected from ray theory (Figures 26a, 26b and 26c, which repeat Figure 13). Similarly, Drummond (1979b) noted that the subcritical reflections at the P^I/P^* cusp on line CD (Figure 26d) were quite large. They are observed within 40 km of the blast, whereas the ray theoretical cusp falls at about 120 km. In Figure 26c,

the arrowed phase is interpreted as a P^I reflection, but the ray theoretical cusp is at twice the epicentral distance. These large amplitudes mean that either the boundaries are sharp, giving rise to large amplitude subcritical phases, and/or low velocity zones exist within the crust and the boundaries are therefore much shallower than interpreted. With the current data, it is not possilbe to distinguish between these alternatives, although low velocity channels extensive enough to halve the critical distance would seem unlikely to be caused by thermal effects in such a geothermally cold region, and would have be due to changes in lithology. The effects of temperature on seismic velocities is treated in more detail in the next chapter.

The Pn arrivals throughout the Pilbara Craton are fairly weak, except along line A,G to B. The record section along line BC, which crosses the Capricorn Orogen with approximatley the same azimuth as line GB crosses the Pilbara Craton, also has Pn arrivals with substantial amplitudes (Figures 5d, 5e). Velocity gradients are therefore implied below the crust/mantle boundary, as well as above it (Drummond, 1979b).

5.4 BRIGHT CUSPS CAUSED BY LATERAL STRUCTURE

Mereu (1969) showed that topography on a boundary can cause amplitude changes, and even triplications, along travel time branches. In section 5.1, caution was expressed that the velocity/depth models derived by synthetic seismogram modelling would be valid only if the effects of vertical structure overprinted the effects of lateral structure. The purpose of this section is to briefly examine whether the bright cusps interpreted in Figures 20, 21, 22 and 23 could be caused by the effects of lateral structure.

In all profiles, the bright cusps occur at about 200 km. If the energy which is focussed at these bright cusps is assumed to bottom halfway between the shotpoint and the epicentral distance of the bright cusps, the bottoming points must be about 100 km from the shotpoints. In all but Figure 21, this would mean that the bottoming point of the rays was near the axis if the Hamersley Basin. In Figure 14a, this corresponds to a basin shaped depression in the intracrustal boundary. While no comparable basin shaped depression has been interpreted at the crust/mantle boundary, a topography of 1 or 2 km would be within the error limits of the intercept method interpretation (Section 4.2).

Figure 27 explores empirically the effects of refractor topography

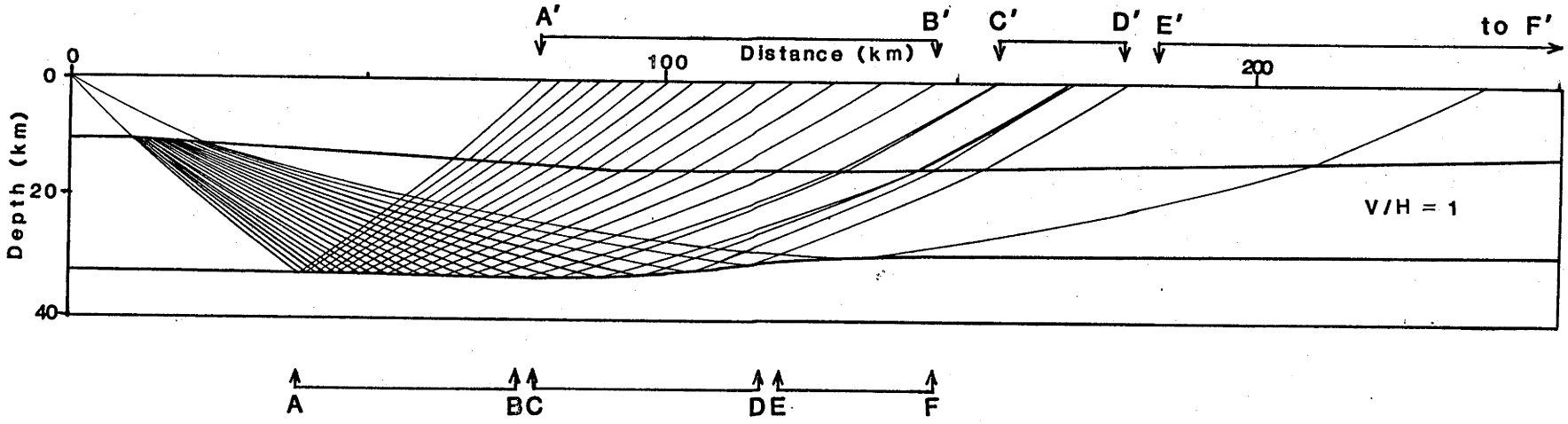

Figure 27. An example of how reflector topography can produce bright cusps. The model is based loosely on the model for line GHD (Figure 14a)

on the concentration of seismic rays at the surface. It must be stressed that while the model in Figure 27 is based loosely on the model in Figure 14a, no attempt was made to accurately model the travel times. The topography on the intracrustal boundary is that interpreted in Figure 14a. The Moho dips from about 28 km in the north (right hand end) to 32 km in the south (left hand end), and has superimposed on it a sinusoidal-type topography with an amplitude of less than 2 km and a wavelength of 70 km. It is represented by straight line segments 10 km long. The upper and lower crusts have velocity gradients from 6.0 to 6.0 km s^{-1} and 6.35 to 6.65 km s^{-1}, respectively; these are typical of the gradients of the velocity/depth functions in Section 5.3 (without the second order increase of velocity with depth required to cause the bright cusps). For convenience, first order discontinuities were used between the layers.

Only the ray paths for mantle reflections are shown. Those which bottom between A and B, where there is no reflector topography, emerge at the surface between A' and B'. Note that the distance between A' and B' is greater that that between A and B. Rays which bottom between C and D, where the reflecting surface is concave upwards, emerge between C' and D', and because the distance from C' to D' is less than that between C and D, there is some focussing of the seismic energy. This can be seen in some cases where rays which impinge on different straight line segments of the interface emerge at almost the same point at the surface. Rays which strike the reflector between E and F, where the surface is concave downwards, are scattered and emerge between E' and F', and because E'F' is very much greater than EF, there will be a sudden diminution of amplitudes of the reflected waves beyond D'.

Countless models could no doubt be found to improve the focussing effects observed by the reflector between C and D, but Figure 27 illustrates that focussing can be caused by structures which are concave towards the energy source, and scattering of the energy will be caused by structures which are convex towards the energy source. No preference can be given to models with either vertical or lateral structure. The second order increases of velocity with depth in the velocity/depth models used to produce the bright cusps of Section 5.2 have little effect on the depths of the seismic boundaries, and the refractor topography required to produce bright cusps in the regions where there is no such second order increases is very small. Consequently, the velocity/depth models of Figure 5.2 are likely to be good approximations to the real earth regardless of whether the bright cusps are caused by lateral or vertical (or both lateral and vertical) structures.

6. COMPOSITION OF THE CRUST

Geological mapping gives us an insight into the geochemical and metamorphic nature of the upper crust, but our knowledge of the lower crust is limited. Geophysical surveys provide us with the tools to probe the nature of the lower crust and perhaps the most useful geophysical parameters for defining its composition are estimates of its density and seismic velocity, which is generally in the range 6.5 to 7.0 km s^{-1}. However, as Tarney & Windley (1977) point out: "Possible materials in the lower crust which would satisfy the seismic and density constraints are:

(a) gabbro

(b) amphibolite

(c) mafic granulite

(d) eclogite or peridotite intercalated with sialic crust, and

(e) a garnet-rich crust of intermediate composition."

Hence rocks from a range of compositions and metamorphic grades have velocities and densities that match those of the lower crust. This was confirmed by Drummond & Shelley (1981) who found that the seismic properties of the crust of the Pilbara and northern Yilgara Cratons, even when considered with the observed gravity field and with the requirement that isostasy is complete, could not define a unique composition for the lower crust. Little wonder that Tarney & Windley (1977) wrote: "It is probably true to say that we know more about the composition of the oceanic crust, and even about the composition of the mantle, than we do about the lowest 15 km of the continents."

The purpose of this chapter is to study the constraints that the velocity/depth functions from the amplitude studies of the previous chapter place on the chemical composition and metamorphic nature of the lower crust of the Pilbara Craton.

The velocity/depth functions for the Pilbara Craton are reproduced in Figure 28. The model for shotpoint B (Newman) northwest along line BDF

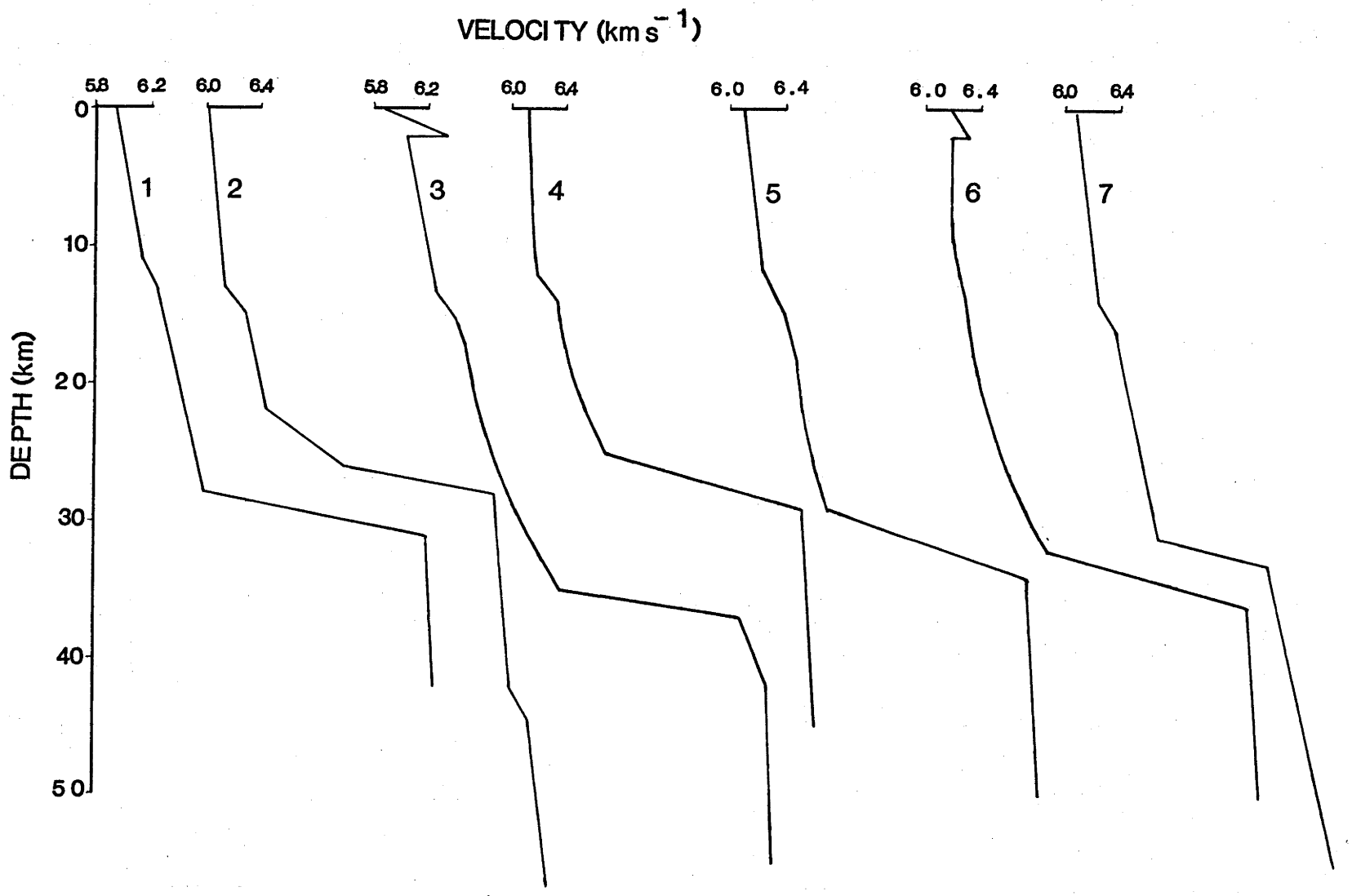

Figure 28. Velocity/depth models for the Pilbara Craton. The models are for: 1 Shotpoint A (Sunrise Hill and Shay Gap), along line AB; 2 Shotpoint G (Goldsworthy), along line GB; 3 Shotpoint B (Newman), along line BG (Model 1); 4 Shotpoint G (Goldsworthy), along line GHD; 5 Shotpoint D (Tom Price), along line DHG; 6 Shotpoint D (Paraburdoo) , along line DHG, and 7 Shotpoint F (Pannawonica), along line FDB.

was not included because the masking effects of the lower crust by the Hammersley Basin rocks meant that the models produced for the line were non-unique. All of the velocity/depth models show a steady increase of velocity with depth (apart from the decrease at the base of the Hamersley Basin rocks on profiles 3 and 6). Models such as these are traditionally interpreted as indicating an upper sialic crust overlying a more mafic (simatic) lower crust, with the effects of pressure causing the steady increase of velocity with depth through the two layers. It is therefore a useful exercise to study the effects of pressure and temperature on seismic velocities. Before this can be done, the pressure and temperature derivatives of the seismic P-wave velocities, and the pressure and temperature gradients must be defined.

6.1 VELOCITY DERIVATIVES

Manghnani & others (1974), and Drummond & Shelley (1981) preferred the velocity derivatives of Anderson, Sammis & Jordan (1972) whose partial temperature and pressure derivatives of P-wave velocity are respectively

$$\left(\frac{\partial V}{\partial T}\right)_P = -4 \times 10^{-4} \text{ km s}^{-1} \text{ deg}^{-1}$$

and

$$\left(\frac{\partial V}{\partial P}\right)_T = 1 \times 10^{-1} \text{ km s}^{-1} \text{ GPa}^{-1}$$

The temperature derivatives at 0.2 GPa and between 0 and 300°C reported by Christensen (1979) for rocks with a range of chemical compositions from acidic to ultramafic are slightly higher than the temperature derivative of Anderson & others (1972). Above 300°C, the confining pressures in Christensen's (1981) experiment were not sufficient to stop the different thermal expansions of the minerals in the rock from creating intergranular cracks, so that the temperature

derivatives above 300°C are unreliable. Christensen's (1979) pressure derivatives of velocity measured in the range 0.3 to 0.8 GPa are all higher than the values of Anderson & others (1972), but the value of 1×10^{-1} km s^{-1} GPa^{-1} measured in two samples in the range 1 to 3 GPa are identical to those of Manghnani & others (1974). This could imply that cracks and pores in the rock samples studied were still closing during the measurements at the lower pressures, so that the value of 1×10^{-1} km s^{-1} GPa^{-1} measured at the higher pressure range is the preferred of Christensen's values.

Matsushima (1981) measured the compressional and shear wave velocities in several specimens of igneous rocks and volcanic glasses at temperatues to 900°C and 2 GPa. He did not quantify any values of the velocity derivatives, but (very) approximate values scaled from his diagrams are:

$$\left(\frac{\partial V}{\partial T}\right)_{1.05\text{GPa}} = -2.5 \times 10^{-4} \text{ km s}^{-1} \text{ deg}^{-1}$$

for both rhyolite (his Fig. 11), which is of acidic composition, and diabase (his Fig. 12), which is of basic composition, and

$$\left(\frac{\partial V}{\partial P}\right)_{400^\circ\text{C}} = 1.5 \times 10^{-1} \text{ km s}^{-1} \text{ GPa}^{-1}$$

for rhyolite (his Fig. 7). The values at 1.05 GPa and 400°C were cited because, as will be shown later, these are the estimated pressure and temperature near the base of the crust of the Pilbara Craton.

Anderson & others' (1972) value of the temperature derivative of velocity is bracketed by that of Matsushima (1981), which is lower, and Christensen's (1979) values, which are higher. Both Matsushima's and Christensen's pressure derivatives agree with that of Anderson and others (1972). Thus the values quoted by Anderson & others

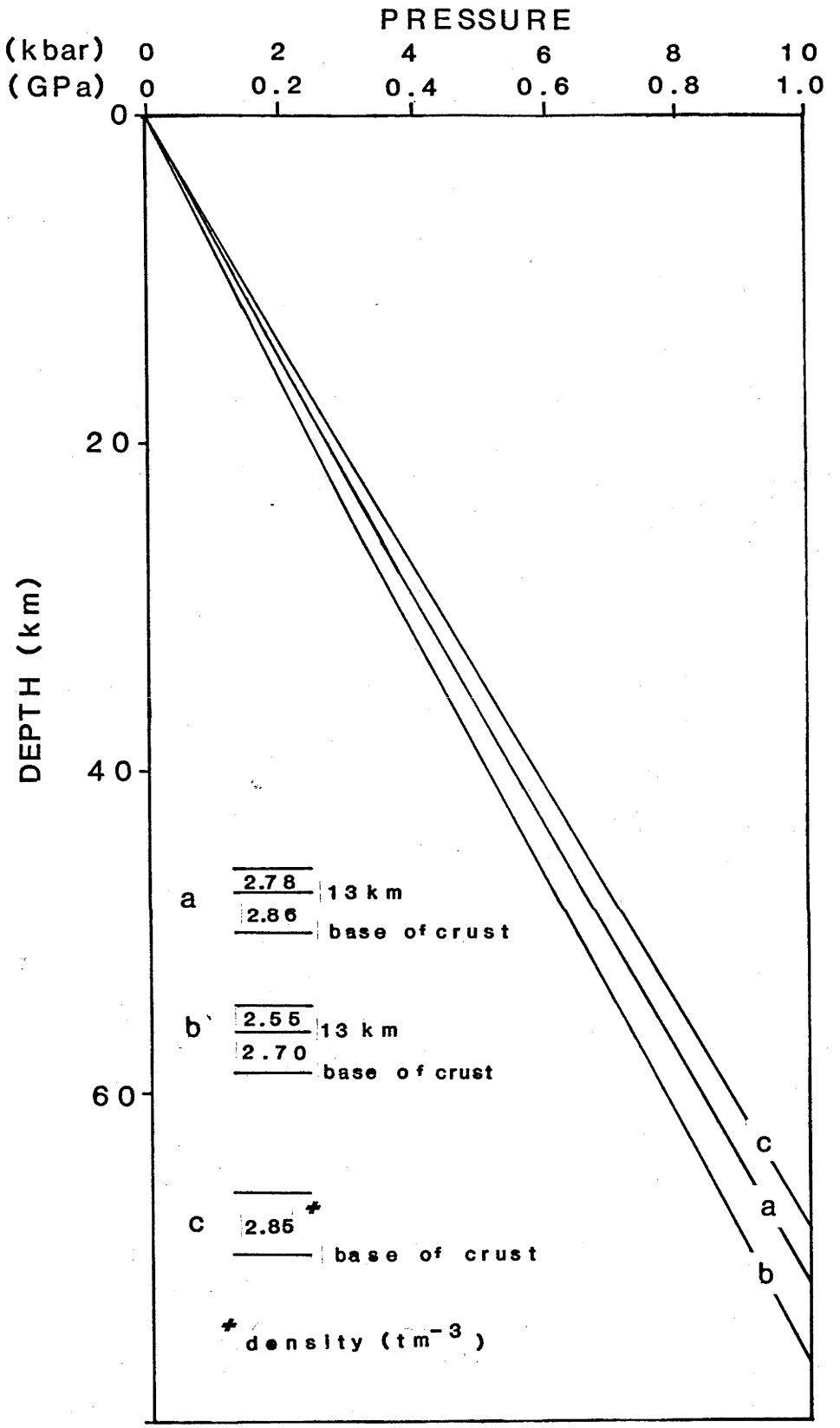

Figure 29. Pressure gradients for the three crustal models given in the lower left hand corner of the diagram. Curves a and b are for Gravity Models A & B of Drummond & Shelley (1981), respectively.

(1972) for the temperature and pressure derivatives of the compressional wave velocities seem appropriate at all pressures, temperatures, and for all chemical compositions likely within the crust, and they were adopted for the present study.

6.2 PRESSURE AND TEMPERATURE GRADIENTS

6.2.1 Pressure gradient:

Density models of the earth are usually based on seismic models, so that using them to generate pressure gradients to correct seismic models can be a circular argument. This situation is not helped by using the measured gravity as a further control. Drummond & Shelley (1981) matched the seismic model for line GBC with the measured gravity and found that several quite different density models could be proposed to fit both the seismic and gravity data. The pressure gradients due to their Gravity Models A and B are shown as lines a and b, respectively, in Figure 29. Also shown is the pressure curve for a crust of uniform density 2.85 tm^{-3} (line c).

None of the pressure gradients can be preferred. Profile b is derived from a crust of low density, and therefore probably represents a lower limit to the likely pressure gradients, while gradient c probably represents an upper limit. Curve a, which lies between them, was adopted as the pressure gradient for this study.

The three pressure gradients in Figure 29 diverge downwards from the surface, with the maximum differences at the base of the crust. If profiles b and c are the outer limits of likely pressure gradients, the maximum error likely in choosing profile a for making pressure corrections is 0.006 km s^{-1} at 1 GPa, which is negligible.

6.2.2 Temperature gradient:

Estimation of the temperature gradient in northwest Australia is difficult because of the limited number of heat flow probes in the region, and the almost complete lack of measurements of surface heat production in the near surface rocks. The heat flow data in Australia were summarised by Sass, Jaeger & Munroe (1976). Further heat flow measurements in the Pilbara region reported by Cull & Denham (1979) confirmed that heat flow in the

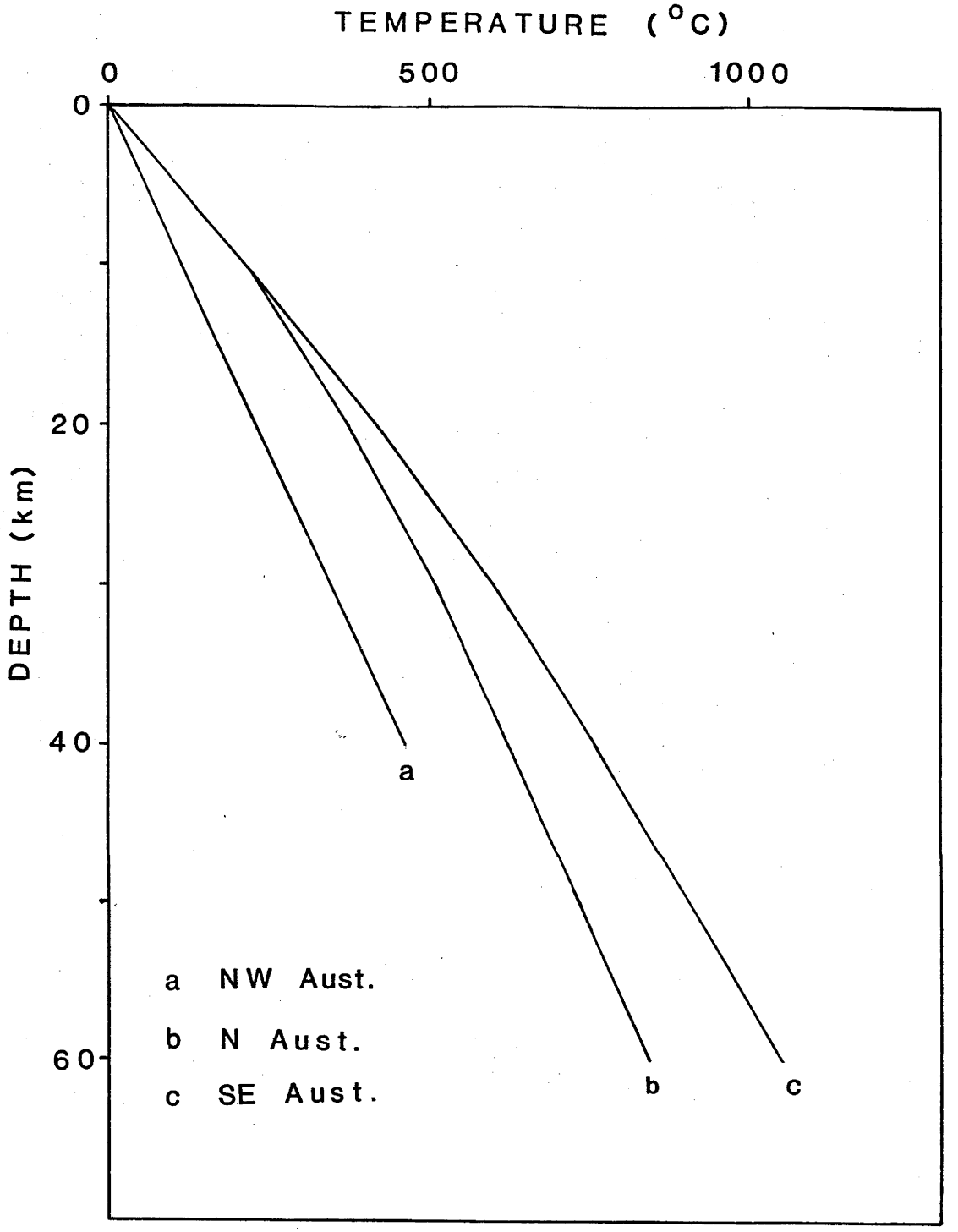

Figure 30. Adopted geothermal gradients for (a) the Pilbara Craton, (b) northern Australia, and (c) southeast Australia.

region is between 40 and 50 mW m^{-2}, or about one heat flow unit. Jaeger (1970) measured surface heat production in rocks from four drill holes in the shield to the south ranging from 0.6 to 9 μWm^{-3} (1.4 to 21.9 heat generation units), while Lambert (1971) calculated it to be 2.5 μWm^{-3}.

By assuming that the thermal conductivity of crustal rocks is 2.5 W m^{-1} K^{-1} (i.e. 6 heat conductivity units), and that the concentration of radioactive heat producing elements declines exponentially below 4.5 km depth, Sass & others (1976) produced a family of geothermal gradients for the Western Australian shield based on a range of acceptable surface heat generation values. The curve for an average surface heat production value of 4.2 μWm^{-3} (10 heat generation units) reaches a temperature of 460°C at 40 km depth. This is a slightly higher gradient than that of Jessop & Lewis (1978) which produces a temperature of 400°C at 50 km depth under the Yilgarn Craton. The differences are due to different assumed values of thermal conductivity and different distributions of heat producing elements. However, commensurate with the low heat flow for the region, the geothermal gradients of Sass & others (1976) are the lowest calculated for Australia, and are probably reasonable.

The adopted geotherm in this study is shown as curve a in Figure 30. It has a linear increase in temperature from 0°C at the surface to 460°C at 40 km depth. It therefore differs slightly from Sass & others' (1976) median curve in which the temperature gradient is slightly higher near the surface, and slightly lower at depth due to the concentration in their model of heat producing elements near the surface. The largest error in assuming this geothermal gradient will not derive from the assumption of linearity, but rather from the wrong choice of surface heat production. This could cause an error of 30°C at 40 km depth, which will cause an error of only 0.01 km s^{-1} in adjusting the velocity/depth models to 25°C.

6.3 THE EFFECT OF PRESSURE AND TEMPERATURE ON THE CRUSTAL VELOCITY/DEPTH MODELS.

With the pressure and temperature derivatives of the velocity and the pressure and temperature gradients defined, it is now possible to discuss the velocity/depth functions. In Figure 31, they are all plotted on the same axes to show, firstly, that at any depth within the crust the maximum difference in apparent velocity over the Pilbara Craton is

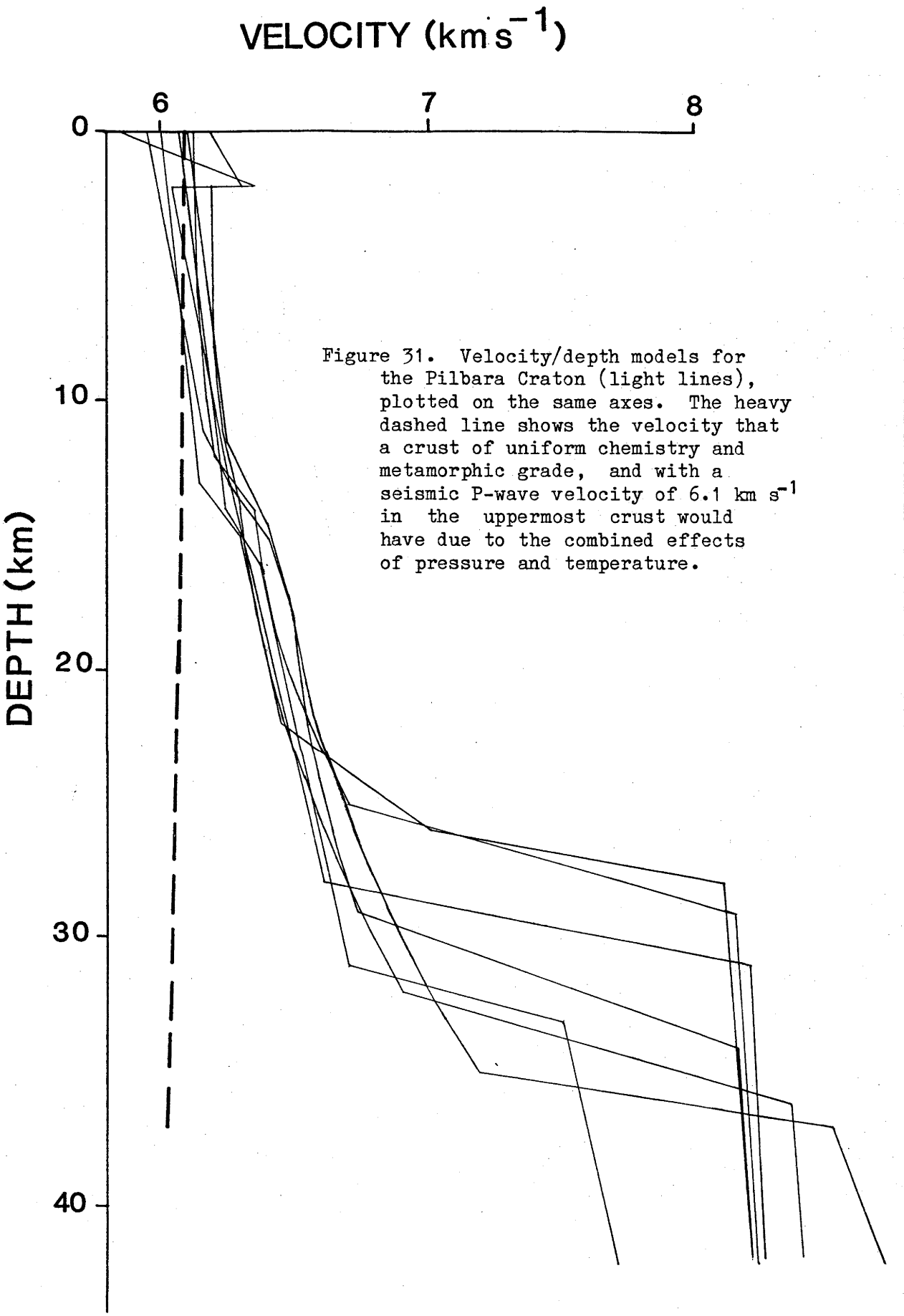

Figure 31. Velocity/depth models for the Pilbara Craton (light lines), plotted on the same axes. The heavy dashed line shows the velocity that a crust of uniform chemistry and metamorphic grade, and with a seismic P-wave velocity of 6.1 km s^{-1} in the uppermost crust would have due to the combined effects of pressure and temperature.

generally less than 0.2 km s^{-1}. The lower crust of the Pilbara Craton therefore has a very uniform velocity/depth distribution, implying a very uniform composition at depth. Secondly, the velocities in the lower crust are generally less than 6.7 to 6.8 km s^{-1}, only approaching or exceeding 7.0 km s^{-1} in the deepest part of the crust. These are apparent velocities, and the effects of dip will alter them such that the highest velocities in the deepest crust (profiles 3, 5 and 6 in Figure 28) will probably be reduced when the effects of the Moho dip are considered. The velocities of the lower crust are therefore quite low when compared with other, younger parts of the world - e.g. southeast Australia (Finlayson & others, 1980; Finlayson & McCracken, 1981), northern Australia (D.M. Finlayson, C.D.N. Collins, personal communications; see later), under the Canadian Rocky Mountains (Mereu & others, 1977) - and even when compared with other Precambrain shield areas, e.g. under the Canadian shield (Berry & Fuchs, 1973).

Positive velocity gradients are often assumed to be caused by the effects of pressure at depth, but these must first be offset by the effects of temperature. If the crust was composed entirely of rock with a seismic velocity of 6.1 km s^{-1} at the surface, its seismic velocity at 33 km depth would be 6.04 km s^{-1}. This is shown by the heavy, dashed line in Figure 31. Thus, even in the radiogenically depleted shield, the temperature gradient is sufficiently high for the negative temperature derivative to counter the velocity increase due to increasing pressure at depth. Christensen's (1979) derivatives would give a bigger decrease with depth. Matsushima's (1981) derivatives would give a slight increase with depth, but not enough to account for the observed velocity increase.

The observed increase of velocity with depth must therefore be explained in terms of changing chemical content at depth, or increasing metamorphic grade with depth. Drummond (1979, 1981) suggested that the low seismic velocities of the crust were indicative of a crust of overall acid to intermediate chemical composition undergoing metamorphism to granulite facies at about 13 km depth, although he did not rule out the possibility of chemical change with depth.

It is difficult to separate the effects of chemical change from the effects of metamorphism. It must be done on the basis of empirical relations derived from a variety of experimental data, the publication

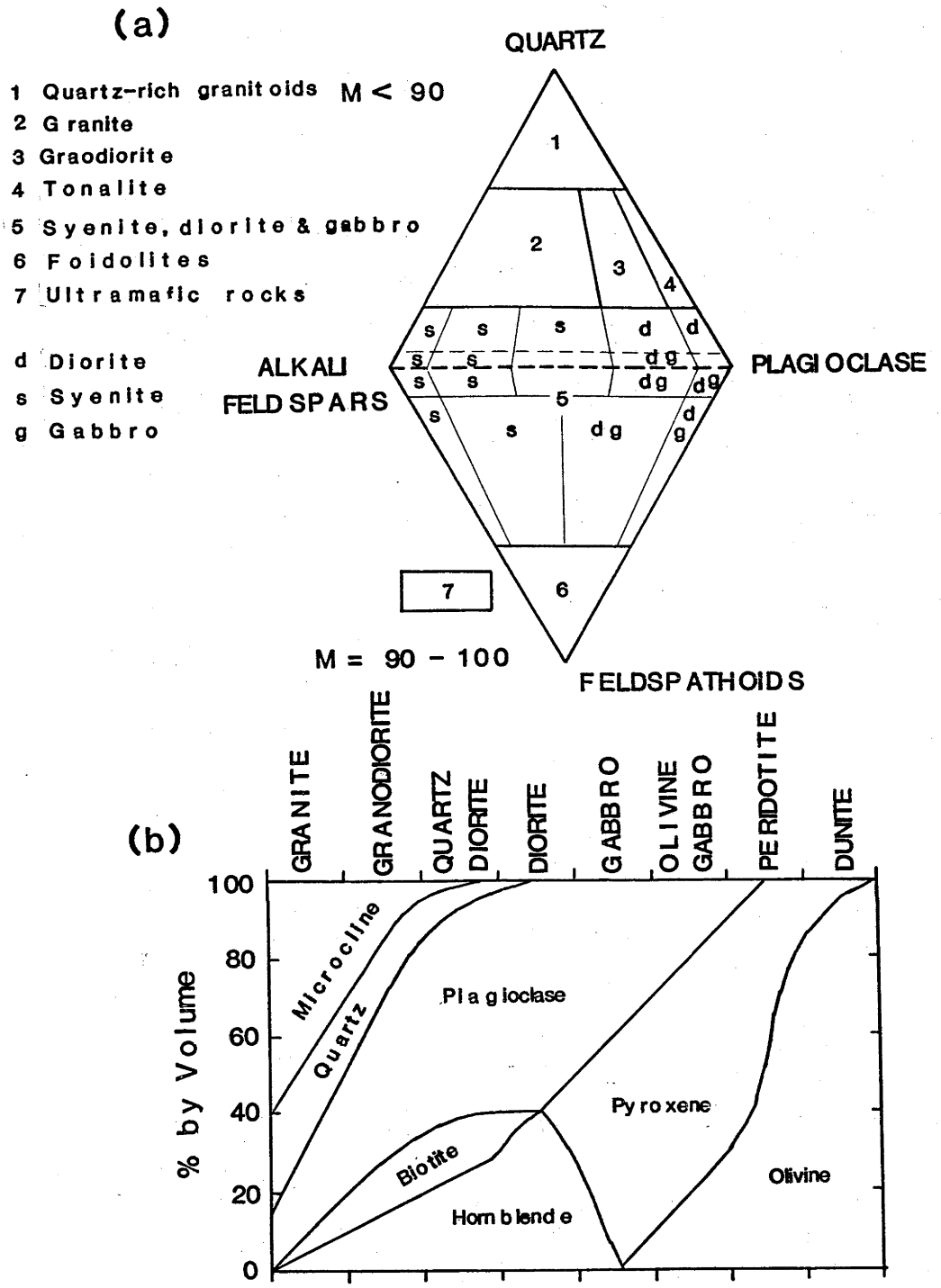

Figure 32. Classification of igneous rocks: (a) IUGS (1973) classification of plutonic rocks; (b) classification of Berry & Mason (1959), modified by Christensen (1965).

of which does not always separate the two effects. The effects of chemical and metamorphic changes was therefore pursued separately.

6.3.1 Classification of Igneous Rocks

Many classification systems have been used in the past in the naming of igneous rocks, so a note on the systems used is in order.

In 1972, the Subcommission on the Systematics of Igneous rocks of the International Union of Geological Sciences (IUGS) adopted as a standard the classification of plutonic rocks outlined in Figure 32a (IUGS, 1973). This classification is based on the relative concentrations of quartz, plagioclase, alkali feldspars and feldspathoids in rocks. While being eminently suitable for use by petrologists, the classification is of limited use to geophysicists. This is because density and seismic velocity, which are the key parameters measured in rocks by geophysicists, are linked to the mean atomic weight of the rock, and the mean atomic weight of a rock is very sensitive to the amount of iron in the rock (Birch, 1961; see Drummond & Shelley, 1981 in Appendix 4 for a brief description). Iron is mostly bound up in ferromagnesian minerals, mainly amphibolites, pyroxenes and olivine, which do not feature in the IUGS classification. As well, several fields of different rock types discussed below, most noticably those of diorite and gabbro, overlap in the IUGS classiciation.

Most of the experimental petrology and empirical velocity/density measurements discussed below were published before the acceptance of the classification in Figure 32a. Christensen's (1965) work was based on the classification shown in Figure 32b, which he modified from that of Berry & Mason (1959). This classification extends the spectrum of rock types classified to ultrabasic rocks, which are classified separately in the IUGS System, and is based on the amount of ferromagnesian minerals as well as the relative proportions of quartz, alkali feldspar, plagioclase and feldspathoids. While early experimental petrology and empirical velocity/density measurements did not specify which system of rock classification they used, it was probably similar to that in Figure 32b, because they made a clear distinction between diorite and gabbro as will become obvious in the following discussion. It must therefore be pointed out that the rock types referred to below are not necessarily those implied by the IUGS System.

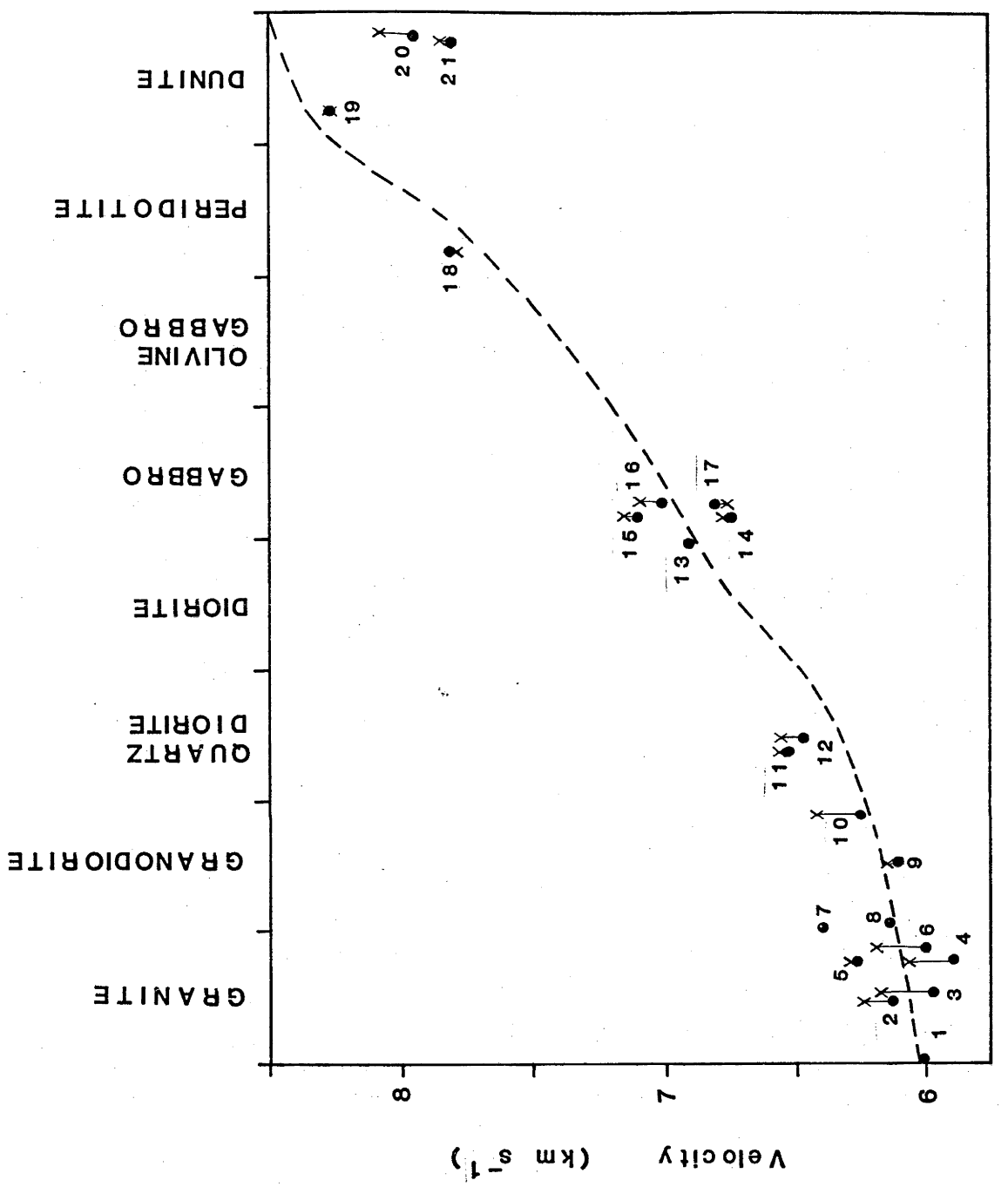

Figure 33. Compressional wave velocities versus chemical composition, after Christensen (1965, Fig. 12). The dots signify measurements in samples at 0.15 GPa and 25°C. The crosses connected by straight lines to the dots represent measurements of the same samples at 1 GPa adjusted to 415°C, the temperature at 1 GPa on the adopted geotherm for the Pilbara Craton. The sample numbers are as for Christensen (1965). The dotted line was derived theoretically by Christensen (1965) for mineral assemblages corresponding to the rock types indicated, as defined by the rock classification in Figure 32.

6.3.2 Chemical change with depth.

The change in chemical composition at depth through the crust is not well known, despite the division, early in seismological history, of the crust into a sial and sima based on the observation of higher velocities at depth in the crust. Christensen (1965, Fig. 12) showed the effect of changing chemistry on the compressional wave velocities measured in cored specimens at 0.15 GPa and 25°C. His diagram is reproduced here as Figure 33. The dashed curve shows the theoretically calculated velocities for rocks of the mineralogical compositions defined for these rock types in Figure 32b and agrees sufficiently well with the empirical velocities to be used as a means of extrapolating across areas where there are no samples.

It might be argued that, at 0.15 GPa, the cracks and pores in the rocks sampled were not completely closed, and that only at much higher pressures do the laboratory measured velocities approach those at depth in the earth. In several of the specimens used by Christensen, seismic velocities were measured at pressures up to, and at times exceeding 1 GPa. For these specimens, the velocities at 1 GPa, adjusted to a temperature of 415°C, which is the temperature at 1 GPa for the adopted geotherm for the Pilbara Craton, are plotted as crosses in Figure 33. In most cases, the crosses plot above the dots, showing that the cracks were not closed at 0.15 GPa. Pressures intermediate between .15 and 1 GPa will give rise to velocities which mostly plot between the dots and the crosses.

The measured seismic velocites in Figure 28 can now be compared with those in Figure 33.

The upper crust is composed of soda rich granites, which make up the bulk of the granitoids (Glikson, 1979), and greenstones which form only a small proportion of the volume of the upper crust. The observed upper crustal velocities are consistent with the bulk mineralogy of the upper crust being near that of granite. If the increase of velocity with depth is due purely to chemical changes, it can be accounted for by a steady increase in the ferromagnesian content across Figure 33 to quartz diorite, and perhaps diorite. If gabbro is present in the crust, it must be located only in the deepest crust.

The seismic boundary at 10 to 15 km depth could be explained by a sharper than normal increase in the mafic content of the rock, perhaps from granite or granodiorite above to quartz diorite or diorite below.

The above discussion assumes that the metamorphic grade does not change with depth, which of course it must. The results of Birch (1960, 1961) and Manghnani & others (1974) showed that the metamorphic grade of a rock affects its seismic velocity, so that increasing the mafic content does not by itself cause an increase in seismic velocity; rather, it can result in a decrease in the seismic velocity.

6.3.3 Metamorphic change with depth.

Blockley (1975) noted that surface rocks in the Pilbara Block had "low to medium grade" metamorphism, which is only a very general statement and of little use in defining the metamorphic character of the rocks. In the Hamersley Basin, the metamorphic grade is generally sub-greenschist facies, only reaching greenschist facies in those rocks which have previously been buried at great depths (Horwitz & Smith, 1978). The metamorphic grade present at depth today under the southern Pilbara Craton must therefore be of a higher grade than greenschist facies.

Amphibolites can have velocities which approach those typical of the lower crust (Tarney & Windley, 1977; Christensen & Fountain, 1975; Mueller, 1977), and are likely components of the mid- to lower-crust of southeast Australia (Ferguson & others, 1979). However, amphibolites are stable only in hydrous conditions at high temperatures and pressures, and Precambrian shields are generally thought to be anhydrous. Under these conditions, amphibolites convert to the granulite facies (Ringwood, 1975).

Numerous workers have suggested that granulites exposed at the surface of several Precambrian shields were originally derived from deep in the crust, and are therefore representative of the lower crust of shields (eg. Lambert, 1971; Glikson & Lambert, 1976; Tarney & Windley, 1979). Other evidence that granulites form the lower crust comes in the form of granulite nodules in kimberlite magmas which sampled the lower crust (Dawson, 1977), and in the concurrence of observed seismic velocities with those measured in the laboratory in samples of granulite under pressure (Christensen & Fountain, 1975).

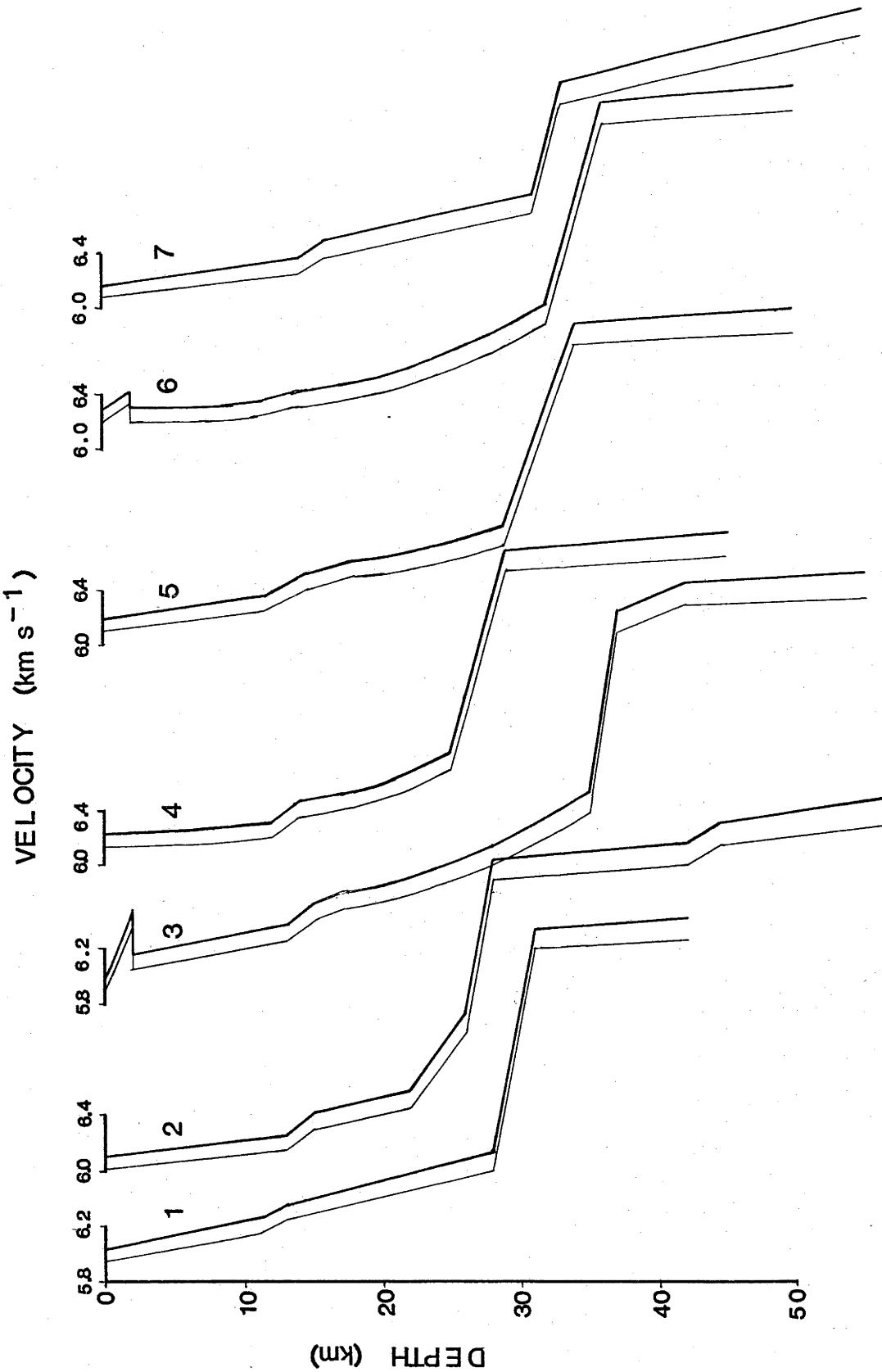

Figure 34. Velocity/depth models for the Pilbara Craton. Light lines are the measured profiles; heavy lines show the velocities adjusted to 1 GPa and 25°C. Profile numbers are as for Figure 28.

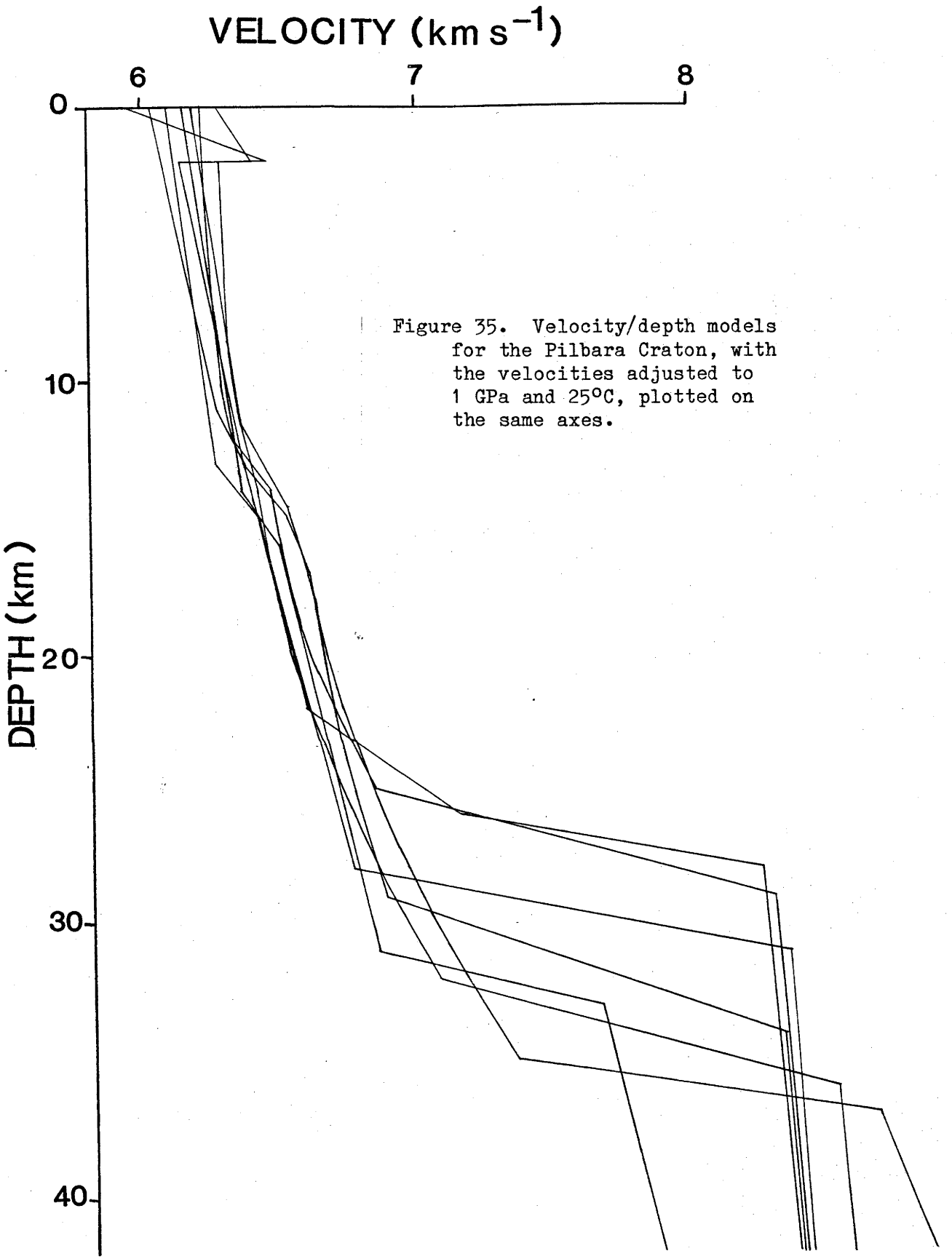

Figure 35. Velocity/depth models for the Pilbara Craton, with the velocities adjusted to 1 GPa and 25°C, plotted on the same axes.

The results of measurements of seismic velocities in samples of granulites and eclogites at the pressures likely in the lower crust are useful for estimating the metamorphic grades and compositions likely in the lower crust. The most notable of such experiments were those of Birch (1960); Manghnani & others (1974) summarise Birch's results and include them with their own results in their Figure 6, which presents the velocities and densities of granulites and eclogites, as functions of composition, at 1GPa and 25°C. In Figure 34, the observed velocity/depth models of Figure 28 are shown as thin lines; the thicker lines offset to the right are the velocity/depth models adjusted to 1 GPa pressure and 25°C, and are the velocity/depth models to be used for comparison with the results on Manghnani & others (1974). They are shown plotted on the same axes, in the fashion of Figure 31, in Figure 35. The velocities in Figure 35 are slightly higher throughout the crust than those in Figure 31.

Figure 36 summarises Figure 6 of Manghnani & others (1974). The empirical velocity/density curves for mean atomic weights of 21 and 22 are shown.

The balloons which define the eclogite, granulite and basalt fields in Figure 36 are based on the plotted points in Figure 6 of Manghnani & others (1974). For larger populations, the granulite and eclogite balloons would probably overlap. The values plotted as dots within and loosely defining the granite balloon are the values for samples clearly identified as granites by Birch (1960). Both the seismic velocities and the densities of the granites were corrected to 1 GPa by correcting for the effects of sample shortening under pressure using the estimated 0.6% shortening quoted for granites by Birch (1960, p.1092).

The broad arrows in the lower right hand corner show the direction of increasing metamorphic grade, parallel to the velocity/density curves, and increasing mafic (iron) content at right angles to them and in the direction of increasing mean atomic weight. Also shown are six arrows which indicate the directions of change that might be expected through the crust based on either the observed change in seismic velocity or the expected increase in density through the crust. The nature of a crust of random upper crustal composition, and changing at depth in the direction indicated by each of the six small arrows will now be considered:

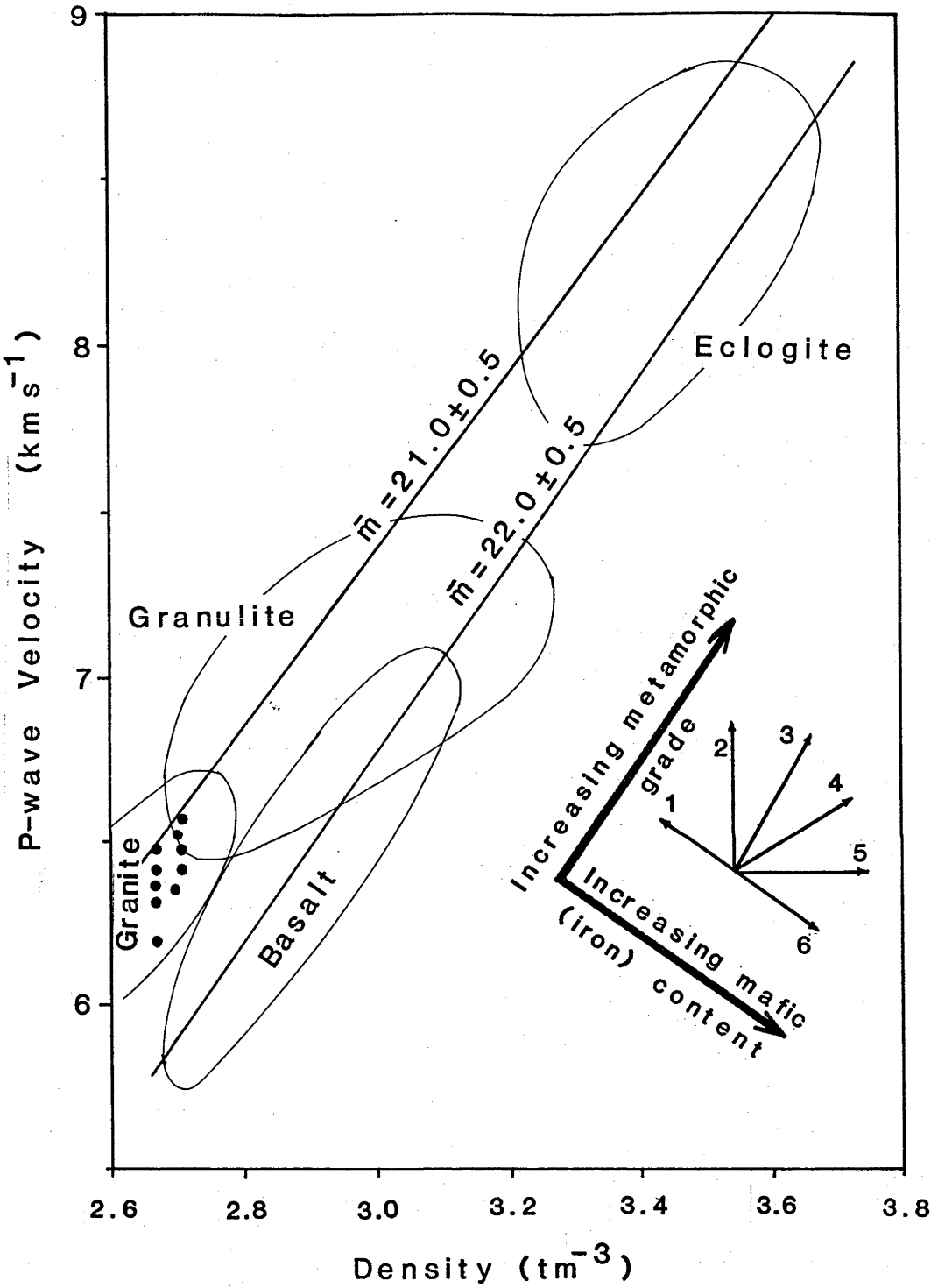

Figure 36. Velocity/density relations for mean atomic weights of 21 and 22 at 25°C and 1 GPa, after Manghnani & others (1974), Fig. 6. The balloons marked 'basalt', 'granulite' and 'eclogite' show the appromixmate positions of the populations of these rocks in Figure 6 of Manghnani & others (1974). The dots defining the granite balloon are from Birch (1960), with density corrections applied for sample shortening due to pressure. The large arrows indicate the directions of increasing isochemical metamorphic grade and increasing mafic (iron) content at constant metamorphic grade. The small arrows numbered 1 to 6 are discussed in the text.

Arrow 1: this model would have higher seismic velocities at depth, but also lower densities, causing a density inversion with the density at the base of the crust less than that near the surface. This is not only intuitively unlikely (eg. Tarney & Windley, 1977), but is also likely to be tectonically unstable over long periods of geological time because it is a high stress state. However, although unlikely throughout the entire crust, a profile represented by arrow 1 may be acceptable for the upper few kilometres of the crust, because the decreasing greenstone to granite ratio with depth near the surface (Glikson & Lambert, 1976) may cause a slight density inversion for which there is no corresponding seismic low velocity zone.

Arrow 2: Such a crust would have a constant density gradient, which would be gravitationally stable, and increasing velocity with depth. As with arrow 1, it indicates decreasing mean atomic weight with depth, and may therefore also represent a possible upper crustal model.

Arrow 3: This would be a crust of uniform chemistry, but the seismic velocity would inrease with depth because of the increasing metamorphic grade. Thus, if the metamorphic conditions are favourable, the velocity could reach 7.0 km s^{-1} within the granulite facies of a rock with the chemistry of granite. The density would also increase with depth giving a gravitationally stable crust.

Arrow 4: The velocity in the crust indicated by arrow 4 would increase with depth due to both increasing mafic material (increasing mean atomic weight), and increasing metamorphic grade. As with arrow 3, the density also increases with depth. However, despite the increasing mafic content, the metamorphic grade would have to reach granulite facies before velocities of about 7.0 km s^{-1} were reached.

Arrow 5: The crust indicated by arrow 5 is unacceptable because the velocity does not increase with depth, even though the density does.

TABLE 11: Compressional wave velocities at 1 GPa and 25°C in common rock types metamorphosed to granulite and eclogite facies, based on the results of experimental petrology.

Rock Type	Velocity ($km\ s^{-1}$) as Felsic Granulite	Eclogite	Reference
Anhydrous Granite	6.51	6.61	1
Diorite	6.6	7.2	2
Gabbroic Anorthosite	6.8	7.4	2
Gabbro	6.9	8.3	3
Quartz Tholeiite	~7.0	~8.0	4

References:
1 Green & Lambert, 1965
2 Green, 1970
3 Ringwood & Green, 1966
4 Ringwood & Green, 1964

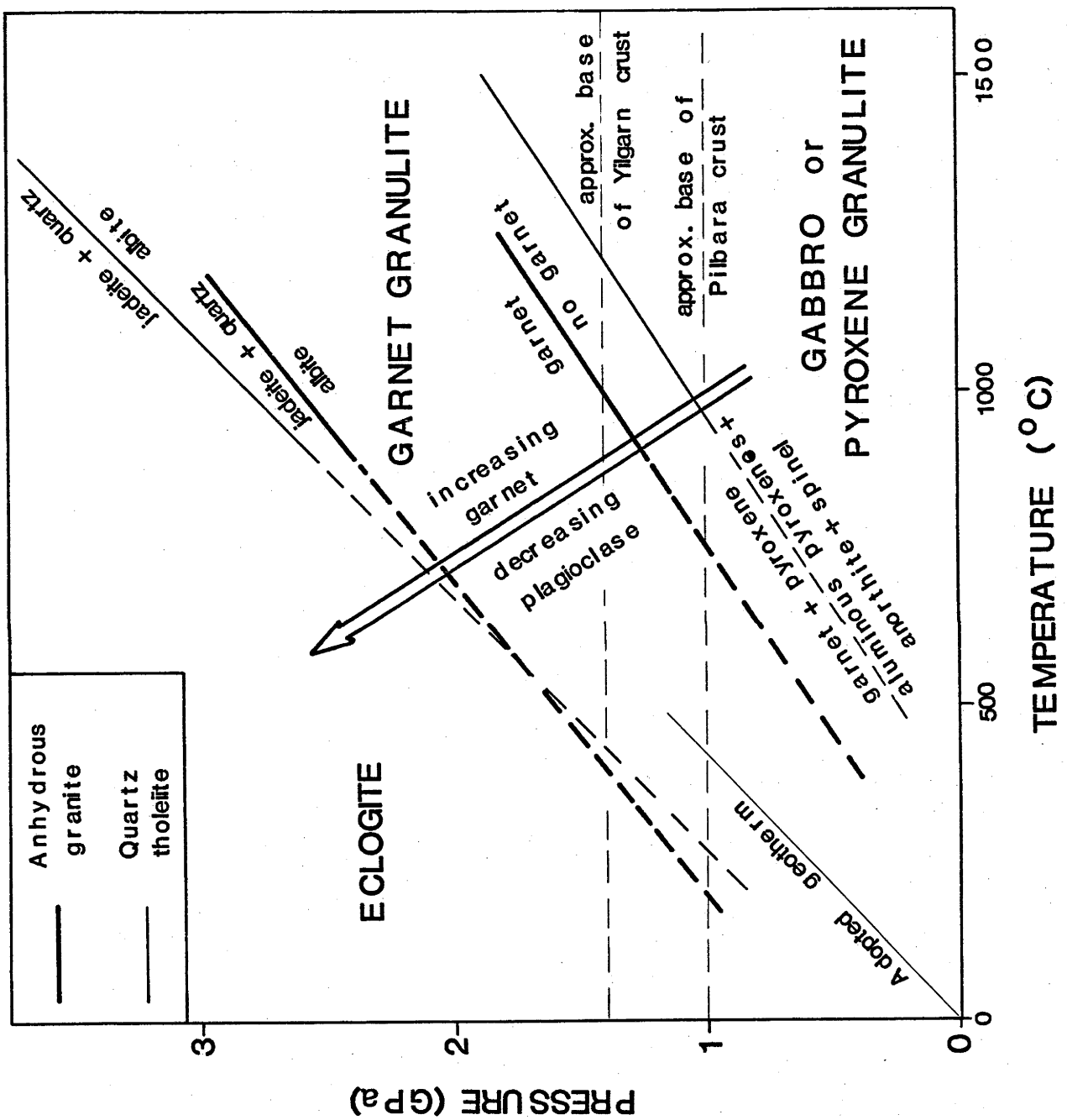

Figure 37. Experimentally determined stability fields of granulite and eclogite The heavy phase boundaries are for anhydrous granite (Green & Lambert, 1965), and the light phase boundaries are for quartz tholeiite (Ringwood, 1975). Solid lines indicate the pressures and temperatures of the experiments; broken lines mark the extrapolations by the original workers to lower temperatures and pressures. The lower boundaries mark the incoming of garnet and the upper line the disappearance of plagioclase. The large arrow shows the direction of increasing garnet and decreasing plagioclase. The adopted geotherm for the Pilbara Craton is shown in the lower left hand corner.

Arrow 6: Arrow 6 indicates the situation, alluded to above, where, although the mafic content increases with depth, the velocity decreases. Thus, if the mafic content increases with depth through the crust, and the seismic velocity also increases, higher metamorphic grades are implied.

If the increasing seismic velocity at depth is to be explained in terms of increasing mafic content and/or increasing metamorphic grade with depth, the crustal chemical and metamorphic profile at depth must lie somewhere between the conditions indicated by arrows 3 and 5. So far, the treatment has been qualitative only; for example, while it shows that increasing metamorphic grade can account for the increasing seismic velocities at depth, it does not indicate whether such metamorphic changes are likely in the lower crust. The results of experimental petrology must be employed to do this.

6.4 THE COMPOSITION OF THE CRUST OF THE PILBARA CRATON

A lot of experimental information is available on the phase transformations at high pressures and temperatures in rocks of basic composition, but very little has been done on rocks of acid or intermediate composition (Ringwood, 1975). The results available to date are summarised in Table 11, where the seismic velocities at 25°C and 1 GPa are given for metamorphosed rocks of various compositions. These velocities can be compared directly with the velocity/depth profiles of Figure 35 which are also at 25°C and 1 GPa.

Green & Lambert (1965) studied the phase changes likely in an anhydrous granite at temperatures of 950 and 1100°C and pressures up to 4 GPa. The stability fields are drawn as heavy unbroken lines in Figure 37; also included, as fine, unbroken lines are the stability fields for quartz tholeiite (Ringwood, 1975). The broad arrow shows the direction of increasing garnet, which first forms at the lower phase boundary, and decreasing plagioclase, which disappears at the upper phase boundary. Garnet appears at higher pressures (or lower temperatures) for acidic rocks than for the basaltic rocks, but disappears at about the same conditions. Consequently, the pressure and temperature stability field boundaries are slightly different for rocks of different compositions.

The adopted geotherm is also shown in Figure 37, as are the approximate pressures expected at the base of the crust in both the Pilbara and Yilgarn Cratons. To study the effects of phase changes on rocks in the crust, it is necessary to extrapolate the data from the high pressure and temperature experiments to lower pressures and temperatures, a procedure admitted by Green & Lambert (1965) to be dubious. They nevertheless did project their curves to lower pressures and temperatures; their projections are shown as broken lines in Figure 37, as are those of Ringwood (1975).

(Note: Herzberg, 1978, in his study of the stability fields of pyroxene, found that the phase boundaries of the gabbro/eclogite transition may be curved and called for a reinvestigation of the transition. Yoder & Tilley, 1962, suggested that, at low temperatures and pressures, the phase boundaries were not as steep as shown in Figure 37).

The geotherm does not intersect either of the projected stability field boundaries; rather, it is sub-parallel to both of them. However, even if the projections of the stability field boundaries to low pressures and temperatures are only broadly correct, the lower part of the crust clearly must lie within the stability field of granulites, and probably in a region of garnet stability (Green & Lambert, 1965).

The upper crust is probably of granitic composition, as shown above. Green & Lambert (1965) estimated that rocks of granitic composition would have velocities (calculated for 1 GPa pressure) of about 6.5 km s^{-1} in the granulite facies before garnet started to form. Velocities such as this are not observed until below the mid-crustal seismic boundary (Figure 35).

Drummond's (1979, 1981) interpretation of the mid-crustal seismic boundary as a metamorphic boundary caused by the metamorphism of an acidic to intermediate crust to granulte therefore seems reasonable. The transitional nature of the seismic boundary is in keeping with this finding, especially if the phase boundary is transitional and the geotherm, being sub-parallel to it, cuts it obliquely. The upper crust would therefore seem to be of overall granitic composition.

Between the mid-crustal boundary and the crust/mantle boundary, the seismic velocity generally increases by about 0.4 km s^{-1}. Green & Lambert (1965) estimated that the incoming of garnet at higher pressures would push the seismic velocity for a granitic rock to 6.6 km s^{-1} (for 1 GPa pressure). In Figure 35, the lower crustal velocities are commonly 6.7 to 6.9 km s^{-1}, so that the velocities expected of a granulite of granitic composition would not be high enough to account for the observed seismic velocities,. Thus an increase in the mafic content with depth in the lower crust is implied. This will increase the amount of garnet available (Green, 1970), thereby increasing the seismic velocity.

Ringwood & Green (1966) suggest that gabbro (or basalt) will be stable as eclogite in the lower crust under anhydrous conditions, and will therefore have a seismic P-wave velocity of about 8.3 km s^{-1}. Quartz tholeiite before the incoming of garnet would have a seismic velocity of 7.0 km s^{-1}. The steady increase in garnet through the garnet stability field would increase the velocity to 8 km s^{-1} (Ringwood & Green, 1964). Green (1970) studied diorite and gabbroic anorthosites under lower crustal conditions and calculated that their stable mineralogical assemblages would give rise to velocities of 6.6 to 7.2 and 6.8 to 7.4 km s^{-1} respectively (Table 11).

From the limited results available from experimental petrology, basic rocks appear to have velocities in the lower crust which are too high. The velocities of acidic rocks are too low, so that an intermediate composition in the lower crust is implied. Green's (1970) studies suggest that the most mafic composition likely at the base of the Pilbara crust is that of diorite.

6.5 COMPOSITION OF THE CRUST OF THE YILGARN CRATON

The limited seismic data available for the northern Yilgarn Craton cannot define a detailed velocity/depth function. However, as the seismic velocities in the top 32 km appear to be broadly comparable with those in the Pilbara Craton, the same interpretation of rock types probably applies in the Yilgarn Craton. That is, the uppermost crust is of granitic composition, and is metamorphosed to felsic granulite facies at about 15 km depth. At greater depths, the crust may become more mafic.

Drummond (1979) suggested that the seismic boundary at about

32 km depth, where the seismic velocity increases to about 7 km s^{-1}, was the eclogite facies equivalent of the rocks of higher crustal levels. Petrologists usually expect eclogites to be of basic or ultrabasic composition, so Drummond (1981) called the facies garnet granulite, implying that the plagioclase was replaced by garnet to give the higher velocities. The replacement of feldspar by garnet is not sharp, (Ringwood, 1975), so that if the seismic boundary is caused by the presence of eclogite facies at 32 km depth, it must be transitional, and velocity gradients are to be expected within the layers.

The seismic velocities indicated for the lower crust for diorite and anorthositic gabbro are sufficiently high to account for the observed seismic velocities. Thus the lower crust of the Yilgarn Craton need not be much more mafic than that of the Pilbara Craton.

Drummond & Shelley (1981) suggested in their Gravity Model B that the crust of Yilgarn Craton could be more mafic than that of the Pilbara Craton. However, they preferred a density model in which, if the Yilgarn Craton was more mafic, the increased mafic content was restricted to the lower crust. A composition of gabbroic anorthosite would seem to be the most mafic composition possible on the grounds of the experimental petrology results discussed above.

6.6 THE NATURE OF THE CRUST/MANTLE BOUNDARY

The foregoing discussion on the composition of the lower crust of the Piblara Craton, taken with the shape of and velocity contrast across the crust/mantle boundary in the velocity/depth functions in Figure 28 makes it possible to comment on the probable nature of the crust/mantle boundary below the Pilbara Craton.

Two hypotheses have been proposed to explain the nature of the crust/mantle boundary: it is either a chemical change, or a phase boundary from, say, basalt above to eclogite below.

Lovering (1958) and Kennedy (1959) forwarded reasonable arguments that the Moho seismic discontinuity was caused by the metamorphic phase transition from basalt to eclogite. Notwithstanding the fact that this hypothesis is inadequate for all areas of the earth (Wyllie, 1971), it fails to explain the crust/mantle boundary under the Pilbara Craton in two ways.

The width and shape of the Moho provide the first line of evidence which can be used to study the nature of the crust/mantle boundary. The average thickness of the crust/mantle boundary in the models in Figure 28 is 3 km. It is no more than 5 km wide on any of the profiles.

Several workers have studied and commented on the shape of the velocity change expected to accompany the density profile across the garnet granulite stability field. Although the likely shape of the density profile remains uncertain, the invoking of the phase change as the cause of the crust/mantle boundary can be invalidated in all cases.

Yoder & Tilley (1962) recognised that the incoming of garnet would make a large contribution to the velocity increase due to the phase change, but they were of the "opinion ... that, although the transformation may extend over a broad pressure range, the effective change in velocity may be realised over a smaller pressure range " , and that the phase change to eclogite could be responsible for a crust/mantle boundary with a thickness of only a few kilometers.

However, they had no measurements of the width of the effective velocity change. Ringwood (1975) argued that the velocity change accompanying the phase change from gabbro (basalt) to eclogite is gradual, and occurs over the entire width of the garnet granulite field.

In Figure 37, the phase boundaries between the fields of gabbro (or pyroxene granulite) and garnet granulite, and between garnet granulite and eclogite converge when projected to lower pressures and temperatures. Ringwood & Green (1966) proposed, arbitrarily, a convergence that was proportional to the absolute temperature; this is somewhat less than that determined by their high pressure and temperature experiments. On the basis of their chosen phase boundary gradients, the phase change is broader at lower crustal and upper mantle conditons than it would be if they had used the experimentally determined gradients. However, they strenuously defended their choice of gradients by a number of arguments, to which they still adhere

(Ringwood, 1975; see also Wyllie, 1971). On the basis of their chosen phase boundary gradients and assuming that the velocity change occurs across the entire garnet granule field, the crust/mantle boundary observed in the Pilbara Craton is too thin to be a phase change.

Ito & Kennedy (1970), at variance with Ringwood & Green (1966), suggested that the incoming of garnet, which controls the density of the rock, and therefore its seismic velocity, is not gradual. They proposed two density jumps, one when garnet first appears, and the other when plagioclase finally disappears (see Wyllie, 1971 & Ringwood, 1975 for arguments for and against this proposal). The crust/mantle boundary, as modelled in the Pilbara Craton, generally has a steady increase of velocity from about 6.7 - 6.9 $km.s^{-1}$ to over 8.0 $km\ s^{-1}$; it has no recognisable steps. Therefore, on the basis of the shape of the crust/mantle boundary, as suggested by Ito & Kennedy's studies, it cannot be a phase boundary.

The second line of evidence that can be used to study the nature of the crust/mantle boundary in the Pilbara Craton is the velocity contrast across it, based on the conclusion reached above that the lower crust is less mafic than basalt, and is probably dioritic. Green (1970) calculated that a dioritic rock at $900^{o}C$ and 1.8 GPa would have a density of 2.88 $t\ m^{-3}$. These conditions are close to the phase boundary at which plagioclase finally disappears, that is, close to the eclogite facies boundary Therefore, if the phase boundaries are transitional, it is just below the density of a dioritic rock in the eclogite facies. Extrapolating to lower pressures, Green (1970) calculated that this density represents a velocity of 7.0 $km\ s^{-1}$ at 1 GPa, and this is therefore near, albeit just below, the velocity expected from a dioritic rock in the eclogite facies. The observed isotropic velocity below the Moho is 7.99 $km\ s^{-1}$ (Chapter 7) which is much higher. The upper mantle must therefore be more mafic than the lower crust to explain the velocity contrast.

Consequently, on the basis of the velocity contrast across the Moho, and its shape and thickness, the crust/mantle boundary under the Pilbara Craton must be a chemical boundary.

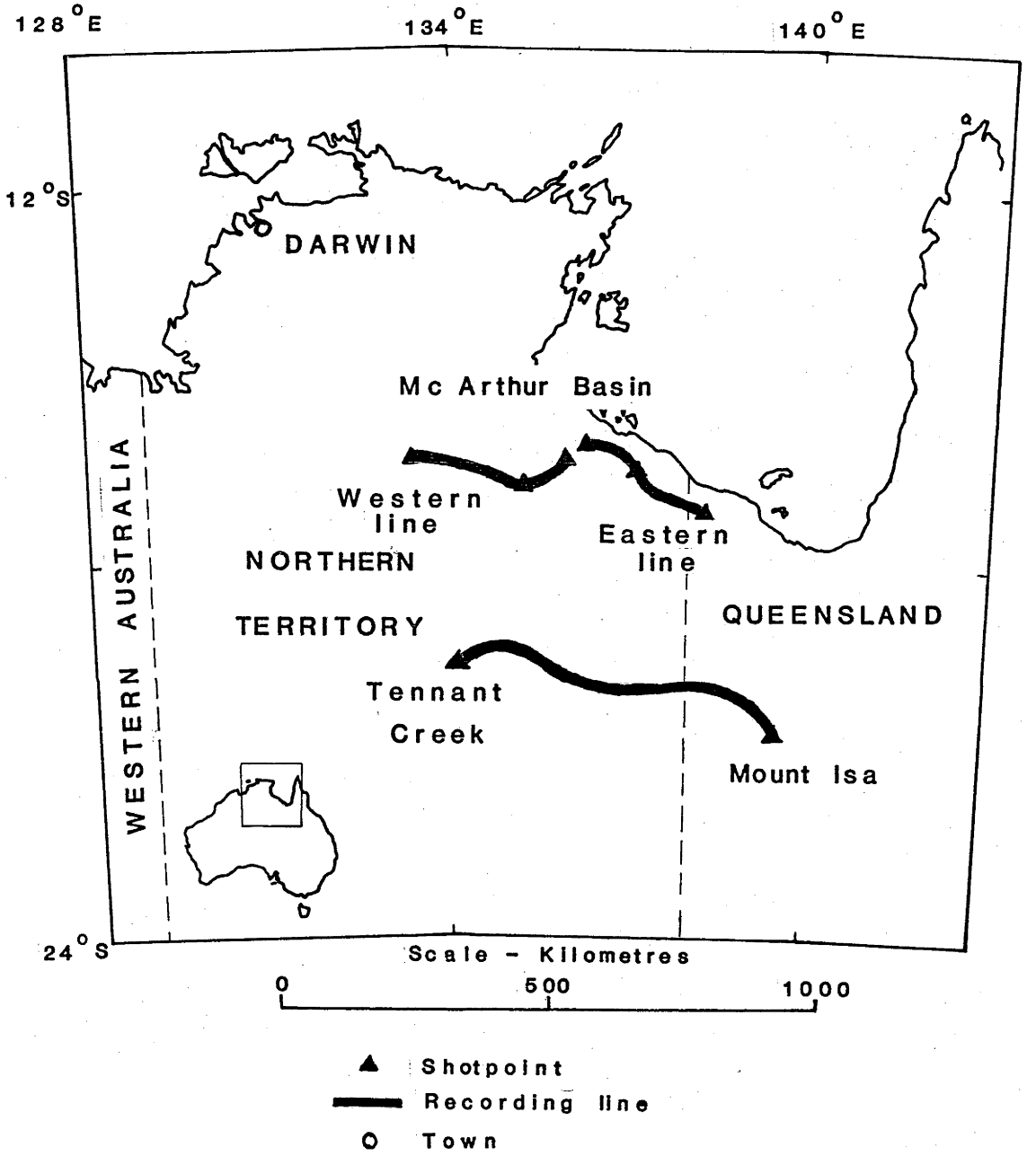

Figure 38. Distribution of seismic refraction lines in northern Australia.

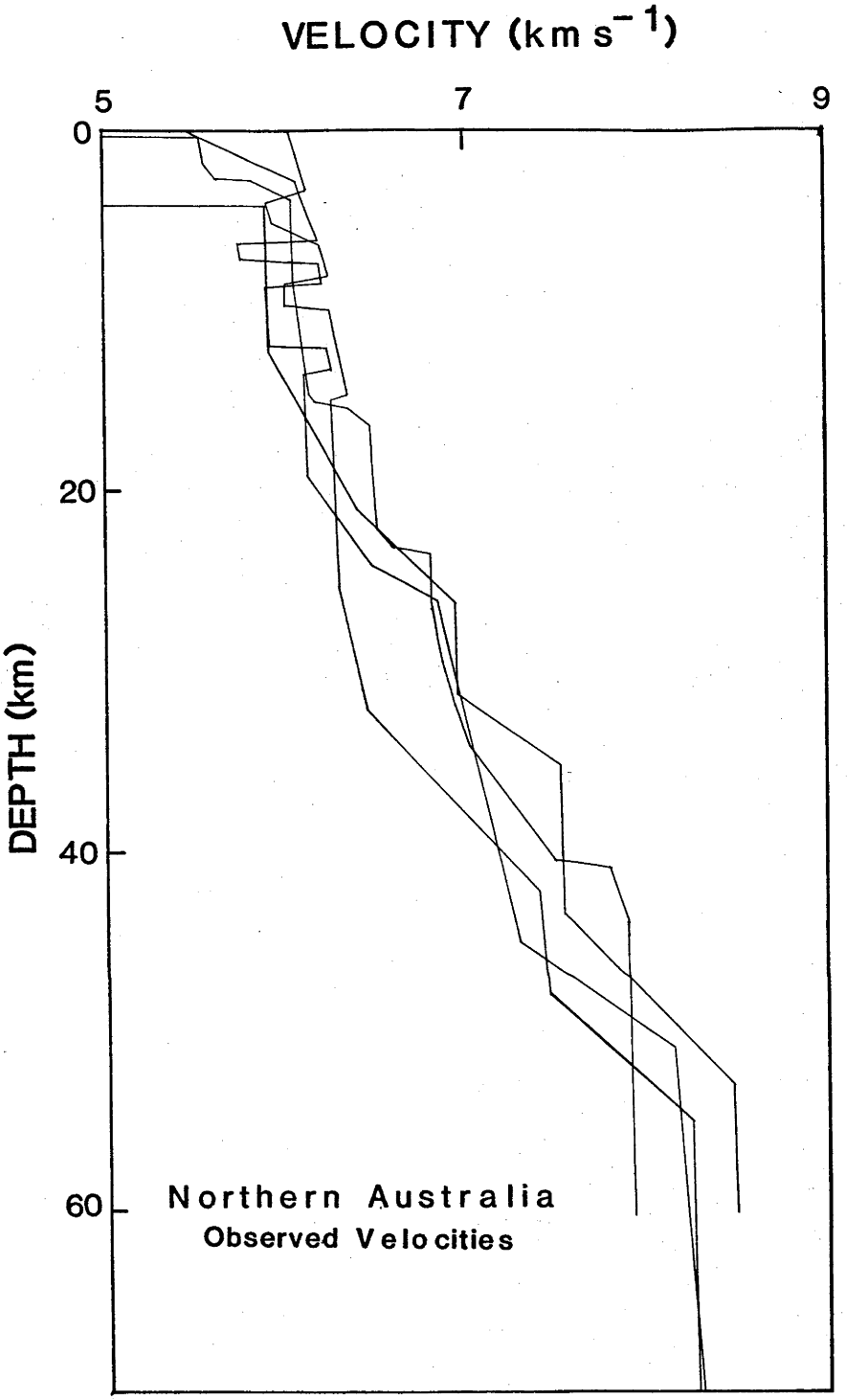

Figure 39. Observed velocity/depth models for northern Australia. The sedimentary section on two of the models was excluded.

6.7 COMPARISON WITH YOUNGER REGIONS OF AUSTRALIA

The foregoing discussion of the composition of the crust within the Pilbara Craton was possible because the similarity of the velocity/depth functions derived for all parts of the craton implied that the crust had a uniform composition at any depth. If there had been only one refraction profile within the Pilbara Craton, the arguments about the chemical composition would have been weakened by the doubt that the effects of lateral structure were influencing the adopted velocity/depth distribution. Within Australia, seismic refraction coverage of equivalent or better quality and areal extent is available in two other regions. They are in the north, where mid- to late-Proterozoic cover rocks overlie the Archaean and early Proterozoic basement in the North Australian Orogenic Province (Plumb,1979), and in the Palaeozoic Lachlan Fold Belt of the Tasman Geosyncline in southeast Australia. The purpose of this section is to compare the velocity/depth profiles of the Pilbara Craton with those from the younger regions, and to comment on the apparent differences they imply about the chemistry and evolution of the lower crust.

Figure 38 shows the location of seismic refraction profiles in northern Australia. The velocity/depth models derived by synthetic seismogram modelling of the data from these lines are shown in Figure 39, and were kindly made available before publication by D.M. Finlayson and C.D.N. Collins, both of BMR (personal communications, 1982).

The velocity/depth models form a tightly knit family of curves; the general similarities of the curves outweigh their specific differences. The velocity increases steadily through the crust, which is about 50 km thick. While the upper crustal velocities are approximately the same as those in the upper crust of the Pilbara Craton, those in the lower crust are much higher than those in the lower crust of the Pilbara craton.

Heat flow in the region is higher than that in the Pilbara region (Cull & Denham, 1979). This may be due in part to higher concentrations of redioactive elements in the upper crust, but Sass & others (1976) predicted a family of geothermal gradients for northern Australia which are higher than those of the western shield. Their median gradient is shown as curve b in Figure 30 and was adopted for the region. Commensurate with the higher seismic velocities compared to those of the Pilbara Craton, a higher crustal density and therefore higher pressure gradient (curve c, Figure 29) was assumed for northern Australia.

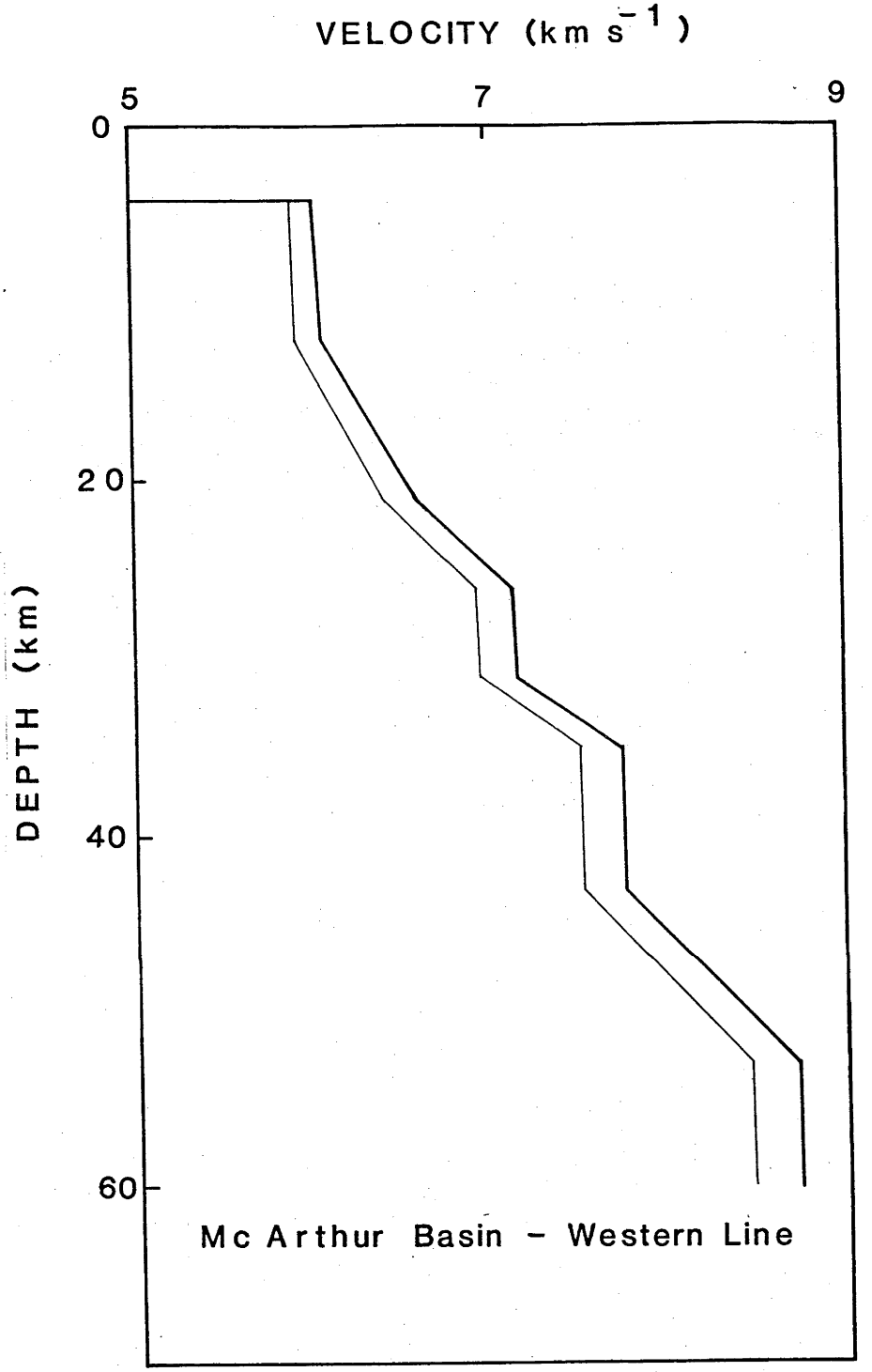

Figure 40. Velocity/depth model for the western line in the Mc Arthur Basin. The light line is the observed model; the heavy line is the model with the velocities adjusted to 25°C and 1 GPa.

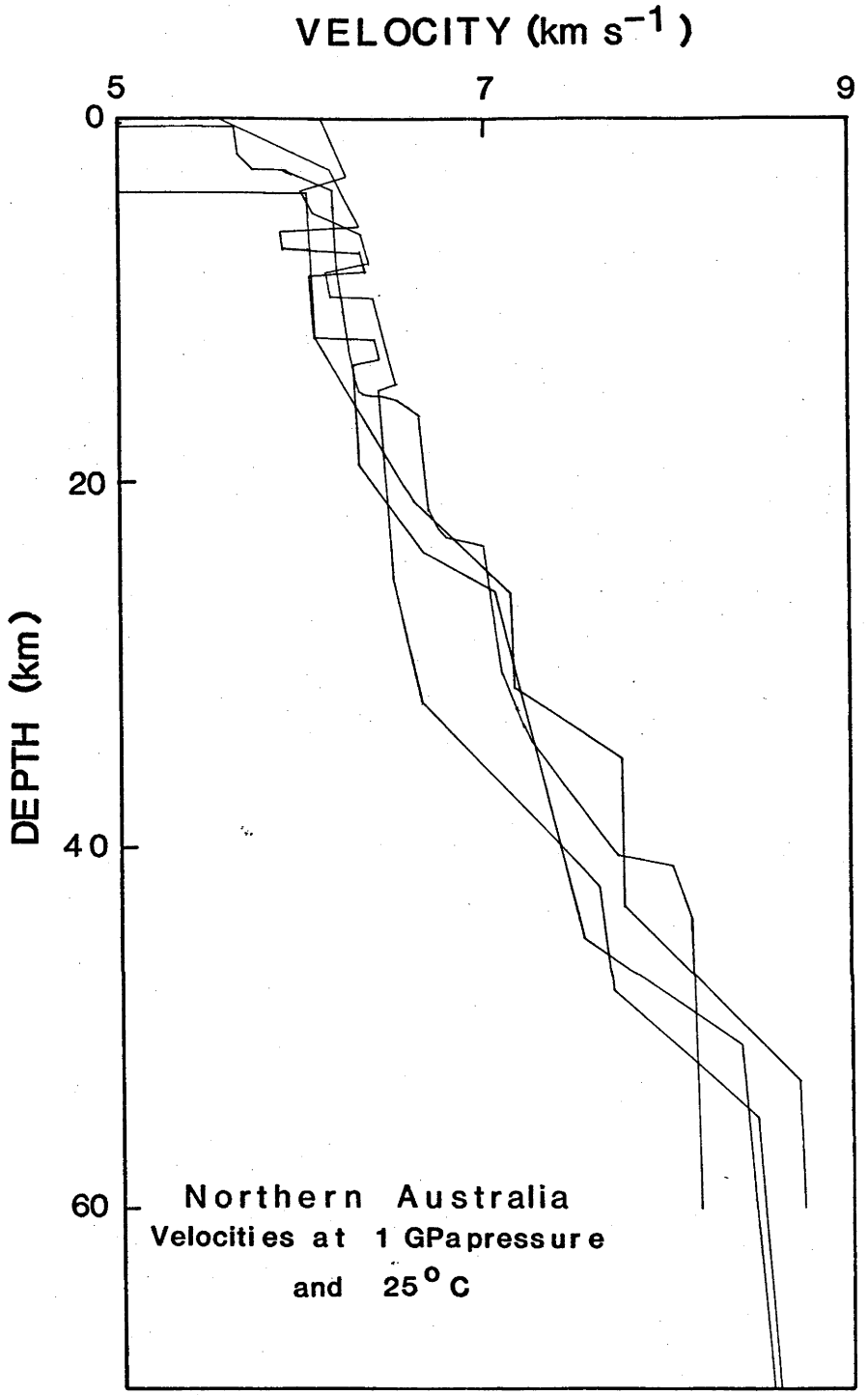

Figure 41. Velocity/depth models for northern Australia, with the velocities adjusted to 25°C and 1 GPa.

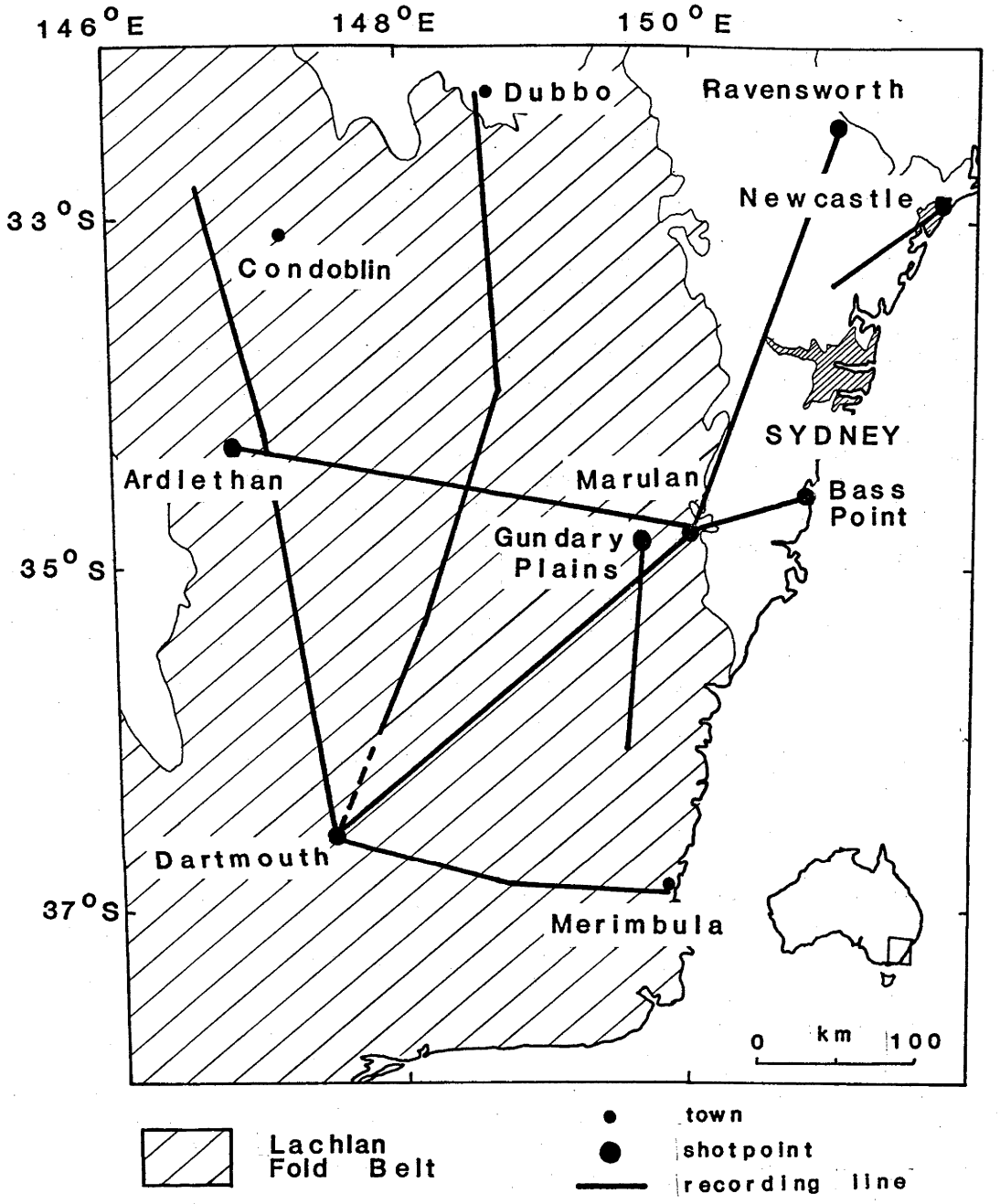

Figure 42. Distribution of seismic refraction lines in southeast Australia. Only models from the lines which fall within the Lachlan Fold Belt (shaded area) were considered.

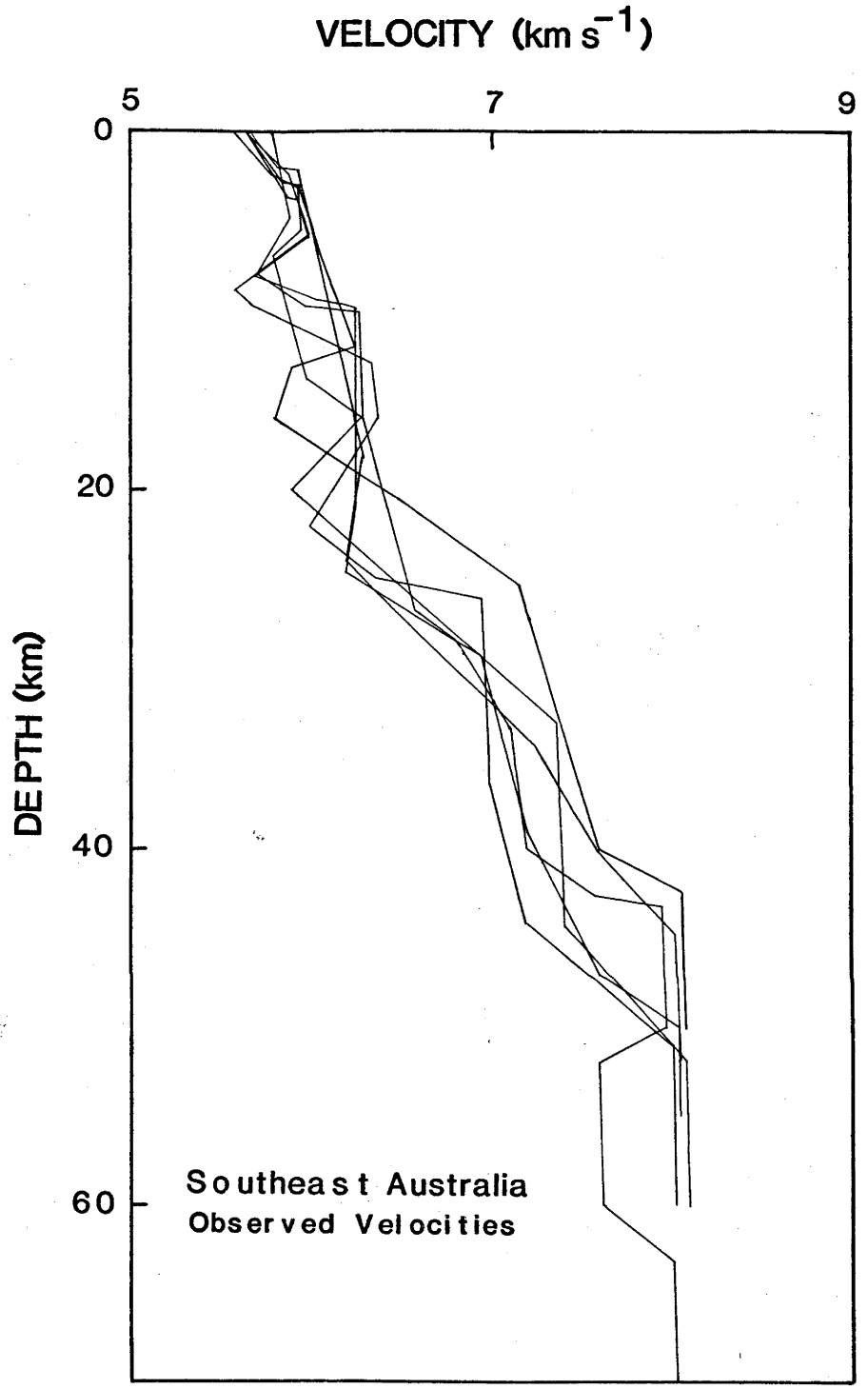

Figure 43. Observed velocity/depth models for the Lachlan Fold Belt.

Using these adopted pressure and geothermal gradients, and the velocity derivatives adopted in Section 6.1, the velocity/depth profiles of Figure 39 were adjusted to 1 GPa pressure and 25°C, so that direct comparison could be made with the profiles from the Pilbara Craton, and with the velocity and density results from experimental petrology (Table 11) and laboratory measurements of velocity and density in rock samples (eg. Birch, 1961; Manghnani & others, 1974). It is important to note that, as with the adjustment of the Pilbara data, the pressure and temperature gradients are sufficiently well constrained that, even if they are in error, the effect on the conclusions reached below are negligible. The magnitude of the adjustment is shown for the western line of the Mc Arthur Basin survey in Figure 40. It reaches about 0.4 km s^{-1} at the base of the crust. The velocities at 1 GPa and 25°C for all of the profiles are shown in Figure 41.

The important differences to note between these profiles and those from the Pilbara Craton is that (i) the crust is much thicker than in the Pilbara Craton, (ii) while velocities above 6.9 km s^{-1} are rare within the crust of the Pilbara Craton, they are common below about 25 km in northern Australia, and grade downwards into regions of even higher velocity; velocities between 7 and 8 km s^{-1} are common in the lower crust of northern Australia, and (iii) the crust mantle boundary is very transitional compared to that at the base of the Pilbara crust

The distribution of seismic refraction lines in southeastern Australia is shown in Figure 42. Results from these lines were published by Finlayson & others (1979), Finlayson & others (1980) and Finlayson & Mc Cracken (1981). Most of the refraction lines are within the Lachlan Fold Belt, and only the results from the lines within the fold belt will be considered, thus ensuring that the discussion is limited to the velocity/depth profile for a single tectonic province. However, the velocity/depth model for the line between Marulan and Ravensworth, which crosses the Sydney Basin, is very similar to those for the Lachlan Fold Belt, and the following discussion therefore might readily be appiled to a much larger area. The velocity/depth models for the Lachlan fold Belt are shown in Figure 43.

As with the models for the Pilbara and North Australian Cratons, the velocity/depth models were converted to 1 GPa pressure and 25°C. The pressure gradient used was curve c in Figure 29, and the geothermal gradient used was curve c in Figure 30, and is a median curve for the region derived

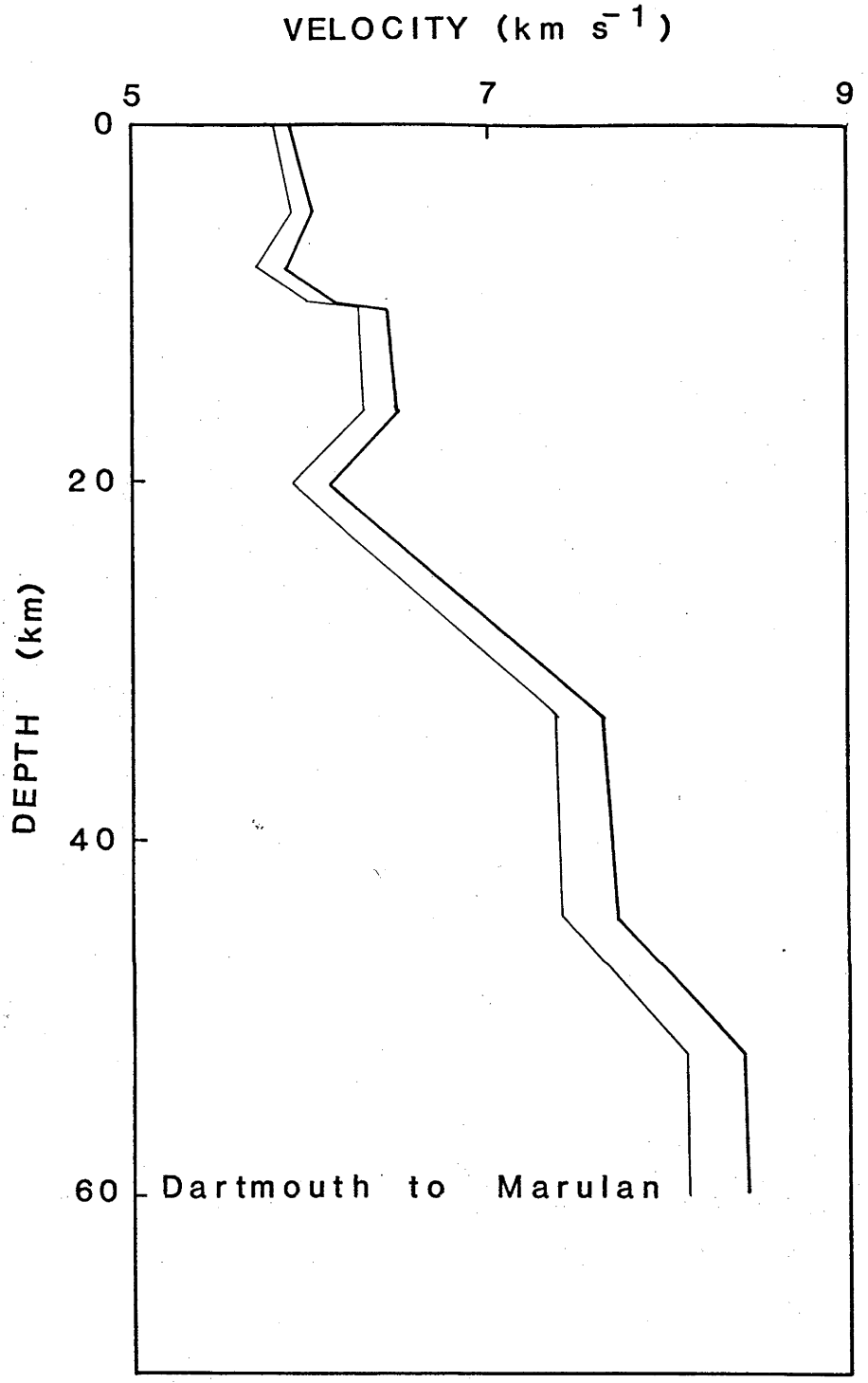

Figure 44. Velocity/depth model for the line from Dartmouth to Marulan. The light line is the observed profile; the heavy line is the observed profile with the velocities adjusted to 1 GPa and 25°C.

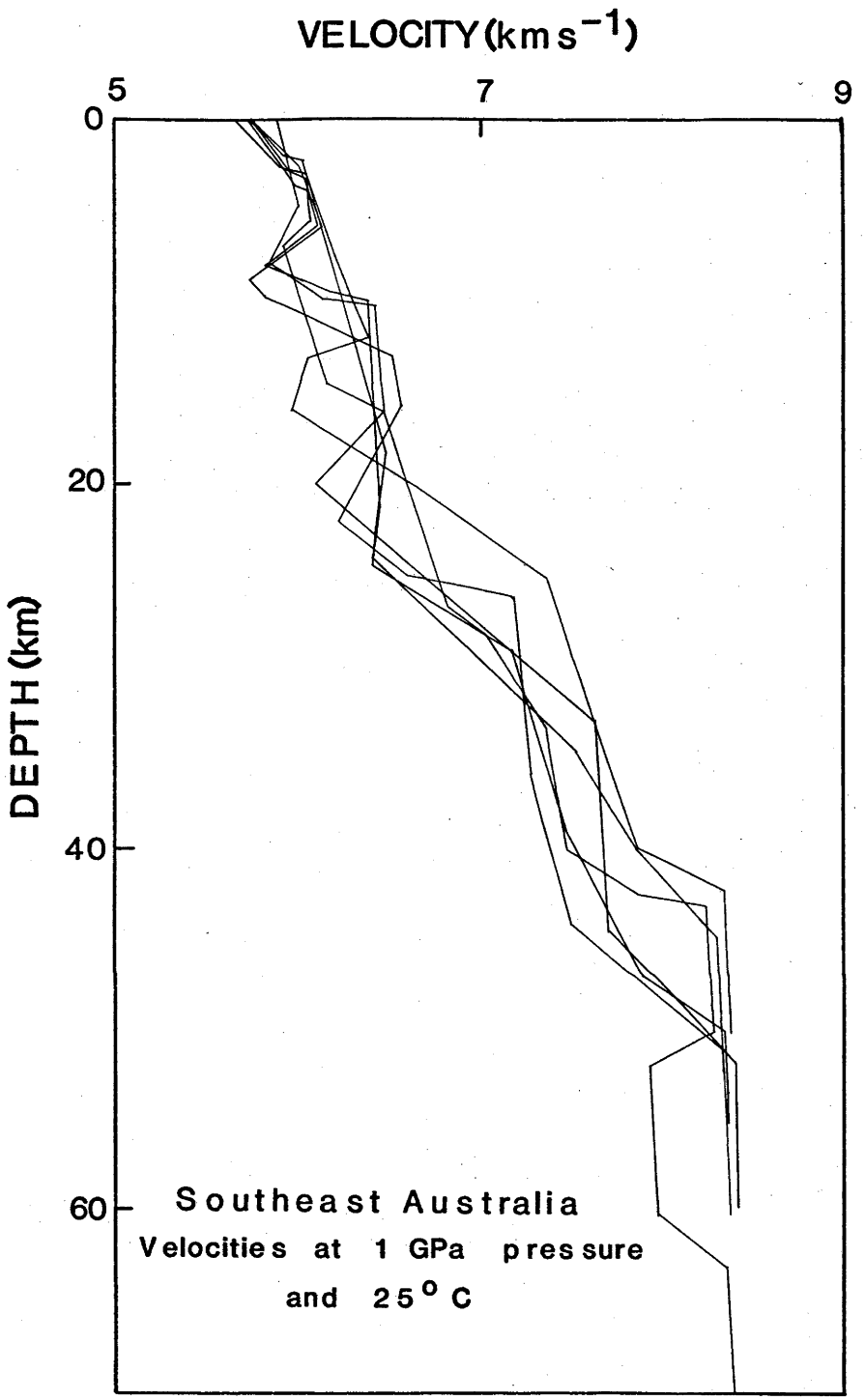

Figure 45. Velocity/depth models for the Lachlan Fold Belt of southeast Australia adjusted to 1 GPa and 25°C.

by Sass & others (1976). As with the other regions, the wrong choice of pressure and geothermal gradients within the family of those likely for the region would have made no difference to the final conclusions. The magnitude of the adjustment to 1 GPa and 25°C for the model from the profile of Dartmouth blasts northwards to Marulan is shown in Figure 44, and the family of curves at 1 GPa and 25°C is shown in Figure 45

The velocity/depth models from southeast Australia are all similar and ensure that the generally increasing velocity with depth is a universal effect throughout the region. The crust in southeast Australia is thinner than that in northern Australia, but thicker than that of the Pilbara Craton. The velocities of the lower crust are much higher than those of the lowest Pilbara crust, and the velocity gradients of the lower crust in southeastern Australia are similar to those from northern Australia, and higher than those of the Pilbara Craton.

Bamford & Prodehl (1977) and Prodehl (1977) concluded that, for non-orogenic regions of North America and Europe, old regions such as Precambrian shields had thick crusts and transitional crust/mantle boundaries while younger regions (eg. Hercynian Europe and the Colorado Plateau) have thin crusts and sharp crust/mantle boundaries. The implication of this generalisation is that as the crust becomes older, the lower crust and upper mantle continue to interact; the crust becomes thicker and the lower crust denser, and the crust/mantle boundary becomes transitional as rocks from the mantle, which are less dense than the mantle but denser than the lower crust are intruded into the lower levels of the crust. However, the velocity/depth models for the Pilbara Craton, when compared with those from younger parts of Australia, are in direct contradiction of Bamford & Prodehl's (1977) and Prodehl's (1977) generalisation. In Australia, therefore, the thinnest crust, with the sharpest crust/mantle boundary, is in the oldest region. A brief discussion of the implications about the evolution of the continental crust drawn from the generalisations made about the crust of North America and Europe is therefore warranted.

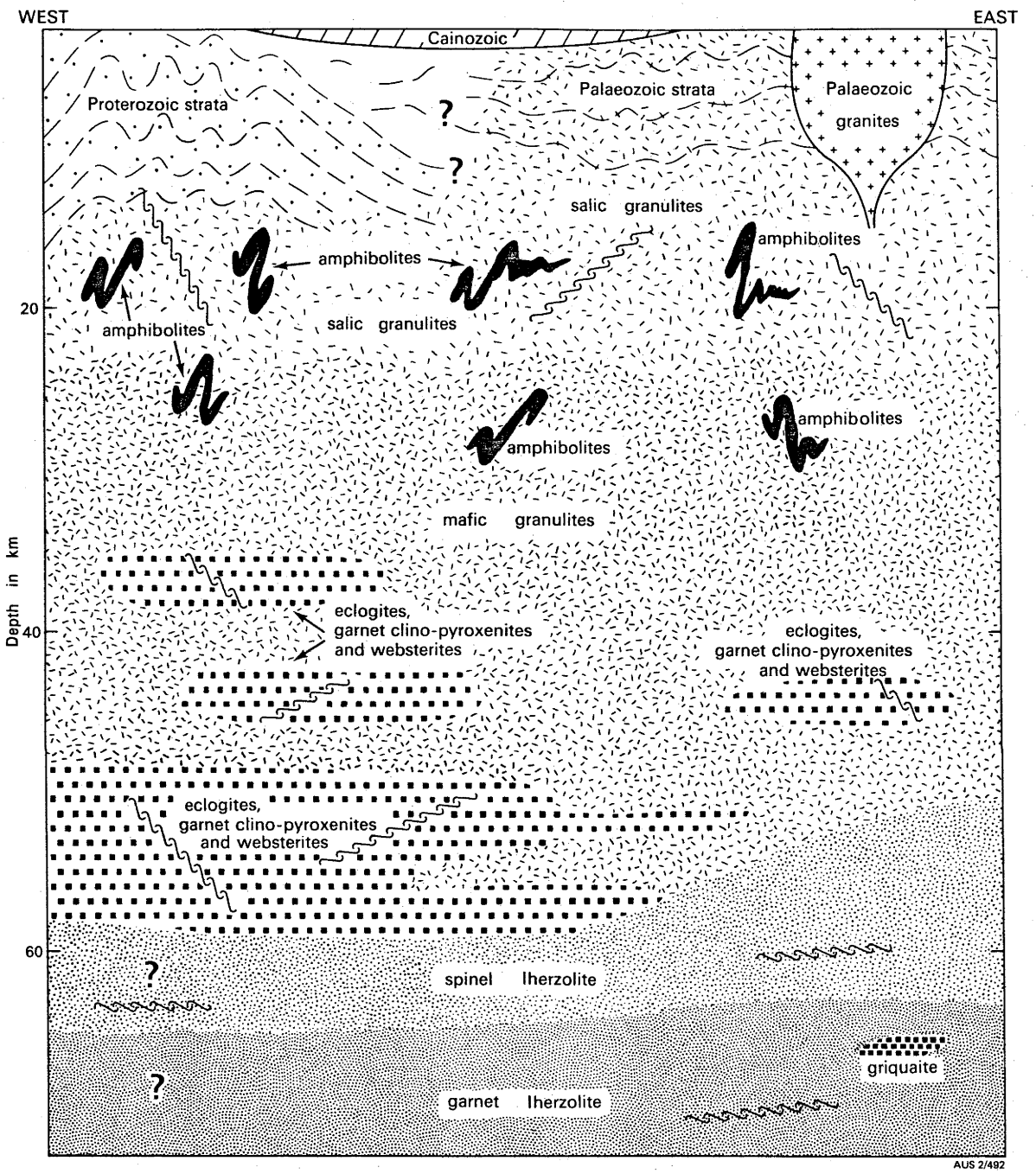

Figure 46. Idealised cross section from Port Augusta (SA) to Jugiong (NSW) with inferred crust - upper mantle lithologies. Stratigraphic relationships in the Murray Basin are uncertain as are the subcrustal granite geometries. Lithologic boundaries between granulites, amphibolites, eclogites, and lherzolites are drawn as gradational in the absence of contrary evidence. Question marks also indicate lack of evidence, in the form of sampled nodules, for lherzolites in South Australian kimberlitic occurrences (Ferguson & others, 1979, Figure 18).

Figure 46 was taken from Ferguson & others (1979), and is their diagrammatic crustal cross section for southeastern Australia based on lower crustal nodules from kimberlite pipes. In it, they suggest that the upper crust is composed of rocks which are generally close to granitic composition, but with depth, the metamorphic grade increases and the overall mafic content increases. However, they suggest that the increase of mafic content was not an even and gradual change, but was caused by blocks of mafic and ultramafic rocks. The proportion of these blocks probably increases with depth. With this model, they tried to explain the seismic models of southeast Australia. A refracted seismic wave travelling through such a lower crust would have a velocity which is the weighted average of all of the crustal components it penetrated, and waves which travelled through the deepest crust would have higher velocities than those which samples the middle crust, so that velocity gradients would be interpreted.

Thus the Precambrian shield of northern Australia and the now stable Lachlan Fold Belt of southeast Australia seem to fit the classification of Bamford & Prodehl (1977) and Prodehl (1977), but the Pilbara Craton does not. While the overall composition of the lower crust of the Pilbara Craton is more mafic than the upper crust, and the increase in mafic content may be due to increasing numbers of blocks of mafic and ultramafic rocks, the proportion of mafic and ultramafic rocks in the lower crust must be minimal or the velocity of the lower Pilbara crust would soon become too high. This follows from the seismic velocities in Table 11. For some reason, the tectonic processes which cause the underplating necessary to produce a lower crust similar to that for southeast Australia must have been absent in the earliest Precambrian.

One of the characteristics of Archaean cratons which distinguishes them from younger regions is that after cratonisation, they remained aloof from further tectonic processes which affected their regions. They are ringed by mobile belts which testify to the ongoing tectonism, and all of the subsequent volcanism, folding, faulting and sedimentation occurred around their edges. In the area of the 1977 crustal survey, the Capricorn Orogenic Belt is a classic example of such a mobile belt. Like the younger areas of northern and southeastern Australia, it has a transitional crust/mantle

boundary due to velocity gradients in the lower crust (Drummond, 1979b), testifying to participation of the lower crust and upper mantle in the Proterozoic tectonism (see also Horwitz & Smith, 1978; Wellman, 1978). However, the lower crust of the Pilbara Craton was not affected by the younger tectonism. Thus, as the Australian continent evolved and grew, the Pilbara Craton was like a pod floating on the turmoil and tectonism which surrounded it. If this is so, it raises the conjecture that other cratons or blocks which are surrounded by mobile belts, and therefore did not participate in the ongoing tectonism, should also have sharp crust/mantle boundaries. The Yilgarn Craton and the Kimberley Block to the north are two such examples.

The reasons why some crust should continue to interact with the mantle while other crust does not remain unknown. However, one suggestion is linked to the evolution of the crust with time. Archaean cratons with granitoid/greenstone terrains and surrounded by mobile belts did not form after about 2500 m.y. The mobile belts which surround the cratons are mostly Proterozoic, and were in turn superseded by different kinds of tectonic provinces as the earth moved towards the plate tectonic processes of recent times. Perhaps the tectonism of the earliest Precambrian was unable to permeate the barrier of density contrast at the crust/mantle boundary of the Pilbara Craton. However, it will be suggested later in Chapter 9 that it did affect the subcrustal lithosphere of the Pilbara Craton.

7. UPPER MANTLE ANISOTROPY.

The previous chapters showed that the crust of the Pilbara Craton has a fairly uniform velocity structure. The same cannot be said of the velocity structure of the upper mantle under the Pilbara Craton. The reversed Pn velocity along line GB (Figure 2) is 8.34 km s^{-1} (Drummond, 1979b), while that along line FDB is 7.8 km s^{-1} (Drummond & others, 1981). It is 8.2 km s^{-1} along line GD.

Drummond & others (1981) suggested two explanations for the differences in Pn velocities. Either they are due to anisotropy, or the Pn velocity varies throughout the region and is lowest under the Hamersley Basin because of iron depletion or different metamorphic grades under the craton associated with the tectonics of the Hamersley Basin formation. Both anisotropy and lateral variation of Pn velocities have been noted before (Fuchs, 1979).

One feature of note in Figure 28 in the previous chapter is the seismic disocontinuity at about 45 km depth in the model for shotpoint G (Goldsworthy) along line GBC. It is not interpreted on any other record section presented so far, although arrivals from it are possibly present on the section from shotpoint B along the same line. The sub-Moho phase may therefore have azimuthal dependence.

In this chapter, the possibility of upper mantle anisotropy is canvassed for both Pn and the sub-Moho phase observed along line GBC.

7.1 ANISOTROPY IN Pn

In Figure 47, all of the reduced Pn travel times (reduction velocity 8.0 km s^{-1}), including those from fan profiles as well as those from the on-line profiles, are plotted as functions of azimuth, both between 0 and 360° (part a), and with the values from 180 to 360° folded between 0 and 180° (part b). In part a, two peaks are clear, at about 120° and 300°, while troughs occur at about 40° and 240°. The reduced Pn travel times therefore show a definite dependence on azimuth, and the suspicion of anisotropy is reinforced.

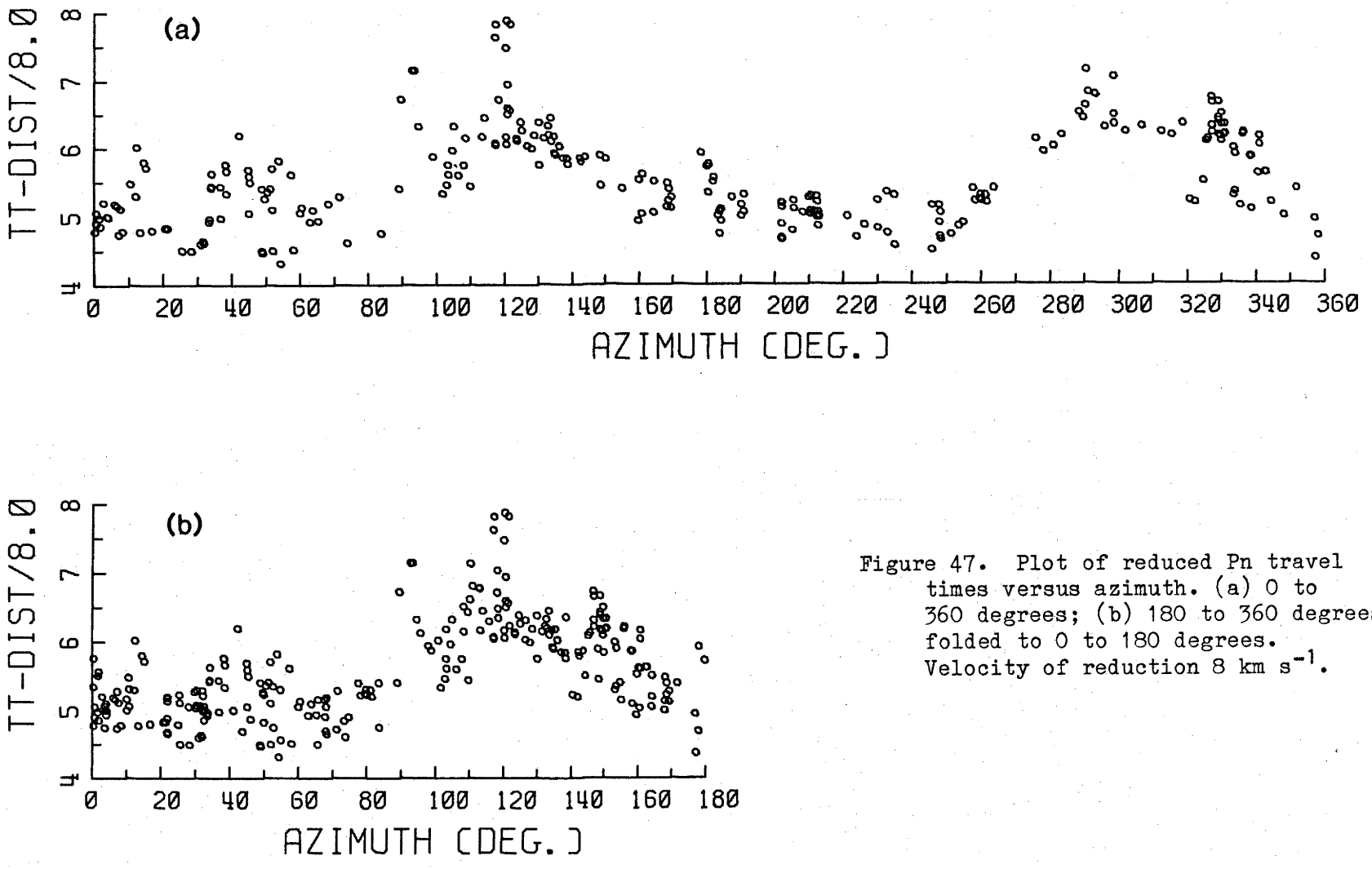

Figure 47. Plot of reduced Pn travel times versus azimuth. (a) 0 to 360 degrees; (b) 180 to 360 degrees folded to 0 to 180 degrees. Velocity of reduction 8 km s^{-1}.

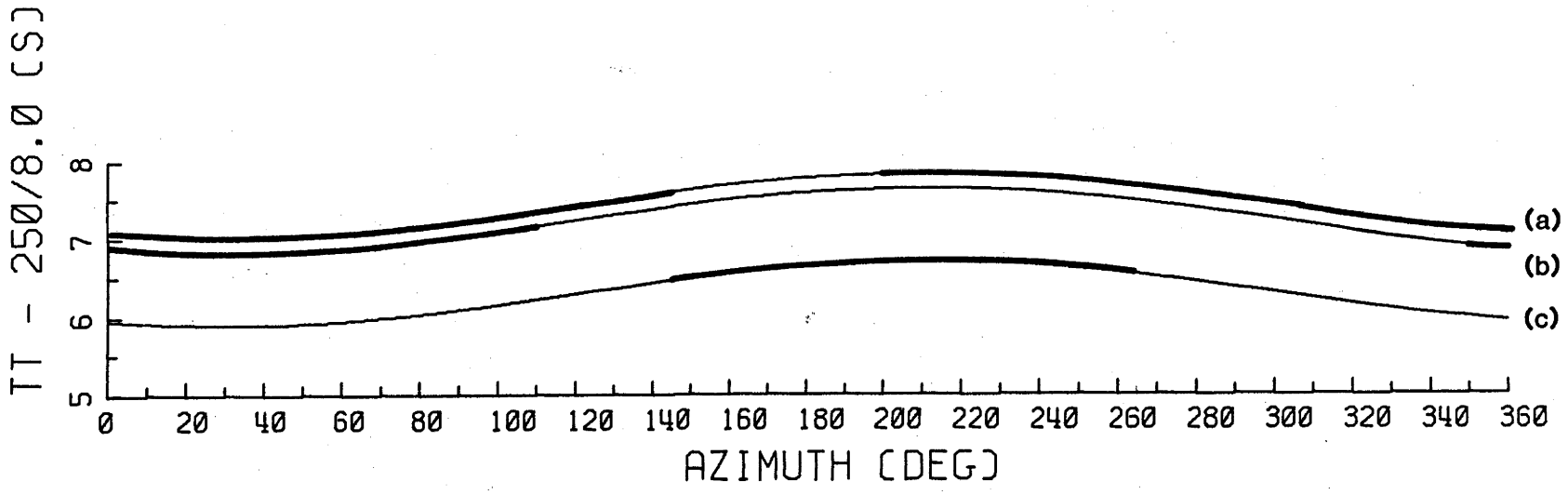

Figure 48. Plot of reduced Pn travel times for a model with an upper crustal layer with a velocity of 6.0 km s^{-1} overlying, at 13 km depth, a lower crustal layer of 6.4 km s^{-1} velocity. Moho dip is 1 degree at an azimuth of 210 degrees, and the Pn velocity is 8.0 km s^{-1}. The three curves are for Moho depths of (a) 33, (b) 32 and (c) 27 km. The heavy parts of the curves indicate those azimuths for which Pn travel times were recorded from shots in areas where the Moho has these approximate depths. Velocity of reduction 8.0 km s^{-1}.

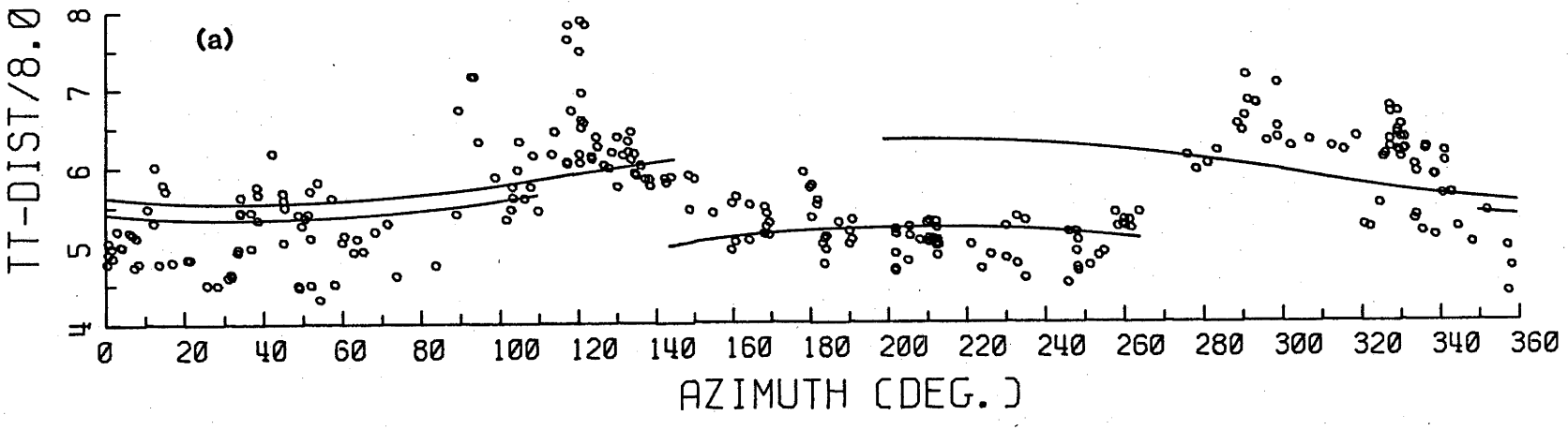

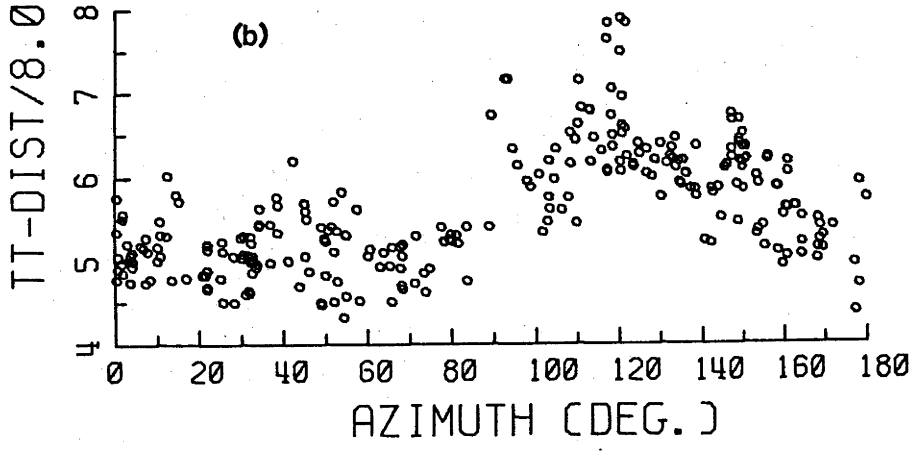

Figure 49. Reduced Pn travel times versus azimuth; (a) 0 to 360 degrees, (b) with 180 to 360 degrees folded to 0 to 180 degrees. Velocity of reduction 8 km s^{-1}. The superimposed curves are the heavy parts of the modelled travel time curves of Fig. 48 adjusted by -1.5 s, and show that the apparent dependence of velocity on azimuth may result from Moho dip.

However, the crust/mantle boundary dips southwards at about or just less than one degree. Larger reduced Pn travel times might therefore be expected along the axis of the Hamersley Basin on profile FDB, where the crust is thickest than, say, for either of lines GB or GD, where one of the ends of each profile lies over a shallower crust/mantle boundary. Moreover, the axis of the Hamersley Basin strikes at 120° (or 300°) and therefore corresponds to the positions of the peaks in Figure 47. The apparent azimuthal dependence of Pn in Figure 47 may therefore be structurally induced.

The travel time for a Pn ray through a model with a dipping interface is easily calculated. Such a model for the crust of the Pilbara Craton , based on the models from the intercept method of interpretation of Chapter 4 could be expressed simply as a two layered crust with velocities of 6.0 and 6.4 km s^{-1} with the intracrustal boundary at 13 km depth, and the crust/mantle boundary dipping at one degree from 27 km depth under shotpoints A and G. The intercept method profiling indicates that the dip is in a southerly direction, but as the the axis of the Hamersley Basin strikes at 120°, the dip direction may be 210°, perpendicular to the basin strike direction.

The reduced travel times at 250 km distance, for three shotpoints, corresponding to (a) shotpoints A and G, where the crust is 27 km thick, (b) shotpoint D (Tom Price), where it is 32 km thick, and (c) shotpoints B, F and D (Paraburdoo), 33 km thick, are shown in Figure 48. The change in reduced travel time through 360° is about 0.7 s for each site. The thick parts of the curves indicate the azimuths over which Pn arrivals from the respective shotpoints were observed. The total variation in modelled reduced travel times is more than one second.

In Figure 49, the modelled reduced travel times marked with heavy line in Figure 48 are shown superimposed on the measured travel times (with an adjustment of 1.6 s to the modelled times to account for a mismatch because of the simplicity of the model). Clearly, the variations of reduced Pn travel times with azimuth correlate with those expected from the effects of the measured structure.

One way of demonstrating the amount of structural effect in the azimuthal travel time dependency in Figure 47 is to subtract the modelled times for the model used in Figures 48 and 49 from the measured times, and display

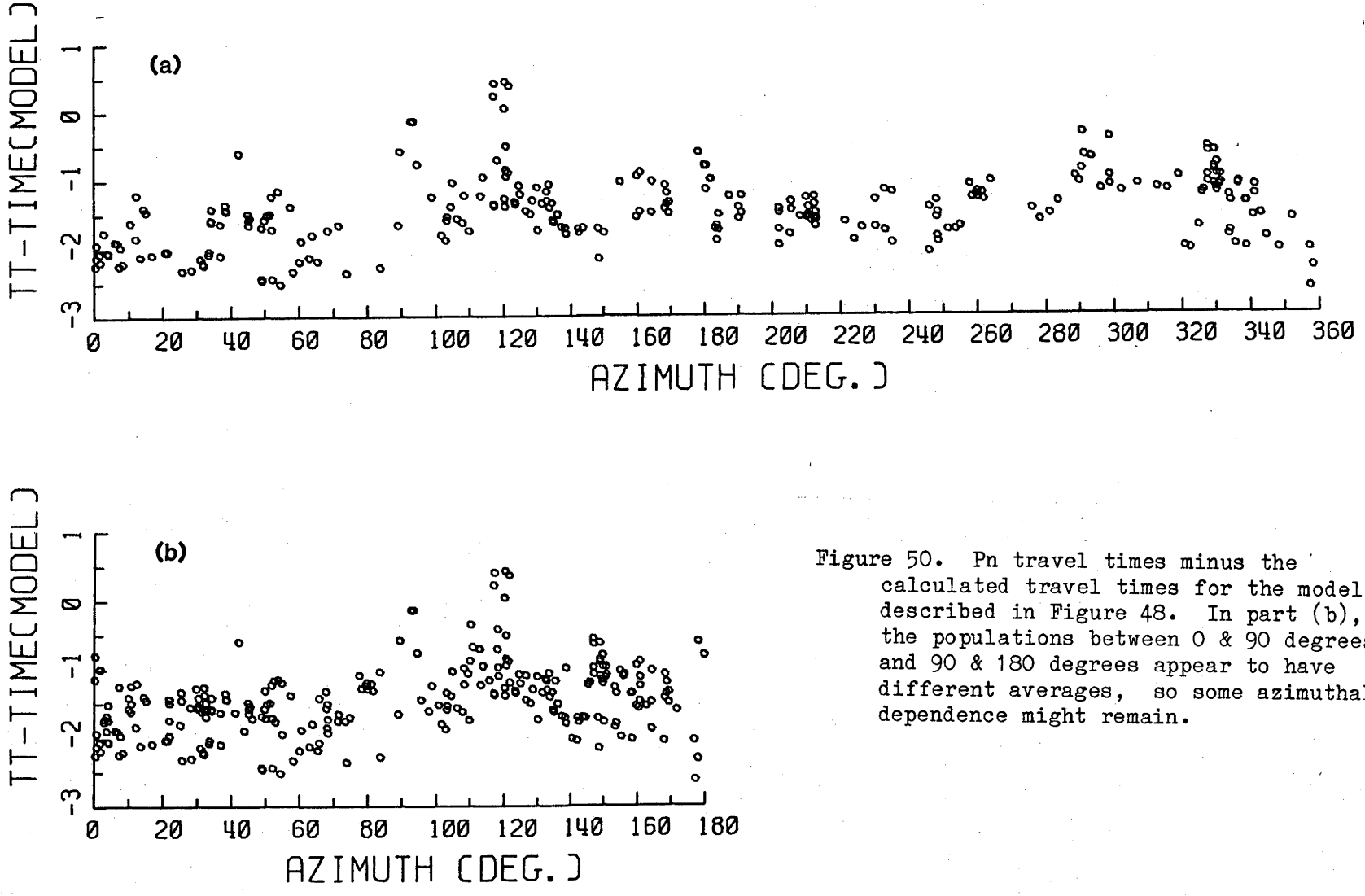

Figure 50. Pn travel times minus the calculated travel times for the model described in Figure 48. In part (b), the populations between 0 & 90 degrees and 90 & 180 degrees appear to have different averages, so some azimuthal dependence might remain.

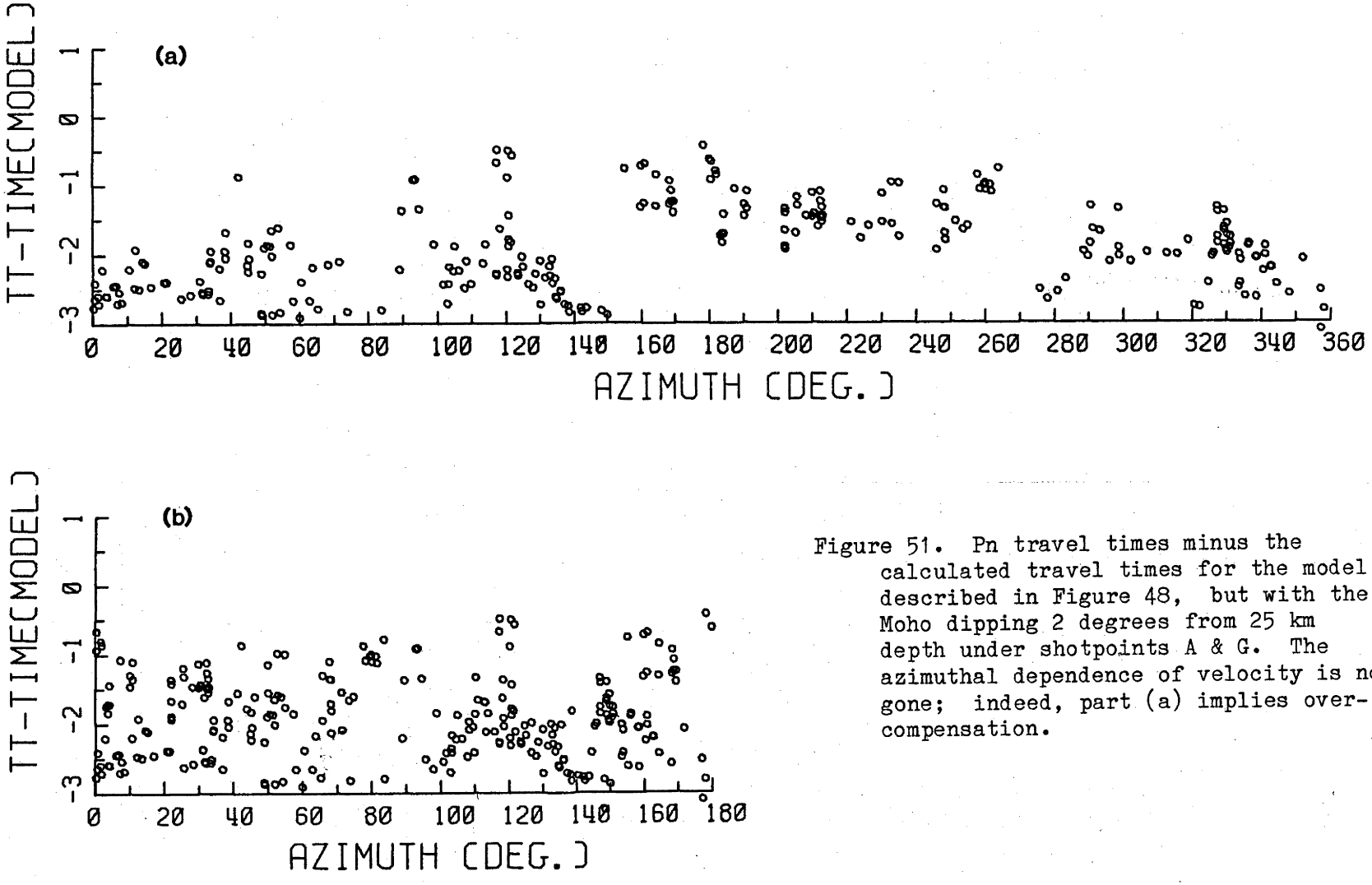

Figure 51. Pn travel times minus the calculated travel times for the model described in Figure 48, but with the Moho dipping 2 degrees from 25 km depth under shotpoints A & G. The azimuthal dependence of velocity is now gone; indeed, part (a) implies over-compensation.

the residuals as functions of azimuth. This is done in Figure 50. Most of the dependence has disappeared in part a. However, in part b, the residuals between 0 and 80° have a lower average than those between 100 and 180°, so some azimuthal dependence remains. In Figure 51, the residuals for a similar model but with a 2° dip on the crust/mantle boundary, do not show any remaining azimuthal dependency; rather, in part a the trend of Figure 47 has been slightly reversed, with the residuals between 160 and 260° now forming a high where a trough once lay. Consequently, a dip of between 1 and 2° is required before all of the apparent azimuthal velocity dependence can be explained by the effects of structure; ie., the crust/,mantle boundary under the southern Pilbara Craton would have to be 10 to 12 km deeper than it is under the northern craton. This is more dip than the intercept method models can tolerate. The conclusion, therefore, is that the apparent azimuthal dependence has a major structural component, but it may also have an anisotropic component.

The Pn data should therefore be interpreted by a technique which will give a estimation of both the structure and the azimuthal dependence of velocity. The time term method of interpretation is such a technique. A full description of the time term method, its historical development and theory, are given in Appendix 6. Before describing the time term interpretation, a brief description of the Pn data set and its suitability to the method is appropriate.

7.1.1 The Pn data set.

All Pn arrivals were recognised with the aid of record sections, and then most of the Pn arrivals were timed from original analog playouts of the magnetic tape recordings. The exceptions were those for the ANU stations where the high amplitude traces on the record sections were clearer than the analog records and were used in their stead. On the profile from shotpoint G southwards along profile GBC, Pn arrivals are overtaken beyond about 280 km by refractions from below the sub-Moho boundary. Similar arrivals from the sub-Moho boundary overtake Pn at comparable distances on some traces on some of the fan profiles to be discussed later, so considerable care was taken to ensure that the arrivals were Pn. Similar problems arise in recognising Pn arrivals beyond 300 km in Europe (Hirn & others, 1973; Bamford, 1973a).

All arrivals were timed with an accuracy better than 0.1 s. However, the subjective nature of judging arrival onsets probably increased the error.

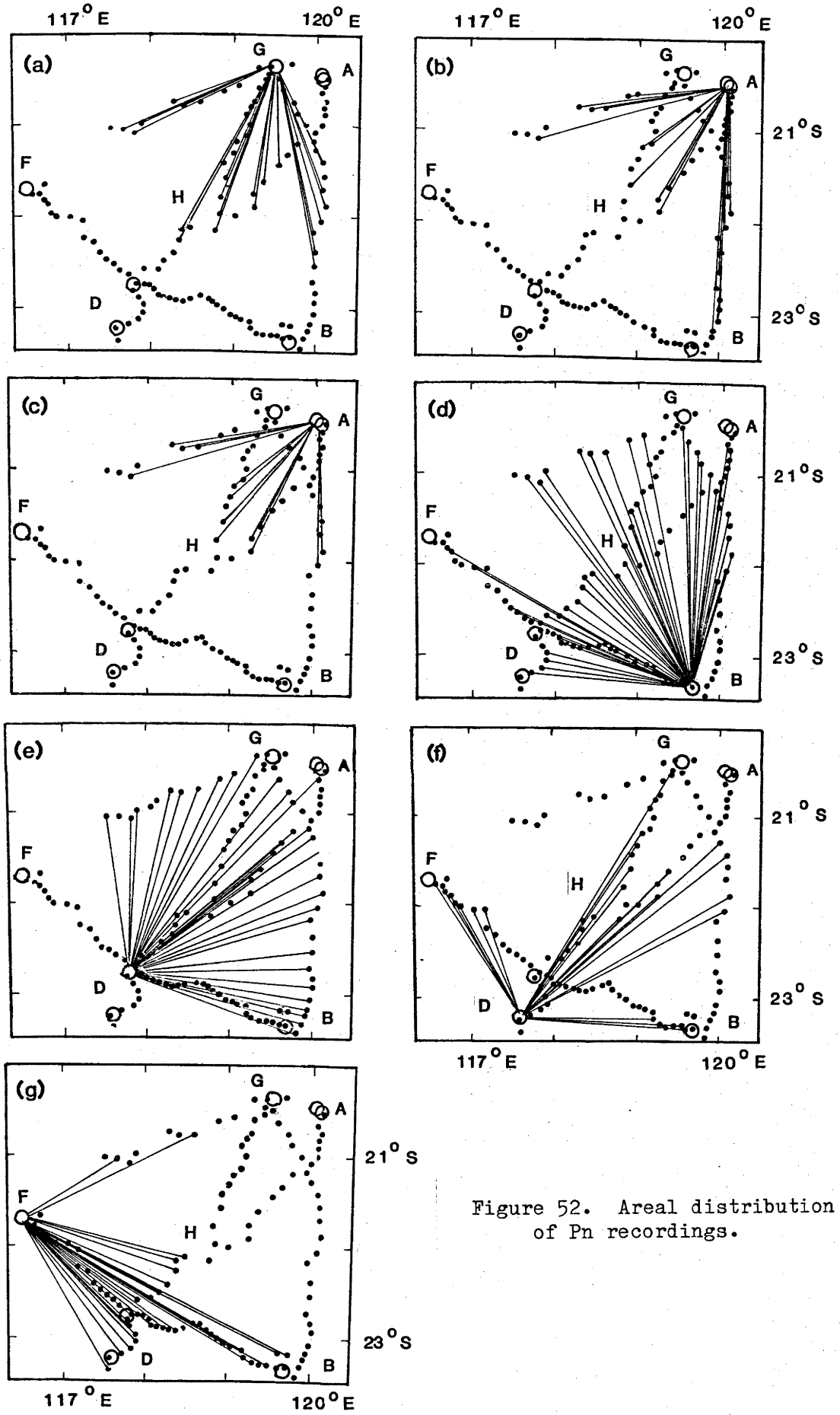

Figure 52. Areal distribution of Pn recordings.

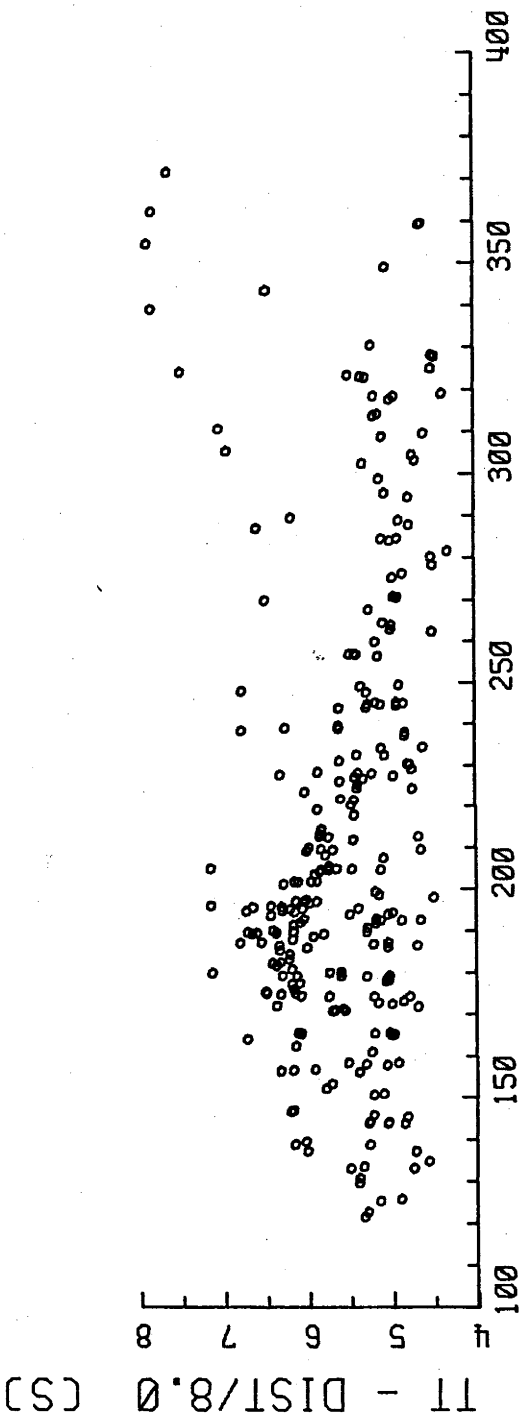

Figure 53. Reduced Pn travel times versus distance. Velocity of reduction 8 km s^{-1}.

As well, the dispersed nature of some of the mining blasts meant that the effective shot positions (ie. the point from which the seismic energy actually emerged) might sometimes have been misjudged. As errors in distance can 'leak' into errors in the time terms, the distance errors can be regarded as errors in travel times; they probably rarely exceeded 0.1 s. The errors in travel times may therefore sometimes exceed 0.2 s, and even 0.3 s for emergent arrivals whose onsets are hard to judge.

Whitcombe & Maguire (1979) introduced the concept of error variance, where the error variance defines the expected error of the entire data set. A measure of the error variance of Pn travel times can be judged from the repeatability of readings, not of the same arrivals several times over, as suggested by Whitcombe & Maguire (1979), but in the case of several explosions from the same shotpoint recorded at some stations. On 55 occasions stations recorded more than one blast from some shotpoints. From the resulting travel times the error standard deviation was calculated as 0.20 ± 0.16 s, giving an error variance of 0.04 s^2. This error variance can possibly be reduced because the differences in the travel times due to slightly different shot locations throughout the mines (and therefore different epicentral distances) were not considered. They are generally small, contributing less than 0.05 s, but in as many as 15 cases may have contributed all of the error.

The areal distribution of the data is shown in Figure 52 in the form of maps of the area with lines joining the shotpoints to the stations which recorded their blasts. The diagram shows clearly that, while each shotpoint was well recorded, all of the shotpoints with the possible exception of shotpoint B (Newman) were not well recorded across the entire survey area. Most of the recognised Pn recordings are limited to within 250 km of the blast (Figure 53), due to both the small amplitudes of Pn arrivals and their subsequent loss in noise, and their being replaced as first arrivals on some profiles by the faster phase from the sub-Moho boundary.

The poor areal distribution of Pn data meant that a test for lateral variations in the upper mantle velocity, such as that proposed by Morris & others (1969), would have been invalid, because it most probably would have indicated lateral variations which reflected the apparent velocities from each shotpoint towards the centre of the survey area.

The azimuthal distribution of Pn data is quite good, with most azimuth ranges amply represented (Figure 54). In Figure 54, only 186 travel times are

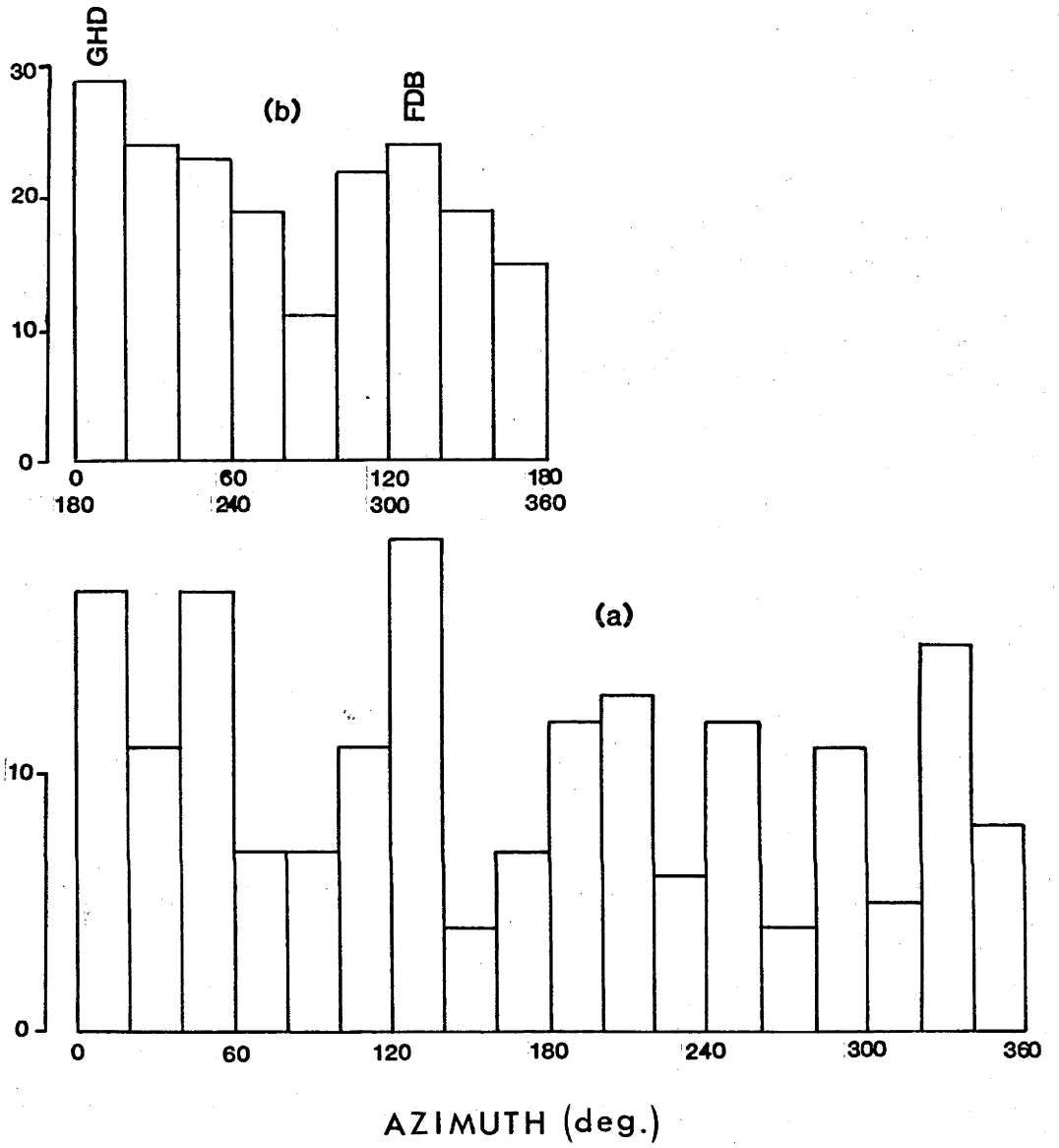

Figure 54. Histograms of the azimuths of Pn travel times. (a) between 0 and 360 degrees; (b) 180 to 360 degrees folded to between 0 and 180 degrees.

represented, compared to 264 in Figure 47. Because 55 shot-station combinations have more than one travel time-distance pair, some had to be culled , or the additional data points would have weighted some shotpoint/station connections at the expense of others. While objective weighting of data is often used to improve time term solutions, it should not be applied purely through the fortuitous recording of extra blasts at some shotpoints. The culling of data was done objectively, often on the basis of residuals in the travel times compared to those for the other times for the shotpoint-station pair, and at other times because the arrivals were not as clear as others on the record sections.

7.1.2 Limitations of the time term method.

The time term method is often regarded as a panacea for those who have a large amount of seismic refraction data to interpret, but do not really understand the seismic refraction method. The early pioneers of the technique, Willmore & Bancroft (1960), feared that this would happen, and that the method would be used as a 'melting pot' technique with all of the data fed into a calculator or computer to produce the correct result at the turn of a handle. Several publications have since criticised the method because the interpreters who used it did not apply the correct care and attention required, both in designing their experiments and in the laboratories interpreting their data, so that their results were not correct.

Most of the criticisms that are made of the time term interpretations arise because the interpreters did not take note of the three assumptions made in deriving the time term equation. They are set out in Appendix 6, but are repeated here to stress their importance:

(i) the velocity varies only with depth (perpendicular to the refractor) within the critically refracted cone under the shot or station;
(ii) the velocity in the base refractor is constant; and
(iii) the slope and curvature of the refracting surface are small.

It is non-adherence to the third assumption that causes most problenms.

O'Brien (1968) first showed that the method can produce erroneous results. He reinterpreted the 1963 Lake Superior Experiment data that had been used in the benchmark papers of Berry & West (1966a,b) and Smith & others (1966) on the time term method, and found that errors had been introduced into the original interpretations because of the assumption that the dips in the refractor are small. Bamford (1973b) showed that a model similar to O'Brien's

could be obtained by the time term method if an iterative approach was used (see Appendix 6). Reiter (1970) made model studies and also saw the importance of adhering to, or at least accommodating, the assumptions outlined above.

Whitcombe & Maguire (1979) also used model studies to research the errors that can arise in both the structure and velocity estimates due to the effects of refractor topography. They suggested comparing the error variance with the solution variance in a statistacal F test. A good fit of the model to the data will give a solution variance which is not statistically greater than the error variance. They stressed, however, that a a good fit of the model to the data does not necessarily mean that the model is the correct one. Likewise, the correct solution does not necessarily have the lowest solution variance.

Whitcombe & Rogers (1981) addressed the problem of structurally induced apparent anisotropy. Synclinal, anticlinal and dipping refractors with isotropic velocities can appear anisotropic, as shown above for the dipping crust/mantle boundary under the Pilbara Craton, and the best solutions for data derived from models with isotropic velocities often have anisotropic, rather than isotropic, velocities, even when the time term surface closely resembles the correct surface. As well, one problem not addressed by most workers is anisotropy in the medium above the refractor. This can cause 'ghost' anisotropy in the refracting layer.

Bath (1978) considered the problems of converting time terms to refractor depths. Berry & West (1966a, b) realised that their refractor depths were likely to be minimum values. The main sources of error are:

(i) Unrecognised embedded low velocity zones can cause the calculated depths to be too large. The only low velocity zone recognised in the Pilbara Craton is the one caused by the Hamersley Basin cover rocks. An average value of seismic velocity within the low velocity zone based on the velocity/depth models from the other profiles seems appropriate.

(ii) If a uniform velocity is assumed for the layer above the refractor, but a velocity gradient is present, the calculated depths will be too small. The error can be reduced by using the average velocity above the refractor, rather than the velocity at the top of the layer, but will not be removed entirely. Bath (1978) shows how to make the correct calculations, but they require complete knowledge of the velocity structure, which is only known approximately in the Pilbara Craton, especially in the southeast Hamersley Basin.

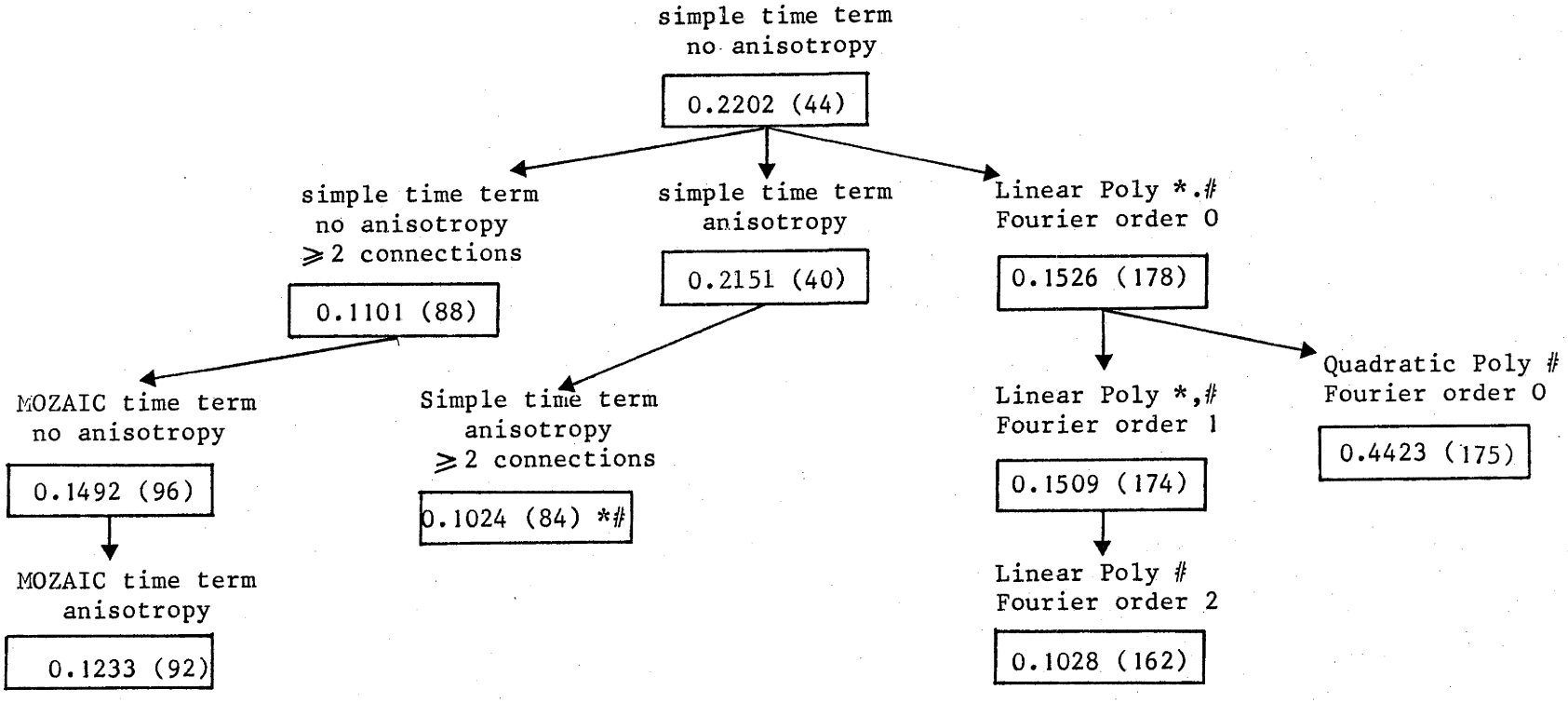

* Iterate F for these solutions

\# These solutions are for a critical distance of 80 km

Figure 55. Hierarchy of time term solutions showing variances (to 4 decimal places) and the number of degrees of freedom (in brackets).

TABLE 12: Details of all uniterated time term solutions.

Solution Number	Type of solution	Combined offset dists.	No. of obs.	Deg. of freedom	Variance	* ≥1SD	* ≥2SD	≥3SD	V=7.99 + † Sin2θ +	Cos2θ +	Sin4θ +	Cos4θ
1	Simple time term, no anisotropy, ALL DATA	NA	186	44	0.2202	10	0	0	0.0	0.0	0.0	0.0
2	Simple time term, no anisotropy, ≥ 2 connections	NA	142	88	0.1101	32	1	0	0.0	0.0	0.0	0.0
3	MOZAIC time term, no anisotropy	NA	155	96	0.1493	26	4	0	0.0	0.0	0.0	0.0
4	Simple time term, anisotropy, ALL DATA	80	186	40	0.2151	8	0	0	0.1083	0.0577	-0.0322	-0.0099
5	Simple time term, anisotropy, ALL DATA	100	186	40	0.2157	8	0	0	0.1190	0.0669	-0.0392	-0.0086
6	Simple time term, anisotropy, ALL DATA	120	186	40	0.2164	8	0	0	0.1288	0.0787	-0.0491	-0.0057
7	Simple time term, anisotropy, ≥ 2 connections	80	142	84	0.1024	35	1	0	0.1083	0.0577	-0.0322	-0.0099
8	Simple time term, anisotropy, ≥ 2 connections	100	142	84	0.1027	37	0	0	0.1190	0.0669	-0.0392	-0.0086
9	Simple time term, anisotropy ≥ 2 connections	120	142	84	0.1030	38	0	0	0.1288	0.0787	-0.0491	-0.0057
10	MOZAIC time term, anisotropy	80	155	92	0.1233	31	2	0	0.1425	0.0970	-0.0571	0.0121
11	MOZAIC time term, anisotropy	100	155	92	0.1222	35	2	0	0.1570	0.1114	-0.0646	0.0142
12	MOZAIC time term, anisotropy	120	155	92	0.1210	36	2	0	0.1714	0.1303	-0.0739	0.0171
13	Linear polynomial	80	186	178	0.1526	42	9	1	0.2016	0.1241	-0.0959	0.0366
14	Linear polynomial	100	186	178	0.1493	42	13	1	0.2231	0.1424	-0.1090	0.0384
15	Linear polynomial	120	186	178	0.1464	42	11	1	0.2474	0.1661	-0.1257	0.0387
16	Linear polynomial + double Fourier of order 1	80	186	174	0.1509	43	7	1	0.2042	0.1407	-0.0998	0.0336
17	Linear polynomial + double Fourier of order 1	100	186	174	0.1472	41	8	1	0.2279	0.1558	-0.1141	0.0435
18	Linear polynomial + double Fourier of order 1	120	186	174	0.1432	42	10	1	0.2485	0.1753	-0.1278	0.0543
19	Linear polynomial + double Fourier of order 2	80	186	162	0.1028	43	6	1	0.1520	0.1361	-0.0613	0.0260
20	Linear polynomial + double Fourier of order 2	100	186	162	0.0993	38	6	1	0.1803	0.1158	-0.0784	0.0475
21	Linear polynomial + double Fourier of order 2	120	186	162	0.0998	41	7	1	0.2271	0.0889	-0.1098	0.0656

* The number >1SD includes those >2SD and >3SD, but the number >2SD does not include those >3SD.

† Solutions 13 to 21 for polynomial and Fourier surfaces were calculated for the axes rotated 30^0 clockwise, ie. rotated to the tectonic azimuth. However, θ refers to the azimuth relative to north.

(iii) The problems arising from using the method in areas of large refractor dip have already been alluded to. To circumvent these problems, the time term method was applied only within the confines of the Pilbara Craton where the profile models from the intercept method interpretation had dips of only one degree or less on the crust/mantle boundary.

(iv) The assumption of one layer rather than two above the refractor can cause the estimated depths of the refractor to be too large. Consequently, when the depths were calculated (see later), a two layered crust was assumed.

The points noted above draw attention to the limitations of the time term method. These limitations are often unquantifiable; we do not know that we have the wrong answer because we do not know what the correct answer is. In the time term analysis described below, care was taken to keep in mind the assumptions of the time term technique. The results obtained should have meaningful qualitative implications, although the models need not necessarily be quantitatively correct.

7.1.3 The time term interpretation.

Time term inversions of the Pn data were made for a variety of models, ranging from simple time term solutions where the individual shotpoint and station time terms were calculated, to MOZAIC solutions and the fitting of time term surfaces with anisotropy in the refractoring layer. The hierachy of solutions is shown in Figure 55 where the solution variances and number of degrees of freedom are also shown. Full details of the (uniterated) solutions are given in Table 12.

In all of the time term solutions discussed below, an isotropic velocity of 7.99 km s^{-1} was used. This is the velocity derived by linear regression analysis of the 186 data points used in the inversions. If all of the 264 recorded Pn travel times are regressed, the velocity is 8.00 km s^{-1}. By assuming the isotropic velocity, the difficulty noted in Appendix 6, noteably that the time term equation 16 in the appendix is non-linear in 1/V and cannot therefore be solved by linear techniques for 1/V, has been circumvented.

Solutions 1 & 2:

Solution 1 is based on all 186 data pairs, and time terms are calculated for every shotpoint and station. In solution 1, 44 stations recorded

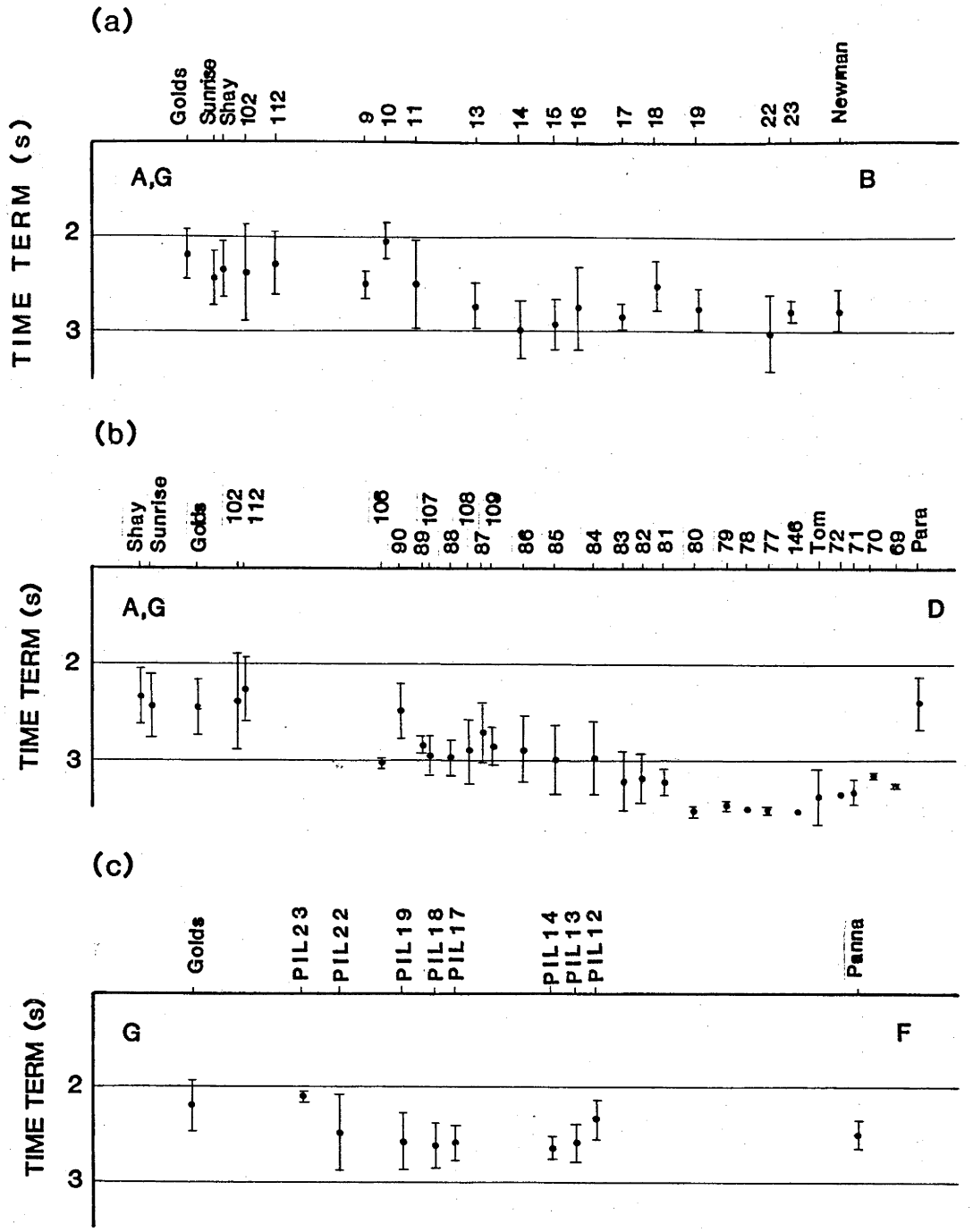

Figure 56. Time term profiles for lines GB, GD and GF for the solution for simple time terms with no anisotropy for the stations with more than one connection. The error bars are the RMS residuals for the travel times to the shots and stations.

only one Pn arrival. As the time terms for these stations have zero degrees of freedom, the travel time-distance data for them do not contribute to the time terms for the shots. In solution 2, those 44 stations with only one connection were omitted. Solutions 1 and 2 are identical for those shots and stations which have more than one connection, and the difference in the solution variances reflects the different numbers of degrees of freedom.

The time terms for solution 2 are shown as time term profiles in Figure 56. The error bars are the root mean square residuals for each shotpoint or station. The crust dips from north to south, as expected. The dips, for reasonable estimates of crustal velocities, is greater than 10 km along profile AD. The time term solution is therefore trying to accommodate the variation of Pn times with azimuth with structure on the crust/mantle boundary as discussed above.

The variances for solutions 1 and 2 are significantly greater than the error variance of 0.04 s^2 calculated above, but as all residuals lie within two standard deviations for solution 1, and all but one lie within two standard deviations for solution 2, the solutions might reasonably be regarded as good solutions.

Solution 3:

The number of degrees of freedom can be increased , and extra data included, in the MOZAIC time term method. The Pilbara data do not lend themselves to MOZAIC solutions as freely as those of Bamford (1976). This is because of the nature of the data distribution (Figure 52). However, the time terms for seven mozaics incorporating 13 extra data pairs, as well as those stations with more than one connection, can be calculated. Solution 3, Table 12 , gives the results.

The variance is greater than that of solution 2, despite the greater number of degrees of freedom. As well, four data pairs have residuals outside two standard deviations, and the time terms for some stations and mozaics, especially around shotpoint B, have differences of more than two seconds over very short distances, implying that the solution is not very good.

Solutions 4, 5 & 6; 7, 8 & 9; and 10, 11 & 12.

Anisotropic velocity functions were introduced into each of solutions

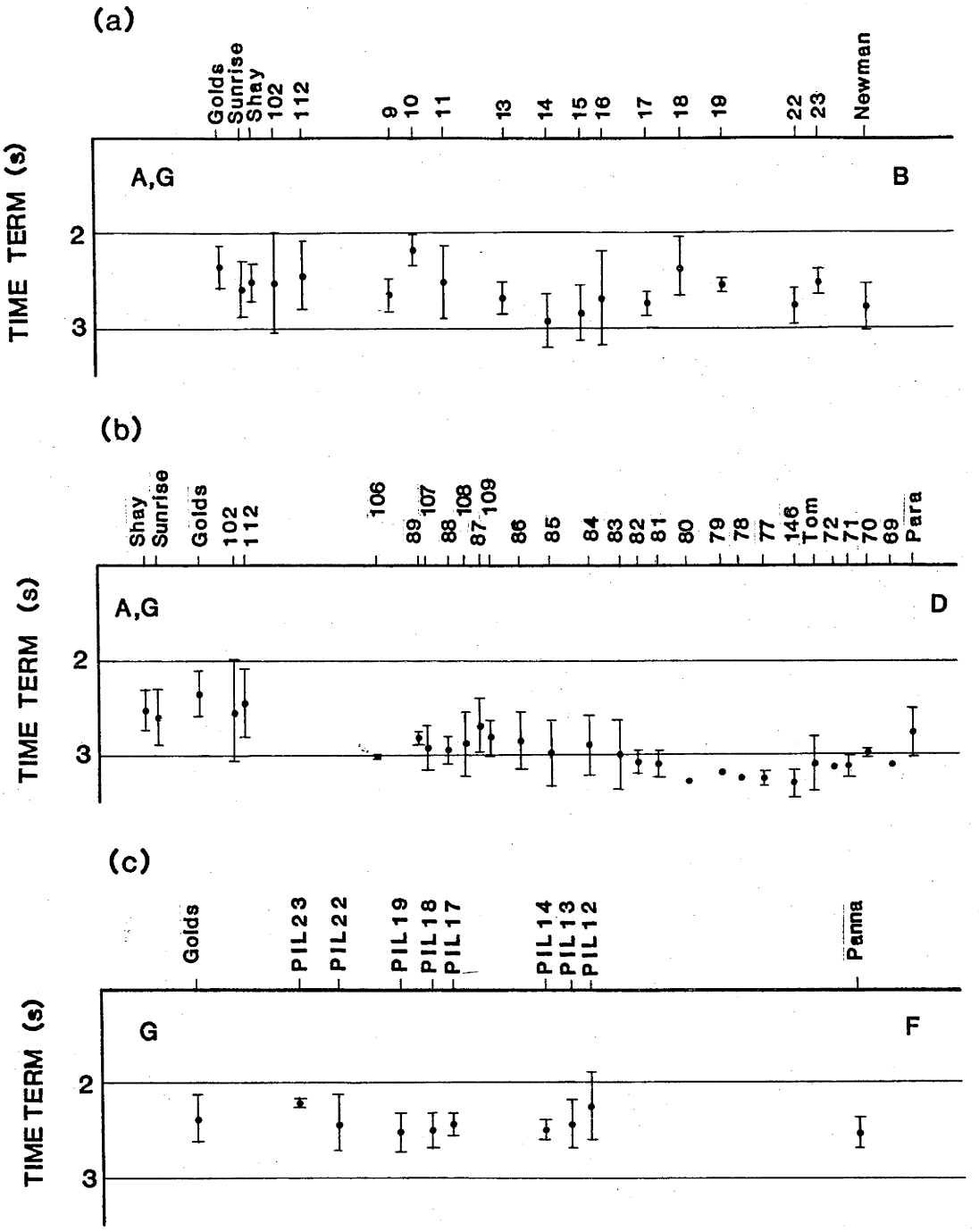

Figure 57. Time term profiles GB, GD and GF for the uniterated solution for simple time terms and anisotropy, for the stations with more than one connection. The error bars are the RMS residuals for the travel times to the shots and stations.

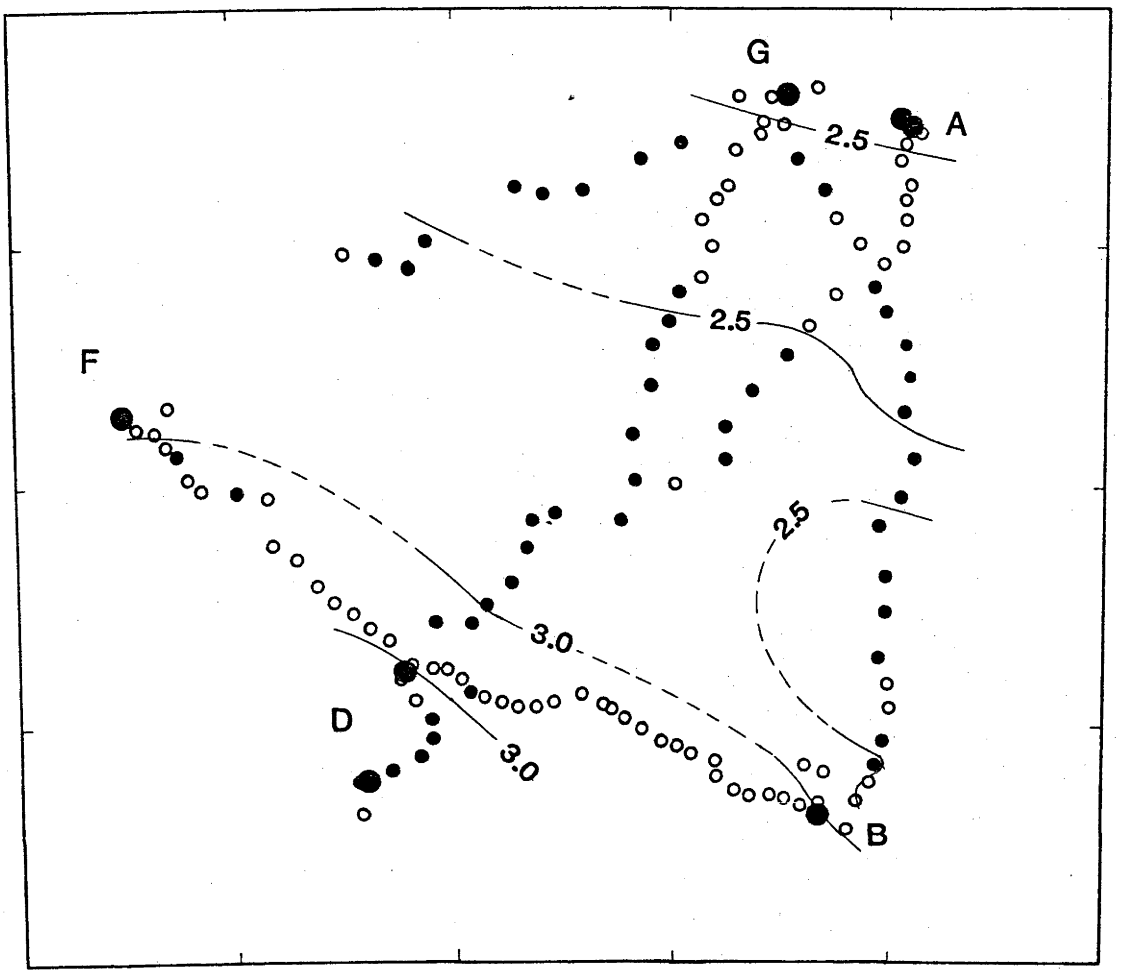

Figure 58. Time term contours for the uniterated solution for simple time terms, with anisotropy, for the stations with more than one connection. The contours are dotted in areas of sparse or no data. Contour interval 0.5 s. Dots indicate stations which participated in the solutions, circles those that did not.

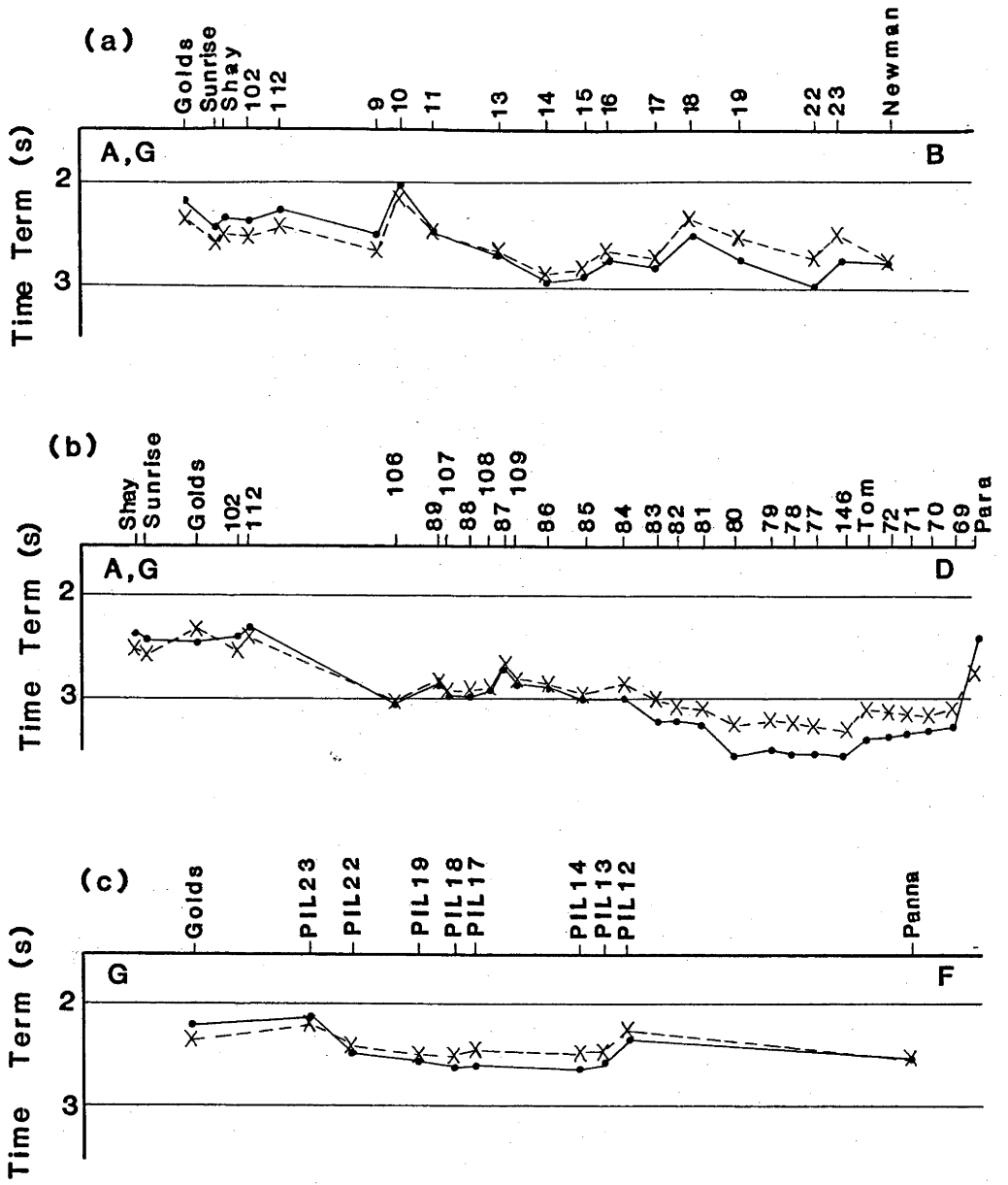

Figure 59. Comparison of the time term profiles for the solutions for simple time terms, with (crosses) and without (dots) anisotropy, for the stations with more than one connection.

1, 2 and 3. Estimates of the sum of the offset distances under each shot and station were required, and 80 km was tried as a first approximation (solutions 4, 7 and 10). This is because the interpreted critical distances for the profiles A and G are about 80 km. On some of the other profiles, the interpreted critical distances are greater, so values of 100 and 120 km were also tried (solutions 5, 6, 8, 9, 11, and 12).

In all cases, the introduction of the anisotropic velocity functions into the solutions improved the variance, but not significantly so at the 95% confidence level (based on F tests on the solution variances). The variation of the combined offset distances did not significantly alter the solution variances, and, by inspection, did not seem to overly affect the anisotropy coefficients.

Note that the anisotropy coefficients of solutions 4 and 7, 5 and 8, and 6 and 9 are the same. This is because the extra data in the former solutions have zero degrees of freedom and do not contribute to the calculation of the anisotropy functions or the shot time terms, as noted for solutions 1 an and 2. The solutions for which the stations have more than one connection (ie. solutions 7, 8 and 9) have the lowest variances, and very few data to be rejected on the basis of residuals greater than two standard deviations.

The time terms for solution 7 are shown as time term profiles in Figure 57, and as a contoured map in Figure 58. In Figure 59, the time term profiles for solutions 2 and 7 are shown on the same axes. Note that while the general features are the same for both solutions, for example, the dip on the refractor is to the south, and a general low occurs in the time terms of profile AD between stations 80 and 77, the dip to the south towards B and D is least in Solution 7. For reasonable assumptions of crustal velocities, based on the crustal velocity/depth models from the amplitude studies (Chapter 5), the dip in Figure 57 would be about 6 km, which is what would be expected from the intercept method interpretation.

Thus, the inclusion of anisotropy in the time term solution confirms the qualitative analysis of the reduced Pn travel times in Figure 47. That is, a solution can be found (solution 2) which will fit the data and explain the azimuthal dependence of travel times entirely in terms of structure. That structure is more than can be accommodated in the the models from other methods of interpretation. However, the inclusion of anisotropy terms reduces the structure to acceptable levels (solution 7), and explains the rest of the

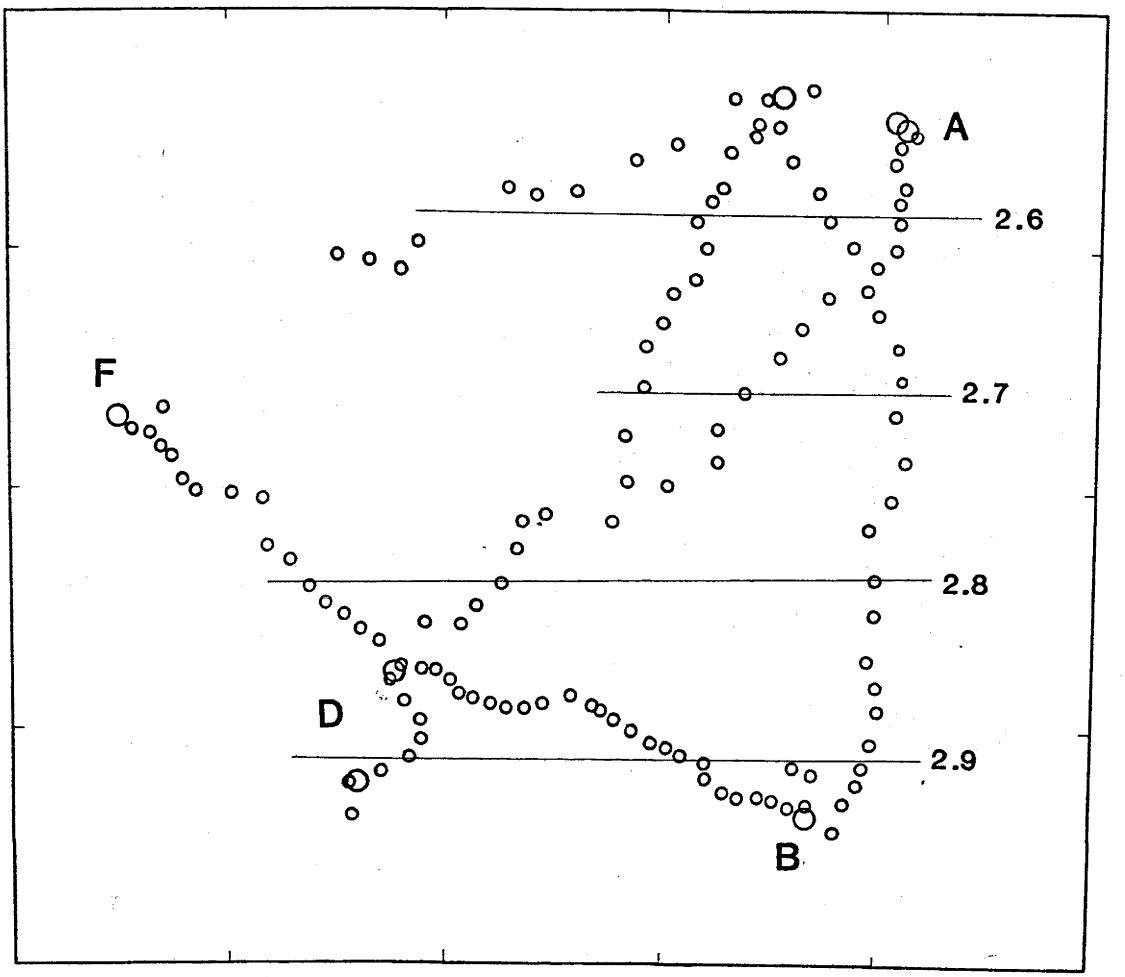

Figure 60. Contours of the uniterated solution for a linear polynomial time term surface with anisotropy. This solution occurs for the axes of the coordinate system rotated to any azimuth. Contour interval 0.1 s.

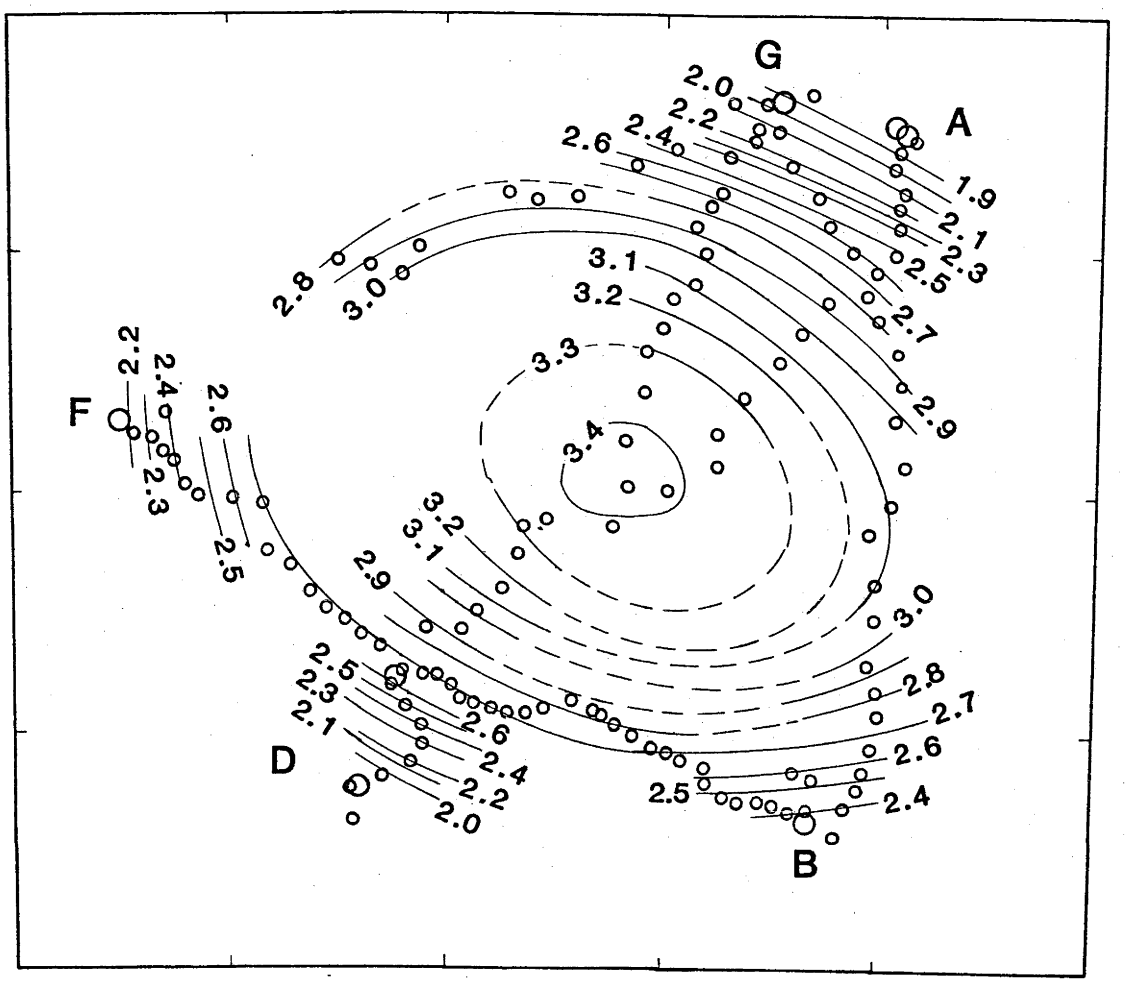

Figure 61. Contours for the uniterated solution for a quadratic polynomial time term surface with anisotropy, for the axes rotated 30 degrees clockwise. Contour interval 0.1 s. Contours are absent or weak in areas of few stations.

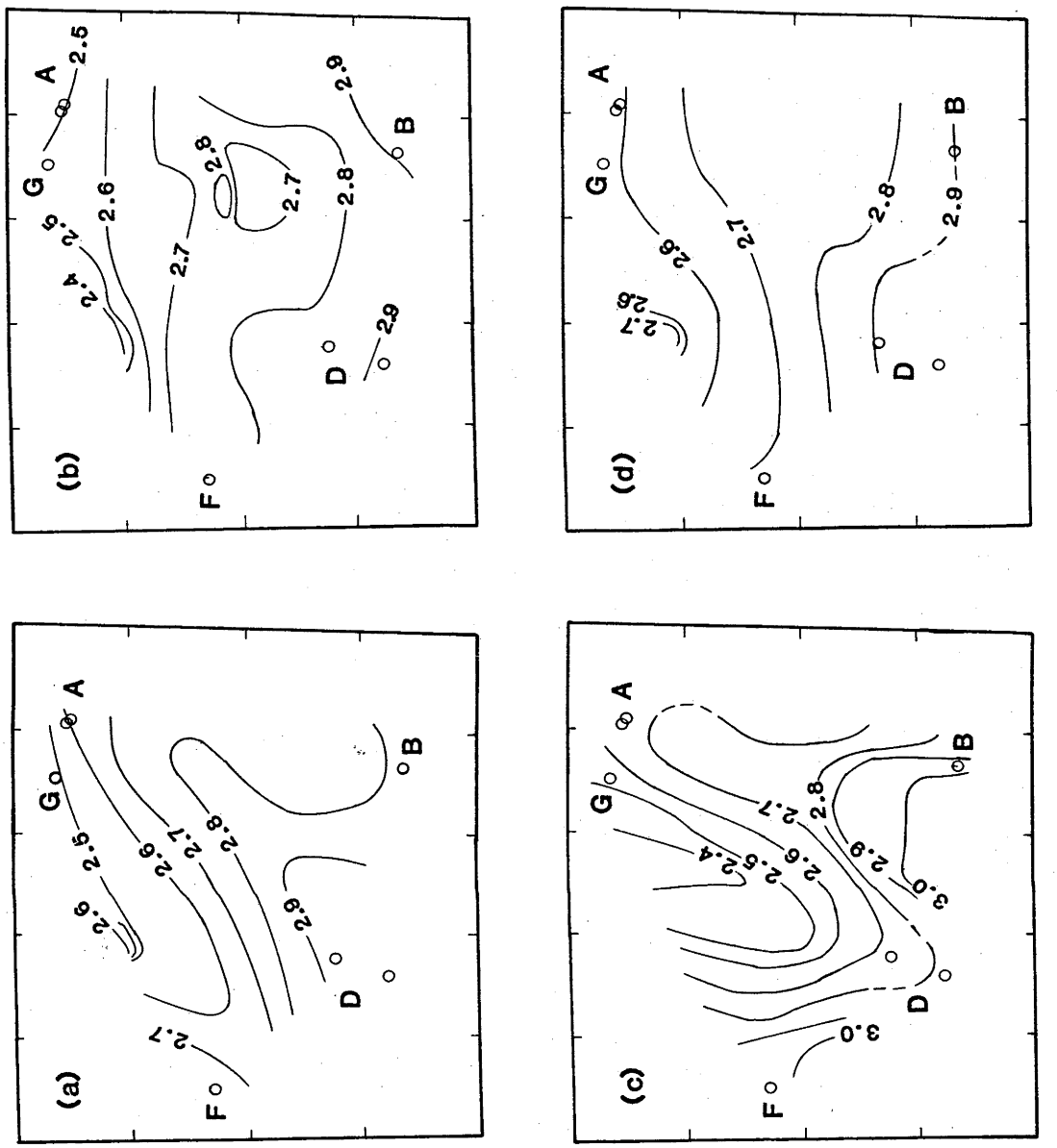

Figure 62. Contours for the uniterated solution for a linear polynomial plus first order double Fourier time term surface with anisotropy, with the axes rotated (a) 0, (b) 30, (c) 60 and (d) 90 degrees clockwise. Contour interval 0.1 s.

TABLE 13: Details of the solutions for time term surfaces.

Solution Number	Description of surface	>2SD	Degrees of Freedom	Variance	V = 7.99 + sin 2θ+	cos 2θ+	sin 4θ+	cos 4θ
1	Linear polynomial, axes at all azimuths	9	178	0.1526	0.2016	0.1241	-0.0959	0.0366
2	Quadratic polynomial, Y axis 30 degrees east of north	10	175	0.4513	0.4122	0.1501	-0.1360	-0.0068
3	Linear polynomial plus double Fourier surface of order 1							
	(a) Y axis 0° E of north	9	174	0.1502	0.2279	0.1222	-0.1002	0.0261
	(b) Y axis 30°E of north	7	174	0.1509	0.2042	0.1407	-0.0997	0.0336
	(c) Y axis 60°E of north	7	174	0.1413	0.1479	0.0977	-0.0813	0.0196
	(d) Y axis 90°E of north	9	174	0.1503	0.2279	0.1223	-0.1002	0.0261
4	Linear polynomial plus double Fourier surface of order 2 Y axis 30° E of north	6	162	0.1028	0.1520	0.1361	-0.0613	0.0260

azimtuhal dependence of Pn travel times in terms of azimuthal variations of velocity.

Raitt & others (1969) introduced the concept of fitting mathematical time term surfaces because many of the recording stations for surveys at sea have only one connection. This is similar to the situation here, where 44 recording stations have only one connection. The advantage of surface fitting is that all data can be used in the inversion. Another advantage is that the number of coefficients required to express the surface is usually much smaller than the number of shot and station time terms, so the number of degrees of freedom is greater.

One disadvantage of surface fitting is that some forms of surfaces, noteably double Fourier surfaces, have azimuthal dependence (Whitten, 1969). This is because the maximum X and Y dimensions of the survey area must be normalised to 2π for double Fourier surfaces, and the maximum X and Y dimensions can change considerably with the orientation of the axes. Tests of azimuthal dependence of various types of surfaces were made by calculating solutions with the axes rotated so that the Y axis was at angles of 0, 30, 60 and 90 degrees east of north. The results are shown in Table 13 and Figures 60 to 63, where all solutions are for a combined offset distance of 80 km. Note also that the azimuth referred to by the term 0 in Table 13 is with respect to north, and not the Y axis of the coordinate system.

All solutions for linear polynomial surfaces are identical; solution 1 in Table 13, shown as a time term contour map in Figure 60, is the solution for the Y axis 30 degrees east of north. Solution 2 is for a quadratic surface, and its large variance is interpreted as indication that the data are not well conditioned for such a surface. Contours of the surface (Figure 61) show the surface as an almost circular depression with very shallow edges. The solution shown has the axes rotated 30 degrees. Solutions for other azimuths are similar.

The four solutions marked 3a, 3b, 3c and 3d in Table 13, shown as contoured time term surfaces in Figures 62a, 62b, 62c and 62d, respectively, are are for linear polynomial plus first order double Fourier surfaces. The solutions have similar variances, and apparently similar anisotropy terms, but the shapes of the surfaces differ. The surface in Figure 62b, that is, for the axes rotated 30 degrees, most closely resembles the surface from the simple time term solution in which anisotropy was included (Figure 58). The surface

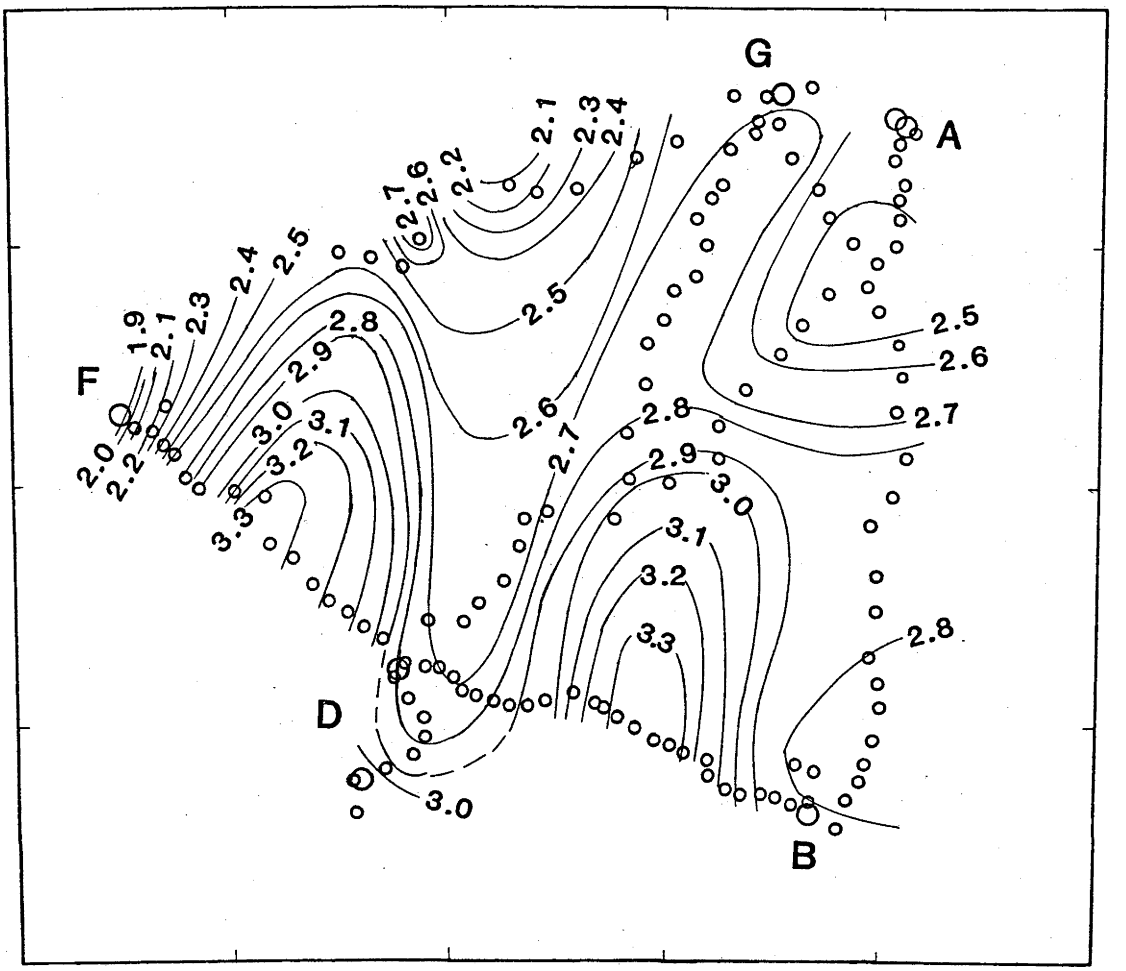

Figure 63. Contours for the uniterated solution for a linear polynomial plus second order double Fourier time term surface with the axes rotated 30 degrees clockwise.

dips south by about 0.5 s of time term. Coincidentally, the axes for this solution are at right angles and parallel to the tectonic azimuth as defined by the axis of the Hamersley Basin. Consequently, all future time term surfaces were calculated with the axes rotated clockwise by 30 degrees.

Intuitively, the linear polynomial plus second order double Fourier surface (solution 4, Table 13, and Figure 63) seems more complicated than the distribution of data would realistically support, with structures in areas where no shotpoints or recording stations were located.

Solutions 13 to 21 in Table 12 are for combinations of linear polynomial plus double Fourier surfaces of order 0, 1 and 2, and combined offset distances of 80, 100 and 120 km. In all cases, the solution variances decreased as the combined offset distances increased, but the number of data points that should have been rejected because their residuals were greater than two standard deviations increased.

Because the decrease in solution variance with increasing combined offset distance was small, and because the number of data with residuals greater than two standard deviations was least for the solutions with the combined offset distances of 80 km, solutions 13 and 16 were chosen for iteration in the fashion described in Appendix 6. The solution for simple time terms with an anisotropic refractor and more than one connection was also to be iterated, and, for consistency, solution 7, with the combined offset distance of 80 km, was chosen.

In all solutions, including those not chosen for iteration, the dip due to the increase in time terms from north to south across the area was less than about 12 km. In the solutions to be iterated, it was about 5 or 6 km. The assumption in the time term method that the slope and curvature of the refractor are small implies that the surface distances between the shots and stations are identical to the distances along the refractor between the feet of the normals from the shots and stations to the refractor. The maximum error from this assumption arises for solutions 1 and 2, and would be about 0.15 km. For every shot/station pair, this is probably less than the combined errors in the positions of the station and the shot. The error will probably leak into the time terms, where it will have an effect of 0.02 s. No iteration of the distance value is therefore necessary in any of the solutions, and the assumption of negligible refractor topography is therefore valid.

TABLE 14: Final time term solutions

Solution Number	Description of solution	Degrees of Freedom	Variance	V = 7.99 + sin 2θ+	cos 2θ+	sin 4θ+	cos 4θ
1	Simple time term with anisotropy ⩾ 2 connections	83	0.0957	0.1075 ±.0070	0.0637 ±.0026	-0.0251 ±.0022	-0.0182 ±.0008
2	Linear polynomial surface	167	0.0969	0.2293 ±.0085	0.1390 ±.0054	-0.0922 ±.0011	0.0595 ±.0027
3	Linear polynomial plus first order double Fourier surface	163	0.0907	0.2481 ±.0064	0.1407 ±.0097	-0.1051 ±.0047	0.0546 ±.0021

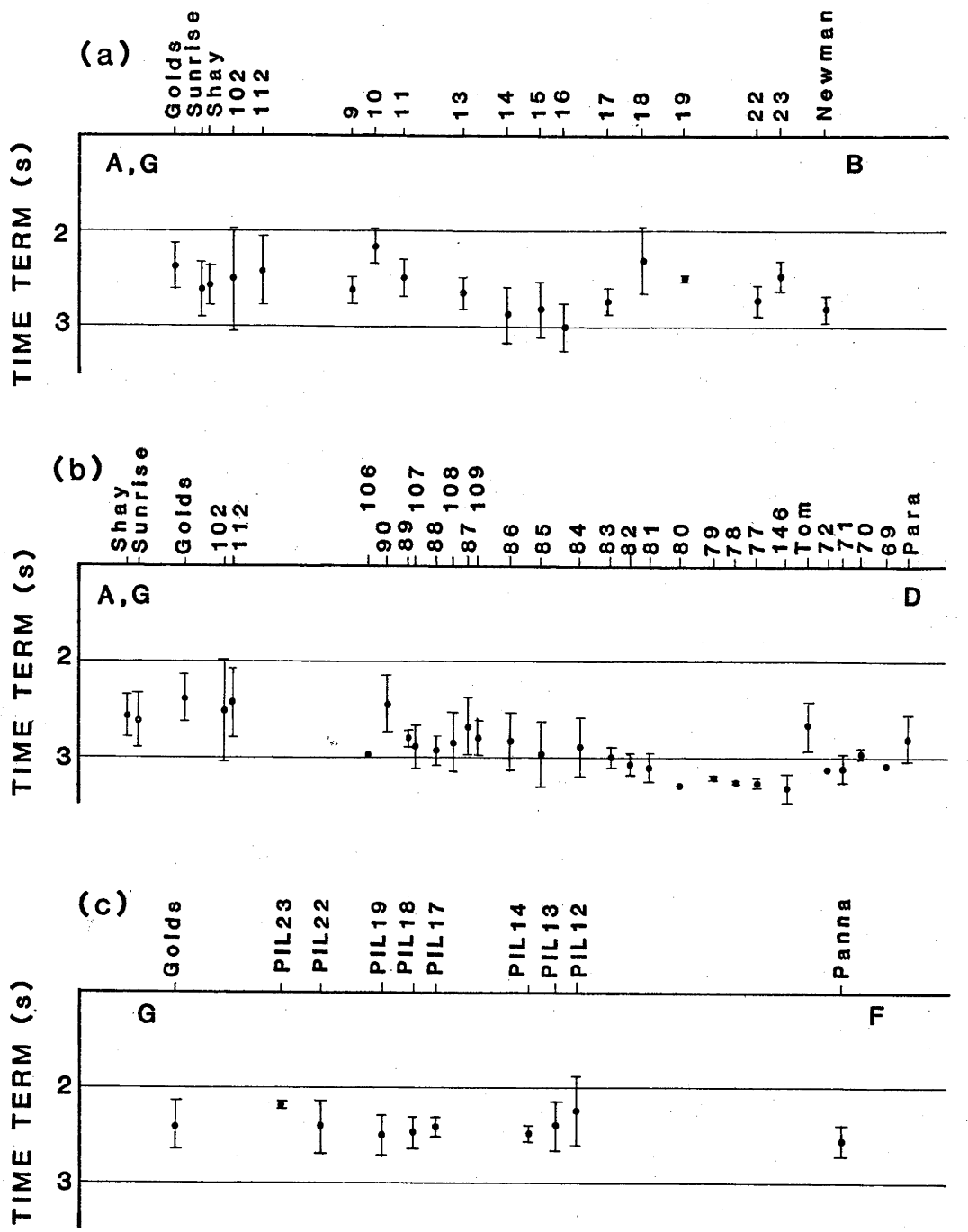

Figure 64. Time term profiles for the solution, after iteration, for simple time terms, with anisotropy, for the stations with more than one connection. Error bars are the RMS residuals.

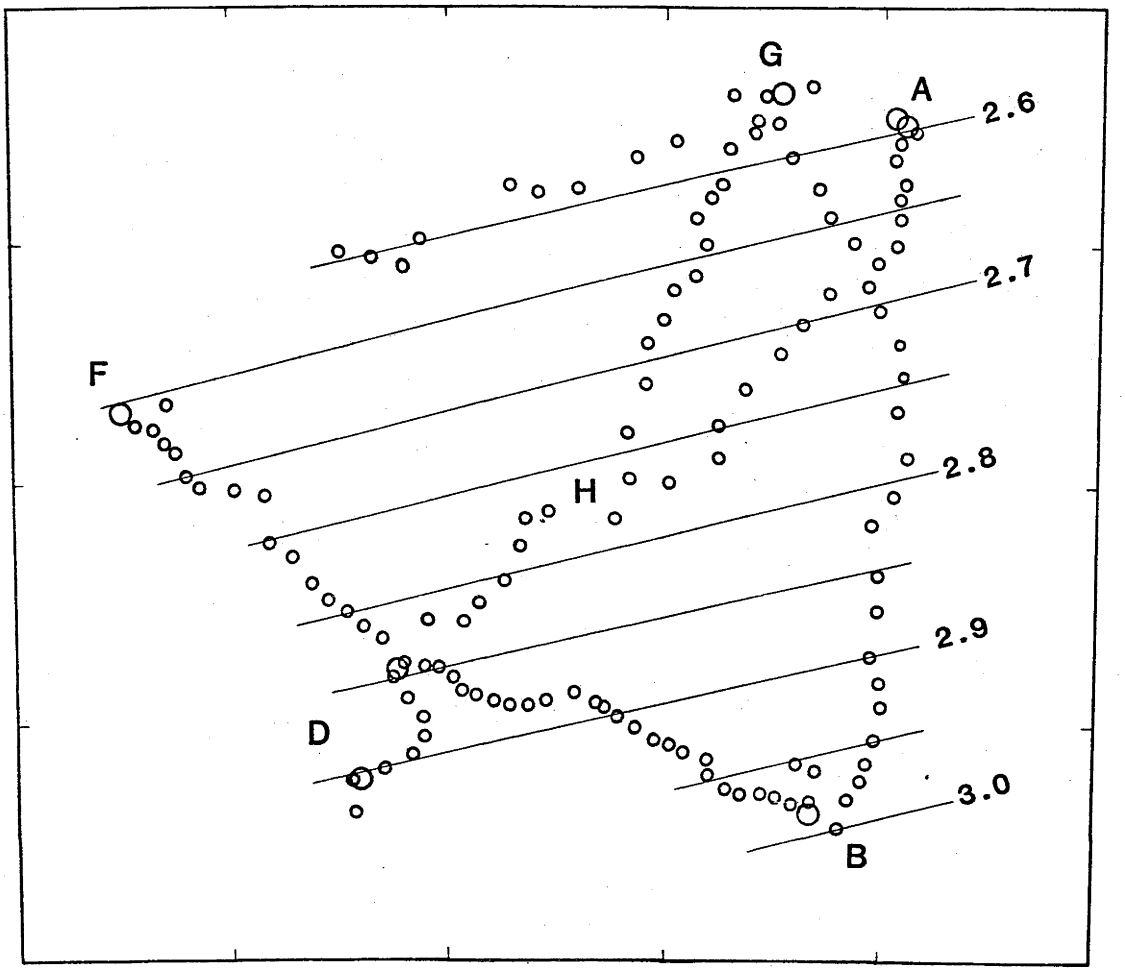

Figure 65. Time term surface for the solution, after iteration, for a linear polynomial surface, with anisotropy. Contour interval 0.05 s.

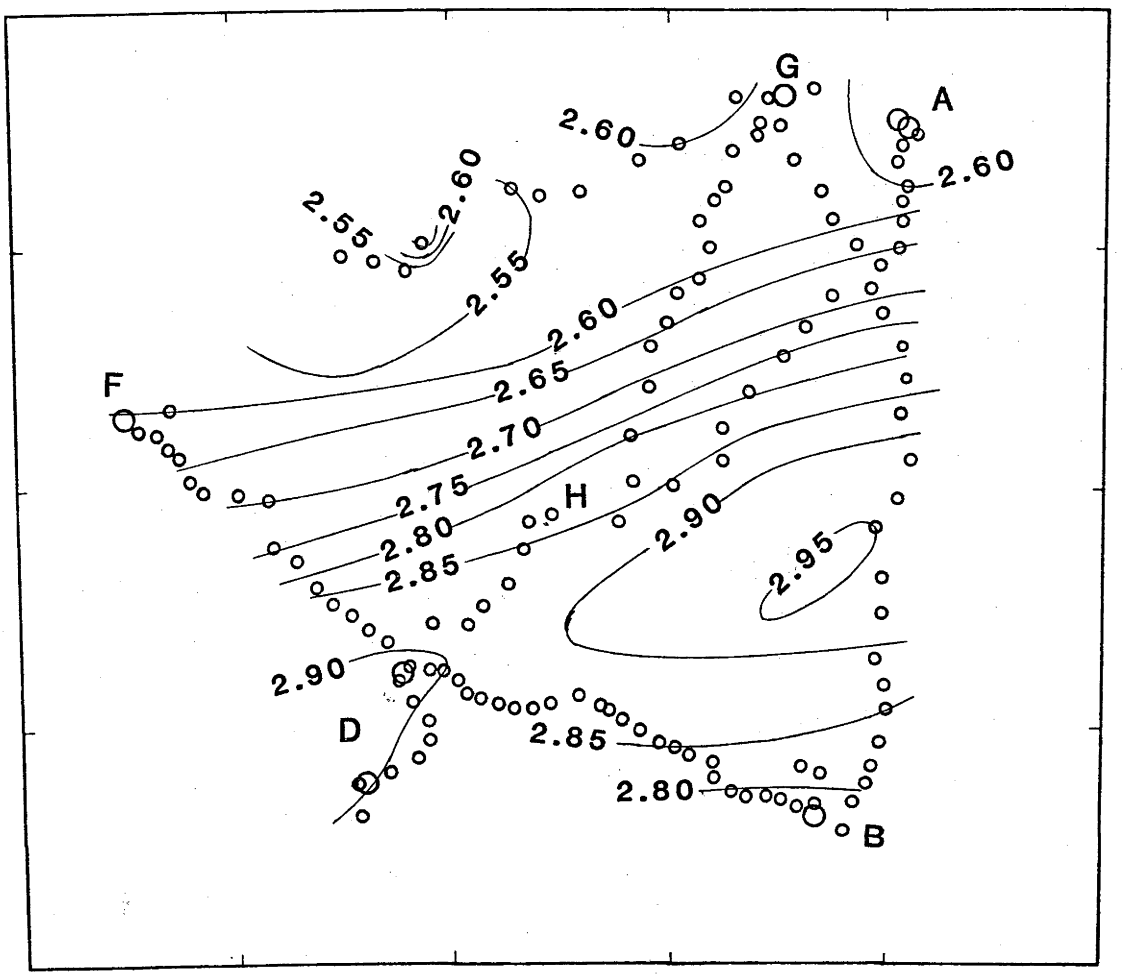

Figure 66. Time term surface for the solution, after iteration, for a linear polynomial plus first order double Fourier surface with the axes rotated 30 degrees clockwise, and with anisotropy. Contour interval 0.05 s.

The other parameter which should be iterated is the combined offset distance. However, the calculation of offset distance is as critically dependent on a knowledge of the velocity structure above the refractor as the calculation of refractor depths, as discussed by Bath (1978). The offset distances were calculated by assuming a two layered crust, with the boundary between the layers at 13 km depth, and the velocities in the layers of 6.15 and and 6.60 km s^{-1}. These are the average velocities in the layers defined by the amplitude studies of Chapter 6. They will give a slight underestimate of the offset distances; however, the offsets calculated using the velocities from the intercept method will be even greater underestimates because the method gives the velocities only in the upper parts of the refractor.

With time-distance data with residuals greater than two standard deviations rejected, only one iteration was necessary to reduce the incremental changes in the iterated offset distances to less than the likely error in their estimation. The details of the final solutions are given in Table 14, which also contains estimates of the standard errors in the anisotropy coefficients.

The final solution for the case of simple time term, with an anisotropic refracting layer, and with all stations with only one connection rejected, is shown in Figure 64 (Table 14, solution 1). The solution is very similar to the uniterated solution (soltuion 7, Table 12). The solutions for the linear polynomial with double Fourier surfaces of order 0 and 1 are shown as as contoured time term surfaces in Figures 65 and 66, respectively (Table 14, solutions 2 & 3, respectively).

The two surface solutions are similar, with the contours trending approximately east northeast to west southwest. Iterating the surface solutions and rejecting loose data therefore rotated the trends of the surfaces as defined by the uniterated solutions, so that the contours now cut the tectonic azimuth at approximately 45 degrees. The dip of the surfaces are about 0.4 s from north to south across the area. This is less than the dip on the model for simple time term and anisotropy in the refractor (solution 1, Table 14).

It must be stressed that all solutions in Tables 12 and 14 have variances that are greater than the estimated error variance of 0.04, although most fall within or very close to the upper limit of the error variance (0.13). The fact that very few data have residuals which fall outside two standard deviations implies to the writer at least that the models are in fairly good agreement with the data.

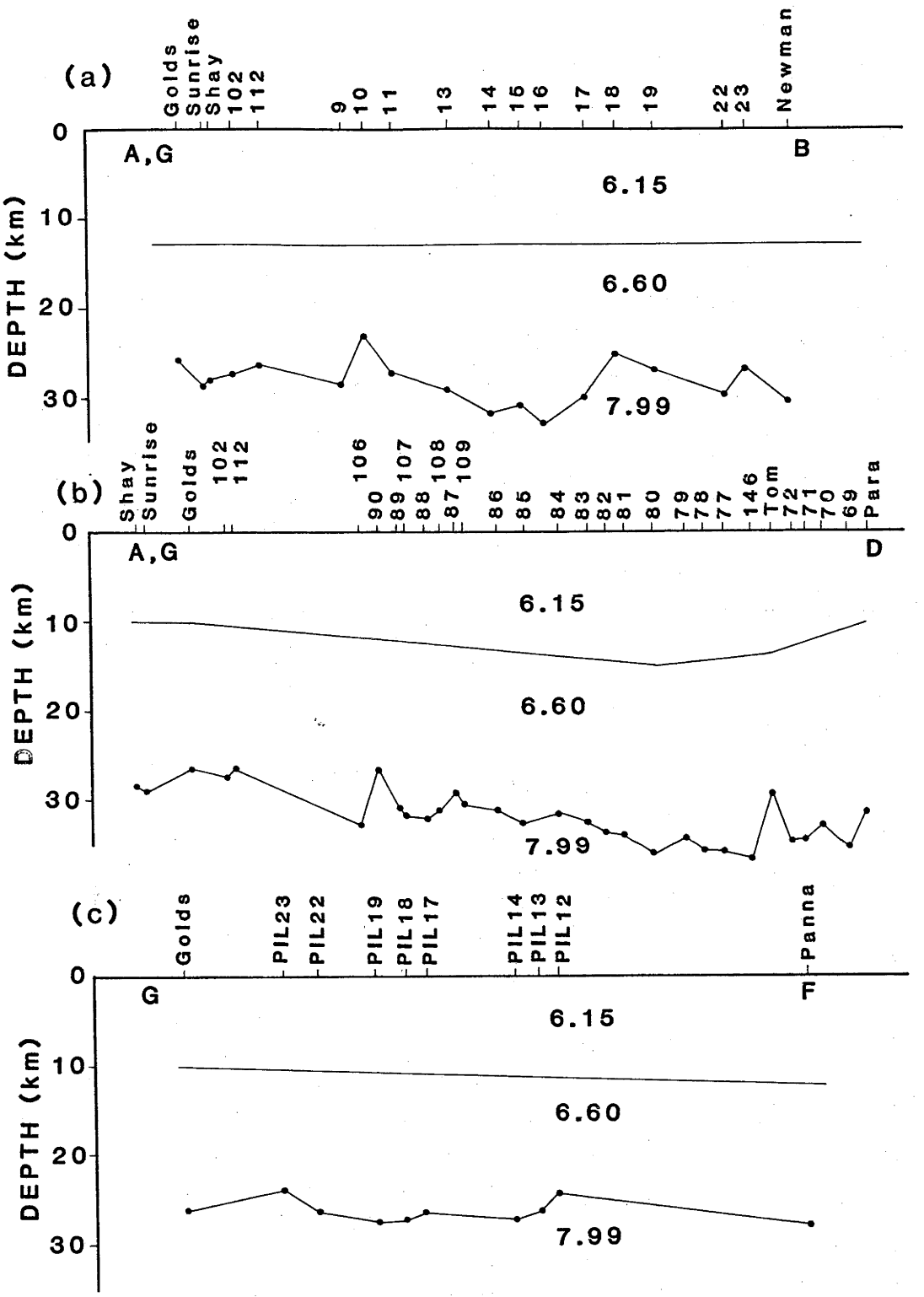

Figure 67. Depth profiles for lines GB, GD and GF. The form of the intra-crustal boundary comes from the intercept method interpretation; the form of the crust/mantle boundary is from the solution for time terms, with anisotropy, for the stations with more than one connection. The crustal velocities are mean values from the velocity/depth models from the amplitude studies.

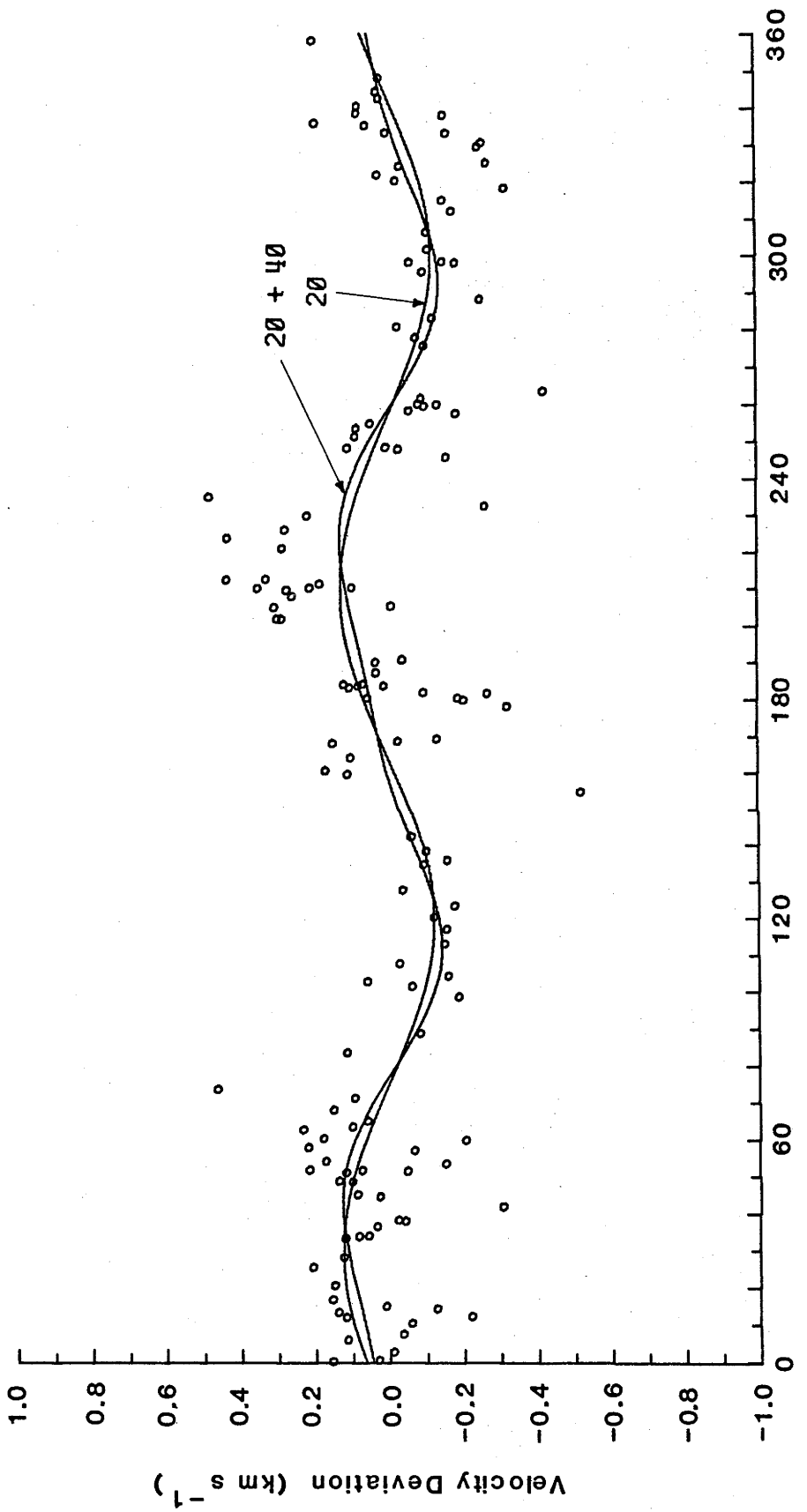

Figure 68. Velocity scattergram for the solution for simple time terms with anisotropy for the stations with more than one connection. The dots represent the velocity perturbation registered by the Pn travel times. The superimposed curves are the variations of the velocity with azimuth (see text for details).

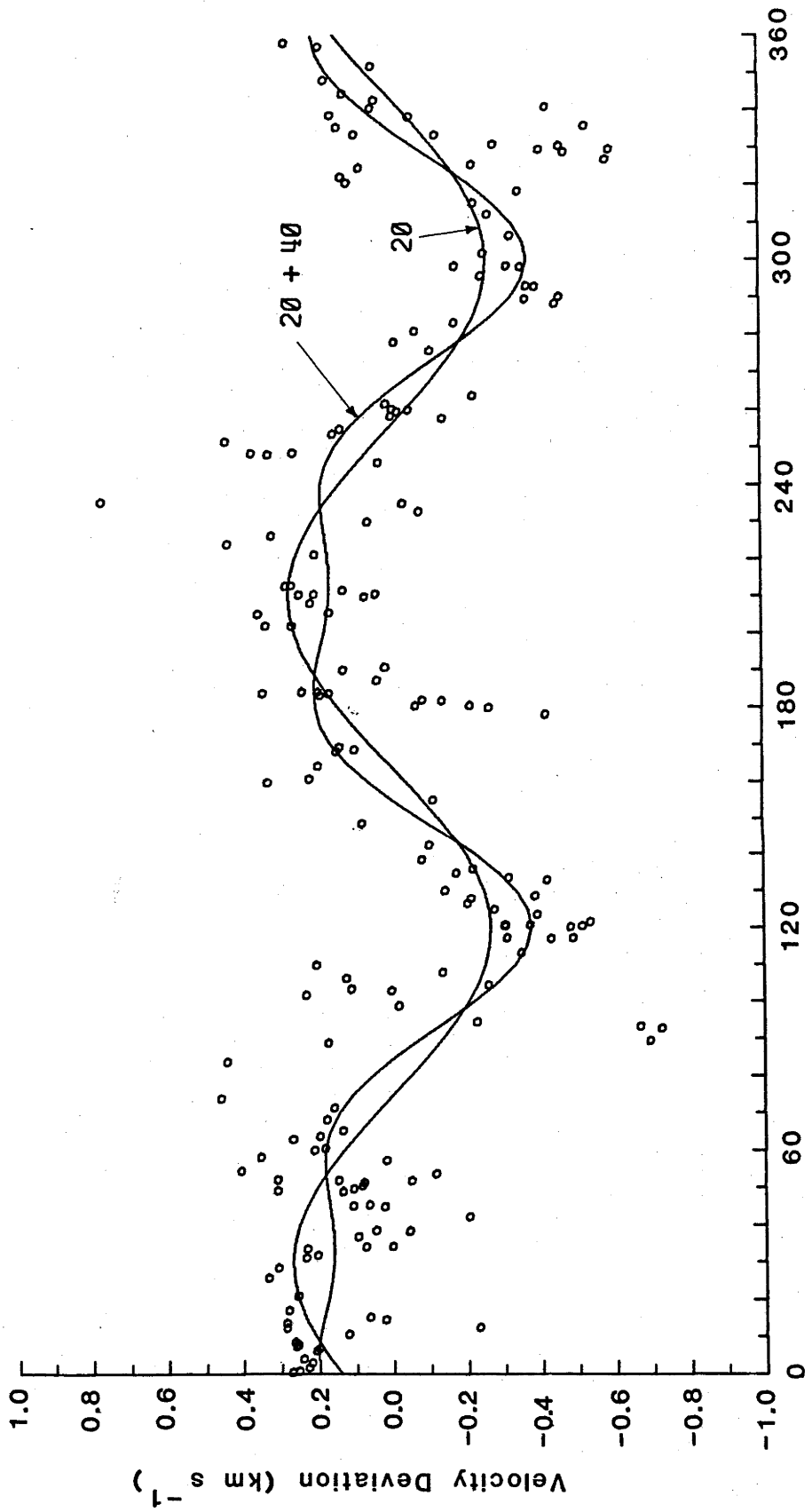

Figure 69. Velocity scattergram for the solution for a linear polynomial time term surface with anisotropy. Details as for Fig. 68.

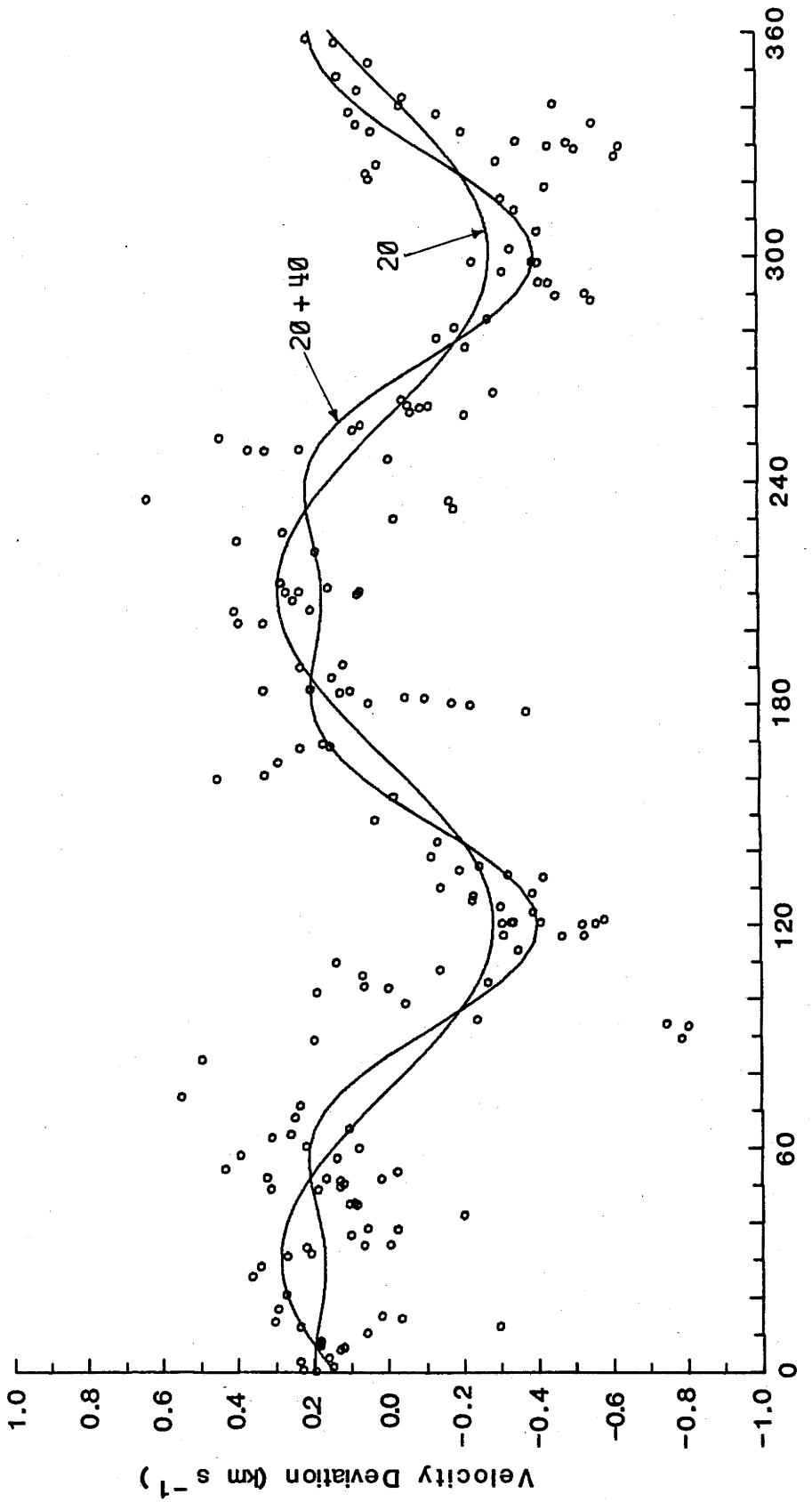

Figure 70. Velocity scattergram for the solution for a linear polynomial plus first order double Fourier time term surface with anisotropy. Details as for Fig. 68.

Statistical F tests between the different solutions generally showed that, with the exceptions of the MOZAIC solutions and the quadratic polynomial surface, all of the solutions were equally good.

The time term profiles in Figure 64 (simple time term with an anisotropic refractor, and with the stations with only one connection rejected) were converted to depths by assuming the depths to the mid-crustal refractor derived from the intercept method interpretation, and the velocities of 6.15 and 6.60 km s^{-1} used before to calculate the offset distances. The depth profiles are shown in Figure 67. The crust between shotpoints A and G and shotpoint B varies between about 25 and 33 km thick, although the surface has considerable topography which may not be real. The profile between shotpoints A and G and shotpoint D dips from about 27 to about 35 km. Note that the trough apparent in the time term profiles in Figure 59, especially between stations 80 and 77 on profile AD is almost completely caused by the depression in the upper crustal layer. The models from the time term interpretation are therefore similar to those from the intercept method interpretation.

Scattergrams (Appendix 6, Section A6.4, Equation 22) were produced for the three iterated solutions (Table 14), and are shown in Figures 68, 69 and 70. The superimposed curves are the azimuthal variations of velocity defined by

$$C'\sin 2\theta + D'\cos 2\theta + E'\sin 4\theta + D'\cos 4\theta,$$

where C', D', E' and F' are the coefficients defined in Table 14 and θ is the azimuth. The solution for all terms, plus that for the 2θ terms only, are shown. The amplitudes of the variations differ between solutions, and is a minimum for the solution for simple time term with anisotropy in the refracting layer and stations with only one connection rejected (Figure 68). This is consistent with the solution having more dip than the surfaces in the other solutions. However, the most significant aspect of the diagram is not the amplitude of the implied anisotropy, but its direction. All solutions have maxima at 30 and 210 degrees. It might be argued that because solution 3 of Table 14 had axes rotated to these azimuths, and because it was dependent on the azimuth of the coordinate system used, this correlation is not significant. However, solutions 1 and 2 in Table 14 are not dependent on the orientation of the axes. Consequently, the highest velocity is perpendicular to the axis of the Hamersley Basin, and the lowest velocity is parallel to its axis.

Thus, although the time term method cannot conclusively prove the existence of anisotropy in Pn under the Pilbara Craton, it certainly shows that anisotropy is a strong probability. The velocity variation may be as much as +0.30 to -0.40 km s^{-1} (Figure 70) or as little as +0.12 to -0.15 km s^{-1} (Figure 68).

7.2 ANISOTROPY IN THE REFRACTOR BELOW THE CRUST/MANTLE BOUNDARY

Anisotropy has been implied in the sub-crustal lithosphere in Europe (Fuchs, 1979). However, the presence of anisotropy is far from certain. The models from several long seismic refraction profiles have high velocity layers interbedded with low velocity layers (Hirn & others, 1973; Ansorge, 1975; Faber & Bamford, 1979; Faber, 1978). Such models do not by themselves imply anisotropy, but the velocities in the high velocitiy layers are much higher than those likely for randomly oriented crystalline aggregates with the mineralogical compositions of the upper mantle. However, single crystals of olivine and pyroxene have considerable seismic anisotropy, with the maximum velocity exceeding that interpreted in the high velocity zones of the sub-crustal lithosphere. Fuchs (1977, 1979) therefore suggested that the high velocity zones were regions where the crystals were aligned with their maximum velocity directions either parallel or sub-parallel to the seismic profile direction. The low velocity zones are presumably regions where they are either aligned in a different direction, or are randomly oriented.

One problem with the European data, admitted by Fuchs (1979), is that the lithospheric profiles from which the data interpreted for anisotropy were gathered are not duplicated with common depth point recordings on other profiles at other azimuths. In the survey area at present under consideration, the system of on-line profiles and fan profiles allows a qualitative analysis of the sub-Moho boundary observed along several azimuths, with several of the fan profiles having common depth points.

The on-line profile on which the sub-Moho boundary was first recognised was from shotpoint G (Goldsworthy) southwards along line GBC (Figure 19). Figure 71 is a record section of traces from a blast at the same shotpoint, but recorded as a fan profile along line BD. The numbers at the bottoms of the traces indicate the order of the recording stations along line BD. Trace 1 is from a station very close to shotpoint B; trace 10 is close to

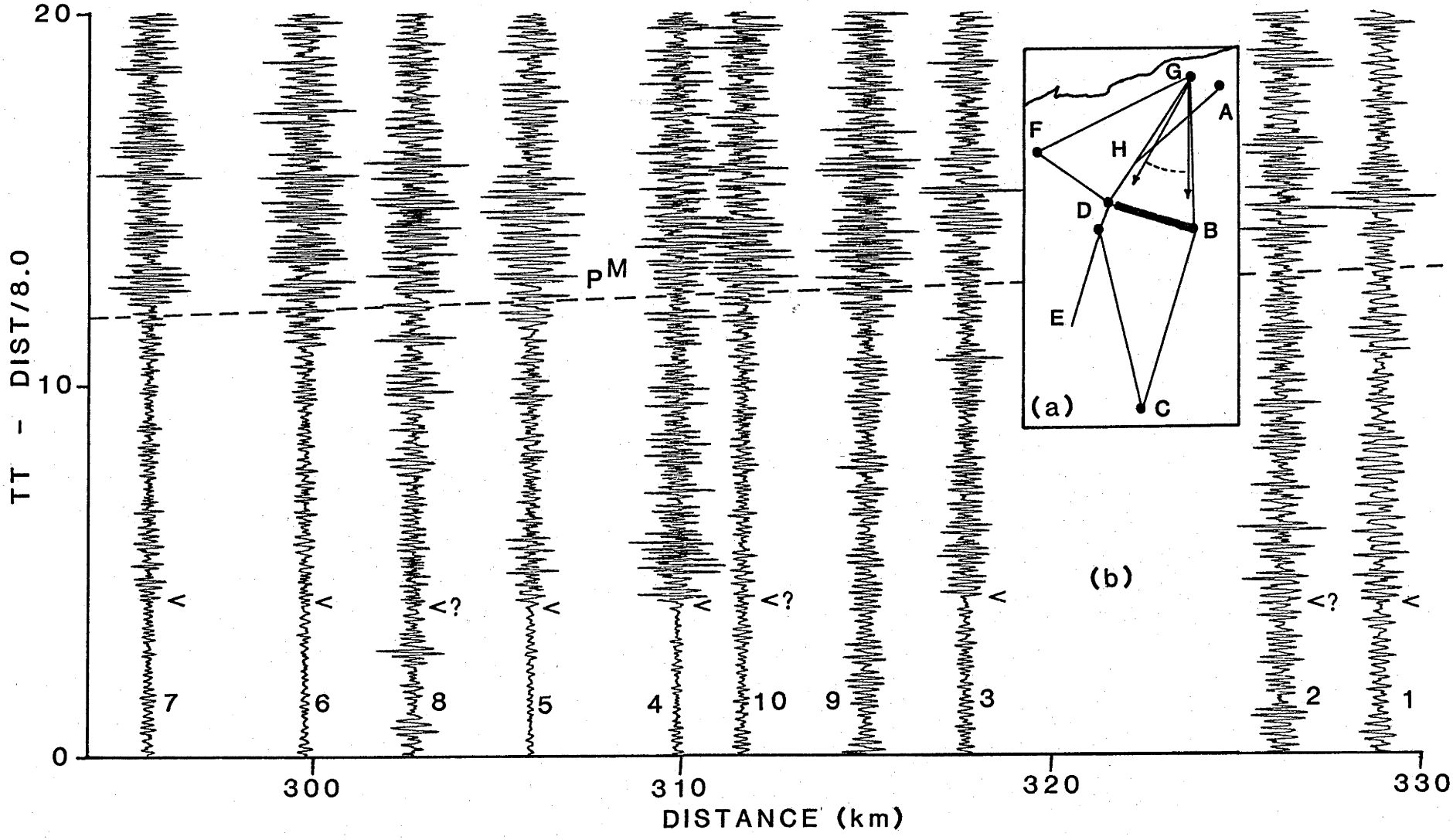

Figure 71. (a) Location diagram for (b) record section of recordings of a blast at shotpoint G (Goldsworthy) to the south along line BD. The numbers at the bottoms traces indicate, in increasing order, the order of the of the stations from B towards D. The arrows indicate interpreted reflections from the sub-Moho boundary.

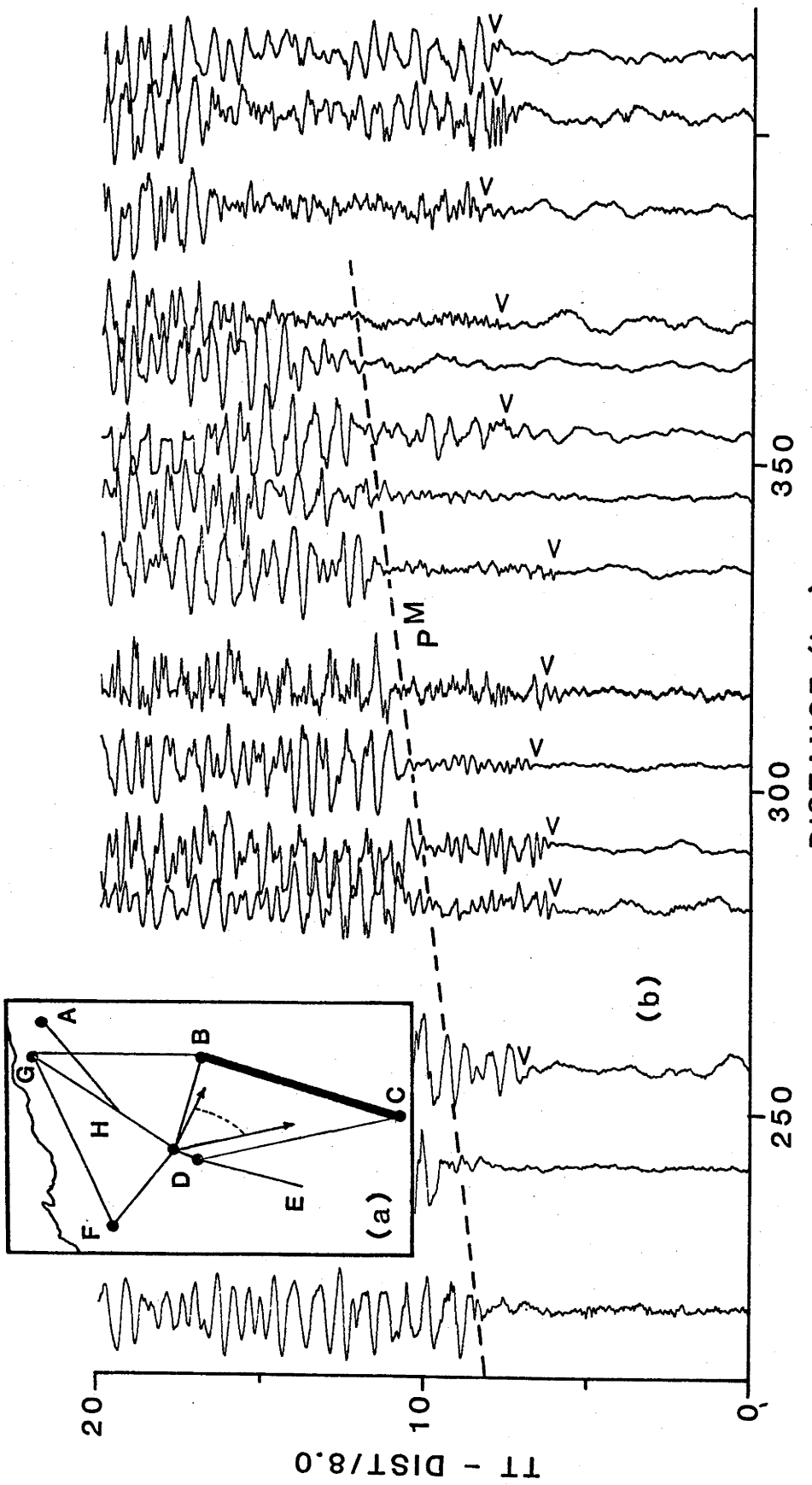

Figure 72. (a) Location diagram for (b) record section of recordings of a blast at shotpoint D (Tom Price) to the southeast along fan profile BC. The arrows indicate interpreted reflections from the sub-Moho boundary.

shotpoint D. The arrivals at about 4 s (marked with an arrow on some traces) are interpreted as reflections off the crust/mantle boundary. The distance range of this record section is small, so it is reasonable to assume that the reflections off the crust/mantle boundary are all of comparable amplitude, and, as most of the trace amplitudes in Figure 71 were set so that the Moho reflections have the same amplitudes, they form a reference on each trace against which the amplitudes of the reflections off the boundary can be compared.

The sub-Moho reflections with the largest amplitudes relative to the crust/mantle boundary reflections are on the traces near the eastern end of the profile (traces 3, 4 & 5), but the amplitudes decrease to the west (traces 6, 7 & 8), and are very small on trace 10. This is confirmed by on-line recordings along profile GDE (Figure 21), where the sub-Moho reflected phase was not observed. Thus, the amplitudes of reflections from the sub-Moho boundary seem azimuth dependent.

Profile GBC is oriented approximately north/south, and in Figure 71 the boundary was observed for ray paths that trend just west of south. They are also observed on profiles that trend to the east of south. In Figure 72, the fan profile from shotpoint D (Tom Price) recorded along line BC shows large amplitude phases at about 6 s reduced travel time preceding the crust/mantle boundary reflections at about 8 to 14 s reduced time. Two factors are worthy of note. Firstly, the reduced times of the reflections from the sub-Moho boundary are about 6 s in the distance range 250 to 310 km, which is 1 to 2 s later than at comparable distances for line GBC (Figure 19) and in Figure 71, which both cross the Pilbara Craton, and secondly, they have an approximate two second delay beyond about 350 km. This implies that the boundary has topography. It must be deeper under the Capricorn Orogen than under the Pilbara Craton, and even deeper under the northern Yilgarn Craton.

The on-line profile GBC was reversed by blasts at shotpoint B (Newman). However, although the reversed record section (Figure 20) has large amplitude Pn arrivals, no large sub-Moho boundary reflections were interpreted. This might be because they were moved beyond the recording distances of this line by the effects of dip or structure, or perhaps the second arrivals which were noted 0.6 s after the Pn arrivals are the reflections, and their apparent velocity was rendered close to that of Pn by the effects of structure.

Figure 73 shows a fan profile from shotpoint B along line DG. The

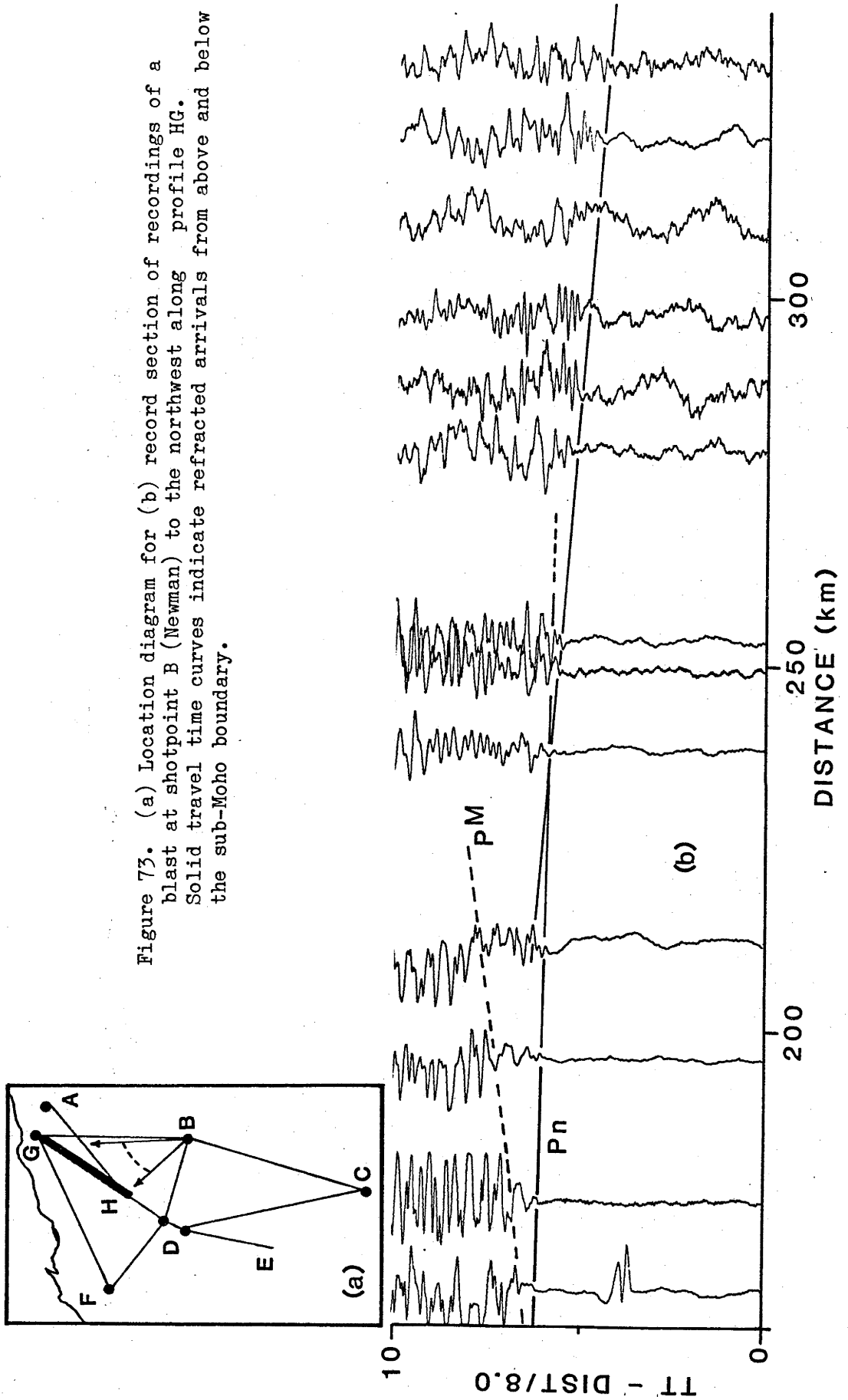

Figure 73. (a) Location diagram for (b) record section of recordings of a blast at shotpoint B (Newman) to the northwest along profile HG. Solid travel time curves indicate refracted arrivals from above and below the sub-Moho boundary.

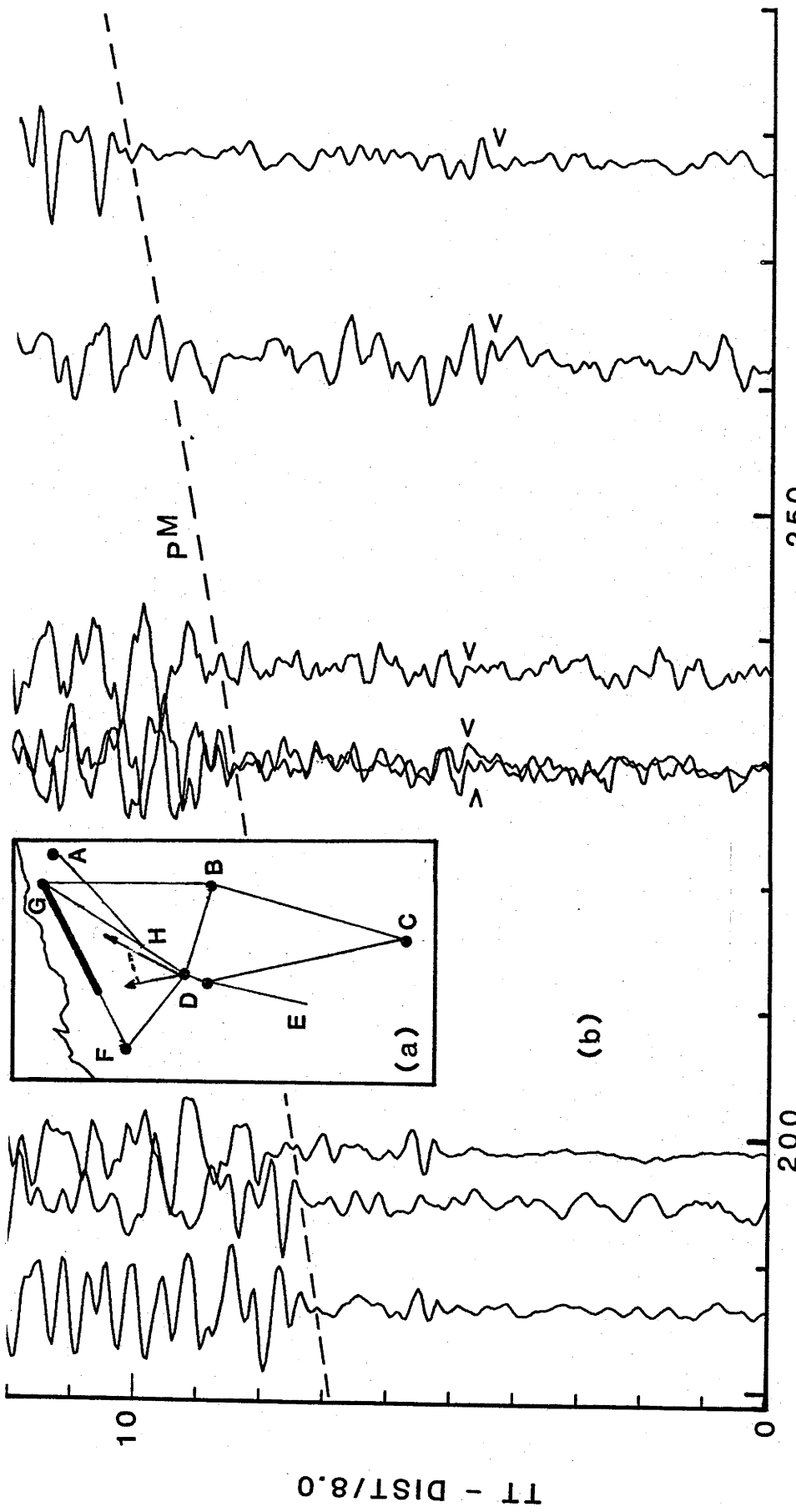

Figure 74. (a) Location diagram for (b) record section of recordings of a blast at shotpoint D(Tom Price) to the northwest along fan profile FG. The arrows indicate the interpreted reflections from the sub-Moho boundary.

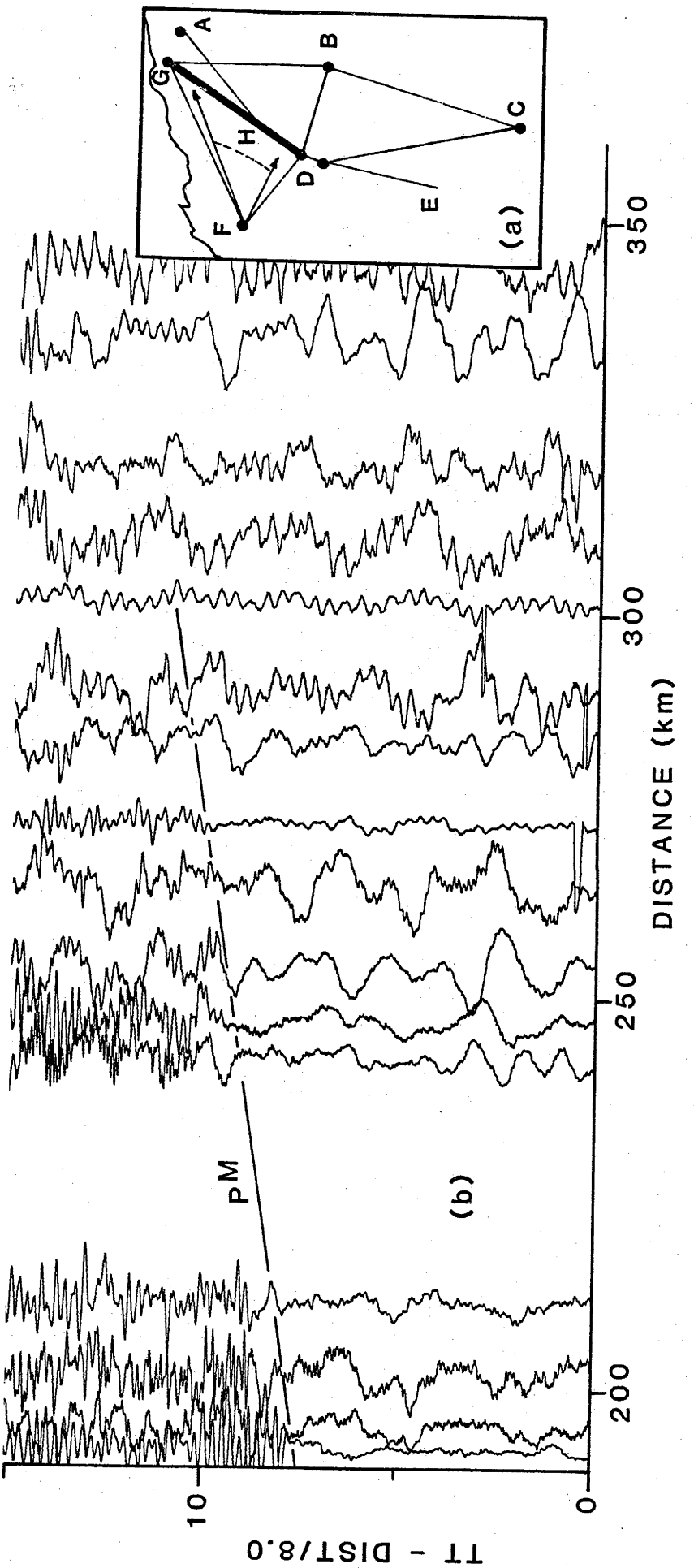

Figure 75. (a) Location diagram for (b) record section of recordings of a blast at shotpoint F (Pannawonica) to the northeast along fan profile DG.

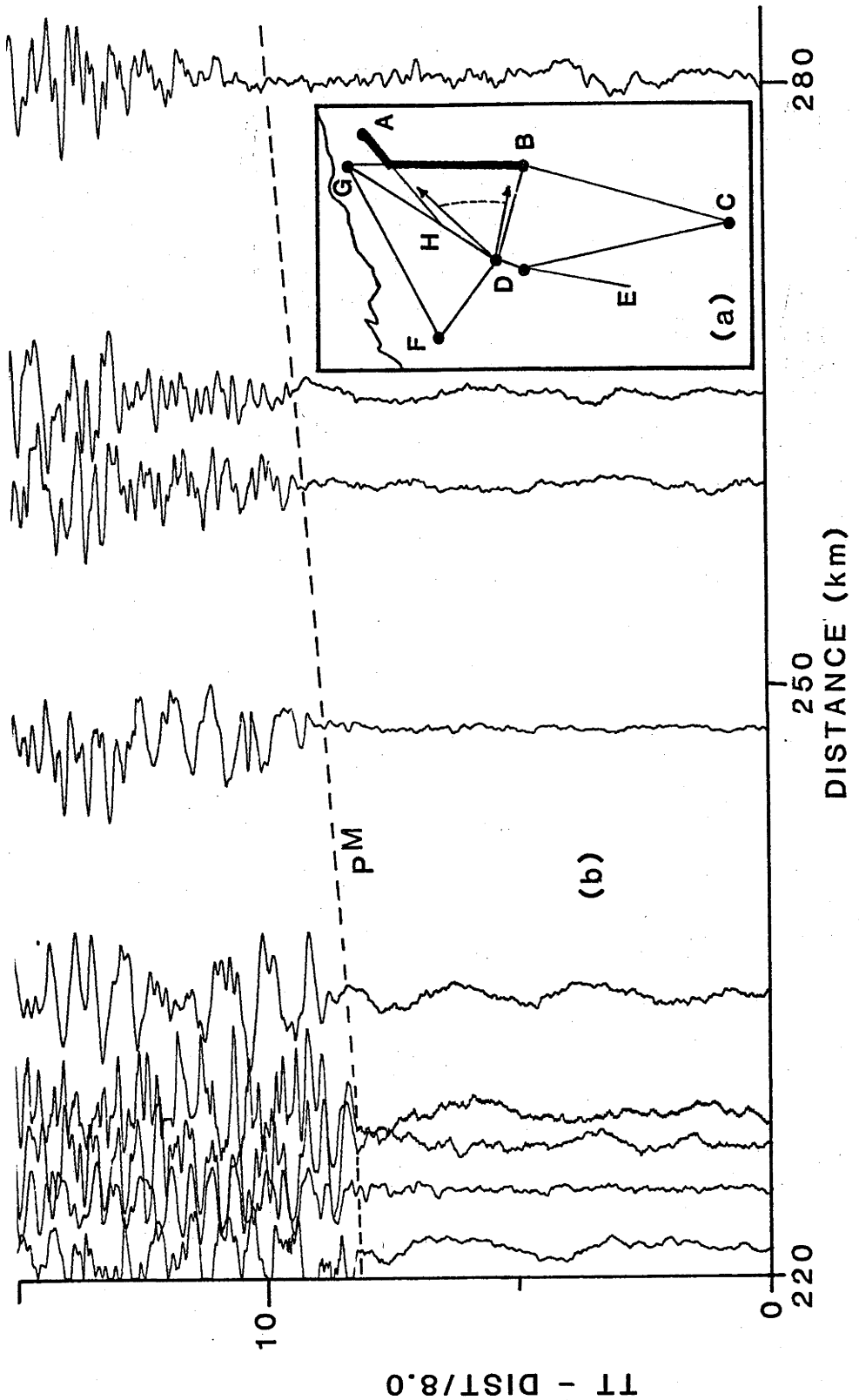

Figure 76. (a) Location diagram for (b) record section of recordings of a blast at shotpoint D (Tom Price) to the northeast along fan profile AB.

stations at smaller distances were close to point H, and those at the greatest distances were near shotpoint G. This profile therefore presents the azimuths immediately to the west of those in Figure 20 for line BG. It shows clearly the reflections off the sub-Moho boundary, and a change in the apparent Pn velocity (of about 8 km s^{-1}) to the much higher apparent velocities of arrivals from below the sub-Moho boundary.

Figure 74 shows traces at about the same range of azimuths for shotpoint D (Tom Price), at stations along the northeastern end of line FG. The arrivals at about 5 s are interpreted as sub-Moho boundary reflections, although this profile is not as convincing as the one in Figure 73.

The above discussion showed that arrivals that can be interpreted as reflections from a sub-Moho boundary were observed on profiles that trend from north/south counterclockwise to about 40 degrees west of north. Profiles at other azimuths show little or no sign of the boundary.

The on-line profiles GDE and FDB (Figures 21 to 25) showed no signs of the sub-Moho boundary. Figure 75 shows the fan profile for shotpoint F northeastwards along line DHG. No large amplitude arrivals are evident in the 4 to 6 s reduced time range. Similarly, Figure 76, for shotpoint D (Tom Price) recorded at similar azimuths along line GB shows no arrivals from the boundary.

Reflections will only be recorded from boundaries that have positive velocity contrasts with the underlying strata. Suppose that the velocity below the sub-Moho boundary is isotropic. The strata above the boundary are probably anisotropic, and the minimum velocity above the reflector, and hence the maximum velocity contrast across the boundary, are likely to occur at an azimuth of 60 degrees west of north. Although the above analysis is qualitative, the direction of maximum velocity contrast appears to be between north and 40 degrees west of north, so the rocks below the lower boundary may also be anisotropic.

The reflections from the sub-Moho boundary will presumably have the greatest amplitudes at those azimuths where the velocity contrasts are maximum. This will depend on the relative directions of the anisotropies above and below the boundary. At one extreme, the range of velocity contrasts will be minimal when the anisotropies are parallel; for the same amount of anisotropy above and below the boundary, there will be no change

of velocity contrast with azimuth. At the other extreme, with the anisotropies perpendicular, the maximum velocity contrast will occur in the direction where the velocity minimum in the upper layer overlies the velocity maximum in the lower layer. The minimum velocity contrast, which could conceivably be negative, ie. a low velocity zone would form, would occur along the azimuth where the maximum velocity in the upper medium overlies the minimum velocity in the lower medium. Such a situation would, for example, explain why Pn arrivals are very weak on some profiles. Between these extremes lies a host of alternatives, some of which could even conceivably alter the apparent directions of maximum and minimum velocities in the lower layer. Hence it is not possible to say with any certainty what the direction of anisotropy is below the sub-Moho boundary, but it appears that the direction of maximum velocity is between 0 and 40 degrees west of north.

Therefore, the conclusions reached in this chapter are twofold. Firstly, anisotropy is likely below the crust/mantle boundary, with the direction of maximum velocity 30 degrees east of north. Secondly, another boundary is present below the crust/mantle boundary, and it probably has both topography and an anisotropic velocity, with the direction of maximum velocity between north and 40 degrees west of north.

8. SHEAR WAVES.

The preceding interpretation considered only compressional waves; no attention was paid to shear waves. This is usually the case with seismic studies of the crust, because the onsets of S-wave arrivals are generally buried in the coda of the foregoing P-waves making the estimation of shear velocities difficult. This chapter looks briefly at the shear waves recorded across the Pilbara Craton, and estimates of the shear velocities within the crust and uppermost mantle of the Pilbara Craton will then be made.

Record sections of shear waves along lines GB, GD and FDB are displayed in Figures 77 to 83. In all of these record sections, the traces were digitally filtered in the bandpass 0.5 to 8.0 Hz and their amplitudes adjusted so that every trace has the same maximum peak to trough amplitude. All record sections have reduced time scales, the velocity used for reduction being 4.6 km s^{-1}. Velocities and intercepts for the refracted waves were scaled from larger versions of these record sections and are listed in Table 15.

Figure 77 depicts the record section of shotpoint G (Goldsworthy) blasts recorded southwards along line GB. The surface waves have a velocity of 3.13 km s^{-1}. The onset times of some Sg phases (arrowed) can be interpreted; the apparent Sg phase velocity is 3.85 km s^{-1}. Clear S^M phases are present, and Sn phases (arrowed, with an asterisk) identified on four traces have an apparent velocity of 4.62 km s^{-1} and an intercept of 9.36 s.

Figure 78 shows the record section of shotpoint B (Newman) blasts recorded along line BG. Phases (arrowed) on traces near 80 and 120 km are colinear with the origin and other phases (arrowed) beyond 270 km. The phases nearer to the shotpoint are identified as Sg and the farther phases as S^I arrivals near the asymptote with the Sg phase. Thus, the upper crustal velocity is estimated to be 3.63 km s^{-1}. Very clear S^M phases are observed. The forward cusp is a bright cusp, and is near 240 km, which is slightly beyond that of the P^M forward cusp which falls near 200 km. Phases (arrowed, with an asterisk) beyond 270 km may be Sn arrivals, in which case the Sn velocity and intercept time are 4.75 km s^{-1} and 10.56 s, respectively. This is consistent with the P-wave data for the same line, in which the Pn velocity northwards is greater than that southwards, and the intercept time for the southern shotpoint is greater than that for the northern shotpoint, implying that the crust/mantle boundary must dip southwards across the Pilbara Craton.

TABLE 15: Shear wave velocities and intercept times

Shotpoint & direction		Line	Phase	Velocity km s^{-1}	Intercept s
G	south	GB	Surface waves	3.13	0.0
G	south	GB	Sg	3.58	0.0
G	south	GB	Sn	4.62	9.36
B	north	BG	Sg	3.63	0.0
B	north	BG	Sn	4.75	10.56
G	south	GD	S^M	3.72	2.0
D (Tom Price)	north	DG	S^M	3.81	2.3
D (Paraburdoo)	north	DG	Sg	3.41	0.0
F	southeast	FDB	Sg	3.59	0.0

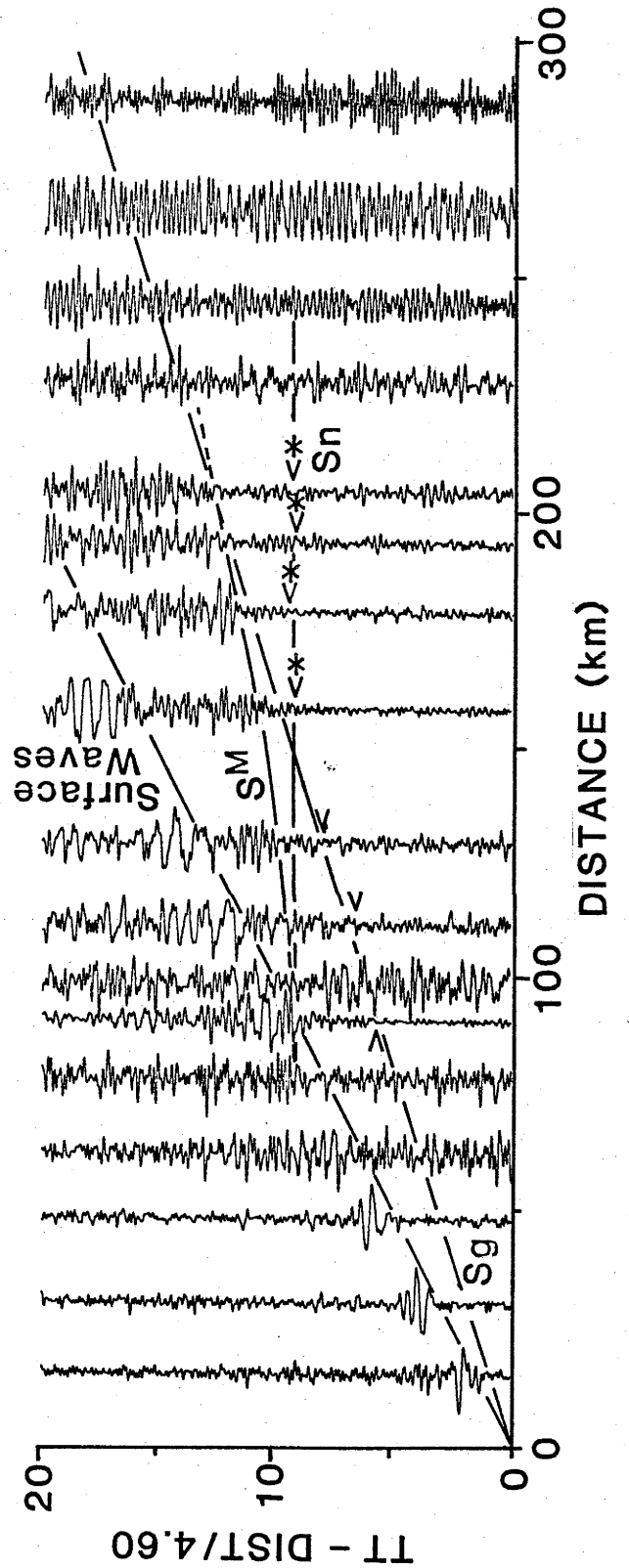

Figure 77. Record section of shear waves from shotpoint G (Goldsworthy), along line GB. Trace normalised, digital filter 0.5 to 8.0 Hz, velocity of reduction 4.6 km s^{-1}.

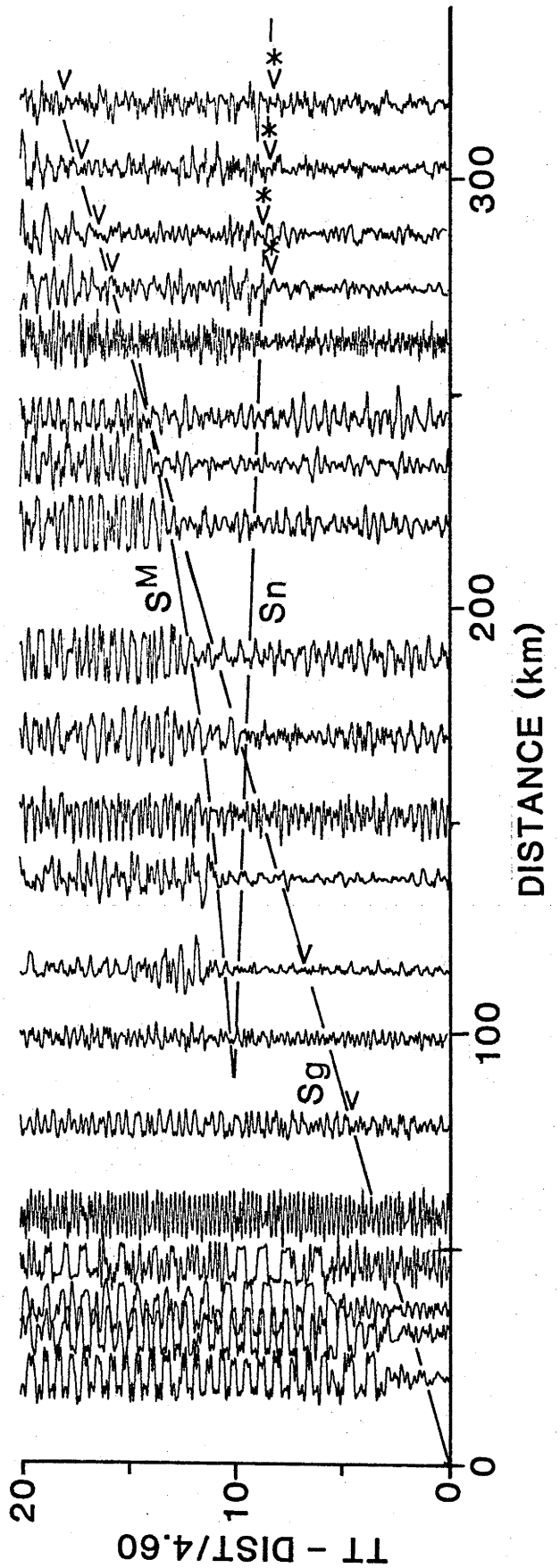

Figure 78. Record section of shear waves from shotpoint B (Newman), along line BG. Trace normalised, digital filter 0.5 to 8.0 Hz, velocity of reduction 4.6 km s^{-1}.

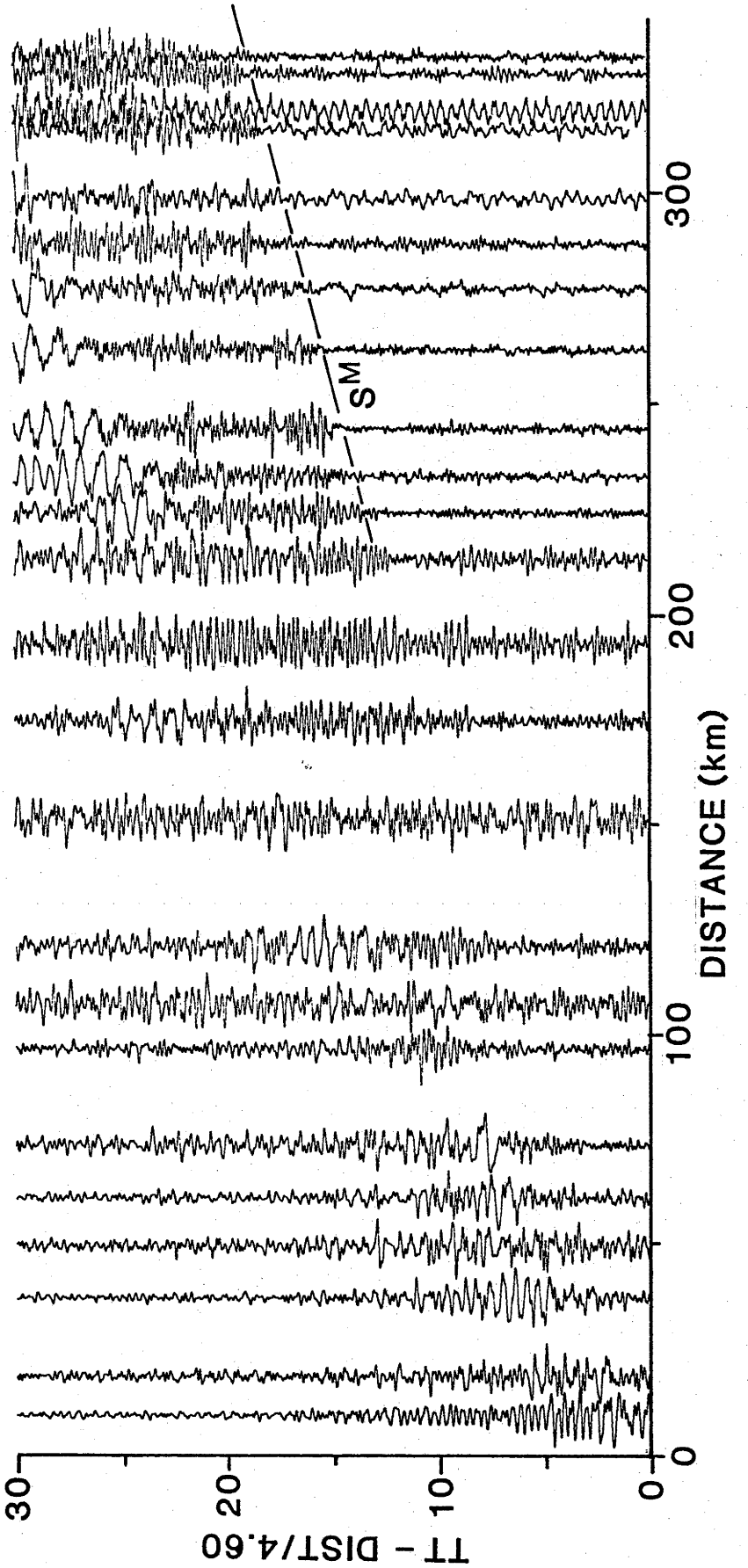

Figure 79. Record section of shear waves from shotpoint G (Goldsworthy), along line GHD. Trace normalised, digital filter 0.5 to 8.0 Hz, velocity of reduction 4.6 km s^{-1}.

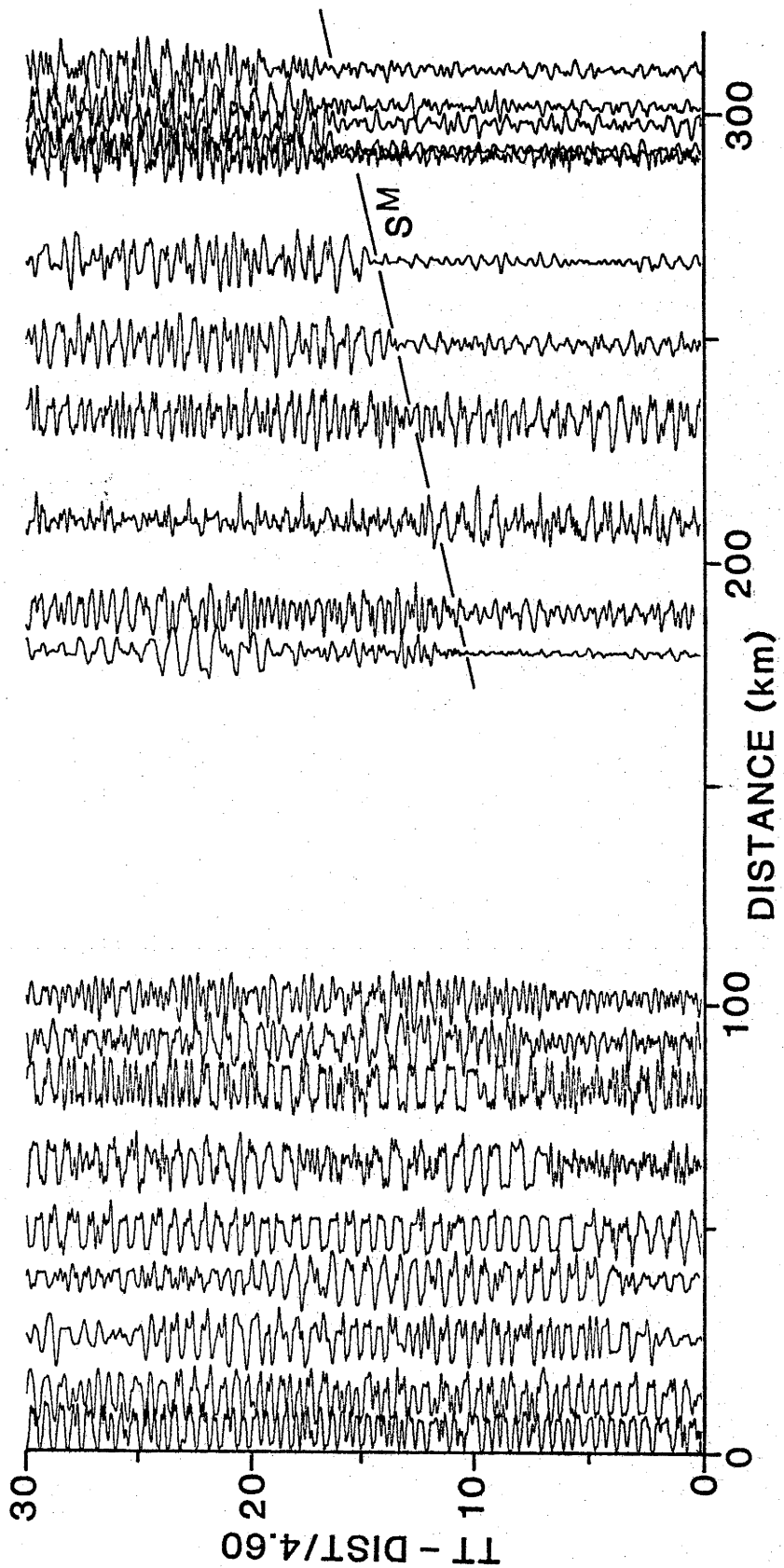

Figure 80. Record section of shear waves from shotpoint D (Tom Price), along line DHG. Trace normalised, digital filter 0.5 to 8.0 Hz, velocity of reduction 4.6 km s^{-1}.

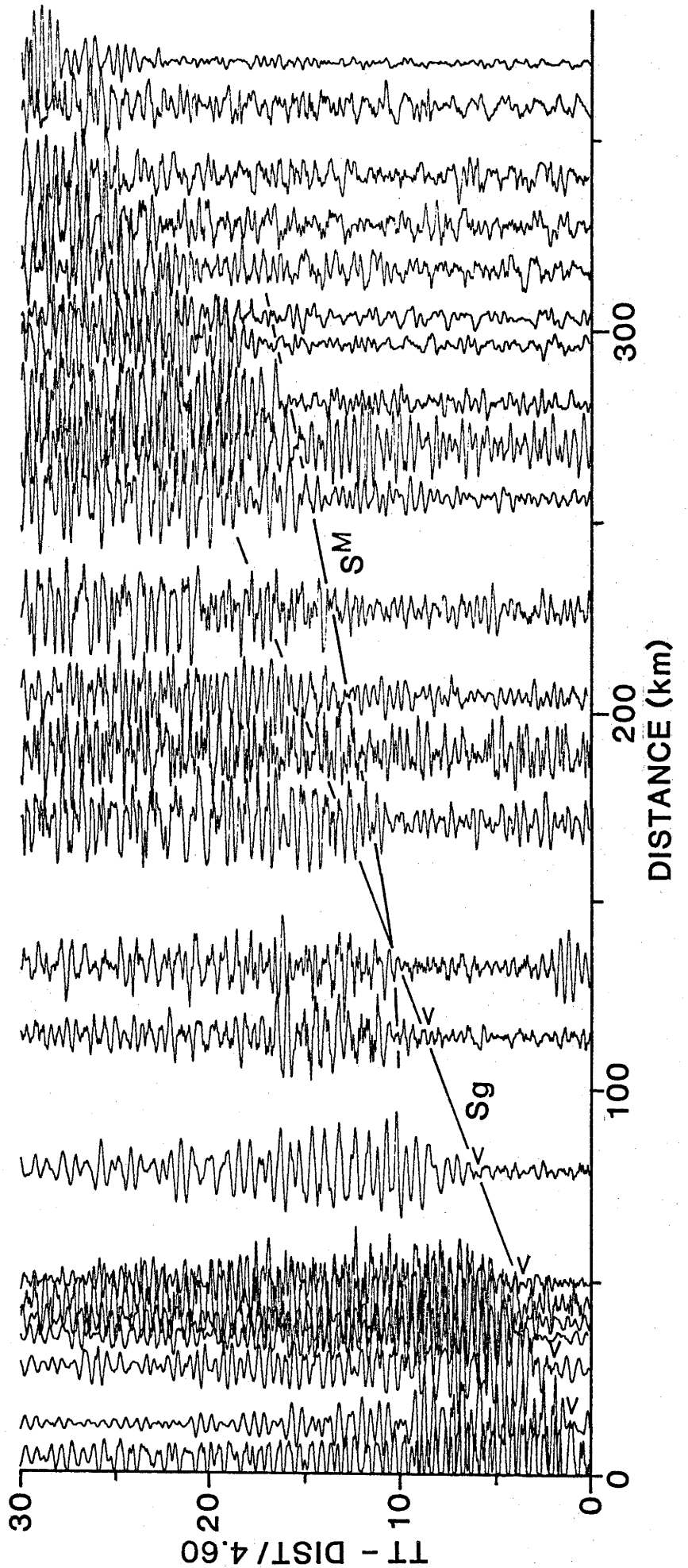

Figure 81. Record section of shear waves from shotpoint D (Paraburdoo), along line DHG. Trace normalised, digital filter 0.5 to 8.0 Hz, velocity of reduction 4.6 km s^{-1}.

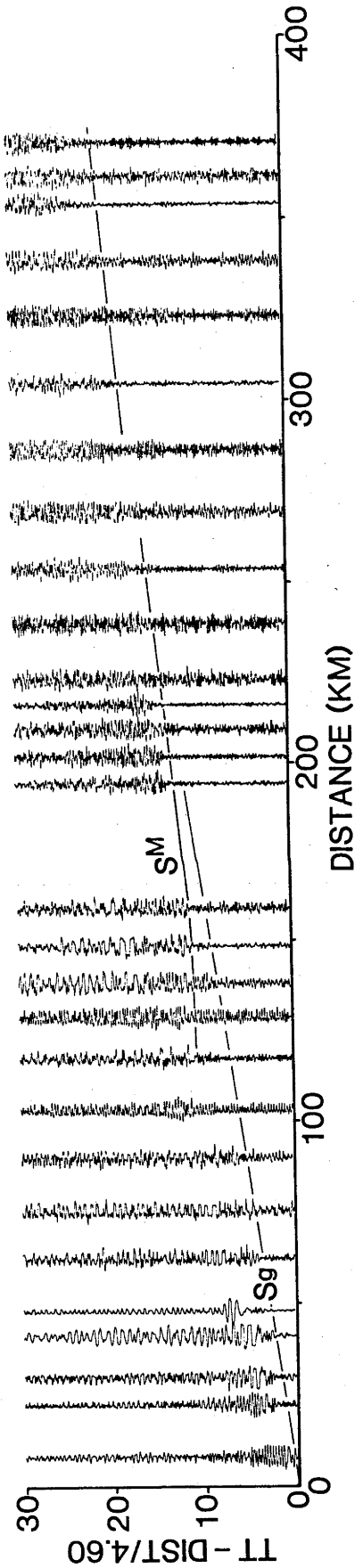

Figure 82. Record section of shear waves from shotpoint F (Pannawonica), along line FDB. Trace normalised, digital filter 0.5 to 8.0 Hz, velocity of reduction 4.6 km s^{-1}.

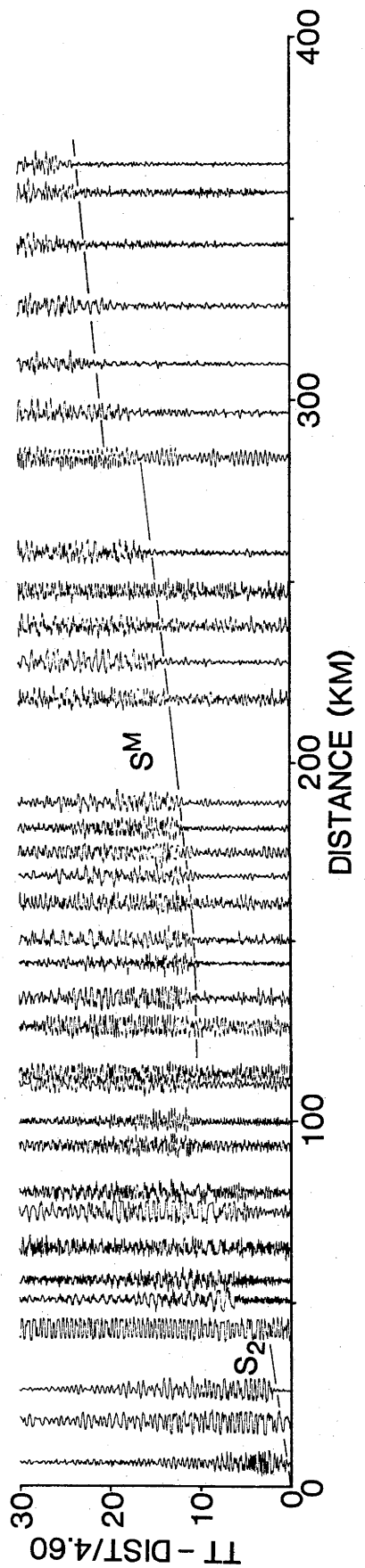

Figure 83. Record section of shear waves from shotpoint B (Newman), along line BDF. Trace normalised, digital filter 0.5 to 8.0 Hz, velocity of reduction 4.6 km s^{-1}.

An alternative interpretation is that these arrivals are reflections off the sub-Moho boundary observed in the P-wave data along the same line for Goldsworthy blasts (Figure 19) but not for Newman blasts (Figure 20).

Figures 79 and 80 show the record sections for shotpoint G (Goldsworthy) and shotpoint D (Tom Price) along line GD. In these record sections, the only correlations that can be made between traces are for phases beyond about 180 km, where, in each record section, phases with apparent velocities of 3.7 to 3.8 km s^{-1} and intercept times near 2 s are observed. The large amplitudes and the intercept times of these phases suggest that they might be S^M phases near the asymptote with the S* phase. If this is so, the S-wave velocity in the lower crust must be about 3.7 to 3.8 km s^{-1}.

Shear waves northwards from shotpoint D (Paraburdoo) along line DG are are shown in Figure 81. Near source Sg phases have an apparent velocity of 3.4 km s^{-1}. Clear S^M phases are also observed.

Figure 82 shows shear waves recorded from shotpoint F (Pannawonica) to the southeast along line FDB. The Sg phase velocity is 3.59 km s^{-1}, and clear S^M phases are also observed. Bundles of energy at 20 to 25 s beyond 300 km are probably the shear wave equivalents of the underside reflections from the Hamersley Basin cover rocks observed in the P-wave data. They are also observed in Figure 83, the record section of shotpoint B (Newman) blasts along the same line reversing the record section in Figure 82. Also observed in Figure 83 are the S_2 phases from within the Hamersley Basin strata. The S_2 phases die out beyond 40 km, indicating that the Hamersley Basin rocks provide a high velocity, upper-crustal lid for S-waves in the same way as they do for P-waves.

The velocities in Table 15 are too poorly constrained to be used to develop a shear wave velocity model for the crust of the Pilbara Craton. However, some generalisations can be made. Apparent shear wave velocities in the upper crust are generally close to 3.6 km s^{-1}, although the value of 3.4 km s^{-1} for Paraburdoo northwards is much lower. In the lower crust, the velocity is between 3.7 and 3.8 km s^{-1}, and an intracrustal shear wave discontinuity seems likely. The reversed Sn velocity along line GB is about 4.7 km s^{-1}. This may not be representative of the isotropic shear wave velocity in the upper mantle under the Pilbara Craton; the reversed P-wave velocity of 8.4 km s^{-1} for the same line is much greater than the isotropic velocity of 7.99 km s^{-1}. Indeed, well constrained estimates of the Sn velocity

from lines GD and FDB could corroborate the Pn anisotropy discussed in the previous chapter. The direction of the maximum Sn velocity should parallel the minimum Pn velocity, and the minimum Sn velocity should parallel the maximum Pn velocity direction (Leven & others, 1981).

9. EVOLUTION OF THE PRECAMBIRAN CRUST OF NORTHWEST AUSTRALIA - CONSTRAINTS FROM THE SEISMIC MODELS.

9.1 CONSTRAINTS FROM THE INTERCEPT METHOD MODELS.

Drummond (1981) combined the crustal models from the intercept method interpretation into a fence diagram, which is shown here as Figure 84. His description and discussion of the models shed some light on some of the tectonic processes active in the Precambrian. Figure 85, which is Figure 11 of Drummond (1981) is a cartoon sketch of a north/south profile through the survey area, and summarises Drummond's (1981) interpretation of the seismic models in terms of the geology. Drummond's (1981) description now follows:

"Pilbara Craton

The Pilbara Craton is 28 km thick in the north and 30-33 km thick in the south, where its boundary with the Capricorn Orogen is interpreted as the zone where the crust thickens sharply to the south. This is about 40 km to the south of the Sylvania Dome in the east, and corresponds to the northern boundary of the Ashburton Trough in the west. The crust/mantle boundary under the craton, therefore, has a dip of slightly less than one degree to the south. The dip is observed on all profiles except FDB, which lies approximately east/west and on which there is no significant dip from the west on the crust/mantle boundary.

An intracrustal boundary is indicated by the increase of seismic velocities from between 6.0-6.2 km s^{-1} to 6.4-6.55 km s^{-1} within the Pilbara Craton. The depth to the boundary varies throughout the region. Drummond (1979b) modelled it as 13 km deep under the eastern Pilbara Craton, but suggested that it could dip from 9 km in the north to 14 km in the south. The latter values are more in agreement with the depths from the central Pilbara Craton (Figure 14a), where the boundary dips from 10 km in the north to 15 km to the south of Tom Price. It shallows to the south of Newman in the east (Figure 6) and between Tom Price and Paraburdoo (Figure 14a). Along the southern edge of the craton, it is deepest between Newman and Tom Price, shallows to 7 km to the west of Tom Price, and then deepens again to 11 km in the west (Figure 10).

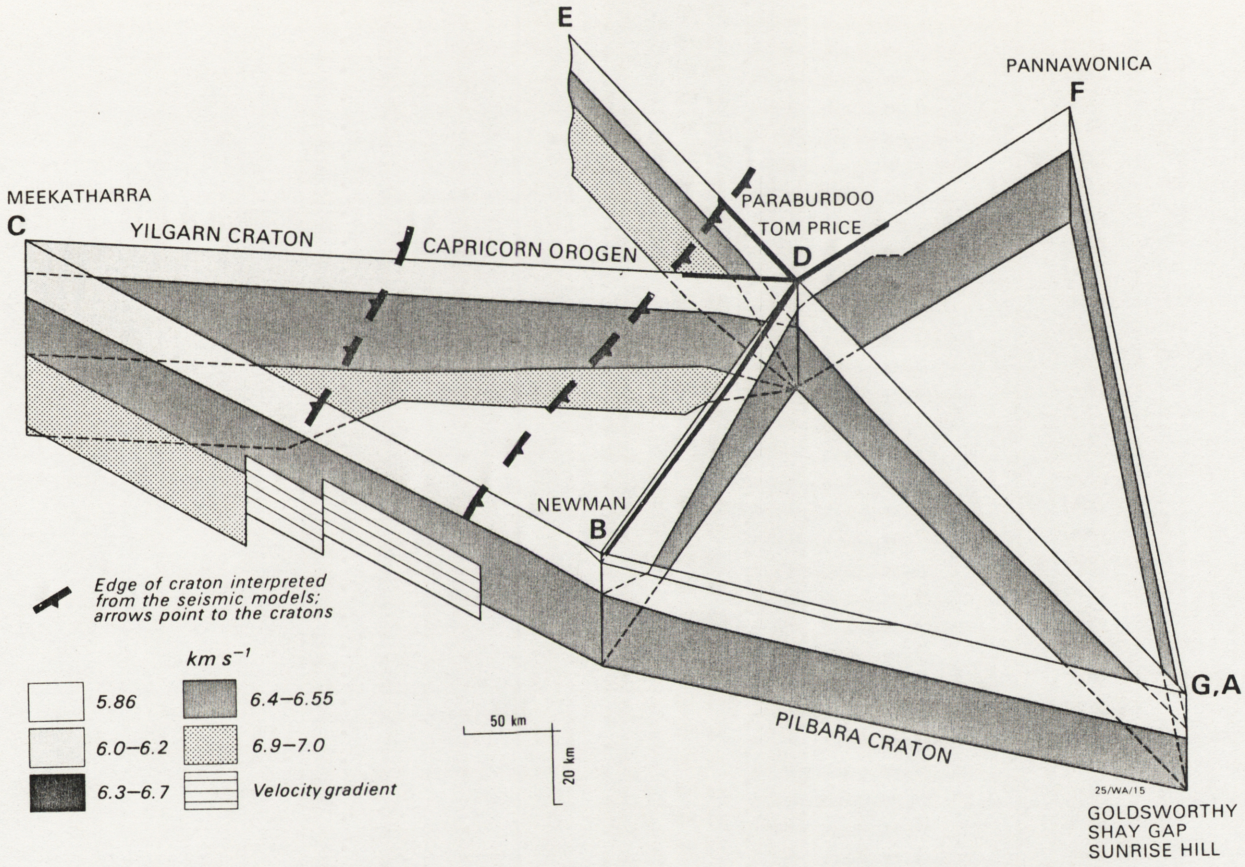

Figure 84. Fence diagram of all of the seismic models from the intercept method interpretation. The interpreted margins of the cratons are based on crustal thickness. The edge of the Pilbara Craton corresponds to the southern margin of thin crust, and the northern edge of the Yilgarn Craton corresponds to the northern margin of thick crust. The Capricorn Orogen between the cratons has crust of intermediate thickness (Drummond, 1981, Figure 10.)

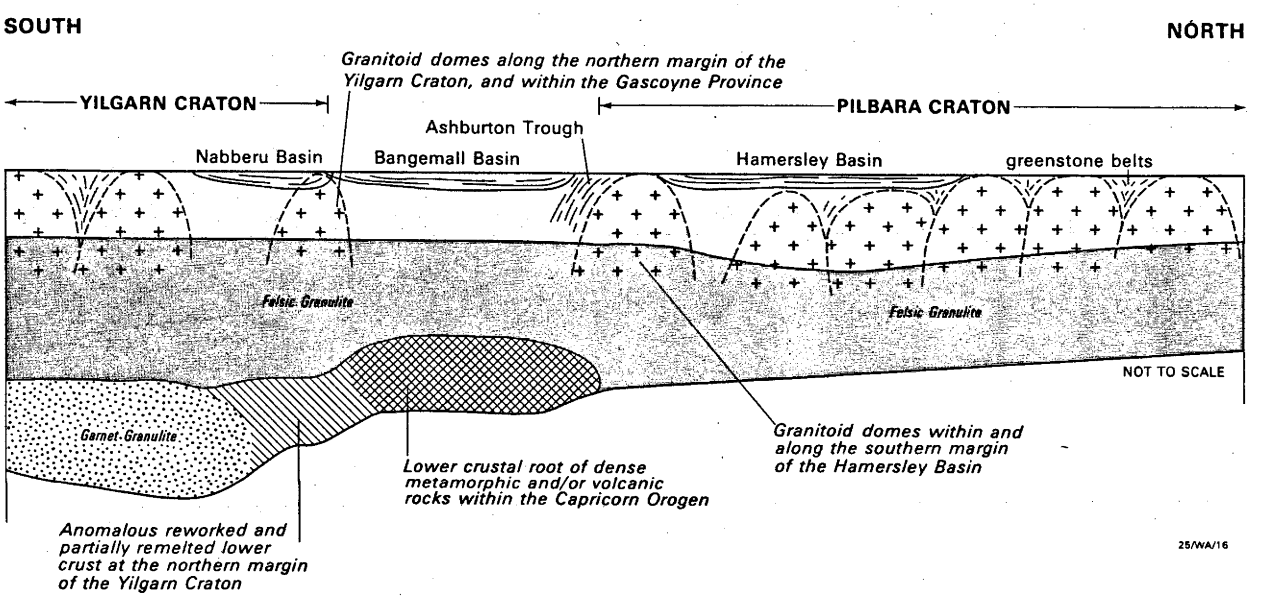

Figure 85. Cartoon sketch of a north/south section of crust through the survey area, in which the seismic models are interpreted in terms of the geology (Drummond, 1981, Figure 11).

Southwards across the Pilbara Craton, the top of the intracrustal boundary defines a basin-like structure with a general southeast/northwest axis. The basin cuts the seismic profiles west of Newman and north of Tom Price. The basin-like structure corresponds to the deepest part of the Hamersley Basin inferred from Trendall's (1975) isopach maps and structural diagrams. Horwitz & Smith (1978) defined an Archaean ridge along the southern edge of the Pilbara Craton which corresponds to the shallowing of the intracrustal boundary south of Newman and south and west of Tom Price.

The highest velocites (6.55 km s^{-1}) observed below the intracrustal boundary occur along the southern basement ridge and the axis of the Hamersley Basin. These velocities are due to the higher metamorphic grades in the lowermost crust, caused by the depression of the crust into higher pressure and temperature regimes during the formation of the Hamersley Basin (Drummond & others, 1981). Uplift occurred after the filling of the Hamersley Basin, and can be divided into two types, regional isostatic rebound and localised diapirism of basement rocks.

Regional isostatic rebound followed the filling of the basin. This can be inferred from the exposure at the surface of some of the stratigraphically lowest members of the Hamersley Basin sequence. As well, R.E. Smith & others (personal communication) used the metamorphic grades mapped at surface exposures to estimate uplifts of 10-12 km west of Tom Price, and 5-7 km, near Newman. The second type of uplift was localised diapirism of basement rocks to form Archaean inliers within the Hammersley Basin. The largest of these is the Sylvania Dome, but several smaller ones are observed or inferred to the west and east of Tom Price. Those near Tom Price correspond to the region where the intracrustal boundary shallows to 7 km depth along profile FDB (Figures 10 and 84).

The diapirism may have been caused by density inversions near the surface. Where rocks of the Hamersley Basin are seismically distinct from the underlying basement rocks, they have velocities which are higher than those of the basement. They are highest in the southeast of the basin. Further west and north, the velocities of the P_1 and P_2 wavegroups

decrease as the metamorphic grade decreases (Drummond & others, 1981), and the basin rocks have not achieved sufficiently high velocities to be seen to be independent of the underlying Archaean basement. Gravity data also infer that the Hamersley Basin rocks are denser than the Archaean Basement (Drummond & Shelley, 1981).

Yilgarn Craton

The crust of the Yilgarn Craton is much thicker (¨50 km) than the crust of the Pilbara Craton, and extends further north than the area mapped by Gee (1979b) as the Yilgarn Block. Intracrustal seismic boundaries occur at 10-16 km and at 32 km depth.

In the Proterozoic, the northern limit of the stable Yilgarn Craton was probably just south of the present day northern edge of the Nabberu Basin. A zone along the northern edge of the Yilgarn Craton, where the crustal thickness is intermediate between that of the Yilgarn Craton and the thinner crust of the Capricorn Orogen, probably represents part of the northern Yilgarn Craton which was reworked by tectonism in the Proterozoic. It corresponds to a large, negative gravity anomaly to the north of the Yilgarn Block. Fraser (1973) suggested that the anomaly was too intense to be purely a gravity edge effect of the Yilgarn Craton, and Horwitz & Smith (1978) correlated it with 'certain granitic and metamorphic rocks of the Gascoyne Province'.

The area contains, in the Gascoyne Province, granitoid intrusions, which have been interpreted as remelted basement and younger sediments (de Laeter, 1976; Williams & others, 1978), and, further east, the Marymia Dome at the northern edge of the Nabberu Basin. It also includes the northwestern part of the Nabberu Basin, where the sedimentary rocks and underlying basement were intensely deformed (Hall & Goode, 1978). The southern belt of stable basement in the western Bangemall Basin falls within and marks the northern limit of this zone.

Capricorn Orogen

No shotpoints were located in the Bangemall Basin or Ashburton Trough, and because the basin and trough rocks do not cause any noticeable deviation of the travel-times from those expected from normal crystalline basement, no estimate of the present day basin and trough thickness is possible.

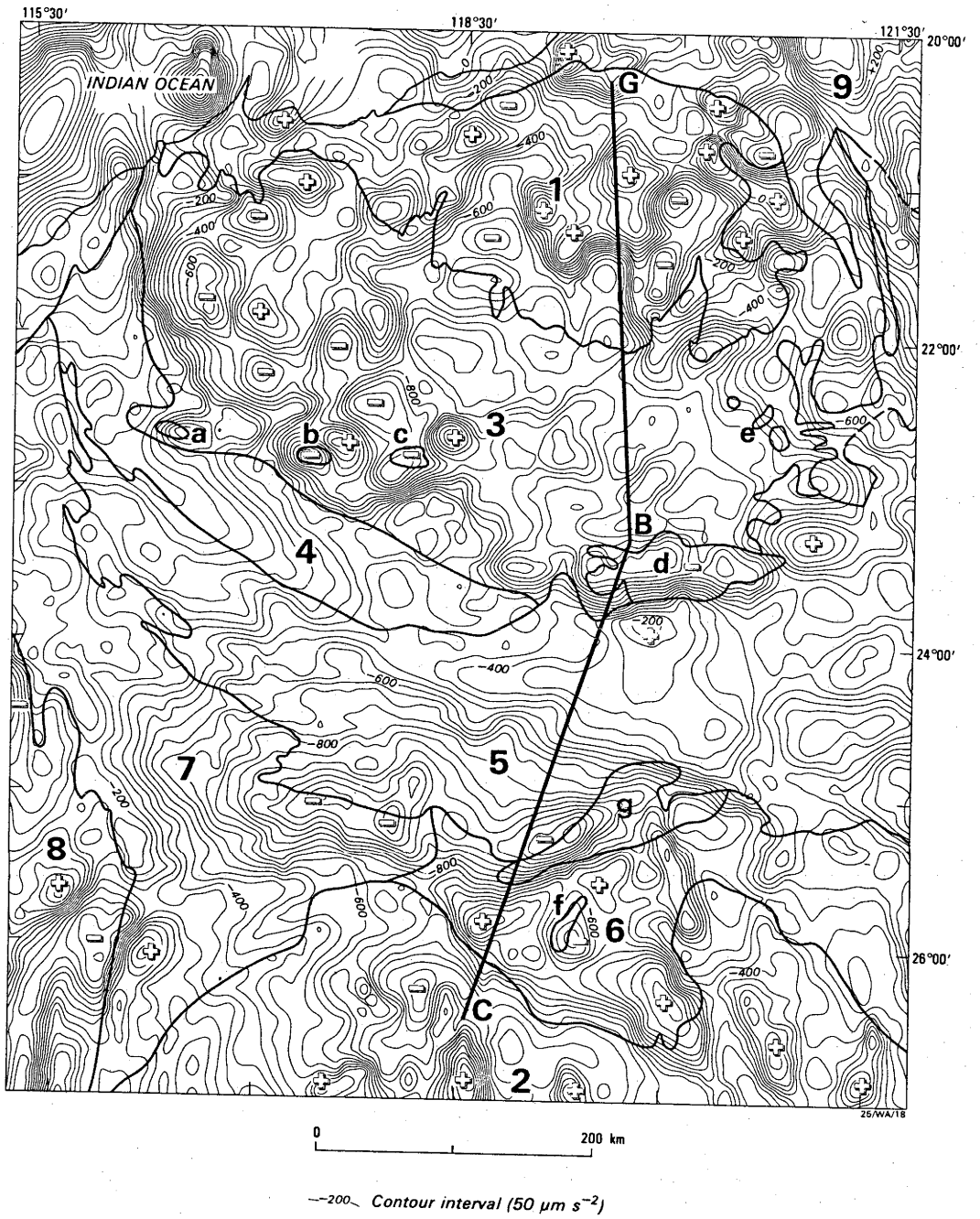

Figure 86. Simple Bouguer gravity map (Bouguer density 2.67 t m^{-3}) onshore and free-air gravity map offshore, with the geology superimposed. The geological provinces are: 1. Pilbara Block; 2. Yilgarn Block; 3. Hamersley Basin; 4. Ashburton Trough; 5. Bangemall Basin; 6. Nabberu Basin; 7. Gascoyne Province; 8. Carnarvon Basin; and 9. Canning Basin. The Archaean domes marked in the Proterozoic basins are: a. Wyloo Dome; b. Rocklea Dome; c. Milli Milli Dome; d. Sylvania Dome; e. Rat Hill Anticline; f. Goodwin Dome; and g. Marymia Dome.
G. Goldsworthy; B. Newman; C, Meekatharra (Drummond & Shelley, 1981, Figure 1).

The lower crust in the Capricorn Orogen is characterised by high velocities and, by inference, dense rocks. Wellman (1978) attributed the denser crust in the orogen to higher metamorphic grades. Horwitz & Smith (1978) favoured an evolutionary model for the orogen, in which the Pilbara and Yilgarn Cratons were welded into a stable basement by the end of the Archaean and then rifted to form the Capricorn Orogen. From the gravity map (BMR, 1975), they inferred dense lower crust in the orogen, and attributed it to intrusions of basic magmas into the lower crust during the rifting. However, the intrusions could also have occurred if the cratons had not been welded, but had been free to move relative to each other to relieve the stresses which must have build up during tectonism."

9.2 FURTHER CONSTRAINTS WHEN THE GRAVITY FIELD IS CONSIDERED.

9.2.1 The Gravity Field.

The gravity field of the region gives further control on the nature of the crust and upper mantle when it is considered with the seismic models from the intercept method interpretation. The gravity coverage of the region consists of readings on a 11 km grid (Fraser, 1979a; 1979b), and road and helicopter traverses with a station spacing of 1 to 4 km, shown in Figure 1, and described by McCracken (in Drummond, 1979c). The Bouguer anomaly map of the region is shown in Figure 86.

Fraser (1979a; 1979b) gave a qualitative description of the short wavelength features of the gravity field. The contour pattern on the Pilbara and Yilgarn Blocks reflects the granitoid/greenstone stratigraphy. Gravity highs correspond to greenstone belts and gravity lows to granitoid domes, and the regions of highest gradient between highs and lows faithfully follow the margins between the granitoid domes and greenstone belts and reflect their steep nature. Thus, in the Pilbara Block, the gravity field is characterised by ovoid-shaped gravity lows and highs, whereas, in the Yilgarn Block, the gravity anomalies are more elongate, reflecting the general north/south trend of the greenstone belts.

In the Hamersley Basin, the gravity contour pattern reflects

the degree of deformation in the basin strata. Thus, in the northern part of the basin outcrop area, where the strata have a fairly uniform southerly dip, the contour pattern is relatively undisturbed, but farther south the contour pattern becomes more complex as the strata become more deformed. In the south of the basin outcrop area, the contour pattern is characterised by circular gravity highs and lows, the highs corresponding to synclines in the dense basin strata, and the lows to granitic Archaean inliers (a, b, c and d in Figure 86), or anticlines which probably have cores of Archaean basement. Similar correlations can be made in the Nabberu Basin. In the east of the basin, ie. in the Earaheedy Sub-basin, the strata dip gently northwards off the Yilgarn Craton, but in the Glengarry Sub-basin, the Goodwin Dome, an inlier of basement, correlates with a gravity low, and the Marymia Dome, at the northern Edge of the basin, correlates with the eastern end of another gravity low.

The Proterozoic mobile belts and Phanerozoic sedimentary basins which ring the cratons correlate with longer wavelength gravity highs and lows. In the Phanerozoic basins, the longer wavelength anomalies probably reflect the horizontally uniform, thick sedimentary piles, and consequent removal of the presumably more complex basement to greater depths from the surface. In the Capricorn Orogenic Belt, the longer wavelengths may also reflect abrupt changes in average crustal density between the Pilbara and Yilgarn Cratons, and their regional isostatic compensation (Wellman, 1978).

Wellman (1976) showed that, in central and western Australia, $3^{\circ} \times 3^{\circ}$ areas were mainly isostatically compensated at the base of the crust. Dooley (1977) suggested that the depth of isostatic compensation may be greater than 160 km. Drummond & Shelley (1981) used the seismic models to consider the implications of both of these theories on the depth of isostatic equilibrium. Their gravity models for the profile GBC (marked on Figure 86) are shown in Figure 87 together with the seismic model on which they were based. Note that in the gravity models, little attention was given to the short wavelength anomalies, especially in the Pilbara Block and Hamersley Basin, as they are due to near surface features.

Figure 87. The seismic model (Drummond, 1979b) and two gravity models for line GBC. Model A has a root of high density upper mantle compensating the effects of the thick crust under end C, and in model B different velocity/density functions (see text) were assumed for each end of the line. The calculated and measured curves agree in the principal features, but the short wavelength effects were not modelled. Both models require a high density slab representing the Nabberu Basin near end C, and model B requires a low density prism to represent the Marymia Dome (Drummond & Shelley, 1981, Figure 3).

SEISMIC MODEL

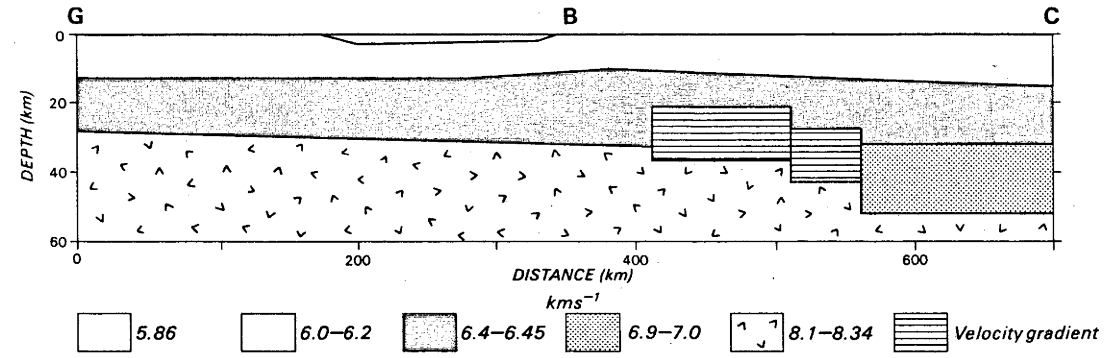

GRAVITY MODEL A

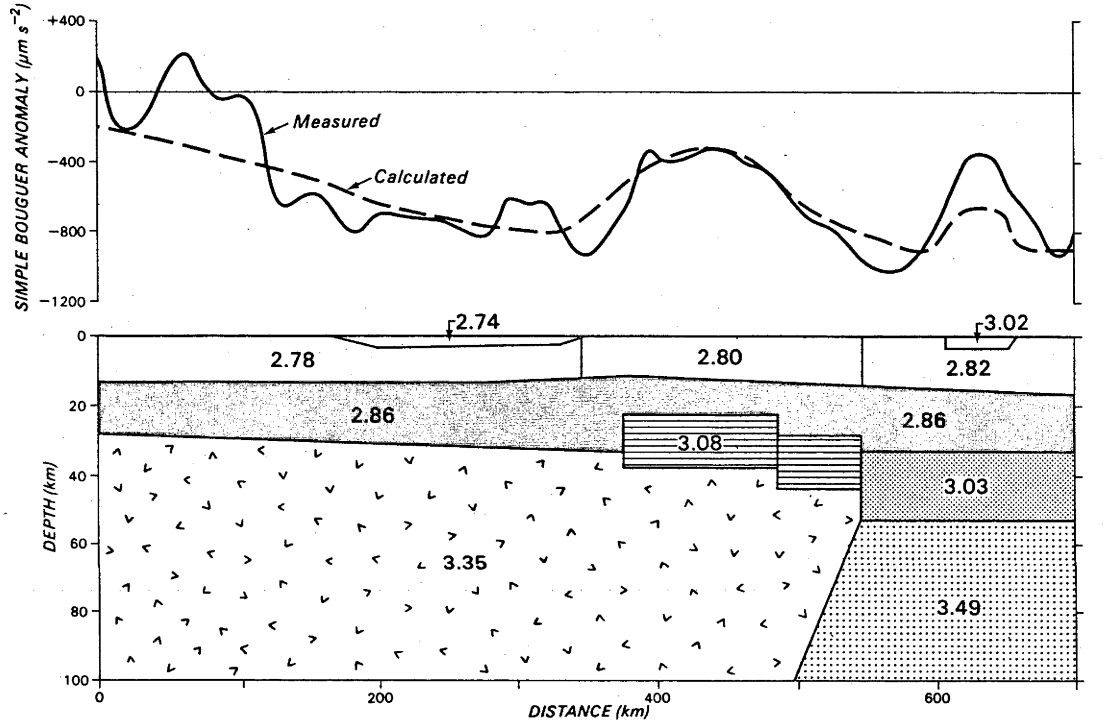

GRAVITY MODEL B

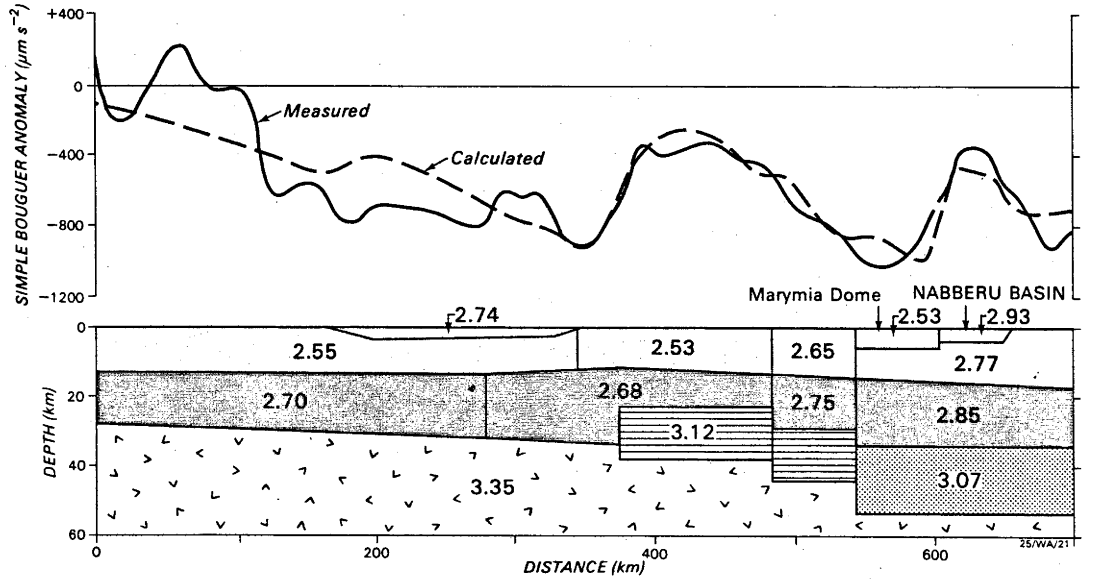

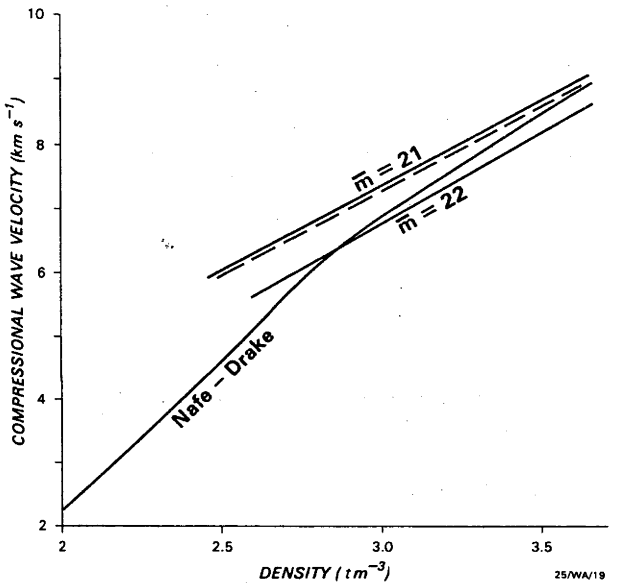

Figure 88. Velocity/density curves of Nafe-Drake (In Talwani & others, 1959) and Manghnani & others (1974) for mean atomic weights of 21 and 22. The dashed line was adopted for the Pilbara Craton.

9.2.2 Isostatic compensation complete below the base of the crust.

If one empirical volocity/density relationship applies throughout the region, at 52 km depth, which is the depth of the crust/mantle boundary under the northern Yilgarn Craton, pressures for unit columns of rock are 1.59, 1.54 and 1.51 GPa in the northern Pilbara Craton, southern Pilbara Craton, and northern Yilgarn Craton, respectively. While these pressures agree to within 5%, and may be within experimental error if the effects of velocity gradients in the Yilgrarn Craton could be considered, they imply that the gravity field should decrease by 3000 μm s^{-2} along profile GBC. The measured decrease is only about 800 μm s^{-2}. However, if the depth of compensation is in the upper mantle, the difference of about 2200 μm s^{-2} can be explained by different densities within the upper mantle beneath the two cratons. In Gravity Model A in Figure 87, compensation is assumed (arbitrarily) to be complete at 100 km depth, and the Yilgarn Craton overlies denser mantle than the Pilbara Craton. The velocity/density relationship of Nafe & Drake (in Talwani & others, 1959) was used to convert the crustal velocities to densities.

9.2.3 Isostatic compensation complete at the base of the crust

If isostatic compensation is complete at the base of the crust, the rocks of the Yilgarn Craton must be denser than those of the Pilbara crust, while still having similar seismic velocities, in order to account for the apparent pressure differences at 52 km depth along the profile. This is possible if they have different mean atomic weights; Gravity Model B, in Figure 87, is based on this premise. Figure 88 shows the velocity/density curves (at 1 GPa pressure) derived by Manghnani & others (1974). In Gravity Model B, the densities of the Pilbara Crust were based on the dashed curve, those for the Yilgarn Craton were based on the curve for a mean atomic weight of 22. The difference in the mean atomic weights was assumed for the whole crust; it could equally have been applied only to the lower crustal rocks, so that, say, the base of the crust in the Yilgarn Craton is very much more mafic than that of the Pilbara Craton.

9.2.4 Implications of the gravity modelling

Drummond & Shelley (1981) discussed the agreement between the seismic and gravity models, and decided that they agreed within the errors

of the experiment, and within the precision to which the short wavelength anomalies were modelled. The models have several implications; Drummond & Shelley (1981) wrote:

"Assuming that the region is in isostatic equilibrium, the seismic model and the gravity field, when considered together, may be indicative of either isostatic compensation being fully achieved deep in the upper mantle, or different bulk chemistry in the cratons and isostatic compensation at the crust/mantle boundary. In model B (Figure 87) the density in the upper crust of the Pilbara Craton (2.55 $t.m^{-3}$) is very low compared with the densities measured in hand samples from the region (Drummond, 1979c), suggesting a compromise between models A and B. We favour a model similar to model A, but with some chemical stratification in the lower crust and the base of the crust in the Yilgarn Craton perhaps reaching $\bar{m}$ = 22.

In gravity model A, the depth of compensation was set arbitrarily, and for convenence, at 100 km. Dooley (1977) suggested that the depth of compensation in the Western Australian Shield was in the upper mantle, but he could do no more than to suggest that it was probably below 160 km depth. Unfortunately, the current seismic data cannot be more definitive.

Although a unique structural profile of the crust and upper mantle cannot be derived from the seismic and gravity data, the models in Figure 87 do have implications for theories of evolution of the crust and upper mantle in the region. Gee (1979a) listed four differences between the Pilbara and Yilgarn Blocks from which different evolutionary histories for the cratons can be inferred:

(i) the western Yilgarn Block has large areas of high grade gneiss terrain, for which there is no equivalent in the Pilbara Block;

(ii) most of the granitoids in the Yilgarn Block are younger than the majority of those in the Pilbara Block;

(iii) the maturity of the clastic sequences within the greenstone belts of the cratons implies

that the Pilbara Block developed more towards crustal stability than the Yilgarn Block; and

(iv) The granitoids of the Pilbara Block are near-circular, whereas those of the Yilgarn Block have distinct linear trends.

Drummond & others (1981) added a fifth: the crust of the Pilbara Craton is much thinner than the crust of the Yilgarn Craton.

The arguments presented above for the depths of the isostatic equilibrium imply also that the Pilbara region differs from the Yilgarn region either in the chemistry of the crust, which can be regarded as a sixth difference between the cratons, or in the metamorphic grade or chemistry of the upper mantle.

Jordan (1975, 1978) suggested that sub-continental mantle to depths possibly as great as 400 km evolves in parallel with the overlying continental crust. Because the sub-continental mantle becomes less dense than the surrounding mantle, it does not mix with the rest of the mantle, but is transported with the continents during plate motions. The features of the mantle established during the formation of the crust are frozen in. The differences in the upper mantle structure or chemistry under the cratons in northwest Australia may therefore indirectly imply different evolutionay processes for the cratons. This is an alternative sixth difference between the cratons.

The upper mantle under the Pilbara Craton may be less dense than that under the Yilgarn Craton, because of iron depletion. The upper mantle would, therefore, be implicated as the reservoir which provided the iron for the large volumes of basin volcanics and banded iron formations of the Hamersley Basin."

If the different densities in the upper mantle in Gravity Model A indicate that matter was removed from the mantle and deposited as basic volcanics and banded iron formations on the Archaean basement, it would account for a pile of rocks 3.5 km thick, with a density of 2.8 t m^{-3}, covering the entire Pilbara Craton. This is about the volume of the Fortescue and Hamersley Groups, as inferred by the cross-sections and stratigraphic columns of Trendall & Blockley (1970) and Trendall (1975).

(Although the basin formed with a depression with about 7 km of strata in the centre and less at the edges.)

9.3 THE EVOLUTION OF NORTHWEST AUSTRALIA - DISCUSSION

The seismic models cannot by themselves define a unique evolutionary model for northwest Australia. The region took from before 3500 m.y. to 1000 m.y. ago to form, and in that time many processes acted and interacted. However, several important stages of crustal development can be recognised in that time, and the seismic models can be used to qualify the types of processes that could have occurred. The purpose of this section is to make some of the qualifications.

9.3.1. The Archaean

The Archaean cratons around the world all have granitoid/greenstone terrains, and it is perhaps this similarity that is their most striking feature. However, when the cratons are studied in more detail, differences become apparent. In northwest Australia, the Pilbara and Yilgarn Cratons are now recognised to have as many as six major differences which point to their separate development. Differences between other Archaean cratons are now being recognised, and on several scales. For example, Hyde (1980) found that the nature of sedimentary rocks in the Abitibi greenstone belt in northwest Ontario indicated that small, unstable continental fragments formed in the Canadian shield, while evidence from South Africa suggested larger, more stable continental fragments formed in South Africa. At the smaller scale of greenstone belts, Padgham (1980) found that "Continued work in the Slave Province during the last decade suggests there are important differences between the geology of the Slave Province and that of other Archaean crustal blocks. Slave volcanic belts do not fit models proposed for the Superior and other craton volcanic belts. In fact, Slave volcanic belts vary so much in composition from one belt to another that three or four models may be required."

As well, the Archaean/Proterozoic boundary is not isochronous. Taylor and McLennan (1981) found that the change in tectonic style from Archaean to post-Archaean was reflected in the bulk chemistry of the crust, as inferred from the rare earth element patterns of sedimentary rocks, and this occurs at different times in different continents.

The different times of cratonisation in different cratons is reflected by the difficulties of setting the Archaean/Proterozoic boundary, as discussed in Chapter 2. Thus the boundary for the Pilbara Craton is older than that for the Yilgarn Craton. Internationally, it used to be set at 2400 m.y., but it is now officially 2500 m.y., which is unsuitable for Western Australia (Gee, 1980). In the USSR, it is set at 2600 m.y. (Keller, 1979).

There is no doubt that the period between 3000 m.y. and 2500 m.y. ago was a time of massive growth of continental crust (Taylor & McLennan, 1981). For example, much of the granitoid intrusion and crustal growth in the Yilgarn Craton, especially in the eastern half, occurred towards the end of this time period. However, the Pilbara Craton was probably fairly well cratonised by 3000 m.y., or, at the latest, 2800 m.y. - the greenstone belts had formed and most of the granitoid domes were in place. The thermal event that caused the emplacement of granitoid magmas in the Yilgarn and other cratons at this time had a different effect on the Pilbara Craton. Part of the lower crust was melted, and the partial melt intruded into the crust, but probably the effect with the most significance was the formation of the Hamersley Basin across the protocontinental crust of the Pilbara Craton. The crust of the Pilbara and Yilgarn Cratons therefore responded differently to the thermal event which peaked at about 2600 m.y. (Figure 3). This implies that the response of the cratons around the world to the evolutionary processes which were forming them to a large extent depended on the maturity of the cratons, ie. the distances they had progressed along the path to cratonisation.

9.3.2 The Hamersley Basin

The study of intracrustal sedimentary basin development was somewhat overshadowed for several years by the study of basins at continental margins and island arcs, because these two classifications account for the majority of sedimentary basins occurring now and in the past, and their evolution is also linked to plate tectonics which, in the last few years, has been at the forefront of earth sciences research. Many of the conclusions reached studying these other basins cannot validly be applied to intracontinental basins, because the effects of plate tectonic processes are not present within the confines of the continents.

The physical characteristics of the basin must be known before evolutionary processes can be considered, and many can be defined from the geological mapping. The Hamersley Basin was an ovoid basin, about 550 km long with the depositional axis trending about N120°E, and it was about 350 km wide. According to the diagrammatic cross sections of Trendall (1975b), it was not symmetric; the deepest part of the basin lay about one third of the way from the southern boundary. The basin strata consisted of up to 4200 m (14,000 ft, Trendall, 1968) of basalt, tuffs and derived mudstone of the Fortescue Group, up to 2500 m (8,350 ft, Trendall & Blockley, 1970) of Hamersley Group banded iron formations, fine grained sediments, dolomites and acid volcanics, and about 400 - 500 m (Trendall, 1975b) of clastic sediments of the Turee Creek Group. The maximum thickness of the basin was approximately 7200 m. This is in keeping with geobarometry estimates from the metamorphic grade of Fortescue Group rocks cropping out in the Tom Price area, which show that the depth of burial was about 7 km (see Drummond & others, 1981). It is less than the 15 km claimed by Button (1976) and the 12 km of Trendall (1968), but their estimates included 9000 m of Wyloo Group clastic sediments which are now recognised as mostly occurring in the structurally separate Ashburton Trough which abuts the southern edge of the Pilbara Craton, and not in the Hamersley Basin (Trendall, 1979).

Trendall & Blockley (1970) provide the following information. The earliest Fortescue Group volcanics were extruded onto an eroded Archaean landscape, and were confined to the axis of the basin that was later to form across the entire Pilbara Craton. Small, shallow, isolated basins formed in the early stages of basin development, but the basin gradually grew until, at the end of the Fortescue Group deposition, the lavas and their intercalated sediments were being deposited across the craton, and subsidence was outstripping the deposition rate. There is some evidence that the basin contracted in the transition from Fortecsue Group to the Hamersley Group.

The Hamersley Group contains banded iron formations throughout its stratigraphic column, and these indicate that the water depth rarely exceeded 250 m in the deepest part of the basin, and was seldom less than 50 m in the present outcrop area. The basin was almost closed, with access to the ocean in the northwest. Currents within the basin were less than 1 m s^{-1}. Compaction rate within the banded iron formations could have been as much as 95%, and the subsidence rate could have been 6,500 - 20,000 years per metre. This would give a time span of deposition in the basin of 47 to 144 m.y., which seems somewhat less than might be expected from the geochronological data that will be discussed later.

The tectonic regime must have been very stable. Banded iron formations require quiescent conditions, and within the banded iron formations microbanding at scales of less than a millimetre has been correlated over distances as great as 300 km.

The almost complete lack of clastic material in the Hamersley Group implies that there were no peripheral land masses shedding sediment into the basin. This could be for many reasons: there may not have been any peripheral bulges providing regional isostatic compensation for the subsiding geosyncline; the surrounding region may have been desert so that no erosion was occurring; or, thirdly, rivers that were present may have been too sluggish to carry sediment. The last two reasons seem unlikely in a basin that may have lasted over 100 m.y. - surely in that time there would have been some storms or disturbances to transport sediment into the basin. The first theory, that there were no significant land masses, is therefore preferred.

Important igneous events which allow the dating and therefore timing of the vents that shaped the basin are: Fortescue Group basalts may be as old as 2750 m.y. (Richards, 1977; Richards & others, 1981; R.T.Pidgeon, ANU, personal communication, 1978) and date a thermal event which heated and partially melted the upper mantle under the Pilbara Craton. The same thermal event also partially melted the lower crust of the Pilbara Craton, forming the younger granitoid suite between 2600 and 2800 m.y. ago (de Laeter & Blockley, 1972; de Laeter & others, 1975). These two events seem coeval, although there is no known contact between the lower Fortescue Group volcanics and any of the younger granitoids to allow a comparison of their relative stratigraphic positions (Hickman & de Laeter, 1977). The thermal event which caused these events appears to be a world-wide phenomenon; it was responsible for most of the crustal growth in the eastern Yilgarn Craton (Figure 3). Mareschal (1981) suggested that there would be a slight time delay between the effect of the thermal event on the upper mantle and the effect on the lower crust. If the time delay exists, it is obscured by the errors in the isotopic ages.

Rocks of basaltic composition were intruded as dolerite dykes and sills at all levels of the Hamersley Basin strata. Some dykes cut only the lowermost Fortescue Group rocks, others cut the higher members of the Hamersley

Group. The dykes occur as swarms, with some dykes many kilomteres long; for example, the Black Range Dyke can be traced for 70 km, but its southern end is now faulted, so that it may have been longer. The dominant trend of the dykes is north northeast, at right angles to the axis of the Hamersley Basin, although some occur at other azimuths (Figure 90). Some of these dykes are thought to be feeders for the basal volcanics of the Fortescue Group (Lewis & others, 1975).

The Woongarra Volcanics, which are composed of dacite, rhyolites with intercalated tuffs and a bed of banded iron formation, occur near the top of the Hamersley Group. They were deposited basinwide, and their Rb/Sr age of 2000 m.y. (Compston & Arriens, 1968) with a low initial ratio implies a younger age limit of the basin. This age, coupled with the approximate 2750 m.y. age of the lower Fortescue Group imply that the basin had a depositional life of at least 750 m.y. This is at variance with the depositional life of 47 - 144 m.y. implied above from subsidence rates.

An age of 2235 m.y. for a granite from the Sylvania Dome was interpreted by Blockley & others (1980) as the time of uplift of the Sylvania Dome. When considered with the age of the Woongarra Volcanics, it implies that the Sylvania Dome was uplifted in the south of the basin before deposition elsewhere in the basin had ceased.

The life of a sedimentary basin can by subdivided into several steps:

(i) creation of an initial subsidence to form a depression;
(ii) filling of the depression with sediment;
(iii) further subsidence caused by the extra load of sediments; and
(iv) isostatic adjustment, which presumably applies from the beginning of the process and continues until the basin ceases as a depocentre and, in the case of the Hamersley Basin, is uplifted.

Many processes may be invoked to explain the initial subsidence. Some will cause more subsidence than others, but as the total thickness of the sedimentary pile depends on the depth of the initial subsidence, it is perhaps wise to consider the depth of the initial subsidence required to produce a basin with a final thickness of 7000 m. In the following discussion, the initial subsidence is defined as the depth of the basin which would form if no sediment or water were to fill it.

TABLE 16: Mean densities of specific rock types from the Pilbara region, based on the values tabulated by Drummond (1979c).

Rock type	Number of samples	Density $t\ m^{-3}$	Standard Deviation
Banded iron formation	13	3.08	0.33
Basic extrusive volcanic*	9	2.88	0.06
Acid extrusive volcanic	2	2.83	-
Sedimentary rocks	19	2.58	0.25

* not all from within the confines of the Hamersley Basin outcrop area.

According to Beaumont & Sweeney (1978), the maximum thickness of sediment that can form in an isostatically compensated basin is determined by assuming that the basin is ultimately in pointwise, Airy isostatic equilibrium. The maximum thickness T is

$$T = H \cdot dm / (dm - ds),$$

where H is the initial subsidence,
dm is the density of the underlying mantle substratum, and
ds is the density of the sediments that form in the depression.
If the initial depression is filled with water, the final thickness of the basin can be as great as

$$T = H (dm - dw) / (dm - ds),$$

where dw is the density of water (Mc Kenzie & others, 1980). We wish to calculate H.

The rocks of the Hamersley Basin strata are dense because of the high proportion of basalts and banded iron formations. Estimates of the densities of the basin strata are given in Table 16, and are based on measurements of the densities of the rocks from the region reported by Drummond (1979c). While the sampling is not exhaustive, and may not be representative of the basin rocks, it is clear from Table 16 that the densities of the banded iron formations and basic volcanics are very high. Using the proportions of each rock type in the Fortescue Group (Trendall, 1975b) and the Hamersley Group (Trendall & Blockley, 1970), an average density of 2.76 t m^{-3} can be derived for the Hamersley Basin strata. The densities were measured in samples which were collected at the surface and might therefore be slightly weathered and cracked, so that this average density might be slightly low; an average density of 2.8 t m^{-3} was adopted for the Hamersley Basin strata.

An upper mantle density of 3.35 t m^{-3} might be assumed. The initial subsidence required to produce a basin 7 km thick is therefore 1.15 km.

Some of the processes that can cause subsidence of the crust to form a depression are shown in cartoon fashion in Figure 89. Many other mechanisms may be possible, and often several could apply at the same time. A few of the processes in Figure 89 can be ruled out immediately.

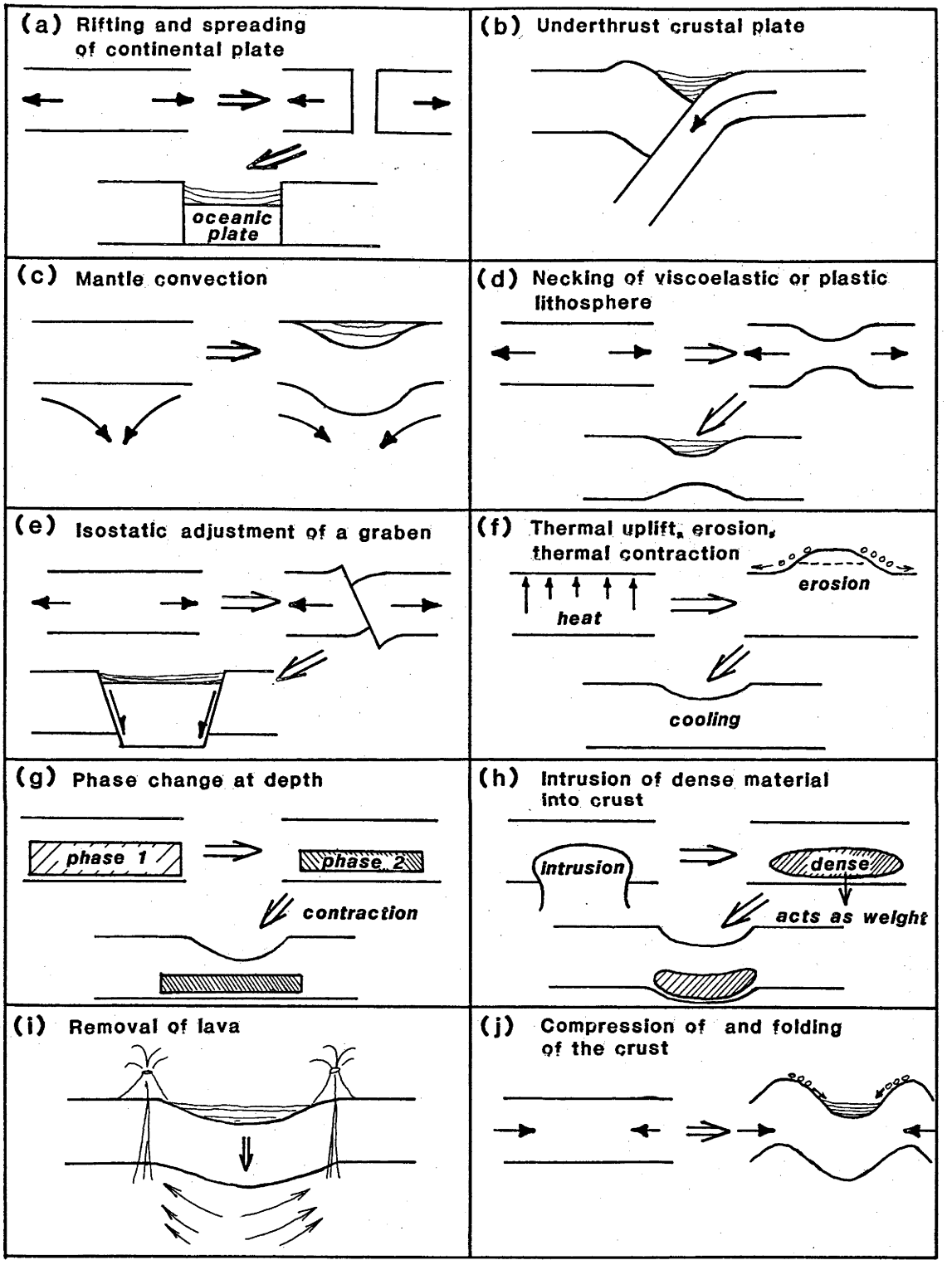

Figure 89. Cartoon sketches of ten methods whereby a depression can be created to start basin subsidence. Details are given in the text.

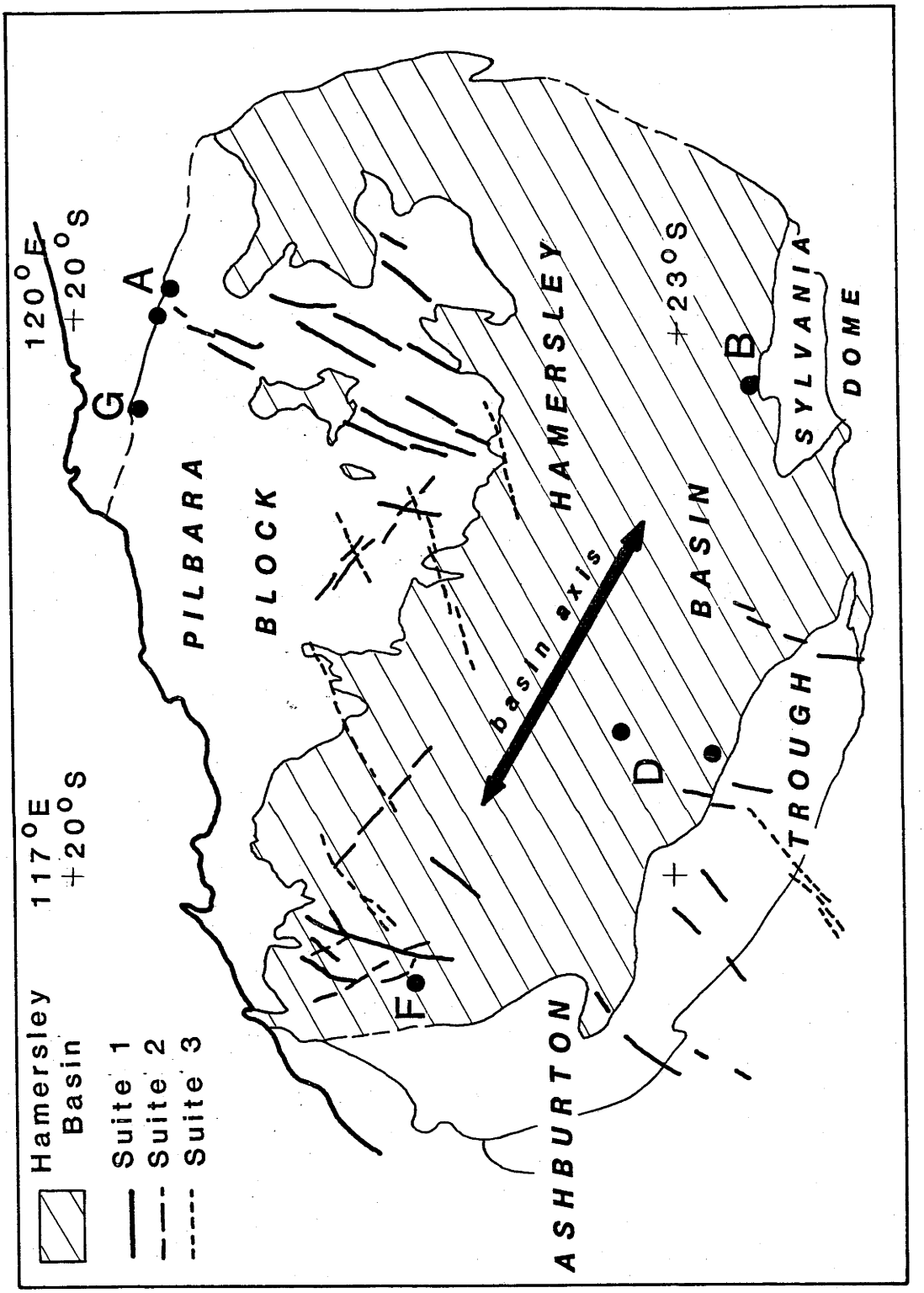

Figure 90. Map of the major dolerite dyke swarms in the Pilbara Block and Hamersley Basin. Hatched area is the present outcrop area of the Hamersley Basin.

Model a, in which the crust thins due to rifting and formation of oceanic crust is inappropriate, because the crust under the present day Hamersley Basin has continental thickness and seismic velocities. In model b, the depression is the trench between a continental block and a subducting slab. This can be ruled out because (i) such trenches usually contain very deep water, and the Hamersley Basin was shallow, (ii) after the palaeotrench becomes inactive, the crust underneath may not have a continental signature, and (iii) volcanism associated with subduction zones is andesitic, not basaltic. Mantle convection, as shown in model c, can be ruled out as the driving mechanism of basin formation because the basin would form over the coldest part of the underlying convection cell, which is the least likely place that partial melting to produce the Fortescue Group basalts would occur.

Model (d), necking of a viscoelastic or plastic lithosphere by tensional stresses, has been treated quantitatively by Mc Kenzie (1978), and may be appropriate for some continental basins. However, an extension of the crust to double its length is required to produce a basin with only 4.5 km of sediments. This type of evolutionary model can therefore be rejected for several reasons. Firstly, there is no evidence from the seismic data that the crust under the axis if the Hamersley Basin has been thinned by one half, corresponding to an extension of two. Secondly, if the crust of the Pilbara Craton had been extended to twice its original length, the geological fabric of the surface rocks would have been destroyed, and it is unlikely that the features recognisable at the surface today would still be recognisable. A third reason for rejecting this model is that the direction of tensional stress at the time of basin formation can be implied from the dolerite dykes which formed throughout the life of the basin. Most of the dykes trend north northeast (suite 1 in Figure 90), at right angles to the axis of the basin. It is reasonable to assume that the dykes would form at right angles to the tension axis, so that if the basin was formed through tension, the dykes would parallel the axis of the basin. Other suites of dykes, which may be coeval, have different directions, and their significance is touched upon later.

Grabens (model e) can form in compressional environments (Bullard, 1936), but their preferred mode of formation is by isostatic adjustment of a faulted crust in tension (Heiskanen & Vening Meinsz, 1958). As just explained explained, the Hamersley Basin probably formed parallel to the tension axis, an and not at right angles to it.

Model f depicts the thermal expansion of the lithosphere by heating, erosion of the uplifted portion, and then cooling to produce a depression. Mareschal (1981) showed that the thermal expansion, and therefore uplift, begins in the lithosphere as soon as the thermal event begins. The thermal expansion will occur in the crust somewhat later. The Pilbara Craton was subjected to heating at the beginning of basin formation, as shown by the Fortescue Group lavas and the younger granitoids. Foucher & Le Pichon (1972) placed an upper limit of 1 km on the depth of depression likely from this process, but they assumed a temperature increase insufficient to cause melting of the lithosphere. As the lithosphere in the Pilbara Craton was partially melted, a slightly greater subsidence might be expected if this process was active. Thus model f represents a likely process active at the start of the Hamerlsey Basin.

Middleton (1980) combined the effects of thermal expansion and erosion with the effects of a phase change at depth (model g). If the rocks of the crust are hydrated, they may be forced into a higher metamorphic grade by an elevation of temperature. The effects of heating are therefore to cause subsidence because of contraction of the crust to a higher density phase, followed by thermal cooling and contraction. Thus a basin forms in two stages. In the Hamersley Basin, the two stages may be represented by the formation of the Fortescue Group and subsequent partial regression of the basin, which was noted by Trendall & Blockley (1970), followed by rejuvenation of the basin because of cooling, and the deposition of the Hamersley Group.

The lower crustal velocity of 6.55 km s^{-1} observed along the axis of the Hamersley Basin is higher than elsewhere in the lower crust under the Pilbara Craton, and may be indicative of higher metamorphic grades in the lower crust under the basin (Drummond & others, 1981). It would imply that the lower crust under the basin is 0.04 t m^{-3} denser than rocks elsewhere in the lower crust under the Pilbara Craton (based on the Nafe-Drake velocity/density curve in Figure 88). Suppose the denser layer is 20 km thick. If it was to be compensated by an unfilled basin at the surface, the basin would be

$$(0.04 \times 20.0) / 2.85 = 0.3 \text{ km}$$

deep, 2.85 t m^{-3} being the assumed density of the crust, and this alone is not a sufficiently deep depression to cause an isostatically compensated basin 7 km deep. However, when acting in parallel with the effects of thermal

expansion, erosion and cooling of the lithosphere, it could produce a sufficiently deep initial subsidence.

Model h depicts the sagging of the crust under the weight of dense intrusions into the lower crust. It is an unlikely model for the Hamersley Basin formation because of the low mafic content of the lower crust. A more likely version of this model, in which the dense rocks are deposited on the land surface is shown in model i.

Trendall & Blockley (1970) preferred a model similar to model i to explain the formation of the Hamerlsey Basin, because it allows the basin to subside because material is removed from the lower lithosphere below the basin, and deposited in the basin. This is a simple mass transfer, and it is therefore possible for the basin to remain in isostatic equilibrium throughout its life as a depocentre without forming peripheral bulges which would, through erosion, provide clastic material to the basin. Certainly a process such as this must have contributed at least partially to the formation of the basin. The depression which must have been present at the end of the Fortescue Group deposition could have been no more than 250 m deep, the maximum water depth for banded iron formations (Trendall & Blockley, 1970). If the 250 m depression was filled with water at the time, which seems likely because the Hamersley Group seems mostly conformable on the Fortescue Group, an extra 1.1 km of sediments with a density of 2.8 t m^{-3} could have been deposited through filling of the depression and further weighing down of the crust. Even if the initial 250 m depression was not filled with water, a maximum thickness of 1.5 km of sediments could be expected. This is less than one half of the thickness of the sediments in the Hamersley and Turee Creek Groups. Thus, although a mass transfer model can account for a large portion of the volcanic pile, an extra driving mechanism is needed to fully account for the sediments, and the most likely mechanisms were thermal uplift, erosion followed by cooling and contraction, and possibly a phase change at depth. These, acting in parallel, can more than account for the initial subsidence required to explain the Hamersley basin as an isostatically compensated basin formed by subsidence of an initial depression by the weight of sediments.

All of the processes just described assume that throughout its formation, the basin was in isostatic equilibrium. A mechanism must then be invoked to explain the uplift of the basin after deposition ceased. Some of the uplift might have been through vertical tectonics caused by the density

inversion due to the dense basin rocks overlying less dense basement, in the fashion described by Mareschal & West (1978). Such localised uplift could account for localised Archaean domes such as those marked in Figure 86, but it cannot account for the regional uplift that occurred basin-wide. A change in the form of the isostatic compensation from regional to local may have occurred, as the region tended towards the lowest stress state. An alternative explanation is that the entire region has been rising throughout geological time as the lithosphere thickens through underplating. This is considered again later. Yet another explanation is that the basin did not form in isostatic equilibrium.

In model j, a mechanism is proposed in which the crust is compressed into a series of folds, with basins and ridges forming. Such a mechanism was first detailed by Heiskanen and Vening Meinsz (1958). It is unlikely to work in nature if the lithosphere is elastic because the stresses required to deform an elastic lithosphere are very large. However, if plastic flow can occur, the stresses required are very much smaller. The results of Heiskanen & Vening Meinsz (1958) can be summarised qualitatively. During compression, the first effects in continents will be elastic compression, and this will cause thickening of the lithosphere, which will in turn lead to the elevation of the surface and the formation of a compensating root in the mantle. The thickness of the root will be several times the height of the elevation, and this will cause an asymmetry in the stress pattern through the lithosphere such that the deviatoric compressive stress at the surface is greater than that at the base of the lithosphere. This will cause a greater shortening at the surface than at depth, and a geosyncline will form. The plastic component of deformation soon becomes greater than the elastic component, and if the compressive stress continues the geosyncline will descend more and more rapidly, until the downwarping becomes catastrophic. As the geosyncline continues to develop, the base of the geosyncline will be heated by its surroundings, and, being less dense than the mantle it is now entering, will flow to the sides, elevating the regions on either side of the geosyncline, providing a source of sediments for the geosyncline. The extra weight of sediments fuels the motor of the geosyncline.

If at any stage the compressive stress, which is the force holding the region out of isostatic equilibrium, is removed, the region will tend towards isostatic equilibrium by uplfiting the geosyncline. That is, the final uplift of the basin is an integral part of the mechanism of Heiskanen & Vening Meinsz (1958). It remains to see if this mechanism can be applied to

the geological and geophysical data of the Hamersley Basin.

The most important factor is whether a compressive stress was active. Deviatoric stresses in the uppermost continental crust of the world today are generally horizontal and compressive (Mc Garr & Gay, 1978), although tension can occur near rifts (Richardson & others, 1979). While the reasons for the predominance of horizontal compressive stresses are not clear, there is no reason to assume that compressive stresses were not also prevalent in the continental crust of the Precambrian; this is the principle of uniformitarianism. In an elastic lithosphere, the trough will form at right angles to the deviatoric compressive stress; in a plastic lithosphere, this may not be so. In the Hamersley Basin, the large number of dolerite dykes at right angles to the basin axis seem ample evidence that the region was being compressed at right angles to the basin axis. The basin formed at right angles to the compressive stress because, as will now be explained, the crust at the beginning of the basin formation may not have been plastic.

The second feature of this model of geosyncline development which has to be explained is the mechanism by which the compressive stress can be turned on to start the process. This may not be difficult if the stress is continuous, and the rheological properties of the crust change.

The collision of the crust of the Pilbara Craton with the primaeval crust of the Yilgarn Craton, which probably occurred before 2400 m.y. ago (Mc Elhinny & Mc Williams, 1977; Embleton, 1978) could have been the cause of the compressive stress. This stress may not have been enough to deform the crust, which may still have been fairly cold, but it may have been enough to control the orientation of the first dolerite dykes. However, as the world-wide thermal event between 2800 and 2600 m.y.ago developed, and the lower crust partially melted, the crust became sufficiently soft and weak for buckling to begin. After deformation, the stress distribution within the lithosphere would have been altered, with the stress pattern shown schematically in Figure 91a (after Beaumont, 1979) superimposed on the regional compressive stress pattern, and the new stress distribution would have influenced the direction of future dolerite dyking. For example, dykes approximately parallel to the basin margin (suite 2, Figure 90) would have been influenced by the tensional stress regime in the upper lithosphere along the margins of the basin. The geosyncline never reached the catastrophic stage; the compressive stress ceased - perhaps it was relieved by the buckling and shortening of the lithosphere - and the Hamersley Basin was left out of isostatic equilibrium. Uplift then occurred.

The seismic data cannot differentiate between the two sets of evolutionary models which may have caused the Hamersley Basin. In the first, the basin formed by the isostatic adjustment of an initial subsidence, perhaps caused by thermal uplift, erosion and then cooling and contraction allied to phase changes at depth and mass transfer between the upper mantle and the surface. This process does not explain the subsequent uplift of the basin, but it does not require that peripheral bulges be formed around the basin. In the second process, subsidence was caused by buckling of the crust, and the basin formd out of isostatic equilibrium. It therefore explains the final uplift of the basin, but small peripheral bulges may be formed by the process. both of the sets of evolutionary processes suit the seismic models, in which the crust has no significant change of thickness under the axis of the basin. It may be that, given the thermal conditions at the time of basin formation, both processes were active, and acting in parallel.

9.3.3 The cause of upper mantle anisotropy.

It now remains to explain the cause of the anisotropy in the upper mantle seismic velocities. The anisotropy in Pn seems so closely linked in direction with the Hamersley Basin axis that it must be due to either the cause or is an effect of the basin formation.

Velocity anisotropy in rocks is presumably caused by the alignment of crystals which themselves exhibit velocity anisotropy. The mineral dominating the anisotropic effect in rocks is olivine (Peselnick & others, 1974), and olivine crystals can be aligned by several methods. Under uniaxial compression, olivine will syntectonically recrystallise so that the slow axes of the minerals will parallel the compression (Ave 'Lallemant & Carter, 1970), while the other axes form girdles about that direction. This will cause apparent velocity anisotropy in the rock such that the maximum velocity will be parallel to the direction of minimum or tensional stress. Under shear, the olivine crystals will align themselves by a power law creep mechanism such that the fast axes will align at low angles of inclination to the direction of flow (Peselnick & others, 1974; Nicolas & Poirer, 1976).

The stress patterns expected in a viscoelastic lithosphere overlying a fluid substratum, and deformed by a point load, are shown in Figure 91a, and the resulting inferred rheology is shown in Figure 91b (Beaumont, 1979).

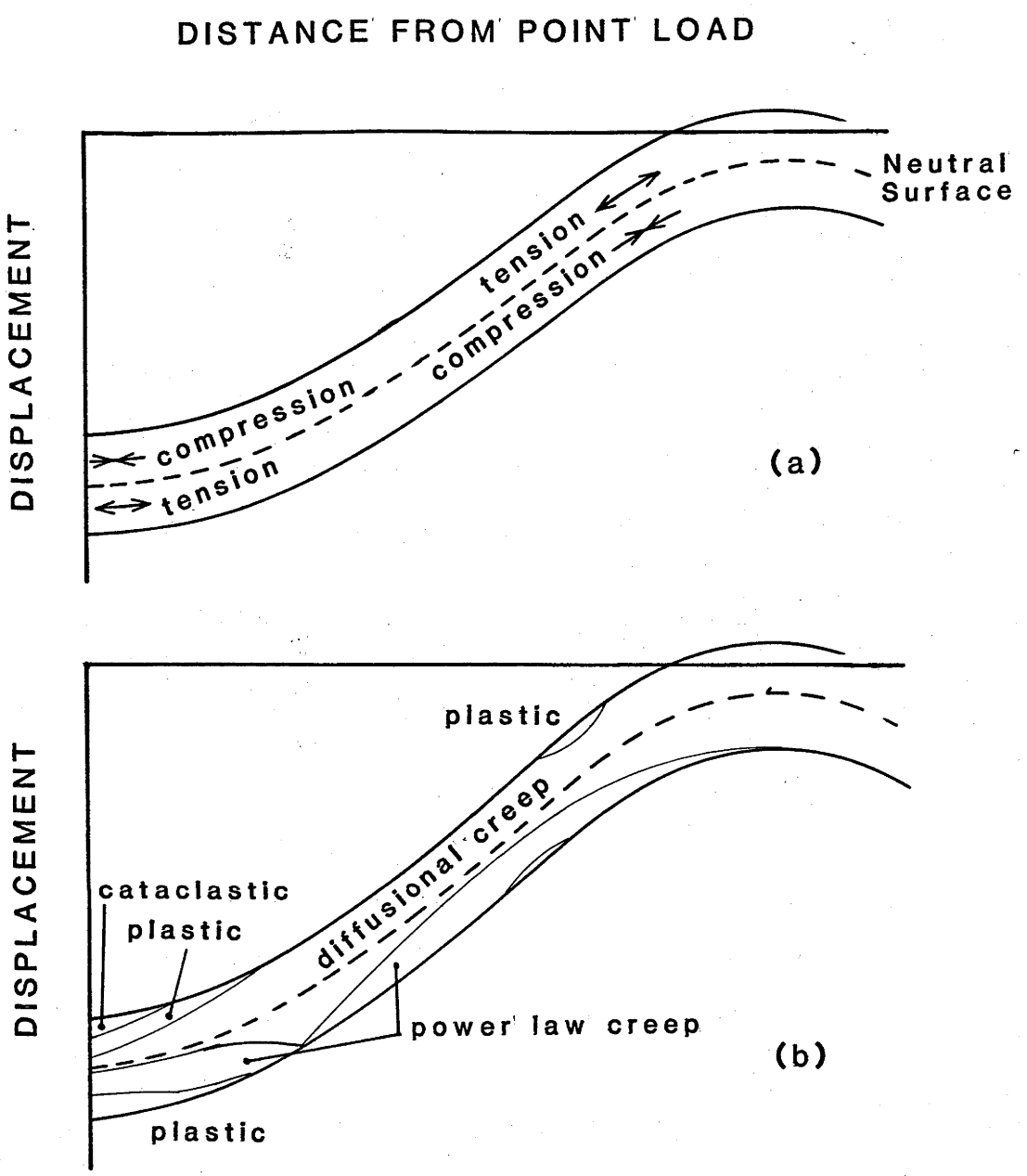

Figure 91. Diagrammatic representation of (a) the stress distribution and (b) the inferred rheology within a viscoelastic lithosphere overlying a fluid substratum and deformed by a point load, based on the results of Beaumont (1979). The neutral surface is the surface of zero deviatoric stress.

The lower lithosphere under the basin will be in tension, and if this stress is maintained long enough, the olivine crystals will recrystallise so that the maximum velocity will be at right angles to the axis of the basin, as observed. If the temperature is high enough, the lower part of the lithosphere will flow plastically. Because of the density differences between the base of the lithosphere and the upper mantle it is intruding, the direction of flow will be laterally away from the base of the syncline. Thus, this mechanism will also cause the crystals to align so that the direction of maximum velocity will be at right angles to the basin.

The observed anisotropy is about 2% of the isotropic velocity, and is much less than would be expected for a rock composed of pure olivine, where, if all of the crystals were perfectly aligned, an anisotropy of more than 10% could be expected. The upper mantle is unlikely to be composed of pure olivine; pyroxenes probably make up a large proportion of the upper mantle and are not as easily aligned as olivine (Carter & Ave 'Lallemant, 1970), so that, on these grounds alone, the maximum velocity is unlikely to be achieved. Other factors which may also have reduced the anisotropy to that observed are incomplete alignment of the crystals because of limited amounts of flow, and the change in the stress pattern in the lithosphere from tensional along the axis of the basin to compressional at the margins.

The ansiotropy in the sub-Moho boundary, which has a probable maximum velocity between north and 40 degrees west of north, parallels no apparent major tectonic feature in the Pilbara Craton. However, dolerite dykes of suite 3 in Figure 90 have a common azimuth with this anisotropy, being parallel to the apparent direction of the minimum velocity. The direction of minimum velocity is also subparallel to major lineaments (the Tangadee and Flint Hill lineaments) in the Bangemall Basin (Brakel & Muhling, 1976). The lithosphere was probably thin at the time of the formation of the Hamersley Basin (Cook & Turcotte, 1981). This is confirmed by the conclusion just reached for the cause of seismic anisotropy in Pn, which, if correct, places the neutral boundary (Figure 91), which is near the middle of the lithospheric plate, at or above the crust/mantle boundary during the formation of the Hamersley Basin. It is suggested that the base of the lithosphere was at the sub-Moho boundary which is now at 45 km depth. As the lithosphere thickened, the lower lithosphere was influenced by later tectonic events, and it is further suggested that the sub-Moho boundary anisotropy was due to such an event. Unfortunatley, insufficient information about the relative ages of the dolerite dykes in the Pilbara Craton is available from the geological maps of

the region (Kriewaldt & Ryan, 1967; Hickman & Lipple, 1975) to confirm whether the dolerite dykes of suite 3 are older than those of suites 1 and 2, and therefore whether the sub-Moho boundary is older than the top layer of the mantle.

The conclusions reached above concerning the Hamersley Basin evolution have important implications for the mechanisms for formation of other continental basins, especially the Transvaal Basin in South Africa. Many parallels have been drawn between the Hamersley and Transvaal Basins (Trendall, 1968; Button, 1976). The basins both formed across Archaean cratons and have similar ages, stratigraphic sequences, rock types, and even some types of mineralisation are similar. As well, the seismic crustal profile for the Transvaal region defined by Hales & Sacks (1958) bears remarkable similarity to that of the Pilbara Craton. In the eastern transvaal, the upper crust has a velocity of 6.03 km s^{-1} (6.0 - 6.1 km s^{-1} in the Pilbara), the lower crust has a velocity increasing from 6.72 to 7.19 km s^{-1} at depth (6.4, possibly reaching 6.7 - 7.2 in the Pilbara), and the upper mantle Pn velocity in the eastern transvaal is 7.96 km s^{-1} compared with an isotropic velocity of 7.99 km s^{-1} in the Pilbara Craton. The crustal thickness of 36 - 37 km in the eastern Transvaal is also similar, although slightly greater than that of the Pilbara Craton. Button (1976) speculated that, because there were so many similarities between the geology of the two basins, many types of mineral occurrences common to only one of the basins may yet be undiscovered in the other. It now becomes interesting to speculate whether the mechanisms suggested above for the formation of the Hamersley Basin might also be applied to the Transvaal Basin, and whether anisotropy might be expected in the upper mantle under the Kaapvaal Craton.

9.3.4 Lateral and vertical changes in the upper mantle.

The upper mantle under the region contains considerable lateral and vertical inhomogeneity. The seismic boundary about 15 km below the Moho is present throughout the region, and its topography follows that of the Moho, being deeper under the Capricorn Orogen than under the Pilbara Craton, and even deeper under the Yilgarn craton. Further structure may be present below this boundary. Drummond & others (1982) concluded that the velocity at 100 km depth under the continental margin to the north was 8.25 km s-1 along a northerly azimuth. Insufficient data exist to link and compare this velocity with the 8.35 km s^{-1} at 44.5 km depth observed along the same azimuth on line GBC. However, the two velocities are sufficinetly different to raise the

question of whether further lateral or vertical changes, or further anisotropic layers with different directions of anisotropy are likely in the upper mantle. If they do exist, the depth of isostatic equilibrium may be even deeper than 160 km as suggested by Dooley (1977).

The consideration of isostasy leads to the conclusion that the upper mantle under the Pilbara Craton is less dense that that under the Yilgarn Craton. Studies of the contrast across the edges of Precambrian cratons have been made elsewhere in the world. The crust in the boundary between the Superior and Grenville Provinces in Canada is thicker that that within the provinces, but the two provinces have very similar characters (Berry & Fuchs, 1973). However, seismic velocity differences between the West African Craton and the bounding Mauritanide Orogenic Belt of Palaeozoic age in Senegal may persist to several hundred kilometres' depth (Briden & others, 1981).

The presence of contrast at great depths across some craton margins and not across others implies that the evolutionary processes that generate the crust leave their marks on the upper mantle. Any detailed study of the evolution of a region should therefore be a study of the entire lithosphere.

10. CONCLUSIONS

Throughout this thesis, many conclusions have been reached about the nature of the crust and upper mantle in the Precambrian shield of northwest Australia, and the implications these conclusions have for crustal evolution in the region. The purpose of this chapter is to summarise those conclusions and their implications. They are:

(1) The Pilbara Craton has a much thinner crust than the Yilgarn Craton. The crust in the intervening Capricorn Orogenic Belt is intermediate in thickness.

(2) The different crustal thicknesses, when considered with isostatic models of the region, imply that the upper mantle under the Pilbara Craton is less dense than the upper mantle under the Yilgarn Craton.

(3) The differences in the upper mantle densities under the cratons imply that the upper mantle was the source of the iron of the Hamersley Basin. No process suitable for extracting and concentrating the iron is suggested by the seismic models, but the basic volcanism of the lower Hamersley Basin was probably the main process for transporting the iron to the surface.

(4) The different crustal thicknesses of and upper mantle densities under the cratons are further evidence that the cratons formed separately before their amalgamation before or about 2400 m.y. ago.

(5) The lower crust of the Capricorn Orogen has high seismic velocities and is dense, probably due either to higher metamorphic grades or mafic intrusions caused by Proterozoic tectonics

(6) The northern margin of the Yilgarn Craton was deformed along a zone about 50 km wide during the Proterozoic orogeny, but no such zone is recognisable in the seismic models along the southern edge of the Pilbara Craton.

(7) The upper crust of the Pilbara Craton has a granitic composition. At 10-15 km depth, it is metamorphosed to felsic granulite. Below this depth, the amount of garnet increases, causing an increase in the

seismic velocity. The mafic content also increases, causing a further increase in the amount of garnet, until the lower crust of the craton is of dioritic composition.

(8) The crust/mantle boundary under the Pilbara Craton is a chemical discontinuity.

(9) The lower crust of the Pilbara Craton is much less mafic than the lower crust in younger regions of Australia. The differences imply that different tectonic processes were active in the Archaean.

(10) The Pn seismic velocity under the Pilbara Craton is anisotropic, with the direction of maximum velocity at right angles to the axis of the Hamersley Basin.

(11) A sub-Moho boundary occurs about 15 km below the Moho, and its topography follows that of the Moho.

(12) The mantle below the sub-Moho boundary is anisotropic, with the direction of maximum velocity apparently between north and 40 degrees west of north.

(13) The response of cratons around the world to discrete global thermal events depended on their cratonic maturity. The response to the thermal event between 2800 and 2600 m.y. ago in the Yilgarn Craton was to form new crust, while in the Pilbara Craton the Hamersley Basin formed.

(14) Several processes may have contributed to the formation of the Hamersley Basin. The most likely are:

(a) Isostatic adjustment of an initial depression gradually filled with sediments. The initial depression may have been caused by any or all of (i) thermal uplift followed by erosion, and then cooling and contraction; (ii) a metamorphic change within the crust to a denser less voluminous phase; and (iii) a mass transfer process in which rocks were taken from the upper mantle and deposited on the land surface immediately above, and

(b) Compression and then folding by a compressive stress, causing a basin to form out of isostatic equilibrium. With the relaxation or accomodation of the stress, the crust rose isostatically.

There is no reason why scenarios (a) and (b) could not have acted in parallel.

(15) The geological parallels between the Hamersley Basin and the Transvaal Basin, and the similarities of the seismic characters of the underlying cratons, suggest that similar processes may have acted to form the Transvaal Basin.

(16) The anisotropy in Pn may be due to syntectonic recrystallisation and/or power law creep in the tensional environment in the uppermost mantle under the Hamersley Basin during basin subsidence.

(17) The anisotropy under the sub-Moho boundary is probably due to a later tectonic event.

(18) The lithosphere under the Pilbara Craton was probably very thin in the early Precambrian. The base of the lithosphere at the end of the Hamersley Basin formation is now at 45 km depth.

(19) The current base of the lithosphere in central and western Australia is now below a seismic discontinuity at about 200 km depth (Drummond & others, 1982).

(20) The vertical and horizontal structure that can be gleaned from the seismic and gravity data suggest that the upper mantle structure is as complex as that of the upper crust.

(21) Notwithstanding the comparisons and predictions of conclusions 8 and 15 above, the different thicknesses of the crusts of the Pilbara and Yilgarn Cratons, and the nature of the crust/mantle boundary suggest that any generalisations about the nature of the crust/mantle boundary or type classifications of the seismic signature of the crust such as those of Bamford & Prodehl (1977), Prodehl (1977) and Mueller (1977) are premature.

(22) The evolution of the lithosphere is inextricably linked to the evolution of the crust, so that a study of the evolution of continents must begin with a study of both.

11. REFERENCES.

AKI,K., & RICHARDS, P.G., 1980- QUANTITATIVE SEISMOLOGY, VOLUME 1. W.H. Freeman & Company, 557p.

ANDERSON, D.L., SAMMIS,C., & JORDAN, T., 1972- Composition of mantle and core. In ROBERTSON, E.C. (editor)- THE NATURE OF THE SOLID EARTH. Mc Graw Hill, New York, 41 - 66.

ANHAEUSSER, C.R., 1973- The evolution of the early Precambrian crust of southern Africa. Philosophical Transactions of the Royal Society of London, A273, 359 - 388.

ANSORGE, J., 1975- Die Feinstruktur des obersten Erdmantels unter Europa und dem mittleren Nordamerika. University of Karlsruhe, Ph D. Thesis (unpublished).

ANSORGE, J., BONJER, K.-P., & EMTER, D., 1979- Structure of the uppermost mantle from longe-range seismic observations in southern Germany and the Rhinegraben area. Tectonophysics, 56, 31 - 48.

ARRIENS, P.A., 1971- The Archaean geochronology of Australia. Geological Society of Australia, Special Publication, 3, 11 - 23.

AVE 'LALLEMANT, H.G., & CARTER, N.L., 1970- Syntectonic recrystallization of olivine and modes of flow in the upper mantle. Geological Society of America, Bulletin, 81, 2203 - 2220.

BACKUS, G.E., 1965- Possible forms of seismic anisotropy of the uppermost mantle under oceans. Journal of Geophysical Research, 70, 3429 - 3439.

BAMFORD, S.A.D, 1971- An interpretation of first-arrival data from the Continental Margin Refraction Experiment. Geophysical Journal of the Royal Astronomical Society, 24, 213 - 229.

BAMFORD, D., 1973a- Refraction data in Western Germany - a time-term interpretation. Journal of Geophysics, 39, 907 - 927.

BAMFORD, S.A.D, 1973b- An example of the iterative approach to time-term analysis. Geophysical Journal of the Royal Astronomical Society, 31, 365 - 372.

BAMFORD, D., 1976- MOZAIC time-term analysis. Geophysical Journal of the Royal Astronomical Society, 44, 433 - 446.

BAMFORD, D., 1977- Pn velocity anisotropy in a continental upper mantle. Geophysical Journal of the Royal Astronomical Society, 49, 29 - 48.

BAMFORD, D., & PRODEHL, C., 1977- Explosion seismology and the continental crust-mantle boundary. Geological Society of London, Journal, 134, 139 - 151.

BATH, M., 1978- An analysis of the time term method in refraction seismology. Tectonophysics, 51, 155 - 169.

BEAUMONT, C., 1979- On rheological zonation of the lithosphere during flexure. Tectonophysics, 59, 347 - 365.

BEAUMONT C., & SWEENEY, J.F., 1978- Graben generation of major sedimentary basins. Tectonophysics, 50, T19 - T23.

BERRY, L.G., & MASON, B., 1959- MINERALOGY. W.H. Freeman & Company, San Francisco. 630p.

BERRY, M.J., 1971- Depth uncertainties from seismic first-arrival refraction studies. Journal of Geophysical Research, 76, 6464 - 6468.

BERRY, M.J., & FUCHS, K., 1973- Crustal structure of the Superior and Grenville Provinces of the northeastern Canadian shield. Seismological Society of America, Bulletin, 63, 1393 - 1432.

BERRY, M.J., & WEST, G.F., 1966a- An interpretation of the first-arrival data of the Lake Superior experiment by the time-term method. Seismological Society of America, Bulletin, 56, 141 - 171.

BERRY, M.J., & WEST, G.F., 1966b- A time-term interpretation of the first-arrival data of the 1963 Lake Superior experiment. In STEINHART, J.S., & SMITH, T.J. (editors)- The earth beneath the continents. American Geophysical Union, Monograph, 10, 166 - 180.

BIRCH, F., 1960- The velocity of compressional waves in rocks to 10 kilobars, Part 1. Journal of Geophysical Research, 65, 1083 - 1102.

BIRCH, F., 1961- The velocity of compressional waves in rocks to 10 kilobars, Part 2. Journal of Geophysical Research, 66, 2199 - 2224.

BLOCKLEY, J.G., 1975 - Pilbara Block. In Geology of Western Australia. Geological Survey of Western Australia, Memoir, 2, 81 - 93.

BLOCKLEY, J.G., TRENDALL, A.F., DE LAETER, J.R., & LIBBY, W.G., 1980- Two "anomalous" isochrons from the vicinity of Newman. Geological Survey of Western Australia, Annual Report, 1979, 93 - 96.

BMR., 1975- Gravity map of Australia, 1:5 000 000 scale. Bureau of Mineral Resources, Australia, Canberra.

BRAILE, L.W., & SMITH, R.B., 1975- Guide to the interpretation of crustal refraction profiles. Geophysical Journal of the Royal Astronomical Society, 40, 145 - 176.

BRAKEL, A.T., & MUHLING, P.C., 1976- Stratigraphy, sedimentation, and structure in the western and central part of the Bangemall Basin, Western Australia. Geological Survey of Western Australia, Annual Report, 1975, 70 - 79.

BRIDEN, J.C., WHITCOMBE, D.N., STUART, G.W., FAIRHEAD, J.D., DORBATH, C., & DORBATH, L., 1981- Depth of geological contrast across the West African Craton margin. Nature, 292, 123 - 128.

BULLARD, E.C., 1936- Gravity measurements in East Africa. Philosophical Transactions of the Royal Society of London, Series A, 235, 445 - 531.

BULLEN, K.E., 1960 - Note on cusps in seismic travel times. Geophysical Journal of the Royal Astronomical Society, 3, 354 - 359.

BUTTON, A., 1976 - Transvaal and Hamersley Basins - review of basin development and mineral deposits. Minerals, Science and Engineering, 8, 262 - 293.

CARTER, N.L., & AVE 'LALLEMANT, H.G., 1970- High temperature flow of dunite and peridotite. Geological Society of America, Bulletin, 81, 2180 - 2202.

CHAPMAN, H.J., DE LAETER, J.R., GORTON, M.P., ANDERSEN, L.S., BETTENAY, L.F., BICKLE, M.J., BINNS, R.A., & GROVES, D.I., 1980- Isotopic study of granitic rocks from the central Yilgarn Block, Western Australia. In GLOVER, J.E., & GROVES, D.I. (editors)- Second International Archaean Symposium, Perth, 1980. Extended Abstracts. Geological Society of Australia and I.G.C.P., Archaean Geochemistry Project, 15 - 17.

CHRISTENSEN, N.I., 1965- Compressional wave velocities in metamorphic rocks at pressures to 10 kilobars. Journal of Geophysical Research, 70, 6147 - 6164.

CHRISTENSEN, N.I., 1979- Compressional wave velocities in rochs at high temperatures and pressures, critical thermal gradients, and crustal low-velocity zones. Journal of Geophysical Research, 84, 6849 - 6857.

CHRISTENSEN, N.I., & FOUNTAIN, D.M., 1975- Constitution of the lower continental crust based on the experimental studies of seismic velocities in granulite. Geological Society of America, Bulletin, 86, 227 - 236.

COLLINS, C.D.N., 1979- Adaption of the synthetic seismogram program "REFLEX" to the CSIRO CYBER 76 computer. Bureau of Mineral Resources, Australia, Record, 1979/7 (unpublished).

COMPSTON, W., & ARRIENS, P.A., 1968- The Precambrian geochronology of Australia. Canadian Journal of Earth Sciences, 5, 561 - 583.

COOK, F.A., & TURCOTTE, D.L., 1981- Parameterized convection and the thermal evolution of the earth. Tectonophysics, 75, 1 - 17.

COOPER, J.A., JAMES, P.R., & RUTLAND, R.W.R., 1980- Rb/Sr dating of granitic intrusions in relation to the stratigraphic and deformational history of the Pilbara region. In GLOVER, J.E., & GROVES, D.I. (editors)- Second International Archaean Symposium, Perth, 1980. Extended Abstracts. Geological Society of Australia and I.G.C.P. Archaean Geochemistry Project, 14 - 15.

COOPER, J.A., NESBITT, R.W., PLATT, J.P., & MORTIMER, G.E., 1978- Crustal development in the Agnew region, Western Australia, as shown by Rb/Sr isotopic and geochemical studies. Precambrian Research, 7, 31 - 59.

CULL, J.P., & DENHAM, D., 1979- Regional variations in Australian heat flow. BMR Journal of Australian Geology & Geophysics, 4, 1 - 13.

DANIELS, J.L., 1975- Gascoyne Province. In Geology of Western Australia. Geological Survey of Western Australia, Memoir, 2, 107 - 114.

DANIELS, J.L., & MACLEOD, W.N., 1965- Newman, Western Australia. Geological Survey of Western Australia, 1: 250 000 Geological Series, Explanatory Notes.

DAWSON, J.B., 1977- Sub-cratonic crust and upper mantle models based on xenolith suites in kimberlitic and nephelinitic diatremes. Geological Society of London, Journal, 134, 173 - 184.

DE LAETER, J.R., 1976- Rb-Sr whole-rock and mineral ages from the Gascoyne Province. Geological Survey of Western Australia, Annual Report, 1975, 126 - 130.

DE LAETER, J.R., & BLOCKLEY, J.G., 1972- Granite ages within the Archaean Pilbara Block, Western Australia. Geological Society of Australia, Journal, 19, 363 - 370.

DE LAETER, J.R., FLETCHER, I.R., ROSMAN, K.J.R., WILLIAMS, I.R., GEE,R.D., & LIBBY, W.G., 1981- Early Archaean gneisses from the Yilgarn Block, Western Australia. Nature, 292, 322 - 324.

DE LAETER, J.R., LEWIS, J.D., & BLOCKLEY, J.G., 1975- Granite ages within the Shaw Batholith of the Pilbara Block. Geological Survey of Western Australia, Annual Report, 1974, 73 - 79.

DE LAETER, J.R., LIBBY, W.G., & TRENDALL, A.F., 1981- The older Precambrian geochronology of Western Australia. In GLOVER, J.E., & GROVES, D.I. (editors)- Archaean Geology. Second International Archaean Symposium. Geological Society of Australia, Special Publication, 7, 145 - 157.

DE LAETER, J.R., PEERS, R., & TRENDALL, A.F., 1974- Petrography, chemical composition, and geochronology of two dolerite sills from the Precambrian Weeli Wolli Formation, Hamersley Group. Geological Survey of Western Australia, Annual Report, 1973, 82 - 91.

DE LA HUNTY, L.E., 1965- Mount Bruce, Western Australia. Geological Survey of Western Australia. 1:250 000 Geological Series Explanatory Notes.

DOOLEY, J.C., 1952- Calculation of depth and dip of several layers by refraction seismic method. In THYER, R.F., & VALE, K.R. - Geophysical surveys, Oakland - Coorabin coalfield, New South Wales. Bureau of Mineral Resources, Australia, Bulletin, 19, Appendix.

DOOLEY, J.C., 1977- Implications of Australian seismic and gravity measurements for the structure and composition of the upper mantle. BMR Journal of Australian Geology & Geophysics, 2, 1 - 5.

DRUMMOND, B.J., 1979a- Structural relations between the Archaean Pilbara and Yilgarn Cratons, Western Australia, from deep seismic sounding. Australian National University M Sc. Thesis (unpublished).

DRUMMOND, B.J., 1979b- A crustal profile across the Archaean Pilbara and northern Yilgarn Cratons, northwest Australia. BMR Journal of Australian Geology & Geophysics, 4, 171 - 180.

DRUMMOND, B.J., 1979c- Pilbara Crustal Survey, 1977: Operational Report. Bureau of Mineral Resources, Australia, Record, 1979/54 (unpublished).

DRUMMOND, B.J., 1981- Crustal structure of the Precambrian terrains of northwest Australia from seismic refraction data. BMR Journal of Australian Geology & Geophysics, 6, 123 - 135.

DRUMMOND, B.J., MUIRHEAD, K.J., & HALES, A.L., 1982- Evidence for a seismic discontinuity near 200 km depth under a continental margin. Geophysical Journal of the Royal Astronomical Society, 69, in press.

DRUMMOND, B.J., & SHELLEY, H.M., 1981- Isostasy and structure of the lower crust and upper mantle in the Precambrian terrains of northwest Australia. BMR Journal of Australian Geology & Geophysics, 6, 137 - 143.

DRUMMOND, B.J., SMITH, R.E., & HORWITZ, R.C., 1981- Crustal structure in the Pilbara and northern Yilgarn Blocks from deep seismic sounding. In GLOVER, J.E., & GROVES, D.I. (editors)- Archaean Geology. Second International Archaean Symposium. Geological Society of Australia, Special Publication, 7, 33 - 41.

EMBLETON, B.J.J., 1978- The palaeomagnetism of 2400 m.y. old rocks from the Australian Pilbara craton and its relation to Archaean - Proterozoic tectonics. Precambrian Research, 6, 275 - 291.

EWING, M., WOOLLARD, G.P., & VINE, A.C., 1938- Geophysical investigations in the emerged and submerged Atlantic coastal plain. Geological Society of America, Bulletin, 50, 257 - 295.

FABER, S., 1978- Refraktionsseismische Untersuchung der Lithosphare unter den britischen Inseln. University of Karlsruhe, Ph D. Thesis (unpublished).

FABER, S., & BAMFORD, D., 1979- Lithospheric structural contrasts across the Caledonides of northern Britain. Tectonophysics, 56, 17 - 30.

FERGUSON, J., ARCULUS, R.J., & JOYCE, J., 1979- Kimberlite and kimberlitic intrusives of southeastern Australia: a review. BMR Journal of Australian Geology & Geophysics, 4, 227 - 241.

FINLAYSON, D.M., & COLLINS, C.D.N., 1980- A brief description of BMR portable seismic tape recording systems. Australian Society of Exploration Geophysicists, Bulletin, 11, 75 - 77.

FINLAYSON, D.M., COLLINS, C.D.N., & DENHAM, D., 1980- Crustal structure under the Lachlan Fold Belt, southeastern Australia. Physics of the Earth and Planetary Interiors, 21, 321 - 342.

FINLAYSON, D.M., & MC CRACKEN, H.M., 1981- Crustal structure under the Sydney Basin and Lachlan Fold Belt, determined from explosion seismic studies. Geological Society of Australia, Journal, 28, 177 - 190.

FINLAYSON, D.M., PRODEHL, C., & COLLINS, C.D.N., 1979- Explosion seismic profiles, and implications for crustal evolution in southeastern Australia. BMR Journal of Australian Geology & Geophysics, 4, 243 - 252.

FOUCHER, J.P., & LE PICHON, X., 1972- Comment on 'Thermal effects of the formation of Atlantic continental margins by continental break up' by N.H. Sleep. Geophysical Journal of the Royal Astronomical Society, 29, 43 - 46.

FRASER, A.R., 1973- A discussion on the gravity anomalies of the Precambrian shield of Western Australia, Bureau of Mineral Resources, Record, 1973/105 (unpublished).

FRASER, A.R.,1979a- Reconnaissance gravity survey in northwest Western Australia, 1969. In FRASER, A.R., & PETTIFER, G.R., Reconnaissance gravity surveys in Western Australia and South Australia, 1969 - 1972. Bureau of Mineral Resources, Australia, Bulletin, 196 Part B, 13 - 25.

FRASER, A.R., 1979b- Reconnaissance gravity surveys in central and southwest Western Australia, 1971 - 1972. In FRASER, A.R., & PETTIFER, G.R.- Reconnaissance gravity surveys in Western Australia and South Australia 1969 - 1972. Bureau of Mineral Resources, Australia, Bulletin, 196 Part C, 27 - 45.

FUCHS, K., 1968- Das Reflexions und Transmissionsvermogen eines geschichteten Mediums mit beliebiger Tiefen-Verteilung der elastischen Moduln und der Dichte fur schragen Einfall ebener Wellen. Journal of Geophysics, 34, 389 - 413. English translation by FEEKEN, E.H., 1979- The reflectivity and transmittance of a stratified medium with variable depth distribution of moduli of elasticity and density for inclined incidence of plane waves. In COLLINS, C.D.N., 1979- Adaption of the synthetic seismogram program "REFLEX" to the CSIRO CYBER 76 computer. Bureau of Mineral Resources, Australia, Record, 1979/7 (unpublished).

FUCHS, K., 1977 - Seismic anisotropy of the subcrustal lithosphere as evidence for dynamical processes in the upper mantle. Geophysical Journal of the Royal Astronomical Society, 49, 167 - 179.

FUCHS, K., 1979- Structure, physical properties and lateral heterogeneities of the subcrustal lithosphere from long-range deep seismic sounding observations on continents. Tectonophysics, 56, 1 - 15.

FUCHS, K., & MULLER, G., 1971- Computation of synthetic seismograms with the reflectivity method and comparison with observations. Geophysical Journal of the Royal Astronomical Society, 23, 417 - 433.

GARDNER, L.W., 1939- An areal plan of mapping subsurface structure by refraction shooting. Geophysics, 4, 247 - 259.

GEE, R.D., 1979a- Tectonics of the Western Australian shield. Tectonophysics, 50, 327 - 369.

GEE, R.D. (compiler), 1979b- Geological map of Western Australia, 1:2 500 000 scale. Geological Survey of Western Australia, Perth.

GEE, R.D., 1979c- The geology of the Peak Hill area. Western Australia Department of Mines, Annual Report, 1978, 99 - 106.

GEE, R.D., 1980- Summary of the Precambrian stratigraphy of Western Australia. Geological Survey of Western Australia, Annual Report, 1979, 85 - 90.

GEE, R.D., DE LAETER, J.R., & DRAKE, J.R., 1976- Geology and geochronology of altered rhyolite from the lower part of the Bangemall Group near Tangadee, Western Australia. Geological Survey of Western Australia, Annual Report, 1975, 112 - 117.

GIESE, P., PRODEHL, C., & STEIN, A. (editors), 1976- Explosion seismology in central Europe. Data and results. Crustal and upper mantle structure in Europe. European Seismological Commission, Monograph, 1, Springer-Verlag, Berlin.

GLIKSON, A.Y., 1975- Greenstone Belts. In WINDLEY, B.F. (editor)- The early History of the Earth. John Wiley & Sons, London, 257 - 277.

GLIKSON, A.Y., 1979- Early Precambrian tonalite-trondhjemite sialic nuclei. Earth Science Reviews, 15, 1 - 73.

GLIKSON, A.Y., & LAMBERT, I.B., 1976- Vertical zonation and petrogenesis of the early Precambrian crust in Western Australia. Tectonophysics, 30, 55 - 89.

GRACHEV, A.F., & FEDOROVSKY, V.S., 1981- On the nature of greenstone belts in the Precambrian. Tectonophysics, 73, 195 - 212.

GREEN, D.H., 1972- Archaean greenstone belts may include equivalents of lunar maria?. Earth and Planetary Science Letters, 15, 263 - 270.

GREEN, D.H., & LAMBERT, I.B., 1965- Experimental crystallization of anhydrous granite at high pressures and temperatures. Journal of Geophysical Research, 70, 5259 - 5268.

GREEN, T.H., 1970- High pressure experimental studies on the mineralogical constitution of the lower crust. Physics of the Earth and Planetary Interiors, 3, 441 - 450.

GROVES, D.I., ARCHIBALD, N.J., BETTENAY, L.F., & BINNS, R.A., 1978- Greenstone belts as ancient marginal basins or ensialic rift zones. Nature, 273, 460 - 461.

GSWA, 1975- Geology of Western Australia. Geological Survey of Western Australia, Memoir, 2, 541p.

HALES, A.L., & SACKS, I.S., 1958- Evidence for an intermediate layer from crustal structure studies in the eastern Transvaal. Geophysical Journal of the Royal Astronomical Society, 2, 15 - 33.

HALL, W.D.M., & GOODE, A.D.T., 1978- The early Proterozoic Nabberu Basin and associated iron formations of Western Australia. Precambrian Research, 7, 129 - 184.

HALLBERG, J.A., & GLIKSON, A.Y., 1981- Archaean granite-greenstone terrains of Western Australia. In HUNTER, D.R. (editor)- Precambrian of the southern hemisphere. Elsevier, Amsterdam, 33 - 96.

HALLBERG, J.A., JOHNSTON, C., & BYE, S.M., 1976- The Archaean Marda Igneous Complex, Western Australia. Precambrian Research, 3, 111 - 136.

HAMILTON, P.J., EVENSEN, N.M., O'NIONS, R.K., GLIKSON, A.Y., & HICKMAN, A.H., 1980- Sm-Nd dating of the Talga-Talga Subgroup, Warrawoona Group, Pilbara Block, Western Australia. In GLOVER, J.E., & GROVES, D.I. (editors)- Second International Archaean Symposium, Perth, 1980. Extended Abstracts. Geological Society of Australia and I.G.C.P. Archaean Geochemistry Project, 11 - 12.

HEISKANEN, W.A., & VENING MEINSZ, F.A., 1958- THE EARTH AND ITS GRAVITY FIELD. Mc Graw Hill Book Company, New York, 470p.

HERZBERG, C.T., 1978- Pyroxene geothermometry and geobarometry: experimental and thermodynamic evaluation of some subsolidus phase relations involving pyroxenes in the system CaO - MgO - Al_2O_3 - SiO_2. Geochimica et Cosmochimica Acta, 42, 945 - 957.

HICKMAN, A.H., & DE LAETER, J.R., 1977- The depositional environment and age of a shale within the Hardey Sandstone of the Fortescue Group. Geological Survey of Western Australia, Annual Report, 1976, 62 - 68.

HICKMAN, A.H., & LIPPLE, S.L., 1975- Explanatory notes on the Marble Bar 1:250 000 geological sheet, Western Australia. Geological Survey of Western Australia, Record, 1974/20 (unpublished).

HIRN, A., STEINMETZ, L., KIND, R., & FUCHS, K., 1973- Long range profiles in western Europe: II. Fine structure of the lower lithosphere in France (southern Bretagne). Zeitschrift für Geophysik, 39, 363 - 384.

HOLMES, A., 1965- PRINCIPLES OF PHYSICAL GEOLOGY. Thomas Nelson & Sons, London, 2nd edition, 1288p.

HORWITZ,R.C., 1975- Provisional geological map at 1:250 000 of the northeast margin of the Yilgarn Block, Western Australia. CSIRO Minerals Research Laboratories, Division of Mineralogy, Report, FP 10.

HORWITZ, R.C., & SMITH, R.E., 1978- Bridging the Yilgarn and Pilbara Blocks, Western Australia. Precambrian Research, 6, 293 - 322.

HUNTER, D.R., 1974- Crustal development in the Kaapvaal Craton: the Archaean. Precambrian Research, 1, 259 - 294.

HYDE, R.S., 1980- Sedimentary facies in the Archaean Timiskaming Group and their tectonic implications, Abitibi greenstone belt, northeastern Canada. Precambrian Research, 12, 161 - 195.

ITO, K., & KENNEDY, G.C., 1970- The fine structure of the basalt - eclogite transition. Mineralogical Society of America, Special Paper, 3, 77 - 88.

IUGS, 1973- Plutonic rocks. Classification and nomenclature recommended by the IUGS Subcommission on the Systematics of Igneous Rocks. Geotimes, 18 (10), 26 - 30.

JAEGER, J.C., 1970- Heat flow and radioactivity in Australia. Earth and Planetary Science Letters, 8, 285 - 292.

JESSOP, A.M., & LEWIS, T., 1978- Heat flow and heat generation in the Superior Province of the Canadian shield. Tectonophysics, 50, 55 - 77.

JORDAN, T.H., 1975- The continental tectosphere. Reviews of Geophysics and Space Physics, 13, 1 - 12.

JORDAN, T.H., 1978- Composition and development of the continental tectosphere. Nature, 274, 544 - 548.

KELLER, B.M., 1979- Precambrian stratigraphic scale of the USSR. Geological Magazine, 116, 419 - 429.

KENNEDY, G.C., 1959- The origin of continents, mountain ranges, and ocean basins. American Scientist, 47, 491 - 504.

KIND, R., 1976- Computation of reflection coefficients for layered media. Journal of Geophysics, 41, 191 - 200.

KRIEWALDT, M., & RYAN, G.R., 1967- Pyramid, Western Australia. Geological Survey of Western Australia, 1:250 000 Explanatory Notes, SF/50-7.

LAMBERT, I.B., 1971- The composition and evolution of the deep continental crust. Geological Society of Australia, Special Publication, 3, 419 - 428.

LEGGO, P.J., COMPSTON, W., & TRENDALL, A.F., 1965- Radiometric ages of some Precambrian rocks from the northwest division of Western Australia. Geological Society of Australia, Journal, 12, 53 - 65.

LEVEN, J.H., JACKSON, I., & RINGWOOD, A.E., 1981- Upper mantle seismic anisotropy and lithosphere decoupling. Nature, 289, 234 - 239.

LEWIS, J.D., ROSMAN, K.J.R., & DE LAETER, J.R., 1975- The age and metamorphic effects of the Black Range dolerite dyke. Geological Survey of Western Australia, Annual Report, 1974, 80 - 88.

LOBERG, B.E.H., 1980- A Proterozoic subduction zone in southern Sweden. Earth and Planetary Science Letters, 46, 287 - 294.

LOVERING, J.F., 1958- The nature of the Mohorovicic Discontinuity. American Geophysical Union, Transaction, 39, 947 - 955.

MACLEOD, W.N., & DE LA HUNTY, L.E., 1966- Roy Hill, Western Australia. Geological Survey of Western Australia, 1:250 000 Geological Series Explanatory Notes.

MAIR, J.A., & LYONS, J.A., 1981 - Crustal structure and velocity anisotropy beneath the Beaufort Sea. Canadian Journal of Earth Sciences, 18, 724 - 741.

MANGHNANI, M.H., RAMANANANTOANDRO, R., & CLARK, S.P., 1974- Compressional and shear wave velocities in granulite facies rocks and eclogites to 10 kbar. Journal of Geophysical Research, 79, 5427 - 5446.

MARESCHAL, J.-C., 1981- Uplift by thermal expansion of the lithosphere. Geophysical Journal of the Royal Astronomical Society, 66, 535 - 552.

MARESCHAL, J.-C., & WEST, G.F., 1978- A model for Archaean tectonism. Part 2. Numerical models of vertical tectonism in greenstone belts. Canadian Journal of Earth Sciences, 17, 60 - 71.

MATSUSHIMA, S., 1981- Compressional and shear velocities of igneous rocks and volcanic glasses to 900oC and 20 kbar. Tectonophysics, 75, 257 - 271.

MC CULLOCH, M.T., & COMPSTON, W., 1981- Sm-Nd age of Kambalda and Kanowna greenstones and heterogeneity in the Archaean mantle. Nature, 294, 322 - 327.

MC CULLOCH, M.T., & WASSERBURG, G.J., 1978- Sm-Nd and Rb-Sr chronology of continental crust formation. Times of addition to continents of chemically fractionated mantle-derived materials are determined. Science, 200, 1003 - 1011.

MC ELHINNY, M.W., & MC WILLIAMS, M.O., 1977- Precambrian geodynamics - a palaeomagnetic view. Tectonophysics, 40, 137 - 159.

MC GARR, A., & GAY, N.C., 1978- State of stress in the earth's crust. Annual Reviews of Earth and Planetary Science, 6, 405 - 436.

MC KENZIE, D., 1978- Some remarks on the development of sedimentary basins. Earth and Planetary Science Letters, 40, 25 - 32.

MC KENZIE, D., NISBET, E., & SCLATER, J.G., 1980- Sedimentary basin development in the Archaean. Earth and Planetary Science Letters, 48, 35 - 41.

MEREU, R.F., 1969- Effect of Mohorovicic topography on the amplitude of seismic P waves. Journal of Geophysical Research, 74, 4371 - 4376.

MEREU, R.F., MAJUMDAR, S.C., & WHITE, R.E., 1977- The structure of the crust and upper mantle under the highest ranges of the Canadian Rockies from a seismic refraction survey. Canadian Journal of Earth Sciences, 14, 196 - 208.

MIDDLETON, M.F., 1980- A model of intracratonic basin formation, entailing deep crustal metamorphism. Geophysical Journal of the Royal Astronomical Society, 62, 1 - 14.

MORRIS, G.B., RAITT, R.W., & SHOR, G.G. Jnr., 1969- Velocity anisotropy and delay time maps of the mantle near Hawaii. Journal of Geophysical Research, 74, 4300 - 4316.

MOTA, L., 1954- Determination of dips and depths of geological layers by the seismic refraction method. Geophysics, 19, 242 - 254.

MUELLER, S., 1977- A new model of the continental crust. In HEACOCK, J.G. (editor)- The earth's crust. American Geophysical Union, Monograph, 20, 289 - 317.

MUELLER, S., & LANDISMAN, M., 1966- Seismic studies of the earth's crust in continents. I: Evidence for a low-velocity zone in the upper part of the lithosphere. Geophysical Journal of the Royal Astronomical Society, 10, 525 - 538.

MUELLER, S., & LANDISMAN, M., 1971- An example of the unified method of interpretation for crustal seismic data. Geophysical Journal of the Royal Astronomical Society, 23, 365 - 371.

MUIRHEAD, K.J., & SIMPSON, D.W., 1972- A three quarter watt seismic station. Seismological Society of America, Bulletin, 62, 985 - 990.

NICOLAS, A., & POIRER, J.P., 1976- CRYSTALLINE PLASTICITY AND SOLID STATE FLOW IN METAMORPHIC ROCKS. John Wiley & Sons, London, 444p.

NIEUWLAND, D.A, & COMPSTON, W., 1980- The geological history of part of the Jimperding Metamorphic Belt, west Yilgarn Block. In GLOVER, J.E., & GROVES, D.I. (editors)- Second International Archaean Symposium, Perth, 1980. Extended Abstracts. Geological Society of Australia and I.G.C.P. Archaean Geochemistry Project, 12 - 13.

O'BRIEN, P.N.S., 1968- Lake Superior crustal structure - a reinterpretation of the 1963 seismic experiment. Journal of Geophysical Research, 73, 2669 - 2689.

OVERSBY, V.M., 1975- Lead isotope systematics and ages of Archaean acid intrusives in the Kalgoorlie - Norseman area, Western Australia. Geochimica et Cosmochimica Acta, 39, 1107 - 1125.

OVERSBY, V.M., 1976- Isotopic ages and geochemistry of Archaean acid igneous rocks from the Pilbara, Western Australia. Geochimica et Cosmochimica Acta, 40, 817 - 829.

PADGHAM, W.A., 1980- Crustal evolution, Slave Province. In GLOVER, J.E., & GROVES, D.I. (editors)- Second International Archaean Symposium, Perth, 1980. Extended Abstracts. Geological Society of Australia and I.G.C.P. Archaean Geochemistry Project, 73 - 74.

PESELNICK, L., NICOLAS, A., & STEVENSON, P.R., 1974 - Velocity anisotropy in a mantle peridotite from the Ivrea Zone: Application to upper mantle anisotropy. Journal of Geophysical Research, 79, 1175 - 1182.

PIDGEON, R.T., 1973- U-Pb study of zircons from the Kambalda granite. Australian National University, Annual Report (unpublished).

PIDGEON, R.T., 1978a- 3450 m.y.-old volcanics in the Archaean layered greenstone succession of the Pilbara Block, Western Australia. Earth and Planetary Science Letters, 37, 421 - 428.

PIDGEON, R.T., 1978b- Geochronological investigations of granite batholiths of the Archaean granite - greenstone terrain of the Pilbara Block, Western Australia. In SMITH, I.E.M., & WILLIAMS, J.G. (editors)- Proceedings of the 1978 Archaean Geochemistry Conference. University of Toronto, 360 - 362.

PLUMB, K.A., 1979- Structure and tectonic style of the Precambrian shields and platforms of northern Australia. Tectonophysics, 58, 291 - 325.

PRODEHL, C., 1977- The structure of the crust-mantle boundary beneath North America and Europe as derived from explosion seismology. In HEACOCK, J.G. (editor)- The earth's crust. Its nature and physical properties. American Geophysical Union, Geophysical Monograph, 20, 349 - 369.

RAITT, R.W., SHOR, G.G. Jnr., FRANCIS, T.J.G., & MORRIS, G.B., 1969- Anisotropy of the Pacific upper mantle. Journal of Geophysical Research, 74, 3095 - 3109.

REITER, L., 1970- An investigation into the time term method in refraction seismology. Seismological Society of America, Bulletin, 60, 1 - 13.

RICHARDS, J.R., 1977- Lead isotopes and ages of galenas from the Pilbara region, region, Western Australia. Geological Society of Australia, Journal, 24, 465 - 473.

RICHARDS, J.R., 1982- Common-lead isotope ratio measurements. Australian National University Research School of Earth Sciences, Annual Report, 1981 (unpublished), 186 - 187.

RICHARDS, J.R., FLETCHER, I.R., & BLOCKLEY, J.G., 1981- Pilbara galenas: Precise isotopic assay of the oldest Australian leads; Model ages and growth - curve implications. Mineralium Deposita, 16, 7 - 30.

RICHARDSON, R.M., SOLOMON, S.C., & SLEEP, N.H., 1979- Tectonic stress in the plates. Reviews of Geophysics and Space Physics, 17, 981 - 1019.

RINGWOOD, A.E., 1975- COMPOSITION AND PETROLOGY OF THE EARTH'S MANTLE. Mc Graw-Hill, New York. 618p.

RINGWOOD, A.E., & GREEN, D.H., 1964- Experimental investigations bearing on the nature of the Mohorovicic discontinuity. Nature, 201, 566 - 567.

RINGWOOD, A.E., & GREEN, D.H., 1966- An experimental investigation of the gabbro-eclogite transformation and some geological implications. Tectonophysics, 3, 383 - 427.

SASS, J.H., JAEGER, J.C., & MUNROE, R.J., 1976- Heat flow and near-surface radioactivity in the Australian crust. United States Department of the Interior, Geological Survey, Open-File Report, 76-250.

SCHEIDEGGER, A.E., & WILLMORE, P.L., 1957- The use of a least squares method for the interpretation of data from seismic surveys. Geophysics, 22, 9 - 22.

SMITH, T.J., STEINHART, J.S., & ALDRICH, L.T., 1966- Lake Superior crustal structure. Journal of Geophysical Research, 71, 1141 - 1172.

STEINHART, J.S., 1964- Lake Superior seismic experiment, shots and travel times. Journal of Geophysical Research, 69, 5335 - 5352.

TALWANI, M., SUTTON, G.H., & WORZEL, J.O., 1959- A crustal section across the Puerto Rico Trench. Journal of Geophysical Research, 64, 1545 - 1555.

TARNEY, J., & WINDLEY, B.F., 1977- Chemistry, thermal gradients and evolution of the lower continental crust. Geological Society of London, Journal, 134, 153 - 172.

TAYLOR, S.R., & MC LENNAN, 1981- The composition and evolution of the continental crust: rare earth element evidence from sedimentary rocks. Philosophical Transactions of the Royal Society of London, Series A, 301, 381 - 399.

TRENDALL, A.F., 1968- Three great basins of Precambrian banded iron formation deposition: A systematic comparison. Geological Society of America, Bulletin, 79, 1527 - 1544.

TRENDALL, A.F., 1975a- Precambrian. In Geology of Western Australia. Geological Survey of Western Australia, Memoir, 2, 25 - 32.

TRENDALL, A.F., 1975b- Hamersley Basin. In Geology of Western Australia. Geological Survey of Western Australia, Memoir, 2, 119 - 143.

TRENDALL, A.F., 1975c- Preliminary geochronological results from two Pilbara porphyry bodies. Geological Survey of Western Australia, Annual Report, 1974, 103 - 106.

TRENDALL, A.F., 1979- A revision of the Mount Bruce Supergroup. Geological Survey of Western Australia, Annual Report, 1978, 63 - 71.

TRENDALL, A.F., & BLOCKLEY, J.G., 1970- The iron formations of the Precambrian Hamersley Group, Western Australia with special reference to the associated crocidolite. Geological Survey of Western Australia, Bulletin, 119.

TUREK, A., 1966- Geochronology of the Kalgoorlie area. Australian National University Ph D. Thesis (unpublished).

WATERS, B.R., 1976- Possible late Precambrian subduction zone in South West Africa. Nature, 259, 471 - 473.

WELLMAN, P., 1976- Regional variation of gravity, and isostatic equilibrium of the Australian crust. BMR Journal of Australian Geology & Geophysics, 1, 297 - 302.

WELLMAN, P., 1978- Gravity evidence for abrupt changes in mean crustal density at the junction of Australian crustal blocks. BMR Journal of Australian Geology & Geophysics, 3, 153 - 162.

WHITCOMBE, D,N., & MAGUIRE, P.K.H., 1979- The response of the time term method to simulated crustal structures. Seismological Society of America, Bulletin, 69, 1455 - 1473.

WHITCOMBE, D.N., & ROGERS, D.E., 1981- The effects of refractor topography and overburden anisotropy on time-term solutions of refractor anisotropy. Geophysical Journal of the Royal Astronomical Society, 67, 449 - 464.

WHITTEN, E.T.H., 1969- Trends in computer applications in structural geology. In MERRIAM, D.F. (editor)- Computer applications in the earth sciences. Plenum Press, New York, 223 - 249.

WIGGINS, R.A., & HELMBERGER, D.V., 1974- Synthetic seismogram computation by expansion in generalised rays. Geophysical Journal of the Royal Astronomical Society, 37, 73 - 90.

WILLMORE, P.L., & BANCROFT, A.M., 1960- The time term approach to refraction seismology. Geophysical Journal of the Royal Astronomical Society, 3, 419 - 432.

WILLIAMS, S.J., ELIAS, M., & DE LAETER, J.R., 1978- Geochronology and evolution of the eastern Gascoyne Province and the adjacent Yilgarn Block. Geological Survey of Western Australia, Annual Report, 1977, 50 - 56.

WYLLIE, P.J., 1971- THE DYNAMIC EARTH: TEXTBOOK IN GEOSCIENCES. John Wiley & Sons, New York, 416p.

YODER, H.S., & TILLEY, C.E., 1962- Origin of basalt magmas: an experimental study of natural and synthetic rock systems. Journal of Petrology, 3, 342 - 532.

APPENDIX 1

Drummond, B.J., 1979 - A crustal profile across the Archaean Pilbara and northern Yilgarn cratons, northwest Australia. BMR Journal of Australian Geology and Geophysics, 4, 171-180.

Note: This paper summarises the work undertaken by the author for a Master of Science Degree awarded in the Australian National University in 1979. As such it cannot be considered for examination for the Doctor of Philosophy Degree for which this thesis is submitted. However, it forms part of the interpretation of the data from the 1977 field work and is referred to in the text, and in the other appendices. It is included here for completeness.

Reprinted from
BMR Journal of Australian Geology & Geophysics, 4, 1979, 171-180

A crustal profile across the Archaean Pilbara and northern Yilgarn cratons, northwest Australia

B. J. Drummond

Two Archaean cratons are exposed in the Precambrian shield of Western Australia: the Pilbara in the north and the Yilgarn in the south. They are separated by the Capricorn Orogen. Seismic recordings of quarry blasts in the north of the West Australian shield indicate that the upper crustal rocks have seismic velocities of 6.0 km s^{-1}, and are probably of acid to intermediate chemical composition. They overlie a lower crust, presumed to be granulitic, which has a seismic velocity of 6.4 km s^{-1} at 13 km depth in the north of the Pilbara Craton and 16 km in the north of the Yilgarn Craton. The northern Yilgarn has a third layer, with a seismic velocity of about 7.0 km s^{-1}, at the base of the crust. This may represent a higher grade (eclogite?) phase, or it may indicate injection of basic material into the base of the crust. The crust-mantle boundary at the base of the Pilbara Craton and Capricorn Orogen appears to be transitional—it shows velocity gradients rather than a first-order velocity discontinuity.

Within the Pilbara Craton, the crust is about 28 km thick in the north and 33 km in the south. South of the Pilbara Craton, the crust thickens under the Capricorn Orogenic Belt, and again under the northern Yilgarn Craton where it is 52 km thick. The form of the structures in the zone of thickening cannot be determined uniquely from the present data. Three models incorporating faults or monoclines and a wedge of 7.0 km s^{-1} material at the base of the crust have been derived. The different crustal thicknesses of the cratons suggest that they formed separately and were then tilted towards the Orogenic Belt.

Introduction

The Precambrian shield is exposed over much of Western Australia. The shield region has both economic and scientific importance. In the north, twenty-five minerals have been reported in economic proportions (The Pilbara Study Group, 1974). The most abundant is iron ore, now mined and exported in considerable quantities. In addition, the geology and geochemistry of the Archaean areas of the shield are being extensively studied by the Geological Survey of Western Australia, CSIRO, BMR and various Australian universities.

BMR carried out a seismic refraction and gravity survey in the region in 1977 to investigate the structures of the crust and upper mantle in the region, and if possible, to shed light on the tectonic processes which influenced the formation of the early crust in the area.

Seven open-cut iron ore mines in the region regularly fire large quarrying blasts; these were used as energy sources for the seismic survey. One specially prepared blast was also used. Lines of portable seismographs were established along traverses which crossed most of the major geological provinces in the region. Gravity readings were made along many of the roads in the area.

This paper presents the results of the interpretation of the seismic data from one traverse. The gravity data, and the data from the other traverses are being processed and will be published elsewhere.

Geology

The survey area (Fig. 1) may be divided geologically into two Archaean cratons—the Pilbara and Yilgarn Cratons—separated by the Hamersley, Bangemall and Nabberu Basins and the Gascoyne Province (Trendall, 1975a), which define the Proterozoic Capricorn Orogenic Belt (Gee, in press).

The Pilbara Block contains the oldest isotopically dated rocks in Australia (Pidgeon, 1978a). They are

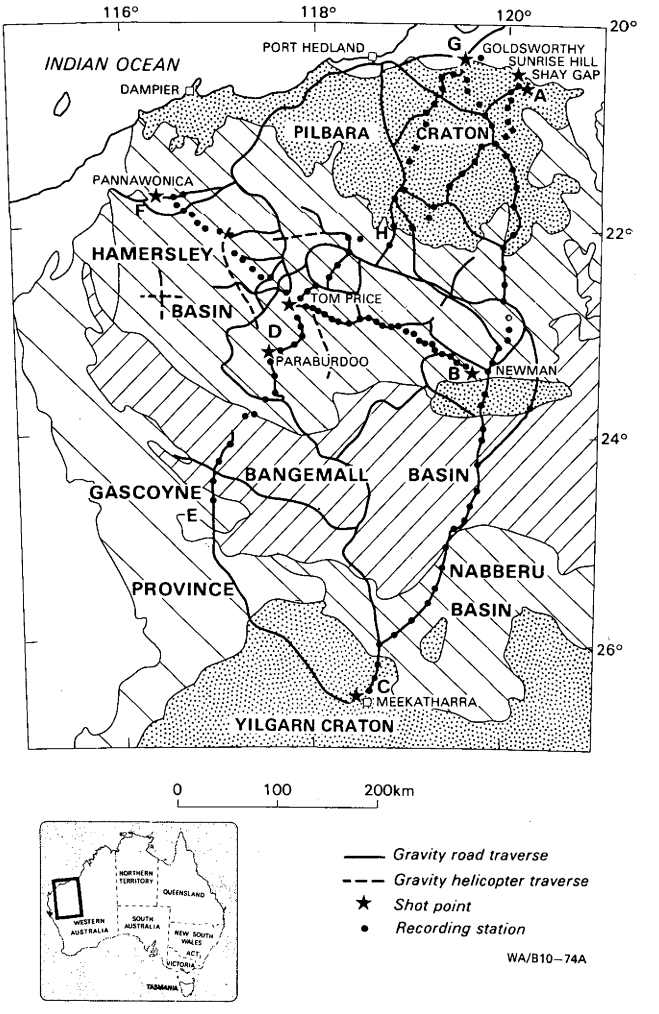

Figure 1. Geology and survey design.

volcanic and sedimentary rocks which are intruded by and overlap large granitoid batholiths (Blockley, 1975). The batholiths contain several phases of granites. The isotopic ages of the granites range from 2700 to 3400 m.y. (De Laeter & Blockley, 1972; De Laeter & others, 1975; Oversby, 1976; Pidgeon, 1978b; Hallberg & Glikson, in press).

Granites and greenstone successions also make up the stratigraphy of the Yilgarn Block; in the central and eastern, and northwestern parts of the block, the greenstone belts have distinct trends—NNW-SSE, and NNE-SSW, respectively (cf elsewhere in the Yilgarn, and the Pilbara). This is reflected in the regional gravity and magnetic patterns (BMR 1975a, 1975b). The southwest of the Yilgarn Block is a high-grade granulite terrain containing only remnants of the supracrustal succession. Isotopic ages of the granites in the Yilgarn Block range from 2500 to 2800 m.y. (Arriens, 1971; Oversby, 1975).

Overlapping the southern part of the Pilbara Block are early Proterozoic sediments and volcanics of the Hamersley Basin (Trendall, 1975b). The sediments and volcanics form three groups: the lowermost Fortescue Group, with volcanic rocks interspersed with sediments, the Hamersley Group, with large, basin-wide accumulations of banded iron formations, and the Wyloo Group which was restricted to a rapidly subsiding sub-basin in the south of the Hamersley Basin.

The sediments in the north of the Hamersley Basin dip southwards at a few degrees. South of the axis of the basin, the dips are to the north and become steeper until, near the southern boundary of the basin, the folding is intense and dips close to the vertical are common. In places, overturning to the north occurs. The Hamersley Basin sediments are variably metamorphosed. In the north, the metamorphism is prehnite-pumpellyite facies, increasing southwards to amphibolite facies in the Gascoyne Province (Horwitz & Smith, 1978).

On the southern side of the Capricorn Orogenic Belt, the sediments of the Nabberu Basin unconformably overlap the Yilgarn Craton (Hall & Goode, 1978). In the south of the basin, the sediments are predominantly sub-horizontal to gently dipping to the north. Farther north, the intensity of folding and the metamorphic grade increases. In the north and northwest of the basin, the folding is intense and the Archaean basement is increasingly included in the deformation (Hall & Goode, 1978). The metamorphic grade reaches granulite facies in the west.

In the west of the survey area, the Gascoyne Province (Daniels, 1975a) contains migmatised Archaean (?) rocks and remnants of the Wyloo and younger Bangemall Groups; the rocks are extensively faulted and folded, and metamorphic grade is variable.

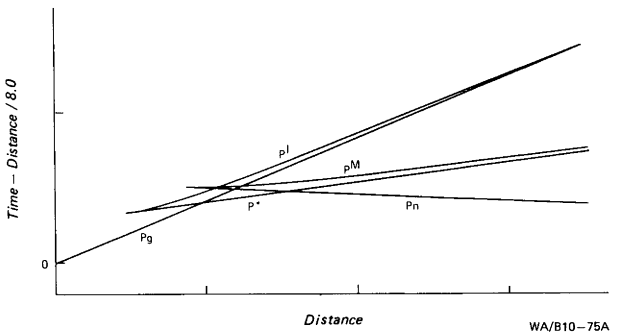

Figure 2. Principal wave groups.

The rocks of the Bangemall Basin (Daniels, 1975b) are mostly fine-grained sediments, but there are some conglomerates, breccias, tuffaceous sandstones and acid volcanics. They are the youngest Precambrian rocks in the area, unconformably overlying the rocks of the Hamersley and Nabberu Basins.

Since the deposition of the Bangemall Group, the area has been a positive landmass; it is mostly covered by Tertiary and Quaternary sand and soil.

The crustal survey

The field work undertaken in 1977 will be described in detail by Drummond (in preparation) and only a summary is given here. The positions of the seismic stations are superimposed on the geological map (Fig. 1).

Only 15 recorders were used as mobile stations. Consequently, not all of the sites on any line could be occupied simultaneously. Equipment was moved along the lines after sufficient blasts had been recorded at each site; 137 seismic stations were occupied. One hundred and fifteen quarry blasts at seven iron ore mines within the region were used as seismic sources. A blast was specially prepared and fired in a disused mine shaft near Meekatharra.

Traverse ABC, interpreted in this paper, crossed the Pilbara Block, Hamersley, Bangemall and Nabberu Basins and the northern Yilgarn Block. Goldsworthy, Shay Gap and Sunrise Hill blasts were used as sources in the north, Newman blasts as sources in the centre. The Meekatharra blast was used to reverse the recordings of Newman blasts along line BC. Station spacing was generally about 20 km, but less near the blast sites.

Seismic data processing

The recording stations used BMR-designed slow-speed seismic tape recorders. Two channels of vertical seismic data, at gain levels 24 db apart, as well as internal clock and radio-time signals, were recorded. The seismic traces for on-line shots along line ABC were digitised and record sections prepared for interpretation. Representative data from line ABC are presented in Figure 3.

Differing nomenclature is used in the literature to describe the wave groups commonly observed in crustal seismic investigations. The nomenclature used here is modified from that of Giese (1976). Figure 2 is a diagrammatic time-distance graph showing the principal wave groups observed in the Pilbara region.

Pg waves are refracted through the crystalline basement. In the Pilbara region, they generally occur as first arrivals to about 130 km, and have phase velocities of about 6 km s^{-1}. P* waves are refracted through the lower crust. Giese (1976) does not differentiate the phase from the Pg wave group. They are seldom observed as first arrivals, and have velocities of around 6.4 km s^{-1}. P^I waves are supercritical (wide-angle) reflections from the lower crustal layer. Pn waves penetrate the uppermost part of the mantle. They occur as first arrivals beyond about 130 km and have velocities generally greater than 8 km s^{-1}. P^M waves are supercritical reflections from the Moho.

Shots with clearly recorded codas were used to build composite record sections shown for lines ABC and GBC in Figure 3. Amplitudes were not normalised for shot weights, recorder gains or distance. The traces have been filtered digitally in the bandpass 0.5 t

Source and direction		Phase	Velocity km s^{-1}	(Std error)	Intercept s	(Std error)	RMS residual s	No. of points
Goldsworthy	South	Pg	6.01	(0.02)	0.03	(0.05)	0.11	26
Goldsworthy	South	Pn[1]	8.20	(0.05)	5.92	(0.17)	0.16	17
Goldsworthy	South	Pn[2]	8.52	(0.04)	7.40	(0.23)	0.11	11
Sunrise Hill	South	Pg	6.01	(0.02)	0.18	(0.04)	0.10	23
Shay Gap	South	Pg	6.05	(0.02)	0.19	(0.04)	0.11	27
Shay Gap	South	Pn	8.18	(0.11)	5.68	(0.40)	0.18	6
Newman	North	Pg	5.86	(0.04)	—0.13	(0.09)	0.20	20
Newman	North	Pn	8.49	(0.05)	6.99	(0.17)	0.18	18
Newman	South	Pg	6.08	(0.04)	0.04	(0.10)	0.23	20
Newman	South	Pn[3]	8.46	(0.07)	7.73	(0.19)	0.08	7
Newman	South	Pn[4]	7.25	(0.05)	2.75	(0.31)	0.10	9
Meekatharra	North	Pg	6.12	(0.02)	0.17	(0.06)	0.10	11
Meekatharra	North	Pn	8.68	(0.11)	10.60	(0.58)	0.31	6
Meekatharra	South	Pn	8.08	(0.03)	6.37	(0.22)	0.11	7

Table 1. Velocities and intercepts along line ABC, from linear regression analyses.

1. Data north of Newman; 2. Data south of Newman; 3. Data between 175 and 255 km; 4. Data beyond 255 km.

8.0 Hz. The arrival times of the principal wave groups were determined from analog chart records. The travel times were then calculated and the apparent phase velocities and intercepts determined by least squares linear regression analysis.

A summary of the results from the regression analysis appears in Table 1. The analysis was applied mainly to first-arrival data, although some second and subsequent arrivals were included when their onsets could be defined. Consequently, only Pg and Pn phases were considered. The velocities and intercepts of the P* phase were scaled directly from the record sections.

Interpretation methods

For interpretation, line ABC was split into segments AB and BC. Most interpretative methods, e.g. the Reciprocal Method (Hawkins, 1961), the Time-Term Method (Scheidegger & Willmore, 1957) and the method described by Ewing & others (1938), Dooley (1952), and Mota (1954), require reversed travel-time data. The data along line ABC are not usually reversed. Along the segment AB, Pg occurs as first arrivals to about 130 km, and Pn as first arrivals beyond 130 km. Because the segment is about 330 km long, Pg arrivals are reversed only for the sections of the line where they occur as second or subsequent arrivals whose onset times are poorly defined. The Pn phase from either end of the traverse bottoms in different parts of the upper mantle and is therefore not truly reversed. The P* phase has poor timing because it is never a first arrival.

The Reciprocal and Time-Term methods, which are based on the discrete travel-times from the shots to the stations, are therefore inappropriate to interpret the data along line AB, and also along segment BC, where similar considerations apply. However, the third method mentioned above is based on the apparent velocities and intercept times of the seismic energy in both directions along the lines. If it is assumed that similar phases at either end of each segment of the line are reciprocal pairs, and the refractors are continuous between the shots, this method can be used to derive plane-layered models, which provide the basis for further modelling.

The depths, dips and velocities of the refractors under the shot points were calculated. The Pn data for segment BC could not be assumed to be reversed, and other assumptions, discussed later, were made. The models derived from the inversion of the seismic data were then modelled using ray-tracing techniques and the models adjusted to fit the record sections in Figure 3. Several models are shown in Figure 4. Their upper crustal features along segments AB and BC, and their lower crustal features along segment AB are similar; their crust/mantle boundary features along segment BC are different. The travel time curves derived from the models are superimposed on the record sections in Figure 3.

Seismic interpretation

The record sections (Fig. 3) present some of the data recorded along line ABC; in most cases high-gain recordings are shown. Second and subsequent arrivals are sometimes seen more clearly on the low-gain traces or on recordings of other shots. The following descriptions of the record sections therefore refer to the entire data set, and not just the records shown in Figure 3. The record sections are reduced travel-time plots. The factor (Distance/8.0) has been subtracted from the time axis for each trace. In the following discussion, reduced travel-times are quoted.

Line AB (and GB)—Goldsworthy to Newman

Figure 3a shows recordings of Goldsworthy blasts southwards along line GBC. Recordings beyond 500 km were poor and are not shown. Pg phases occur as first arrivals to about 130 km, and can be traced farther as second and subsequent arrivals. They have an apparent phase velocity of 6.01 km s^{-1}, and an almost zero intercept time (Table 1). Because velocities of about 6 km s^{-1} are representative of crystalline basement, the near zero intercept indicates that the basement is very close to the surface. The P*/P^{I} cusp is best observed on a low-gain trace at about 90 km. The cusp may occur closer to the blast, but the over-modulation on closer recordings obscures the true nature of the traces. A velocity of 6.4 km s^{-1} and an intercept of 1.0 s were assigned to the P* phase. Large amplitude phases in the 6 to 8 s range between 120 and 200 km are interpreted as P^{M} arrivals. The P^{M}/Pn cusp occurs in over-moduled coda at about 80 km and 6s. Pn is observed as first arrivals beyond 140 km. The Pn phase between Goldsworthy and Newman has a velocity of 8.20 km s^{-1} and an intercept of 5.92 s. South of Newman, the Pn velocity increases slightly (Table 1), although the point at which this occurs is difficult to define.

Record sections of Shay Gap and Sunrise Hill blasts southwards along line AB show similar travel-time features (Fig. 3b), but because these blasts are smaller than at Goldsworthy the amplitudes of the traces are smaller. Although this obscures some of the more

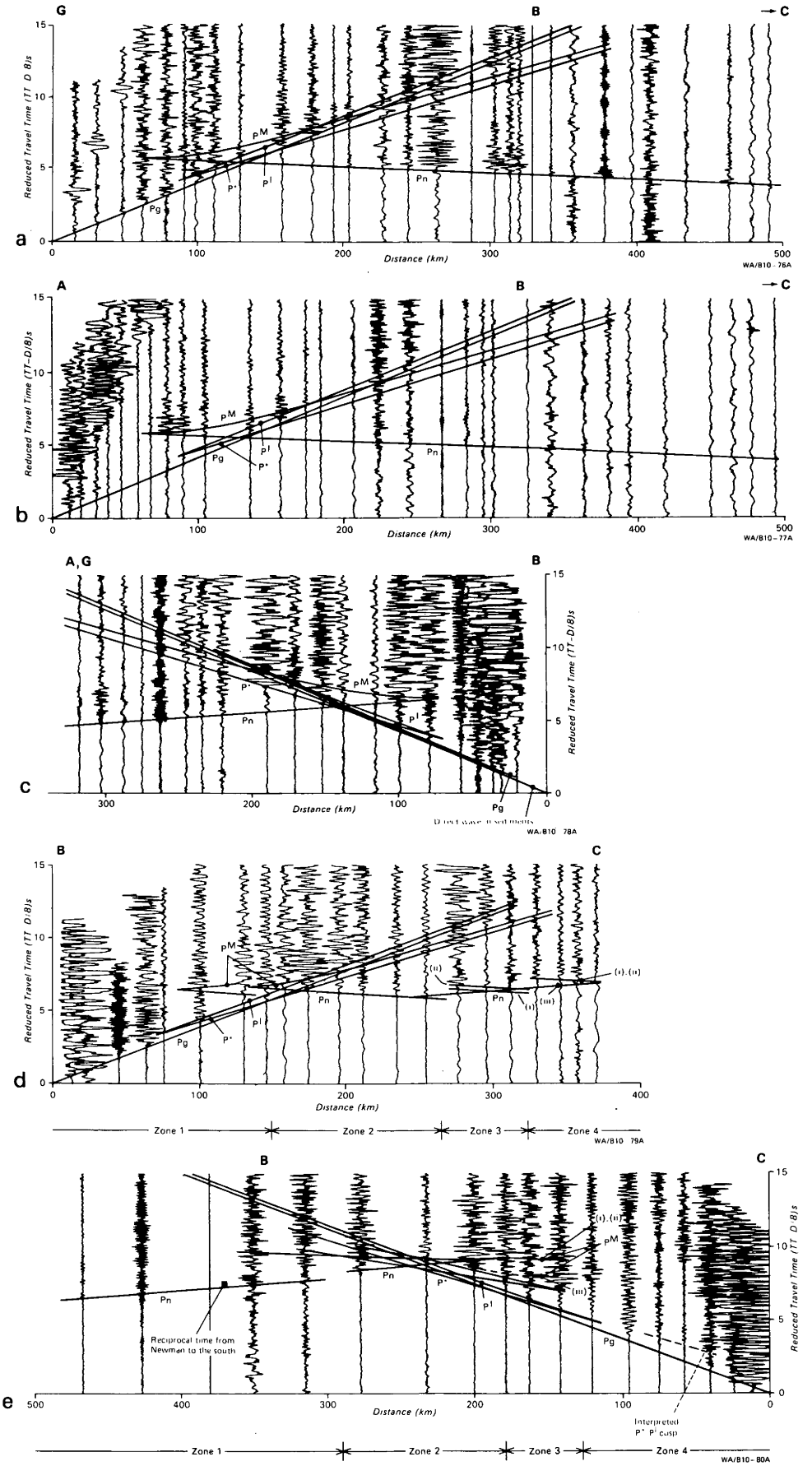

Figure 3. Records sections along line ABC. The travel time curves superimposed on the record sections in 3a, 3b, a 3c were calculated for the model in Figure 4a. In 3d and 3e, the travel time curves numbered i, ii and are for the models in Figures 4a, 4b and 4c respectively.

emergent arrivals, it allows better definition of the P^M wavegroup and the P^M/Pn cusp. The velocities and intercepts are similar to those from the Goldsworthy data (Table 1).

Newman blasts recorded northwards along line AB are shown in Figure 3c. They had large areal extents, with blasting on benches several kilometres apart making up one shot, and very long burning times, with delays sometimes totalling over a second. The Newman shots therefore often produced very emergent arrivals.

The Pg phase velocity, as measured from first arrivals, is 5.86 km s^{-1}. This is lower than that derived from Goldsworthy, Shay Gap and Sunrise Hill blasts, and also from south of Newman and north of Meekatharra. It could be caused by either the emergent arrivals, whose onsets were picked later than they in fact occur, or the sediments of the Hamersley Basin, which crop out in the region; the sediments are often iron-rich, metamorphosed, and have compressional wave velocities in hand specimens approaching those of the crystalline basement (Drummond, in preparation). The Pg phase has a slightly negative intercept time (Table 1), indicating a decrease in apparent velocity and therefore density away from the shots. This is consistent with increasing thicknesses of sedimentary rocks to the north of Newman.

The P* phase appears to be present, but its velocity and intercept were difficult to determine because of the unclear nature of the onsets. An apparent phase velocity of 6.4 km s^{-1} and intercept of 1 s were adopted, although the velocity could be as high as 6.45 km s^{-1} and the intercept as large as 1.65 s. The upper surface of the lower crustal layer was therefore interpreted as horizontal, although its depth could increase southwards from Goldsworthy to Newman by as much as 5 km.

The Pn phase northwards from Newman is quite clear, and has a phase velocity of 8.49 km s^{-1} and intercept time of 6.99 s. The Pn arrivals from Newman northwards seem to have two phases, separated by 0.6 s. To demonstrate this, traces from two shots have been plotted in Figure 3c, one between 160 and 250 km and the other beyond 250 km. The arrivals out to 250 km have a low-frequency phase followed by one of higher frequency. Beyond 250 km both phases have high frequencies, although the second phase is only clear on the trace at 300 km. The duality of the arrivals may be caused by source effects, because traces from different shots have different waveforms. Alternatively, because it may also be interpreted on some traces of Goldsworthy blasts in Figure 3a (see for example the traces at 230, 240, and 340 km), it may be caused by a complex velocity-depth function at the crust/mantle boundary; this interpretation is supported by large amplitude arrivals in the 6 to 8s range between 80 and 200 km, which do not readily fit the P^M wave group as modelled. The large amplitude phases are not present in the Goldsworthy data.

The simplest interpretation of the data from segment AB is that the crust is two-layered; the upper layer has a seismic P-wave velocity of 6.0 km s^{-1}, and the lower layer a velocity of 6.4 km s^{-1}. The lower layer has a horizontal interface at 13 km depth, but it may dip from about 9 km under Goldsworthy to 14 km under Newman. The crust/mantle boundary dips from 28 km in the north to about 33 km in the south. The upper mantle velocity is 8.34 km s^{-1} (Fig. 4). A layer of sediments north of Newman may be incorporated into the

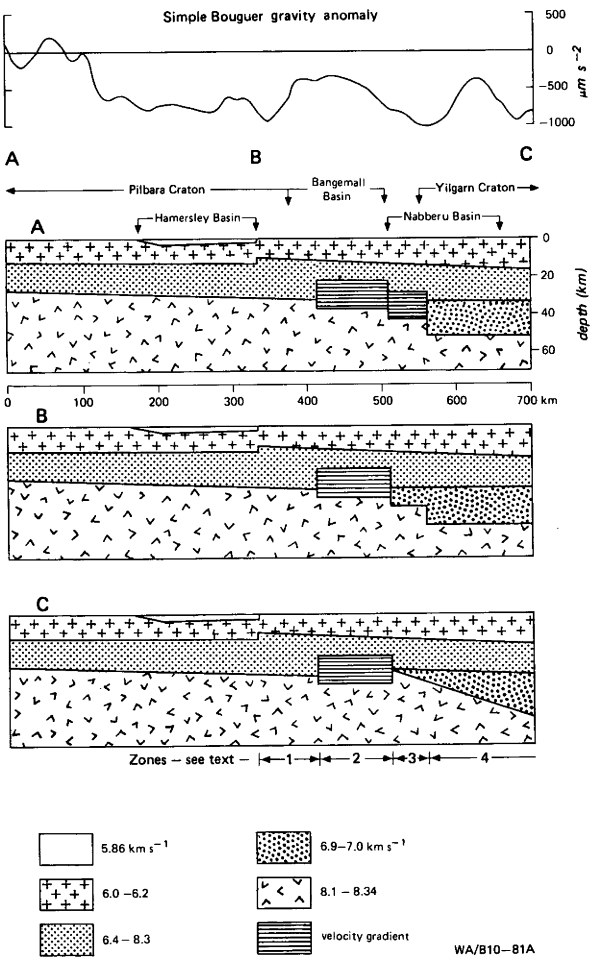

Figure 4. Gravity profile and seismic crustal models along line ABC.

model to explain the low upper crustal velocity from the Newman data. Trendall (1975b) shows diagrammatically that a maximum thickness of 2 to 3 km of Hamersley Basin sediments is likely to the north of Newman. Incorporation of the sediments into the model does not significantly perturb the theoretical travel-times.

The travel-time curves superimposed on the record sections (Fig. 3a, 3b, and 3c) were calculated using ray-tracing techniques on section AB of the model in Figure 4a. The model is satisfactory for first-arrival data, and for the Pg phase. However, the fit of the model travel-times to the reflected phases, and particularly the P^M phase, is not satisfactory. The P^M phase is about 1 s earlier than the time-distance curve for the model. This indicates that velocity gradients, in which the velocity increases with depth, may be present at the base of the crust. A gradient at the base of the crust will draw the P^M phase closer to the Pn phase. This is demonstrated in Figure 5 by modelling the Goldsworthy, Sunrise Hill, and Shay Gap with a plane, horizontal layered model with the velocity/depth function shown in Figure 5a. The function has a linear increase in velocity from 6.4 km s^{-1} to 8.20 km s^{-1} over a depth range of 15 km at the base of the crust. The P^M phase now fits the observed curve more closely than in Figures 3a and 3b, but the P^M/Pn cusp is not so well modelled.

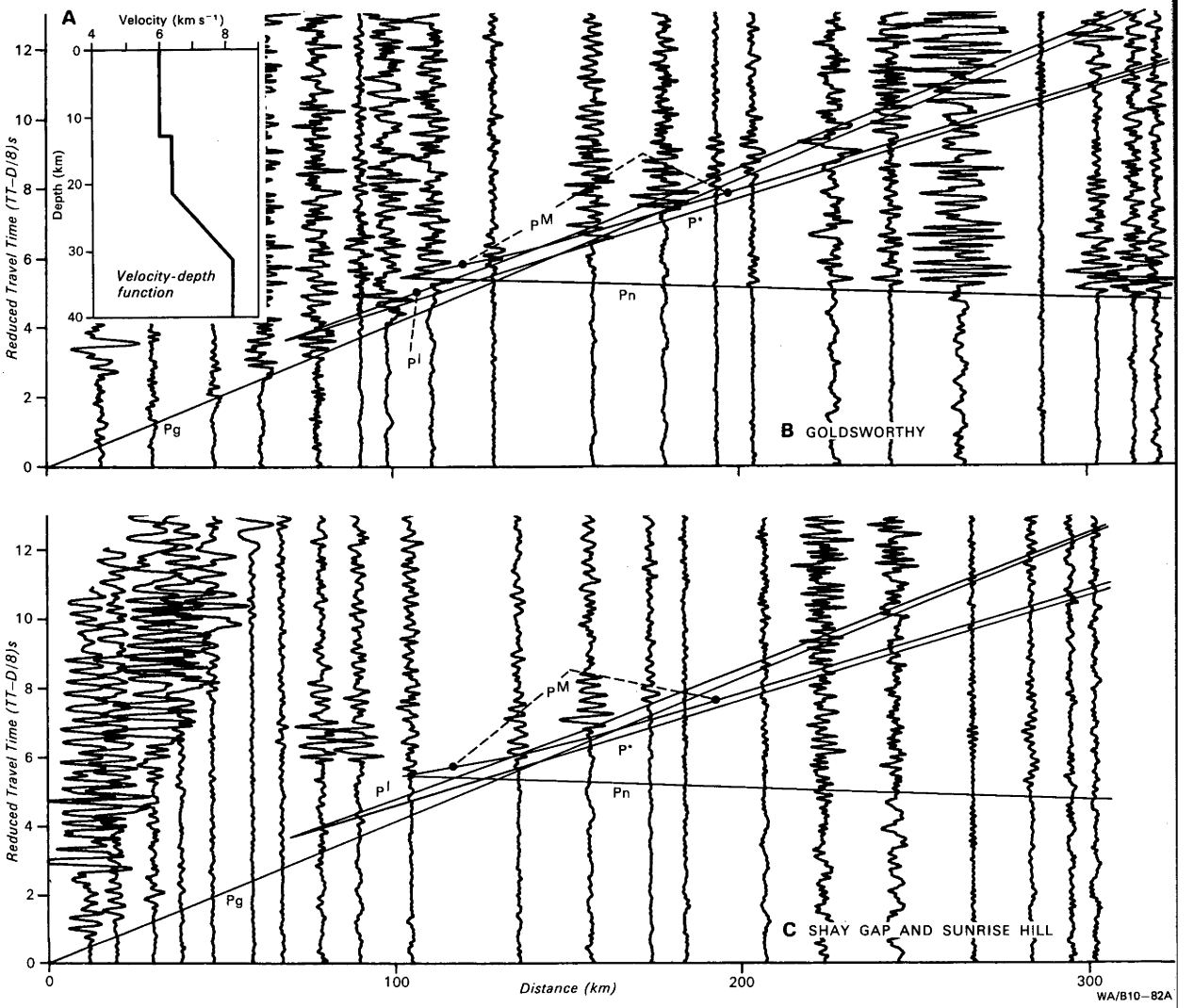

Figure 5. Effects of a velocity gradient at the crust/mantle boundary along line AB.

Line BC—Newman to Meekatharra

South of Newman, the Pg velocity is 6.08 km s^{-1} (Fig. 3d, Table 1) and the intercept is close to zero. At about 70 km, the Pg phase seems to disappear, to be replaced about 0.5 s later by another set of arrivals with a phase velocity of 6.4 km s^{-1} and an intercept of 1 s. The disappearance of the Pg phase may be owing to spreading of the wavefronts. However, it may also have several other causes, for example the crystalline basement may be downfaulted south of Newman. This does not seem unreasonable in view of other anomalies in the record section to be discussed later. A step of 0.5 s represents a throw on the fault of over 8 km. The step in the travel times may also be caused by a low velocity zone in the upper crust. Both of these causes, however, require low density material in the upper crust in the region of a high gravity anomaly (Fig. 4). Consequently, because of the similarity of its velocity and intercept time to those for the P* group north of Newman, the wave group beyond 75 km has been interpreted as the P* phase.

Beyond 170 km, the first arrivals are the Pn wave group, which has a phase velocity of 8.46 km out to 250 km, beyond which it abruptly decreases to 7.25 km s^{-1} and the Pn arrivals are increasingly delayed. Several interpretations are possible. The Moho may have a change in dip. For a two-layered crust, with seismic velocities similar to those along segment AB overlying a mantle with a seismic velocity of 8.3 km s^{-1}, a change in dip of 6 degrees is sufficient to account for the abrupt change in the apparent velocity of the Pn phase. Alternatively, two steps in the travel-time curve, of the type expected from fault-like structures, may be interpreted at 260 and 320 km, implying three regions at the crust/mantle boundary separated by fault-like structures.

Large-amplitude arrivals in the 7 to 9 s range between 100 and 280 km are interpreted as the P^M wave group. Difficulties in fitting the interpreted P^M/Pn cusp to the apparent Pn curve between 170 and 240 km, and fitting the curve P^M reflections to all of the observed arrivals have required the interpretation of a third step in the Pn travel-time curve at 130 km, implying a fourth region in the crust/mantle boundary defined by a fault-like structure. This is supported by the record section from Meekatharra.

To describe the features observed in the Meekatharra blast data (Fig. 3e) in terms of the features on the Newman record section (Fig. 3d), four zones have been defined (Fig. 3d and 3e). They do not correspond to the same regions on the surface in the two record sections because the crust is thicker in the south of segment BC.

Zone 1 extends about 80 km south of Newman. Zones 2 and 3 are about 100 and 50 km long respectively, and Zone 4 extends about 140 km north from Meekatharra. When the appropriate offsets are applied to the groups of reflection phases on the two record sections, they are shown to bottom in the same zones.

In Figure 3e (the Meekatharra blast data), the Pg phase is emergent and has a velocity of 6.12 km s^{-1}. A slightly higher value of 6.18 km s^{-1} was eventually adopted for modelling purposes because it provided a better fit to some later arrivals. The P* phase has a velocity of 6.4 km s^{-1} and an intercept of 1.65 s. A lower crustal reflected phase, defined by a suite of large amplitude arrivals at about 7 to 8 s between 140 and 200 km, was also interpreted. No refracted phase could be uniquely defined for this group, but a velocity of 7.0 km s^{-1} and an intercept of about 5 s were derived by drawing a tangent to the reflected phase at the interpreted cusp. The P^M/Pn cusp occurs at about 10 s and 140 km; it is more obvious on the low-gain traces than the high-gain traces plotted. At about 200 km, the interpreted Pn phase velocity increases slightly, and at about 300 km a step, corresponding to the zone 1/zone 2 boundary inferred in the Newman data (Fig. 3d), occurs in the travel-time data. The Pn velocity of 8.68 km s^{-1} corresponding to the zone 1 section of the Moho is greater than that observed from Newman blasts recorded northwards (8.49 km/s).

If the features in the record sections along segment BC were caused by the effects of vertical velocity structure, the record sections from Newman southwards and Meekatharra northwards would be similar. However, because of the obvious differences, the features cannot be explained in terms of vertical velocity structure; they must be caused by lateral structures within the crust and upper mantle. The following procedure was therefore followed to interpret and model the segment BC. The Pg and P* phases recorded south from Newman and north from Meekatharra have similar velocities, so the upper and lower crustal layers with velocities of 6.1 and 6.4 km s^{-1} respectively were assumed to be continuous between the two blasting centres. This assumption is necessary, because no information is available about the upper crust in the centre of the profile. The lower crustal layer, responsible for the P* refractions of 6.4 km s^{-1} velocity, was modelled as being 10 km deep under Newman and 16 km deep under Meekatharra (Fig. 4a and c).

The model immediately to the north of Newman, without the sedimentary basin, was extended southwards for 80 km. This corresponds to the point at which the Pg phase dies out (Fig. 3d); the model also satisfies the Pn data from the Meekatharra blast. 80 km south of Newman, a delay of 0.4 s observed in the Pn data was interpreted as indicating a deepening of the Moho by 4 km to about 37 km (Fig. 4a, b and c). No information about the true velocities is available; therefore, the lower crustal layers south of this point were assumed to be horizontal, and the estimates of the apparent velocity were used as the true velocities. To fit the reflections more closely, a gradient was necessary at the base of the crust in zone 2. That adopted was a linear increase in velocity from 6.4 km s^{-1} to 8.3 km s^{-1} over a 15 km depth range. In zones 3 and 4, several models fit the data. The Moho may have fault or monocline-type structures, with a thickening of the crust by about 6 km at the zone 2/zone 3 boundary, and a further thickening at the zone 3/zone 4 boundary of 9 km to 52 km under Meekatharra (Fig. 4a and b). The nature of the material at the base of the crust in zone 3 cannot be defined from the data available. The model in Figure 4a has a velocity gradient, and the model in Figure 4b has 7.0 km s^{-1} material. Alternatively, the crust/mantle boundary may have a change of dip, with a wedge of 7.0 km s^{-1} material at the base of the crust (Fig. 4c). The theoretical travel times for the right-hand sides (segment BC) of the models in Figure 4 have been superimposed on the record sections in Figures 3d and 3e; the fit is generally good. However, the P^M times for one model (Fig. 4c) are about 1 s earlier than recorded in Figure 3e. The times south from Newman for this model are also slightly early. The model could be made to fit the data by simply thickening the southern end of the lower crustal wedge of 7.0 km s^{-1} material. However, making the crust too thick might be difficult to explain geologically, isostatically, and tectonically because of the crustal thicknesses to the north under the Pilbara Craton and under the southern Yilgarn Craton (Mathur, 1974; Mathur & others 1977).

Another feature of the travel-time data not well modelled is the interpreted P^*/P^I cusp north from Meekatharra (Fig. 3c). The cusp derived from the model does not extend far enough back towards the origin.

Composite model along profile ABC

When the models for segments AB and BC were adjusted to give a close fit of the theoretical times to the data from each segment (within 0.2 s for first arrival data), they were joined and further tested by modelling the travel times for Goldsworthy blasts south of Newman. The curvature in the observed travel times beyond Newman was also present in the modelled times, although to a lesser extent, with deviations of the modelled times from the measured times of up to 0.3 a. Unfortunately, the arrivals beyond 500 km were generally poor and the models could not be tested more exhaustively.

The models in Figure 4 may be summarised as follows. An upper crustal layer of 6.0 km s^{-1} is present at the surface along the profile, except to the north of Newman where the Hamersley Basin sediments crop out, and perhaps 80 km to the south of Newman, where a thick pile of low-velocity rocks may occur. A lower crustal phase, with a velocity of 6.4 km s^{-1}, is observed at all shot points, and is refracted from a crustal layer 9 to 13 km deep under Goldsworthy, Shay Gap, and Sunrise Hill, and 16 km deep under Meekatharra. The step in the refractor under Newman in the models results from the process in which segments AB and BC were interpreted independently. It is probably not real, and the refractor is probably continuous between Goldsworthy and Meekatharra. This would make the calculated travel times from the full model fit the Goldsworthy arrivals beyond Newman more closely. The crust is 28 km thick near the northern mines, and thickens to 33 km about 80 km to the south of Newman, where it abruptly thickens to 37 km, and a velocity gradient is probably present at the base of the crust. One hundred kilometres farther south, the crust again thickens. The lower crust may be a wedge of 7.0 km s^{-1} material or the crust/mantle boundary may have several faults or monoclines.

The upper mantle velocity along segment AB is 8.34 km s^{-1}. Along segment BC, 8.3 km s^{-1} was adopted in zones 2, 3 and 4 in the models in Figures 4a and 4b; 8.34 km s^{-1} was used in zone 1. Gregson (1978)

reported the arrival times of the Meekatharra blast energy at the seismological observatories up to 700 km to the south on the Yilgarn Craton. Using a revised origin time slightly different to the preliminary one Gregson used, an apparent velocity of 8.08 km s^{-1} and an intercept time of 6.37 s were calculated for the Pn phase across the Yilgarn Craton. The intercept time is considerably less than that for Meekatharra blast data to the north, implying that this is an up-dip velocity, so that the true velocity is probably lower. The effect of earth curvature would also increase the apparent velocity when measured over such large distances, so that the true velocity is probably somewhat less than 8.08 km s^{-1}. The apparent velocity (8.08 km s^{-1}) was used as the velocity in the upper mantle in zones 3 and 4 in the model in Figure 4c.

Discussion

The boundaries between the zones in the models in Figure 4 have so far been referred to as "fault-like structures". No information is available about the true nature of these structures; only their sense is apparent; in all cases the deeper side of the crust/mantle boundary is to the south. Their width must be less than the station spacing, which is about 20 km along line BC. The geological map of Australia (BMR, 1976) shows that the line crossed two major faults, one of which corresponds to the zone 2/zone 3 boundary. The zone 1/zone 2 boundary corresponds to a fault zone reported by Brakel & Muhling (1976). R. E. Smith (CSIRO, personal communication, 1979) calls it the Mount Vernon-Brumby Creek Fault, and reports that it continues for 200 km. The zone 1/zone 2 and zone 2/zone 3 boundaries therefore correspond to the known surface expressions of major faults. The zone 3/zone 4 boundary does not.

The Proterozoic sedimentary basins were not convincingly observed in the seismic data. A sedimentary basin 2 to 3 km thick was included in the model north of Newman without having to adjust the depths of the other refractors in the model by more than a kilometre. Perturbations that could be related to Bangemall Basin sediments may be interpreted in the Pg data south of Newman.

The southern limit of the Bangemall Basin outcrop area corresponds to the zone 2/zone 3 boundary, but the northern edge of the basin outcrop area is offset about 40 km to the north of the zone 1/zone 2 boundary. The basin has a broad 600 um s^{-2} gravity high centred over it (Fig. 4). Because the seismic velocities imply uniform densities in the upper crust, the transition zone at the base of the crust must represent denser crustal material than on either side of the zone. This interpretation is supported by Wellman (1978), who predicted on gravity evidence that the Capricorn Orogenic Belt between the Archaean cratons had a thicker, more dense crust than the cratons. Because the only lateral density differences in the seismic models occur at the base of the crust, it can also be inferred that the velocity gradient proposed at the crust-mantle boundary under the Pilbara Block is not as broad as the one at the base of zone 2.

The Nabberu Basin is interpreted from the geology as overlapping the northern edge of the Yilgarn Block, and its northern limits seem to correspond fairly well with the zone 2/zone 3 boundary. It may be that the tectonism which folded the sediments and the Archaean basement of the Nabberu Basin (Hall & Goode, 1978) also left its imprint on the lower crust in the form of seismically anomalous material at the base of the crus in zone 3.

The Pilbara Block is interpreted as extending 80 km south of Newman. This is about 30 km farther south than implied by the outcrop of Archaean granite inliers in the Hamersley Basin. The Yilgarn Block is interpreted from the geology as extending northwards under the Nabberu Basin to include granite inliers of supposed Archaean age. This is in fairly close agreement with the zone 3/zone 4 seismic boundary.

Crustal composition

Hickman & Lipple (1975) presented diagrammatic cross-sections of the crust in the northeastern part of the Pilbara Block. Presumably based on the structure of the greenstone belts and on the foliation patterns in the granites, the sections show the granites and the synclinal keels of the greenstone belts extending to 30 km depth. Their models imply that the crust is likely to have an average acid to intermediate composition. Ringwood (1975) predicted that a purely basaltic lower crust was unlikely because, in a region of low heat flow, a dry mafic lower crust in thermodynamic equilibrium would exist as eclogite and have seismic P-wave velocities of about 8.4 km s^{-1}. Ringwood's favoured model for the lower crust in old, stable regions is one of acid to intermediate chemical composition, composed principally of granulites and eclogites with seismic P velocities in the range 6.5 to 7.2 km s^{-1}.

The interpretation of lower crustal material as granulites is supported by Tarney & Windley (1977), and Dawnson (1977), although they favour some basification of the lower crust in continental areas. The velocity of 6.4 km s^{-1} in the lower crustal layer in the Pilbara and Yilgarn Blocks is slightly less than that expected for Ringwood's model; a velocity gradient at the base of the crust would bring the models closer to agreement.

Glikson & Lambert (1976) proposed, in agreement with the model of Hickman and Lipple (1975), that the granite to greenstone ratio increases with depth in the Pilbara and Yilgarn Cratons. They also predicted an increase in the metamorphic grade to amphibolite and even granulite facies, with depth. The lower crust may therefore be more acidic than Ringwood (1975) Tarney & Windley (1977), and Dawson (1977) predicted; this would account for the lower observed velocities.

The seismic data in th e Pilbara Block are therefore consistent with a crust of average acid to intermediate chemical composition, with a transition, probably from amphibolite to granulite, at about 13 km.

The transition to granulite is also present in the northern Yilgarn Block, although it is slightly deeper. It is underlain at about 30 km by a third crustal layer with a velocity of about 7.0 km s^{-1}. Mathur (1974) interpreted the crustal structure along several seismic and gravity profiles in the southern Yilgarn Block. He also derived a three-layer crustal model, although his lower crustal velocities of 7.3 to 7.5 km s^{-1} were higher than in the models in Figure 4. Glikson & Lambert (1976) found Mathur's lower most crustal layer anomalously dense, and suggested that it might result from the accumulation of basic magmas at the crust mantle boundary during the break up of Gondwana land. Tarney & Windley (1977) favour a mechanism whereby the crust becomes chemically stratified during its creation. The mafic material. being dense, is restricted to the lower crust. The velocities in the nort

of the Yilgarn Block are lower than the southern values, and are consistent with Ringwood's (1975) model. The simpler explanation of the lowermost crustal layer being caused by further phase changes, perhaps to eclogite grade, of a thick, somewhat chemically stratified crust with the increased pressure and temperature likely at the base of a thick crust, is attractive. It eliminates the need to invoke a tectonic mechanism for injecting basic material into the base of the entire Yilgarn Block, but not the Pilbara Block.

Structural development

Palaeomagnetic data (McElhinny & McWilliams, 1977; Embleton, 1978) imply that the Pilbara and Yilgarn Blocks are unlikely to have formed at widely separated locations and subsequently been brought closer together by plate-tectonic movements.

However, they do not rule out the possibility that the blocks may have formed as one craton which was later rifted, as proposed by Horwitz & Smith (1978). The present data cannot define the nature of the crust in the Capricorn Orogenic Belt with sufficient clarity to determine whether it represents an ancient rift system. However, the different thicknesses of the cratons and the divergent isotopic ages for the rocks within the cratons tend to imply separate development of the cratons in their approximate relative positions.

Glikson & Lambert (1976) suggested that the arcuate style of the greenstone belts and the generally greater isotopic ages of the granites of the Pilbara Block indicated that the rocks formed at a deeper level of the crust than the rocks to the south in the Yilgarn Block. They were subsequently uplifted and exposed by erosion. This has now been discounted by Hallberg & Glikson (in press), but requires further investigation in the light of different crustal thicknesses in the Pilbara and northern Yilgarn Cratons.

The seismic model indicates that the base of the Pilbara Block has a dip to the south. A. Y. Glikson (BMR, personal communication, 1979) suggested that the increasing granite-greenstone ratio northwards across the Pilbara Craton, as evidenced by the largely granite terrains in the north of the survey area, is further evidence of southerly dip. The dip from the seismic modelling is about the same as the dip observed in the Hamersley Basin sediments over the craton, implying that the entire craton was tilted to the south following the deposition of the sediments.

The base of the Yilgarn Craton has been shown (Fig. 4) as either horizontal (Fig 4a and b) or dipping steeply to the south (Fig. 4c). The survey data do not allow a unique interpretation of the dip and these dips were assumed in the interpretation. They are presented here as possible models for the northern part of the Yilgarn Craton. The intercept times of the Meekatharra blast data to the north and south, and the presence of a higher grade lower crustal granulite terrain in the southwest of the Yilgarn Craton (Glikson & Lambert, 1976) suggest that the dips in Figure 4 are local features and that, overall, the Yilgarn Craton as a structural unit has been tilted to the northeast. The tilting occurred after the deposition of the Nabberu Basin sediments, which dip northwards on the Yilgarn Craton.

The Pilbara and Yilgarn Cratons therefore seem to have developed separately in their approximate relative positions, and were tilted towards their common mobile belt, the Capricorn Orogenic Belt, after the deposition of the lower and middle Proterozoic sediments in the mobile belt.

Acknowledgements

The BMR is indebted to the iron-mining companies of the Pilbara without whose support the seismic survey would not have been possible. The staff of Goldsworthy Mining Limited, Cliffs Robe River Associates, Hamersley Iron Pty Ltd, and Mount Newman Mining Company Pty Ltd gave of their own time on several occasions to make the survey a success.

I acknowledge the efforts of my colleagues at the BMR who undertook the field work during 1977, and their support and comments during the interpretation of the data. The interpretation was undertaken while I was a full-time research scholar at the Australian National University (ANU) in receipt of an Australian Public Service Board Postgraduate Scholarship. I thank the staff and students of the ANU, and particularly K. J. Muirhead and J. Cleary, whose guidance and comments were most useful. A. Y. Glikson critically read the manuscript and made many useful comments and suggestions. The figures were drawn by M. Moffat.

References

ARRIENS, P. A., 1971—The Archaean geochronology of Australia. *Geological Society of Australia, Special Publications*, **3**, 11-23.

BLOCKLEY, J. G., 1975—Pilbara Block. *In* Geology of Western Australia. *Western Australia Geological Survey, Memoir* **2**, 81-93.

BMR, 1975a—Gravity map of Australia, 1:5 000 000. *Bureau of Mineral Resources, Geology & Geophysics, Canberra, Australia.*

BMR, 1975b—Magnetic map of Australia, 1:2 500 000 (4 sheets). *Bureau of Mineral Resources, Geology & Geophysics, Canberra, Australia.*

BMR, 1976—Geology of Australia, 1:2 500 000 (4 sheets). *Bureau of Mineral Resources, Australia, Canberra.*

DANIELS, J. L., 1975a—Gascoyne Province. *In* Geology of Western Australia. *Western Australia Geological Survey, Memoir* **2**, 107-14.

DANIELS, J. L., 1975b—Bangemall Basin. *In* Geology of Western Australia. *Western Australia Geological Survey, Memoir* **2**, 147-59.

DAWSON, J. B., 1977—Sub-cratonic crust and upper mantle models based on xenolith suites in kimberlite and nephelinitic diatremes. *Journal of the Geological Society of London*, **134**, 173-84.

DE LAETER, J. R., & BLOCKLEY, J. G., 1972—Granite ages within the Archaean Pilbara Block, Western Australia. *Journal of the Geological Society of Australia*, **19**, 363-70.

DE LAETER, J. R., LEWIS, J. D. & BLOCKLEY, J. G., 1975—Granite ages within the Shaw Batholith of the Pilbara Block. *Geological Survey of Western Australia, Annual Report*, 1974, 73-9.

DOOLEY, J. C., 1952—Calculation of depth and dip of several layers by refraction seismic method. *In* THYER, R. F., & VALE, K. R., 1952—Geophysical Surveys, Oakland-Coorabin coalfield, New South Wales. *Bureau of Mineral Resources, Australia, Bulletin*, **19**.

BRAKEL, A. T. & MUHLING, P. C., 1976—Stratigraphy, sedimentation, and structure in the western and central part of the Bangemall Basin, Western Australia. *Geological Survey of Western Australia Annual Report*, 1975, 70-79.

DRUMMOND, B. J., 1979—Structural relations between the Archaean Pilbara and Yilgarn Blocks, Western Australia, from deep seismic sounding. *Australian National University, MSc. Thesis* (unpublished).

DRUMMOND, B. J., in preparation—Pilbara Crustal Survey, 1977—Operational Report. *Bureau of Mineral Resources, Australia, Record.*

EMBLETON, B. J. J., 1978—The palaeomagnetism of 2400 m.y. old rocks from the Australian craton and its relation to Archaean-Proterozoic tectonics. *Precambrian Research*, **6**, 275-91.

EWING, M., WOOLLARD, G. P., & VINE, A. C., 1938—Geophysical investigations in the emerged and submerged Atlantic coastal plain. *Bulletin of the Geological Society of America*, **50**, 257-95.

GEE, R. D., in press—Tectonics of the Western Australian Shield.

GIESE, P., 1976—Models of crustal structure and main wave groups. *In* GIESE, P., PRODEHL, C., & STEIN, A. (Editors)—Explosion seismology in Central Europe. Data and results. Crustal and upper mantle structure in Europe. *European Seismological Commission, Monograph*, **1**, *Springer-Verlag, Berlin*, 196-200.

GLIKSON, A. Y., & LAMBERT, I. B., 1976—Vertical zonation and petrogenesis of the early Precambrian crust in Western Australia. *Tectonophysics*, **30**, 55-89.

GREGSON, P. J., 1978—Mundaring Geophysical Observatory, Annual Report 1977. *Bureau of Mineral Resources, Australia, Record*, **1978/73**.

HALL, W. D. M., & GOODE, A. D. T., 1978—The early Proterozoic Nabberu Basin and associated iron formations of Western Australia. *Precambrian Research*, **7**, 129-84.

HALLBERG, J. A., & GLIKSON, A. Y., in press—Archaean granite-greenstone terrains of Western Australia. *In* HUNTER, D. R. (Editor)—Precambrian of the southern hemisphere. *Elsevier, Amsterdam.*

HAWKINS, L. V., 1961—The reciprocal method of routine shallow seismic refraction investigations. *Geophysics*, **26**, 806-19.

HICKMAN, A. H., & LIPPLE, S. L., 1975—Explanatory notes on the Marble Bar 1:250 000 geological sheet, Western Australia. *Geological Survey of Western Australia. Record*, **1974/20** (unpublished).

HORWITZ, R. C., & SMITH, R. E., 1978—Bridging the Yilgarn and Pilbara Blocks, Western Australia. *Precambrian Research*, **6**, 293-322.

MATHUR, S. P., 1974—Crustal structure in southwestern Australia from seismic and gravity data. *Tectonophysics*, **24**, 151-82.

MATHUR, S. P., MOSS, F. J., & BRANSON, J. C,. 1977—Seismic and gravity investigations along the Geotraverse, Western Australia, 1969. *Bureau of Mineral Resources, Australia, Bulletin* **191**.

MCELHINNY, M. W., & MCWILLIAMS, M. O., 1977—Precambrian geodynamics—a palaeomagnetic view. *Tectonophysics*, **40**, 137-59.

MOTA, L., 1954—Determination of dips and depths of geological layers by the seismic refraction method. *Geophysics*, **19**, 242-54.

OVERSBY, V. M., 1975—Lead isotope systematics and ages of Archaean acid intrusives in the Kalgoorlie-Norseman area, Western Australia. *Geochimica et Cosmochimica Acta*, **39**, 1107-25.

OVERSBY, V. M., 1976—Isotope ages and geochemistry of Archaean acid igneous rocks from the Pilbara, Western Australia. *Geochimica et Cosmochimica Acta*, **40**, 817-29.

PIDGEON, R. T., 1978a—3450 m.y. old volcanics in the Archaean layered greenstone succession of the Pilbara Block, Western Australia. *Earth and Planetary Science Letters*, **37**, 421-8.

PIDGEON, R. T., 1978b—Geochronological investigations of granite batholiths of the Archaean granite-greenstone terrain of the Pilbara Block, Western Australia. *In* SMITH, I. E. M., & WILLIAMS, J. G. (Editors)—Proceedings of the 1978 Archaean Geochemistry Conference. *University of Toronto*, 360-2.

RINGWOOD, A. E., 1975—COMPOSITION AND PETROLOGY OF THE EARTH'S MANTLE. *McGraw-Hill, New York.*

SCHEIDEGGER, A. E., & WILLMORE, P. L., 1957—The use of a least squares method for the interpretation of data from seismic surveys *Geophysics*, **22**, 9-22.

TARNEY, J., & WINDLEY, B. F., 1977—Chemistry, thermal gradients and evolution of the lower continental crust. *Journal of the Geological Society of London*, **134**, 153-72.

THE PILBARA STUDY GROUP, 1974—The Pilbara Study: Report on the industrial development of the Pilbara (to the Governments of Australia and Western Australia). *Australian Government Publishing Service, Canberra.*

TRENDALL, A. F., 1975a—Precambrian: Introduction. *In* Geology of Western Australia. *Western Australia Geological Survey, Memoir* **2**, 25-32.

TRENDALL, A. F., 1975b—Hamersley Basin. *In* Geology of Western Australia. *Western Australia Geological Survey, Memoir* **2**, 119-43.

WELLMAN, P., 1976—Regional variation of gravity, and isostatic equilibrium of the Australian crust. *BMR Journal of Australian Geology and Geophysics*, **1**, 297-302.

WELLMAN, P., 1978—Gravity evidence for abrupt change in mean crustal density at the junction of Australian crustal blocks. *BMR Journal of Australian Geology and Geophysics*, **3**, 153-62.

APPENDIX 2

Drummond, B.J., Smith, R.E., and Horwitz, R.C., 1982 - Crustal structure of the Pilbara and northern Yilgarn Blocks from deep seismic sounding. In, Glover, J.E., and Groves, D.I. (editors) - Archaean Geology. Second International Archaean Symposium. Geological Society of Australia, Special Publication, 7, 33-41.

CRUSTAL STRUCTURE IN THE PILBARA AND NORTHERN YILGARN BLOCKS FROM DEEP SEISMIC SOUNDING

B. J. Drummond,[1] R. E. Smith,[2] & R. C. Horwitz[2]

[1] *Bureau of Mineral Resources, Geology and Geophysics, PO Box 378, Canberra City, ACT 2601: currently at Research School of Earth Sciences, Australian National University, PO Box 4, Canberra, ACT 2600*

[2] *CSIRO Institute of Earth Resources, Division of Mineralogy, Private Bag, PO Wembley, Western Australia 6014*

ABSTRACT

Two seismic refraction profiles in the Pilbara and northern Yilgarn Cratons of northwest Australia reveal major velocity-depth features in the crust. The Pilbara Craton has a 28-33 km thick, two-layered crust, but in the northern Yilgarn Craton the crust is thicker (50 km) and three-layered. The lower crust in the Proterozoic mobile belt between the cratons has high velocity gradients implying a dense lower crust.

Along the axis of the Hamersley Basin, the crust has a velocity inversion close to the surface, and lateral changes in near-surface seismic velocities correspond to zoning in the burial metamorphism of the Hamersley Basin volcanic and sedimentary rocks. Partial melting and metamorphic grade are used to explain velocities in the lower crust that are different from those under the eastern Pilbara Block.

The differences in the crustal thicknesses and the number of crustal layers in the Pilbara and Yilgarn Cratons are evidence of separate crustal histories of the cratons during the Archaean.

INTRODUCTION

The Pilbara region of northwest Australia is one of the most geologically interesting and important areas of Australia—it has the oldest isotopically dated rocks in Australia and therefore may represent the primeval continental crust of Australia; it is also one of Australia's principal mineral provinces.

In 1977, the Australian Bureau of Mineral Resources, Geology and Geophysics (BMR) and the Research School of Earth Sciences, Australian National University (ANU) undertook a survey to study the crustal and upper mantle structure in the Precambrian shield of northwest Australia. The aims of the survey were to define the structural relations between the Archaean Pilbara and Yilgarn Cratons, and to compare the crustal parameters of the exposed parts of the cratons with those of the crust under the Proterozoic sedimentary basins in the region.

This paper sets out some of the results and develops crustal models for the region.

GEOLOGY

Several Precambrian provinces occur in northwest Australia; those discussed here are shown in Figure 1. Most nomenclature used for the provinces follows that of Gee (1979*a*) and amendments are discussed in the text. The oldest rocks crop out in the Archaean Pilbara Block which has a granite/greenstone stratigraphy. Rb-Sr isotopic ages of the bulk of the granites (Arriens, 1971; de Laeter & Blockley, 1972; de Laeter *et al.*, 1975) are about 3100 Ma, although some granites were emplaced later at about 2700 Ma. U-Pb ages (Oversby, 1976; Pidgeon, 1978*a*; 1978*b*; 1978*c*) imply older ages of about 3300-3400 Ma for the bulk of the granites.

The Yilgarn Block in the south also has a granite/greenstone stratigraphy, but both Rb-Sr and U-Pb isotopic ages of granites (Arriens, 1971; Oversby, 1975) suggest that granites equivalent in age to the younger granites of the Pilbara dominate in the Yilgarn Block.

Volcanics, banded iron formations, and sediments of the Hamersley Basin overlie the southern half of the Pilbara Craton. Archaean inliers within the Hamersley Basin, and trends in the Bouguer gravity anomaly field (BMR, 1975) suggested to Horwitz & Smith (1978, Fig. 1, p. 294) that the craton extended south to include the Sylvania Dome, and hence that the Hamersley Basin, as later redefined by Gee (1979*a*, 1979*c*), is within the confines of the Pilbara Craton.

The slightly younger Ashburton Trough

(Doust, 1975) abuts the southwest margin of the Hamersley Basin and contains the sediments of the Wyloo Group. Smith & Horwitz (1975) demonstrated that it coincides with the western part of a gravity feature which Fraser (1976) labelled the Ashburton Regional Gravity Ridge. Horwitz & Smith (1978) named it the Wyloo Trough and extended it to the Glengarry Sub-basin of the Nabberu Basin (Hall & Goode, 1978) where similar sediments, believed to be of the same general age, overlap the northern Yilgarn Block.

Sedimentary rocks of the Bangemall Basin unconformably overlie the rocks of the Hamersley and Nabberu Basins and mask their structural relations. The Gascoyne Province, in the west of the surveyed region, contains metamorphosed and folded relics of Archaean basement, lower Proterozoic sediments and volcanics, and rocks of the Bangemall Basin (Daniels, 1975; de Laeter, 1976; Williams *et al.*, 1978). Horwitz & Smith (1978, Fig. 1) extended the Gascoyne Province eastward to include the Goodin and Marymia Domes of Gee (1979*b*).

Palaeogeographic reconstructions by Horwitz & Smith (1978) showed that, during the early sedimentation in the Hamersley Basin, a basement high extended north-northwest from about the northern edge of the Sylvania Dome, and that the southern margin of the Pilbara Craton was tilting or subsiding toward the Ashburton Trough. This is allied to an increase in metamorphic grade towards the south (Smith, 1975*a*) and an increase in deformation (Daniels, 1966). A similar but reversed picture occurs in the sedimentary cover of the Yilgarn Craton (Hall & Goode, 1978; Horwitz & Smith, 1978), and thus folding and metamorphism indicate that the Gascoyne Province lies along an east-west axis of mirror-image symmetry.

THE CRUSTAL SURVEY

During the crustal survey, seismic refraction data and data from road and helicopter gravity traverses were collected (Fig. 1). The Pilbara region has seven open-cut iron ore mines which regularly fire large quarrying blasts suitable for use as seismic sources. To extend the survey

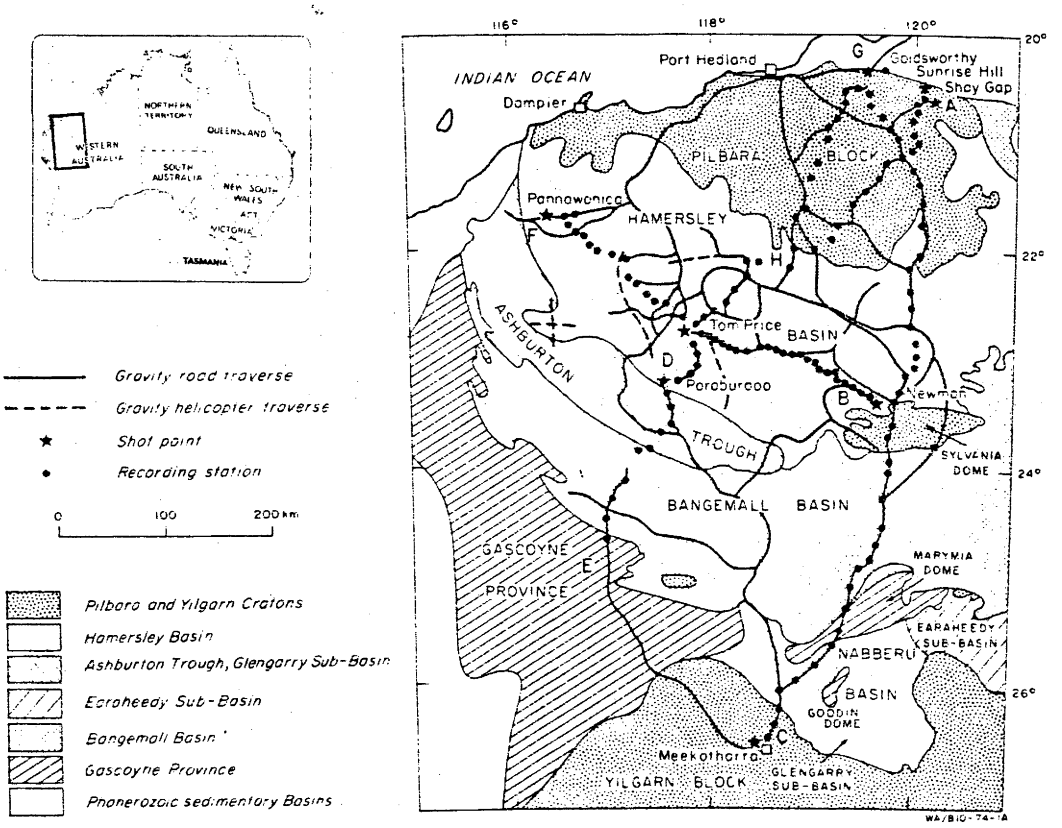

Fig. 1. Geology and survey design.

farther south, a specially prepared blast was fired at Meekatharra on the northern Yilgarn Block.

The field work was described by Drummond (1979*b*, 1979*c*). Portable field seismographs were deployed at intervals of less than 20 km along three lines (Fig. 1). The principal line (GBC) extended from Goldsworthy to Meekatharra, crossing the eastern Pilbara Block and Hamersley Basin, the Bangemall and Nabberu Basins, and the northern Yilgarn Block. Farther west, a second line (GHDE) extended south to the Gascoyne Province. The third BMR line (FDB) lay along the axis of the Hamersley Basin outcrop area.

Several methods were used to interpret the data. The models presented here were derived using the intercept method (Mota, 1954). They are two-dimensional representations of the crust and have several layers in which the velocities generally do not vary with depth. However, studies using synthetic seismogram computer modelling indicate that velocity gradients are likely in the crust, at the crust/mantle boundary, and in the upper mantle. They are also evident from the positions of reflected phases and travel-time cusps in some of the data presented here.

SECTION GBC

The first model for line GBC was derived and presented by Drummond (1979*a*), but because line GBC is the principal seismic profile in the survey, this model is reviewed here. Because of the approach to the original interpretation, some of the layers had small steps which have now been smoothed out. Three possible models were presented by Drummond (1979*a*), and their revised equivalents are shown in Figure 2.

Seismic velocities in the upper crust along the profile are between 6.0 and 6.2 km s^{-1}, except to the north of Newman, where a slightly lower velocity (5.86 km s^{-1}) and small negative intercept indicate thickening Hamersley Basin rocks to the north. This agrees with the palaeogeographic reconstruction for the region of Horwitz & Smith (1978).

A lower crustal layer (6.4 km s^{-1}) is present along the profile, at depths ranging from 13 km in the north (at G) to 15 km in the south (at C).

From the data available, the differences between the three alternative models for the lower crust along segment BC in Figure 2 cannot be resolved. While they differ in detail, they all show a thickening of the crust from north to south. Velocity gradients and material with a seismic velocity of about 7 km s^{-1} imply a dense lower crust in the south of the segment.

The crust is 28 km thick in the north of the

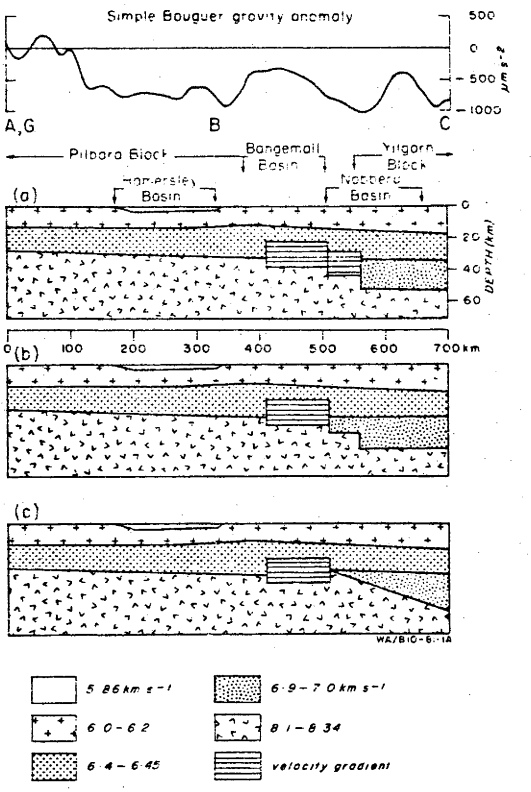

Fig. 2. Alternative models along seismic lines ABC and GBC, based on those of Drummond (1979*a*).

Pilbara Block, and thickens to 33 km to the south of B, where the steps in models a and b increase its thickness to 37, 43, and finally 52 km at C. The thicknesses may be revised slightly by synthetic seismogram modelling; results so far suggest that increases of up to 10% may be required.

The upper mantle velocity along segment GB is 8.34 km s^{-1}. Travel-times from the Meekatharra blast to seismological observatories to the south indicated an upper mantle velocity of 8.1 km s^{-1} under the Yilgarn Block. Consequently, the upper mantle velocity may decrease from north to south along segment BC.

The outcrop areas of the geological provinces have been marked in Figure 2. The Pilbara Craton, whose rocks crop out along much of segment GB, is considered to extend about 80 km south of B, to the most northerly step in the lower crust. This is about 40 km south of the Sylvania Dome, and corresponds to the southern limit of the Northern Facies of the Bangemall Basin (see Brakel & Muhling, 1976).

The northern Yilgarn Craton is three-layered and its northern margin is near the Marymia Dome (Fig. 1). The zones of dense lower crust in

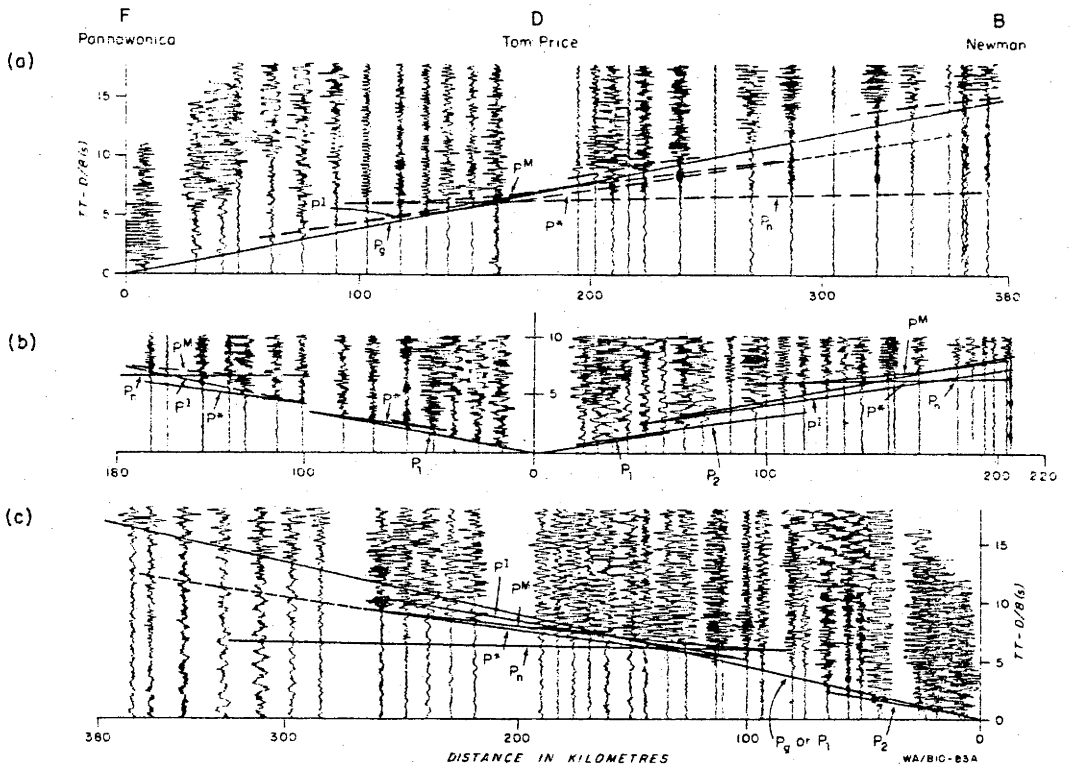

Fig. 3. Seismic record sections along line FDB of blasts at (a) Pannawonica, to the southeast towards Newman; (b) Tom Price, to the northwest towards Pannawonica (LHS) and to the southeast towards Newman; and (c) Newman, to the northwest towards Pannawonica. The amplitudes of the traces are as recorded, except in (c) where they have been trace-normalized to enlarge the phases beyond 270 km. The travel time curves superimposed on the record sections are for the model in Figure 4.

the centre of segment BC correspond to the Bangemall and northern Nabberu Basin outcrop areas.

SECTION FDB

Some of the data from line FDB are presented as record sections in Figure 3. The velocities and intercept times for the observed phases were scaled from the record sections, and the travel-time equations are listed in Table I. A preliminary model derived from these data is shown in Figure 4. The nomenclature used to describe the seismic phases is as follows. P_1 arrivals have an apparent velocity of about 5.9 km s^{-1} and have travelled directly through the near-surface sediments. The P_2 phases have a higher apparent velocity (6.3 to 6.7 km s^{-1}), and have travelled through near-surface rocks which are underlain by lower-velocity rocks. Pg arrivals are refracted through the top of the crystalline basement. The P^1 phases are reflected off a lower crustal interface, and the P* phases (6.5 km s^{-1}) are refracted through the lower crust. P^M arrivals are wide-angle reflections from the Moho, and Pn arrivals are Moho refractions. Not all phases were

TABLE I

Seismic travel time equations

Phase	Pannawonica eastward	Tom Price westward	Tom Price eastward	Newman westward
P_1	absent	absent	tt = D/5.88 − 0.31 s	absent
P_2	absent	tt = D/6.32	tt = D/6.49 + 0.42 s	tt = D/6.76 + 0.1 s
Pg	tt = D/6.07 s	absent	absent	absent
P*	tt = D/6.51 + 1.2 s	tt = D/6.54 + 0.6 s tt = D/6.57 + 1.2 s	tt = D/6.39 + 0.91 s	tt = D/6.77 + 3.1 s
P_n	tt = D/7.64 + 5.5 s	tt = D/8.0 + 6.1 s	absent	tt = D/7.96 + 6.0 s

observed at each shot-point (Table 1, Fig. 3), and with differences of up to 2 s in the times for reciprocal pairs of near-surface phases there must be lateral variations in the upper crust.

The P_1 phase was observed to the east of Tom Price, and the P_2 phase both to the east of Tom Price and the west of Newman. Interpretation of the travel-time data shows that the P_2 phase results from a shallow, high-velocity layer 0.5 to 1 km deep under Newman and 2 to 3 km deep to the east of Tom Price. These depths are approximately the thicknesses of the Hamersley Basin volcanic and sedimentary rocks in the region (Daniels & MacLeod, 1965; MacLeod & de la Hunty, 1966; de la Hunty, 1965). For 60 km west of Tom Price, the high-velocity layer is modelled as 1 km thick, but may be thicker, and beyond 60 km no estimate of the basin thickness is possible because it has a seismic velocity indistinguishable from that of the basement.

In Figure 5, the laboratory measurements of seismic velocities and densities in hand specimens from the region are plotted as bars, in their approximate stratigraphic order. Basement under the basin consists of granitic rocks and their metamorphosed equivalents, gneiss and, in places, quartzite. The predominantly basic volcanic Fortescue Group forms the basal unit of the Hamersley Basin, and is overlain by the banded iron formations, mudstone, siltstone, and sandstone of the Hamersley Group. The seismic velocities are likely to increase with increasing pressure, and therefore with increasing depth of burial, as the microfractures and cracks in the rocks close up, but because this will affect all of the rock types, the relative order of the velocities and densities should be unaltered. The basic volcanics and banded iron formations have the highest velocities and densities, and velocity inversions are likely where they overlie granitic basement.

Four zones of burial metamorphism (subgreenschist to greenschist facies) have been recognised in the rocks of the Hamersley Basin (Smith, 1975*b*; Smith *et al.*, 1978). The lowest-grade metamorphic zones are recognised on the northern side of the basin. With increasing grade they are now called: pumpellyite-prehnite zone ZI; pumpellyite-epidote zone ZII; pumpellyite-actinolite zone ZIII; and the greenschist facies proper, the actinolite zone ZIV. Rocks of zones ZIV and ZIII occupy most of the southern side of the basin.

The intersection of three of the metamorphic zones with the section FDB is shown diagrammatically in Figure 6. The progressive increase in metamorphic grade may explain the observed increase in seismic velocity from west to east in the near-surface high-velocity layer. ZII corresponds to the observed velocity of 6.07 km s^{-1}, and is indistinguishable from basement; ZIII corresponds to the 6.3 km s^{-1} velocity, and ZIV to the

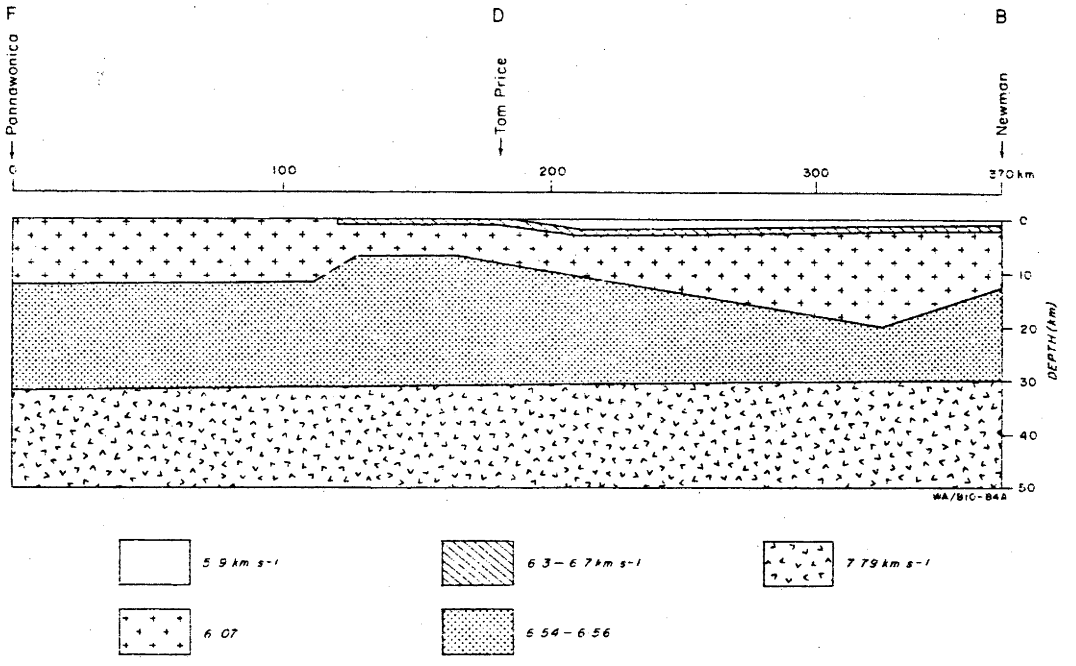

Fig. 4. Crustal model along line FDB based on the seismic data in Figure 3 and Table 1.

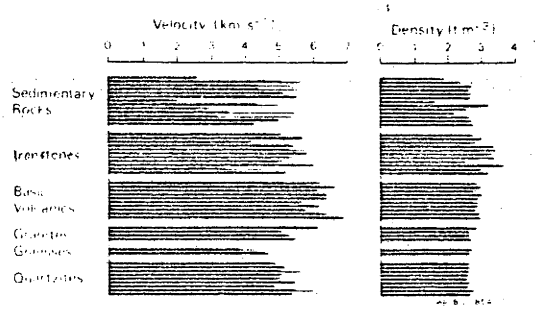

Fig. 5. Bar graph of corresponding laboratory measurements of velocities and densities of 49 hand specimens from the survey region. Seismic velocity was measured both parallel and at right angles to the layering in layered samples, and is illustrated in the figure by the split ends of some of the velocity bars.

6.5 to 6.7 km s^{-1} velocity material. The surface layer of 5.9 km s^{-1} between Tom Price and Newman may correspond to the Hamersley Group.

No estimate of the velocity of the material below the Hamersley Basin is possible. In the model, 6.07 km s^{-1} was used; it is the value measured east from Pannawonica and generally agrees with the upper crustal velocities from line GBC (Fig. 2). Subsequent inversion of the P* data gives a lower crustal layer 12 km deep under Pannawonica. About 60 km west of Tom Price, it shallows to 7 km over a maximum distance of 20 km (Fig. 4). The region where the lower crustal layer shallows around Tom Price corresponds to areas of Archaean basement outcrop and doming of the Hamersley Basin rocks. East of Tom Price, the lower crustal layer deepens, possibly reaching 20 km before shallowing again to 13 km at Newman, the depth determined from line GBC. The velocity in the lower crustal layer is 6.55 km s^{-1}.

The 7.8 km s^{-1} velocity layer is 31 km deep under Pannawonica, and 32 km deep under Newman. Although the depth under Newman agrees well with the depth of the crust/mantle boundary under Newman along profile GBC, the 7.8 km s^{-1} velocity is very much less than the upper mantle velocity of 8.3 km s^{-1} along section GB. Upper mantle P-wave anisotropy of 0.5 km s^{-1} may therefore be implied in the lithosphere below the Pilbara Craton. Anisotropy of this magnitude has been observed in both oceanic (*e.g.* Morris *et al.*, 1969) and continental (*e.g.* Bamford, 1977) lithospheres, and is generally attributed to alignment of olivine crystals. Confirmation of anisotropy in the lithosphere below the Pilbara Craton will have to await more comprehensive analysis of all the available data.

An alternative explanation is that the lower 7.8 km s^{-1} velocity is confined only to the axis of the Hamersley Basin. Fuchs (1979), in a review of seismic studies of continental lithospheres, reports that lateral changes of several tenths of a kilometre per second can be observed in upper mantle velocities from regions only several tens of kilometres apart. The lateral velocity heterogeneity in the Pilbara Craton is unlikely to be due to high present-day crustal temperatures in the Hamersley Basin, because heat flow in the region is uniformly low (Cull & Denham, 1979). However, it may be due to lower crustal and upper mantle chemical inhomogeneities which pinch out towards the eastern edge of the basin.

Drummond (1979*a*) suggested a tectonic model for the region based on crustal thicknesses and dips in which he inferred that the Pilbara Craton was tilted to the south.

The dip of 0.8° on the base of the crust is similar to the dip on Hamersley Basin remnants in the north of the Pilbara Block and represents a subsidence of at least 5 km along the southern boundary of the craton. However, the presence

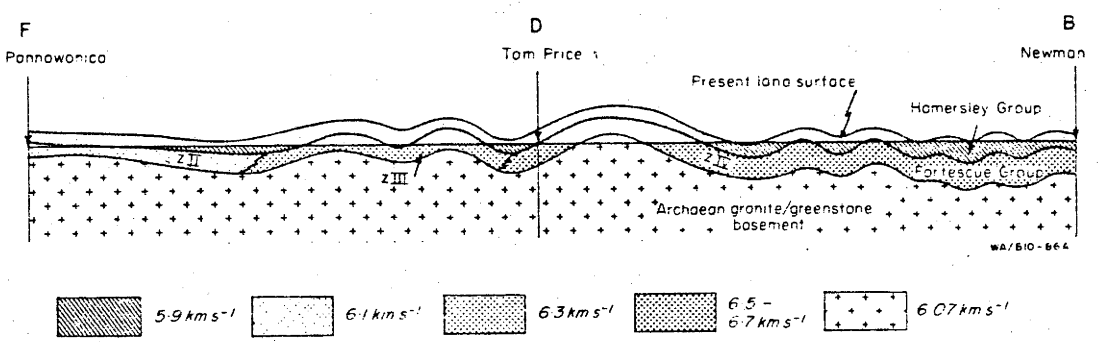

Fig. 6. Diagrammatic cross-section along line FDB illustrating the correspondence of the increase in metamorphic grade to the increase in near-surface seismic velocity. The metamorphic grades in the figure are represented as: ZII pumpellyite-epidote zone; ZIII pumpellyite-actinolite zone; and ZIV actinolite zone.

of Archaean inliers within the Hamersley Basin, which correspond to the shallowing of the lower crustal layer near Tom Price in Figure 4, the sedimentary thicknesses (Horwitz & Smith, 1978, Figs. 6 & 7), and the low-grade burial metamorphism of the Hamersley Basin rocks all suggest that the subsidence was much greater, especially along the southern margin of the craton, and that the crust has rebounded. A maximum rebound, based on metamorphic grades, of 10 to 12 km to the west of Tom Price, and perhaps 5 to 7 km near Newman, has been estimated. The 7.8 km s^{-1} velocity may therefore represent lower crustal rocks depressed sufficiently during the Proterozoic for partial melting to have occurred. The partial melting could account for the acid Woongarra Volcanics (Trendall, 1975). The remaining lower crustal rocks would then be anomalously dense, giving rise to seismic velocities of 7.8 km s^{-1}. As well, the lower crustal velocity (6.55 km s^{-1}) along profile FDB is slightly higher than to the northeast under the eastern Pilbara Block (6.4 km s^{-1}). This probably results from a higher metamorphic grade caused by the depression of the material into a higher temperature and pressure regime.

DISCUSSION

These studies have considered mainly the Pilbara Craton and its Proterozoic cover rocks, and we are therefore able to suggest a possible scenario of events for the tectonic evolution of the Pilbara Craton from the end of the Archaean. We have not tested all aspects of the scenario and propose it mainly as a basis for further discussion.

The movements associated with the vertical tectonics interpreted along Section FDB are approximately half the thickness of the present-day crust in the Pilbara Craton. The forces required to produce such movements are unlikely to have originated within the crust, and a high heat flux is suggested as the factor influencing the creation of the Hamersley Basin. High heat flux would have caused partial melting of the upper mantle, producing the basalts of the Fortescue Group. The basalts spilled out over the Archaean basement, which, weakened by the high heat flux, would have subsided; the metamorphic pattern suggests that the subsidence was greater in the south than in the north. The Hamersley Basin sedimentary and volcanic sequences accumulated and were progressively metamorphosed as they were in turn depressed and buried. The rocks of the lower crust would have been depressed sufficiently to have partially melted, giving rise to acid volcanism. With the passing of the thermal event, basin subsidence ceased. The crust, depressed into the more dense mantle, began to rise as local isostatic compensation was replaced by lower-stress regional compensation. The uplift would not be by the full extent of the original subsidence because of the redistribution of mass from the mantle onto the top of the crust, and the ability of the cooler and therefore stronger crust to support the load. The balance of the subsidence is represented by the 5 km of tilt measured by the seismic profiling.

Models for the evolution of the region must reconcile major differences in the geology and structure between the Pilbara and Yilgarn Block. Gee (1979*c*) listed four of them: (i) The western Yilgarn Block has large areas of high-grade Archaean gneiss terrain—no similar rocks have been found in the Pilbara Block; (ii) granites form the bulk of the rocks in the crust of both the Pilbara and Yilgarn Blocks, but all reliable dates for those of the Yilgarn Block fall in the range 2600 to 2700 Ma, while most of those of the Pilbara Block have ages greater than 3000 Ma; (iii) the clastic sequences within the greenstone belts of the Pilbara Block are more mature than those of the Yilgarn Block, implying to Gee (1979*c*) that the Pilbara Block developed more toward crustal stability than the Yilgarn Block (such stability also being evident from the broad, simple burial-metamorphic pattern: see Smith, 1975*b*) and (iv) the Pilbara Block has near-circular granite batholiths, but those of the Yilgarn Block have distinct linear trends.

To these four points can now be added two more, which may be related. Firstly, the crust of the Pilbara Craton is 28 to 33 km thick, but that of the Yilgarn Craton is more than 50 km thick in the north (Fig. 2) and 40 km thick in the south (Mathur, 1974). The crust in the Yilgarn Craton is therefore much thicker than the crust in the Pilbara Craton. Secondly, excluding the rocks of the Hamersley Basin, the Pilbara Craton is two-layered (Figs 2 & 4), but three layers are present in the Yilgarn Craton (Fig. 2, and Mathur, 1974). A third, thin, lower crustal layer can be used to explain anomalous amplitudes of some seismic phases immediately to the north of Newman, but it appears to be a local feature and not of significance to the structure of the Pilbara Craton as a whole.

The difference in the crustal thickness, especially in the northern Yilgarn Craton, is due mainly to the thick, high-velocity (7 km s^{-1}) lower crustal layer. The lower crustal layer of Mathur (1974) in the southern Yilgarn Craton has a higher seismic velocity (7.4 km s^{-1}), and in the southwestern Yilgarn Craton is very close to the surface. Glikson & Lambert (1976) proposed that

MACLEOD, W. N., & DE LA HUNTY, L. E., 1966: Roy Hill, Western Australia—1:250000 Geological Series. *Explan. Notes geol. Surv. West. Aust., SF50-12.*

MATHUR, S. P., 1974: Crustal structure in southwest Australia from seismic and gravity data. *Tectonophys., 24,* 151-182.

MCELHINNY, M. W., & MCWILLIAMS, M. O., 1977: Precambrian geodynamics—a palaeomagnetic view. *Tectonophys., 40,* 137-159.

MORRIS, G. B., RAITT, R. W., & SHOR, G. G., 1969: Velocity anisotropy and delay-time maps of the mantle near Hawaii. *J. geophys. Res., 74,* 4300-4316.

MOTA, L., 1954: Determination of dips and depths of geological layers by the seismic refraction method. *Geophys., 19,* 242-254.

OVERSBY, V. M., 1975: Lead isotopic systematics and ages of Archaean acid intrusives in the Kalgoorlie-Norseman area, Western Australia. *Geochim. cosmochim. Acta, 39,* 1107-1125.

_____, 1976: Isotopic ages and geochemistry of Archaean acid igneous rocks from the Pilbara, Western Australia. *Geochim. cosmochim. Acta, 40,* 817-829.

PIDGEON, R. T., 1978*a*: 3450 m.y. old volcanics in the Archaean layered greenstone succession of the Pilbara Block, Western Australia. *Earth planet. Sci. Lett., 37,* 421-428.

_____, 1978*b*: Geochronological investigations of granite batholiths of the Archaean granite-greenstone terrain of the Pilbara Block, Western Australia; *in* Smith, I. E. M., & Williams, J. G. (Eds) *Proceedings of the 1978 Archaean Geochemistry Conference,* 360-362. University of Toronto.

_____, 1978*c*: Big Stubby and the early history of the earth. *Open-File Rep. U.S. geol. Surv., 78-701,* 334-335.

SMITH, R. E., 1975*a*: Exploration guides for Keweenawan-type copper deposits in the Proterozoic Fortescue Group of Western Australia, Preliminary Report. *Rep. CSIRO miner. Res. Lab., FP 8.*

_____, 1975*b*: Metamorphism of the Proterozoic Fortescue Group, Western Australia—a reconnaissance study. *Rep. CSIRO miner. Res. Lab., FP 9.*

SMITH, R. E., GREEN, A. A., ROBERTS, G., & HONEY, F. R., 1978: Use of Landsat-1 imagery in exploration for Keweenawan-type copper deposits. *Remote Sens. Environment, 7,* 129-144.

SMITH, R. E., & HORWITZ, R. C., 1975: Structural synthesis for the deposition of the Wyloo and Bangemall Groups. *Abstr. First Aust. geol. Conv. Prot. Geol., geol. Soc. Aust.,* 77.

TRENDALL, A. F., 1975: Main areas of Proterozoic sedimentary rocks, Hamersley Basin; *in* Geology of Western Australia. *Mem. geol. Surv. West. Aust., 2,* 119-143.

WILLIAMS, S. J., ELIAS, M., & DE LAETER, J. R., 1978: Geochronology and evolution of the eastern Gascoyne Province and the adjacent Yilgarn Block. *Ann. Rep. geol. Surv. West. Aust. for 1977,* 50-56.

it was formed by the injection of basic magma during the break up of Gondwanaland in the Phanerozoic. However, Drummond (1979*a*) suggested that the layering within the cratons represents the metamorphic effects on a crust of broadly uniform acid to intermediate chemical composition so that the third crustal layer may be a metamorphic effect and not a change in chemistry. Certainly any tectonic model which proposes the injection of magma, whether basic or acidic, into the base of the crust has to inject it selectively at the base of the Yilgarn Craton and not at the base of the Pilbara Craton, which, from palaeomagnetic data (McElhinny & McWilliams, 1977; Embleton, 1978), was in its present position relative to the Yilgarn Block from about 2400 Ma ago.

ACKNOWLEDGMENTS

We acknowledge the invaluable assistance of our colleagues at the Bureau of Mineral Resources, Geology and Geophysics (BMR), the Research School of Earth Sciences at the Australian National University (ANU) in Canberra, and the CSIRO Division of Mineralogy in Perth. K. J. Muirhead, R. Arculus, and D. M. Finlayson critically read the manuscript. The seismic interpretation was performed while BJD was on full-time study leave at the ANU under the Australian Public Service Postgraduate Scholarship Scheme. This work is published with the permission of the Director of the BMR. Jane Prowse typed the manuscript and Gill Clark drew the figures.

REFERENCES

ARRIENS, P. A., 1971: The Archaean geochronology of Australia. *Spec. Publs geol. Soc. Aust., 3,* 11-23.

BAMFORD, D., 1977: Pn velocity anisotropy in a continental upper mantle. *Geophys. J. R. astr. Soc., 49,* 29-48.

BMR, 1975: Gravity map of Australia, 1:5 000 000. Bur. miner. Resour. Geol. Geophys. Aust., Canberra.

BRAKEL, A. T., & MUHLING, P. C., 1976: Stratigraphy, sedimentation and structure in the western and central part of the Bangemall Basin, Western Australia. *Ann. Rep. geol. Surv. West. Aust. for 1975,* 70-79.

CULL, J. P., & DENHAM, D., 1979: Regional variations in Australian heat flow. *BMR J. Aust. Geol. Geophys., 4,* 1-13.

DANIELS, J. L., 1966: The Proterozoic geology of the North-West Division of Western Australia. *Proc. Australas. Inst. Min. Metall., 219,* 17-26.

DANIELS, J. L., 1975: Gascoyne Province; *in* Geology of Western Australia. *Mem. geol. Surv. West. Aust., 2,* 107-114.

DANIELS, J. L., & MACLEOD, W. N., 1965: Newman, W.A.—1:250 000 Geological Series. *Explan. Notes geol. Surv. West. Aust., SF50-10.*

DE LAETER, J. R., 1976: Rb-Sr whole-rock and mineral ages from the Gascoyne Province. *Ann. Rep. geol. Surv. West. Aust. for 1975,* 126-130.

DE LAETER, J. R., & BLOCKLEY, J. G., 1972: Granite ages within the Archaean Pilbara Block, Western Australia. *J. geol. Soc. Aust., 19,* 363-370.

DE LAETER, J. R., LEWIS, J. D., & BLOCKLEY, J. G., 1975: Granite ages within the Shaw Batholith of the Pilbara Block. *Ann. Rep. geol. Surv. West. Aust. for 1974,* 73-79.

DE LA HUNTY, L. E., 1965: Mount Bruce, W. A. —1:250 000 Geological Series. *Explan. Notes. geol. Surv. West. Aust., SF50-11.*

DOUST, Q., 1975: Economic implications of the geology of the Duck Creek Syncline, Ashburton Trough, Western Australia. *Abstr. First Aust. geol. Conv. Prot. Geol., geol. Soc. Aust.,* 77.

DRUMMOND, B. J., 1979*a*: A crustal profile across the Archaean Pilbara and northern Yilgarn Cratons, northwest Australia. *BMR J. Aust. Geol. Geophys., 4,* 171-180.

———, 1979*b*: Pilbara Crustal Survey, 1977: Operational Report. *Rec. Bur. miner. Resour. Geol. Geophys. Aust., 1979/54* [unpublished].

———, 1979*c*: Structural Relations Between the Archaean Pilbara and Yilgarn Cratons, Western Australia, from Deep Seismic Sounding. MSc. Thesis, Aust. Nat. Univ. [unpublished].

EMBLETON, B. J. J., 1978: The palaeomagnetism of 2400 m.y. old rocks from the Australian Pilbara Craton and its relation to Archaean-Proterozoic tectonics. *Precamb. Res., 6,* 275-291.

FRASER, A. R., 1976: Gravity provinces and their nomenclature. *BMR J. Aust. Geol. Geophys., 1,* 350-352.

FUCHS, K., 1979: Structure, physical properties, and lateral heterogeneities of the subcrustal lithosphere from long-range deep seismic sounding observations on continents. *Tectonophys., 56,* 1-15.

GEE, R. D. (COMPILER), 1979*a*: Geological map of Western Australia, 1979, 1:2 500 000. Geol. Surv. West. Aust., Perth.

———, 1979*b*: The geology of the Peak Hill area. *Ann. Rep. geol. Surv. West. Aust. for 1978,* 55-62.

———, 1979*c*: Structure and tectonic style of the Western Australian shield. *Tectonophys., 58,* 327-369.

GLIKSON, A. Y., & LAMBERT, I. B., 1976: Vertical zonation and petrogenesis of the early Precambrian crust in Western Australia. *Tectonophys., 30,* 55-89.

HALL, W. D. M., & GOODE, A. D. T., 1978: The Early Proterozoic Nabberu Basin and associated iron formations of Western Australia. *Precamb. Res., 7,* 129-184.

HORWITZ, R. C., & SMITH, R. E., 1978: Bridging the Yilgarn and Pilbara Blocks, Western Australia. *Precamb. Res., 6,* 293-322.

MACLEOD, W. N., & DE LA HUNTY, L. E., 1966: Roy Hill, Western Australia—1:250000 Geological Series. *Explan. Notes geol. Surv. West. Aust., SF50-12.*

MATHUR, S. P., 1974: Crustal structure in southwest Australia from seismic and gravity data. *Tectonophys., 24,* 151-182.

MCELHINNY, M. W., & MCWILLIAMS, M. O., 1977: Precambrian geodynamics—a palaeomagnetic view. *Tectonophys., 40,* 137-159.

MORRIS, G. B., RAITT, R. W., & SHOR, G. G., 1969: Velocity anisotropy and delay-time maps of the mantle near Hawaii. *J. geophys. Res., 74,* 4300-4316.

MOTA, L., 1954: Determination of dips and depths of geological layers by the seismic refraction method. *Geophys., 19,* 242-254.

OVERSBY, V. M., 1975: Lead isotopic systematics and ages of Archaean acid intrusives in the Kalgoorlie-Norseman area, Western Australia. *Geochim. cosmochim. Acta, 39,* 1107-1125.

_____, 1976: Isotopic ages and geochemistry of Archaean acid igneous rocks from the Pilbara, Western Australia. *Geochim. cosmochim. Acta, 40,* 817-829.

PIDGEON, R. T., 1978*a*: 3450 m.y. old volcanics in the Archaean layered greenstone succession of the Pilbara Block, Western Australia. *Earth planet. Sci. Lett., 37,* 421-428.

_____, 1978*b*: Geochronological investigations of granite batholiths of the Archaean granite-greenstone terrain of the Pilbara Block, Western Australia; *in* Smith, I. E. M., & Williams, J. G. (Eds) *Proceedings of the 1978 Archaean Geochemistry Conference,* 360-362. University of Toronto.

_____, 1978*c*: Big Stubby and the early history of the earth. *Open-File Rep. U.S. geol. Surv., 78-701,* 334-335.

SMITH, R. E., 1975*a*: Exploration guides for Keweenawan-type copper deposits in the Proterozoic Fortescue Group of Western Australia, Preliminary Report. *Rep. CSIRO miner. Res. Lab., FP 8.*

_____, 1975*b*: Metamorphism of the Proterozoic Fortescue Group, Western Australia—a reconnaissance study. *Rep. CSIRO miner. Res. Lab., FP 9.*

SMITH, R. E., GREEN, A. A., ROBERTS, G., & HONEY, F. R., 1978: Use of Landsat-1 imagery in exploration for Keweenawan-type copper deposits. *Remote Sens. Environment, 7,* 129-144.

SMITH, R. E., & HORWITZ, R. C., 1975: Structural synthesis for the deposition of the Wyloo and Bangemall Groups. *Abstr. First Aust. geol. Conv. Prot. Geol., geol. Soc. Aust.,* 77.

TRENDALL, A. F., 1975: Main areas of Proterozoic sedimentary rocks, Hamersley Basin; *in* Geology of Western Australia. *Mem. geol. Surv. West. Aust., 2,* 119-143.

WILLIAMS, S. J., ELIAS, M., & DE LAETER, J. R., 1978: Geochronology and evolution of the eastern Gascoyne Province and the adjacent Yilgarn Block. *Ann. Rep. geol. Surv. West. Aust. for 1977,* 50-56.

APPENDIX 3

Drummond, B.J., 1981 - Crustal structure of the Precambrian terrains of northwest Australia from seismic refraction data. BMR Journal of Australian Geology and Geophysics, 6, 123-135.

Reprinted from
BMR Journal of Australian Geology & Geophysics, 6, 1981, 123-135

Crustal structure of the Precambrian terrains of northwest Australia from seismic refraction data

B. J. Drummond

The crust of the Pilbara Craton is 28-33 km thick, and its boundary with the upper mantle dips south at slightly less than one degree. The southern edge of the craton is marked by a sharp increase in crustal thickness about 40 km south of the Sylvania Dome in the east and along the northern boundary of the Ashburton Trough in the west. Seismically, the crust has two layers, an upper one with P-wave velocity 6.0-6.1 km s^{-1}, and a lower of 6.4-6.6 km s^{-1}. The boundary between them is depressed beneath the deepest part of the Hamersley Basin, and rises along the southern part of the basin and craton, beneath a topographic ridge of higher grade metamorphic rocks. The velocities in the lower crustal layer are highest along the southern part of the Hamersley Basin, an area known to have been depressed during the formation and filling of the basin, and then uplifted. The crust of the northern Yilgarn Craton is at least 50 km thick and, seismically, has three layers. The uppermost layer has P-wave velocities of 6.1-6.2 km s^{-1}, the middle layer, at 10-16 km depth, 6.4 km s^{-1}, and the lowest, at 32 km depth, 6.7-7.0 km s^{-1}. A zone of crust, about 50 km wide, along the northern margin of the craton was extensively reworked during Proterozoic orogenesis, and is now characterised by thinner crust than the rest of the Yilgarn Craton, extensive granitoid emplacement, intense deformation and folding of the upper crustal rocks, and low gravity values. The Capricorn Orogen between the cratons is marked by high velocities in the lower crust, probably caused by dense mafic intrusions or a higher metamorphic grade. The seismic layering within the crust is most likely caused by increasing metamorphic grade with depth. The crust is probably of average acid to intermediate chemical composition, and has a low metamorphic grade at the surface. The velocities are attributed to metamorphic grade increasing to felsic granulite at 9-16 km depth, and garnet granulite at 32 km depth in the Yilgarn Craton.

Introduction

During 1979, seismic refraction measurements were made along five profiles in the Pilbara region of Western Australia (Drummond, 1979a). Seven open-cut iron-ore mines in the northern Pilbara Block and the Hamersley Basin regularly fired large quarrying blasts, and these were used as seismic sources.

The seismic survey was planned so that the refraction profiles would traverse all the Precambrian geological provinces in the region. The survey design is superimposed on the geological map in Figure 1. BMR recorded along lines ABC, FDB and ADHE (Drummond, 1979a), and the Research School of Earth Sciences at the ANU recorded along lines GF and DC. Drummond (1979b) and Drummond & others (1981) used the intercept method (Mota, 1954) to interpret the data from lines ABC and FDB, and extended their interpretation by using computer ray tracing through their models to test for lateral structural changes.

In this paper the results of the earlier interpretations are summarised, the data from the three remaining traverses (ADHE, DC and FG) are interpreted, and the results from all five profiles are used to derive a picture of the crustal structure of the region.

Geology

The regional geology is shown in Figure 1. The tectonic nomenclature follows that of Gee (1979a, c); accordingly, a 'block' is the exposed part of an old, stabilised region called a 'craton'. In the survey area, two Archean cratons, the Pilbara and Yilgarn Cratons, are overlapped and separated by younger sediments and volcanics of several sedimentary basins.

The greenstone belts of the Pilbara Block have provided Australia's oldest isotopic ages of 3400 to 3500 m.y. (Richards, 1977; Pidgeon, 1978a; Hamilton & others, 1980), and sinuously enclose large, ovoid domes of younger, intrusive granitoid, with isotopic ages grouped around 3000 m.y. (Oversby, 1975; Pidgeon, 1978b; de Laeter & Blockley, 1972; de Laeter & others 1980, 1981) and 2600-2800 m.y. (Oversby, 1975; de Laeter & Blockley, 1972; de Laeter & others, 1980). The younger granitoids are a minor proportion of the granitoids of the Pilbara Block, and may have resulted from partial remelting of the older crust (de Laeter & Blockley, 1972).

The Yilgarn Block, which extends about 1000 km south of the area shown in Figure 1, also has a granitoid/greenstone stratigraphy. In the north, the majority of the granitoids have isotopic ages of about 2600 m.y. (Compston & Arriens, 1968; Oversby, 1975; de Laeter & others, 1980).

Volcanic and sedimentary rocks and banded iron formations of the Hamersley Basin overlap the southern edge of the Pilbara Block. Trends in the regional gravity pattern (Fraser, 1973; Wellman, 1978), and inliers of Archaean basement (e.g. the Sylvania Dome) indicate that the Pilbara Craton forms the basement of the Hamersley Basin. The rocks of this basin have marked lateral continuity, and are thought to have originally covered most of the Pilbara Craton. They are now restricted to the southern part of the craton, where the basin was deepest (Trendall, 1975; Horwitz & Smith, 1978). Where the basal unconformity of the basin is exposed, the basal volcanics are restricted to the centre of greenstone belts, implying that the granitoid plutons were still rising when the basin formed (Trendall, 1975). The intensity of folding in the basin increases southwards (Trendall, 1975).

Abutting the southern edge of the Hamersley Basin is the Ashburton Trough (the Wyloo Trough of Horwitz & Smith, 1978), which contains thick clastic sediments, turbidites, and olistostromes. The Ashburton Trough is younger than the Hamersley Basin, and

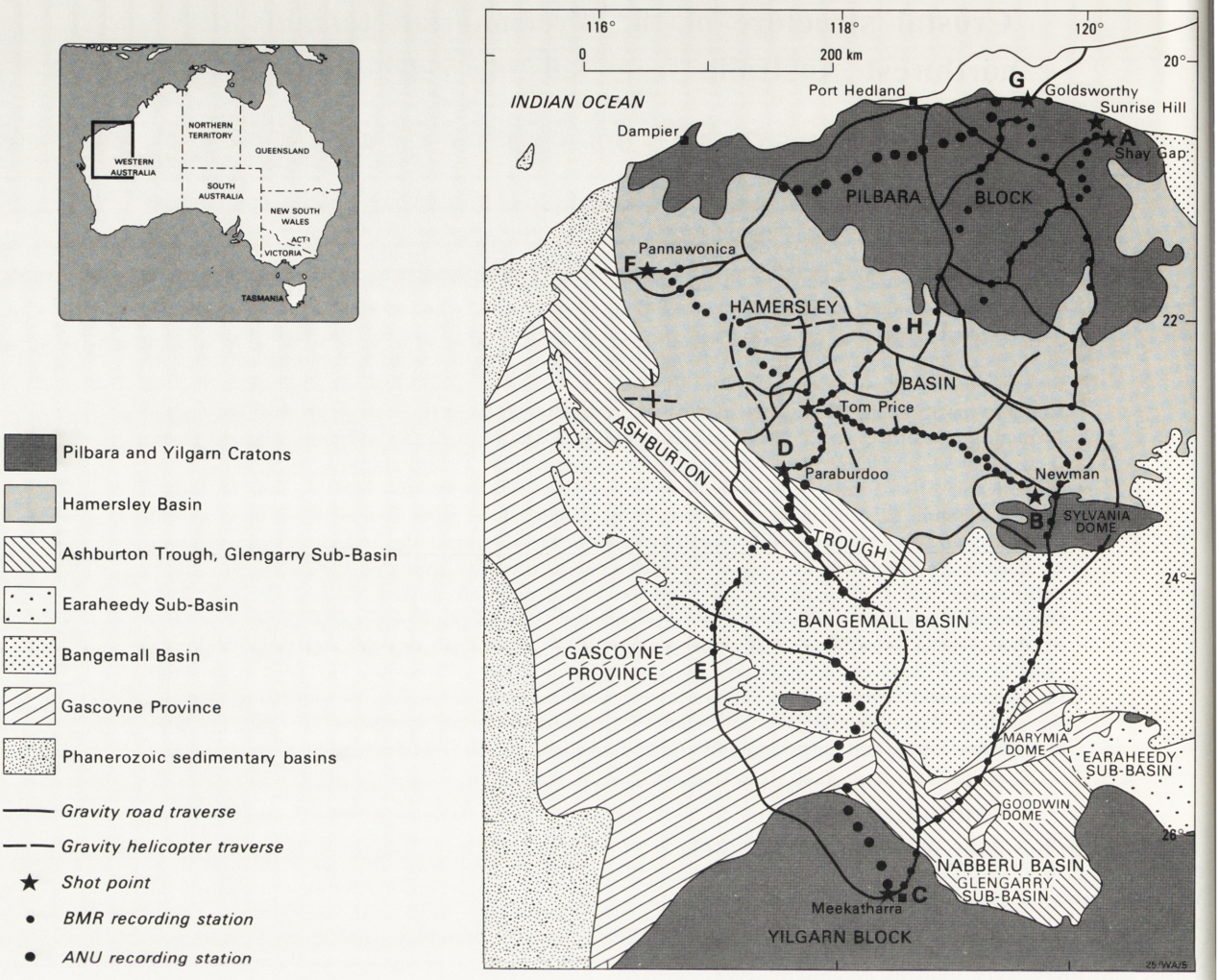

Figure 1. Geology and survey design.

is possibly contemporaneous with the Glengarry Sub-basin of the Nabberu Basin, which bounds the northern edge of the Yilgarn Craton (Gee, 1979a).

The Glengarry Sub-basin contains clastic sediments, volcanic rocks, and turbidites, which dip gently off the Yilgarn Craton. The dip and deformation of the sediments increase northwestwards across the basin (Hall & Goode, 1978; Gee, 1979b) and, although the structural relations between the Nabberu Basin and the Hamersley Basin are masked by the younger cover of the Bangemall Basin, Horwitz (1975) was able to show a mirror image symmetry of the structures in the two basins.

Clastic sediments, dolomites and cherts are the principal rock types of the Bangemall Basin; volcanic rocks are not common. Changes of facies and structural style reflect the stability of the basement on which the basin formed. Stable basement parallelled the southern boundary of the Pilbara Craton in the north, and the northern edge of the Yilgarn Craton in the south. The western and central portions of the basin had an active basement (Brakel & Muhling, 1976).

The Gascoyne Province in the west of the survey area contains reworked Archaean basement rocks, and reworked sediments from the Bangemall and Nabberu Basins and Ashburton Trough (Daniels, 1975; Williams & others, 1979). Granitoids which crop out in the province were derived from reworked Archaean basement, possibly mixed with younger magmatic or supracrustally reworked material (de Laeter, 1976; Williams & others, 1978).

The Gasycoyne Province, Bangemall Basin, and Ashburton Trough occupy the Proterozoic Capricorn Orogenic Belt (Gee, 1979c). Palaeozoic sedimentary basins bound the region on the west, north, and east.

Seismic wavegroup nomenclature

The nomenclature used in this paper is similar to that used by Drummond & others (1981), which is derived from Giese (1976).

Pg — Direct waves, which travel through the near-surface crystalline basement with velocities of 6.0-6.2 km s^{-1}.

P* — Waves critically refracted at an intracrustal boundary, and with velocities of 6.4-6.55 km s^{-1}.

P^I — Waves reflected from the intracrustal boundary and travelling with velocities intermediate between those of the Pg and P* wavegroups.

Pn — Waves critically refracted at the crust/mantle boundary, and having apparent velocities in the range 7.6-8.6 km s^{-1}.

P^M — Waves reflected from the crust/mantle boundary, and with apparent velocities in-

termediate between those of the P* and Pn wavegroups.

P_1,P_2 — Near-surface wavegroups observed where the Hamersley Basin strata are underlain by lower velocity rocks. P_1 waves have velocities of about 5.9 km s^{-1}, and P_2 waves have velocities of 6.3-6.7 km s^{-1}.

PL — Near-critical point reflections from a deep crustal layer in the northern Yilgarn Craton. They have apparent velocities of about 7.0 km s^{-1}.

Results

Line ABC, including blasts at G (Shay Gap, Sunrise Hill, Goldsworthy-Newman-Meekatharra)

The data from line ABC (and line GBC) were interpreted by Drummond (1979b), and a slightly revised model, shown here as Figure 2, was given by Drummond & others (1981).

In the north, along segment Shay Gap-Newman, the crust is 28 km thick at Shay Gap, 32 km thick at Newman, and is two-layered. The upper crust has a seismic velocity of 6.0 km s^{-1}, and at about 13 km depth the velocity increases to 6.4 km s^{-1}. The upper mantle velocity is 8.34 km s^{-1}. The Hamersley Basin north of Newman is represented by a thin layer with a low (5.86 km s^{-1}) velocity.

Along the segment from Newman to Meekatharra, the Pn arrivals are delayed beyond 250 km, and as no such delay is apparent in the Pn data in the reverse direction, crustal thickening to the south is inferred. Crustal thickening is consistent with intercept times from recordings of Newman and Meekatharra shots, and with delays of teleseismic arrivals from earthquakes in the Fijian region (Drummond, 1979c), and the Indonesian Arc to the north (Drummond & others, in prep.). Ray tracing has shown that, in the most likely models, the crust thickens from about 33 km south of Newman to more than 50 km at Meekatharra. The principal differences in the models occur in the lower crust along the segment between Newman and Meekatharra.

The seismic velocity in the upper crust between Newman and Meekatharra is 6.1-6.2 km s^{-1}. At 10 km depth in the north and at 16 km depth in the south, the velocity increases to 6.4 km s^{-1}. In the south of segment BC, a lower crustal layer, with a velocity of about 7 km s^{-1}, is implied by a band of large-amplitude reflections at about 7 s and 140-200 km. The crust in the south is therefore three-layered. The upper mantle velocity may decrease from 8.34 to 8.1 km s^{-1} southwards along segment BC.

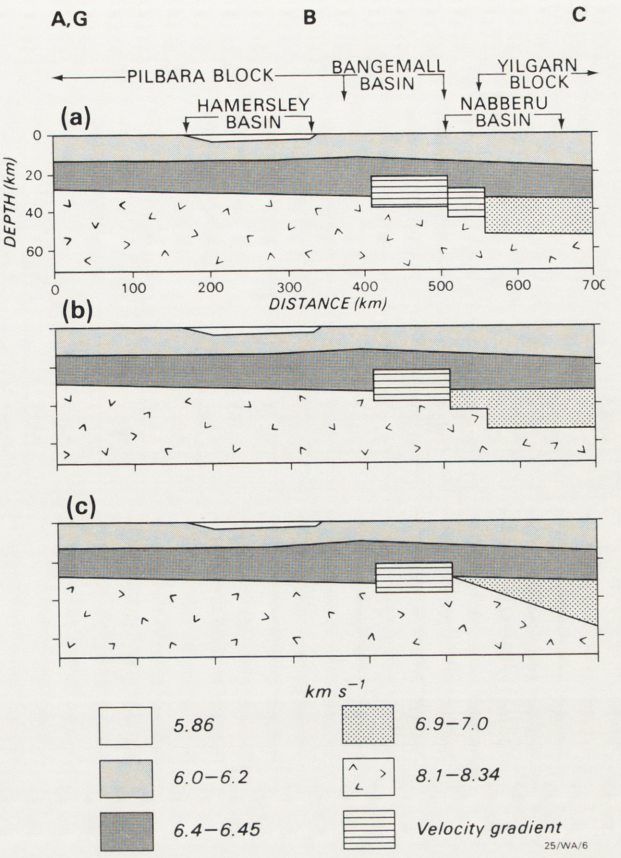

Figure 2. Three alternative seismic models for line GBC (and line ABC).
The models are those of Drummond & others (1981).

Line FDB (Pannawonica-Tom Price-Newman)

Drumond & others (1981) reported the results from line FDB, and Figure 3 shows their model. It is preliminary, because several features of their record sections could not be explained by ray-tracing methods alone.

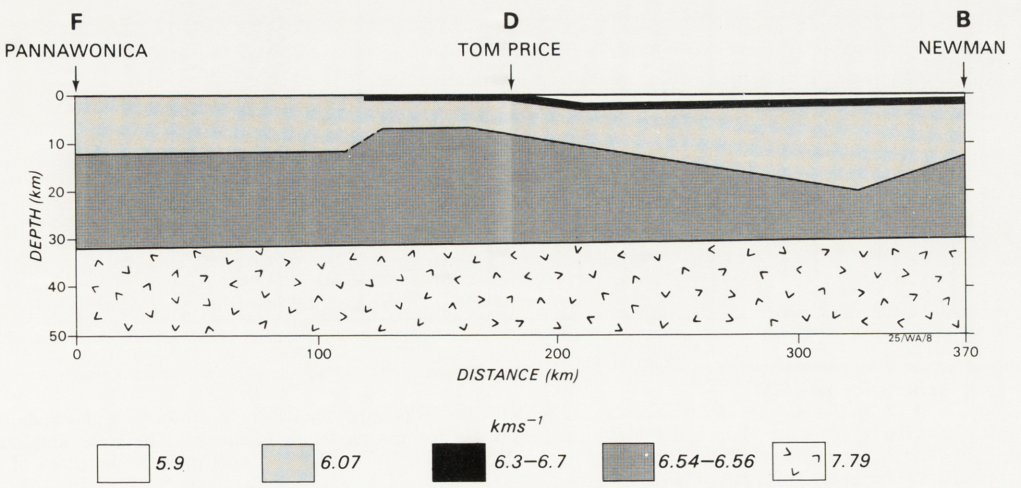

Figure 3. The crustal model derived by Drummond & others (1981) for line FDB.

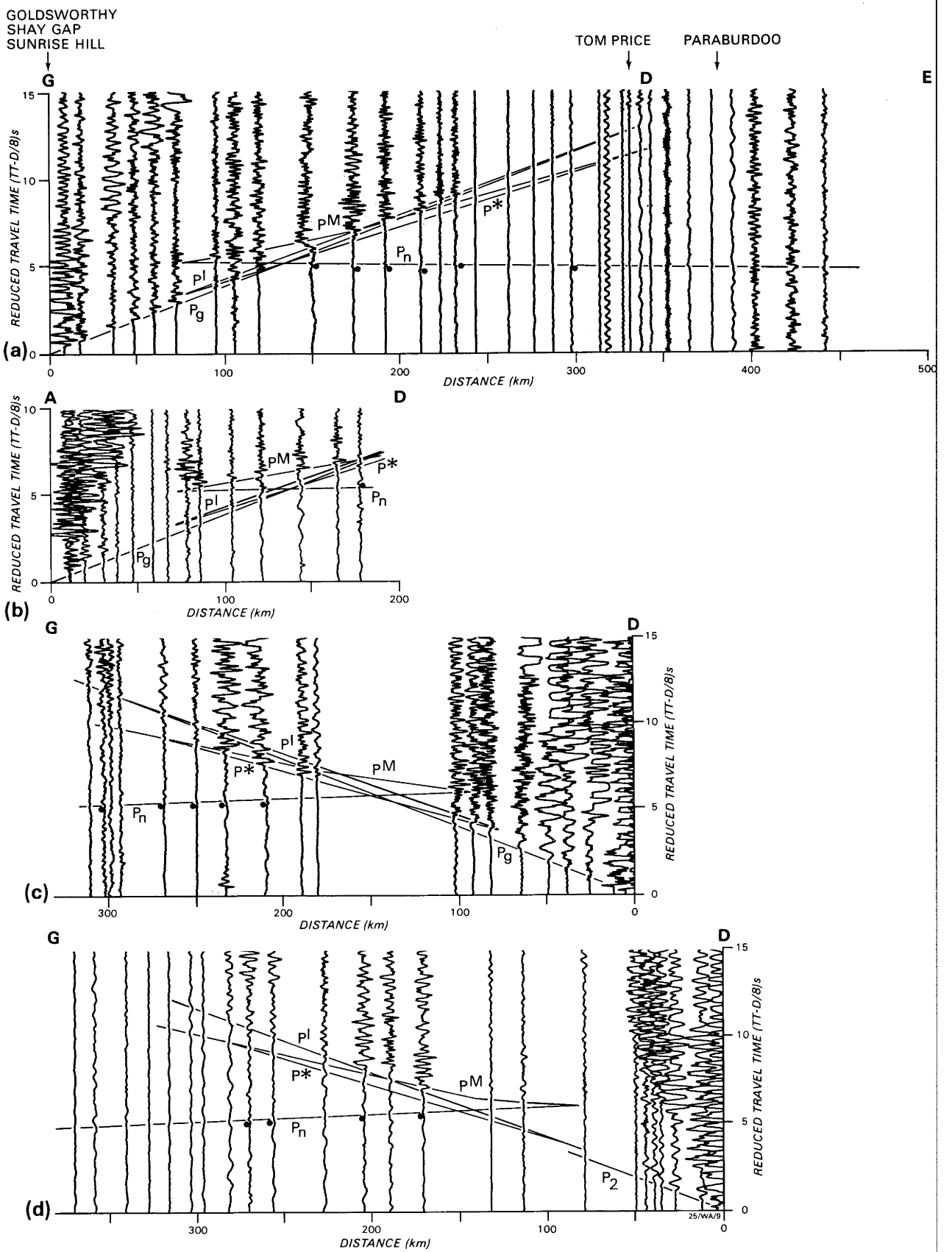

Figure 4. Record sections for line GD.
Sections a, b, c and d are for shotpoints G southwards, A southwards, Tom Price northwards and Paraburdoo northwards respectively. The superimposed travel-time curves are for the model in Figure 8a. The trace amplitudes are as recorded, and all traces were digitally filtered in the bandpass 0.5 to 8 Hz. The dots indicate the times of P_n arrivals picked from these and large amplitude records.

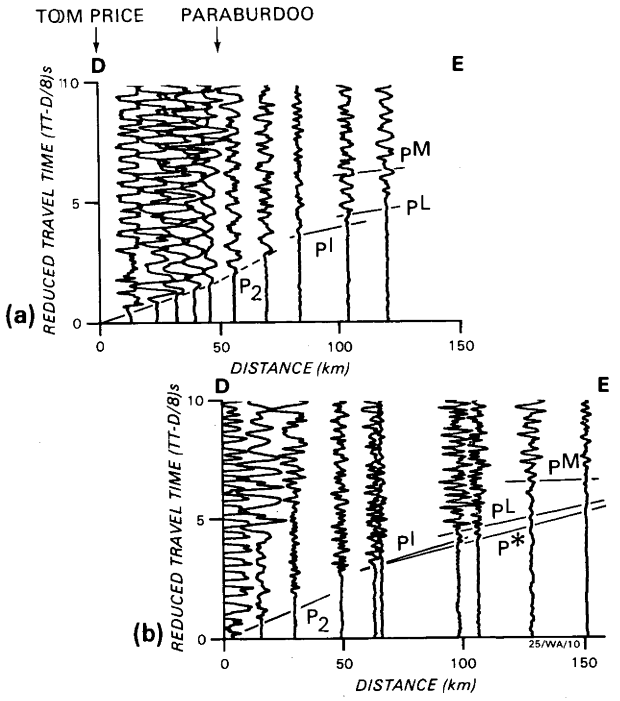

Figure 5. Record sections for line DE.
Section a is for Tom Price southwards, and section b is for Paraburdoo southwards. The superimposed travel-time curves are for the model in Figure 8b. The trace amplitudes are as recorded, and all traces were digitally filtered in the bandpass 0.5 to 8 Hz.

Between Tom Price and Newman, thin, near-surface layers with velocities of 5.9 and 6.3-6.7 km s^{-1} are interpreted as Hamersley Basin banded iron formations and volcanic and sedimentary rocks. They overlie a deeper crust in which the seismic velocities are less; the velocity of 6.07 km s^{-1} used throughout the profile was the unreversed velocity measured in the western part of the basin from a blast at Pannawonica. A lower crustal layer under the basin has a slightly higher velocity (6.54-6.56 km s^{-1}) than the corresponding layer under Newman measured along the north-south profile (Figure 2).

The boundary between the upper (6.07 km s^{-1}) and lower crustal layers has considerable topography. It is 12 km deep under Pannawonica, and shallows to 7 km depth to the west of Tom Price. Further east it deepens, perhaps reaching 20 km before shallowing to about 13 km under Newman.

Sub-Moho refracted arrivals are poorly observed along this profile, the reversed upper mantle seismic velocity was estimated at 7.8 km s^{-1}, which is considerably lower than along profile ABC. The crust/mantle boundary was modelled with very little topography; it is 31 km deep under Pannawonica, and 30 km deep under Newman. It may deepen slightly in the centre of the profile.

Lines GDC (including blasts at A) and DE (Goldsworthy-Tom Price-Meekatharra; and Tom Price towards SW)

The data from lines GD, DE, and DC are depicted as record sections in Figures 4, 5 and 6 respectively and the velocities and intercepts for the refracted phases and the P^L phase identified in, and scaled from, these record sections are listed in Table 1. In all cases, and in the following discussion, the travel times are reduced by the factor, distance/8.0. In Figures 4 and 5, the traces were digitally filtered in the bandpass 0.5 to 8.0 Hz, and the trace amplitudes are not normalised; normalised amplitudes were used in some cases in the identification and correlation of phases, but these are not shown here. In Figure 6, all record sections have had the trace amplitudes normalised so that the maximum amplitude for each trace is the same; the traces in Figure 6 were filtered in the bandpass 1.0 to 8.0 Hz. The models derived from the record sections are shown in Figure 7. The travel-time curves superimposed on the record sections in Figures 4, 5, and 6 were derived by computer ray tracing through the models in Figure 7; the following discussion serves to illustrate the wave groups used to derive the models.

Representative record sections from the line between Goldsworthy and Tom Price (GD) are shown in Figure 4. Two mines are located near D. The northern one is at Tom Price, and the southern one at Paraburdoo (Figure 1). They were treated as separate shotpoints and record sections from both are depicted.

The record section of blasts from the Goldsworthy shotpoint (G) is presented in Figure 4a. Coherent seismic energy was not observed beyond 240 km. The near-surface Pg phase is clearly seen as a first arrival to the crossover point with Pn at about 130 km. The Pn phases are very weak; dots indicate the arrivals that can be identified on larger scale records. A P^*/P^I cusp can be identified about 0.5 s after Pg, at about 70 km, and the P^M phase is clearly seen as large amplitude later arrivals in the 80-240 km distance range.

The smaller blasts at shoptpoint A (Shay Gap and Sunrise Hill), generate less seismic energy and, therefore, smaller amplitude arrivals than those at Goldsworthy. The P^M phase is, therefore, more clearly seen because the earlier arrivals do not obscure it (Figure 4b).

The Tom Price record section for line GD is shown in Figure 4c. The modelled P^M travel-times are about 0.5 s later than the recorded times. This was interpreted by Drummond (1979b) for data from shotpoint G along line GB as evidence for positive velocity gradients in the lower crust. The P^I wavegroup is clearly identified as a high-frequency phase following the low-frequency Pg arrivals.

In the record section of the Paraburdoo blasts recorded northwards (Figure 4d), the first arrivals from the shotpoint to about 50 km show a very rapid fall off in amplitude. This is indicative of a low-velocity zone in the upper crust north of the shotpoint. As will be shown in Figures 5 and 6, the near-source first arrivals probably belong to the P_2 phase which travels through the high-density, high-velocity, near-surface Hamersley Basin rocks. The P^*/P^I cusp is not clearly seen in this record section. The P^M phase is clearly seen, but the Pn phase is very weak.

The record section of Tom Price shots recorded southwards on line DE is shown in Figure 5a. The P_2 phase is recorded with strong amplitudes to about 60 km, whereafter it is delayed and its amplitudes weaken. The delay and weakening of amplitudes is also observed southwards from Paraburdoo (Figure 5b), but at only a few stations within 20 km of the blast. The delay and fall off in amplitudes corresponds, for both shotpoints, with the southern boundary of the Hamersley Basin about 10-15 km south of Paraburdoo (Gee, 1979a). The near-source upper crustal phase has, therefore, been interpreted as the P_2 phase, and not the

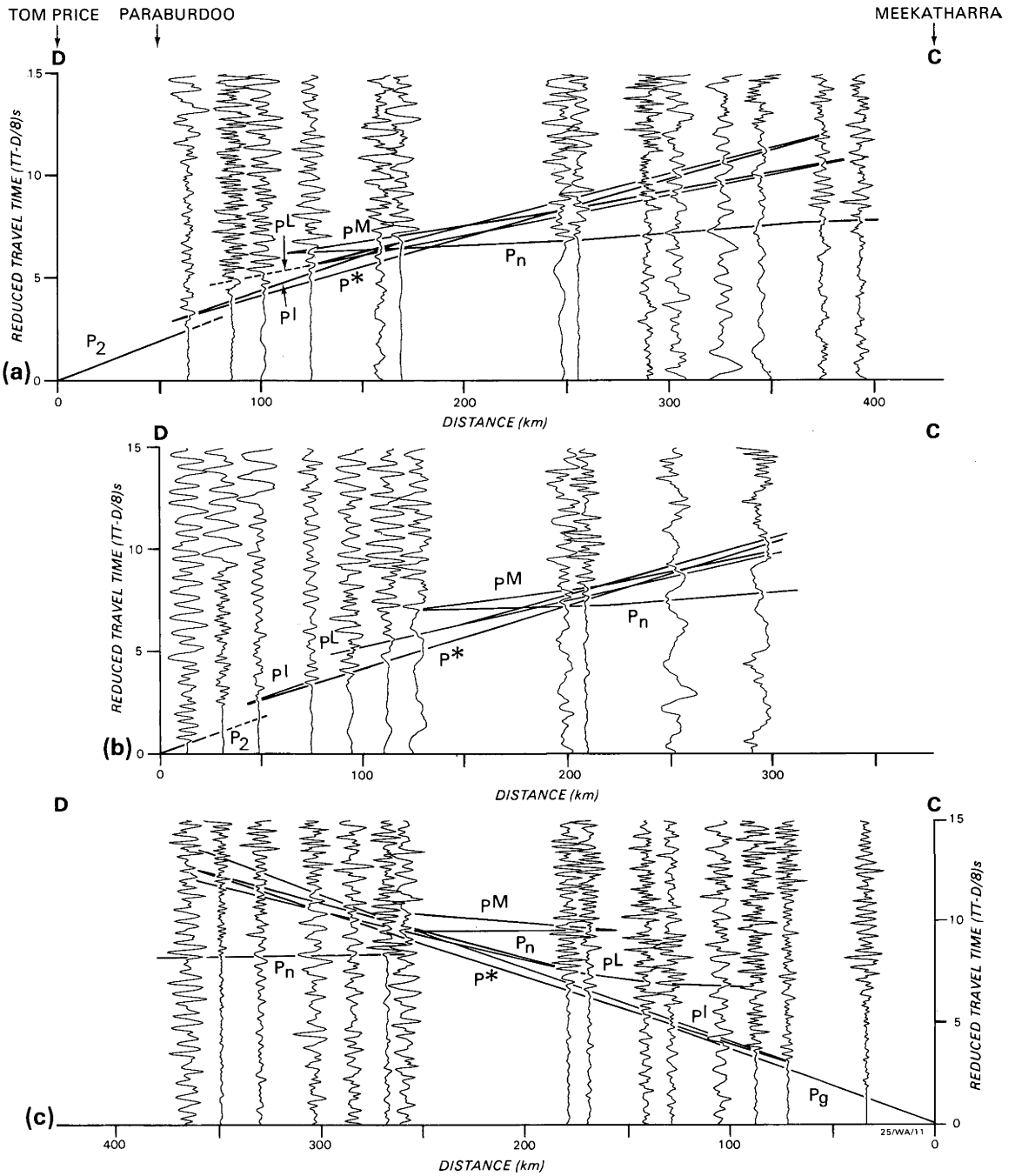

Figure 6. Record sections from line DC.
The sections a, b and c are for Tom Price southwards, Paraburdoo southwards, and shotpoint c northwards, respectively. The superimposed travel-time curves are for the model in Figure 8a. The trace amplitudes have been normalised so that the maximum amplitude is the same for all traces, and the traces in section c were digitally filtered in the bandpass 1.0 to 8.0 Hz. For some recorders, one of the horizontal components had clearer arrivals than the vertical component and has been plotted in its place. Note that the P^L cusp (the dashed curve) is closer to the shotpoint than predicted by the model.

Pg phase. This is the main reason for interpreting the near-source first arrivals in Figure 4d as P_2. Some of the lower crustal phases can also be identified in Figure 5b, in particular, the P^I and P^L phases.

Figure 6 contains the data from the ANU line between Paraburdoo and Meekatharra (DC). In Figure 6a, the P_2 phase is identified by only one early arrival, but it is identified with confidence because, at that point, the ANU line is coincident with the BMR line DE, on which the data in Figure 5a were recorded. The Pn phase is observed as strong arrivals on two traces at 240 to 260 km, but beyond that it is not clear. The traces at 375 and 395 km have large amplitude arrivals at about 8.5 s, which are delayed in time relative to Pn between 120 and 260 km, but may still be Pn arrivals. Figure 6a is similar to the record section from the line between Newman and Meekatharra (BC), where large-amplitude Pn phases are clearly evident, and can be correlated from trace to trace, and Pn is delayed beyond 250 km (Drummond, 1979b).

The P^L phase is very clearly seen in Figure 6a; the cusp on the travel-time curve for the model (Figure

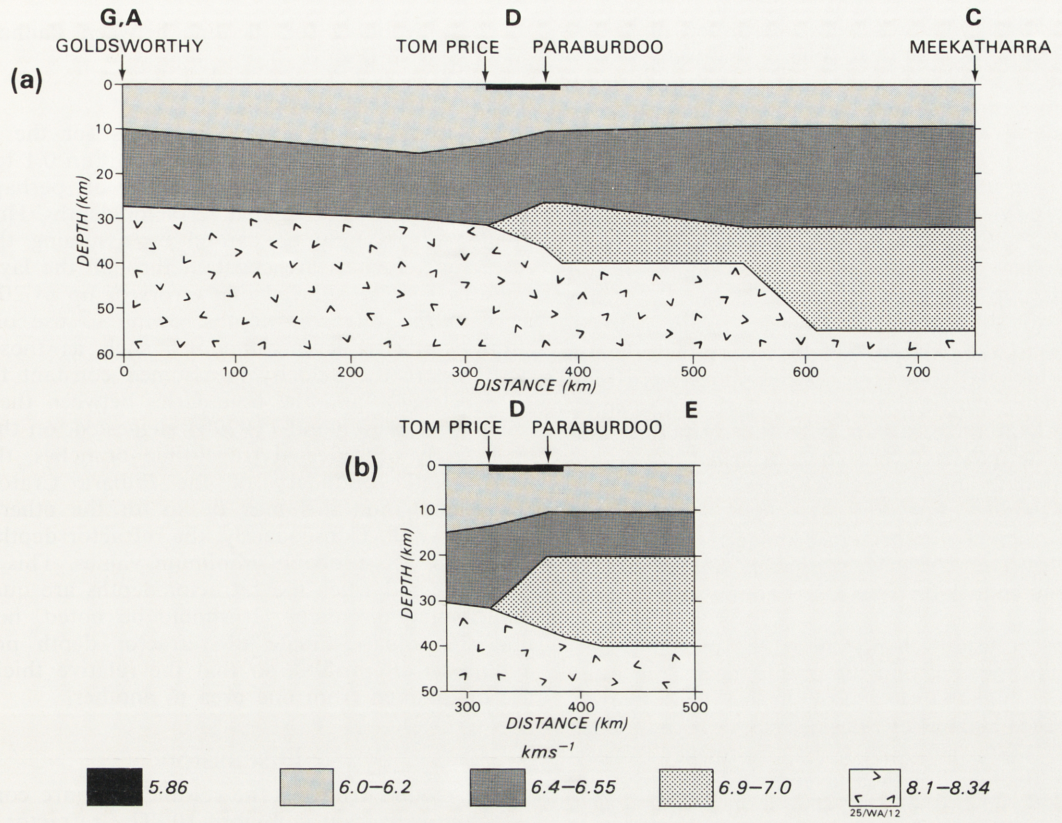

Figure 7. Seismic model for lines GDC and DE.
Figure 7a is the model for line GDC, and Figure 7b is the model for line DE.

LINE GD (Goldsworthy, Shay Gap and Sunrise Hill to Tom Price and Paraburdoo)

	Goldsworthy southwards		*Shay Gap & Sunrise Hill southwards*		*Tom Price northwards*		*Paraburdoo northwards*	
	V	*ti*	*V*	*ti*	*V*	*ti*	*V*	*ti*
P_2							6.19	0.0
Pg	6.11	0.0	6.15	0.0	6.10			
P*	6.36	1.0			6.55	1.6	6.54	1.2
Pn	8.13	5.5			8.23	6.2	8.23	6.2

LINE DE (Tom Price and Paraburdoo southwards)

	Tom Price southwards		*Paraburdoo southwards*	
	V	*ti*	*V*	*ti*
P_2	6.25	0.0		
Pg				
P*			6.25	1.2
Pn				

LINE DC (Tom Price and Paraburdoo to Meekatharra)

	Tom Price southwards		*Paraburdoo southwards*		*Meekatharra northwards*	
	V	*ti*	*V*	*ti*	*V*	*ti*
P_2						
Pg					6.13	0.0
P*	6.54	1.30	6.54	1.30	6.37	0.85
PL	6.99	3.40	6.99	3.40	7.04	4.46
Pn	7.89	6.23	7.89	6.80	8.17	10.15[1]
					8.12	8.70[2]

[1] Later arrivals between 120-180 km.
[2] First arrivals beyond 180 km.

Table 1. Velocities (km s^{-1}) and intercepts (seconds) scaled from record sections (Figures 4, 5 & 6).

7) is at 130 km, but the clearest P^L phases are observed between 80 and 100 km. The P^L cusp is also closer to the blast than the model would predict in Figure 6b, the southwards record section of Paraburdoo blasts. This may imply that the lower crustal, 7.0 km s^{-1}, layer should be shallower in the model. Pn is not clear in Figure 6b.

The record section for shotpoint C at Meekatharra is shown in Figure 6c. The Pg phase is weak, but it is nevertheless clear on large scale plots. The P^L cusp is clearer on the lower gain records, and the P^M phase is not as clear as it is for the same shotpoint along line CB towards Newman (Drummond, 1979b). Pn is observed clearly on only two traces—those at 265 and 350 km.

The data from Figure 4 were interpreted by taking reciprocal pairs of refracted phases between Goldsworthy and Tom Price (GD), and inverting them, using the intercept method, for refractor depths, velocities, and dips. The data from line DE are unreversed, and were interpreted by assuming that the layers were horizontal and that the apparent velocities were refractor velocities. The Pn delays at distances beyond 250 km in Figure 6a imply structures on the crust/mantle boundary; the boundaries between the layers and the crust/mantle boundary at either end of line from Tom Price to Meekatharra (DC) were assumed to be horizontal and the velocities to be the refractor velocities. The models from these various lines were then combined. The calculated depths were assumed to apply only beyond the offset distances to the refractors, and the composite models were then adjusted using ray tracing so that the final models (Figure 7) satisfied the travel-time data.

Figure 7a depicts the preferred model for line GDC (Goldsworthy-Tom Price-Meekatharra) and Figure 7b the preferred model for line DE (Tom Price towards the SW).

The upper crustal velocity along the profile is 6.0-6.1 km s^{-1}. In the centre of the profile, near Tom Price (D), a thin, high-velocity, near-surface layer corresponds to the Hamersley Basin rocks. It has been modelled as 1 km thick, but it may be thicker. Assessment of the thickness of such layers is difficult with ray tracing alone, and further modelling with synthetic seismograms is required. A lower crustal layer, with velocities of 6.37-6.55 km s^{-1} is present along the profile. It is 10 km deep under shotpoint G at Goldsworthy, deepens to 15 km about 260 km south of G, but then shallows again to 10 km between Tom Price and Meekatharra (DC). An even deeper crustal layer, with a velocity of 6.7-7.0 km s^{-1} is present along DC. It is 10 km thick south of Tom Price (D), and thickens rapidly in the centre of the line, to be 20-25 km thick under Meekatharra (C). The interpreted upper mantle velocity along the Goldsworthy-Tom Price-Meekatharra line varies between 8.0 and 8.2 km s^{-1}. The crust/mantle boundary is 28 km deep under Goldsworthy, deepens steadily to 31.5 km under Tom Price, and then rapidly to 40 km, and then to 55 km southwards towards Meekatharra.

The model for line DE (Figure 7b) is similar to the equivalent part of line DC to the east, except that the lowermost, 6.98 km s^{-1}, crustal layer is thicker. This may not be significant, because the seismic line is unreversed.

Line FG (Pannawonica-Goldsworthy)

Only 15 stations were installed along line FG. The data are shown in Figure 8. The recorders were set up along the northeastern half of the line, but not all operated successfully, and consequently, it is not possible to interpret the data with any degree of confidence. The model adopted for the line is shown in Figure 9 and was derived by taking the refractor depths under Pannawonica (F) from line FDG (Figure 3), and those under Goldsworthy (G) from line GDC (Figure 7), and assuming that the refractors were plane layered between F and G. The velocities used were averages of those from the northern part of line GDC (Figure 7) and the western part of line FDB (Figure 3). The travel-time curves for the model were then derived by computer ray tracing, and are superimposed on the record sections. They are generally consistent with the observed data, so the model in Figure 9 is taken to be the best available for the line between Pannawonica and Goldsworthy.

Accuracy of the models

The refracted travel-time branches for the models in Figure 7 fit the observed data to within 0.1 to 0.2 s, thereby implying an accuracy of one or, perhaps, two kilometres in the calculated refractor depths. However, greater errors may be caused by assuming that the refractor velocities are constant through the layers.

Berry (1971) showed that errors of up to 20% can arise in the refractor depths, owing to use of oversimple velocity/depth functions, such as those used here, where the velocity is assumed constant through each refractor and the boundaries between the layers are sharp. Drummond (1979b) suggested, on the basis of a study of reflected travel-time branches, that the crust/mantle boundary of the Pilbara Craton was transitional, and this may be so for the other boundaries as well. Consequently, the refractor depths from this study are probably minimum values. This should be considered when the refractor depths are quoted in the ensuing discussion. It should be noted, however, that the under-estimate of refractor depth probably applies to all profiles, so that the relative thicknesses are maintained from one area to another.

Discussion

The models from all the seismic lines are combined as a fence diagram in Figure 10. The refractor depths generally agree at the junction of the profiles within the accuracy of the modelling. Figure 11 depicts the interpretation of the seismic models in terms of the geology .

Pilbara Craton

The Pilbara Craton is 28 km thick in the north and 30-33 km thick in the south, where its boundary with the Capricorn Orogen is interpreted as the zone where the crust thickens sharply to the south. This is about 40 km to the south of the Sylvania Dome in the east, and corresponds to the northern boundary of the Ashburton Trough in the west. The crust/mantle boundary under the craton, therefore, has a dip of slightly less than one degree to the south. The dip is observed on all profiles except FDP, which lies approximately east/west and on which there is no significant dip from the west on the crust/mantle boundary.

An intracrustal boundary is indicated by the increase of seismic velocities from between 6.0-6.2 km to 6.4-6.55 km s^{-1} within the Pilbara Craton. The depth to the boundary varies throughout the region. Drummond (1979b) modelled it as 13 km deep under the eastern Pilbara Craton, but suggested that it could dip from 9 km in the north to 14 km in the south. The latter values are more in agreement with the depths from the central Pilbara Craton (Figure 7a), where the boundary dips from 10 km in the north to 15 km to the north of Tom Price. It shallows to the south of Newman in the east (Figure 2) and between Tom Price and Paraburdoo (Figure 7a). Along the southern edge of the craton, it is deepest betwen Newman and Tom Price, shallows to 7 km to the west of Tom Price, and then deepens again to 11 km in the west (Figure 3).

Southwards across the Pilbara Craton, the top of the intracrustal boundary defines a basin-like structure with a general southeast/northwest axis. The basin cuts the seismic profiles west of Newman and north of Tom Price. The basin-like structure corresponds to the

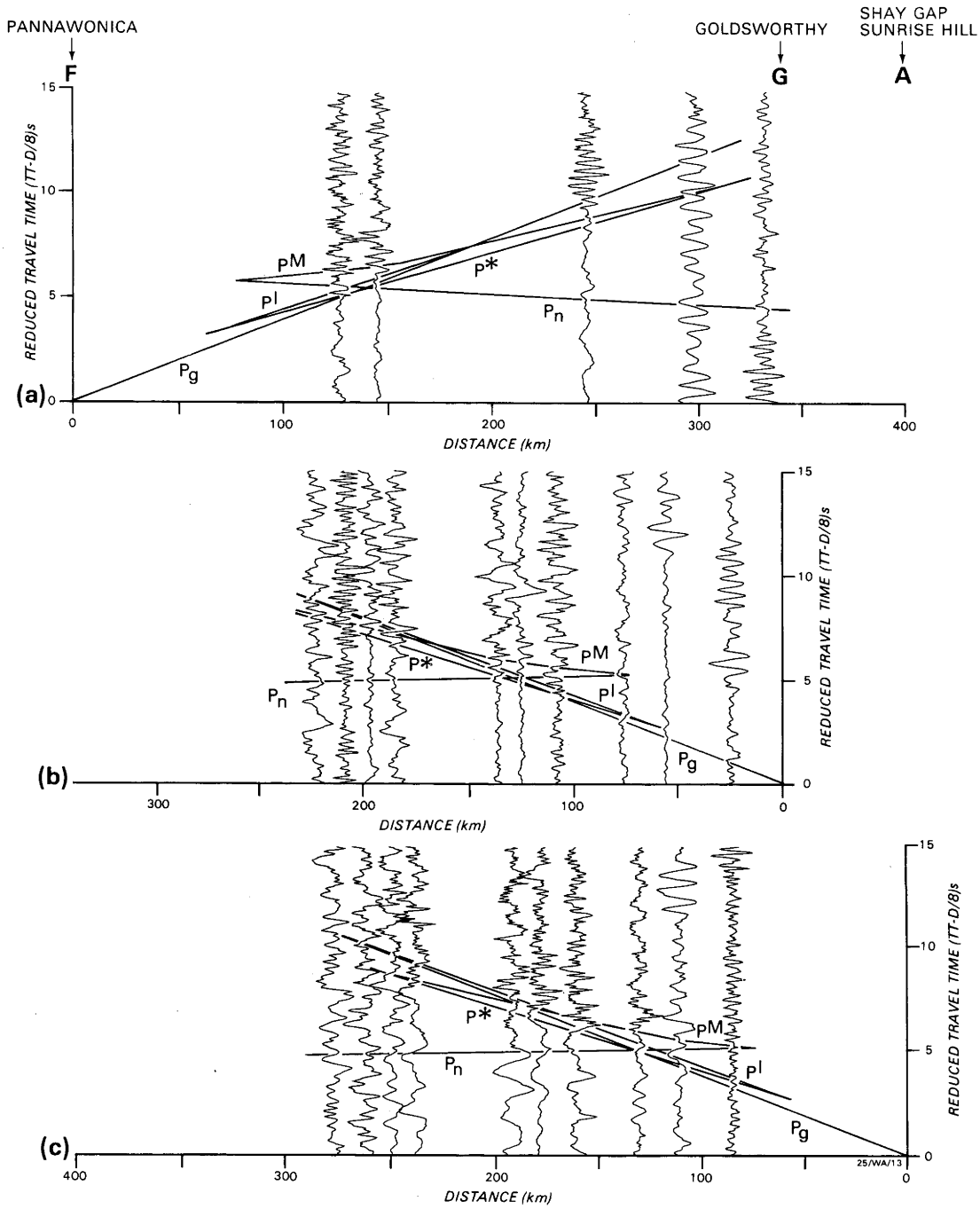

Figure 8. Record sections from line FG.
Sections a, b and c are for shotpoint F northeast, G southwest, and A southwest respectively. The superimposed travel-time curves are for the model in Figure 9. The trace amplitudes have been normalised as in Figure 6. For some recorders, one of the horizontal components had clearer arrivals than the vertical component and has been plotted in its place.

deepest part of the Hamersley Basin inferred from Trendall's (1975) isopach maps and structural diagrams. Horwitz & Smith (1978) defined an Archaean ridge along the southern edge of the Pilbara Craton which corresponds to the shallowing of the intracrustal boundary south of Newman and south and west of Tom Price.

The highest velocities (6.55 km s^{-1}) observed below the intracrustal boundary occur along the southern basement ridge and the axis of the Hamersley Basin. These velocities are due to higher metamorphic grades in the lowermost crust, caused by the depression of the crust into higher pressure and temperature regimes during the formation of the Hamersley Basin (Drummond & others, 1981). Uplift occurred after the filling of the Hamersley Basin, and can be divided into two types, regional isostatic rebound and localised diapirism of basement rocks.

Regional isostatic rebound followed the filling of the basin. This can be inferred from the exposure at the surface of some of the stratigraphically lowest members of the Hamersley Basin sequence. As well, R. E. Smith & others (personal communication) used the metamorphic grades mapped at surface exposures to estimate uplifts of 10-12 km, west of Tom Price, and 5-7 km, near Newman. The second type of uplift was localised

diapirism of basement rocks to form Archean inliers within the Hamersley Basin. The largest of these is the Sylvania Dome, but several smaller ones are observed or inferred to the west and east of Tom Price. Those near Tom Price correspond to the region where the intracrustal boundary shallows to 7 km depth along profile FDB (Figures 3 and 10).

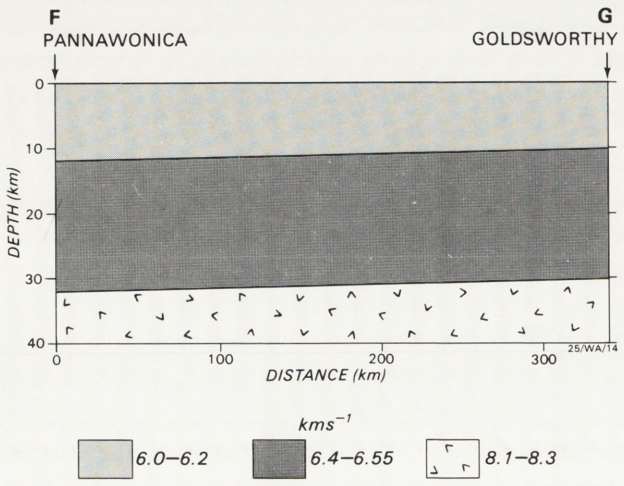

Figure 9. Seismic model for line FD.
The model was not derived from the data in Figure 8, but is an average of the models for the northern end of line GD and the western end of line FD (see the text).

The diapirism may have been caused by density inversions near the surface. Where rocks of the Hamersley Basin are seismically distinct from the underlying basement rocks, they have velocities which are higher than those of the basement. They are highest in the southeast of the basin. Further west and north, the velocities of the P_1 and P_2 wavegroups decrease as the metamorphic grade decreases (Drummond & others, 1981), and the basin rocks have not achieved sufficiently high velocities to be seen to be independent of the underlying Archaean basement. Gravity data also infer that the Hamersley Basin rocks are denser than the Archaean basement (Drummond & Shelley, 1981).

Yilgarn Craton

The crust of the Yilgarn Craton is much thicker (> 50 km) than the crust of the Pilbara Craton, and extends further north than the area mapped by Gee (1979a) as the Yilgarn Block. Intracrustal seismic boundaries occur at 10-16 km and at 32 km depth.

In the Proterozoic, the northern limit of the stable Yilgarn Craton was probably just south of the present day northern edge of the Nabberu Basin. A zone along the northern edge of the Yilgarn Craton, where the crustal thickness is intermediate between that of the Yilgarn Craton and the thinner crust of the Capricorn Orogen, probably represents part of the northern Yilgarn Craton which was reworked by tectonism in the Proterozoic. It corresponds to a large, negative gravity anomaly to the north of the Yilgarn Block. Fraser (1973) suggested that the anomaly was too intense to

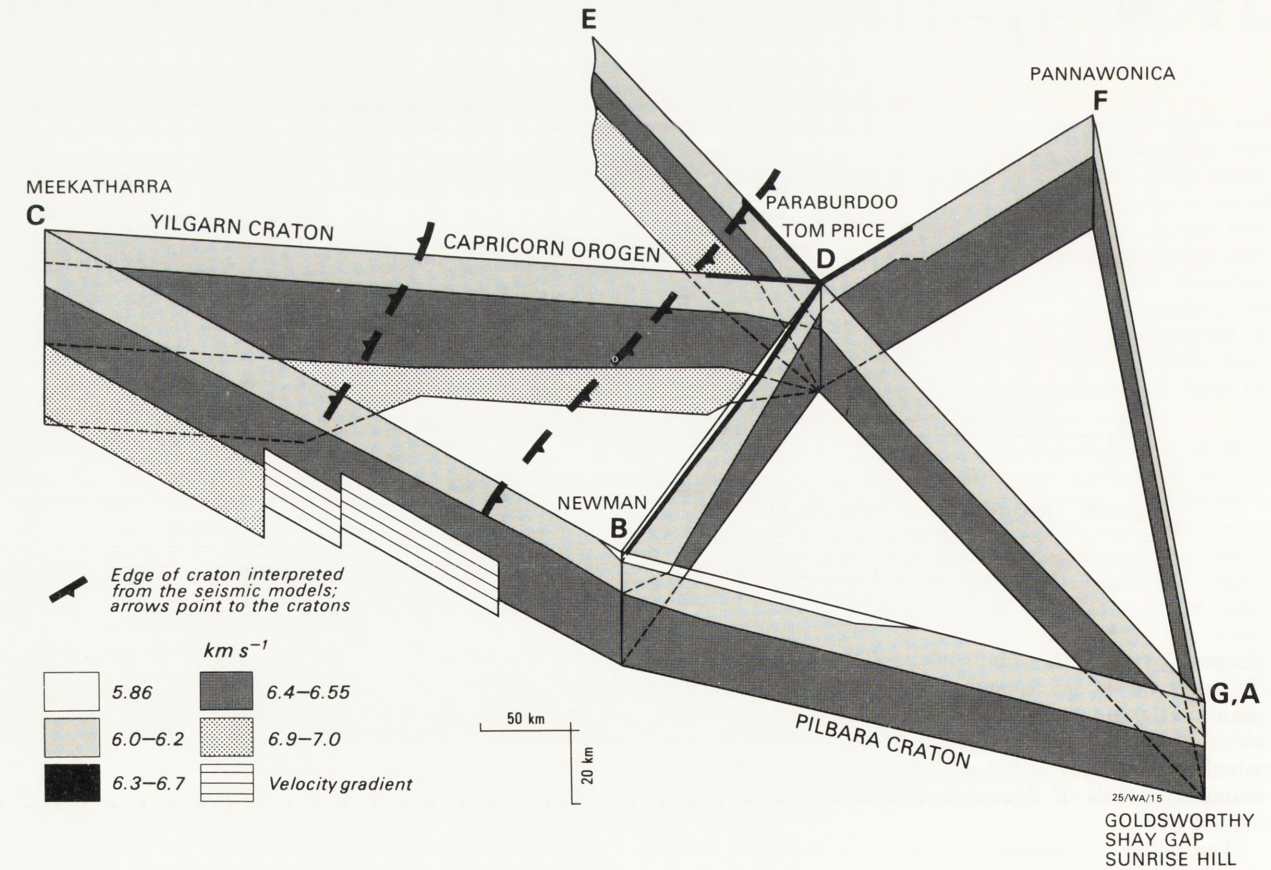

Figure 10. Fence diagram of all of the seismic models from the Intercept Method interpretation of the data from the 1977 Pilbara Crustal Survey.
The interpreted margins of the cratons are based on crustal thicknesses. The edge of the Pilbara Craton corresponds to the southern margin of thin crust, and the northern edge of the Yilgarn Craton corresponds to the northern margin of thick crust. The Capricorn Orogen between the cratons has crust of intermediate thickness.

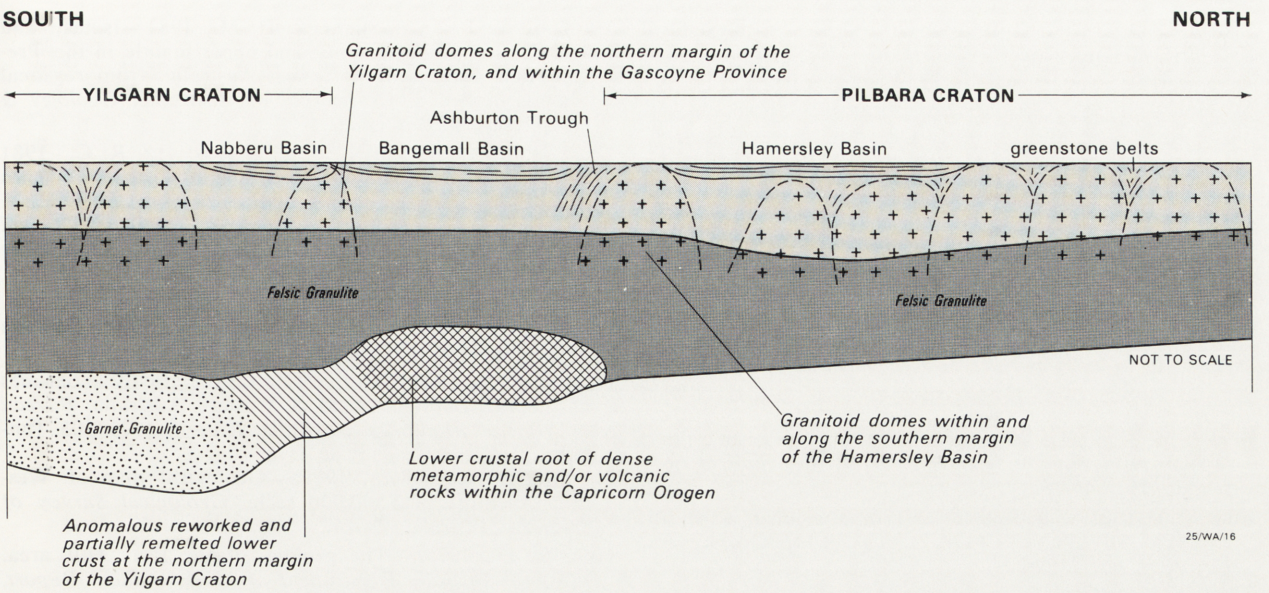

Figure 11. Cartoon sketch of a north/south section of crust through the survey area, in which the seismic models are interpreted in terms of the geology.

be purely a gravity edge effect of the Yilgarn Craton, and Horwitz & Smith (1978) correlated it with 'certain granitic and metamorphic rocks of the Gascoyne Province'.

The area contains, in the Gascoyne Province, granitoid intrusions, which have been interpreted as remelted basement and younger sediments (de Laeter, 1976; Williams & others, 1978), and, further east, the Marymia Dome at the northern edge of the Nabberu Basin. It also includes the northwestern part of the Nabberu Basin, where the sedimentary rocks and underlying basement were intensely deformed (Hall & Goode, 1978). The southern belt of stable basement in the western Bangemall Basin falls within and marks the northern limit of this zone.

Capricorn Orogen

No shotpoints were located in the Bangemall Basin or Ashburton Trough, and because the basin and trough rocks do not cause any noticebale deviation of the travel-times from those expected from normal crystalline basement, no estimate of the present day basin and trough thicknesses is possible.

The lower crust in the Capricorn Orogen is characterised by high velocities and, by inference, dense rocks. Wellman (1978) attributed the denser crust in the orogen to higher metamorphic grades. Horwitz & Smith (1978) favoured an evolutionary model for the orogen, in which the Pilbara and Yilgarn Cratons were welded into a stable basement by the end of the Archaean and then rifted to form the Capricorn Orogen. From the gravity map (BMR, 1975), they inferred dense lower crust in the orogen, and attributed it to intrusions of basic magmas into the lower crust during the rifting. However, the intrusions could also have occurred if the cratons had not been welded, but had been free to move relative to each other to relieve the stresses which must have built up during tectonism.

Chemical composition of the crust

The seismic velocities in the upper crust throughout the region, excluding those in the Hamersley Basin, range from 6.0 to 6.2 km s^{-1}. Drummond (1979b) suggested that they represent an upper crust of overall acid to intermediate chemical composition and low metamorphic grade. Below the intracrustal boundary at 9-16 km depth throughout the region, the seismic velocity increases to 6.4 km s^{-1}, and 6.55 km s^{-1} under the axis of the Hamersley Basin. Drummond (1979b) attributed the increase in velocity to the metamorphism of the acid to intermediate crust to felsic granulite. A chemical change was ruled out, because more basic rocks would have higher seismic velocities (Christensen & Fountain, 1975).

Underlying the felsic granulite layer at 32 km depth along the northern Yilgarn Craton is the thick, lower crustal layer with seismic velocities of 6.7-7.0 km s^{-1}. Drummond (1979b) suggested that this layer was caused by 'eclogite'-grade metamorphism of rocks with compositions similar to or slightly more basic than the upper crust. Drummond & others (1981) called it, perhaps less ambiguously, garnet granulite. Garnet granulites of acid to intermediate chemical composition readily give seismic velocities of about 7 km s^{-1} at depths greater than 30 km (pressures greater than 10 kbar). Basic garnet granulites often have much higher seismic velocities, and eclogite velocities at pressures of 10 kbar can exceed 8.00 km s^{-1} (Birch, 1961; Christensen, 1965; Manghnani & others, 1974; Christensen & Fountain, 1975). However, Drummond & Shelley (1981) combined the seismic and gravity data, and suggested that some chemical layering was possible in the Yilgarn Craton, with the lower crust more basic than the upper crust.

Acknowledgements

The BMR is indebted to the iron mining companies of the Pilbara, without whose support the seismic survey would not have peen possible. I acknowledge the generous assistance of Goldsworthy Mining Limited, Cliffs Robe River Associates, Hamersley Iron Pty Ltd, and the Mount Newman Mining Company Pty Ltd.

I am grateful to my colleagues at the BMR who assisted in the field work, and also made useful suggestions during the interpretation; in particular, I thank D. M. Finlayson, P. Wellman, J. B. Connelly, J. W. Williams, and especially C. D. N. Collins who made his ray tracing program SEISRAY available to me. The interpretation was performed while I was a full time

postgraduate research scholar at the Research School of Earth Sciences at the Australian National University, and was supervised by Dr K. J. Muirhead. Dr A. L. Hales of the Geosciences Program, University of Texas at Dallas, and formerly Director of the Research School of Earth Sciences, generously made available the ANU data, and, together with Dr J. Cleary, offered useful advice. The postgraduate research was supported by an Australian Public Service Postgraduate Scholarship.

References

BERRY, M. J., 1971—Depth uncertainties from seismic first-arrival refraction studies. *Journal of Geophysical Research,* 76, 6464-8.

BIRCH, F., 1961—The velocity of compressional waves in rocks to 10 kilobars, Part 2. *Journal of Geophysical Research,* 66, 2199-224.

BMR, 1975—Gravity map of Australia, 1:5 000 000. *Bureau of Mineral Resources, Australia, Canberra.*

BRAKEL, A. T., & MUHLING, P. C., 1976—Stratigraphy, sedimentation, and structure in the western and central part of the Bangemall Basin, Western Australia. *Geological Survey of Western Australia Annual Report,* 1975, 70-9.

CHRISTENSEN, N. I., 1965—Compressional wave velocities in metamorphic rocks at pressures to 10 kilobars. *Journal of Geophysical Research,* 70, 6147-64.

CHRISTENSEN, N. I., & FOUNTAIN, D. M., 1975—Constitution of the lower continental crust based on experimental studies of seismic velocities in granulite. *Bulletin of the Geological Society of America,* 86, 227-36.

COMPSTON, W., & ARRIENS, P. A., 1968—The Precambrian geochronology of Australia. *Canadian Journal of Earth Sciences,* 5, 561-83.

DANIELS, J. L., 1975—Gascoyne Province. *In* Geology of Western Australia. *Geological Survey of Western Australia, Memoir* 2, 107-14.

DE LAETER, J. R., 1976—Rb-Sr whole-rock and mineral ages from the Gascoyne Province. *Geological Survey of Western Australia Annual Report,* 1975, 126-30.

DE LAETER, J. R., & BLOCKLEY, J. G., 1972—Granite ages within the Archaean Pilbara Block, Western Australia. *Journal of the Geological Society of Australia,* 19, 363-70.

DE LAETER, J. R., LIBBY, W. G., TRENDALL, A. F., & FLETCHER, I. R., 1980—The older Precambrian geochronology of Western Australia. *In* GLOVER, J. E., & GROVES, D. I. (editors), *Second International Archaean Symposium, Perth, 1980. Extended Abstracts. Geological Society of Australia and I.G.C.P., Archaean Geochemistry Project,* 9-10.

DE LAETER, J. R., LIBBY, W. G., & TRENDALL, A. F., 1981—The older Precambrian geochronology of Western Australia. *In* GLOVER, J. E., & GROVES, D. I. (editors), Archaean Geology. *Second International Archaean Symposium. Geological Society of Australia, Special Publication,* 7, in press.

DRUMMOND, B. J., 1979a—Pilbara Crustal Survey, 1977—Operational Report. *Bureau of Mineral Resources, Australia, Record,* 1979/54 (unpublished).

DRUMMOND, B. J., 1979b—A crustal profile across the Archaean Pilbara and northern Yilgarn Cratons, northwest Australia. *BMR Journal of Australian Geology & Geophysics,* 4, 171-80.

DRUMMOND, B. J., 1979c—Structural relations between the Archaean Pilbara and Yilgarn Cratons, Western Australia, from deep seismic sounding. *M.Sc. Thesis, Australian National University* (unpublished).

DRUMMOND, B. J., & SHELLEY, H. M., 1981—Isotasy and structure of the lower crust and upper mantle in the Precambrian terrains of northwest Australia, from regional gravity studies. *BMR Journal of Australian Geology & Geophysics,* 6, this issue.

DRUMMOND, B. J., SMITH, R. E., & HORWITZ, R. C., 1981—Crustal structure in the Pilbara and northern Yilgarn Blocks from deep seismic sounding. *In* GLOVER, J. E., & GROVES, D. I. (editors) Archaean Geology. *Second International Archaean Symposium. Geological Society of Australia Special Publication,* 7, in press.

DRUMMOND, B. J., MUIRHEAD, K. J., & HALES, A. L., in prep.—Evidence for a seismic discontinuity near 200 km under a continental margin.

FRASER, A. R., 1973—A discussion on the gravity anomalies of the Precambrian Shield of Western Australia. *Bureau of Mineral Resources, Australia, Record,* 1973/105 (unpublished).

GEE, R. D. (compiler), 1979a—Geological map of Western Australia, 1:2 500 000 scale. *Geological Survey of Western Australia, Perth.*

GEE, R. D., 1979b—The geology of the Peak Hill area. *Western Australia Department of Mines Annual Report,* 1978, 99-106.

GEE, R. D., 1979c—Tectonics of the Western Australian shield. *Tectonophysics,* 50, 327-69.

GIESE, P., 1976—Models of crustal structure and main wave groups. *In* GIESE, P., PRODEHL, C., & STEIN, A. (editors), Explosion seismology in Central Europe. Data and results. Crustal and upper mantle structure in Europe. *European Seismological Commission, Monograph,* 1, 196-200.

HALL, W. D. M., & GOODE, A. D. T., 1978—The early Proterozoic Nabberu Basin and associated iron formations of Western Australia. *Precambrian Research,* 7, 129-84.

HAMILTON, P. J., EVENSEN, N. M., O'NIONS, R. K., GLIKSON, A. Y., & HICKMAN, A. H., 1980—Sm-Nd dating of the Talga-Talga Subgroup, Warrawoona Group, Pilbara Block, Western Australia. *In* GLOVER, J. E., & GROVES, D. I. (editors), *Second International Archaean Symposium Perth, 1980. Extended Abstracts. Geological Society of Australia and I.G.C.P., Archaean Geochemistry Project,* 11-12.

HORWITZ, R. C., 1975—Provisional geological map at 1:2 500 000 of the northeast margin of the Yilgarn Block, Western Australia. *CSIRO Minerals Research Laboratories, Report,* FP 10.

HORWITZ, R. C., & SMITH, R. E., 1978—Bridging the Yilgarn and Pilbara Blocks, Western Australia. *Precambrian Research,* 6, 293-322.

MANGHNANI, M. H., RAMANANANTOANDRO, R., & CLARK, S. P., 1974—Compressional and shear wave velocities in granulite facies rocks and eclogites to 10 kbar. *Journal of Geophysical Research,* 79, 5427-46.

MOTA, L., 1954—Determination of the dips and depths of geological layers by the seismic refraction method. *Geophysics,* 19, 242-54.

OVERSBY, V. M., 1975—Lead isotopic systematics and ages of Archaean acid intrusives in the Kalgoorlie-Norseman area, Western Australia. *Geochimica et Cosmochimica Acta,* 39, 1107-25.

PIDGEON, R. T., 1978a—3450 m.y. old volcanics in the Archaean layered greenstone succession of the Pilbara Block, Western Australia. *Earth and Planetary Science Letters,* 37, 421-8.

PIDGEON, R. T., 1978b—Geochronological investigations of granite batholiths of the Archaean granite-greenstone terrain of the Pilbara Block, Western Australia. *In* SMITH, I. E. M., & WILLIAMS, J. G. (editors), *Proceedings of the 1978 Archaean Geochemistry Conference, University of Toronto,* 360-2.

RICHARDS, J. R., 1977—Lead isotopes and ages of galenas from the Pilbara region, Western Australia. *Journal of the Geological Society of Australia,* 24, 465-73.

TRENDALL, A. F., 1975—Hamersley Basin. *In* Geology of Western Australia. *Geological Survey of Western Australia, Memoir* 2, 119-43.

WELLMAN, P., 1978—Gravity evidence for abrupt changes in mean crustal density at the junction of Australian crustal blocks. *BMR Journal of Australian Geology & Geophysics,* 3, 153-62.

WILLIAMS, S. J., ELIAS, M., & DE LAETER, J. R., 1978—Geochronology and evolution of the eastern Gascoyne Province and the adjacent Yilgarn Block. *Geological Survey of Western Australia Annual Report,* 1977, 50-6.

WILLIAMS, S. J., WILLIAMS, I. R., & CHIN, R. J., 1979—Explanatory notes on the Mount Phillips 1:250 000 geological sheet. *Geological Survey of Western Australia, Record* 1978/13.

APPENDIX 4

Drummond, B.J., and Shelley, H.M., 1981 - Isostasy and structure of the lower crust and upper mantle in the Precambrian terrains of northwest Australia, from regional gravity studies. BMR Journal of Australian Geology and Geophysics, 6, 137-143. (With the following erratum published in Volume 6, number 3).

CORRECTION

Volume 6, Number 2: In the paper by B. J. Drummond & H. M. Shelley, on page 141, the value of 3 x 10^{-3} km s^{-1} $kbar^{-1}$ quoted for the pressure derivative of velocity is the shear wave velocity derivative. A value of 10^{-2} km s^{-1} $kbar^{-1}$, corresponding to the compressional wave velocity derivative, was used for adjusting the crustal model seismic velocities to 10 kbar pressure.

Reprinted from
BMR Journal of Australian Geology & Geophysics, 6, 1981, 137-143

Isostasy and structure of the lower crust and upper mantle in the Precambrian terrains of northwest Australia, from regional gravity studies

B. J. Drummond & H. M. Shelley

Published seismic models for the northwest region of Australia are somewhat at variance with proposed isostatic models for the region. Two density models are examined to explain the difference. In one, the thick, low-density crust of the Yilgarn Craton is compensated at depth by a region of high-density upper mantle rocks, and in the other the composition of the Yilgarn Craton is slightly more iron rich (either at the base or to a lesser extent throughout) than the crust of the Pilbara Craton. A compromise model is preferred in which the crust, particularly in the Yilgarn Craton, is chemically stratified with the denser, more basic rocks at the base. In this model the upper mantle under the Yilgarn Craton is denser than that under the Pilbara Craton and isostatic equilibrium is reached at depths greater than the base of the crust.

The differences in the crust or the mantle throughout the region provide more evidence that the cratons had separate evolutionary histories. The upper mantle under the Pilbara Craton may be less dense than that under the Yilgarn Craton because of iron depletion, and may have been the source of iron for the basic volcanics and banded iron formations in the Hamersley Basin, which overlies the Pilbara Craton.

Introduction

Two Archaean cratons, the Pilbara and Yilgarn Cratons, crop out in Western Australia (Gee, 1979a); their outcrop areas in the northwest part of the State are shown in Figure 1 of Drummond (1981, this issue). Following Gee (1979b), a 'block' is taken as the exposed part of a stabilised 'craton'. Brief summaries of the geology are given by Drummond (1979c, 1981) and comprehensive descriptions can be found in Gee (1979b) and GSWA (1975).

The blocks have large granitoid domes between which greenstone belts of sedimentary and volcanic rocks are draped. Sedimentary and volcanic rocks of the late Archaean to lower Proterozoic Hamersley Basin cover the southern part of the Pilbara Craton, except for small Archaean inliers within the basin, e.g. the Sylvania Dome. The northern part of the Yilgarn Craton is overlain by the Proterozoic sedimentary and volcanic rocks of the Nabberu Basin (Hall & Goode, 1978; Gee, 1979b). These, and the younger Proterozoic rocks of the Ashburton Trough and Bangemall Basin, which occupy the Capricorn Orogenic Belt, mask the structural relations between the cratons.

A seismic refraction and gravity survey conducted in 1977 (Drummond, 1979a) aimed to study the structural relations between the cratons by delineating the crustal structure within and between the cratons. In the seismic models of Drummond (1981), the crust of the Pilbara Craton varies between 28 km thick in the north and 33 km thick in the south. In contrast, the northern Yilgarn Craton has a crust between 50 and 55 km thick, and the crust in the intervening Capricorn Orogenic Belt is 40 km thick. A zone with crustal thickness intermediate between that of the Yilgarn Craton and the crust of the Capricorn province lies along the northern edge of the Yilgarn Craton and contains evidence for remelting of the crust and tectonic activity in the Proterozoic.

The velocity in the upper crust is 6.0–6.2 km.s^{-1}, and increases to 6.4–6.55 km.s^{-1} at 10 to 16 km depth throughout the region, and to 6.7–7.0 km.s^{-1} at 32 km depth in the Yilgarn Craton. Drummond (1981) proposed that the velocity increase with depth was due to increasing metamorphic grade related to the increasing pressure and temperature with depth.

The gravity coverage of the area consists of data from regional helicopter gravity surveys with an 11-km grid spacing (Fraser, 1979a, b), some detailed mining company data, and road and helicopter traverses with station spacing of 1–4 km (McCracken, *in* Drummond, 1979a). The Bouguer anomaly gravity map for the region is shown in Figure 1.

Fraser (1979a,b) gave a qualitative description of the short wavelength features of the gravity field. Over the Pilbara Block, gravity highs correlate with greenstone belts and gravity lows with granitoid intrusions. In the Hamersley Basin, gravity lows correlate with granitic Archaean inliers (a, b, c, d, in Figure 1) and anticlines with granitic cores in the Hamersley Basin strata; gravity highs correlate with synclines in the dense basin strata (Fraser, 1979a). Similar correlations can be made in the Yilgarn Craton and Nabberu Basin.

Gravity highs and lows of longer wavelength ring the cratons. Wellman (1978) suggested that they reflect abrupt changes in average crustal density between crustal blocks, and their regional isostatic compensation.

The purpose of this paper is to compare the theoretical gravity signature of the seismic models with the measured gravity field, and, from this, draw conclusions about isostatic compensation and the composition and structure of the lower crust and upper mantle of the region. Some conclusions are then drawn about the evolutionary processes which generated the crust.

Pressure calculations

Wellman (1976) showed that, for Western Australia, isostatic compensation was mainly complete at the base of the crust for 3° x 3° areas. Using the Nafe-Drake velocity/density relationship (*in* Talwani & others, 1959a) (Fig. 2), pressures for unit columns of rock at 52 km depth are 1.59, 1.54, and 1.51 GPa in the northern Pilbara Craton, southern Pilbara Craton, and northern Yilgarn Craton, respectively, for model (a) of Drummond (1979c). These pressures agree with

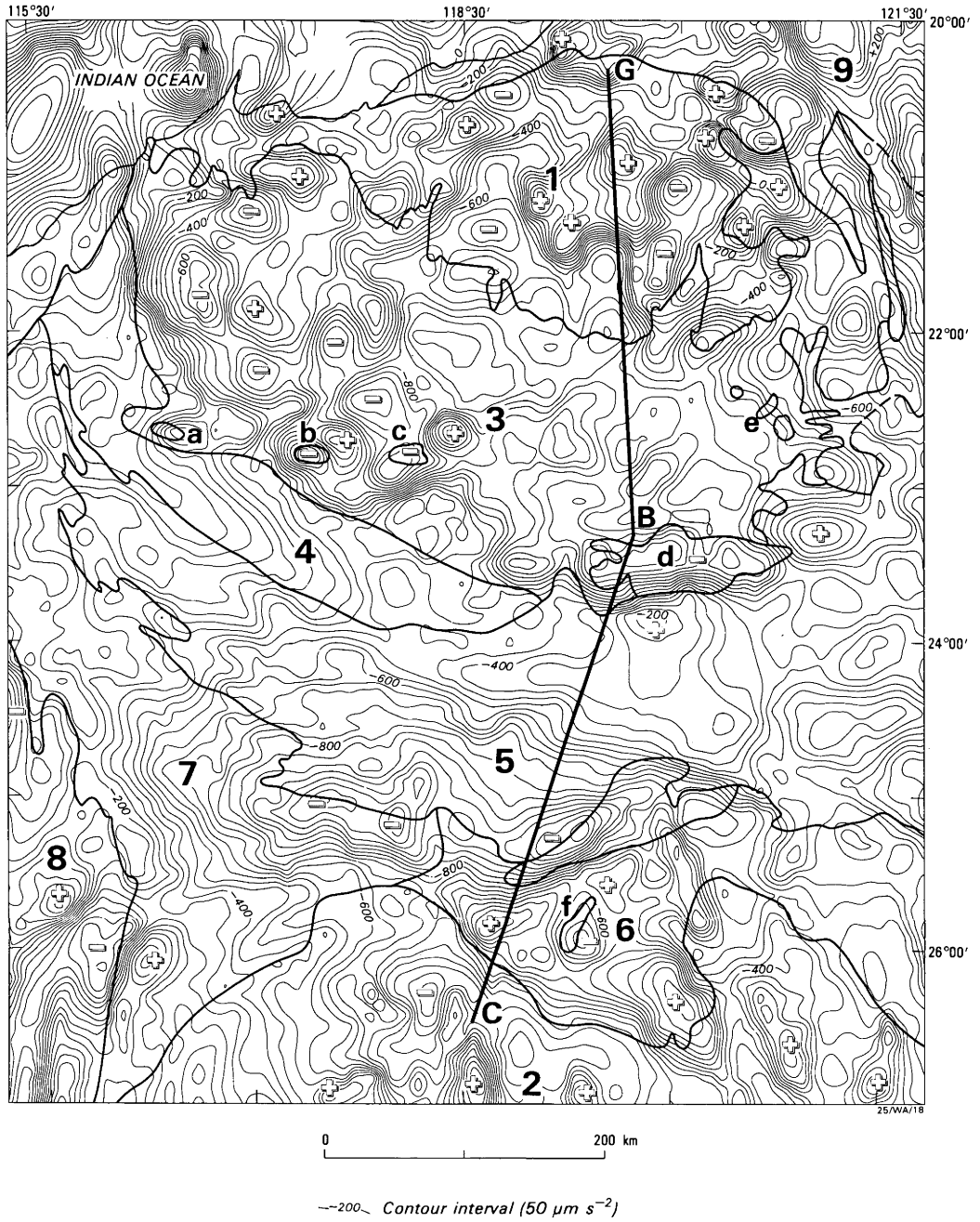

Figure 1. Simple Bouguer gravity map (Bouguer density 2.67 t.m^{-3}) onshore and Free-air gravity map offshore, with geology superimposed. The geological provinces are: 1. Pilbara Block; 2. Yilgarn Block; 3. Hamersley Basin; 4. Ashburton Trough; 5. Bangemall Basin; 6. Nabberu Basin; 7. Gascoyne Province; 8. Carnarvon Basin; and 9. Canning Basin.
The Archaean domes marked in the Proterozoic basins are: a. Wyloo Dome; b. Rocklea Dome; c. Milli Milli Dome; d. Sylvania Dome; e. Rat Hill Anticline; f. Goodwin Dome; and g. Marymia Dome. G. Goldsworthy; B. Newman; C. Meekatharra.

each other to within 5 percent, but the differences between them would result in gravity decreasing by more than 3000 μm.s^{-2} from the northern Pilbara Craton southwards to the northern Yilgarn Craton. The measured decrease is only about 800 μm.s^{-1}, with regional Bouguer anomaly values ranging from about 0 μm.s^{-2} in the north to about 800 μm.s^{-2} in the south. This leaves a discrepancy of about 2000 μm.s^{-2} between the measured gravity and the gravity expected from the seismic model.

The seismic velocity structure in the upper 32 km of the Yilgarn Craton is similar to that of the Pilbara Craton. The differences below 32 km produce a mass deficiency, which generates the gravity difference along the profile. Seismic intercept times for upper mantle P-waves from shotpoints at Newman and Meekatharra, delays in upper mantle P-wave arrivals south of Newman and Tom Price, travel-times northwards and southwards from Meekatharra, and travel-time residuals for teleseismic arrivals from Fiji and the Indonesian Arc all indicate that the crust must thicken considerably between Newman and Meekatharra (Drummond, 1979b, c, 1981; Drummond & others, in prep.). However, the intercept time for upper mantle P-waves from

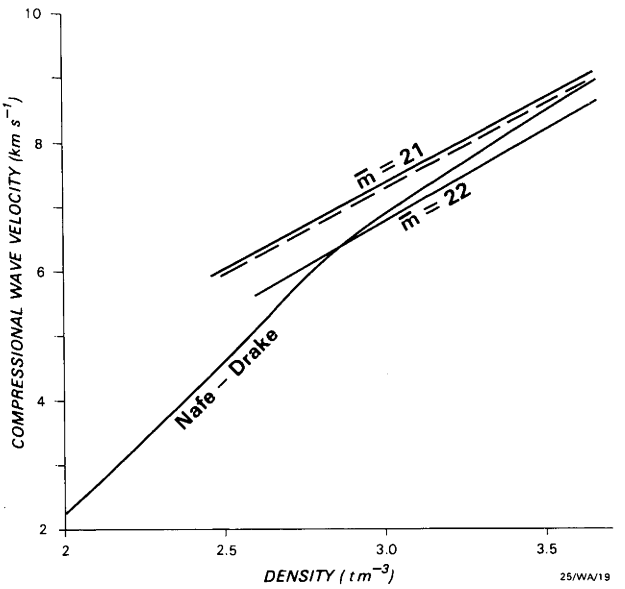

Figure 2. Velocity/density curves of Nafe-Drake (*in* Talwani & others, 1959a) and Manghnani & others (1974) for mean atomic weights of 21 and 22. The dashed line was adopted for the Pilbara Craton.

the blast at Meekatharra recorded southwards is much less than that for similar phases recorded northwards (Drummond, 1979c). This implies that the crust thins south of Meekatharra.

Drummond (1979c, 1981) interpreted seismic first-order velocity discontinuities at all boundaries within the crust. It was recognised that this was probably an oversimplification, and that the velocity and, consequently, density were likely to increase within the crustal layers, and boundaries, especially the crust/mantle boundary, were likely to be transitional. Prodehl (1977) compared the velocity structures under numerous geological provinces in the USA, Europe, Scandinavia, and the Ukraine, and concluded that crust 40–60 km thick is characterised by medium to high seismic velocities and transitional crust/mantle boundaries, and that crust less than 35 km thick is characterised by low seismic velocities and sharper crust/mantle boundaries. If these generalisations are valid, the vertical density gradients should be more prevalent through the thick crust of the Yilgarn Craton than through the thin crust of the Pilbara Craton. Consequently, the density in the lowermost Yilgarn Craton is probably higher than the simple structure described by Drummond (1979c, 1981). However, the effects of this are offset somewhat by the effects that the velocity gradients would have on the depths of the interfaces. Berry (1971) showed that it could be necessary to increase the depths of interfaces by up to 20 percent to account for velocity gradients, and this would regenerate the gravity discrepancy.

The seismic model, based on the available data, stands up to the seismic tests that can be applied, and no simple inadequacies of the model can be found to overcome the mass discrepancy at the southern end of the seismic model.

Two assumptions were made above in calculating the pressure at 52 km depth at the northern and southern boundaries of the Pilbara Craton and at the northern edge of the Yilgarn Craton. The first was that isostasy was complete at the base of the crust, and the other was that a single empirical velocity/density function can be assumed for the whole region. The implications of each of these assumptions on the theoretical calculations for the gravity effect of the seismic model are discussed below.

Compensation below the crust

In the pressure calculations, isostasy was assumed to be complete at 52 km, the base of the thickest crust. However, it may only be complete at greater depths. Very little information is available about the upper mantle structure in the region. Drummond & others (1981) suggested that lateral chemical variations within the upper mantle could account for differences in the upper mantle seismic velocity observed over the Pilbara Craton, but Drummond & others (in prep.) are unable to make any conclusive statement about the structures in the upper mantle above 200 km depth.

Drummond's (1981) seismic model for line GBC (Goldsworthy-Newman-Meekatharra) was tested on the assumption that isostatic equilibrium occurred within the upper mantle. The Nafe-Drake empirical velocity/density relationship (Fig. 2) was used to convert the seismic velocity model into a density model, which is shown as gravity model A in Figure 3. The seismic model is shown for comparison. The calculated gravity profile for the model was generated using the computer program of Milson & Worthington (1977), which utilises the method of Talwani & others (1959b). The measured curve was derived from the contours of the gravity map (Fig. 1); no corrections for regional gradients (Wellman, 1976) were necessary, because the regional gradients along the profile are small compared to the precision with which the curve was fitted.

The short wavelength anomalies in the Pilbara Craton are due to near-surface features such as granitoid domes, greenstone belts, and anticlines and synclines in the Hamersley Basin rocks, and were not accommodated in the gravity model; rather, it is shown that the seismic model can quite easily be made to fit the major features of the gravity field. The general level of the gravity field decreases southwards across the Pilbara Craton. It rises more sharply across the Capricorn Orogen than the seismic model predicts; if the low density Sylvania Dome had been included in the density model, a better match would have been achieved. Note that the high-density lower-crustal layer was moved northwards 30 km relative to the seismic model to match the position of the anomaly.

The thicker crust of the Yilgarn Craton was counterbalanced by a high-density upper mantle root, which extends to 100 km depth. Many other models could have been used for the upper mantle root. The density contrast between the root under the crust of the Yilgarn Craton and the upper mantle under the Pilbara Craton is 0.14 $t.m^{-3}$. The density contrast could be made less and the root made thicker, and the model would still satisfy the measured gravity profile. In addition, if the crust thins to the south of Meekatharra, as may be the case, the root does not need to be as thick or as dense. The northern end of the root must wedge out northwards under the Capricorn Orogen. It could also be modelled as a zone of laterally gradational density contrast (Gendzwill, 1970).

The reversed upper mantle velocity under the Pilbara Craton for a north/south line is 8.34 $km.s^{-1}$ (Drummond, 1979c). Drummond & others (1981) reported

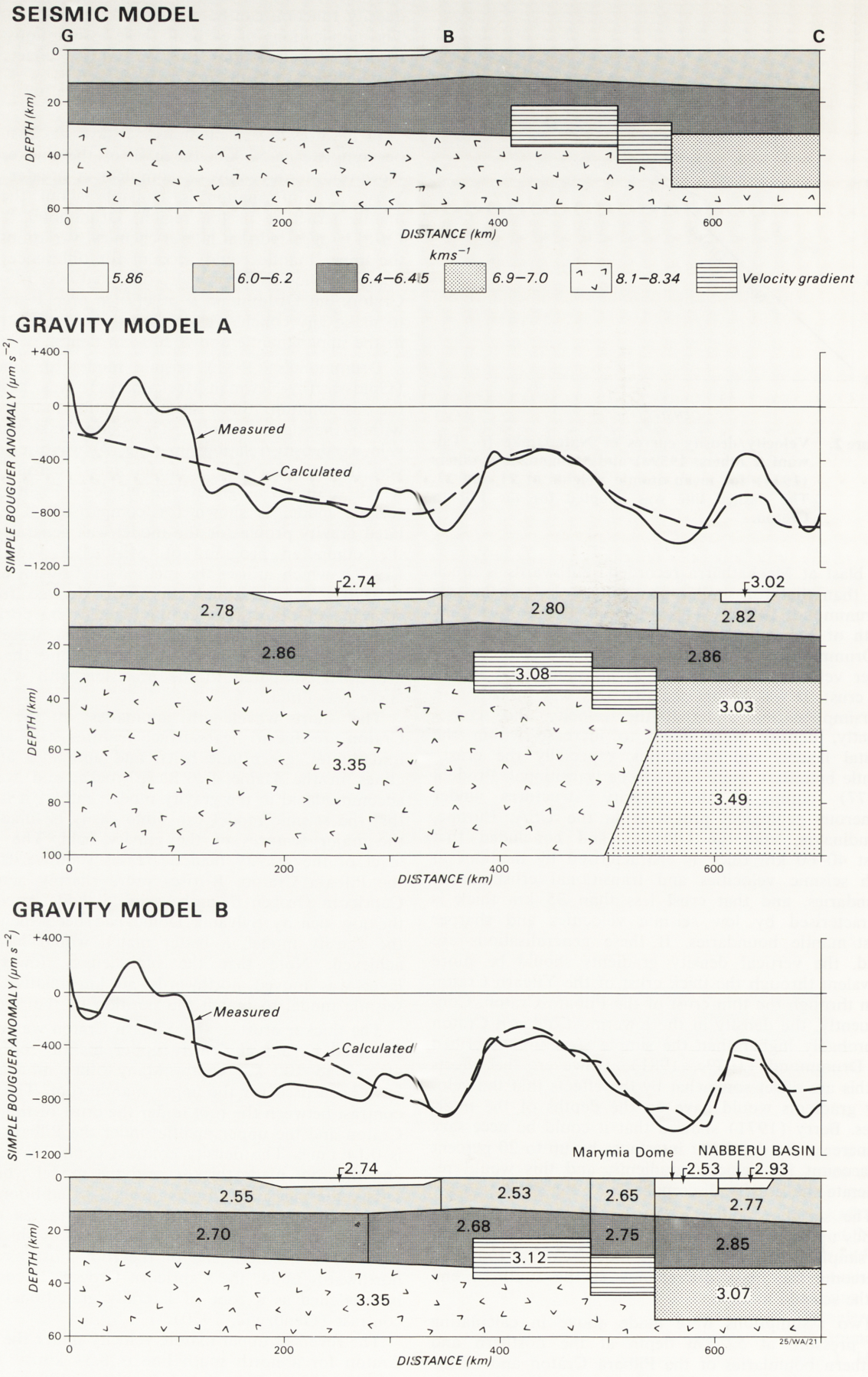
SEISMIC MODEL
G
B
C
DEPTH (km)
DISTANCE (km)
kms⁻¹
5.86
6.0–6.2
6.4–6.45
6.9–7.0
8.1–8.34
Velocity gradient
GRAVITY MODEL A
SIMPLE BOUGUER ANOMALY (μm s⁻²)
Measured
Calculated
2.74
3.02
2.78
2.80
2.82
2.86
2.86
3.08
3.03
3.35
3.49
GRAVITY MODEL B
Marymia Dome
NABBERU BASIN
2.53
2.93
2.55
2.53
2.65
2.77
2.70
2.68
2.75
2.85
3.12
3.07
25/WA/21

a reversed upper mantle Pn velocity of 7.8 km.s^{-1} along the axis of the Hamersley Basin, which lies approximately northwest/southeast. If the differences in the Pn velocity under the Pilbara Craton indicate upper mantle seismic anisotropy, an average velocity for the Pilbara Craton of 8.07 km.s^{-1} is implied.

Gregson (1978) reported the travel times from the Meekatharra shotpoint, recorded at seismological observatories southwards across the Yilgarn Craton. The unreversed velocity of the upper mantle Pn phase is 8.08 km.s^{-1} (Drummond, 1979c), and is similar to the 8.11 km.s^{-1} measured on a north/south line in the southwest Yilgarn Craton, where the east/west Pn velocity is 8.39 km.s^{-1} (Mathur, 1974). This gives a somewhat tenuous average for the upper mantle velocity under the Yilgarn Craton of 8.25 km.s^{-1}, which is greater than under the Pilbara Craton. It should be stressed that the seismic data only indicate that velocity differences could occur in the upper mantle; the present data are too few to interpret the magnitude of the difference with any confidence.

The second assumption made in calculating the pressures at 52 km depth was that one empirical velocity/density function applies throughout the survey area. Many such functions have been proposed in the past, and Dooley (1976) compared some of them. The variations in the functions are striking.

Birch (1961) defined the mean atomic weight of a rock as $\bar{m} = \Sigma(x_i/m_i)^{-1}$ where m_i and x_i are, respectively, the mean atomic weight and proportion of constituent oxide i. Most common rocks have mean atomic weights of between 20 and 22. Birch (1961) showed that the velocity/density function for rocks was dependent on their mean atomic weight. The element on which the mean atomic weight is most dependent is iron: high iron content correlates with high mean atomic weight. The variations in the published empirical velocity/density functions probably reflect variations in rock chemistry.

Manghnani & others (1974) measured the velocities and densities of 17 granulite facies and 15 eclogite facies rocks, and compared these with other published data. They derived velocity/density curves at 10 kbar (Fig. 2) which were similar to those of Birch (1961).

These curves indicate that the density of rocks, for a given seismic velocity, is dependent on the mean atomic weight—rocks with a seismic velocity of, say, 8.0 km.s^{-1} and $\bar{m} = 21$ have a lower density than those with the same velocity and $\bar{m} = 22$. If the upper mantle under the Yilgarn Craton is more iron rich than that under the Pilbara Craton, the density under the Yilgarn Craton will be higher, irrespective of whether the seismic velocity is greater under the Yilgarn Craton.

The effect of different velocity/density curves with isostatic compensation at the base of the crust

The crustal thickness varies throughout northwest Australia, so that, if isostatic equilibrium is complete at the base of the thickest crust, rather than in the upper mantle, the thin crust of the Pilbara Craton must have a lower density than the thick crust of the Yilgarn Craton. However, the seismic velocities to 32 km depth are similar throughout the region, so that the differences in density must be generated by differences in mean atomic weight.

Manghnani & others (1974) analysed the seismic velocities for the crust in the United States. They found that a mean atomic weight of 22 fitted the data from most regions, but a value of 21 was a better fit to the data from the east Basin and Range Province and the northern Colorado Plateau, which have relatively thin crusts (Prodehl, 1977), as in the Pilbara Craton. This is one example of different geological provinces having different mean atomic weights, and therefore different velocity/density functions, with the lowest values of mean atomic weight in areas of thin crust.

A second gravity model (Figure 3, model B) was therefore generated by assuming that the Pilbara and Yilgarn Cratons had different velocity/density functions. For simplicity, the differences were assumed throughout the entire crust, but the crust may be chemically stratified, with the dense, basic rocks restricted to the lower crust. The curve for $\bar{m} = 22$ in Figure 2 was used for the Yilgarn Craton, and the dashed curve was used for the Pilbara Craton. The density values between the cratons were assumed to be intermediate in value.

Corrections for the effects of pressure and temperature on the seismic velocities were made using the pressure derivative of $\beta \times 10^{-2}$ km.s^{-1}kbar^{-1} and the temperature derivative of -4×10^{-4} km.s^{-1}deg^{-1} of Anderson & others (1972), which were favoured by Manghnani & others (1974), and the temperature gradient for the Yilgarn Craton proposed by Jessop & Lewis (1978).

The density model (gravity model B in Figure 3) gives a good fit to the general long-wavelength features of the observed curve. As in model A, the high-density lower-crustal body between the cratons had to be extended 30 km north relative to the seismic model to match the calculated and measured gravity profiles. Note the better fit of the gravity gradient over the Capricorn Orogen compared with gravity model A. A higher density at the base of the crust was assumed than that used in model A, corresponding to a mean atomic weight of 22. A dense, shallow basin was introduced to model the gravity high over the Nabberu Basin, and also a prism of low-density rock corresponding to the Marymia Dome.

Discussion

Within the crust, the gravity models differ from the seismic models only in the northern limits of the dense crustal root in the Capricorn Orogenic Belt. The seismic refraction data (Drummond, 1979c) place the northern limit about 80 km south of Newman, but the resolution of this is limited by the spacing of seismic recording stations, and could be as much as ±20 km. The position of the seismic boundary was, therefore,

Figure 3. The seismic model (Drummond, 1979c) and two gravity models for line GBC. Model A has a root of high-density upper mantle compensating the effects of the thick crust under end C, and in model B different velocity/density functions (see text) were assumed for each end of the line. The calculated and measured curves agree in the principal features, but the short-wavelength effects were not modelled. Both models require a high-density slab representing the Nabberu Basin near end C, and model B requires a low-density prism to represent the Marymia Dome.

set to coincide with the Mount Vernon Fault Zone, which correlates with a major facies change in the Bangemall Basin (Brakel & Muhling, 1976).

The steep gravity gradients at the boundary of the Hamersley Basin and Bangemall Basin in the region of the seismic profile correlate also with the southern boundary of the Sylvania Dome (Fig. 1). The low density basement rocks of the Sylvania Dome, which were not included in the gravity models, probably contribute to the steep gravity gradient. In view of this, and the possible inaccuracy of the boundary in the seismic model, the departure of the gravity models from the seismic model in the region of the Capricorn Orogenic Belt is outside the accuracy of the experiment, and is not significant.

Assuming that the region is in isostatic equilibrium, the seismic model and the gravity field, when considered together, may be indicative of either isostatic compensation being fully achieved deep in the upper mantle or different bulk chemistry in the cratons and isostatic compensation at the crust/mantle boundary. In model B (Fig. 3) the density in the upper crust of the Pilbara Craton (2.55 $t.m^{-3}$) is very low compared with the densities measured in hand samples from the region (Drummond, 1979a), suggesting a compromise between models A and B. We favour a model similar to model A, but with some chemical stratification in the lower crust and the base of the crust in the Yilgarn Craton perhaps reaching $\bar{m} = 22$.

In gravity model A, the depth of compensation was set arbitrarily, and for convenience, at 100 km. Dooley (1977) suggested that the depth of compensation in the Western Australian Shield was in the upper mantle, but he could do no more than to suggest that it was probably below 160 km depth. Unfortunately, the current seismic data cannot be more definitive.

Although a unique structural profile of the crust and upper mantle cannot be derived from the seismic and gravity data, the models in Figure 3 do have implications for theories of evolution of the crust and upper mantle in the region. Gee (1979b) listed four differences between the Pilbara and Yilgarn Blocks from which different evolutionary histories for the cratons can be inferred:

(i) the western Yilgarn Block has large areas of high-grade gneiss terrain, for which there is no equivalent in the Pilbara Block;
(ii) most of the granitoids in the Yilgarn Block are younger than the majority of those in the Pilbara Block;
(iii) the maturity of the clastic sequences within the greenstone belts of the cratons implies that the Pilbara Block developed more towards crustal stability than the Yilgarn Block; and
(iv) the granitoids of the Pilbara Block are near-circular, whereas those of the Yilgarn Block have distinct linear trends.

Drummond & others (1981) added a fifth: the crust of the Pilbara Craton is much thinner than the crust of the Yilgarn Craton.

The arguments presented above for the depths of isostatic equilibrium imply also that the Pilbara region differs from the Yilgarn region either in the chemistry of the crust, which can be regarded as a sixth difference between the cratons, or in the metamorphic grade or chemistry of the upper mantle.

Jordan (1975, 1978) suggested that sub-continental mantle to depths possibly as great as 400 km evolves in parallel with the overlying continental crust. Because the sub-continental mantle becomes less dense than the surrounding mantle, it does not mix with the rest of the mantle, but is transported with the continents during plate motions. The features of the mantle established during the formation of the crust are frozen in. The differences in the upper mantle structure or chemistry under the cratons in northwest Australia may therefore indirectly imply different evolutionary processes for the cratons. This is an alternative sixth difference between the cratons.

The upper mantle under the Pilbara Craton may be less dense than that under the Yilgarn Craton, because of iron depletion. The upper mantle would, therefore, be implicated as the reservoir which provided the iron for the large volumes of basic volcanics and banded iron formations of the Hamersley Basin.

Acknowledgements

We thank the iron ore companies of the Pilbara for their willing co-operation during the field work and are grateful to our colleagues at BMR for their useful discussions and suggestions for field work; in particular, we thank P. Wellman and D. M. Finlayson.

This work was undertaken when one of us (BJD) was a full time research scholar at the Research School of Earth Sciences, Australian National University, under the auspices of an Australian Government Public Service Postgraduate Scholarship. We are indebted to Professor K. Lambeck and Dr K. J. Muirhead of RSES for their support and advice.

References

ANDERSON, D. L., SAMMIS, C., & JORDAN, T., 1972—Composition of mantle and core. *In* ROBERTSON, E. C. (editor), The nature of the solid Earth. *McGraw Hill, New York,* 41-66.

BERRY, M. J., 1971—Depth uncertainties from seismic first-arrival refraction studies. *Journal of Geophysical Research,* 76, 6464-8.

BIRCH, F., 1961—The velocity of compressional waves in rocks to 10 kilobars, Part 2. *Journal of Geophysical Research,* 66, 2199-224.

BRAKEL, A. T., & MUHLING, P. C., 1976—Stratigraphy, sedimentation, and structure in the western and central part of the Bangemall Basin, Western Australia. *Geological Survey of Western Australia Annual Report,* 1975, 70-9.

DOOLEY, J. C., 1976—Variation of crustal mass over the Australian region. *BMR Journal of Australian Geology & Geophysics,* 1, 291-6.

DOOLEY, J. C., 1977—Implications of Australian seismic and gravity measurements for the structure and composition of the upper mantle. *BMR Journal of Australian Geology & Geophysics,* 2, 1-5.

DRUMMOND, B. J., 1979a—Pilbara Crustal Survey, 1977: Operational Report. *Bureau of Mineral Resources, Australia, Record,* 1979/54 (unpublished).

DRUMMOND, B. J., 1979b—Structural relations between the Archaean Pilbara and Yilgarn cratons, Western Australia, from deep seismic sounding. *M.Sc. Thesis, Australian National University* (unpublished).

DRUMMOND, B. J., 1979c—A crustal profile across the Archaean Pilbara and northern Yilgarn cratons, northwest Australia. *BMR Journal of Australian Geology & Geophysics,* 4, 171-80.

DRUMMOND, B. J., 1981—Crustal structure of the Precambrian terrains of northwest Australia from seismic refraction data. *BMR Journal of Australian Geology & Geophysics,* this issue.

DRUMMOND, B. J., SMITH, R. E., & HORWITZ, R. C., 1981—Crustal structure in the Pilbara and northern Yilgarn blocks from deep seismic sounding. *In* GLOVER, J. E., & GROVES, D. I. (editors), Archaean Geology: Second International Archaean Symposium. *Geological Society of Australia Special Publication,* 7, in press.

DRUMMOND, B. J., MUIRHEAD, K. J., & HALES, A. L., in prep.—Evidence for a seismic discontinuity near 200 km depth under a continental margin.

FRASER, A. R., 1979a—Reconnaissance gravity survey in northwest Western Australia, 1969. *In* FRASER, A. R., & PETTIFER, G. R., Reconnaissance gravity surveys in Western Australia and South Australia, 1969–1972. *Bureau of Mineral Resources, Australia, Bulletin,* 196 Part B, 13-25.

FRASER, A. R., 1979b—Reconnaissance gravity survey in central and southwest Western Australia, 1971–1972. *In* FRASER, A. R., & PETTIFER, G. R., Reconnaissance gravity surveys in Western Australia and South Australia, 1969–1972. *Bureau of Mineral Resources, Australia, Bulletin,* 196, Part C, 27-45.

GEE, R. D. (compiler), 1979a—Geological map of Western Australia, 1:2 500 000 scale. *Geological Survey of Western Australia, Perth.*

GEE, R. D., 1979b—Structure and tectonic style of the Western Australian shield. *Tectonophysics,* 58, 327-69.

GENDZWILL, D. J., 1970—The gradational density contrast as a gravity interpretation model. *Geophysics,* 35, 270-5.

GREGSON, P. J., 1978—Mundaring Geophysical Observatory, Annual Report, 1977. *Bureau of Mineral Resources, Australia, Record,* 1978/73 (unpublished).

GSWA, 1975—Geology of Western Australia. *Geological Survey of Western Australia, Memoir,* 2.

HALL, W. D. M., & GOODE, A. D. T., 1978—The early Proterozoic Nabberu Basin and associated iron formations of Western Australia. *Precambrian Research,* 7, 129-84.

JESSOP, A. M., & LEWIS, T., 1978—Heat flow and heat generation in the Superior Province of the Canadian Shield. *Tectonophysics,* 50, 55-77.

JORDAN, T. H., 1975—The continental tectosphere. *Reviews of Geophysics & Space Physics,* 13, 1-12.

JORDAN, T. H., 1978—Composition and development of the continental tectosphere. *Nature,* 274, 544-8.

MATHUR, S. P., 1974—Crustal structure in southwestern Australia from seismic and gravity data. *Tectonophysics,* 24, 151-82.

MANGHNANI, M. H., RAMANANANTOANDRO, R., & CLARK, S. P., 1974—Compressional and shear wave velocities in granulite facies rocks and eclogites to 10 kbar. *Journal of Geophysical Research,* 79, 5427-46.

MILSON, J., & WORTHINGTON, G. A., 1977—Computer programs for rapid computation of gravity effects of two-dimensional and three-dimensional bodies. *Computers & Geosciences,* 3, 269-81.

PRODEHL, C., 1977—The structure of the crust-mantle boundary beneath North America and Europe as derived from explosion seismology. *In* HEACOCK, J. C., The Earth's crust. *American Geophysical Union Geophysical Monograph,* 20, 349-69.

TALWANI, M., SUTTON, G. H., & WORZEL, J. O., 1959a—A crustal section across the Puerto Rico Trench. *Journal of Geophysical Research,* 64, 1545-55.

TALWANI, M., WORZEL, J. L., & LANDISMAN, J., 1959b—Rapid gravity computations for two-dimensional bodies with application to the Mendocino submarine fracture zone. *Journal of Geophysical Research,* 64, 49-59.

WELLMAN, P., 1976—Regional variation of gravity, and isostatic equilibrium of the Australian crust. *BMR Journal of Australian Geology & Geophysics,* 1, 297-302.

WELLMAN, P., 1978—Gravity evidence for abrupt changes in mean crustal density at the junction of Australian crustal blocks. *BMR Journal of Australian Geology & Geophysics,* 3, 153-62.

APPENDIX 5

Drummond, B.J., Muirhead, K.J. and Hales, A.L., 1982 - Evidence for a seismic discontinuity near 200 km depth under a continental margin. Geophysical Journal of the Royal Astronomical Society, 69, in press.

EVIDENCE FOR A SEISMIC DISCONTINUITY NEAR 200 KM DEPTH UNDER A CONTINENTAL MARGIN.

B.J. DRUMMOND[1], K.J. MUIRHEAD[2] AND A.L. HALES[2]*

[1] Bureau of Mineral Resources, Geology and Geophysics,
P.O. Box 378,
Canberra City, ACT 2601
and presently at

[2] Research School of Earth Sciences,
Australian National University,
P.O. Box 4,
Canberra, ACT 2600
*and presently at

[3] Geosciences Program,
University of Texas at Dallas,
P.O. Box 688,
Richardson, Texas 75080
USA

INTRODUCTION

Lehmann (1959) first demonstrated the presence of a seismic discontinuity at about 200 km depth under continental Europe, and in 1962 she suggested that it was also present under continental North America (Lehmann, 1962). Subsequently, numerous seismological studies have demonstrated the discontinuity under the continental regions of the world, and it has become known as the Lehmann Discontinuity. It is also believed to be present under oceans (see, for example, the PEM-O model of Dziewonski, Hales and Lapwood, 1975), but, because of the difficulty of long range seismic profiling at sea, it is usually delineated only by surface wave analysis.

The Lehmann Discontinuity has been delineated under continental Australia by both body wave (Simpson, 1973; Finlayson, Cull and Drummond, 1974; Muirhead, Cleary and Finlayson, 1977; Hales, Muirhead and Rynn, 1980) and surface wave analysis (Goncz and Cleary, 1976; Mills and Fitch, 1977). The most conclusive body-wave evidence for the Lehmann Discontinuity under continental Australia is that of Hales et al. (1980). Their exercise was planned so that the seismic waves travelled almost entirely within the Australian continental plate. Using deep events, they were able to define a velocity increase of about 0.3 km s^{-1} at about 200 km depth. Their CAP-8 model of the discontinuity is shown in Figure 1. The discontinuity is underlain by a low velocity zone which has a gradual onset about 30 km below the discontinuity. Leven (1980) used synthetic seismograms to imply that the onset of the low velocity zone was more

pronounced, but his studies could not fully describe the nature of the low velocity zone. His preferred model, also shown in Figure 1, has a very sharp onset of the low velocity zone about 20 to 30 km below the discontinuity, so that the discontinuity resembles a knee of high velocity superimposed on a smaller velocity which steadily increases with depth.

The low velocity zone below the discontinuity makes it difficult to observe the discontinuity. For surface focus events the seismic body waves refracted below the discontinuity fall off in amplitude soon after becoming first arrivals. By using deep events Hales et al. (1980) were able to observe the discontinuity clearly, because the refracted arrivals are clearly observed as first arrivals for much longer distances. They were also able to define accurately the velocity increase of more than 0.3 km s^{-1} across the discontinuity.

The velocity increase is more than can be readily explained by modern theories of upper mantle geochemistry. When the discontinuity was first discovered, it was regarded as merely the return to "normal" upper mantle velocities at the bottom of a low velocity zone between about 100 and 200 km depth in young continental regions (see, for example, Clark and Ringwood, 1964). However, in the old continental regions of central Australia the low-velocity zone above the discontinuity is not present (Hales et al., 1980), and the velocity increase at about 200 km depth is clearly a seismic discontinuity. Anderson (1979) suggested that the discontinuity is a worldwide feature and represents a chemical change from garnet lherzolite above to eclogite immediately below. However, Leven, Jackson

and Ringwood (1981) have examined this and other chemical models and argued that they do not explain the high velocity contrast across the discontinuity, nor do they explain the low velocity zone below it.

Leven et al. (1981) suggested that the velocity knee in the velocity/depth model of Leven (1980) (Fig. 1) represents the zone of decoupling of the continental lithosphere from the deeper mantle, and that the higher velocities result from anisotropy due to alignment of olivine crystals along the zone of movement. By recognising similar high velocity knee structures at shallower depths in models from refraction surveys for oceanic paths, they implied that oceanic lithosphere is much thinner, (75-104 km), and that the zone of decoupling is therefore shallower under the oceans. Previously, the motion was thought to occur along low velocity layers above the discontinuity, although Jordan (1975 , 1978) suggested that the differences in the chemistry and heat flow between oceans and continents extend to considerable depths, perhaps greater than 400 km. The upper mantle under the continents has been progressively depleted by partial melting, creating continent roots which are lighter than, and therefore cannot mix with, the surrounding mantle. The continental lithosphere may therefore carry with it thick roots of upper mantle material as it translates over the deeper mantle. However, Anderson (1979) proposed that the motion occurs along a zone of low viscosity lying below the discontinuity at about 250 km depth.

Clearly the Lehmann Discontinuity is enigmatic - it is difficult to observe with surface focus events, and it is difficult to explain in terms of present knowledge of upper

mantle geochemistry. It will remain an enigma until sufficient seismic data are collected to define its structure and distribution. This paper presents the first body wave evidence for the discontinuity under a continental margin, where the continental lithosphere merges into oceanic lithosphere.

DATA

On 19 August 1977, a large earthquake occurred south of Sumbawa Island in the Indonesian Archipelago. It had a body wave magnitude of 6.8, and was preceded by a foreshock of magnitude 5.8. Between August 1977 and January 1978, the International Seismological Centre (ISC) bulletins list 402 earthquakes from the original fault zone and a second fault zone about 100 km to the north. At the time of the main earthquake, the Australian Bureau of Mineral Resources, Geology and Geophysics (BMR) and the Research School of Earth Sciences of the Australian National University (ANU) were conducting a seismic survey in the Precambrian shield of northwest Australia to study the crustal structure of the Archaean of northwest Australia (Drummond, 1979a).

All the seismographs used slow-speed magnetic-tape recorders. The ANU seismographs were direct record units at three gain levels; the BMR seismographs recorded frequency modulated signals, and were subject to overmodulation by phases with large amplitudes.

Figure 2 shows the arrangement of the recorders and the positions of the seismic events used in this paper. The stations occupied for Events 1 and 2 were those along lines

A-A' and B-B', plus those stations marked with open circles. Shortly after the main earthquake, the recorders were moved to new sites to continue the crustal survey. The recorders along line N-N' observed Event 3, an aftershock.

Events 1 and 2 occurred on a fault zone along the Java Trench. To the north another fault zone coincides with the 4000 m isobath of a shallower trench. This is the site of Event 3. The Java Trench is the submarine expression of a convergent plate margin along which old oceanic crust (circa 145-150 m.y.) of the Argo Abyssal Plain is being subducted (Larson, 1975; Heirtzler et al., 1978). The southern and eastern limits of the oceanic crust are uncertain. Veevers and Cotteril (1978) suggested that the Scott and Exmouth Plateaus are epiliths, and therefore of oceanic origin and crustal type, but Stagg and Exon (1979), in reply, claimed a continental structure for the Scott Plateau. However, in both cases it is apparent (Figure 2 of Veevers and Cotteril and Figure 2 of Stagg and Exon) that the northwestern Australian continent has a passive margin with oceanic crust (see also Heirtzler et al., 1978) probably somewhere between the 2000 m and 4000 m isobaths.

The seismic recorders were all located on the Precambrian Shield of Western Australia, but Palaeozoic Canning Basin sediments may extend offshore between the Precambrian Shield and the edge of the continent (Gee, 1979). Hence the seismic body waves recorded in northwest Australia originated along the southern edge of an island arc environment, travelled the first half of their paths under

oceanic lithosphere, bottomed approximately under the continental margin, and travelled the last half of their paths under continental crust, mainly beneath the Precambrian Shield.

RESULTS

The ISC hypocentral data for the three earthquakes used in this study are listed in Table 1. Events 1 and 2 are the foreshock and the main event respectively. Event 3 was chosen because it provided data at alternative recording sites and epicentral distances and because the seismic waves from this relatively small event did not overmodulate BMR recorders. However, Event 3 was positioned by use of records from only seven stations, and therefore is probably not as accurately positioned as Events 1 and 2.

Lines AA' and BB' gave almost identical travel-time curves for Event 1, even though they were separated by over 200 km at their northern end. Figure 3 is a composite record section of the recordings of Event 1. Superimposed on the record section are our interpreted travel-time curves. Between 1000 and 1450 km, the first arrivals have an apparent velocity of 8.4 km s^{-1}. This phase is observed as a second arrival beyond 1450 km. Note that beyond 1600 km, it is delayed by the thick crustal section at the southern end of the line (Drummond, 1979b). Beyond about 1500 km, the first arrivals have a higher apparent velocity of about 8.75 km s^{-1}, but this phase is very weak (see the inset), and quickly dies out beyond 1600 km. When projected back towards the event, the travel time curve correlates with large amplitude second arrivals on records in the distance range 1150-1310 km.

Recordings of Event 2 are plotted as a composite section in Figure 4. As with Event 1, the first arrivals out to about 1500 km have an apparent velocity of 8.4 km s^{-1} and, as in Figure 3, this phase continues beyond 1500 km. The higher apparent velocity branch is evident as second arrivals on most traces between 1150 and 1450 km, but no clear first arrivals beyond 1500 km are evident.

We have interpreted the increase in velocity at 1500 km as a cross-over associated with a seismic discontinuity in the upper mantle. The large amplitude second arrival phases, associated with the higher velocity branch in the distance range 1150 to 1450 km in both Figures 3 and 4, lie on the retrograde, reflected branch of the travel time curve. The forward branch, which dies out beyond 1600 km in Figure 3 and 1500 km in Figure 4, represents refracted waves below the interface.

The wide angle reflections from the discontinuity and the refractions below it probably have a critical point cusp between 1100 and 1200 km. Figure 5 is a record section of Event 3. The traces have been filtered in the bandpass 2 to 8 Hz, which encompasses the dominant frequencies for this event. The superimposed travel-time curves have the same apparent velocities as those in Figure 4, but have been transposed later in time by 2.6 s. This implies an uncertainty in the location of the hypocentre of Event 3, as discussed above. The bands of large amplitude reflected arrivals are clearly seen between 1150 and 1300 km.

DISCUSSION

For most Earth models of the Australian region, seismic waves for a surface focus recorded in the distance range between 1000 and 1500 km bottom in the depth range from 80 to 120 km. The apparent velocity of 8.4 km s^{-1} therefore represents a velocity, when corrected for earth curvature, of about 8.25 to 8.3 km s^{-1}. The higher apparent velocity branch represents refractions below a deeper discontinuity. We do not have sufficient data to invert for an Earth model to determine accurately the depth of the interface. However, with events at the depths of our events 1 and 2, the models of Hales et al. (1980) and Simpson (1973) both give crossover distances comparable to the crossover distance of our high velocity phase. In addition, the velocities in our model are comparable to theirs if we assume bottoming depths of 100 and 200 km for the slower and faster phases respectively (Table 2). We therefore conclude that the seismic discontinuity we observed is the "200 km" or Lehmann Discontinuity.

We are unable to comment more fully on the nature of the lithospheric velocity structure above the discontinuity under northwest Australia. Drummond (1979b) observed Pn velocities under the northern Precambrian shield of 8.34 km s^{-1}, which is similar to the velocity observed at an assumed depth of 100 km in this study. However, because of offsets to the refractors, the two studies sampled different parts of the upper mantle, so it is not possible to say whether Drummond's (1979b) Pn velocity and our velocity at about 100

km depth imply constant velocity in the mantle in the depth range 30 to 100 km. Current synthetic seismogram studies of the crustal survey data, and the results of Drummond, Smith and Horwitz (1980), suggest significant lateral and vertical velocity structure in the upper mantle under the northern Precambrian shield of Western Australia. This, coupled with the obvious lateral changes which must occur northwards as the continental crust meets the oceanic crust, makes it difficult to define a more precise lithospheric velocity structure. In particular we can make no comment on whether a low-velocity layer occurs above the discontinuity.

The amplitudes on the refracted branches from below the Lehmann Discontinuity fall-off sharply in the distance range 1500 and 1650 km in Figure 3, and are not clearly seen as first arrivals in Figure 4, implying that there is a low velocity layer under the discontinuity. This was suggested by Hales et al. (1980) and supported by Leven (1980). The fall-off in amplitude could also result from high attenuation of waves which bottom below the 200 km discontinuity. Such an explanation is, however, not supported by the arrivals in Figure 14 of Hales et al. (1980) which show no apparent change in frequency content associated with diminishing amplitudes.

A seismic discontinuity therefore exists at about 200 km depth under the continental margin of northwest Australia; there must be a velocity contrast of about 0.2-0.3 km/s across it.

CONCLUSIONS

Leven et al. (1981) suggested that the Lehmann Discontinuity represents the zone of gliding for the continental lithosphere over the underlying mantle. By correlating their high velocity knee at 200 km depth (Fig. 1) with shallower features under oceanic regions, they implied that the gliding zone for the lithosphere over the deeper mantle shallows under oceans.

We have shown that the Lehmann Discontinuity is present at about 200 km depth under the northwestern margin of continental Australia. This provides one link between the seismic discontinuity already observed under continents and oceans elsewhere in the world. If the discontinuity under continents results from shearing associated with plate motions, and if the shearing zone shallows under oceans, the thesis of Leven et al. (1981) leaves the Lehmann Discontinuity under oceans unexplained.

We are more in agreement with Anderson (1979) - the Lehmann Discontinuity is a worldwide phenomenom, to be found under continents and oceans, and at the continental margins.

ACKNOWLEDGEMENTS

We thank our colleagues at the Australian National University, particularly Ian Jackson and Jim Leven, for their interest and discussions. Many of our colleagues at both the ANU and the Bureau of Mineral Resources contributed to the success of the field work. The contributions of B.J. Drummond to this work were undertaken while he was a full time research scholar under the auspices of a Commonwealth Public Service Postgraduate Scholarship at the ANU, and are published with the permission of the Director, Bureau of Mineral Resources.

REFERENCES

ANDERSON, D.L., 1979. The deep structure of continents. J.geophys.Res., 84, 7555-7560.

CLARK, S.P., & RINGWOOD, A.E., 1964 - Density distribution and composition of the mantle. Rev.Geophys., 2, 35-88.

DRUMMOND, B.J., 1979a. The Pilbara Crustal Survey, 1977, Operational Report. Rec.Bur.Miner.Resour.Aust. 1979/54 (unpubl.).

DRUMMOND, B.J., 1979b. A crustal profile across the Archaean Pilbara and northern Yilgarn cratons, northwest Australia. BMR J.Aust.Geol.Geophys., 4, 171-180.

DRUMMOND, B.J., SMITH, R.E., & HORWITZ, R.C., 1980. Crustal structure in the Pilbara and northern Yilgarn blocks from deep seismic sounding. in GLOVER, J.E. & GROVES, D.I. (editors) - Archaean Geology. Second International Archaean Symposium. Spec.Publ.Geol.Soc. Aust., 7, (in press).

DZIEWONSKI, A.M., HALES, A.L., & LAPWOOD, E.R., 1975. Parametrically simple earth models consistent with geophysical data. Phys.Earth Planet.Int., 10, 12-48.

FINLAYSON, D.M., CULL, J.P., & DRUMMOND, B.J., 1974. Upper mantle structure from the trans-Australia seismic refraction data. J.Geol.Soc.Aust., 21, 447-458.

GEE, R.D. (compiler), 1979. Geological map of Western Australia. 1:2 500 000 scale. Geol.Surv.West.Aust., Perth.

GONCZ, J.H., & CLEARY, J.R., 1976. Variations in the structure of the upper mantle beneath Australia, from Rayleigh wave observations. Geophys.J.R.astr. Soc., 44, 507-516.

HALES, A.L., MUIRHEAD, K.J., & RYNN, J.M.W., 1980. A compressional velocity distribution for the upper mantle. Tectonophysics, 63, 309-348.

HEIRTZLER, J.R., CAMERON, P., COOK, P.J., POWELL, T., ROESER, H.A., SUKARDI, S., & VEEVERS, J.J., 1978. The Argo Abyssal Plain. Earth Planet Sci.Lett., 41, 21-31.

JORDAN, T.H., 1975. The continental tectosphere. Rev.Geophys.Space Phys., 13, 1-12.

JORDAN, T.H., 1978. Composition and development of the continental tectosphere. Nature, 274, 544-548.

LARSON, R.L., 1975. Late Jurassic sea-floor spreading in the eastern Indian Ocean. Geology, 3, 69-71.

LEHMANN, I., 1959. Velocity of longitudinal waves in the upper part of the earth's mantle. Ann.Geophys., 15, 93-118.

LEHMANN, I., 1962. The travel times of the longitudinal waves of the Logan and Blanca atomic explosions and their velocities in the upper mantle. Bull.Seis. Soc.Am., 52, 519-526.

LEVEN, J.H., 1980. The application of synthetic seismograms to the interpretation of crustal and upper mantle structure. Ph.D. Thesis Australia National University (unpubl.).

LEVEN, J.H., JACKSON, I., & RINGWOOD, A.E., 1981. Upper mantle anisotropy and lithospheric decoupling. Nature, 289, 234-239.

MILLS, J.M., & FITCH, T.J., 1977. Thrust faulting and crust-upper mantle structure in East Australia. Geophys.J.R.astr.Soc., 48, 351-384.

MUIRHEAD, K.J., CLEARY, J.R., & FINLAYSON, D.M., 1977. A long-range seismic profile in south-eastern Australia. Geophys.J.R.astr.Soc., 48, 509-520.

SIMPSON, D.W., 1973. P wave velocity structure of the upper mantle in the Australian region. Ph.D. Thesis Australian National University (unpubl.).

STAGG, H.M.J., & EXON, N.F., 1979. Western margin of Australia: Evolution of a rifted arch system: Discussion. Bull.Geol.Soc.Am., 90, 795-797.

VEEVERS, J.J., & COTTERIL, D., 1978. Western margin of Australia: Evolution of a rifted arch system. Bull.Geol.Soc.Am., 89, 337-355.

TABLE 1

Event	Time (UT)				Latitude °S	Longitude °E	Depth km	No. of stns	Mb
			h	m s					
1 (Preshock)	1977 19 Aug		05	08 43.6±0.145	11.21±0.028	118.43±0.029	54±1	281(172)	5.8
2 (main event)	1977 19 Aug		06	08 54.8±0.11	11.16±0.024	118.41±0.023	78±3	523(263)	6.8
3 (aftershock)	1977 7 Sept		08	30 43±1.2	10.4 ±0.14	117.9 ±0.13	33	10(7)	UN

International Seismological Centre determinations of Hypocentres and magnitudes for the earthquakes used in this study.

TABLE 2

	Depth of Lehmann Discontinuity (km)	Velocity at 100 km depth* ($km\ s^{-1}$)	Velocity below Lehmann Discontinuity ($km\ s^{-1}$)	Velocity contrast at Discontinuity ($km\ s^{-1}$)	Velocity difference between 100 & 200 km depths ($km\ s^{-1}$)	Cross-over distance h=54 km	Cross-over distance h=78 km
Hales et al. (1980)	200	8.27	8.62	0.38	0.35	1600	1515
Simpson (1973)	175	8.25	8.53	0.15	0.28	1320	1250
This study	200*	8.25-8.3	8.45-8.55	unknown	0.2-0.3	1450	1450

h = focal depth.

Comparison of the travel-time curves of this study with those of Simpson (1973) and Hales et al. (1980).

(* assumed depth for this study - see text).

Figure Captions

Figure 1: Velocity/depth curves near the 200 km discontinuity for the CAP-8 model of Hales et al. (1980) and the CAPRI model of Leven (1980). The dots mark the velocities at their assumed depths from our study.

Figure 2: Locality map showing the positions of the recording stations and the earthquakes discussed in the text. The approximate edges of the Precambrian Shield are after Gee (1979).

Figure 3: Composite record section of the recordings of Event 1 along lines AA' and BB'. The interpreted travel time curves are superimposed. Their apparent velocities, with depth corrected values in brackets, are marked. The inset shows in more detail the absence of energy of the high velocity branch which is a clear later arrival at shorter distances.

Figure 4: Composite record section of the recordings of Event 2 along lines AA' and BB'. The interpreted travel time curves are superimposed. Their apparent velocities, with depth-corrected values in brackets, are marked.

Figure 5: Record section of the recordings of Event 3 along line NN'. The traces have been digitally bandpass filtered in the range 2 and 8 Hz. The superimposed travel-time curves are as for Fig. 3, but shifted in time by +2.6 s to account for the mislocation of the events.

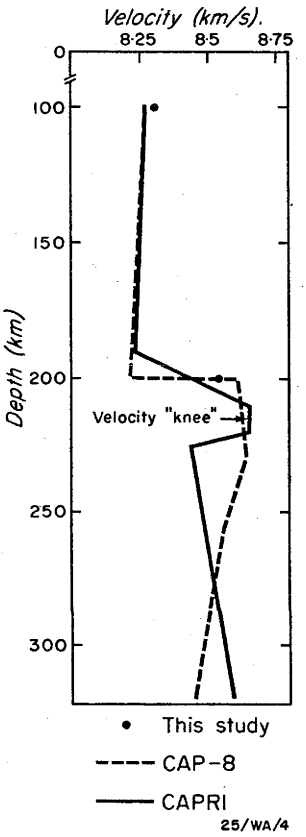
Velocity (km/s).
8·25
8·5
8·75
0
100
150
200
250
300
Depth (km)
Velocity "knee"
This study
CAP-8
CAPRI
25/WA/4

FIGURE 1

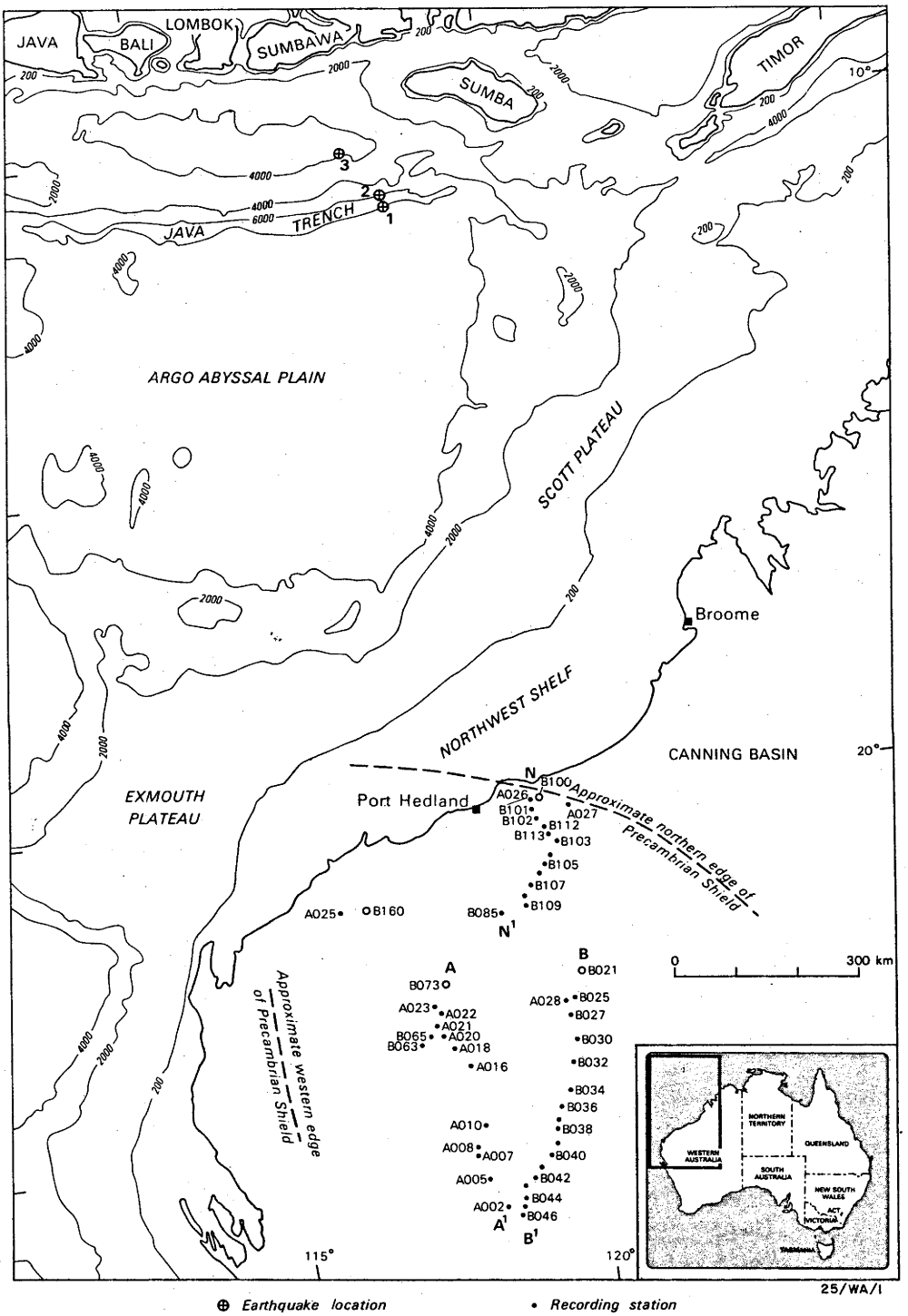
JAVA
BALI
LOMBOK
SUMBAWA
SUMBA
TIMOR
JAVA TRENCH
ARGO ABYSSAL PLAIN
SCOTT PLATEAU
NORTHWEST SHELF
EXMOUTH PLATEAU
CANNING BASIN
Broome
Port Hedland
Approximate northern edge of Precambrian Shield
Approximate western edge of Precambrian Shield
A026
B100
B101
B102
B112
B113
A027
B103
B105
B107
B109
A025
B160
B085
N
N'
A
B
A'
B'
B073
B021
A028
B025
B027
A023
A022
A021
B065
B063
A020
A018
B030
A016
B032
B034
B036
A010
B038
A008
A007
B040
A005
B042
B044
A002
B046
0
300 km
115°
120°
10°
20°
WESTERN AUSTRALIA
NORTHERN TERRITORY
QUEENSLAND
SOUTH AUSTRALIA
NEW SOUTH WALES
ACT
VICTORIA
TASMANIA
25/WA/1
⊕ Earthquake location
• Recording station

FIGURE 2

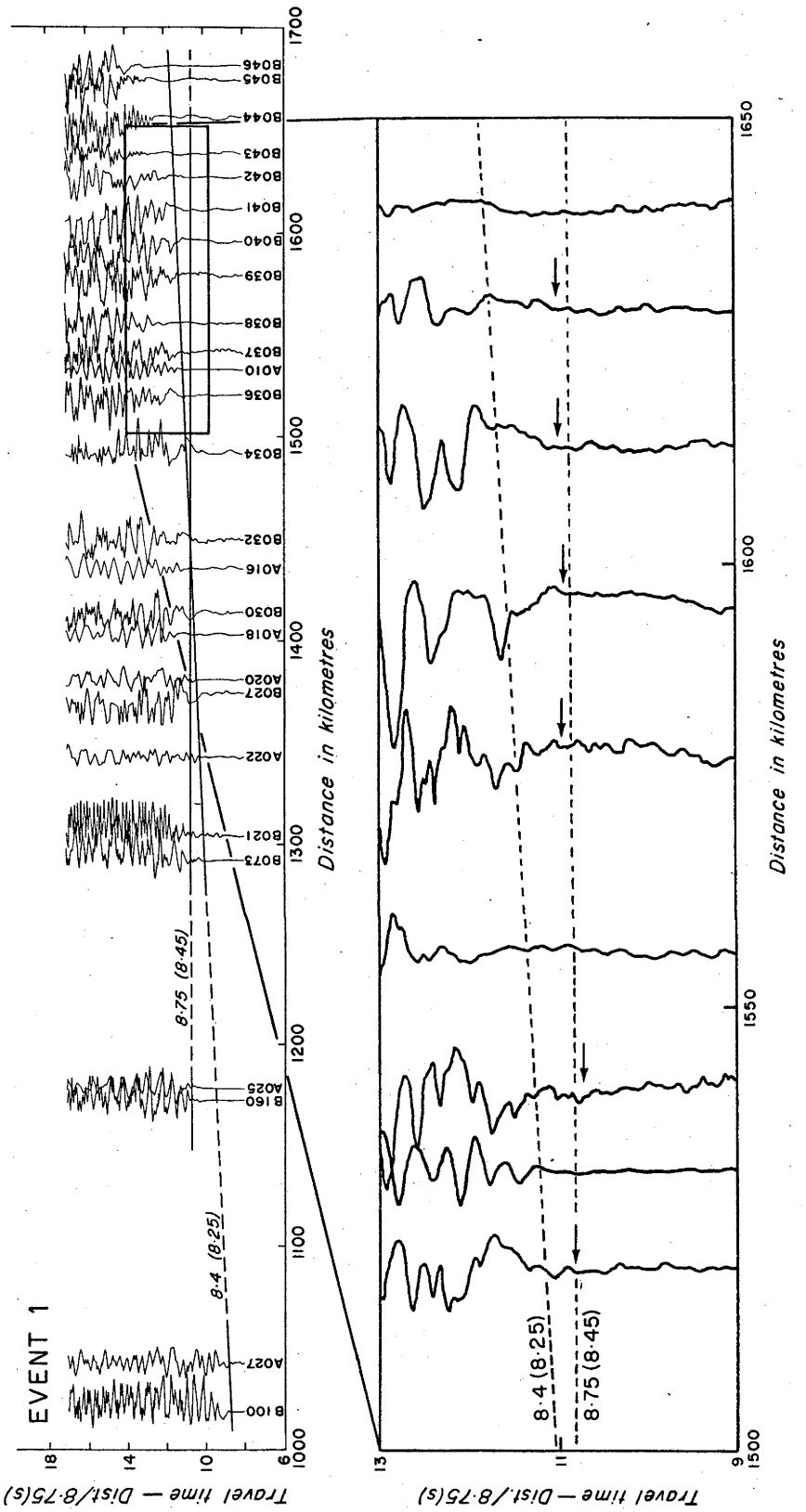
EVENT 1
B046
B045
B044
B043
B042
B041
B040
B039
B038
B037
A010
B036
B034
B032
A016
B030
A018
A020
B027
A022
B021
B073
B160
A025
A027
B100
8·75 (8·45)
8·4 (8·25)
Distance in kilometres
Travel time — Dist./8·75(s)
8·4 (8·25)
8·75 (8·45)
Distance in kilometres
Travel time — Dist./8·75(s)

FIGURE 3

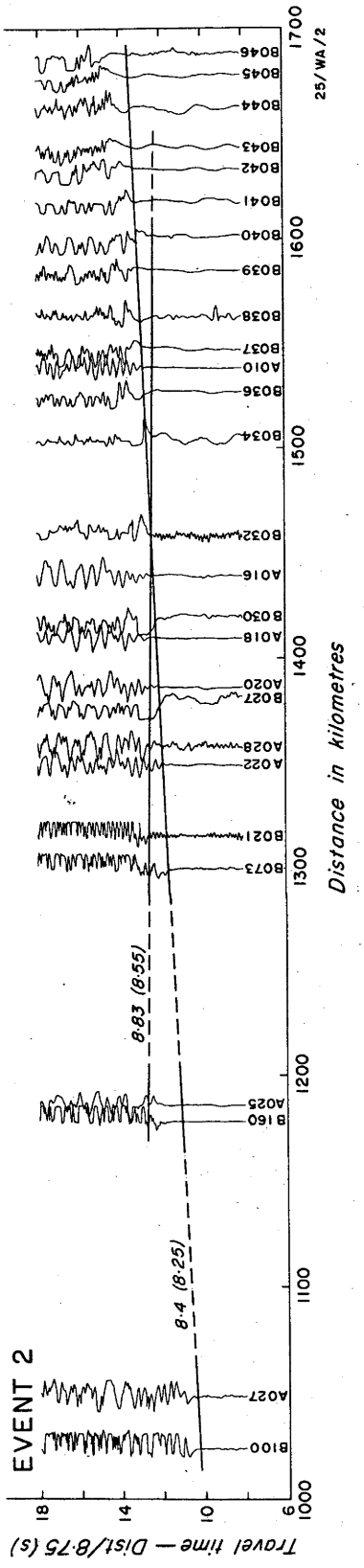
EVENT 2
25/WA/2
Travel time — Dist/8·75 (s)
Distance in kilometres
8·83 (8·55)
8·4 (8·25)
B100
A027
B160
A025
B073
B021
A022
A028
B027
A020
A018
B030
A016
B032
B034
A010
B036
B037
B038
B039
B040
B041
B042
B043
B044
B045
B046
18
14
10
6
1000
1100
1200
1300
1400
1500
1600
1700

FIGURE 4

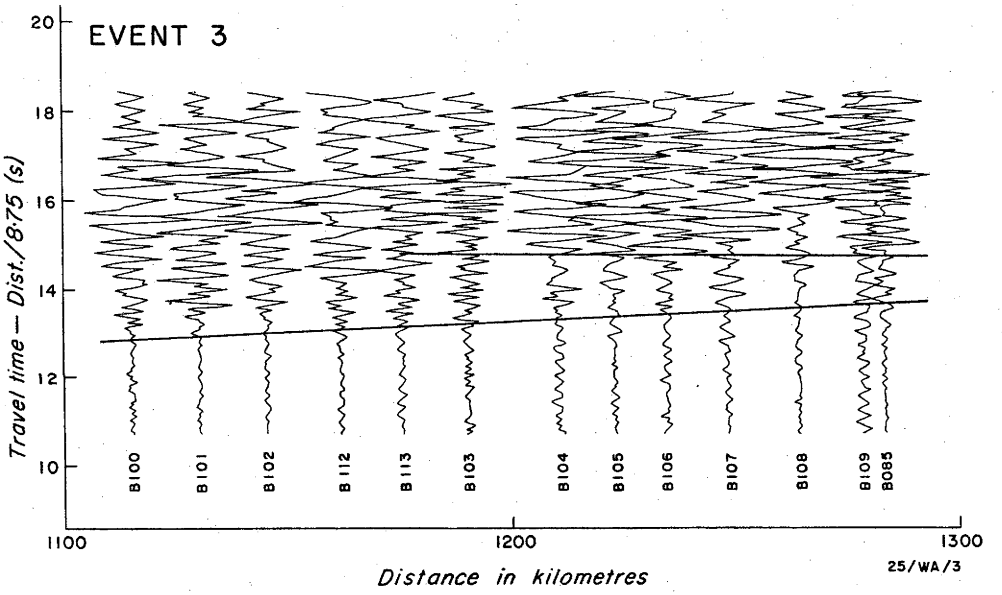
EVENT 3
20
18
16
14
12
10
Travel time — Dist./8·75 (s)
B100
B101
B102
B112
B113
B103
B104
B105
B106
B107
B108
B109
B085
1100
1200
1300
Distance in kilometres
25/WA/3

FIGURE 5

APPENDIX 6

Theory and application of the time term method.

APPENDIX 6 - THEORY AND APPLICATION OF THE TIME TERM METHOD.

A6.1 INTRODUCTION

Gardner (1939) showed that the time for a refracted wave to travel from a shot to a recording station can be partitioned, approximately, into three segments, comprising the time the wave would take to travel the surface distance between the two sites at the refracting velocity, and two terms, which he called delay times, which, if the velocity structure above the refractor is known, can be converted to refractor depths under the shot and station. He then described the design of interconnected networks of shots and stations which would allow the unique calculation of the delay times for the shots and stations.

Scheidegger and Willmore (1957) gave a more rigorous description of the method of calculating delay times, which they called time terms, and the time term method of seismic refraction analysis was spawned. Willmore and Bancroft (1960), in a more expansive treatment, discussed the limitations and accuracy of the technique. The formulation of Scheidegger and Willmore (1957) was set up to handle small amounts of data using a desk calculator. With the advent of large, high speed computers, the number of data that could be readily analysed increased, and the formulation of an analytical procedure by Berry and West (1966a,b) suitable for programming on a computer led to world wide acceptance and usage of the technique.

The method as originally proposed by Scheidegger and Willmore (1957) has since been extended to more complex velocity structures within the refracting layer. In the following description of the technique, these complex velocity structures are discussed, and their methods of solution explained. Several methods of describing the refractor surface are also included.

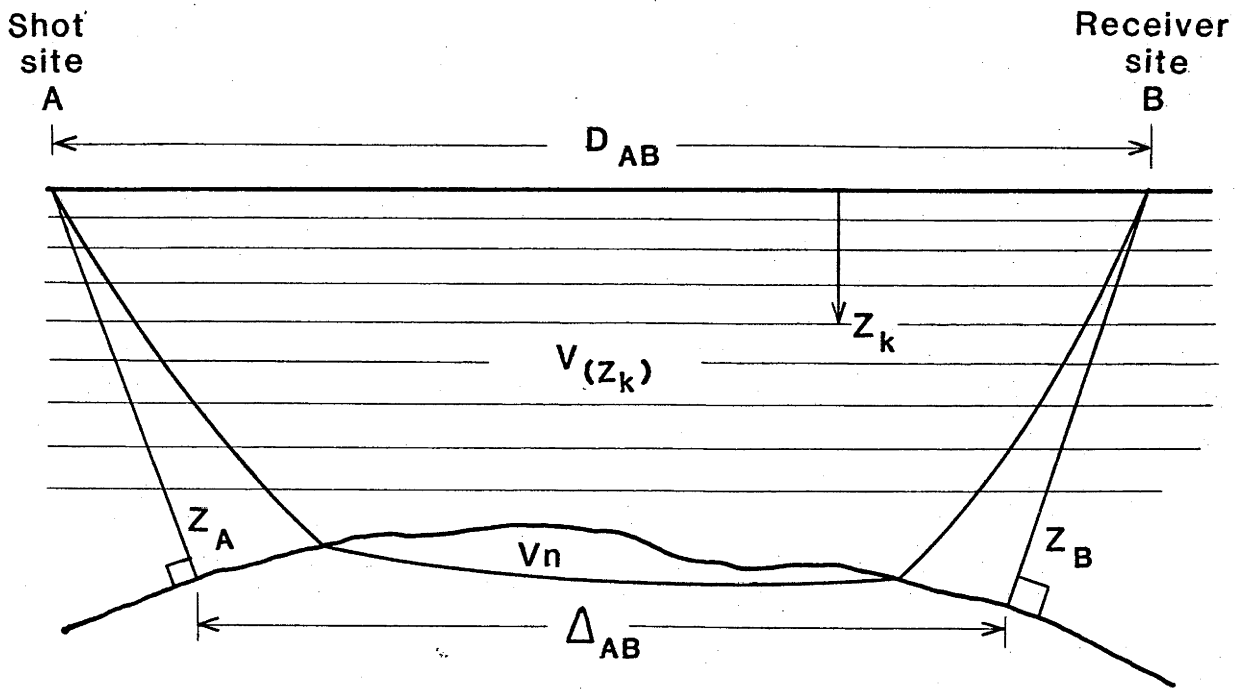

Figure A6.1: Ray path for a wave critically refracted at the nth interface while travelling from a shot at site A to a receiver at site B.

A6.2 CONSTANT VELOCITY IN THE REFRACTING LAYER

The simplest velocity structure that can be proposed within a refractor is one in which the velocity is constant. Figure A6.1 shows the ray path for a wave travelling from a shot at site A to a receiver at site B and critically refracted at the nth interface. The travel time of the wave is given approximately by (Berry and West, 1966a)

$$t_{AB} = \frac{D_{AB}}{V_n} + \int_0^{Z_A} \frac{\sqrt{V_n^2 - V_{(z_A)}^2}}{V_n . V_{(z_A)}} \, d(z_A) + \int_0^{Z_B} \frac{\sqrt{V_n^2 - V_{(z_B)}^2}}{V_n . V_{(z_B)}} \, d(z_B)$$

$$= \frac{D_{AB}}{V_n} + \text{time term at site A} + \text{time term at site B} \qquad (1)$$

where

D_{AB} is the distance between A and B,

$V_{(z_A)}$ is the velocity at depth z_A under site A,

V_n is the velocity in the base refractor, and

Z_A, Z_B are the depths to the refractor at A and B respectively, measured perpendicular to the refractor.

The following assumptions were made in formulating this equation:

(1) The velocity varies only with depth (perpendicular to the refractor) within the critically refracted cone under the shot or station;

(2) The velocity of the base refractor (ie. V_n) is constant; and

(3) The slope and curvature of the refracting surface are small, so that $D_{AB} \simeq \Delta_{AB}$.

Most seismic surveys, and particularly those designed with the time term method of interpretation in mind, consist of a network of shots and receiving stations, so that a family of travel-time equations can be written in the form

$$t_{ij} = \frac{D_{ij}}{V} + \Gamma_i + \Gamma_j \qquad (2)$$

where

t_{ij} is the theoretical travel-time from the ith site to the jth site,

D_{ij} is the distance between the ith and jth sites,

Γ_i, Γ_j are the time terms at the ith and jth sites, respectively, and

V is the velocity in the refractor.

For a survey of M shots and stations, there is a maximum of M(M-1) possible equations of this form; this corresponds to a shot and receiver at every site. In practice, there are usually fewer equations. There are, however, only M time terms to be calculated, as well as the refractor velocity. If there are sufficient equations of this type, they are best solved in a least squares sense by minimising the sums of the squares of the differences between the times calculated from the model and the measured travel times. Berry and West (1966 a,b) give a lucid description of the technique of linear inversion of these equations, and only a brief description is given there.

If T_{ij} is the measured travel-time and R_{ij} is the residual, then

$$R_{ij} = T_{ij} - t_{ij}$$

Berry and West (1966a,b) introduced the term $X_{ij} = T_{ij} - \frac{D_{ij}}{V}$ to combine the observable quantities T_{ij} and D_{ij} so that R_{ij} can be written as

$$R_{ij} = X_{ij} - \Gamma_i - \Gamma_j \qquad (3)$$

Because all shots are seldom recorded at all sites, the quantity γ_{ij} is introduced:

$\gamma_{ij} = 1$ when T_{ij} exists as data,

$\gamma_{ij} = 0$ when it does not, and

$\gamma_{ii} = 0$.

If there are L equations of type 3, the sum of the squares of the residuals is

$$I = \sum_{i=1}^{M} \sum_{j=1}^{M} (x_{ij} - \Gamma_i - \Gamma_j)^2 \gamma_{ij} \qquad (4)$$

I will be a minimum with respect to each time term when

$$\frac{\partial I}{\partial \Gamma_i} = 0 \tag{5}$$

Expanding the right hand side of equation 4, differentiating, and setting the derivative equal to zero yields

$$\sum_{j=1}^{M} \Gamma_j \gamma_{ij} + \Gamma_i \sum_{j=1}^{M} \gamma_{ij} = \sum_{j=1}^{M} x_{ij} \gamma_{ij} \tag{6}$$

This is the ith equation of a set of L simultaneous linear equations which can be expressed in matrix notation as

$$\left[c_{ij}\right]\left[\Gamma_j\right] = \left[\sum_{j=1}^{M} x_{ij} \gamma_{ij}\right] + \left[\sum_{j=1}^{M} x_{ji} \gamma_{ji}\right] \tag{7}$$

where

$$c_{ij} = \gamma_{ij} + \gamma_{ji} , \qquad i \neq j$$

$$c_{ii} = \sum_{j=1}^{M} (\gamma_{ij}+\gamma_{ji})$$

and each term in the matrix on the right hand side of equation 7 is a summation. $\left[c_{ij}\right]$ is a coefficient matrix, and

$$\left[\sum_{j=1}^{M} x_{ij} \gamma_{ij}\right] + \left[\sum_{j=1}^{M} x_{ji} \gamma_{ji}\right]$$

is a data matrix, so that

$$\left[\Gamma_j\right] = \left[c_{ij}\right]^{-1} \left\{\left[\sum_{j=1}^{M} x_{ij} \gamma_{ij}\right] + \left[\sum_{j=1}^{M} x_{ji} \gamma_{ji}\right]\right\} \tag{8}$$

gives the time terms as functions of the measured quantities D_{ij}, T_{ij} and V (all in X_{ij}).

If none of the shots and sations coincides, matrix c_{ij} is singular, and the time terms will be determined only to within an additive constant. This is because the equation

$$t_{ij} = \frac{D_{ij}}{V} + (\Gamma+\alpha) + (\Gamma-\alpha)$$

is also true. The problem can be overcome in one of two ways. If a shot and station are sufficiently close (though not at the same site) that their

time terms might reasonably be assumed to be the same, they can be assigned the same site and matrix c_{ij} will then become connected and nonsingular. Alternatively, one of the time terms must be assigned an arbitrary value, thus reducing the order of the matrix by one and achieving the same result. Some readjustment of the time term network may be necessary after the solution has been obtained.

If the number of data are considerably in excess of the number of time terms, a least squares velocity may be calculated. Rewriting equation 4 as

$$I = \sum_{i=1}^{M} \sum_{j=1}^{M} \left(T_{ij} - \frac{D_{ij}}{V} - e_i + \frac{f_i}{V} - e_j + \frac{f_j}{V}\right) \gamma_{ij}$$

where

$$e_i = c_{ij}^{-1} \sum_{i} (T_{ij}\,\gamma_{ij} + T_{ji}\,\gamma_{ji})$$

and

$$f_i = c_{ij}^{-1} \sum_{i} D_{ij}(\gamma_{ij} + \gamma_{ji})$$

(Note Berry and West, 1966a, have two errors of sign in this equation), differentiating with respect to 1/V, and setting the derivative equal to zero, yields

$$V = \frac{\sum_{j=1}^{M} \sum_{i=1}^{M} (D_{ij}-f_i-f_j)^2 \gamma_{ij}}{\sum_{j=1}^{M} \sum_{i=1}^{M} (D_{ij}-f_i-f_j)(T_{ij}-e_i-e_j)\gamma_{ij}} \qquad (9)$$

which will give the velocity to be used in equation 8 to calculate the time terms. If there are insufficient data to calculate V in this way, it must be calculated in some other way before the time terms can be found.

A6.3 VELOCITY GRADIENT IN THE REFRACTOR

In the foregoing discussion, the velocity was assumed constant throughout the refracting layer. Smith and others (1966) addressed the problem of a refracting layer in which the velocity increases with depth. In practice, this is evidenced in the travel-time data by an increase in apparent velocity with distance, ie.

$$V = V_o + V(D).$$

The simplest form of apparent velocity dependence on distance is a linear dependence:

$$V = V_o + V_1 D$$

Equation 2 becomes

$$t_{ij} = \frac{D_{ij}}{V_o + V_1 D_{ij}} + \Gamma_i + \Gamma_j \qquad (10)$$

This equation could be solved by non-linear inversion, but Smith and others (1966) chose to linearise it and use linear inversion techniques to solve for Γ_i, Γ_j, V_o and V_1. They rewrote it as

$$\Gamma_i + \Gamma_j = t_{ij} = \frac{D_{ij}}{V_o + V_1 D_{ij}}$$

Suppose there are m shots and n stations (M = m+n above), from which L ($\leq$ mxn) observations are made. The observations can be indexed by ℓ=1,2,...L, and let

$$\Gamma_i = B_i , \quad i = 1,2,...m, \quad \text{and}$$

$$\Gamma_j = B_{m+j}, \quad j = 1,2,...n .$$

Smith and others (1966) avoided the singularity noted above by setting B_{m+n}=0. The observational equation can be written

$$\gamma_{\ell i} B_i = t_\ell - \frac{D_\ell}{(V_o + V_1 D_\ell)}$$

where the second subscript of γ_{1i} denotes summation over that subscript. This equation can be linearlised by expanding the second term on the right hand side in a Taylor series expansion:

$$\frac{D}{V_o+V_1 D} = \frac{1}{V} D - \frac{V_1}{V_o^2} D^2 + \frac{V_1^2}{V_o^3} D^3 + \text{higher order terms of } D$$

$$= \lambda_o D + \lambda_1 D^2 + \lambda_2 D^3 + ...$$

The truncated length of this series is dependent on the length of the profiles being studied. Smith and others (1966) found that for reasonable values of V_o and V_1, only the first two terms are rquired for D less than 300 km. For D greater than 500 km, higher order terms may be required. Truncating to two terms yields

$$\gamma_{\ell i} B_i = t_\ell - \lambda_o D_\ell - \lambda_1 D_\ell^2 \qquad (11)$$

for which a least squares solution is to be obtained for m+n-1 time terms B_i and the two velocity parameters λ_o and λ_1. The solution requires some matrix manipulation to calculate λ_o and λ_1 before the time terms can be obtained. Smith and others (1966) describe the process and it will not be repeated here.

A6.4 ANISOTROPY IN THE REFRACTOR

Raitt and others (1969) introduced anisotropic terms into the velocity function in the travel-time equation to study anisotropy in the upper mantle in the Pacific Ocean. Their approach has been followed by many other authors.

For small anisotropy in the P-wave velocity, where the azimuthal deviation of the velocity from the isotropic velocity is less than, say, 10%, the velocity may be written, from equations 19 and 21 of Backus (1965), as

$$V(\theta)^2 = V_o^2 + A + C\cos 2\theta + D\sin 2\theta + E\cos 4\theta + F\sin 4\theta \qquad (12)$$

where

$V(\theta)$ is the anisotropic velocity, which is a function of azimuth,

V_o is the isotropic velocity,

θ is the azimuth, measured clockwise from north, and

A,C,D,E,F are constants which determine 5 of the 21 independent elastic constants of a tensor which expresses the anisotropy of the medium.

Equation 12 has been used by numerous authors in time term analyses of seismic refraction data to study anisotropy. It is a useful exercise to study these forms, the way equation 12 was applied to the travel-time equation, and the approximations that were made in the inversions of the travel-time equations for the constants C, D, E, F and $(V_o^2 + A)$.

Equation 12 may be written

$$V(\theta)^2 = V_o^2 + F(\theta) \qquad (13)$$

where $f(\theta) = A + C\cos 2\theta + D\sin 2\theta + E\cos 4\theta + F\sin 4\theta$.

Then

$$V(\theta) = [V_o^2 + f(\theta)]^{\frac{1}{2}}$$

$$= V_o \left[1 + \frac{f(\theta)}{V_o^2}\right]^{\frac{1}{2}}$$

which may be expanded in a Taylor series as

$$V(\theta) = V_o \left[1 + \tfrac{1}{2}\frac{f(\theta)}{V_o^2} - \frac{1}{8}\frac{f(\theta)^2}{V_o^4} + \ldots\ldots\right]$$

Because equation 12 is valid when $f(\theta)$ is less than about one tenth of V_o, the third term and higher order terms of the expansion can validly be ignored, so that

$$V(\theta) = V_o + \tfrac{1}{2}\frac{f(\theta)}{V_o}$$

ie.

$$V(\theta) = V_o + \frac{1}{2V_o}\left[A + C\cos 2\theta + D\sin 2\theta + E\cos 4\theta + F\sin 4\theta\right]$$

ie.

$$V(\theta) = V + C'\cos 2\theta + D'\sin 2\theta + E'\cos 4\theta + F'\sin 4\theta \qquad (14)$$

where

$$V = V_o + \frac{A}{2V_o}\ ;\ C' = \frac{C}{2V_o}\ ;\ D' = \frac{D}{2V_o}\ ;\ E' = \frac{E}{2V_o}\ ;\ F' = \frac{F}{2V_o}\ .$$

This is equivalent to the equation used by Raitt and others (1969). They wrote

$$V(\psi) = V + C'\sin 2\psi + D'\cos 2\psi + E'\sin 4\psi + F'\cos 4\psi$$

where ψ is the azimuth measured anticlockwise from east.

Applying equation 14 to the travel-time equation 2 gives

$$t_{AB} \simeq \frac{D_{AB}}{V} + \frac{(F_A+F_B-D_{AB})}{V^2}(C'\cos 2\theta + D'\sin 2\theta + E'\cos 4\theta + F'\sin 4\theta) + \Gamma_A + \Gamma_B \qquad (15)$$

where

t_{AB} is the travel-time between sites A and B,

D_{AB} is the distance between sties A and B,

F_A, F_B are the offset distances between sites A and B, respectively, and the points at which the rays meet the refractor, and

Γ_A, Γ_B are the time terms at sites A and B respectively, expressed in terms of the isotropic velocity V.

The derivation of this equation is clearly set out by Raitt and others (1969) and need not be repeated here. Equation 15 differs slightly from equation 13 of Raitt and others (1969), in that they included the term $1/V^2$ in the coefficients C', D', E', and F'.

Bringing the term 1/2V out of the coefficients C', D', E', and F' in equation 15 yields

$$t_{AB} \quad \frac{D_{AB}}{V} + \frac{(F_A+F_B-D_{AB})}{2V^3}(C\cos 2\theta + D\sin 2\theta + E\cos 4\theta + F\sin 4\theta) + \Gamma_A + \Gamma_B \qquad (16)$$

which is the form of the equation used by Bamford (1977). In this equation, D_{AB} and θ are observed quantities; F_A and F_B must be estimated. 1/V, C, D, E, and F, and Γ_A and Γ_B are unknowns.

Raitt and others (1969) used a linear inversion technique to solve their equation 13 for the parameters 1/V, C', D', E', and F', as well as for the time terms. Their approach was followed by many other workers, eg. Morris and others (1969); Berry and Fuchs (1973); Bamford (1973a, 1976); Mair and Lyons (1981). However, when the equation is expressed in the form of equation 16, it is clearly non-linear in 1/V.

Bamford (1977) described V as "the assumed isotropic velocity", from which it might be deduced that he does not calculate 1/V in his inversion, but that the values of $1/V_o$ in his Table 1, which are equivalent to 1/V in this discussion, were derived by other means. If 1/V is known, equation 16 becomes linear in all unknowns and may be solved by linear inversion techniques. It is therefore a useful exercise to use the results of Bamford's (1977) inversion to study the effects of assuming that equation 16 is linear in all parameters including 1/V.

Let

$$a_{i1}x_1 + a_{i2}x_2 + a_{i3}x_3 + \ldots + a_{im}x_m = y_1 , \qquad i = 1,2,\ldots,n \qquad (17)$$

be a set of n simultaneous linear equations, where $n \geq m$, which can be written in matrix notation as

$$[a_{ij}]\ [x_j] = [y_i] \qquad (18a)$$

If $n \neq m$, the n simultaneous linear equations in m unknowns can be converted to m simultaneous linear equations in m unknowns by

$$[a_{ij}]^T\ [a_{ij}]\ [x_j] = [a_{ij}]^T\ [y_i]$$

ie.

$$[b_{ij}]\ [x_j] = [z_j], \qquad i = j = 1,2,\ldots,m \qquad (18b)$$

The optimum solution for equations of the form of 18a is found by minimising the sum of the squares of the differences between the observed quantities Y_i and the theoretical values y_i (or their equivalents Z_i and z_i in 18b); ie. if

$$R_i = Y_i - y_i$$

ie.

$$R_i = Y_i - a_{i1}x_1 - a_{i2}x_2 - \ldots - a_{im}x_m,$$

the optimum solution for x_{ij} occurs when

$$\frac{\partial \sum_{j=1}^{m} R_j^2}{\partial x_{ij}} = 0 = -2a_{ij}(Y_i - a_{i1}x_1 - a_{i2}x_2 - \ldots - a_{im}x_m) \qquad (19)$$

ie. The optimum solution of equation 18 is found by solving a set of m simultaneous linear equations:

$$a_{i1}x_1 + a_{i2}x_2 + \ldots + a_{im}x_m = Y_i \quad , \quad i = 1,2,\ldots,m$$

which may be written in matrix notation

$$[a_{ij}]\ [x_i] = [Y_i] \tag{20}$$

Equation 20 can be solved by the matrix operation

$$[a_{ij}]^{-1}\ [a_{ij}]\ [x_i] = [x_i] = [a_{ij}]^{-1}\ [Y_i]$$

Raitt and others (1969) expressed equation 16 in the form of equation 18 above and solved it by the linear inversion method just outlined. The equation of type 19 for minimising the sum of the squares of the residuals with respect to 1/V is therefore

$$\frac{\partial \sum_{j=1}^{m} R_j^2}{\partial \frac{1}{V}} = 0 = -2 \left[D_{AB} + \frac{3(F_A+F_B-D_{AB})}{2V^2} (C\cos 2\theta + D\sin 2\theta + E\cos 4\theta + F\sin 4\theta) \right]$$
$$\cdot \left[T_{AB} - \frac{D_{AB}}{V} - \frac{(F_A+F_B-D_{AB})}{2V^3} (C\cos 2\theta + D\sin 2\theta + E\cos 4\theta + F\sin 4\theta) - \Gamma_A - \Gamma_B \right]$$

which will give the optimum solution according to the above technique only if

$$\left| D_{AB} \right| >> \left| \frac{3(F_A+F_B-D_{AB})}{2V^2} (C\cos 2\theta + D\sin 2\theta + E\cos 4\theta + F\sin 4\theta) \right| \tag{21}$$

Bamford's (1977) best solution, given in his Table 2, has

$V_o = 8.05$

$C = 3.177$

$D = 3.246$

$E = 0.647$

$F = -0.172$

and was obtained by setting $F_A = F_B = 30$ km, deriving a solution, and using that solution to calculate new offsets from which the above parameters were obtained. Setting $F_A = F_B = 30$ km, at $D_{AB} = 100$, 200, and 300 km, the right hand side of equation 21 is 4%, 7%, and 8% of D, respectively, at $\theta = 16^o$, the azimuth of maximum velocity.

At the distances at which Pn refractions are recorded at sea, the assumption of linearity in equation 16 is probably valid. For the greater distances common in continental surveys, the assumption of linearity may not be valid. In such cases, 1/V must either be assumed or equation 16 solved by non-linear inversion.

From equation 15, the velocity deviation of each measured travel time from that expected for an isotropic refractor can be written as

$$\delta V = \frac{(T_{AB} - D_{AB}/V - \Gamma_A - \Gamma_B)V^2}{(F_A + F_B - D_{AB})} \qquad (22)$$

where T_{AB} is the measured travel time between sites A and B. When plotted as a function of azimuth, these deviations form a "scattergram" and are usually used to illustrate the variation of refractor velocity with azimuth. Another way of demonstrating the anisotropy is to plot the azimuthal component of velocity defined by the 2θ and 4θ terms, ie.,

$$\delta V(\theta) = C'\cos 2\theta + D'\sin 2\theta + E'\cos 4\theta + D'\sin 4\theta \qquad (23)$$

Often the 4θ terms are very much smaller than the 2θ terms and are not calculated (eg. Raitt and others, 1969). $\delta V(\theta)$ is often superimposed on the scattergram.

A6.5 GEOGRAPHICAL VARIATION OF REFRACTOR VELOCITY

Morris and others (1969) introduced a variation of refractor velocity with geographical position into the travel-time equation. If (x_A, y_A) are the position coordinates of site A and (x_B, y_B) are the coordinates of site B, equation 16 may be expanded to

$$t_{AB} \simeq \frac{D_{AB}}{V} + \frac{(F_A+F_B-D_{AB})}{2V^3} (C\cos 2\theta + D\sin 2\theta + E\cos 4\theta + F\sin 4\theta)$$

$$+ E_1\bar{x}_{AB} + E_2\bar{y}_{AB} + E_3\bar{x}^2_{AB} + E_4\overline{x_{AB}y_{AB}} + E_5\bar{y}^2_{AB}) + \Gamma_A + \Gamma_B \qquad (24)$$

where

$$\bar{x}_{AB} = \frac{x_A+x_B}{2}, \quad \bar{y}_{AB} = \frac{y_A+y_B}{2}$$

and E_1, E_2, E_3, ... are the coefficients of the equation which describes the variation of refractor velocity with position. In this equation, a second order polynomial in both the x and y directions is shown. It adds five more unknowns to the list of those to be calculated.

A6.6 TIME TERM SURFACE

Because of the difficulty of reoccupying shot and receiver sites during marine surveys, every recorder seldom registers every shot, so that the number of equations of type 16 may not exceed the number of unknown parameters, including time terms, which have to be calculated. Raitt and others (1969) introduced the concept of a time term surface to circumvent this problem. The concept has since been applied to continental surveys (eg. Berry and Fuchs, 1973; Bamford, 1973a).

Equation 16 represents a family of travel-time equations from which M time terms and 5 anisotropy terms are to be calculated. Raitt and others (1969) replaced the time terms Γ_A and Γ_B by a time term surface which may be represented mathematically by:

(1) a polynomial

$$\Gamma_{(x,y)} = \Gamma_0 + P_1x + P_2y + P_3x^2 + P_4xy + P_5y^2 + \ldots \qquad (25)$$

(2) or as a double Fourier series

$$\Gamma_{(x,y)} = \sum_{n=1}^{N}\sum_{m=1}^{N} [b_{nm}\sin(nUx)\sin(mVy) + c_{nm}\sin(nUx)\cos(mVy)$$

$$+ d_{nm}\cos(nUx)\sin(mVy) + e_{nm}\cos(nUx)\cos(mVy)] \qquad (26)$$

(3) or as a linear combination of polynomial and double Fourier series.

In equations 25 and 26, P_1, P_2, ... etc. are the coefficients of the polynomial expressing the time term surface in terms of position (x,y); b, c, d, e are coefficients of the double Fourier series, U and V scale the survey area dimensions into multiples of 2π, and N is the order of the double Fourier series.

If P is the order of the polynomial, and N is the order of the double Fourier series, the number of terms needed to specify the time term surface is

$$\frac{(1 + P)(2 + P)}{2} + 4N^2$$

For example, for a second order polynomial and second order double Fourier series, 22 terms are needed to specify the time term surface. This is generally fewer than the number of individual time terms.

Raitt and others (1969) set out the procedure for calculating the coefficients and it will not be repeated here.

A6.7 MOZAIC TIME TERM ANALYSIS

Although the method of fitting a mathematical surface to the time terms means that fewer variables have to be calculated, the method has several disadvantages. Witten (1969) stressed that the fitting of a double Fourier surface to a set of data may be affected by the orientation of the axes, and real trends in the data may not be accurately represented. As well, fitting a surface to the data sacrifices "the fundamental, and, furthermore, realistic assumption that delay times at different sites are independent" (Bamford, 1976, his emphasis).

Bamford (1976) introduced the MOZAIC time term method to circumvent these problems. He was faced with the problem, as were Raitt and others (1969), of having a network of shots and stations in which few stations recorded all shots. He reasoned that there would be zones in which, by virtue of the information from geological maps, gravity maps, etc., all shot and recording sites could be expected to have equal time terms. He divided his survey area into a mozaic (hence the name of the method) of these zones and in his inversion calculated the time terms for the zones, rather than for every site. He therefore reduced the number of unknowns in his inversion.

The MOZAIC method requires only a small change to the general time term method. In equation 16, Γ_A and Γ_B are replaced by the time terms for the zones in which sites A and B lie. The equation is otherwise unchanged.

A6.8 IMPROVING THE SOLUTION BY ITERATION

The formulation of equation 1, on which the time term method is based, requires that D = Δ (Fig. A6.1). In regions of significant refractor topography, this may not be the case. Willmore and Bancroft (1960) recognised this and proposed an iterative approach, whereby D was used to calculate a first model, which was in turn used to calculate Δ to be used in a second solution. They showed, using models, that such an iterative procedure rapidly converges to a realistic solution.

The history of the interpretation of the data from the 1963 Lake Superior seismic experiment (Steinhart, 1964) provides a practical demonstration of the need to make several iterations when the refractor has considerable topography. The first solutions of the data, by Berry and West (1966a,b) using equation 2 as the observational equation, and by Smith and others (1966), using equation 11 as the observational equation, yielded models in which the depth to the Moho varied from between 20 to 30 km to between 50 to 60 km. Both solutions involved only one solution of the observational equations; that is, they were not iterated.

O'Brien (1968) reinterpreted the data using the "method of matching structure" in which he used patterns in the travel time residuals to estimate the overburden velocity, the dip of the refractor, and the offset distances. His derived model for the Lake Superior data showed that the models of Berry and West (1966) and Smith and others (1966) had exaggerated Moho topography which was displaced westward.

Bamford (1973b) reinterpreted the Lake Superior seismic data using the iterative time term technique. His first model was similar to that of Smith and others (1966). By iterating the solution, and using realistic limitations on the dips allowed to stabilise the solution, he was able to obtain, after three iterations, a model which was similar to that of O'Brien (1968).

In equation 16, the offset distances F_A and F_B are unknown. They must therefore be assumed. Bamford (1977) showed that varying the chosen values for F_A and F_B changed the coefficients of the anisotropy terms, but the overall form of the anisotropy function, when plotted as velocity against azimuth, was not greatly altered. Berry and Fuchs (1973) found that when initial values for F_A and F_B were used to calculate a model from which new values of F_A and F_B could be calculated, the solutions converged stably within a few iterations.

A6.9 ERROR ANALYSIS, AND CHOOSING THE BEST SOLUTION

Most of the workers contributing to the development of the theory of the time term method have set out ways to calculate the quality of the fit of their models to the data. They usually use the standard deviation or variance of the solution to express the quality of the fit to the complete data set, while the accuracy of any time term is measured by the standard deviation of that term's residuals.

The time term method can yield solutions in which the refractor exhibits:

(1) constant velocity;
(2) variation of velocity with depth, as shown by an increase of apparent velocity with distance;
(3) azimuthal velocity variations (anisotropy); and
(4) geographical variation of velocity (described by a polynomial of any order).

As well, the refracting surface may be described by:

(1) individual time terms;
(2) MOZAIC time terms;
(3) a time term surface expressed as either
    (i) a polynomial of order 1,2,3, etc., or
    (ii) a double Fourier series of order 1,2,3, etc., or
    (iii) a combination of polynomial and double Fourier series.

The method adopted by most workers (eg. Morris and others, 1969; Bamford, 1973a, 1977) is to calculate solutions for velocity functions of increasing complexity to try to reduce the standard deviation of the solution. Morris and others (1969) made statistical F tests between pairs of solutions to determine whether improvements in the standard deviations were significant.

A6.10 CALCULATION OF REFRACTOR DEPTH FROM TIME TERMS

The conversion of the time terms to refractor depths is based on the definition of a time term, ie., from equations 1 and 2,

$$\Gamma_A = \int_0^{Z_A} \frac{\sqrt{V_n^2 - V_{(z_A)}^2}}{V_n V_{(z_A)}} \, d(z_A)$$

Clearly, the accurate calculation of refractor depths is only possible when the velocity structure $V_{(z_A)}$ below each site, time term surface grid point, or MOZAIC time term zone is known in detail. Usually this is not the case, and an average velocity for the upper medium must be assumed. If the shots and stations were deployed along lines, and if the lines were reversed, an average velocity in the upper medium can be calculated with reasonable precision. The time terms are then converted to depths by the relation

$$Z_A = \Gamma_A \frac{V_n V_\alpha}{\sqrt{V_n^2 - V_\alpha^2}}$$

where

Z_A is the depth of the refractor at A,

V_n is the refractor velocity (isotropic velocity V in the case of an anisotropic refracting medium), and

V_α is the average velocity above the refractor.